Grid Type Deep Mixing Applications to Liquefaction Mitigation

Masaki Kitazume, Tokyo Institute of Technology, 2-12-1 Ookayama Meguro Tokyo, Japan, +81 3 5734 2798, kitazume.m.aa@m.titech.ac.jp

Abstract

Many earthquakes take place every year in Japan, in which the 1995 Hyogoken-Nambu earthquake and the 2011 Tōhoku earthquake induced both a humanitarian crisis and massive economic impacts. As liquefaction which occur in a loose and saturated sand layer, induces quite large damages of infrastructures, the importance of liquefaction mitigation has been emphasized to minimize earthquake disasters for many years. Many kinds of ground improvement techniques based on various improvement principles have been developed for earthquake disaster mitigation. Among them, the grid type deep mixing method has been often applied to liquefaction mitigation. In the method, the stiff grid walls are constructed by mixing the soil and binder *in-situ*, which are expected to restrict the shear deformation of the soil within the grid walls so that the pore water pressure generation can be remained small. The high applicability of the method was confirmed in several earthquakes, including the 1995 Hyogoken-Nambu earthquake and the 2011 Tōhoku earthquake. In this paper, the development of the method, some applications of the deep mixing method to earthquake disaster mitigation are briefly introduced.

Keywords: deep mixing method, earthquake, liquefaction, disaster mitigation

INTRODUCTION

In Japan, many earthquakes take place every year in Japan, in which the 1995 Hyogoken-Nambu earthquake and the 2011 Tōhoku earthquake induced both a humanitarian crisis and massive economic impacts. As liquefaction induces quite large damages, the importance of liquefaction mitigation has been emphasized to minimize earthquake disasters for many years. Table 1 shows the amount of damage to port facilities (Noda, 1991). According to the table, the amount of damage when liquefaction takes place is about 20 to 50 times larger than that without liquefaction. This highlights the importance of liquefaction mitigation to minimize earthquake disasters. There are many kinds of soil stabilization techniques developed for liquefaction in Japan. Among them, the deep mixing method (DMM), an *in-situ* cement stabilization techniques, was developed in 1970s in Japan and has frequently been applied to improvements of clayey and sandy soils (Kitazume and Terashi, 2013). The grid type DMM has been often applied to prevent liquefaction, where the grid of stabilized column walls function to restrict generation of excess pore pressure in the soil within the walls by confining the soil particle movement. The improvement effect of the method was first evaluated in the Hyogoken-Nambu earthquake in 1995 and was also evaluated in the Tōhoku earthquake in 2011. In this paper, some successful performance of the deep mixing method to earthquake disaster mitigation in the two earthquakes are briefly introduced.

Table 1. Comparison of amount of damage (Noda, 1991)

Earthquake	Magnitude	Port	Soil type	Max. accel. (gal)	Liquefaction	Damage (million yen)
Niigata, 1964	7.5	Niigata	Sand	159	Yes	49,980*
Tokachi Oki, 1968	7.9	Hachiohe	Sand	233	No	1,980*
Miyagiken Oki, 1978	7.4	Shiogama	Clay	273	No	160*
	7.4	Ishinomaki	Sand	195-210	Yes	3,008*
Urakawa Oki, 1982	7.3	Muroran	Sand	164	No	120
Nihonkai Chubu, 1983	7.7	Akita	Sand	205	Yes	6,400

* converted into 1978 prices.

DEEP MIXING METHOD

The Deep Mixing Method (DMM), an *in-situ* admixture stabilization technique using cement was developed and put into practice in Japan in the middle of 1970s, and has been applied in many construction projects for various improvement purposes (Kitazume and Terashi, 2013). Figure 1(a) and 1(b) show Japanese DM machines for on land and marine constructions, respectively. The special machine used to stabilize soft soil is basically composed of several mixing shafts and blades, a binder-supplying system and a control system.

In one operation, a column shape of stabilized soil is constructed in a ground. Through a series of construction steps, any arbitrary shape of improved ground can be constructed in a ground; block, grid, wall and group column types. The block, grid and wall types are manufactured by overlapping deep-mixed stabilized soil columns. The block type is the most stable against both the external and internal failures among all the patterns. The grid type has almost the same function as the block type with less stabilized soil volume. When the major concern is the consolidation settlement of soft ground under an embankment or a light weight structure, the group column type can provide a good solution.



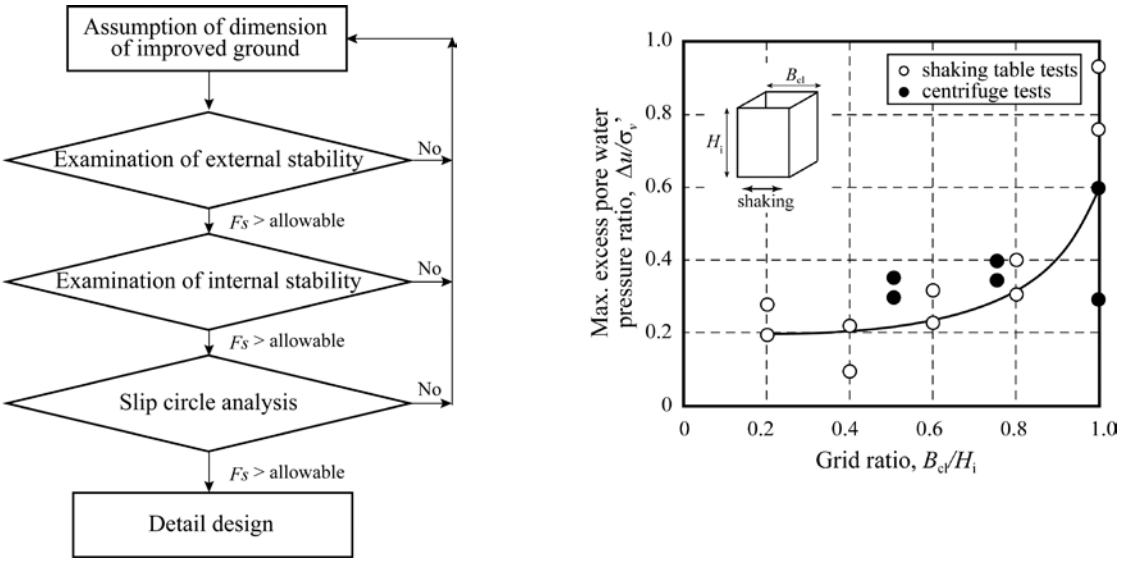
(a) For on land construction **(b) For marine construction**

Fig. 1. Deep mixing machines.

DEVELOPMENT OF GRID TYPE IMPROVEMENT FOR LIQUEFACTION MITIGATION

In the grid type improvement, the spacing of the grid wall is one of the essential factors for the liquefaction design, which the thickness and strength of the grid wall are the other essential factors for the external and internal stabilities. The development of the grid type of improved ground for liquefaction mitigation was initiated by the Ministry of Construction in the late 1980s by a collaborative study with several Japanese construction firms, in which many centrifuge model tests, large scale shaking table tests and numerical analyses were carried out to investigate these factors on the liquefaction (Fujii et al., 1988, ; Koseki et al., 1991; Suzuki et al., 1991; Babasaki et al., 1992; Matsuo and Shimizu, 1994; Matsuo et al., 1996; Namikawa et al., 2005, 2007). According to these reteach, the Ministry of Construction proposed the draft of the design procedure and guideline of the grid type deep mixing improvement in 1999 (Ministry of Construction, 1999). Figure 2(a) shows the design flow of the grid type improvement. In the assumption of dimension of improved ground, the ratio of the grid space and thickness of liquefiable layer is determined by Fig. 2(b), in which the maximum excess pore pressure ratio, $\Delta u/\Delta\sigma_v'$ at the mid depth of potentially liquefiable layer is plotted. The Ministry recommended that the grid ratio, B_{cl}/H_i should be smaller than about 0.8 to assure the effect of liquefaction prevention. In the external stability analysis of the improved ground, three failure modes are examined: sliding, overturning and bearing capacity failures.

In the internal stability analysis, the induced stresses due to the weight of structure and seismic inertia loads in the improved ground are calculated based on the elastic theory. The width of improved ground and the thickness of grid wall are determined so that the induced stresses become lower than the allowable strengths of the stabilized soil. In the slip circle analysis, the overall stability of the improved ground, superstructure and soft ground is evaluated.



(a) Design flow **(b) Relationship between grid ratio and max. pore water pressure ratio**

Fig. 2. Design flow of grid type improvement for liquefaction prevention (Ministry of Construction, 1999).

In order to brush up the design guideline, the research group of the Port and Airport Research Institute carried out a series of centrifuge model tests to investigate the effect of grid spacing on generation of pore pressure and seismic response in a sand layer and proposed a new design guideline in 2006 (Takahashi and Hayano, 2009; Takahashi et al., 2006, 2012a, 2012b; Coastal Development Institute of Technology. 2014). In 2008, a new design procedure was also proposed for building application based on the numerical analyses and case histories (Taya et al., 2008). In the design, the F_L value was calculated by Eqs. [1] and [2], while the coefficients, *F(L)*, *F(G)* and *F(H)*, were derived as Eq. [3] by the numerical calculations incorporating the grid space, the stiffness of the grid and the improvement depth.

$$F_L = \left(\frac{\tau_1}{\sigma_z'}\right) \Big/ \left(\frac{\tau_d}{\sigma_z'}\right)_{\text{Grid}} \quad [1]$$

$$\frac{\tau_d}{\sigma_z'} = \gamma_n \cdot \frac{\alpha_{max}}{g} \cdot \frac{\sigma_z}{\sigma_z'} \cdot \gamma_d \cdot F(L) \cdot F(G) \cdot F(H) \quad [2]$$

$$\gamma_d = 1 - 0.033z$$
$$F(L) = 0.287 \ln L - 0.095$$
$$F(G) = -0.459 \ln G + 4.026$$
$$F(H) = 0.689 \cdot e^{0.016H} \quad [3]$$

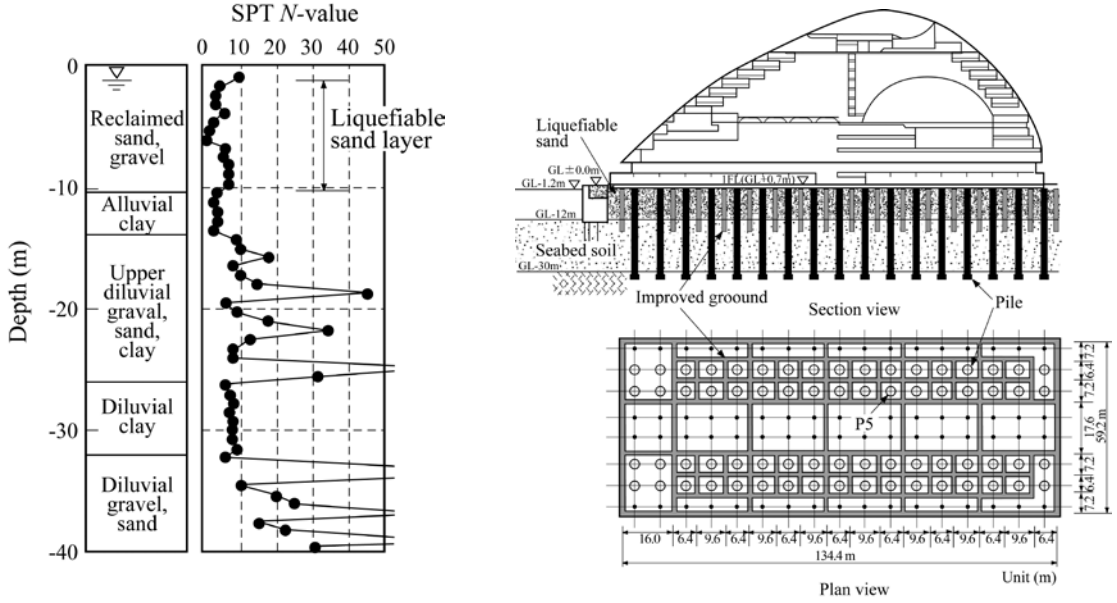
Where G = grid stiffness (MN/m^2), H = thickness of sand layer (m), L = grid space (m), z = depth (m), *F(L)* = coefficient for grid space, *F(G)* = coefficient for grid stiffness and *F(H)* = coefficient for thickness of sand layer.

APPLICATIONS AND PERFORMANCES OF GRID TYPE IMPROVEMENT

Application and Performance to Building in the 1995 Hyogoken-Nambu Earthquake

The grid type of DM improved ground was applied to a building foundation at Kobe port to prevent liquefaction during earthquake. Figure 3(a) shows the soil profile at the site which consisted of 10 to 12 m of soft reclaimed sand and gravel layers over the seabed (Tokimatsu et al., 1996; Suzuki et al., 1996). The seabed layer consisted of alternating layers of clay, sand and gravel. As small SPT *N*-value lower than 10, the top layer had been anticipated to liquefy due to earthquake excitation. The building was supported by cast-in-place reinforced concrete piles with a diameter of 2.5 m extending to dense diluvial sand and gravel at a depth of 33 m for bearing capacity. Its section and plan diagrams are shown in Fig. 3(b) (Suzuki et al., 1996). A grid type improvement was applied to prevent liquefaction in the upper loose fill. More than 1,000 stabilized soil columns with a diameter of 1.0 m were constructed where 200 kg/m^3 of blast furnace slag cement type B was mixed to obtain 2,400 kN/m^2 in q_u for the sand layer and 3,600 kN/m^2 for the clay layer. The improvement area ratio was approximately 0.2. The unconfined compressive strength of the stabilized soil after about six weeks curing was 4,000 to 6,000 kN/m^2 (Suzuki et al., 1996).

At the 1995 Hyogoken-Nambu earthquake, the ground improvement and piles' installation were already completed but the building was under construction. As the reclaimed ground around the building was not improved, liquefaction took place, which caused serious damages of the quay wall near the building as shown in Fig. 4(a). The concrete caisson type quay walls were subjected to the large excess pore water pressure due to the liquefaction, and they on the west, south and east displaced horizontally towards the sea by 1 m, 2 m, and 0.6 m respectively and the ground behind the quay walls settled by 0.5 m, 0.6 m and 0.3 m. Sand boils and ground cracks were observed at the ground surface outside of the building. In the building, however, there was no crack at the surface of the improved ground as shown in Fig. 4(b). The head of the cast-in-place piles supporting the building was found to be intact. Moreover, negligible differential settlement was observed on the first floor of the building.



(a) Ground condition (Tokimatsu et al., 1996) **(b) Plane view of Grid type improved ground (Suzuki et al., 1996)**

Fig. 3. Application of grid type deep mixing to building at Kobe port

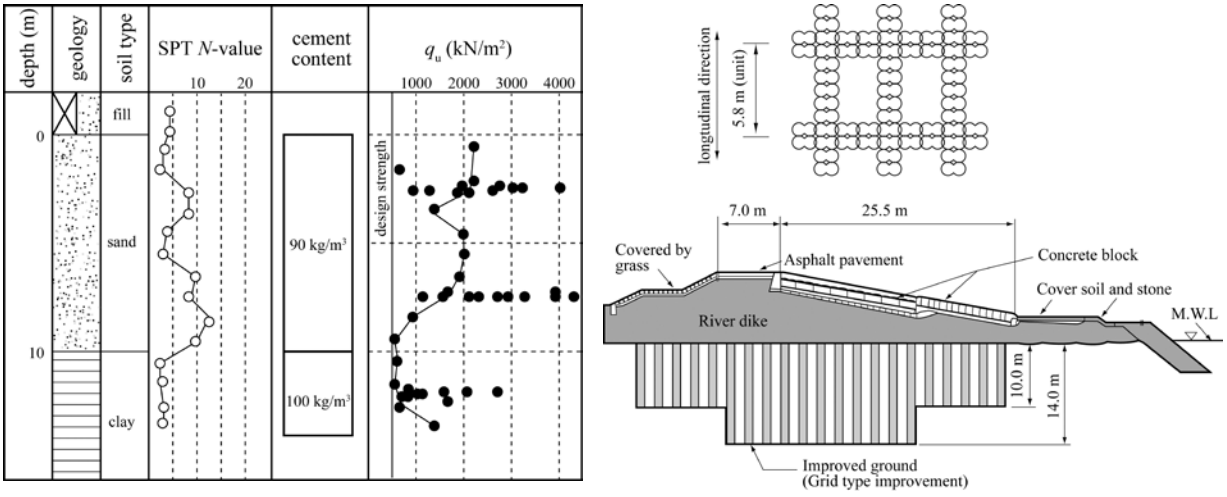


(a) Damage of sea revetment near the building **(b) Parking area in the building**

Fig. 4. Ground deformation after the 1995 Hyogoken-Nambu earthquake

Application to River Embankment after the 1995 Hyogoken-Nambu Earthquake

Yodo River flows from Lake Biwa to Osaka Bay through Osaka City. Due to the 1995 Hyogoken-Nambu earthquake in January 1995, the river dike was heavily damaged with slope failure for the length of 1.8 km due to liquefaction (Kamon, 1996), where the top portion of the river dike sank down about 3 m. The ground condition at the site is shown in Fig. 5(a). As the SPT *N*-value of part of the sandy layer was smaller than 10, it was anticipated that the liquefaction might take place there in future earthquake attacks. Because there were many residential houses in the neighborhood along the river dike, it was necessary to avoid noise and vibratory problems during the construction. This was one of the reasons why the deep mixing method was applied there. The cross section of the improved ground is shown in Fig. 5(b), where grid type improvement was applied to prevent the liquefaction of the ground and to improve the stability of the river embankment. The design strength of the stabilized soil, q_u was 500 kN/m^2. Assuming the strength ratio of the field stabilized soil and laboratory stabilized soil, q_{uf}/q_{ul} was assumed 0.25 in the design, 90 or 100 kg/m^3 of blast furnace slag cement type B was mixed to achieve the design strength for the sandy layer and the clay layer respectively.



(a) Ground condition at the site **(b) Sectional view of DM improved ground**

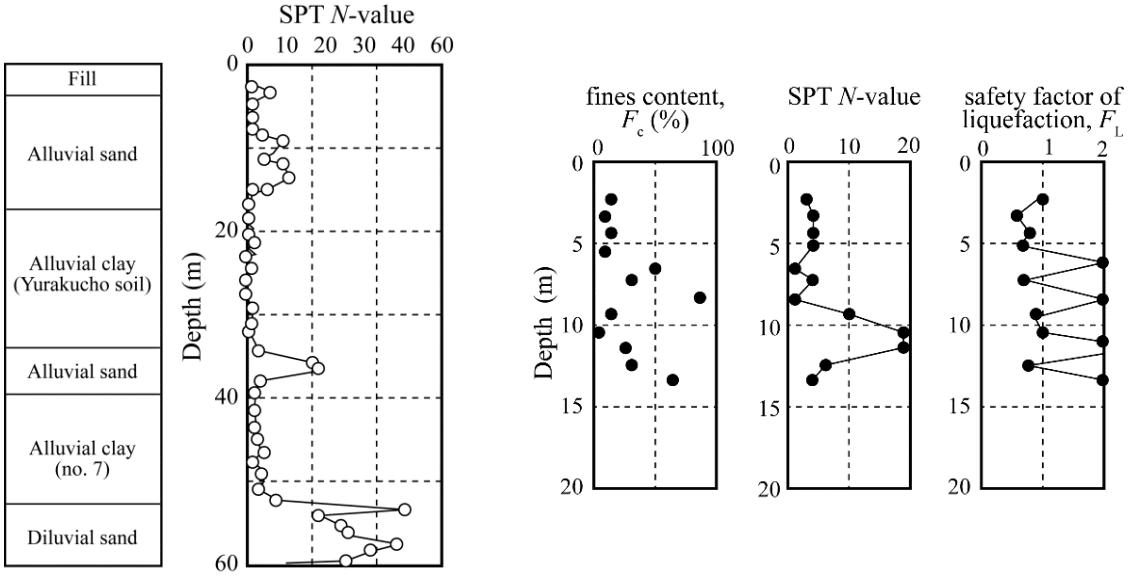
Fig. 5. Application of grid type deep mixing to river embankment at the Yodo River dike

Application and Performance to Building in the 2011 Tōhoku Earthquake

Figure 6(a) shows a four-story parking building with 213 m in length and 71 m in width in Urayasu-city, Chiba Prefecture, which was supported by the pre-stressed high-strength concrete piles with diameters from 500 mm to 1000 mm and lengths from 33 m to 60 m (Uchida et al., 2012; 2013; 2014). Figure 6(b) shows the ground condition, in which a landfill and sand layer were stratified from the surface to a depth GL-14~16 m, and a soft clay layer was distributed over the lower part. The SPT *N*-values of the landfill and sand layer from the surface to around GL-14 m were around 10. Figure 6(c) shows the estimated liquefaction potential of the site according to the Architectural Institute of Japan recommendations for foundations (Architectural Institute of Japan, 2001). The liquefaction potential, F_L became less than 1.0 in the case of the surface acceleration of 200 cm/s^2, and liquefaction might take place in the depth from GL-1.8 m to GL-12 m. The typical 15.6 m by 16.5 m grid-form ground improvement were applied there for liquefaction prevention, which was designed based on the AIJ recommendations for ground improvement (Architectural Institute of Japan, 2006) and the simplified method proposed by Taya et al. (2008). The design unconfined compressive strength of the stabilized soil was 1,800 kN/m^2. The building and the improved ground were subjected to the 2011 Tōhoku earthquake attack. Extensive soil liquefaction was observed in the reclaimed land of Urayasu city. However, neither the ground damage nor building damage were observed after the earthquake, as shown in Fig. 6(a).



(a) Building on grid type deep mixing improved ground



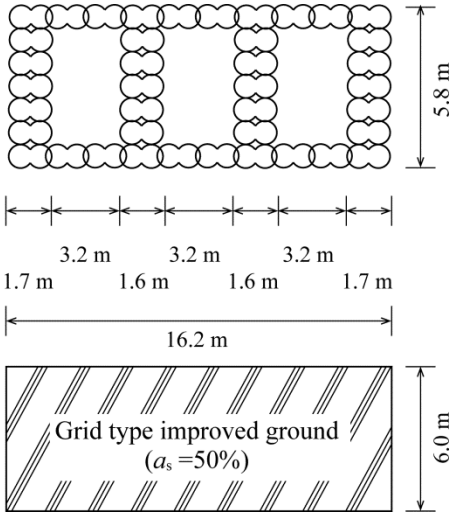
(b) Ground condition at the site **(c) Liquefaction potential at the site**

Fig. 6. Application of grid type deep mixing to building at Urayasu (Uchida et al., 2012).

Application and Performance to Road Embankment in the 2011 Tōhoku Earthquake

Soon after the aftermath of the 2011 Tohoku earthquake and tsunami, the Cement Deep Mixing Association, the Dry Jet Mixing Association and Chemical Grouting Co. Ltd. conducted field surveys in the Tohoku and Kanto areas to investigate any deformation and damage in the deep mixing improved ground and the performance of the improved grounds. Though few slight deformations were found in some grounds, as a whole no serious deformation and damage was found in the improved ground and superstructures even they were subjected to quite large seismic force (Kitazume, 2012; Tokunaga et al., 2015). Here, two applications in the field surveys are briefly introduced.

The road embankment at Soga, Chiba Prefecture, was improved by the grid type deep mixing method for liquefaction prevention. The original ground beneath the embankment contained large amount of fine sand to the depth of -7 m, which was anticipated to be highly liquefied due to earthquake motion. The improved ground has about 5.6 m in width, 6.0 m in height, and the improvement area ratio of 50%, and whose unconfined compressive strength, q_u is 200 kN/m^2 (Fig. 7(a)). No damage was found in the embankment and the improved ground as shown in Fig. 7(b), even subjected to the seismic force of 5.0 upper in Japanese Magnitude-Shindo (seismic intensity scale). As contrast, Figure 7(c) shows heavy damage of the road without improvement located in the neighborhood due to liquefaction.



(a) Layout of ground improvement



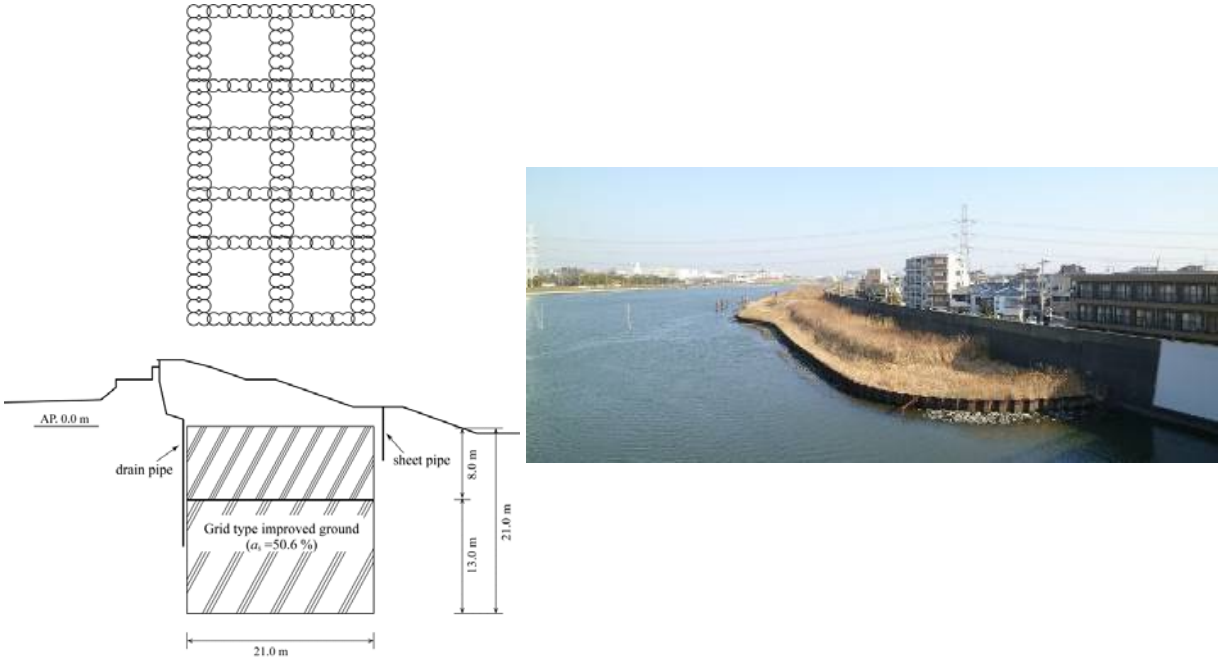


(b) Road at improved are after earthquake **(c) Road at unimproved area after earthquake**

Fig. 7. Application of grid type deep mixing to road embankment at Soga

Application and Performance to River Embankment in the 2011 Tōhoku Earthquake

The foundation for the river embankment in Chiba Prefecture was improved by the grid type DM method as shown in Fig. 8(a), where the width and height of the improved ground were 21.0 m and 21.0 m respectively. The improvement area ratio and the unconfined compressive strength, q_{uck} were 50.6% and 600 kN/m^2 respectively. No damage was found in the embankment and the improved ground, as shown in Fig. 8(b).



(a) Layout of ground improvement **(b) River embankment after earthquake**

Fig. 8. Application of grid type deep mixing to river embankment in Chiba Prefecture

CONCLUDING REMARKS

This manuscript emphasizes the importance of liquefaction mitigation to minimize earthquake disaster. Then it briefly describes the development history of the grid type deep mixing method for liquefaction mitigation. The grid type deep mixing has often been applied to many types of infrastructures and many building foundations, and its high applicability and improvement effect have been evaluated in many earthquakes. Its design, execution and quality control and assurance have been improved based on the accumulated laboratory and field experiments, numerical analyses, field experiences and know-how.

Since the 2011 Tōhoku earthquake, the necessity and importance of earthquake reinforcement and liquefaction mitigation have been highlighted on new infrastructures and existing residential houses. Especially in Urayasu city, the liquefaction countermeasure will be conducted to more than a thousand of residential houses by the grid type deep mixing, as they were damaged by liquefaction. A large number of the numerical analyses and centrifuge tests were performed for the detail design of each house. The detail of the design and construction will be presented in future.

REFERENCES

Architectural Institute of Japan. 2006. Seismic response analysis and design of buildings considering dynamic soilstructure interaction (in Japanese).

Babasaki, R., Suzuki, K. and Suzuki, Y. 1992. Centrifuge tests on improved ground for liquefaction, Proc. of the 10th World Conference on Earthquake Engineering. 1461-1464.

Coastal Development Institute of Technology. 2014. Technical Manual of Floating and Grid Type Deep Mixing Method (in Japanese).

Fujii, N., Kusakabe, O., Keto, H. and Maeda, Y. 1988. Bearing capacity of a footing with an uneven base on slope: Direct comparison of prototype and centrifuge model behavior, Proc. of the Centrifuge 88. 301-306.

Kamon, M. 1996. Effect of grouting and DMM on big construc-tion projects in Japan and the 1995 Hyogoken-Nammbu earthquake. Proc. of the 2nd International Conference on Ground Improvement Geosystems. 2. 807-823.

Kitazume, M. 2012. Soil mixing performance in the 2011 Tohoku earthquake, The Magazine of the Deep Foundations Institute. 77-78.

Kitazume, M. and Terashi, M. 2013. The Deep Mixing Method: CRC Press, Taylor and Francis Group.

Koseki, J., Kubodera, I., Ito, K., Suzuki, K., Nishioka, S. and Fukada, H. 1991. Study of the applicability of deep mixing method as a countermeasure system against liquefaction - Numerical analysis by means of DIANA-J, Proc. of the 26th Annual Conference on Soil Mechanics and Foundation Engineering. 1015-1016 (in Japanese).

Matsuo, O. and Shimizu, T. 1994. Experimental study of design procedures for the deep mixing method used as a liquefaction prevention measure in embankments, Civil Engineering Journal. 36(7) (in Japanese).

Matsuo, O., Shimizu, T., Goto, Y., Suzuki, Y., Okumura, R. and Kuwabara, M. 1996. Deep mixing method as a liquefaction prevention measure, Proc. of the 2nd International Conference on Ground Improvement Geosystems, IS-TOKYO '96. 521-526.

Ministry of Construction. 1999. Design and construction manual of liquefaction prevention techniques (draft), Joint Research Report. 186 p. (in Japanese).

Namikawa, T., Koseki, J. and Suzuki, Y. 2007. Finite element analysis of lattice-shaped ground improvement by cement-mixing for liquefaction mitigation, Soils and Foundations, 47(3). 559-576.

Namikawa, T., Suzuki, Y. and Koseki, J. 2005. Seismic response analysis of lattice-shaped ground improvements, Proc. of the International Conference on Deep Mixing, Best Practice and Recent Advances, (1.2). 263-271.

Noda, S. 1991. Waterfront development and liquefaction, Journal of the Japanese Society of Soil Mechanics and Foundation Engineering, 'Tsuchi-to-Kiso', 39(2). 1-4 (in Japanese).

Suzuki, K., Babasaki, R. and Suzuki, Y. 1991. Centrifuge Tests on liquefaction-proof foundation, Proc. of the Centrifuge 91. 1461-1464.

Suzuki, Y., Saitoh, S., Onimaru, S., Kimura, G., Uchida, A. and Okumura, R. 1996. Grid-shaped stabilized ground improved by deep cement mixing method against liquefaction for a building foundation, Journal of the Japanese Society of Soil Mechanics and Foundation Engineering, 'Tsuchi-to-Kiso', 44(3). 46-48 (in Japanese).

Takahashi, H. and Hayano, K. 2009. Dynamic model tests in centrifuge on lattice-shaped DMM ground improvement for restraining displacement of quay wall, Proc. of the International Conference on Performance-based Design in Earthquake Geotechnical Engineering, IS-Tokyo 2009.

Takahashi, H. Morikawa, Y., Tsukuni, S., Fukutake, K., Suzuki, W. and Takehana, K. 2012a. Experimental study on floating lattice-shaped cement treatment method applied to liquefiable ground, Journal of Japan Society of Civil Engineers, 68(2). I_432-I_437 (in Japanese).

Takahashi, H., Morikawa, Y., Tsukuni, S., Yoshida, M. and Fu-kada, H. 2012b. Approach to reducing improvement depth of lattice-shaped cement treatment method for liquefaction countermeasure, Report of Port and Airport Research Institute, 51(2). 3-39 (in Japanese).

Takahashi, H., Yamawaki, S., Kitazume, M. and Ishibashi, S. 2006. Effects of DMM on liquefaction prevention and proposal on new arrangement of grid-type improvement, Report of Port and Airport Research Institute, 45(2). 135-167 (in Japanese).

Taya, Y., Uchida, A., Yoshizawa, M., Onimaru, S., Yamashita, K. and Tsukuni, S. 2008. Simple method for determining lattice intervals in grid-form ground improvement, Electrical Journal of Geotechnical Engineering, 3(3). 203-212 (in Japanese).

Tokimatsu, K., Mizuno, H. and Kakurai, M. 1996. Building damage associated with geotechnical problems, Soils and Foundations, Special Issue 1. 219-234.

Tokunaga, S., Kitazume, M., Morikawa, Y., Takahashi, H., Nagatsu, T., Honda, N., Onishi, T., Asanuma, T., Kubo, S. and Higashi, S. 2015. Performance of cement deep mixing method in 2011 Tohoku earthquake, Proc. of the Deep Mixing 2015. 1071-1080.

Uchida, A., Odajima, N. and Yamashita, K. 2013. Performance of building foundation with grid-form ground improvement during the 2011 Tohoku pacific earthquake, Architectural Institute of Japan Journal of Technology, 19(42).481-484 (in Japanese).

Uchida, A., Tsukuni, S., Akashi, T., Ohashi, M. and Arai, H. 2014. Simplified evaluation method about effect of liquefaction countermeasure for the grid-form deep mixing walls, Architectural Institute of Japan Journal of Technology, 20(46).921-924 (in Japanese).

Uchida, A., Yamada, T. Odajima, N. and Yamashita, K. 2012. Piled raft foundation with grid-form ground improvement subjected to the 2011 earthquake, Proc. of the 9th International Conference on Urban Earthquake Engineering/4th Asian Conference on Earthquake Engineering. 151-156.

CONSTRUCTION OF HIGH ROAD EMBANKMENT OVER THICK SOFT SILTY CLAY- A CASE STUDY

Radhakrishnan R, Geo-Enviro Engineers P Ltd, Chennai, Tamil Nadu, India, 044-24483522, geoenviro2012@gmail.com.
Gunasekaran C, Geo-Enviro Engineers P Ltd, Chennai, Tamil Nadu, India, gunageoenviro@gmail.com.

ABSTRACT

Calicut Bypass Phase-II project included construction of 7 m high embankment over soft compressible clays up to 18 m in thickness. Approx 1.5 km length of road out of a total 5 km length consisted of abandoned paddy fields which were low lying, waterlogged and marshy in nature. On the basis of excellent results achieved in earlier phases of the by-pass construction, ground improvement work by installing pre-fabricated vertical drains (PVD) was undertaken to stabilize the embankment foundation along the weak clay areas prior to road pavement construction to avoid large post construction settlement as well as to improve the lateral stability during and after embankment construction. This project perhaps stands out as one of the highway projects completed within a very short time period of total 18 months including four month long heavy monsoon period, when embankment construction was not possible and construction of two bridges across rivers. All activities including the ground improvement had to be programmed and completed within the shortest time period possible. The paper discusses details of the extensive ground improvement and soil instrumentation carried out for the project and will illustrate how careful planning and execution can reduce the period required for highway projects involving ground improvement.

Keywords: clay, PVD, ground improvement, embankment, settlement

INTRODUCTION

Phase-II construction of Calicut by-pass was undertaken on a priority basis by the State of Kerala in 2014. The main contract was awarded to M/S ULCCS Ltd, Kozhikode, Kerala and the ground improvement work was awarded to M/S Geo-Enviro Engineers P Ltd, as specialist agency to design and execute the work.

Soil investigation carried out confirmed thick soft clay deposits below GL in three areas along the road alignment totaling approx 1.5 km in length. These areas were low lying, waterlogged and marshy in nature. Highway embankment had to be constructed up to 7 m in height above existing GL to form the proposed road alignment along these areas. On the basis of excellent results achieved in earlier phases of the by-pass construction using pre-fabricated vertical drains or PVD (R. Radhakrishnan, 2006), ground improvement using PVD had been included in the contract to stabilize the embankment foundation along the weak clay areas prior to highway embankment construction to avoid large post construction settlement as well as to improve lateral stability during its construction.

This project stands out as one of the highway projects completed possibly within the shortest time period requiring ground improvement. The entire work including embankment construction over the entire stretch and two bridges across rivers was completed within a period of 18 months with a 4 month long heavy monsoon period, well ahead of the 24 month completion stipulated by the client. All activities including ground improvement had to be programmed and completed within the shortest time period possible. By careful planning no additional surcharge load was required to shorten the consolidation period.

SUB-SOIL CONDITION

Soil investigation established soft clay existing at site was variable in thickness from about 5 m to a maximum depth of 18 m at certain locations. The soft clay was classified as highly compressible CH soil, with high plasticity and natural moisture content. Typical subsoil details from laboratory tests are included in "Table 1". As the soft clay was weak in shear strength, it was necessary to ensure adequate embankment stability during all stages of embankment construction. Stability analyses confirmed that the 7 m high embankment will have to be constructed in three or four stages with waiting periods between stages for clay consolidation to take place under each stage of filling.

Table 1. Typical Soil Parameters

Description	Range	Average Values
Bulk Density, kN/m^3	15-19	17
Liquid Limit, %	32-60	50
Plastic limit, %	26-41	30
Natural Moisture Content, %	28-52	40
Cohesion, kN/m^2	14-22	18
Compression Index	-	0.6
Co efficient of Vertical Consolidation, m^2/year	-	1.0
Initial Void Ratio, e0	-	1.5

PVD DESIGN

Barron (1948) first proposed the general case for soil consolidation using vertical drains. Hansbo (1979) modified Barron's proposal for application with prefabricated vertical drains (PVD) and also considered soil disturbance due to PVD installation. However, as the disturbance factors are difficult to evaluate practically, only the ideal case without considering soil disturbance was employed in the PVD design for this case.

As the period available for the entire by-pass construction was very short, time available for soil consolidation and embankment construction were extremely limited. Since Kerala experiences heavy rains during the south- west monsoon period, earthwork for embankment construction was not possible during the period June to September. This monsoon period was approximately ten months after work started at site. This meant that the entire ground improvement work as well as most of embankment construction had to take place within this ten month period. In order to shorten the waiting periods for clay consolidation between construction stages as well as to keep overall completion as short as possible, the PVD spacing adopted for the project was 1.0m c/c triangular pattern.

The PVD selected for the project was 100 mm wide and 3.5 mm thick with high discharge capacity as shown in "Table 2". Based on design soil parameters, predicted final primary consolidation settlement under full embankment load could vary from 600 mm to 1300 mm depending on final embankment height and clay thickness at different locations. As the maximum expected settlement for thick clay areas

was high, it was important to ensure that the PVD discharge capacity in the kinked condition was adequate for the purpose.

Table 2. Technical specification of PVD Tencate HB 63

Properties	Test Standard	Unit	Value
Composite			
Discharge capacity-straight (240kPa), i=1	ASTM D4716	10^{-6} m^3/s	75
Discharge capacity-kinked (240kPa), i=1	ASTM D4716	10^{-6} m^3/s	60
Tensile strength (full width test)	ASTM D4595	N	2500
Elongation at break	ASTM D4595	%	20
Core compressive strength	ASTM D1621	kPa	475
Filter			
Grab strength (MD)	ASTM D4632	N	310
Trapezoidal tear	ASTM D4533	N	70
Puncture resistance	ASTM D4833	N	80
Apparent opening size	ASTM D4751	µm	90
Water permittivity	ASTM D4491	s^{-1}	0.75
Coefficient of permeability	ASTM D4491	10^{-4} m/s	1.80
Physical			
Nominal width	NA	mm	100
Nominal thickness	ASTM D5199	mm	3.50

PVD INSTALLATION

PVD was installed to the full depth of soft clay using hydraulic PVD stitchers. Hydraulic stitchers install PVD at a constant rate of penetration by static force pushing a steel mandrel without jerk or vibration during installation thus reducing disturbance to surrounding soil by the mandrel. The steel mandrel used was rectangular in cross section and had cross sectional area not exceeding 65 sq.cm as recommended, to ensure minimum disturbance to surrounding soil (FHWA,1986). A disposable anchor plate was attached to the PVD end which closed the mandrel bottom as well as anchored the installed PVD at the desired depth after penetrating the soft clay.

A heavy duty hydraulic excavator was used as base machine to power the stitcher unit for PVD installation. A photo of the PVD stitcher used is included in “Fig. 1”. The maximum depth of PVD penetration was not expected to exceed 20 m. In a good working day, it was possible to install PVD at more than 400 locations in a single shift. Due to the urgency to complete the PVD installation, work continued in two shifts per day. The PVD installation depths were closely monitored with the help of soil investigation data to ensure full penetration in soft clay stratum.



Fig. 1. PVD Installation

GEOTEXTILE SEPARATOR CUM BASAL REINFORCEMENT

The areas of ground improvement were water logged and the clay layers close to ground level were very soft in nature. Initial soil filling approx 0.7 m thick was necessary to provide a safe and stable work platform for heavy machinery to operate under such site condition.

In order to avoid mixing of embankment fill soil with the drainage filter during its placement and compaction, it was necessary to place a suitable geotextile separator between the drainage filter and the earth fill placed above it subsequently. Both non-woven and woven geotextile may be used to act as the separator. However, non-woven geotextile has low tensile strength and undergoes large strain under load, allowing large lateral embankment deflection during its construction over soft clays having poor shear strength. Woven geotextile undergoes lower strain during comparable loading and therefore is a better choice in this respect. Moreover, woven geotextile has higher tensile strength compared to non-woven and can also act as basal reinforcement for the embankment under construction. While choosing the woven geotextile, it is necessary to consider the permeability and apparent opening size to avoid clogging of the drainage filter.

Woven geotextile as shown in “Table 3” was therefore employed based on computerized embankment stability analysis to act as a separator as well as basal reinforcement for the embankment to reduce stresses induced in the soft clay particularly in the initial stages of embankment construction.

DRAINAGE FILTER

A suitable drainage filter is necessary to ensure quick drainage of pore water discharged from installed PVD in order to allow soft clay consolidation to take place without delay. As clean sand was difficult to obtain for this purpose, stone chips (aggregates) 8-10 mm in size and minimum 300 mm in thickness was employed for this purpose over the installed PVD.

Table 3. Woven Geotextile Specification

Description		Test Standard	Value
Mass, kg/m^2		ASTM D5261	0.160
Tensile Strength, kN/m	Warp	ASTM D4565	50
	Weft		40
Elongation at break, %	Warp	ASTM D4565	25
Grab Tensile Strength, N		ASTM D4632	1400
Trapezoidal Tearing Strength, N		ASTM D4533	800
Water Permeability, l/m^2/s		ASTM D4491	37
Index Puncture Resistance, N		ASTM D4833	425
Apparent Opening Size, µm		ASTM D4751	130

EMBANKMENT CONSTRUCTION

As the underlying soft clay was weak in shear strength, it was necessary to consider lateral embankment stability during all stages of its construction. Embankment loading had to be controlled to ensure that shear failure in underlying soft clay does not happen at any stage of embankment filling. Stability computations established the maximum fill levels possible in each stage of embankment loading as well as minimum waiting periods required in between loading stages for the soft clay to gain sufficient strength before the next stage of embankment filling takes place. Minimum Factor of safety considered for each stage of loading was 1.2 and 1.1 under static and seismic condition respectively. Under full embankment load the FS required was 1.3 and 1.1 for static and seismic conditions respectively. Based on this, the embankment construction had to be carried out in 4 stages where soft clay was thick and embankment height maximum. Please refer "Fig.2(c)". The woven geotextile basal reinforcement also helped to improve embankment stability. The required minimum waiting period between stages was 4 weeks.

GEOTECHNICAL INSTRUMENTATION

Platform settlement gauges and Casagrande Piezometers were installed at selected locations to monitor ground settlement and dissipation of pore water pressure respectively during clay consolidation. Settlement gauges were installed approx 0.5 m below ground level and Piezometers were installed within boreholes at depths approximately middle of the soft clay thickness and 1m above the bottom of the soft clay layer. Both instruments were installed as per recommended procedure and in groups for comparison of records at the required locations. The instruments were monitored throughout the embankment construction and clay consolidation for a period of more than 12 months. Typical observed settlement and Piezometer excess pore pressure at one location (Settlement Gauge S_2 and Piezometers P3 and P4), where maximum soft clay depth was 18 m below GL and embankment height was 7 m, are included in "Fig.2(a)"and "Fig.2(b)". P3 & P4 were installed at mid depth and at 1.0 m above bottom of the soft clay layer, respectively.

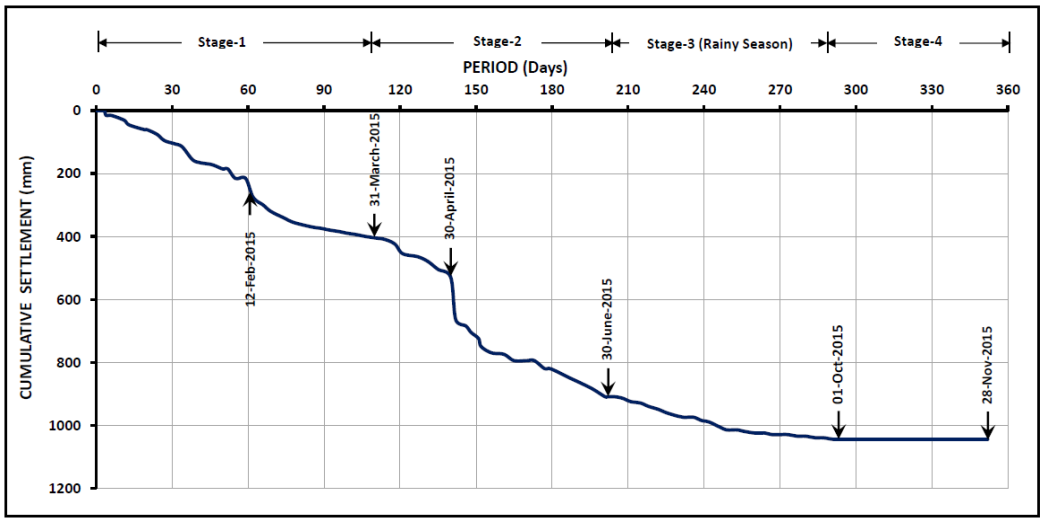


Fig. 2(a). Observed Settlement at Ch 2+820 (S_2)

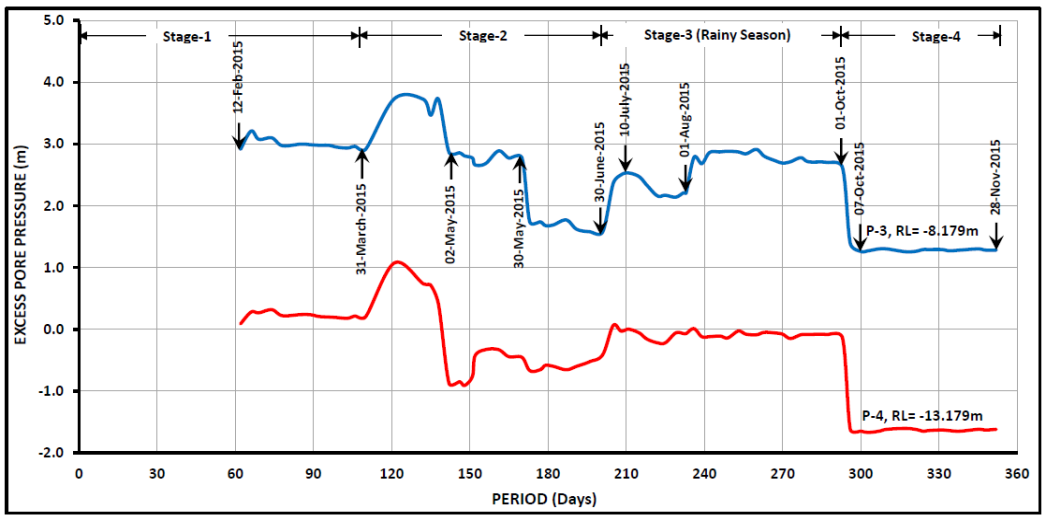


Fig. 2(b). Piezometer Excess Pore Pressure

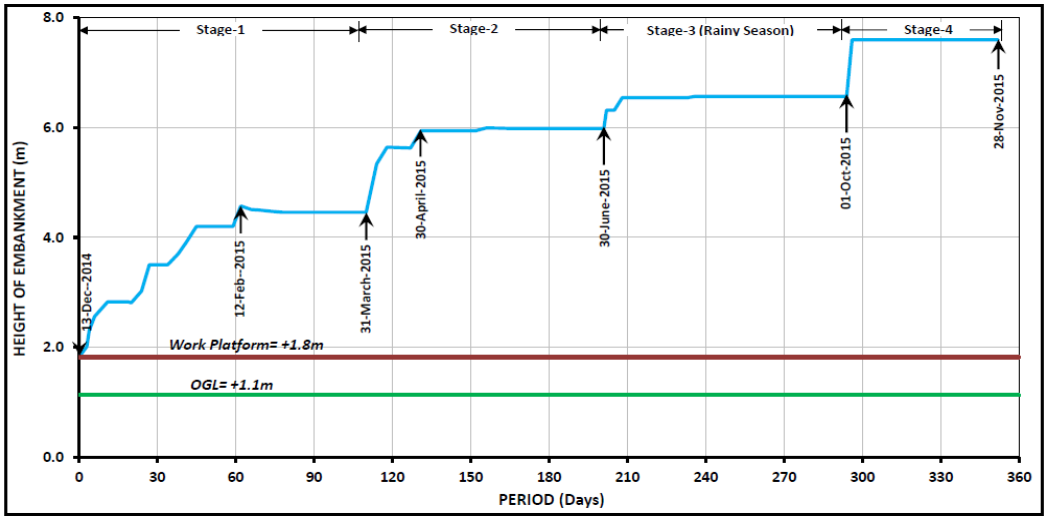


Fig. 2(c). Embankment Fill Height

Comparing with the embankment loading at the same location (Fig.2(c)), it may be clearly observed that both settlement gauge and Piezometers at this location responded in general, as expected in accordance with the embankment loading. "Table 4" below shows the settlement observed under different loading stages. The maximum settlement recorded at this location was 1044 mm under the completed embankment. The degree of consolidation achieved under each stage of embankment loading is included in "Table 4". It is significant to note that no settlement was observed under the final stage of loading as by end of stage-3 already 100% of total primary settlement had taken place.

Figure 2(b) shows the excess pore pressure registered during the period of observation. Due to some delay, Piezometers were installed for the project only two months after Stage-1 embankment construction commenced. In general, the excess pore pressures registered are as expected. However, the pore pressure dissipation appears to be slower initially but was much quicker under the later stages of embankment construction. It may be noted that both the Piezometers- at mid clay layer and 1m above bottom of clay layer- responded similarly to fill level changes. Much lower excess pressures were registered at the lower piezometer (P-4) than the one at mid layer (P-3). Excess pore pressure computations showed some negative excess pressure at times. However, it may be concluded that they may not really be negative pore pressures in soil but could rather be due to observed ground water levels in reference wells established some distance away. The sudden excess pore pressure dissipation noticed at the end of stage-3 is hard to explain and requires further study of the results.

Table 4. Observed Settlement and Degree of Consolidation under stages of loading

Loading Stages	Fill Height, m	Observed Settlement, mm	Degree of Consolidation, %
Stage-1	3.4	404	39
Stage-2	1.5	505	87
Stage-3	0.6	135	100
Stage-4	1.0	Nil	100

DISCUSSION

Figure 3 shows the Degree of consolidation ($\bar{U}$) against the time period for consolidation under the four different stages of embankment construction at Settlement gauge location S_2 as shown in "Fig. 2(a). The same figure also shows the predicted degree of consolidation against period 'ideal case' proposed by Hansbo (1979) when similar embankment is constructed in a single stage. As is noticed the required $\bar{U}$=90% is achieved much earlier in the case of the ideal one stage construction. However sub-soil conditions dictate the construction of the embankment in a number of stages, four in this case. While planning the total construction period, it is therefore important to consider the stages of embankment construction.

Secondly, it may be noted that there was no settlement observed under the final 1m filling under stage-4 construction (Fig.2(a)). A larger final stage loading might have caused further clay consolidation and settlement delaying the embankment construction. It is clearly seen that in cases where embankment construction period is limited, speed of embankment construction should be maximized under earlier stages of loading. The success of this project may be attributed to the fact that most embankment filling took place before the heavy monsoon period giving ample time for full clay consolidation to take place during the monsoon period.

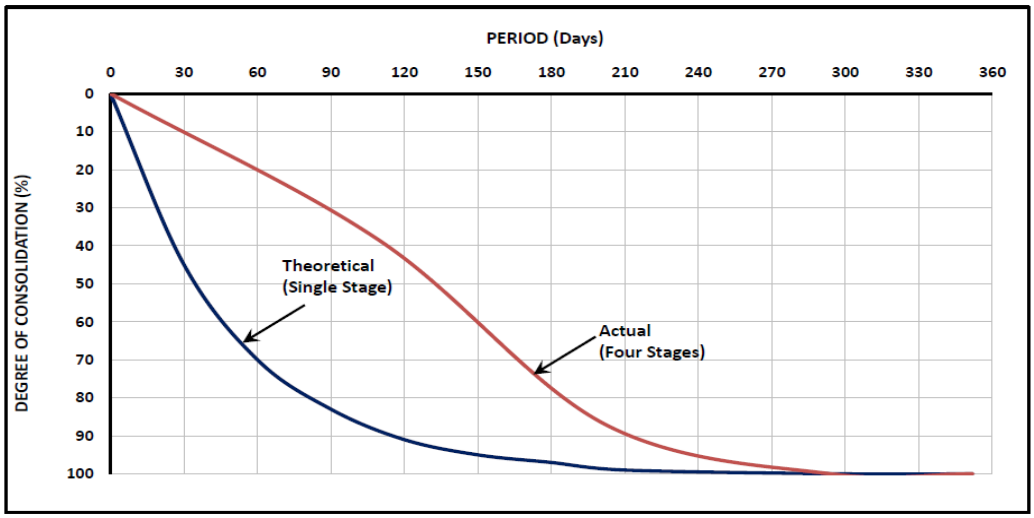


Fig. 3. Comparison of Degree of Consolidation

CONCLUSIONS

The project clearly demonstrates the importance of PVD in reducing the time period required considerably for high embankment construction over thick soft compressible clays. By careful planning, design and execution of ground improvement work using PVD and controlling embankment construction, high embankments can be constructed safely and within shorter construction periods.

Suitable Geotextile material can be incorporated in embankment construction for safety as well as to speed up construction. A woven geotextile was used in this case for the dual purpose- as a separator as well as a basal reinforcement.

Geotechnical instrumentation is an integral part of ground improvement work for purposes of control as well as to ensure that desired results have been achieved. Careful installation and monitoring and good knowledge of geotechnical engineering to interpret results are essential for the success of such works.

ACKNOWLEDGEMENT

The support and understanding of the main contractor M/S ULCCS Ltd and their staff and the interest and close monitoring of the project by the client PWD (NH), Kozhikode, Kerala have been major factors for the successful completion of the project. Their contributions are gratefully acknowledged.

REFERENCES

Barron, R.A., 1948. Consolidation of Fine Grained Soils by Drained Wells. Transactions of the American Society of Civil Engineers, Vol. 113, pp.718-742.

FHWA, 1986. Prefabricated Vertical Drains, Vol. 1. Engineering Guidelines, FHWA/RD-86/168. Federal Highway Administration, Washington. DC.

Hansbo, S., 1979. Consolidation of Clay by Band-shaped Prefabricated Drains. Ground Engineering, Vol. 12, No.5, pp.16-25.

Radhakrishnan, R., 2006. Ground Improvement for Embankments Over Soft Clay. Proceedings. IGC 2006, Chennai, pp. 631-633.

FAILURE ANALYSIS AND STRENGTHENING OF TAILING POND EMBANKMENT BY PREFABRICATED VERTICAL DRAINS AND GEOGRID

Biswajit Das, Tata Consulting Engineers Limited, Kolkata, West Bengal, India, +91 33 6611 5500, biswajitd@tce.co.in
Dr. Anup Kumar Mandal, Tata Consulting Engineers Limited, Kolkata, West Bengal, India, +91 33 6611 5500, akmandal@tce.co.in
Sanjoy Chowdhury, Tata Consulting Engineers Limited, Kolkata, West Bengal, India, +91 33 6611 5500, schowdhury@tce.co.in

ABSTRACT

Tailing pond of an iron ore mine necessitated raising the height of its embankment to create additional storage capacity. The tailing pond is located in eastern India and raising the height of embankment was going on during the month of January, 2014. Upstream method of construction was adopted since there was no space available at the downstream side. During the construction, about 200 m stretch of the north east embankment of height about 5.5 m failed forming a classical slip circle on the upstream side involving about half the top width of the embankment. To find out the root cause of the slope failure, detail geotechnical investigation work was carried out within the embankment as well as in the adjacent areas within the pond. About 7.5m thick very soft tailings were detected below the constructed embankment. Shear strength of the soft tailing was very low and was inadequate to sustain imposed embankment load. This resulted in the failure of the embankment. Analysis of the tailing deposit revealed that even after failure, settlement was continuing due to imposed embankment load. Under normal one-dimensional consolidation, the tailing deposit would have taken about 5.7 years for 90% of primary consolidation. However, in order to mitigate the scarcity of storage space, mining plan required raising the height of the embankment within next six to eight months. Therefore, despite the fact that there was a failure, it was necessary to continue the construction on the underlying weak stratum. The system was redesigned with installation of prefabricated vertical drains (PVDs) to accelerate the consolidation process thereby gaining the in-situ strength. Strength was additionally enhanced by installing geogrids in multiple layers. It stabilized the existing embankment and also ensured construction of additional height over and above the existing embankment.

tailing, embankment, consolidation, prefabricated vertical drain, geogrids.

INTRODUCTION

Beneficiation plant in the Iron mines enhances the mineral content by separation of contaminants and fines. The residue (waste material) is called tailings/tailings depending upon the grain sizes. These tailings in a slurry form are generally disposed in a pond called as tailing pond/tailing pond. Height of embankment of such ponds is increased either by upstream or by downstream or by centrally raising methods in different phases as quantum of deposition in the pond increases with time.

Upstream raising of embankment of iron ore tailing pond was in progress at a Project site in Eastern India when a slip circle failure at one part of the embankment occurred. Primarily mine waste materials were used for the construction work. Length of the failure zone was about 200 – 250 m. The failure pattern closely resembled with a classical slip circle having crest at around the mid-width of the embankment at top and toe towards the upstream side of the embankment. The failure associated with movement of huge quantity of embankment mass and tailings within the pond which in turn created a heaving at some distance within the pond. Construction activities were discontinued and regular monitoring was done by visual inspection to check any occurrence of further distress. Detailed geotechnical investigation was undertaken to find out the root cause of the failure and to check feasibility of further raising of the height

of the embankment. Based on the investigation report, the root cause of the failure was very poor shear strength of the tailings over which the embankment was constructed. The tailings were improved by accelerated consolidation aided by installing prefabricated vertical drains (PVDs) and laying multi- layer high tensile geogrids. Consequently, it was possible to raise the height of the embankment up to a maximum of 6 m over and above the existing embankment.

DEVELOPMENT AFTER THE FAILURE

Longitudinal cracks and sink holes were formed on the embankment top aftermath of failure. The numbers and width of such cracks and radius of sink holes increased with time. This was a clear indication of continuation of further movement/settlement of the embankment, although at a much slower rate. The geotechnical investigation comprised boreholes, standard penetration tests (SPT), collection of soil and tailing samples, field permeability tests and laboratory tests on selected samples.



Fig. 1. The embankment after failure; Heaving within the pond due to failure is visible at the upstream side.



Fig. 2. Longitudinal crack and sink hole in the embankment.

FINDINGS OF GEOTECHNICAL INVESTIGATION

Boreholes were sunk both on the embankment and within the pond to find out strata characteristics. Generally, three type of strata were encountered in the boreholes carried out within the embankment whereas only two types of strata were found in the boreholes carried out within the pond.

Stratum	**Description**	**Stratum**		
		Ave. thickness (m)	**Ave. N-Value**	**Shear parameters**
I	Heterogeneous fill, primarily mine waste, consisting of reddish brown, lateritic soil mixed with pebbles, gravels, boulder, ferruginous nodules, etc.	5.50 m in the embankment. Not encountered in the pond.	30 (range 21 to 49)	$\Phi = 34^0$ (Direct Shear, range 34 to 35)
II	Reddish brown tailing	7.50 m in the embankment 12.50 m in the pond.	4 (range 3 to 6)	C = 23 kPa (Unconsolidated Undrained, range 15 to 25)
III	Reddish brown, heterogeneous fill material mixed with pebbles, gravels, boulder, lateritic soil, etc.	> 5.0	40 to >100	$\Phi = 36^0$ (Direct shear, range 35 to 50)

From the stress history revealed by the consolidation test results, it was established that the preconsolidation pressure of the tailings was lower than the existing effective surcharge pressure. .The overconsolidation ratio (OCR) determined from consolidation test results of tailing deposit (Stratum-II) ranged between 0.11 and 0.55.

ROOT CAUSE ANALYSIS OF FAILURE

Embankment materials of Stratum-I and Stratum-III were well compacted as these layers indicated high N-values and shear strengths. However, low shear strength and OCR (< 1) of Stratum-II indicated that it was very soft. It implied that induced stresses on the tailing due to construction of embankment over it was yet to be fully transferred to the grains and excess pore water pressure still remained to be dissipated. Liquid limit, plastic limit and natural moisture content were about 38%, 20% and 30% respectively. Grain size analysis of tailing deposit revealed average distribution of particle size as Gravel: 2%, Sand:8%, Silt 52% and Clay 38%. Therefore, about 90% of the grains were of finer fraction. Based on the field permeability tests and permeability determined from consolidation test results, coefficient of permeability of the tailing deposit was determined in the range of 1×10^{-7} cm/s. Due to such low permeability and low degree of coefficient of consolidation (0.023 m^2/day), rapid loading from the embankment material resulted in generation of excess hydrostatic pressure which would have taken a long time for dissipation. Since excess pore water pressure corresponds to lower effective normal stress, in situ shear strength of the tailing deposit was expected to be low. Indeed, tri-axial tests on selected undisturbed samples of tailing showed cohesion value between 8 kPa and 25 kPa with nominal angle of internal friction between 3^0 and 7^0.

Raising the height of embankment was undertaken after a short period of cessation of tailing disposal at the pond. As a result, the slurries got hardly any time for consolidation. It was in a semi-viscous state with very low shear strength. Tri-axial tests on selected undisturbed tailing samples collected during the geotechnical investigation work, showed average cohesion of about 25 kPa. Few shear tests showed even lower values of about 15 kPa. Therefore, it may be concluded that during the construction of the embankment, cohesion of the tailing deposit must have had a value of about 20 kPa or so.

Considering cohesion of 20 kPa, following Skempton's bearing capacity equation the ultimate bearing capacity of tailing deposit was determined as

$$q_d = cN_c s_c d_c i_c \quad \text{..... (1)}$$

The length of the embankment resting on the tailing (Stratum-II) is much longer when compared to its width. Hence, footprint of the embankment may be considered as a continuous strip for bearing capacity estimation.

Based on the above, ultimate bearing capacity of the tailing stratum neglecting depth factor is obtained as

$q_d = 20 \times 5.14 = 102.8$ kPa.

Based on the findings of the borehole logs, overburden material placed over the tailing deposit was found to be about 5.5 m. Bulk density of the embankment material was about 24 kN/m^3. Therefore, the imposed load over the tailing deposit was 5.5 x 24 = 132 kN/m^2; much greater than the ultimate bearing capacity. As a consequence, the embankment slope failed.

STUDY ON FEASIBILITY OF FURTHER RAISING OF THE EMBANKMENT:

Due to unexpected failure of the embankment, there was an acute crisis of space for deposition of tailings from the beneficiation plant. An emergency arrangement of diverting tailing slurry to another abandoned tailing pond was made at the earliest.. However, storage capacity of that pond was limited. Therefore, despite a failure it was essential to check the feasibility of raising the height of the pond further by about 6.0 meters. However, it was clear that unless the tailing deposit could be consolidated considerably (at least 90%) under the already imposed embankment load, further raising of it was technically untenable. It was estimated that about 1.5 years would be required for 90% consolidation of the tailing deposit under the already imposed embankment load. Further, it was estimated that 6.0 m additional height would require additional time for settlement. It was estimated that total consolidation settlement of the tailing deposit would be about 1250 mm. Under one-dimensional consolidation about 5.7 years would have been required for 90% of consolidation. Therefore, it was essential that the desired settlement could be achieved by expediting the rate of consolidation and the work of raising the height is allowed within acceptable period in order to meet up the storage problem.

RAPID CONSOLIDATION OF THE TAILING DEPOSIT BY INSTALLATION OF PREFABRICATED VERTICAL DRAINS:

To increase the rate of settlement (in other words, dissipation of excess pore water pressure) it was decided to install prefabricated vertical drains (PVDs). Consolidation of the tailing deposit would also ensure gain in additional shear strength. Preload to be used for consolidation, was designed and constructed in such a way that it forms a part of the permanent embankment. Depending upon the varying reduced level (RL) of the existing embankment, maximum height of the preload was calculated as 6.0 m and was designed to be imposed in phases over the PVDs.

Design of PVDs for the embankment was carried out based on the following considerations:

- 90% of primary consolidation would be over within 2 months of construction of the embankment.
- About 6 month time would be required for the construction of the embankment all along the periphery.
- Though coefficient of permeability in soft clay along horizontal direction is higher than that along the vertical direction, the same has been approximated to be equal as the coefficient of permeability in the vertical direction. This approximation is considered reasonable since tailing characteristics, particularly the grain size distribution curve, usually remain same throughout the life of the plant. Chances of having either varve nature or thin continuous layer of sand or silt in between the slurry deposit are very less.
- Coefficient of consolidation in the horizontal direction, C_h, would be same as the coefficient of consolidation in the vertical direction, C_v assuming co-efficient of volume compressibility as constant. Drain spacing depends on soil disturbance & drain resistance which could not be considered for lack of enough data. As such, to be a little conservative, this assumption is reasonable and is good engineering practice.
- Prefabricated vertical drains (PVDs) would be installed in a triangular grid so that the diameter of the drain influence zone D= 1.05S where S is the centre to centre distance between the drains.

It was estimated that about 18% of primary consolidation would have occurred within two months of embankment construction considering only vertical drainage. We now calculate the required $\bar{u}_h$ which PVD will take care of;

$$\bar{u} = 1 - (1 - \bar{u}_h)(1 - \bar{u}_v) \quad \text{..... (2)}$$

Therefore,

$$\bar{u}_h = 1 - \frac{1 - \bar{u}}{1 - \bar{u}_v}$$

$$\bar{u}_h = 1 - \frac{1 - 0.9}{1 - 0.18} = 0.878$$

For the "ideal case" PVD spacing can be determined by the equation (Barron R.A. 1948):

$$t = \frac{D^2}{8C_h} F(n) \ln\left(\frac{1}{1 - \bar{u}_h}\right) \quad \text{..... (3)}$$

Here,

$C_h = C_v = 0.023\ m^2/day$

Assume FOS = 1.5 on C_h for drain design.

Therefore, $(C_h)_{design} = 0.023/1.5 = 0.015\ m^2/day$

F(n) = drain spacing factor

$$= \ln\frac{D}{d_w} - \frac{3}{4}(simplified) \quad \text{.....(4)}$$

Here,

d_w = equivalent diameter $= \frac{1}{2}(a + b) = \frac{1}{2}(4 + 100) = 52mm = 0.052m$

Considering PVD distribution in a triangular grid with spacing S

$$D = 1.05S$$

Substituting the above values, we get,

$$t = \frac{D^2}{8C_h}\left[\ln\left(\frac{D}{d_w}\right) - \frac{3}{4}\right]\ln\left(\frac{1}{1 - \bar{u}_h}\right) \quad \text{.....(5)}$$

$$t = \frac{D^2}{8x0.015}[\ln(19.23D) - 0.75]\ln\left(\frac{1}{1-0.878}\right)$$

$$t = 17.52D^2[\ln(19.23D) - 0.75]$$

For PVD spacing S = 1.0 m, in triangular grid, drain influence zone D is given by,

D = 1.05S = 1.05 x 1.0 = 1.05

Therefore,

$$t = 17.52(1.05)^2[\ln(19.23x1.05) - 0.75] = 43.56days \approx 44days$$
$$\approx 1\,\tfrac{1}{2}\,months(O.K.)$$

Hence, PVD was designed in triangular grid with 1.0 m centre to centre spacing.



Fig. 3. Installation of PVD is in progress

GAIN IN SHEAR STRENGTH OF TAILING DEPOSIT AFTER CONSOLIDATION

Considering the tailing would behave like "normally consolidated clay", shear strength of the tailing layer would increase linearly with depth from its surface to the bottom as surcharge load from embankment increases. However, improvement of strength will be different below the embankment, at the sloping portion and within the pond tailing. The increase in shear strength may be calculated from the normalized shear strength equations for clay suggested by several researchers like Skempton and Henkel (1953), Bjerrum and Simons (1960), Karlsson and Viberg (1967) etc.

Based on their recommendations, strength of tailing deposit at the mid-depth of the stratum is calculated below:

Surcharge pressure due to 6 m high embankment

P_0 = 6 x 24 kN/m^2 = 144 kN/m^2

Method proposed by	Normalized Equation	Undrained cohesion (Su)
Skempton and Henkel (1953)	$\frac{S_u}{P_o'} = 0.11 + 0.0037 I_p$	38 kPa
Bjerrum and Simons (1960)	$\frac{S_u}{P_o'} = 0.45(I_p)^{0.5}$	41 kPa
Karlsson and Viberg (1967)	$\frac{S_u}{P_o'} = 0.50 w_l$	41.6 kPa
Average undrained cohesion		40.0 kPa

Using Skempton's bearing capacity equation, it was estimated that the safe bearing capacity of the tailing deposit considering a factor of safety of 2.5 would be about 85 kPa. Required bearing capacity to safely withstand a load of 6 m of embankment height considering stresses developed at the mid-depth of tailing was about 115 kPa. Hence, the improved bearing capacity would still be inadequate to sustain safely the embankment weight.

ADDITIONAL INCREASE IN BEARING CAPACITY BY BASE REINFORCEMENT:

Since the strength of the tailing material after consolidation by PVD, would be lesser than the required bearing capacity, it was essential to further increase the bearing capacity by some kind of basal reinforcement. For this purpose, high tensile geogrids were used. Geogrids were preferred over other conventional reinforcing material, such as geotextiles, because of their higher tensile strengths. Design of base reinforcement by geogrid was carried out following the arching theory based on the calculation of vertical stress arising from localized subsidence (i.e. differential settlement). In the 1930s, both Terzaghi in Austria (calculating stresses on deep tunnels) and Martson in the U.S. (calculating stresses on buried pipelines) developed the analytical theory. Their work resulted in the following simplified equation for vertical stress on the surface of the particular underground structure (tunnel or pipe respectively).

$$\sigma_z = 2\gamma_{ave} R\left[1 - e^{-0.5H/R}\right] + qe^{-0.5H/R} \quad \text{..... (6)}$$

Where,
σ_z = vertical stress on the reinforcement layer
γ_{ave} = average unit weight of soil above the settlement area
R = radious of differential settlement zone
H = total height above the settlement area and
q = surcharge pressure placed at the ground surface.

For large values of H (typically $H \geq 6R$) the equation reduces to the following value of constant vertical stress

$$\sigma_z = 2\gamma_{ave} R \quad \text{..... (7)}$$

Knowing the vertical stress, the required tensile strength of geogrid can be calculated as (Koerner, R.M., 1999, Designing with Geosynthetics, Fourth Edition, Prentice Hall)

$$T_{required} = \sigma_z R\ \Omega \quad \text{..... (8)}$$

Where,
$\Omega = 0.25[(2y)/B + B/(2y)]$, where
B = width of settlement void, and
y = depth of settlement void

Few settlement voids had developed at the surface of the existing embankment in the subsequent months following the failure. Based on the site observations, average radius of these holes may be considered as 1.0 m, The proposed embankment was considered to have a maximum height of 6.0 m. Therefore, equation (7) is considered for calculation of vertical stress (H = 6R).

$\sigma_z = 2x24.0x1.0 = 48kPa \qquad [\sigma_z = 2\gamma_{ave}R\ ]$

To transfer this vertical stress into a horizontal force, we use,

$T_{required} = \sigma_z R\,\Omega$

Where, Ω = strain criterion
= 0.97 at 5% strain
= 0.73 at 10% strain

The geogrids were designed for 10% of allowable strain to be developed under ultimate state of stress.

Therefore,

$T_{required}$ = 48 x 1.0 x 0.73 kN/m = 35.04 kN/m

Geogrids to be used would be made of high tensile strength Polypropylene/Polyethylene having minimum ultimate wide-width tensile strength of 125 kN/m. Allowable tensile strength of a geogrid with 125 kN/m ultimate strength (at 10% strain) is given by (Koerner, R.M., 1999, Designing with Geosynthetics, Fourth Edition, Prentice Hall)

$$T_{allow} = T_{ult}\left[\frac{1}{\prod RF_p}\right] \qquad \text{..... (9)}$$

Where

$\prod RF_p$ = cumulative reduction factor
= RF_{ID} x RF_{CR} x RF_{CD} x RF_{BD}

RF_{ID} = reduction factor for installation damage = 1.5
RF_{CR} = reduction factor for creep = 3.0
RF_{CD} = reduction factor for chemical degradation = 1.2
RF_{BD} = reduction factor for biological degradation = 1.2

Therefore,

$\prod RF_p$ = 1.5 x 3.0 x 1.2 x 1.2 = 6.48

$T_{allow} = \frac{125}{6.48}$ kN/m = 19.29 kN/m

No of geogrid layers,

$$= \frac{35.04}{19.29} = 1.82 \approx 2.0nos.$$

Therefore, two layers of geogrids were used having intermediate sand.



Fig. 4. Laying of Geogrid is in progress

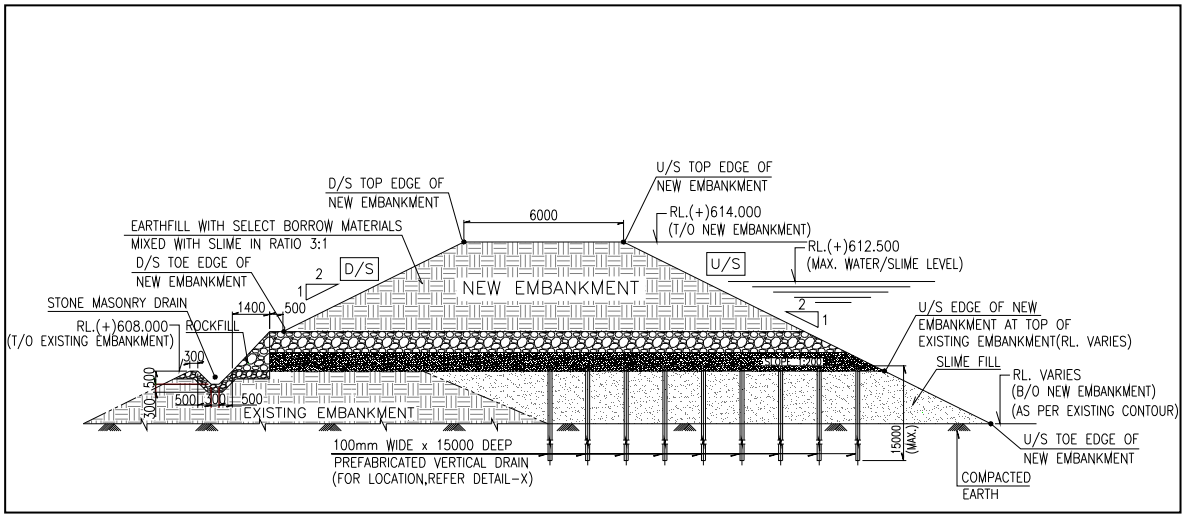


Fig. 5. Sectional view of embankment with geogrid & PVDs



Fig. 6. Finished embankment

INSTRUMENTATION (PIEZOMETERS AND SETTLEMENT GAUGE)

To check the performance of the embankment with respect to degree of consolidation, dissipation of excess hydrostatic pressure, rate of settlement etc. settlement devices and piezometers were installed at the newly constructed embankment top.

CONCLUSIONS

Under the present socio political scenario, land is the most scare resource for any Project and stringent environmental norms do not permit unplanned disposal of industrial waste. As a result upstream method of raising is generally preferred in most of the tailing ponds since it requires less land, lesser quantity of construction materials and less construction time. Upstream method of raising of tailing embankment needs embankment to be constructed over the tailings. However, for raising height of embankment in this method, it is essential that adequate time gap between two successive raisings must be provided for consolidation of the tailings and to achieve adequate bearing capacity. But, in most of the cases, schedule of mine planning is such that time gap in between two successive phases of height raisings do not permit adequate time for consolidation of the beach tailings as well as attainment of adequate bearing capacity to withstand further loads imposed on it. The challenge can be successfully met by proper investigation, analysis, innovative use of proper technology and materials like PVDs and geogrids.

REFERENCES

1. Koerner, R.M., 1999, Designing with Geosynthetics, Fourth Edition, Prentice Hall, Upper Saddle River, New Joursey,07458, USA

2. Barron, R.A., 1948, Consolidation of fine-grained soils by drain wells, ASCE Trans, paper 2346, V.113, pp 718-724.

3. Cedergren, H.R. 1977, Seepage drainage and flow nets, Second Edition, John Wiley and Sons, New York, 534 p.

4. Federal Highway Administration, US Depatment of Transportation, Prefabricated Vertical Drains, Vol-I: Engineering Guidelines, Report No. FHWA/RD-86/168, Final Report August 1986, 107 p.

5. Hansbo, S. 1979, Consolidation of clay by band-shaped prefabricated drains, Ground Engineering, Vol. 12 No. 5, pp 21-25.

6. Casagrande, L. And Poulos, S., 1969, On the effectiveness of sand drains, Canadian Geotechnical Journal, Vol. 6, No.-3, pp 287-326.

7. Mesri, G., and Choi, A.M., 1985,on Soft Clays","Settlement Analysis of Embankments; JGED ASCE GT4, pp. 441-464.

AN UNIQUE FORMULA FOR THE STONE-COLUMN GROUP EFFICIENCY

Abhijit Saha, Irrigation & Waterways Department, Government of West Bengal, India, 9433509798, ovijeet@rediffmail.com.

ABSTRACT

The stone columns improve the performance of foundations on soft and loose soil due to the ability of composite ground to sustain increased structural loads under reduced settlements. The interaction between the two basic elements: the ambient subsoil and installed column, present a complexity of behaviour, both in terms of applied stresses and resulting strains. Moreover, as the same is provided in-group in a regular array beneath foundations, the performance of an individual column is likely to be influenced by the presence of neighbouring columns. The present paper addresses this very issue. Analysis of reported field hydro-test data of large diameter oil storage tanks in soft ground in reference to some existing theories led to the development of the stone-column 'group efficiency factor'. In order that such factor is of general use, it was felt necessary to examine the applicability of the factor to different sizes of groups under varied subsoil conditions. With this in view, some model test results reported in literature of single and group of columns have been analysed and in the process an explicit relationship regarding the stone-column 'group-effect' could be established.

Keywords: soil-column interaction, group-efficiency, analytical methods, settlement reduction

INTRODUCTION

The field application of the stone column technology has gained momentum than the intricate design methodology due to its simplicity in installation and intuitive performance. The ground improvement is due to the complex interaction within the 'unit-cell' comprised of the installed column in ambient ground under sustained vertical stress; in association with the interdependence of problem geometry and material properties of the two different soils-one 'native' and the other 'back-filled'. The beneficial effects are increased load capacity, reduction in total and differential settlements, minimization of post construction settlements effected by accelerating consolidation, reduced risk of soil liquefaction, aiding in improvement of slope stability of embankments and natural slopes and effecting changes in the dynamic response. The 'unit-cell' concept of a tributary soil cylinder encapsulating an installed column with some reasonable assumptions and boundary conditions (Aboshi et al, 1979; Balaam & Booker, 1981; Van Impe & De Beer, 1983; Priebe, 1976; Saha & De, 1994; Saha; 2005, 2006, 2007, 2011, Saha & Das; 2007) deals with the load-settlement behaviour of the composite system. The present investigation is based on published field data from literature & validated with experimental study reported in literature. The study addresses the effect of group interaction of stone columns beneath a large area loading on ground settlement. The hydro-test load-settlement data of 12 large diameter oil storage tanks founded on stone column reinforced soil at Haldia[1] and Kandla[2] refinery sites in India; reported by Som (1997), has been analysed to quantify the group efficiency. The results as obtained are compared with experimental study on 2, 3 and 4 stone column groups at different spacing-diameter ratios in soft clay[3] reported by Rao et al (1997) to validate the above analysis. A unique relationship between the column spacing and group efficiency has been obtained.

[1] A major seaport located approximately 50 kilometres south-west of Kolkata city in Eastern India, near the mouth of the Hooghly River, one of the distributaries of the Ganges

[2] A seaport located on the Gulf of Kutch in Gujarat state, on the north-western coast of India

[3] From eastern coast of India

SETTLEMENT REDUCTION FACTOR (SRF) OF A UNIT-CELL BY VARIOUS ANALYTICAL METHODS

Settlement reduction factor (β) is defined as the ratio of settlement of stone column reinforced ground to that of virgin ground. Settlement reduction factor (β) of a unit-cell (single zone of influence) has a direct bearing with the area-ratio (A_r). The nature of variation of β with A_r, as theoretically obtained by several investigators and also by the author, is presented in Fig.-1. The said methods are based on the unit-cell concept and the nature of variation is similar in all cases. The salient details of the different methods and the input variables considered in each of these are enumerated below.

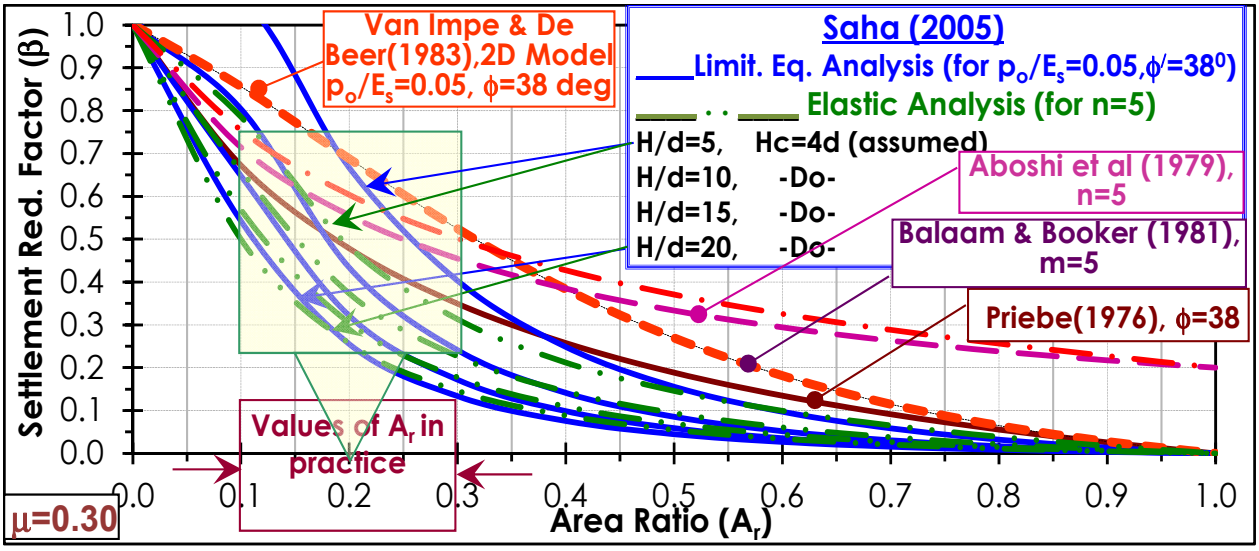


Fig. 1. Settlement Reduction Factor (β) Vs. Area Ratio (A_r) for a singular 'unit-cell'

Priebe's (1976) study considered the column to be rigid-plastic and incompressible and ambient subsoil to be elastic and isotropic. The design variables considered were the area ratio (A_r), Poisson's ratio of ambient subsoil (μ_s) and the angle of frictional resistance of column (ϕ_c). Hence, Priebe's study did not consider the external stress level (p_o) and deformation modulus (E_s) of host soil.

In **Aboshi et al's (1979)** study, the settlement reduction factor is related to the stress concentration ratio (n) and the area replacement factor (A_r). Hence only two variables are considered, out of which 'n' is an input parameter; that in itself is a function of the problem geometry and material properties of native soil and backfilled column.

Van Impe and De Beer (1983) presented a 2-dimensional plain strain model of unit-cell where the stone columns are replaced by stone walls with equivalent area. Two methods of analysis were proposed. First method considered the soil as elastic and the stone column to be at limiting equilibrium, where the design variables are elastic modulus (E_s) and Poisson's ratio (μ_s) of subsoil and effective angle of internal friction of column material (ϕ'_c). The second case considered both the soil and stone column to be elastic and, hence, the material variables are the elastic parameters of ambient soil and stone column, E_s, μ_s and E_c, μ_c respectively. The equivalent area ratio A_r for the 2-D case and the external vertical stress level (p_o) has also been considered as input variables. However, it was assumed that the column bulging occurred along the entire length (H) of column, though in reality only the top horizon or the column head bulges under sustained load.

Balaam and Booker (1981) have proposed a method for predicting the settlement using elastic solution. The design variables considered were the equivalent spacing-diameter ratio S_{eq} (=D_e/d=S_r, where, D_e is the effective distance between columns of diameter d), which may be considered equal to inverse of square-root of area ratio (S_{eq} =1/√A_r), and the elastic parameters of native soil and installed column, E_s, μ_s and E_c, μ_c respectively. The external stress level (p_o), though considered in the analysis, balances out in the expression for settlement reduction factor.

Author's (2005) study considers more parameters than any other methods cited above.
These are:

(i) soil replacement factor or area ratio Ar (=d^2/D_e^2),
(ii) the external vertical stress level (p_o),
(iii) the critical height factor or column critical depth (H_c) to height (H) ratio, h_f (=H_c/H),
(iv) the elastic modulus and Poisson's ratio of ambient subsoil, E_s, μ_s and,
(v). (a) effective angle of frictional resistance of column ϕ'_c, (for a case where the stone column is at its limit of equilibrium while deforming at constant),
(v). (b) dialatancy of column with consequent lateral compression of soil along critical depth (for a case where the stone column head dilates under heavy load),
(v). (c) the elastic parameters of stone column, E_c, μ_c (for a case where soil and column are both assumed elastic),
(v). (d) column capacity and column stress transfer for different degrees of mobilization of column friction by arching theory (Saha, 2006).

Balaam and Booker's (1981) and author's (elastic analysis case) consider almost similar set of input variables. However, author's study considers the upper boundary strain level (p_o/E_s) and the critical height factor (h_f=H_c/H) as additional inputs.

EXPRESSIONS FOR SETTLEMENT REDUCTION FACTOR (β) USED IN THE STUDY

Balaam & Booker's method (1981)

The settlement reduction factor, β is given by,

$$\beta = \frac{\left(\frac{1}{\sqrt{A_r}}\right)\frac{E_s(1-\mu_s)}{(1+\mu_s)(1-2\mu_s)}}{(\lambda_p+2G_p)+(\lambda_s+2G_s)\left(\frac{1}{\sqrt{A_r}}-1\right)-2(\lambda_p+\lambda_s)\left[(\lambda_e-\lambda_s)\left(\frac{1}{\sqrt{A_r}}-1\right)\Big/\left\{2(\lambda_s+G_s-\lambda_e-G_e)+\frac{1}{\sqrt{A_r}}(\lambda_e+G_e+G_s)\right\}\right]}$$

Where, λ= Lame's constant = $\frac{E\mu}{(1+\mu)(1-2\mu)}$, and Shear Modulus = G = $\frac{E}{2(1+\mu)}$. p and s subscripts stand for granular pile and soil respectively.

Author's elastic analysis model (2005)

The expression of settlement reduction factor, β, is given by,

$$\beta = \frac{(2+\psi)\left(\frac{1}{\sqrt{A_r}}-1\right)\left(\frac{H_c}{H}\right)}{\left\{1-\sqrt{A_r}(1+\psi)\right\}^2+(1+\psi)^2 A_r\left[\frac{m\left[1+\left(\frac{1}{\sqrt{A_r}}-1\right)\{2\mu K_o+m(1-2\mu K_o)\}\right]}{(1-2\mu K_o)+m\left\{\left(\frac{1}{\sqrt{A_r}}-1\right)+2\mu K_o\right\}}\right]\left\{(2+\psi)\left(\frac{1}{\sqrt{A_r}}-1\right)\left(\frac{H_c}{H}\right)+2K_o\right\}}$$

Where, ψ is the diametrical strain ($=2\delta_h/d$, and δ_h is the bulge at column head of column diameter d), 'm' is the modular ratio $=E_c/E_s$, and $K_o = \mu_s/(1-\mu_s)$.

GROUP INTERACTION FACTOR (GIF) – DEFINITION

The theoretical prediction of settlement reduction factor of a single column, as plotted Fig.-1, is based on the assumption of frictionless boundary of a single 'cylindrical unit'. Since the bulge at column head of an individual column influences the bulge of the neighbouring column, the bulge at top of a column in a 'unit' of the group would be less than that would have occurred in presence of idealized singular frictionless wall of cylindrical unit. This is due to the existence of adjacent loaded cylindrical units sharing common boundary along the cell periphery. A lower magnitude of bulge means a lower degree of diametrical strain resulting in higher vertical settlement within the practical domain of area ratio – the so-called ***group effect***; in case of unit-cell groups. As such, a hypothetical definition of the GIF beneath a large area uniformly distributed loading has been put forward intuitively from logical considerations. The Group Interaction Factor (GIF) in stone-column reinforcement "α_p" at a point 'p' beneath a large area flexible loading is defined as:

$$\boldsymbol{\alpha_p} = \left\{\frac{\sum_{i=1}^{n}\left(\frac{\delta_a}{\delta_v}\right)_i\left(\frac{p_o}{E_{eq}}\right)_i}{\sum_{i=1}^{n}\left(\frac{p_o}{E_{eq}}\right)_i}\right\}\left\{\frac{A_{r_{center}}}{A_{r_p}}\right\} \qquad [1]$$

Where, $\mathbf{E_{eq.}}$=Equivalent modulus of deformation of composite mass beneath the loaded area =

$$\mathbf{E_s\left(1-\sqrt{A_r}\right)^2+E_cA_r} \qquad [2]$$

And, p_o / E_{eq} =Upper boundary strain level

δ_a =Actual settlement under a given upper boundary strain level (p_o / E_{eq}) at a point 'p' under consideration

δ_v =Predicted settlement at the point 'p' under consideration (by various existing theories)

Ar_{center} = Area ratio provided at the center of the group

Ar_p = Area ratio provided at the point 'p' under consideration

i = Total number of available data sets of settlements of stone column reinforced ground in similar subsoil conditions

The SRF (β) of a unit-cell shall be multiplied by this GIF (α_p) to determine the modified settlement reduction at the point 'p' of the group. The theoretical settlement values, as calculated by using β of Balaam & Booker's method and author's method (*elastic analysis model*) and the reported field load-settlement

data have been synthesized to arrive at an appropriate group interaction factor at a point 'p' under a flexible loaded area for estimation of settlement.

GROUND SETTLEMENTS: ACTUAL Vs. PREDICTED BY ANALYTICAL APPROACHES

The measured hydrotest settlements (Som, 1997) and the ratio of measured to predicted ground settlements of stone column reinforced ground by the two methods have been tabulated in Table 1.

Table 1. Ratio of Measured to Predicted Ground Settlements

TANK			PREDICTED SETTLEMENT (δ_v)				MEASURED HYDROTEST SETTLEMENT (δ_a)		RATIO MEASURED/ PREDICTED				Ar_{centre}/Ar_P (as adopted in stone column design in concerned sites)	
No.	Diameter	Height	Application of Balaam & Booker's Model *(Elastic Analysis)*		Present Study *(Elastic Analysis Model)*				Balaam & Booker's Model *(Elastic Analysis)*		Present Study *(Elastic Analysis Model)*			
	m	m	Centre mm	Edge mm	Centre mm	Edge mm	Centre mm	Edge mm	Centre	Edge	Centre	Edge	Centre	Edge
HALDIA SITE														
A	50	11.4	283	133	291	129	310	157	1.10	1.18	1.06	1.22	1	0.84
B	50	11.4	283	133	291	129	332	182	1.18	1.37	1.14	1.41		
C	55	13.0	342	150	352	146	562	368	1.64	2.44	1.59	2.50		
D	30	11.4	222	98	228	94	255	150	1.15	1.54	1.12	1.59		
KANDLA SITE														
1	55	10	328	152	351	163	314	174	0.96	1.15	0.89	1.06	1	1
2	55	10	328	152	351	163	390	200	1.19	1.32	1.11	1.22		
3	55	10	328	152	351	163	440	216	1.33	1.43	1.27	1.33		
4	55	10	328	152	351	163	460	250	1.41	1.64	1.32	1.54		
5	50	10	321	148	344	159	530	290	1.64	1.96	1.54	1.82		
6	50	10	321	148	344	159	600	310	1.85	2.08	1.75	1.96		
7	50	10	321	148	344	159	425	235	1.32	1.59	1.23	1.47		
8	50	10	321	148	344	159	470	228	1.47	1.54	1.37	1.45		

From above, it can be seen that in all the cases the ratio of measured to predicted ground settlements of stone column reinforced ground is greater than one. This is in line with the remarks and postulations given above while defining group interaction factor. From the results of the field measurements and theoretical analysis it is likely that the bulge at top of an individual column in an *'unit'* of the *group* (under a uniformly distributed load over a large area treated by stone columns) is less than that would have occurred in case of a singular frictionless cell. This is due to the presence of *adjacent* loaded cylindrical units sharing common boundary along the cell periphery.

QUANTIFYING THE GROUP EFFECT

It is reported (Som, 1997) that the final settlement during hydrotesting of 12 large diameter (30 m., 50 m. and 55 m. dia.) oil storage tanks of heights varying from 10m. to 13 m., four at Haldia and eight at Kandla oil refinery sites was arrived at by the formula: $\delta v = \beta \times \rho_{c1} + U\,\% \times \rho_{c2}$, Where, δ_v = settlement of stone-column foundation system during hydrotest, ρ_{c1} = settlement of treated soil upto the depth of stone-column treatment, ρ_{c2} = settlement of untreated soil below stone-column treatment, β = Settlement

Reduction Factor, U%= average degree of consolidation (under appropriate boundary conditions) of soil layer thickness below column tip upto which stress increment due to hydrotest load is negligible.

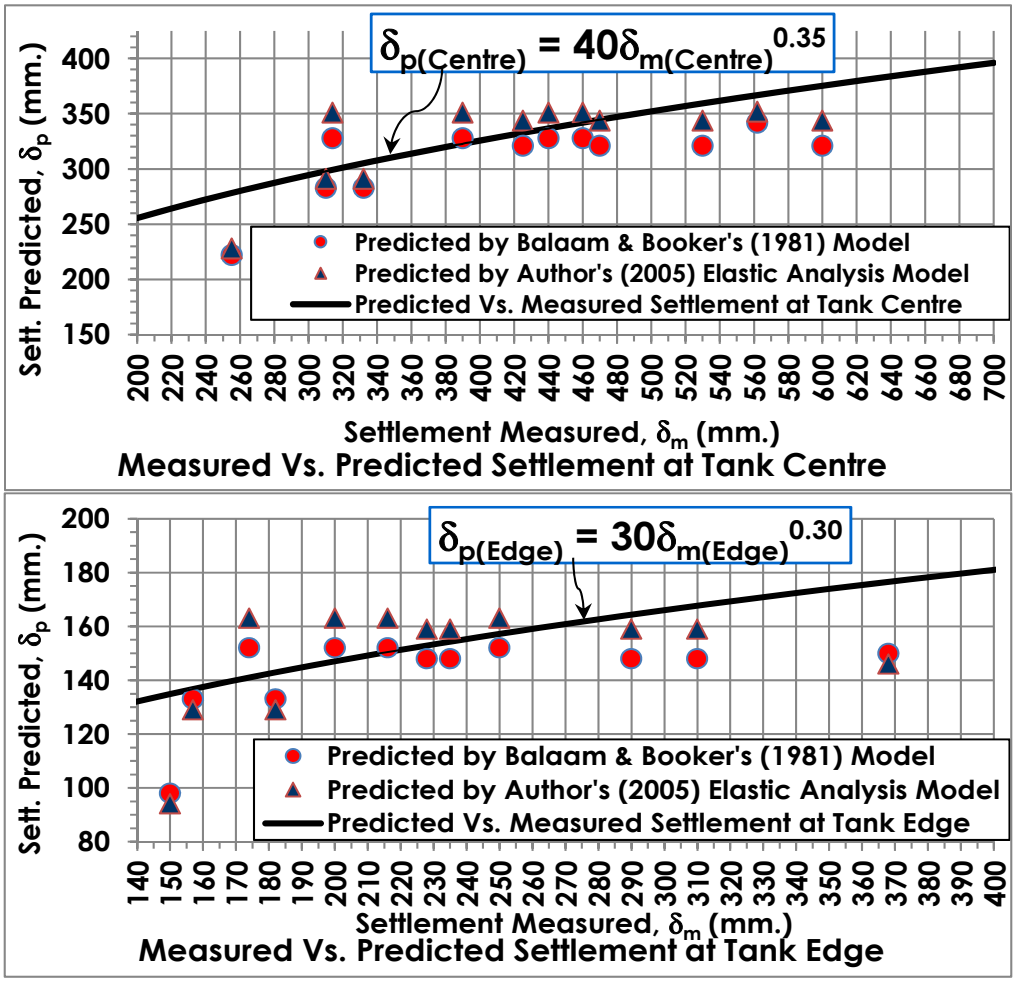


Fig. 2. Measured vs. predicted settlements below large diameter tank centre (top) and tank edge (bottom)

In order to quantify the group effect in the form of an interaction factor, the raw data for all the tank locations were analyzed and the relevant information have been presented in Table 2 and Table 3. In Table 2, the upper boundary strain levels ($p_o/E_{eq.}$) at the centre and edge for all tank locations, calculated from field test data have been presented (p_o is the applied stress under the sand pad and $E_{eq.}$ is the equivalent modulus of elasticity). $E_{eq.}$ has been calculated using Eqn. [2]. For this, the weighted average undrained cohesion (c_u) up to the depth of stone column treatment was calculated first. The modulus of deformation of ambient subsoil (E_s) was assumed as $500c_u$ and modular ratio (E_c/E_s) was assumed as 5. Calculations of E_c and E_s for Haldia and Kandla sites have been presented below. In Table 4, the product of the ratio of actual to predicted settlement (δ_a/δ_v) and upper boundary strain level ($p_o/E_{eq.}$) of all the individual tank sites along-with the ratio of summation of product of δ_a/δ_v and $p_o/E_{eq.}$ to summation of $p_o/E_{eq.}$ at Haldia and Kandla sites have been presented. The group interaction factor α_p as defined in Eqn. [1] has been calculated from the synthesized data presented in Table 3 and Table 1 (last two columns) and tabulated in Table 4. The same is plotted against the respective area ratios in Figure 3.

Calculation of weighted average undrained cohesion (c_u) & deformation modulus of soil (E_s)

HALDIA SITE

Depth of stone-column treatment =17 m.

$$\text{Weighted average } c_u = \frac{\sum_{i=1}^{n} c_{u_i} d_i}{\sum_{i=1}^{n} d_i} = \frac{5\times3+3\times6+5\times4+8.5\times3}{3+6+4+3} = 4.90\text{MT/m}^2$$

(The top 1m. of soil is simply designated as top soil in literature with no description of engineering properties of the same. Hence, the weighted average c_u is calculated for the other four layers falling within the zone of stone column treatment)

$E_s = 500c_u = 500\times4.90 = 2450\ \text{T/m}^2$,

$E_c = 5E_s = 5\times2450 = 12250\ \text{T/m}^2$.

KANDLA SITE

Depth of stone-column treatment =14 m.

$$\text{Weighted average } c_u = \frac{\sum_{i=1}^{n} c_{u_i} d_i}{\sum_{i=1}^{n} d_i} = \frac{1.5\times2+3.5\times1+2\times4}{1.5+3.5+4} = 1.61\text{T/m}^2$$

(The third layer from top is a loose sand layer of 5 meters thickness; hence the weighted average c_u is calculated for the other three layers falling within the zone of stone column treatment)

$E_s = 500c_u = 500\times1.61 = 800\ \text{T/m}^2$,

$E_c = 5E_s = 5\times800 = 4000\ \text{T/m}^2$.

Table 2. Upper Boundary Strain Levels (p_o/E_{eq})

TANK			p_o		A_r		$E_{eq.} = E_s(1-\sqrt{A_r})+E_cA_r$		Upper Boundary Strains ($p_o/E_{eq.}$)	
	m	m	T/m²	T/m²			T/m²	T/m²		
No.	Dia.	Height	Centre	Edge	Centre	Edge	Centre	Edge	Centre	Edge
HALDIA SITE										
A	50	11.4	9.57	4.79	0.168	0.20	2911	3199	0.002992	0.001496
B	50	11.4	9.57	4.79	0.168	0.20	2911	3199	0.002992	0.001496
C	55	13.0	10.98	5.49	0.168	0.20	2911	3199	0.003431	0.001716
D	30	11.4	8.33	4.17	0.168	0.20	2911	3199	0.002605	0.001303
KANDLA SITE										
1	55	10	10.31	5.16	0.225	0.225	1120	1120	0.009208	0.004604
2	55	10	10.31	5.16	0.225	0.225	1120	1120	0.009208	0.004604
3	55	10	10.31	5.16	0.225	0.225	1120	1120	0.009208	0.004604
4	55	10	10.31	5.16	0.225	0.225	1120	1120	0.009208	0.004604
5	50	10	10.12	5.06	0.225	0.225	1120	1120	0.009034	0.004517
6	50	10	10.12	5.06	0.225	0.225	1120	1120	0.009034	0.004517
7	50	10	10.12	5.06	0.225	0.225	1120	1120	0.009034	0.004517
8	50	10	10.12	5.06	0.225	0.225	1120	1120	0.009034	0.004517

Table 3. Synthesis of Data

TANK			$(\delta_a/\delta_v)(p_o/E_{eq})$				$\Sigma\{(\delta_a/\delta_v)(p_o/E_{eq})\}/\Sigma(p_o/E_{eq})$			
No.	Diameter	Height	Synthesized from Balaam & Booker's predicted settlement data		Present Study (Elastic Analysis Model)		Synthesized from Balaam & Booker's predicted settlement data		Present Study (Elastic Analysis Model)	
			Centre	Edge	Centre	Edge	Centre	Edge	Centre	Edge
HALDIA SITE										
A	50	11.4	0.003	0.001	0.003	0.001	1.2827	1.6665	1.2473	1.7195
B	50	11.4	0.003	0.002	0.003	0.002				
C	55	13.0	0.005	0.004	0.005	0.004				
D	30	11.4	0.003	0.002	0.002	0.002				
KANDLA SITE										
1	55	10	0.008	0.005	0.008	0.004	1.3981	1.5866	1.3055	1.4780
2	55	10	0.010	0.006	0.010	0.005				
3	55	10	0.012	0.006	0.011	0.006				
4	55	10	0.012	0.007	0.012	0.007				
5	50	10	0.014	0.008	0.013	0.008				
6	50	10	0.016	0.009	0.015	0.008				
7	50	10	0.012	0.007	0.011	0.006				
8	50	10	0.013	0.007	0.012	0.006				

Table 4. Group Interaction Factor

$$\textbf{GROUP INTERACTION FACTOR} = \alpha_p = \left\{ \frac{\sum_{i=1}^{n} \left(\frac{\delta_a}{\delta_v} \right)_i \left(\frac{p_o}{E_{eq}} \right)_i}{\sum_{i=1}^{n} \left(\frac{p_o}{E_{eq}} \right)_i} \right\} \left\{ \frac{A_{r_{center}}}{A_{r_p}} \right\}$$

SITE	Synthesized from Balaam & Booker's predicted settlement data		Present Study (Elastic Analysis Model)	
	Centre	Edge	Centre	Edge
HALDIA	1.283	1.400	1.247	1.444
KANDLA	1.398	1.587	1.305	1.478

A regression analysis has been carried out using the synthesized data as calculated above and an empirical equation has been deduced which projects the group interaction factor as a function of the area ratio in power trend (Saha & Das, 2000). The same is superimposed in Fig. 3.

$$\alpha = 2.2346 \times A_r^{\,0.2987} \qquad [3]$$

VALIDATION OF PREDICTION WITH EXPERIMENTAL STUDY REPORTED IN LITERATURE

In order that such factor is of general use, it is necessary to examine the proposition to different sizes of groups and at other sub-soil conditions also. With this in view, some model test results of single and group of stone columns from literature (Rao et al, 1997) have been analysed.

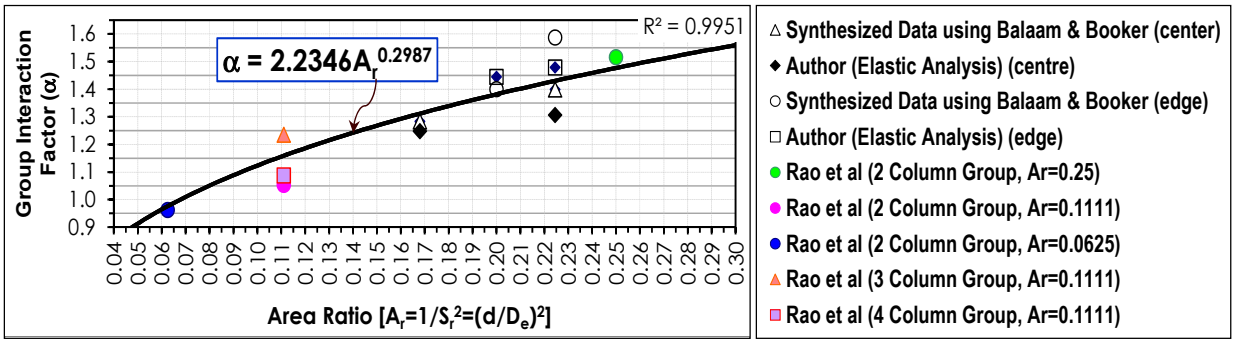


Fig. 3. Group Interaction Factor (α) vs. Area Ratio (A_r)-An unique relationship

The study of Rao et al (1997) consisted of load tests on single and group of model stone-columns in two types of clayey soils from East Coast of India with varying H/d ratios and different consistency indices of soil. The column groups consisted of 2, 3 and 4 columns at different spacing-diameter ratios. The group efficiency factors (GEF, which is equal to the inverse of GIF) for 2-column group were reported as 0.66, 0.95 and 1.04 for spacing of 2d, 3d and 4d respectively and the same for 3 and 4 column group (for 3d spacing) are reported as 0.81 and 0.92 respectively. The said findings of Rao et al have been superimposed on the results of previous full-scale load tests on oil storage tanks and shown in Fig.-3. It transpires that the curve of GIF as predicted from analysis of full-scale load test data may well be regarded as the mean curve of the experimental results obtained by Rao et al (1997). Likewise, the GEF predicted for large area loading treated by stone-columns, as obtained from present study (Fig.-4), agrees with the experimental results of Rao et al. An empirical equation for GEF is obtained as a function of the spacing-diameter ratio. The relationship, for the group efficiency factor (1/α) versus spacing-diameter ratio (S_r) is:

$$1/\alpha = 0.4475 \times S_r^{\,0.5974} \qquad [4]$$

In order to get a group efficiency factor of 1, a column spacing of 3.80 times the diameter is suggested.

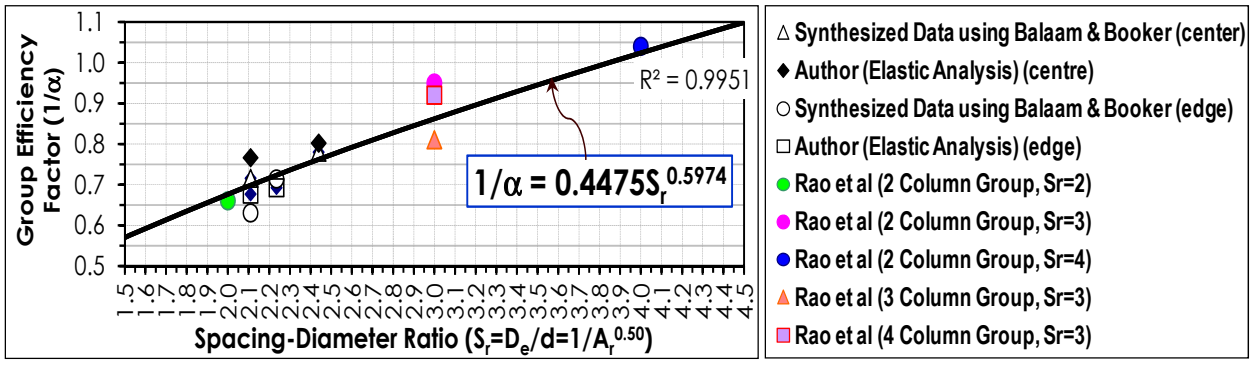


Fig. 4. Group Efficiency Factor (1/α) vs. Spacing-Diameter Ratio (S_r)-A unique relationship

CONCLUSIONS

Settlement of stone-column group may be estimated from analysis of unit-cells using the proposed hypothetical group interaction factor which depends on equivalent modulus of deformation of composite soil and area-ratio of individual unit-cells. Quick yet representative evaluation of group efficiency (and interaction) may be made by the proposed empirical equations.

REFERENCES

Aboshi H., Ichimoto E., Enoki M. & Harada K. (1979). The Composer-A Method to Improve Characteristics of Soft Clay by Inclusion of Large Diameter Sand Columns. Proc. International Conference on Soil Reinforcement: Reinforced Earth & Other Techniques, Paris, France: pp. 211-216.

Balaam N.P. & Booker J.R., (1981). Analysis of Rigid Raft Supported by Granular Piles", Int. Journal of Numerical and Analytical Methods in Geomechanics, 5:379-403.

Priebe, H. (1976). Abschätzung des Setzungverhaltens eines durch Stopfverdichtung verbesserten (Estimating settlements in a gravel column consolidated soil), Baugrundes. Die Bautechnik, 5, 160-162.

Rao, S.N., Reddy, K.M. & Kumar, P.H., (1997). Studies on Group of Stone Columns in Soft Clay, Geotechnical Engineering, Journal of Southeast Asian Geotechnical Society, 28:165-181.

Saha Abhijit & De P. K. (1994). Field & Analytical Study of Stone Columns by Non-Linear Strain. Proc. XIII International Conference on Soil Mech. & Foundation Engg., New Delhi, India, 3:pp.1211-1214.

Saha Abhijit & Das S.C. (2000). Interaction Analysis of Stone Column Groups In Foundations, Proceedings of Indian Geotechnical Conference, Mumbai, India, 1: pp.279-284.

Saha Abhijit (2005). A Study of Behaviour of Stone Columns for Ground Improvement. Ph.D. Thesis, Jadavpur University, India, 197 p.

Saha Abhijit (2006). Analysis of Stone-Column Reinforced Soil by Arching Theory, Proceedings of Indian Geotechnical Conference, Chennai, India, 2: pp. 551-554.

Saha Abhijit & Das S.C. (2007). Analytical Study & Back Analysis of Field Response of Stone-Column Reinf. Ground, Proc. 13th Asian Regional Conference on SMGE, Kolkata, India, 1(II): pp.881-884.

Saha Abhijit (2007). Analysis and Design of Stone-Column Reinforced Ground, Proc. of Seminar on Stone Column: Experiences of the Constructors, Kolkata, India, pp. 13-65.

Saha Abhijit (2011). The time-settlement-load behaviour of stone-column drain-well, Proc. of 14th Asian Regional Conference on Soil Mech. & Geotechnical Engineering, Hong Kong, China, pp. 1843-1846.

Som N. (1997). Ground Improvement by Stone Column for Large Diameter Storage Tank Foundations in Soft Clay. Summer School on Ground Improvement Technology, Paper No. 7, BESU, Shibpur, India.

Van Impe, W. & De Beer, E. (1983). Improvement of Settlement Behaviour of Soft Layers by means of Stone Columns. Proc. 8th Euro. Conf. on Soil Mech. & Fdn. Engg., Helsinki, 1: pp. 309-312.

STATE OF THE ART GROUND IMPROVEMENT TECHNIQUE FOR A RESIDENTIAL COMPLEX: CASE STUDY

Anirudhan I. V., Consultant Geotechnical, Geotechnical solutions, geotechnicalsolutionsch@gmail.com
Madan Kumar Annam, Technical Manager, Keller India, madankumar@kellerindia.com
Hari Krishna Y, Director, Keller India, yhari@kellerindia.com

ABSTRACT

For completion of projects in time with positive results, improvements of productivity and effective project management procedures have become extremely important. This paper discusses a milestone project comprising 198 residential units of stilt plus 4 levels that highlighted the benefits of these key aspects. Success of ground modification procedure benefitting the entire cycle involving End Users, Suppliers, Bankers and Developer is discussed.

Soil profile for a considerable depth comprises weak layers of silty clay and sandy clay with varying consistency. Deep foundations have been an automatic choice of foundation for major buildings constructed in similar environment. After serious geotechnical appraisal, reconsideration of the foundation system with an alternative solution of Ground Improvement was found to be optimal in terms of Cost and Time. Full raft foundation on the improved ground by installation of Vibro Stone Columns (dry bottom feed method) was considered as an alternative foundation system. The ground improvement works were completed within 6 weeks (as against 6 months to that of pile foundations) that was made possible through effective project management. Full size plate load tests were conducted to ascertain effectiveness of the ground improvement works. Success of the foundation system was proved by full scale monitoring of foundation settlement during and after completion of the project over a span of 2 years. This paper describes design considerations, quality control in the construction of Vibro Stone Columns (dry bottom feed method) and performance monitoring of the project thereafter.

Keywords: Vibro stone columns (dry bottom feed method), ground improvement, settlement monitoring.

INTRODUCTION

Generally in weak deposits, deep foundations like bored cast-in-situ piles and driven piles have historically been the foundation choice for major buildings and other structures. Construction of pile foundations is becoming a challenge due to their high cost, large construction time and due to severe environmental issues (noise pollution, ground vibrations and carbon footprint). Since the proposed building complex is located within the proximity of a well-developed residential locality, objections raised by neighborhoods to pile driving activities called for a rethinking on the foundation system.

The top 6m to 8m of soil profile comprises of silty clay / sandy clay having highly varying consistency. GWT was encountered at 3.0m below the existing ground level. Under this situation, the reconsideration of the type of foundation system with respect to the geotechnical analysis gave a thought to assess feasibility of ground improvement system.

GROUND IMPROVEMENT BY VIBRO TECHNIQUES

Ground Improvement refers to a technique that improves the engineering properties like shear strength, stiffness, permeability etc., of the weak soil mass treated, which in turn support foundations for a wide variety of structures. Stone columns acts as drainage path allowing for rapid consolidation by faster dissipation of construction pore water pressure. The improved drainage capabilities of the stone column treated ground provide a much better resistance to liquefaction of the surrounding soil. Performance of

this composite system can be established theoretically and also by full size field plate load tests. Priebe (1995) developed the design of vibro stone columns on theoretical basis which can be adopted to different soil conditions.

VIBRO STONE COLUMNS (DRY BOTTOM FEED METHODOLOGY)

A custom-built machine called Vibrocat has been developed by Keller for installation of vibro stone columns without using water. The Vibrocat comprises a specially constructed track mounted supporting unit, attached with high capacity depth vibrator, which incorporates a stone tube with compression chamber and stone feed hopper ensures properly formed compacted stone columns to the required diameter and depth. A special feature of the dry method is that it does not require water jetting for penetration and hence eliminates the need to handle the collected water. Furthermore, this method can be used most successfully where limited working space is available, especially in developed or urban areas or where no near water source can be found. This technique provides effective drainage paths to ensure rapid consolidation. It also has a built-in real time computer monitoring system to provide quality control on compaction effort throughout the construction process. Sequence of installation of vibro stone columns using dry bottom feed method is illustrated in Fig. 1.

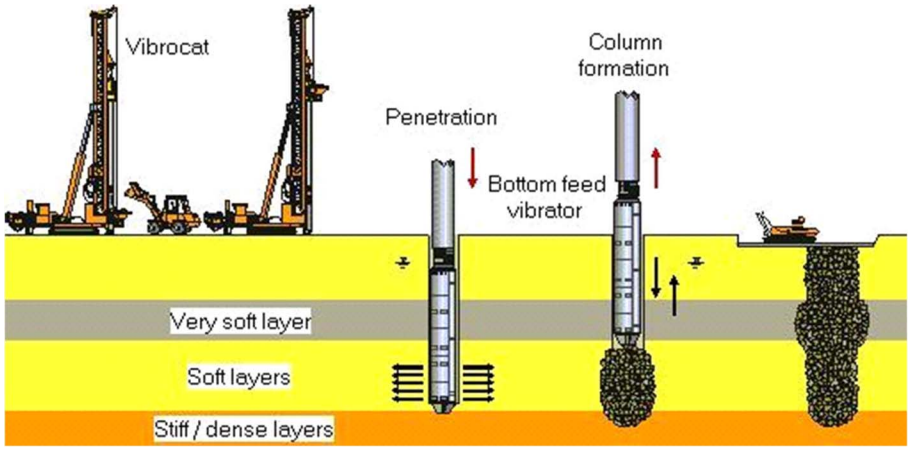


Fig. 1. Sequence of installation of dry vibro stone columns

PROJECT AND SOIL CONDITIONS

Urban Tree Infrastructure Private Limited (Urban Tree), Chennai, proposed to develop a residential project in Chennai. The project comprises of 198 units of Stilt + 4 floors and the approximate area of development is about 2.5 acres. The project site comprises of desiccated clay and medium dense sand up to about 3.5m followed by relatively weak clay and sandy clay up to 6m depth. This top 6m soil with highly varying consistency, followed by 8m thick medium dense sand stiff clay deposits after which there is a 6m thick layer of medium stiff consistency. Denser sand layers and hard clay layers are forming the remaining sub-soil profile.

DESIGN APPROACH

The performance of individual footings (shallow foundations) would not be effective due to weak to very weak soil layers till 6m depth below the existing ground level. Larger settlements were expected in case of raft foundation due to high structural loads. The range of settlement estimated in the investigation report was about 220mm out of which the top 6m to 8m soil attributing about 115mm.

Considering the project boundary conditions, vibro stone columns (dry bottom feed method) was selected as a viable method as an alternative foundation system. In this method, the stone columns are installed by displacement technique (without removing any soil). Hence, the site environment would be comparatively clean and tidy. In addition, benefits with regard to economizing the foundation cost and optimizing construction time was proven invaluable for the project. The load intensity over the foundation raft is about 75 to 85 kPa. The raft foundation was divided into six pours to ease the construction (see Fig. 2).

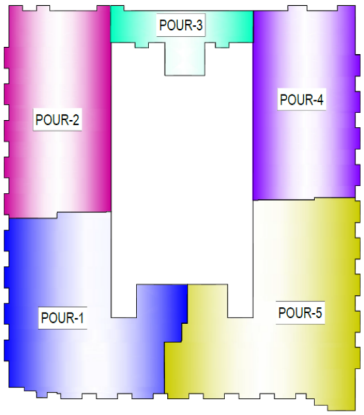


Fig. 2. Footprint of the raft foundation (divided into pours for ease of construction)

Critical review in terms of strength and deformation characteristics for the proposed loading conditions were made using Priebe (1995) design methodology and the final scheme was reviewed and vetted by M/s Geotechnical Solutions, Chennai, a third party specialist Geotechnical Consultancy firm for Geotechnical compliance. Typical scheme and cross section of ground improvement using vibro stone columns using dry bottom feed method adopted for the present project is illustrated in Fig. 3

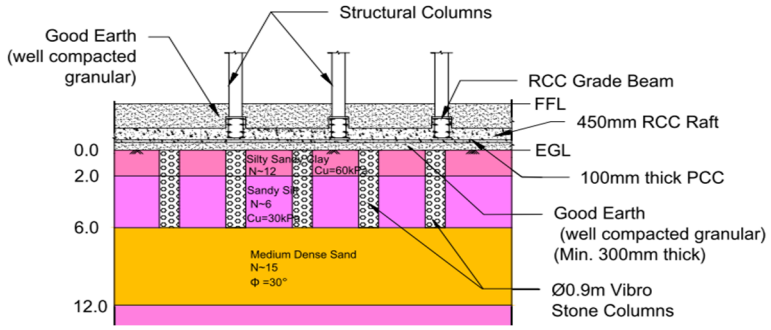


Fig. 3. Typical soil profile showing ground improvement arrangement

QUALITY CONTROL & MONITORING

In order to measure and assure the quality of stone columns installed, it is necessary to adopt stringent quality control and quality assurance procedures to meet the specifications and to satisfy the client's requirement at various stages of execution of the project. An automated computerized recording device fitted to the Vibrocat records the installation of each stone column. This instrument yields a computer record (M4 Graph) of the installation process in a continuous graphical mode, plotting depth versus time and power consumption (compaction effort) versus time.

In addition, routine single column load tests were performed to ascertain the effectiveness of the design and performance of the ground improvement works. The observed settlements are within the acceptable limits for the applied design load intensity of 100 kPa. Load test results are presented in Fig. 4

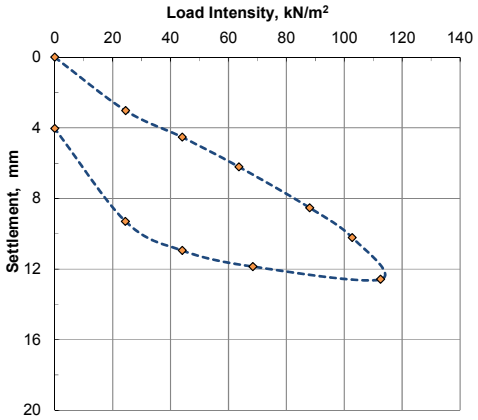


Fig. 4. Results of single column routine plate load test

REAL TIME SETTLEMENT MONITORING

Success of the foundation system needs to be proved by full scale monitoring of foundation settlements during and post completion of the project. Post construction monitoring offers confidence on the engineering assumptions considered during design. In order to monitor the settlements, about 14 points were located on the raft foundation to monitor settlements. Typical arrangement of the selected locations is shown in Fig. 5.

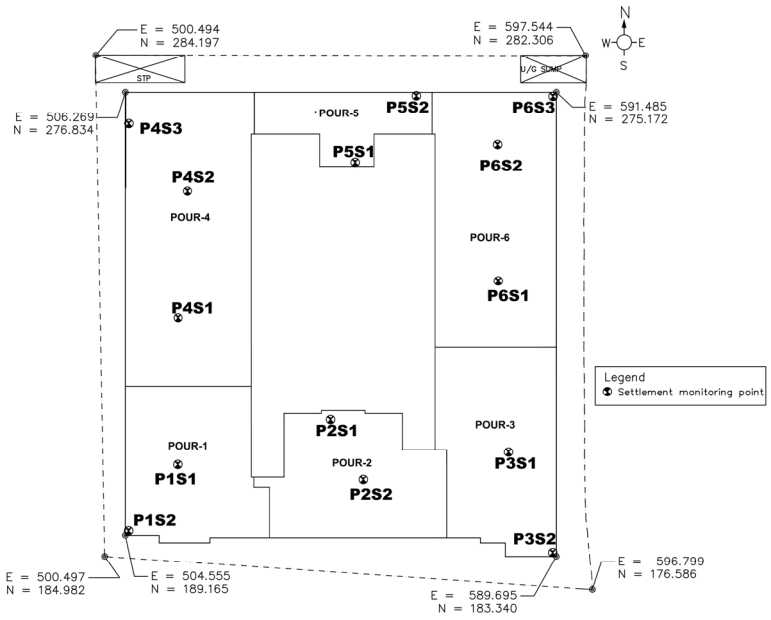


Fig. 5. Settlement monitoring points

The measured settlements are substantially lower than the predicted settlement, which proved the efficiency of the raft foundation resting on improved ground. It can be seen from Fig. 6 that the load in the super structure increases with increase in number of floors and the corresponding settlements are increased. The superstructure load is increased from 0 to 80 kPa in 20 weeks and correspondingly predicted settlements (analytical method) increased from the 0 to 64 mm. However, the observed

settlements are considerably less than the predicted settlements as well as the allowable settlements of 75 to 100 mm for raft foundations resting in clayey soils. Pattern of the observed settlements at one of the pour is presented in Fig. 6. It is suggesting that the long-term settlements will be of much smaller range than that was expected. Vibrocat in action is shown in Fig. 7 and completed structure is shown in Fig. 8.

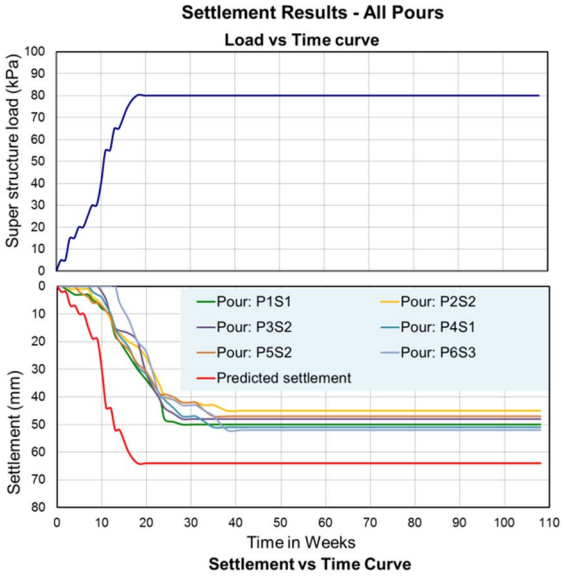


Fig. 6. Results of observed settlements



Fig. 7. Vibro cat in action at project site

CONCLUSIONS

Vibro stone columns proved to be an effective ground improvement solution to support residential buildings on varying weak soil deposits. It is also proven from the results of extensive monitoring that the required performance was achieved. In addition to improving shear strength and compressibility parameters, the ground improvement technique offered acceleration in the overall construction schedule and enabled the project to be completed within stipulated duration.

The ground improvement works were completed within 6 weeks (as against 6 months to that of pile foundations, as scheduled) that was made possible through effective project management. The project got delivered to the end users ahead of time as a result of construction speed of alternative foundation solution (i.e. 6 weeks vs. 6 months) marking a milestone in ground modification. The key success of ground improvement is the savings in time benefitting the entire cycle involving End Users, Suppliers, Bankers and Developers.



Fig. 8: Completed Structure

ACKNOWLEDGEMENTS

The authors wish to thank the developers (Mr Abhishek and Mr Abhinay Mehta, Directors, M/s Urban Tree Infrastructures Ltd.) of the project for their kind permission to publish the information contained in this paper. The authors acknowledge with gratitude to Keller management, for their continuous support and encouragement in finalization of theme of this paper including valuable comments and suggestions that helped the authors to refine and improve the quality of the paper. Thanks are also due to Keller India technical and site team for providing photographs and other execution data.

REFERENCES

1. Hughes JMO & Withers N J, 1975, 'Reinforcing of Soft Cohesive Soils with Stone Columns', Ground Engineering, Volume 7, Issue No. 3
2. Heinz J. Priebe, 1995, The Design of vibro replacement, Ground Engineering, GT 037-13 E
3. IS: 6403: 1981 (Reaffirmed 2002), Indian Standard code of practice for determination of bearing capacity of shallow foundations.
4. IS: 15284 (Part 1): 2003, Indian Standard for design and construction for ground improvement – Guidelines, Part 1: Stone Columns
5. IS: 1904 – 1986 (2006), Code of Practice for design and construction of foundations in soils: general requirements

BACK ANALYSIS OF FIELD INSTRUMENTATION RESULTS DURING RECLAMATION & GROUND IMPROVEMENT WORKS- A CASE STUDY

Aminul Islam, Geotechnical Manager, ITD Cementation India Limited, Mumbai, E-mail: aminul.islam@itdcem.co.in
Prasanta Paul, General Manager, ITD Cementation India Limited, Mumbai, E-mail: prasanta.paul@itdcem.co.in)

ABSTRACT

Nhava Sheva (India) Gateway Terminal Private Limited proposed to construct a container terminal yard, comprising a back-up area at Jawaharlal Nehru Port Terminal (JNPT), Uran, Maharashtra. The proposed container terminal yard is located on a recent reclamation on the Thane Creek, which was developed by land-based reclamation method. The underneath soft marine clay was treated, using vertical band drains and placement of surcharge upon.

Settlement of the reclamation during its construction was monitored using settlement plate installed at +4.8m CD elevation which was above the highest high water level.

This paper examines the settlement behaviour of the reclamation during the ground improvement works. The geotechnical parameters are back-analyzed by the authors from the field settlement results and the concerned preloading details. The back analyzed coefficients of consolidation due to horizontal flow (C_h) are compared with laboratory determined parameters and the estimated value, using Asaoka Method (1978). The authors also studied field compression ratio [$CR= C_c/(1+e_0)$] vs. the compression ratio determined by laboratory test using back-analysis method.

Keywords: **Asaoka method, coefficient of consolidation, back analysis, compression ratio, reclamation**

1. INTRODUCTION

Nhava Sheva (India) Gateway Terminal Private Limited proposed to construct a container terminal yard, comprising a back-up area of approximately 27 hectares, complete with associated buildings and services on a part brownfield/ greenfield site. The back-up area shall include a heavy duty block paved pavement with band beams for electric Rubber-Tyred Gantry Crane (eRTGC) alongwith surface water drainage system and other services including area lighting, provision of fire-fighting facilities , sources for potable water and power.

Based on the Employer's Requirement and the available geotechnical investigation report, ground improvement scheme is designed by the construction contractor. Ground improvement works included the installation of prefabricated vertical drains and subsequent placement of surcharge for accelerating the consolidation of the underlying soft marine clay.

In such ground improvement projects in soft marine clay, the degree of improvement attained by the marine clay has to be ascertained to confirm whether the soil has achieved the required degree of consolidation before proceeding with the surcharge removal. This analysis can be carried out by means of observational methods for which records of ground behaviour can be continuously monitored from the inception of installation of field instrumentation. Field settlement monitoring data can be used to ascertain the settlement of the reclaimed fill from the time of initial installation. The field settlement data can be analyzed to predict the ultimate settlement of the reclaimed land under the surcharge fill. This study aims to evaluate the coefficient of consolidation due to horizontal flow and consolidation parameters by back-analyzing of the field settlement data.

2. SITE LOCATION AND SOIL PROFILE

The project site is located at Jawaharlal Nehru Port which is the largest container port in India and it is located at east of Mumbai, Maharashtra. The port on the Arabian Sea is accessed via Thane Creek. Based on the geotechnical investigation report, 7.0 to 9.5m of compressible soft marine clay is observed in the project boundary. This compressible layer is followed by dense sand/highly weathered rock. The geotechnical parameters of the marine clay are presented is Table 1& Table 2

In absence of radial consolidation test results and based on the previous experience at the adjacent project, coefficient of consolidation due to horizontal flow (C_h) is assumed as 2 times of coefficient of consolidation due to vertical flow (C_v).

Table 1 Geotechnical Parameters (Laboratory Test Results)

Layers	Depth (m CD)		Depth (m)	LL (%)	PL(%)	PI (%)	NMC (%)	Bulk density (t/m^3)
	From	To						
Very soft Marine Clay (Unit 1A)	2.0	-1.0	3.0	104	42	62	92	1.44
Soft Marine Clay (Unit 1B)	-1.0	-6.5	5.5	88	37	51	73	1.56

Table 2 Consolidation property of marine clay (Laboratory Test Results)

Layers	Depth (m CD)		Depth (m)	Compression Index, C_c	Initial Void Ratio, e_0	CR= $C_c/(1+e_0)$	C_v (m^2/yr)	$C_h = 2 \times C_v$ (m^2/yr)
	From	To						
Very soft Marine Clay (Unit 1A)	2.0	-1.0	3.0	0.90	2.63	0.25	1.17	2.34
Soft Marine Clay (Unit 1B)	-1.0	-6.5	5.5	0.68	2.55	0.19	1.57	3.14

3. RECLAMATION METHODOLOGY & CONSTRUCTION STAGES

The suitable fill material is transported through trucks from the local borrow areas to the project site at seashore. The fill material is placed near the leading edge and gently pushed towards the sea by Bulldozers for advancing of the reclamation . This cycle is continued till entire area is reclaimed. Generally, this method is termed as land based reclamation method or end tipping method.

The stages of construction adopted in this project are presented below

- Reclamation up to working level i.e. +4.8m CD
- Installation of Prefabricated Vertical Drains
- Placement of drainage blanket & non-woven geotextile as separator
- Installation of Settlement plates at 80 m x 80m grid
- Placing of Surcharge over drainage blanket and separator above +4.8m CD level
- Removal of Surcharge after achieving required degree of consolidation

4. ASSESSMENT OF FIELD SETTLEMENT DATA

The Asaoka method enables to forecast accurate predictions of the ultimate settlement of marine clay. This method is frequently used in the assessment of the degree of improvement of marine clays under reclaimed fills.

The coefficient of consolidation due to horizontal flow (C_h) can also be determined using Asaoka method.

4.1. Asaoka's Method

Asaoka (1978) has suggested a procedure modified for application to consolidation problems with vertical drains using Barron's (1948) solution for pure radial drainage. The Asaoka procedure generates a straight-line only if the soil behaviour fulfils the assumptions of Terzaghi's (1943) theory of one-dimensional consolidation. The use of the Asaoka method for the assessment of the degree of consolidation of marine clays with vertical drains in land reclamation projects has been described in Port work design manual Part-3 (2002) by The government of the Hong Kong special administrative region. In the Asaoka analysis procedure, the time settlement curve of the settlement gauge is first plotted. Next, a series of settlement values $s_1, s_2, \ldots s_n$ is selected, such that s_n is the settlement at time n and that the time interval, $\Delta t = (t_n - t_{n-1})$ is constant. The next step is to plot the points (s_{n-1}, s_n).

These points should lie on a straight line defined as follows:

$$s_n = s_o + \beta s_{n-1} \quad \ldots\ldots \quad (1)$$

where s_o and β are two constants which depend on the selected time interval Δt.

The ultimate settlement can then be predicted at the intercept of this line and a 45 degree line. The constant β represents the slope of the constructed straight line. As suggested by Magnan and Deroy (1980), the constant β is related to the coefficient of consolidation due to horizontal flow (C_h).

Considering horizontal (radial) drainage only, C_h value shall be determine by following equation

$$C_h = \left(\frac{-D_e^2 \times F(n)}{8}\right) \times \left(\frac{ln\beta}{\Delta t}\right) \quad \ldots \quad (2)$$

where D_e is the diameter of equivalent soil cylinder and F(n) is the drain spacing factor.

4.2. Curve Fitting Method

The field measured settlement curve has been superimposed with the theoretical settlement curve. The theoretical settlement curve has been fitted with the field measured curve by adjusting consolidation parameters such as compression ratio [CR= $C_c/(1+e_0)$] and coefficient of consolidation (C_v & C_h). Generally, this type of analysis is called as curve fitting method or invert analysis.

5. ASSESSMENT OF SETTLEMENT DATA

5.1. Assessment by Asaoka Method

The basic assumption in Asaoka method considers that the settlements follow a negative exponential curve under a constant loading condition. For this study, only the settlement data recorded after reaching the top of the surcharge level is used. A typical settlement and fill elevation vs. date is presented in Figure 1.

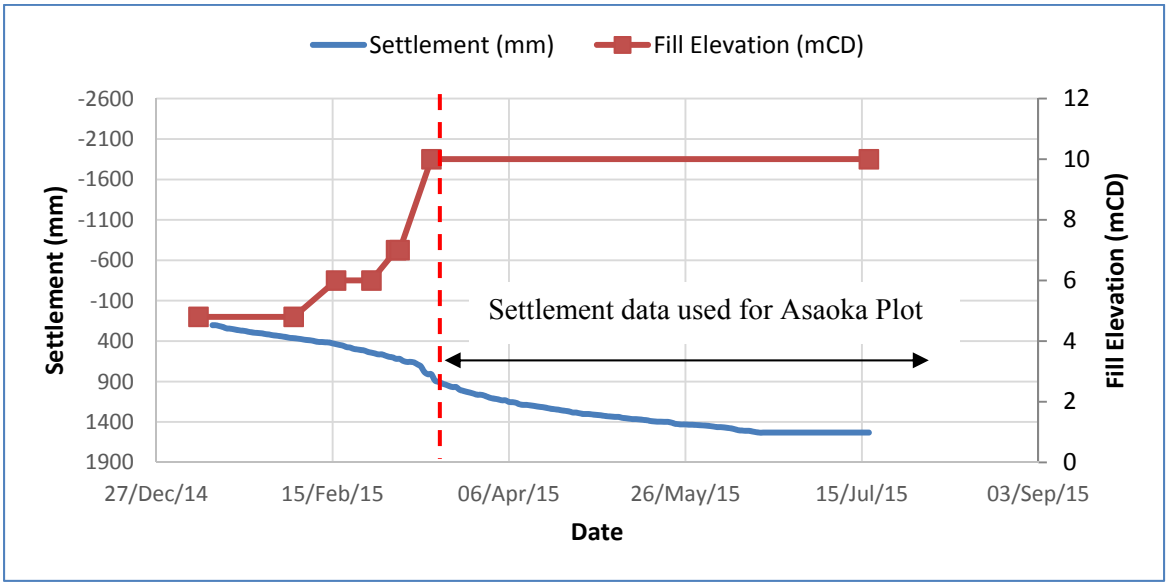


Figure 1 Settlement/Fill Elevation vs Date (Field record)

The constant time interval of 7days is considered for generating Asaoka plots. The entire project is divided into 4 areas and the Asaoka plots are prepared and presented in Figure 2 to 5.

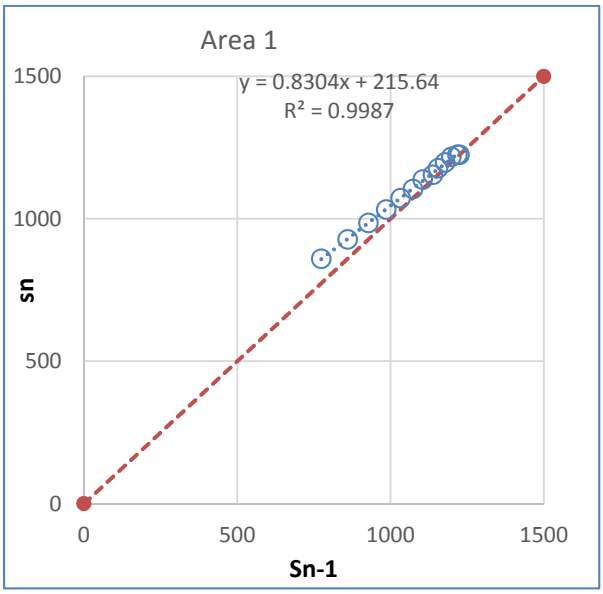


Figure 2 Asaoka Plot for Area 1

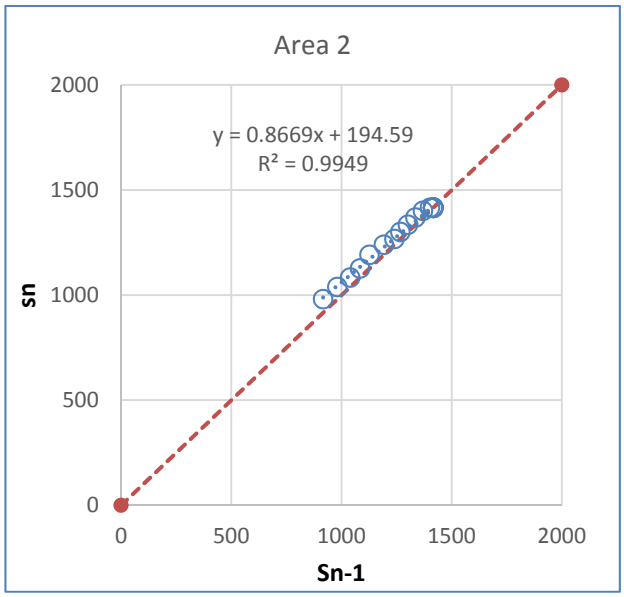


Figure 3 Asaoka Plot for Area 2

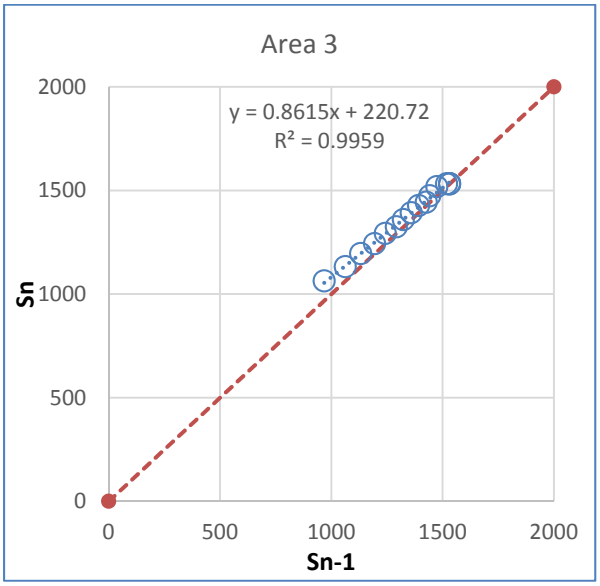


Figure 4Asaoka Plot for Area 3

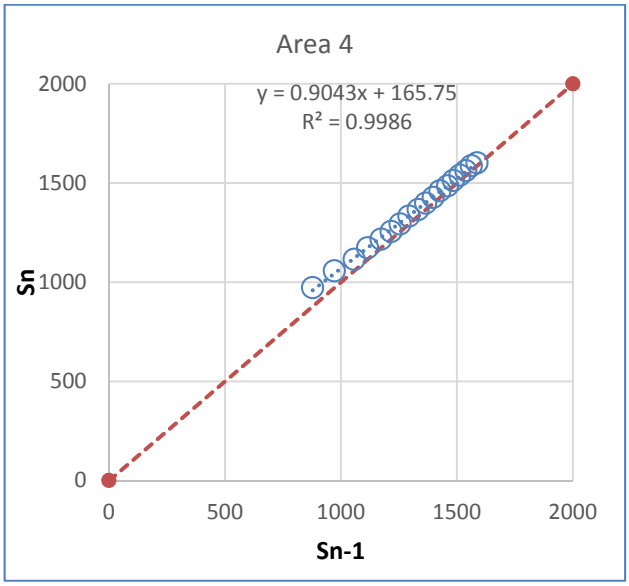


Figure 5 Asaoka Plot for Area 4

5.2. Assessment by Curve Fitting Method

The field measured curve has been plotted over the theoretical settlement plot and a comparative study has been made. The theoretical curve has been calibrated by adjusting the consolidation parameters to fit

the curve with actual field reading. A typical curve fitting has been presented in Figure 6. In absence of exact depth of marine clay at the location of the settlement plates, the authors considered the clay depth from the nearest borehole. The depth of clay has a significant role in this method of analysis, determination of the exact depth of clay at the settlement plate location has been excluded from the ambit of this study due to limitation of resources and time.

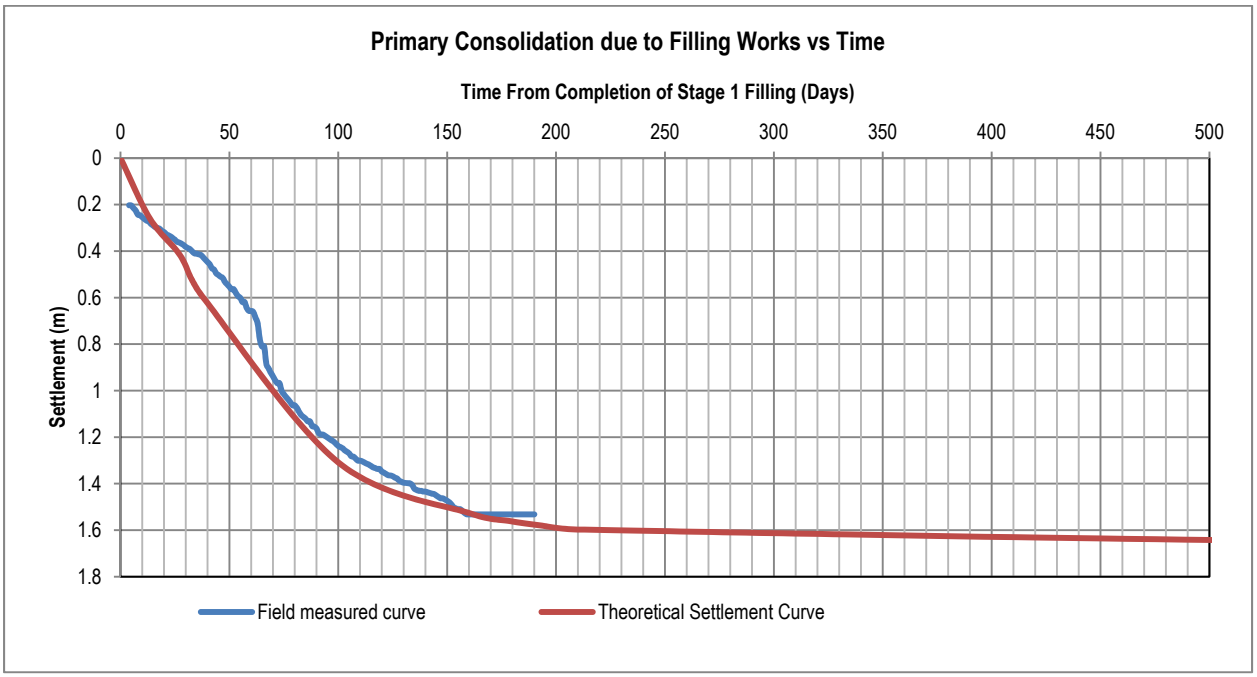


Figure 6 Curve Fitting Method

5.3. Comparison between design parameter & back analyzed parameter

The comparison between laboratory test parameter and back analyzed parameter obtained from curve fitting is presented in Table 3.

Table 3 Comparison between laboratory test & Back Analyzed Parameter

Layers Description	Depth (m CD)		Depth	Laboratory test Parameter			Back Analyzed Parameter (Avg)		
				CR	C_v	C_h	CR	C_v	C_h
	From	To	(m)	-	(m^2/yr)	(m^2/yr)	-	(m^2/yr)	(m^2/yr)
Very soft Marine Clay (Unit 1A)	2.0	-1.0	3.0	0.25	1.17	2.34	0.21	1.18	2.35
Soft Marine Clay (Unit 1B)	-1.0	-6.5	5.5	0.19	1.57	3.14	0.18	1.43	2.85

The calculated coefficient of consolidation due to horizontal flow by Asaoka and curve fitting method is also compared and shown in Table 4.

Table 4 : Comparison C_h Value-Asaoka & Curve Fitting Method

Location	Reference Instrument ID #	Asaoka Method	Curve Fitting Method (Avg.)
		Ch (m^2/yr)	Ch (m^2/yr)
Area 1	SP13	4.24	2.79
Area 2	SP28	3.26	2.66
Area 3	SP20	3.40	2.46
Area 4	SP16	3.43	2.79

SP- Settlement plate

6. SUMMARY AND CONCLUSIONS

This study attempted to use back analysis to evaluate geotechnical parameters of marine clay that has been improved by prefabricated vertical drains. On the basis of this evaluation, the following conclusions can be drawn

1. Authors' findings reveal that the back analyzed compression ratio (CR) from curve fitting method is less than that conceived in the laboratory test parameters. The study reveals that based the laboratory test parameters, the theoretical estimated settlement is found as overestimated.

2. Calculated C_h values by curve fitting method are slightly lower than laboratory test parameters. The authors hypothesize that during reclamation by land based method top layer of marine clay is disturbed and remoulded. The top disturbed layer is contributing to reduce the average of coefficient of consolidations.

3. Authors' findings reveal that Asaoka method predicts higher C_h value compared to the one obtained from curve fitting method.

REFERENCES

Asaoka, A., 1978. Observational procedure of settlement prediction, Soil and Foundations, Journal of the Japanese Society of Soil Mechanics and Foundation Engineering,, Vol. 18, No. 4, pp. 87-101.

Barron, R.A, 1948. Consolidation of fine grained soils by drains wells. Trans ASCE 124, PP 709-739

Indian Standard (IS 15284 Part 2), 2004. Design and construction for ground improvement-guidelines for Preconsolidation using vertical drain.

Magnan, J.P, Deroy, J.M, 1980. Analyse graphic des de consolidation oedometrique. Bull Liason Lab. Ponts et Chaussees, Paris, France, , PP 53-56

Port Works Design Manual, 2002. Part-3: Guide to design of reclamation. The government of the Hong Kong special administrative region, PP 85-94

Terzaghi, K., 1943. Theoretical Soil Mechanics, Wiley, New York.

DETERMINATION OF LIQUEFACTION IN TIME DOMAIN USING SHAKE TABLE TEST, WAVELET ANALYSIS AND NUMERICAL APPROACH

Raj Banerjee, Scientific Officer, Bhabha Atomic Research Center, Mumbai, Maharashtra, India, 02225593548, banerjeeraj1990@rediffmail.com
Aniruddha Sengupta, Professor, Indian Institute of Technology Kharagpur, West Bengal, India, 03222283454, sengupta@civil.iitkgp.ernet.in
Rana Chattaraj, Research Scholar, Indian Institute of Technology Kharagpur, West Bengal, India, 03222283454, chattaraj.rana@gmail.com
G.R.Reddy, Outstanding Scientist, Bhabha Atomic Research Center, Mumbai. Maharashtra, India, 02225595181, rssred@barc.gov.in

ABSTRACT

Earthquake induced liquefaction in saturated granular soils is an important phenomenon which causes severe damage to life and property. In the present study, dynamically induced liquefaction of saturated Kasai River sand is studied in 1-g shake table to assess its liquefaction potential. In the shake table, the soil was subjected to sinusoidal motions of amplitude 0.35g at a frequency of 2Hz. A numerical model using FLAC 2D (Itasca 2005) was performed to simulate the shaking table tests. Reasonably good agreement between the experimental and the numerical results has been observed. Moreover, wavelet analysis has been conducted to identify the occurrence of liquefaction in sand and to correlate the observations found from the experiments. The nonlinear curves used to represent shear strain dependency of stiffness of the Kasai River sand was obtained from cyclic tri axial tests.

Keywords: Shake table test, Small scale model test, Liquefaction, Wavelet, FLAC 2D.

INTRODUCTION

The term Liquefaction is used in conjunction with a variety of phenomena that involve soil deformations due to cyclic disturbance in saturated soil under undrained conditions. The generation of excess pore water pressure is the hallmark of all liquefaction related phenomena and the reduction in the volume or the tendency of cohesionless soil to densify during undrained loading condition as prevails during an earthquake is also well known. Use of shaking table tests to understand liquefaction of soils has been demonstrated by several researchers (Ye et al. 2013; Ha et al. 2011). Mohajeri and Towhata 2003 and Towhata et al. 2006 carried out 1-g shaking table tests on soil models prepared in laminar box to study the rate dependent behavior of liquefied soils. Ueng et al. 2010 used a biaxial laminar shear box mounted on shaking table to study the settlements in saturated clean deposits of sand and related the volumetric strain in liquefied sand to the relative density for various shaking durations and earthquake magnitudes. Maheshwari et al. 2012 reported increase in liquefaction resistance of reinforced sand through shaking table tests and concluded that the type and amount of reinforcement in the soil layer has influence on its liquefaction potential.

The objective of the present study is to compare the behavior of dry and saturated Kasai River sand when subjected to seismic shaking. The Kasai River separates two growing cities, Medinipur and Kharagpur in the state of West Bengal in India. A number of road and railway bridges exist over the river connecting the two cities. The area being in Seismic Zone III, that is, a zone with moderate probability of earthquake, it is important to characterize the behavior of the Kasai River sand during a possible earthquake event especially when a number of bridges are existing over it. Small scale laboratory model tests and numerical analyses using a commercial finite difference algorithm called FLAC2D (Itasca 2005) have been utilized to study the difference in behavior of dry and liquefied Kasai River sand during dynamic loading conditions.

EXPERIMENTAL SETUP

The experimental setup consists of a shake table which essentially comprises of a 1m by 1m steel table mounted on rails. The load carrying capacity of the table is 5ton. The model tests, reported here, were performed in a rigid plexiglass container of dimensions 0.9m x 0.825m x 0.858m (length x breadth x height) with top open. The plexiglass sheets are 16mm thick and glued to each other as well as fixed in a steel frame consisting of steel angles. All the model tests are conducted in a 1-g environment, where the model and the prototype accelerations are kept equal. The scale factor (λ) utilized in the model study to scale down the other parameters is 20 (Iai 1989). The initial case consists of testing the dry sand followed by saturated sand. The model ground was prepared in layers until the test container was filled almost up to a height of 650 mm, with the dry sand at a uniform density of 1600 kg/m^3 (unit weight = 15.7kN/m^3) by compacting the sand to the intended relative density. Two accelerometers, one near the top and another near the bottom were inserted into the soil in horizontal direction to measure the amplification of motion through the sand bed during the test. One accelerometer was placed on the shake table itself to double check the motion of the shaking table. Thermocols, 16mm in thickness, was placed between the plexiglass container and the sand layer on three sides to minimize the reflection/refraction of waves from the side walls (Giri and Sengupta 2010). Liquefaction tests on the sand were carried out on the uniaxial shake table within the same transparent plexiglass container. Pre-calculated amount of water to fully saturate the sand (30.56%) was added to the sand in the test chamber. Three pore water pressure transducers at the middle location of the test chamber and at 11.50, 31.0 cm and 52.0 cm from the top surface of sand was utilized to monitor the pore water pressure development in the sand bed during the shaking. All the liquefaction tests were conducted with water table maintained at the top surface of the sand bed. All the accelerometers was placed at the same positions as before. Figure 1 shows the liquefaction test setup.

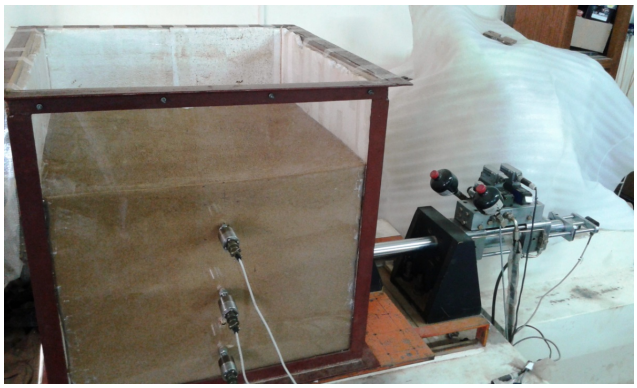


Fig. 1. Liquefaction setup in shaking table

SOIL PROPERTIES

Local uniform grained sand (Kasai River sand) was used in this study. It is classified as poorly graded sand (SP), according to the Unified Soil Classification System (USCS). The specific gravity of the sand was 2.7. In all the model tests, the bulk unit weight and a relative density (D_r) of the sand has been maintained at 15.7kN/m^3 and 48%, respectively. The drained triaxial shear tests were performed on the sand to find its shear strength parameters. The effective cohesion (c') and the effective angle of friction (φ') obtained from triaxial tests are 0.0 kPa and 32^0, respectively. The elastic properties of the soil have been found from the initial part of the stress-strain data. Table 1 shows all the material properties for the Kasai River sand.

Table 1. Geotechnical parameters of the Kasai River sand

Parameters of foundation soil	Value
Mass density(kg/m^3)	1600
Cohesion(Pa) ($c^{'}$)	0
Angle of internal friction	32^o
Modulus of elasticity, E (MPa)	58.76
Poisson's ratio, ν	0.3

Tsuchida (1970) investigated the gradation of soils for which liquefaction behavior was observed during earthquakes in Japan and those exhibiting similar behavior in shaking table. The mean grain size (D_{50}) of the soil was used as an index to distinguish between the liquefiable and non-liquefiable deposits of soil and the range of gradation for potentially liquefiable deposits was proposed by Tsuchida (1970) as shown in Fig. 2.

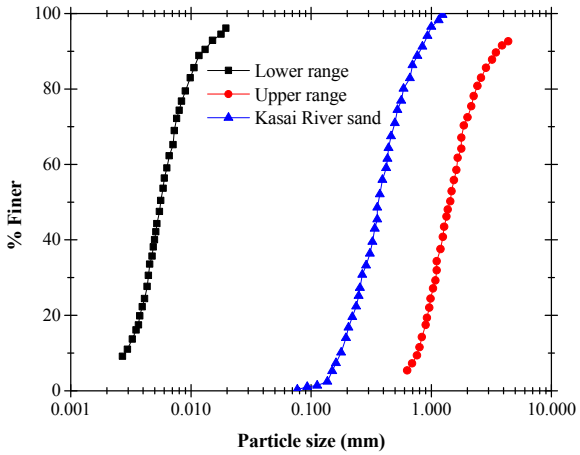


Fig. 2. Gradation of Kasai River sand

As may be seen from the figure, the grain size distribution of Kasai River sand is well within the proposed range, hence under dynamic loading condition the sand is susceptible to liquefaction. Liquefaction resistance curve of Kasai River sand has been found out from cyclic tri axial tests for confining pressure which are matching with the scaled up experimental confining pressures at 26, 46 and 66 kPa deviator stresses. The number of cycles needed for liquefaction in Kasai River sand with the cyclic deviator stress is shown in Fig. 3. The liquefaction was observed in the test by relying on the pore pressure ratio, r_u time history which comes close to unity as the sand liquefies. It shows that the liquefaction resistance of soil decreases with the increase in deviator stress magnitude.

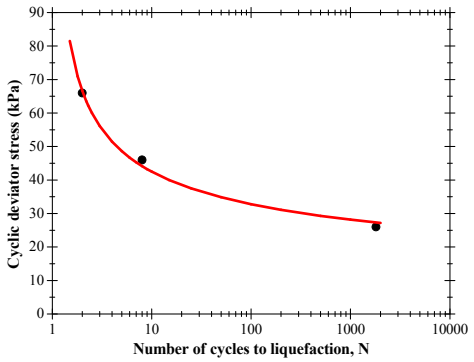


Fig. 3. Liquefaction resistance curve for Kasai River sand

SELECTION OF INPUT MOTION

In the present study, the performance of the Kasai River sand has been studied conservatively for a 0.35g event. As a part of the study, a number of earthquake motions are reviewed and 03 September, 2010 Darfield Christchurch Earthquake (M_w= 7·1, S73W component) motion was selected for studying the dynamic behavior of the dry and liquefied sand. Following the procedure developed by Seed and Idriss (1971) to convert an actual irregular stress time history into repetition of several stress cycles of constant amplitude, the equivalent acceleration time history is constructed whose a_{avg} is calculated as 2/3 of PGA and found to be 0·3503 g with a frequency of 2Hz applied for 10 cycles.

LIQUEFACTION CHARACTERISTICS OF THE FOUNDATION SOIL

The pore water pressure fluctuations at the specified locations were measured during the shake table test and liquefaction of sand was assessed. Measurement of the pore water pressure at 0.115m depth sometimes failed during the test, in which case the reading of this transducer was not taken into account throughout the study. The variation in excess pore water pressure, U_{excess} with time at various depths within the sand bed was recorded using the remaining two transducers, due to malfunctioning of one transducer during the test and is shown in Fig. 4. Thus, the maximum value of excess pore water pressure, U_{excess} and time elapsed in three different stages of liquefaction (t_1, t_2 and t_3) was evaluated for each transducer and is shown in Table 2. The time t_1, t_2 and t_3 are the time for occurence of liquefaction, duration of liquefaction and the time needed for dissipation of excess pore water pressure, respectively.

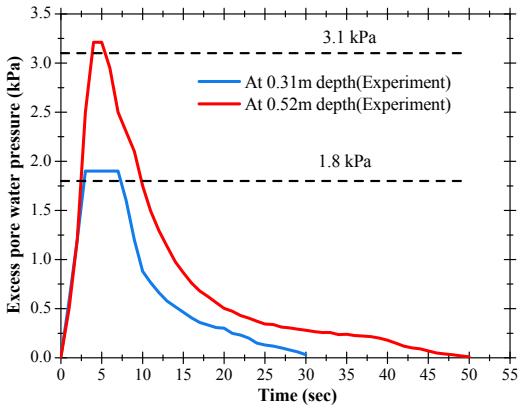


Fig. 4. Variation of excess pore water pressure distributions at various times in the sand

An important observation made from Fig. 4 is that excess pore pressure first develops near the top of the sample then proceeds to the middle and eventually to the bottom implying that liquefaction occurs at shallower depths first and the zone of liquefaction spreads downward from the top, a similar observation made by Florin and Ivanov (1966). The duration for liquefaction occurs longer at shallower depths which is observed in Table 2.

Table 2. Data from experimental observations

Location of pore pressure transducer	Middle (0.31m depth)	Bottom (0.52m depth)
$U_{maximum}$ (kN/m^2)	1.90	3.212
t_1 (sec)	3.0	4.0
t_2 (sec)	4.5	1.5
t_3 (sec)	22.5	44.5

After the application of about 6 to 8 cycles (3 to 4 seconds) of the sinusoidal motion, the sand liquefies. It may be noticed from Table 2 that the dissipation of excess pore water pressure takes longer time with depth. This is attributed to the fact that the drainage path for the middle layer is shorter compared to the bottom one. Thus, experimental observations very well respond to the theoretical basis, and this validates the experimental results for further study on liquefaction.

WAVELET ANALYSIS FOR THE OCCURRENCE OF LIQUEFACTION IN TIME DOMAIN

The wavelet analysis has emerged as a powerful tool to analyze a signal and recent studies suggested an effective use of wavelets for the solution of both linear and nonlinear problems (Grossman and Morlet 1984). A wavelet is a small wave with finite energy, which has its energy concentrated in time or space to serve as a "basis function" for the analysis of transient, nonstationary, or time-varying phenomenon. Each wavelet is located at a different position on the time axis and is local in the sense that it decays to zero when sufficiently far from its center. Wavelet analysis provides immediate access to information that can be obscured by other time-frequency methods such as Fourier analysis. The specific objective for studying the wavelet transform in our study is to identify the occurrence of liquefaction in sand and to correlate the observations found from the experiments. In this study, the acceleration time history for dry and saturated sand has been analyzed using wavelets. The real part of morlet wavelet (Morlet et al. 1982) has been used for the analysis. The equation for the 'Morlet' wavelet is :

$$\psi(t) = \frac{1}{\sqrt{2\pi}} e^{-t^2/2} \cos(\omega t) \qquad [1]$$

Continuous wavelet transform (CWT) is used as a signal processing tool for investigating time-varying frequency spectrum characteristics of the accelerometer signals by considering a numerical approximation to the integral in CWT :

$$W(a,b) = a^{-1/2} \int_{-\infty}^{\infty} s(t)\psi^*\left(\frac{t-b}{a}\right)dt \qquad [2]$$

If the signal set is sampled with sampling interval T_s, then the CWT at the time step $b = kT_s$ is approximated by the sum:

$$W(a,kT_s) = T_s a^{-1/2} \sum_{n=0}^{\infty} s(nT_s)\psi^*\left(\frac{(n-k)T_s}{a}\right) \qquad [3]$$

Putting the value of the Morlet wavelet equation, the equation reduces to:

$$W(a,b) = \frac{\Delta T}{\sqrt{2\pi a}} \sum_{n=0}^{\infty} s(n\Delta T) \exp\left(\frac{-(n\Delta T - b)^2}{2a^2}\right) \cos\left(2\pi f_0 \frac{(n\Delta T - b)}{a}\right) \quad [4]$$

where $\psi^*(t)$ is the complex conjugate of the wavelet equation and ω_0 =5.0.

Time frequency representation of both accelerograms are shown in Fig. 5 in which the peak frequency of 2 Hz has occurred for the entire time domain but for the case of liquefaction, the amplitude of the wave has decreased after 2.8 seconds which indicates the onset of liquefaction for the zone.

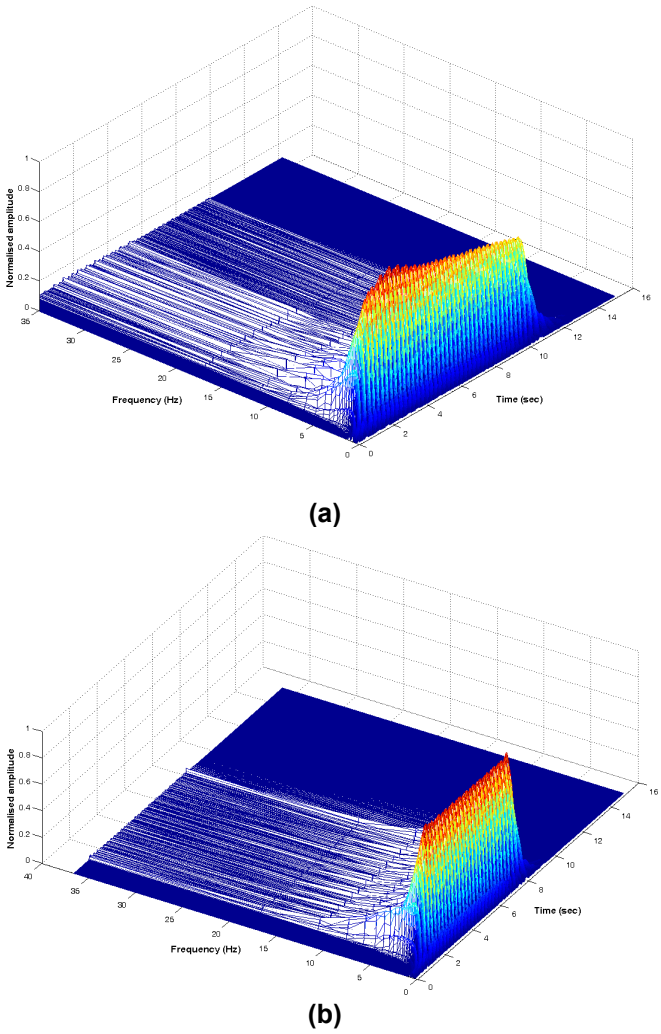


Fig. 5. Time frequency representation of accelerometers for (a) saturated and (b) dry Kasai River sand

As the liquefaction starts, there is a sudden drop in shear wave velocity as well as wave energy which is manifested by the decrease in the amplitude in the time frequency plot which is not observed in the case for dry sand. Hence the soil starts to liquefy at 2.8 seconds (around 6 cycles) which is close to the experimentally obtained value of 3.0 to 4.0 seconds (6 to 8 cycles) from the pore pressure history plot, thus validates the above analysis.

NUMERICAL STUDY OF LIQUEFACTION

Numerical simulation of the laboratory shake table tests on the Kasai River sand leading to its liquefaction has been performed using commercial finite difference software called FLAC2D (Itasca 2005). In order to model numerically the generation of pore water pressures in the sand during dynamic loading "Finn" model was employed. The Finn model was originally developed by Martin et al. (1975) and later modified by Byrne et al. (1991). FLAC2D incorporates this model in the general Mohr Coulomb plasticity model to simulate the generation of pore water pressure.

The locations of the side and bottom boundaries in the numerical analyses was chosen to satisfy the scaled up dimensions of the soil in the shake table test. The sand bed (17m in width and 13m in height), was discretized by 34 x 26 numbers of quadrilateral elements of size 0.5m × 0.5m as shown in Fig. 6. The zone (element) size was chosen in a manner such that it is small enough to allow the acceleration waves at the input frequency to propagate accurately (Itasca 2005). For the dynamic analyses, absorbing boundaries are assumed on the sides. The acceleration-time history applied to the shake table was applied to the bottom of the soil domain after proper scaling of frequency and duration. The magnitude of the maximum acceleration is 3.43 m/s^2 (0.3503g), which is same as mentioned before.

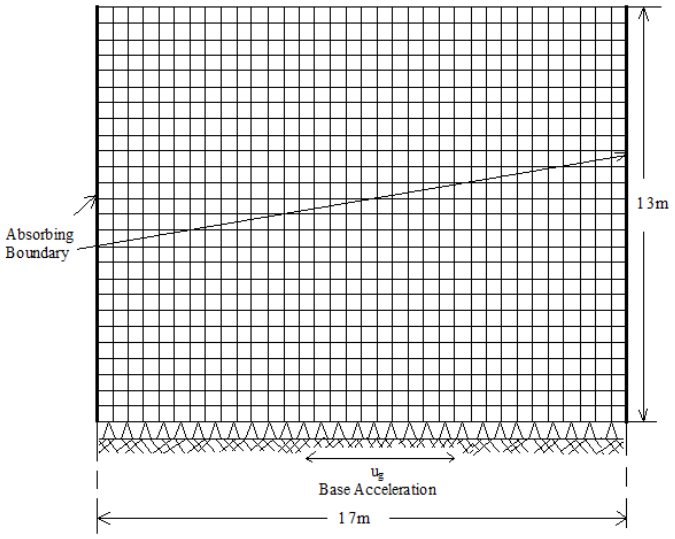
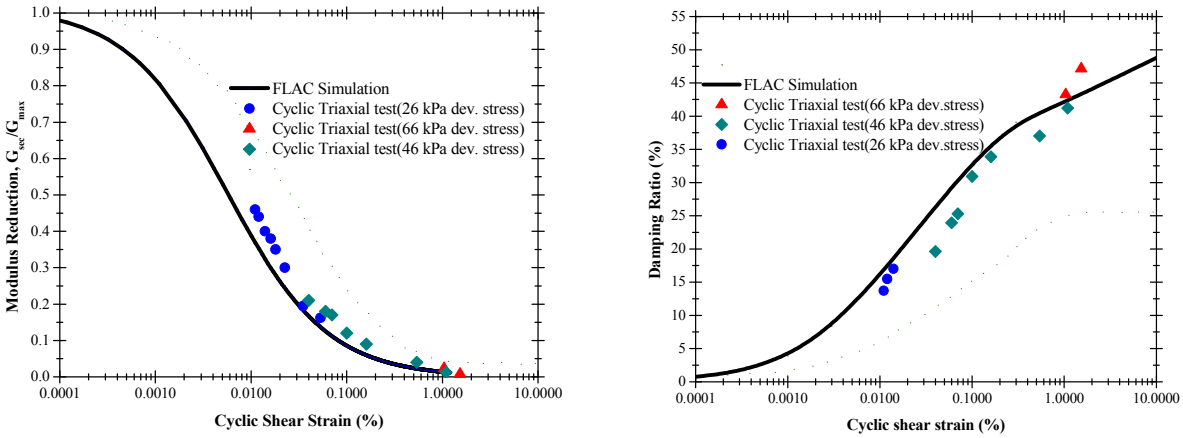


Fig. 6. Numerical discretization of soil domain in FLAC 2D

The hysteretic damping and shake down of strength in the Kasai River sand during dynamic loading was obtained from cyclic tri axial tests. These two nonlinear curves are then fitted with multiple points using "*sigmoidal"* model available in FLAC (Itasca 2005). The "*sigmoidal"* model in FLAC 2D is defined as follows:

$$M_s = \frac{a}{1+\exp(\frac{-(L-x_o)}{b})} \qquad [5]$$

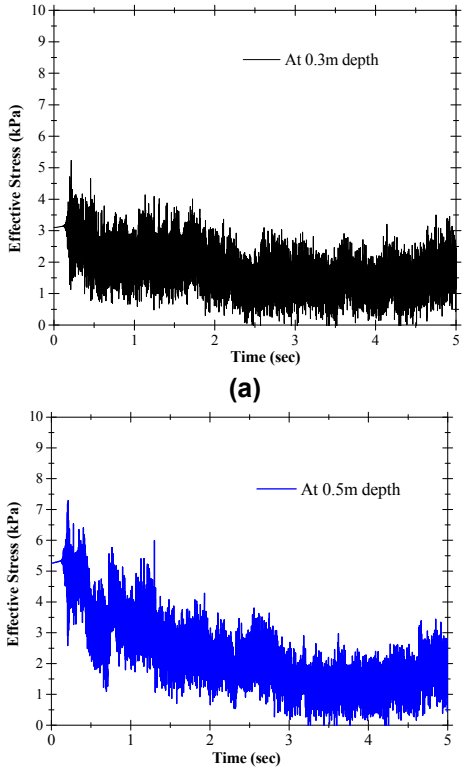
where, L is the logarithmic strain, $L = \log_{10}(\gamma)$, a, b and x_o are the curve fitting parameters whose values for the Kasai River sand are 1.014, -0.525 and -2.650 respectively. Figure 7 shows the test data and the fitted curves utilized in the numerical analyses for the hysteretic damping and modulus degradation of Kasai River sand.



(a) (b)

Fig. 7. Shakedown strength (a) and Hysteretic damping (b) of Kasai River sand

The number of cycles to liquefaction of the sand was estimated from the effective stress-time history at 0.30 and 0.50 m depth, and observing at which instance effective stress is close to zero. Figure 8 shows the effective stress-time history at the two foresaid points in the sand bed which is properly scaled for frequency, duration and stresses, respectively.



(a)

(b)

Fig. 8. Effective stress time history for (a) 0.30m and (b) 0.50m depth of soil

From Fig. 8, it is observed that the soil liquefies at around 2.5 to 3.0 seconds (5 to 6 cycles) for 0.3m depth and at 3.5 to 4.0 seconds (7 to 8 cycles) at a depth of 0.5m respectively, which implies that the soil at a shallower depth liquefies earlier as compared to soil at a deeper location. Thus the zone of

liquefaction spreads downward from the top, a similar observation made by Florin and Ivanov (1966), which is also verified numerically from Fig. 8.

CONCLUSIONS

The engineering behavior of dry and saturated Kasai River sand at 67% relative density is studied experimentally on a shake table and analytically by wavelets when subjected to 10 sinusoidal cycles of amplitude 0.35g at 2Hz. The shake table tests as well as the analytical results show coherently that the Kasai River sand liquefies in about 8 cycles of 0.35g sinusoidal motion at 2Hz.

ACKNOWLEDGMENTS

The shake table facility at the Geotechnical laboratory of IIT Kharagpur utilized in this study is provided by SERB (DST), New Delhi vide a grant no. SR/S3/MERC-0029/2011.

REFERENCES

Bryne, P.M., 1991. A model for predicting liquefaction induced displacement. Proceedings, 2nd International Conference on Recent Advances in Geotechnical Earthquake Engineering and Soil Dynamics, St. Louis, Missouri, pp. 1027-1035.

Florin, V.A. and Ivanov, P.L., 1961. Liquefaction of Saturated Sandy Soils. Proc. 5th International Conference on Soil Mechanics and Foundation Engineering, Paris, Vol. 1,pp. 107-111.

Giri, D. and Sengupta, A., 2010. Dynamic behavior of small-scale model of nailed steep slopes. Geomechanics and Geoengineering: An international journal, 5(2) 99-108.

Grossman, A. and Morlet, J., 1984. Decomposition of Hardy functions into square integrable wavelets of constant shape. SIAM J Math Anal, 15(4) 723-736.

Ha, I.S., Olson, S.M., Seo, M.W., Kim, M.M., 2011. Evaluation of reliquefaction resistance using shaking table tests. Soil Dyn Earthq Eng, 31(4) 682–691.

Iai, S., 1989. Similitude for shaking table tests on soil-structure-fluid model in 1g gravitational field. Soils and Foundations, 29(1) 105–118.

Ishihara, K., Troncoso, J., Kawase, Y., Takahashi, Y., 1980. Cyclic strength characteristics of tailings materials. Soils Foundations, 20(4) 127–142.

Itasca., 2005 User's guide for FLAC version 5.0. Itasca India Consulting, Nagpur, India.

Maheshwari, B.K., Singh, H.P., Saran, S., 2012. Effects of reinforcement on liquefaction resistance of solani sand. J Geotech. Geoenviron. Eng, 13(7) 831–840.

Martin, G.R., Finn, W.D.L., Seed, H.B., 1975. Fundamentals of Liquefaction Under Cyclic Loading. Jl of Geotech and Geoenv Engineering, 101(GT5) 423-438.

Mohajeri, M., Towhata, I., 2003. Shake table tests on residual deformation of sandy slopes due to cyclic loading. Soils Found, 43(6) 91–106.

Morlet, J., Arens, G., Fourgeau, E., Giard, D., 1982. Wave propagation and sampling theory. Geophysics, 47 203-236.

Seed, H.B. and Idriss, I.M., 1971. A simplified procedure for evaluating soil liquefaction potential. J Soil Mech Found Div, 97(9) 1249–1274.

Towhata, I., Sesov, V., Motamed, R., 2006. Model Tests on Lateral Earth Pressure on Large Group Pile Exerted by Horizontal Displacement of Liquefied Sandy Ground. 8th U.S. National Conference on Earthquake Engineering and 100th Anniversary Earthquake Conference,San Francisco, California.

Ueng, T.S., Wu, C.W., Cheng, H.W., Chen, C.H., 2010. Settlements of saturated clean sand deposits in shaking table tests. Soil Dyn Earthq Eng, 30(1) 50–60.

Ye, B., Ye, G., Ye, W., Zhang, F., 2013. A pneumatic shaking table and its application to a liquefaction test on saturated sand. Nat. Hazards, 66(2) 375–388.

GROUND FREEZING COMBINED METHOD FOR URBAN TUNNEL EXCAVATION

Filippo Mira-Cattò, Rodio Geotechik AG, Urdorf, Switzerland, +41786907696,
filippo.miracatto@rodio.ch

Andrea M. R. Pettinaroli, Studio Andrea Pettinaroli srl, Milan, Italy, +393333836384,
a.pettinaroli@stap-engineering.eu

Elena Rovetto, Studio ingegneria Balossi Restelli e Associati, Milan, Italy, +393336545141,
elena.rovetto@studiobalossi.191.it

ABSTRACT

The construction of Powisle station of Metro Warsaw Line 2, in Poland, required the execution of two shafts next to an urban road tunnel adjacent to the Vistula River. The shafts were linked by three conventionally mined tunnels to be excavated 10 m below the water table level, into an upper sandy and sandy silty layer and a lower stiff clayey stratum. After a failed dig attempt under the protection of jet grouting and forepoling, it was decided to deal with the tunnels excavation problem by using the ground freezing technique as a temporary, non-polluting geotechnical treatment, keeping in service the upper road tunnel. The planning of the activities and the executive phases had a significant importance for the success of the work. For work scheduling reasons the mixed system was adopted, i.e. using both the liquid nitrogen system and the brine freezing method. The freezing process management, with a real time evaluation of the soil temperature measured by thermometric strings and an accurate monitoring of the overlying road tunnel structure, allowed the tunnel excavation and lining stages to be performed under difficult conditions, without water leaking from the frozen ground shell, within the expected times and saving extra costs.

INTRODUCTION

The new Underground Line 2 in Warsaw connects the eastern and western part of the town. One of the most critical interferences was the under passing of the Vistula river and of the Wislostrada motorway tunnel, a very congested motorway along the western bank of the river, with the construction of the new station Powisle. The construction of the station required the excavation of two shafts, using the top-down system with the creation of intermediate slabs while deepening the excavation.
The shafts were used for the extraction of four Tunnel Boring Machines (TBMs), two approaching from the Vistula river side (east-side) and two approaching from downtown (west-side); in order to connect the two shafts was foreseen the realization of three tunnels, two for the underground lines and the central one for the exchanging passenger platform. These tunnels were underpassing the “Wislostrada Road Tunnel” and interfered with this tunnel foundation, which consisted of diaphragm walls (DW), the “barrettes” (Figure 1).
Due to the variable geological conditions at the site, the first excavation stage, with a temporary underground support constructed of horizontal jet grouting columns and forepoling, caused the North tunnel face failure, that required an immediate filling of the empty cavities with lean mix concrete under the Wislostrada tunnel slabs. Thereafter, the recovering attempt with the grout injections could not be completed because of the development of heaves induced on the tunnel structures (Bringiotti et al. 2016).
In those conditions the tunnel excavation with traditional technologies appeared to be very problematic, with high risk for the structural safety of the Wislostrada tunnel. This would have meant longer duration for the works and higher costs for the General Contractor as well as for the city Council.
In light of this, the artificial ground freezing appeared to be the best solution. It was proposed to create a shell of frozen soil around the tunnel excavation profiles in order to ensure a safe excavation of the tunnels, using the mixed ground freezing method with Liquid Nitrogen (LN) and brine. Collecting all the

information about the occurred failure and with an accurate additional ground investigation, times and costs could be predicted with a very moderate fluctuation due to unexpected occurrences.

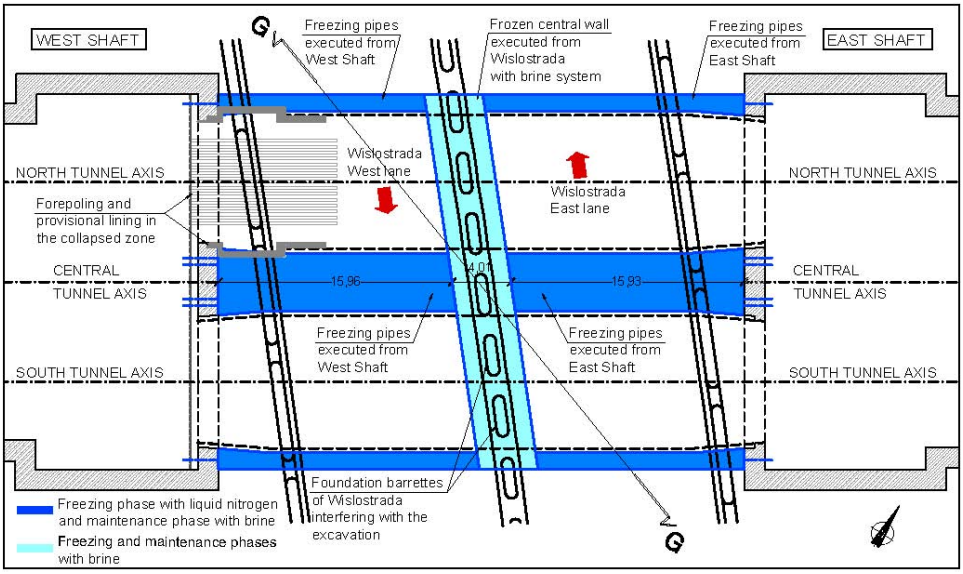


Figure 1: Powisle Station Plan View

GEOLOGICAL CONDITIONS

The ground conditions encountered during the site investigations have been interpreted from the Cone Penetration Tests (CPTs), Drilling Parameters Test (DPTs) and Seismic Tomography records. The ground investigations confirmed a variable complex stratigraphic layout due to the effect of collapsing during the excavation of the North Tunnel and the ground treatments executed before and after it (Figure 2).
In the upper part of the ground profile, below the superficial backfill materials, medium sand with a thickness of 5 m, overlies fine silty sands up to 10 m, and approximately sandy silts up to 13 m. Below this depth, a layer of plastic clay with slight silty content can be found, up to a depth of approximately 18 m. The contact surface between the clay and silty layers is very irregular and is leaning towards south-east; the ground water table is located approximately 2 m below the "Wislostrada Road Tunnel" and all tunnels are completely immersed into ground water (Lombardi et al. 2015).

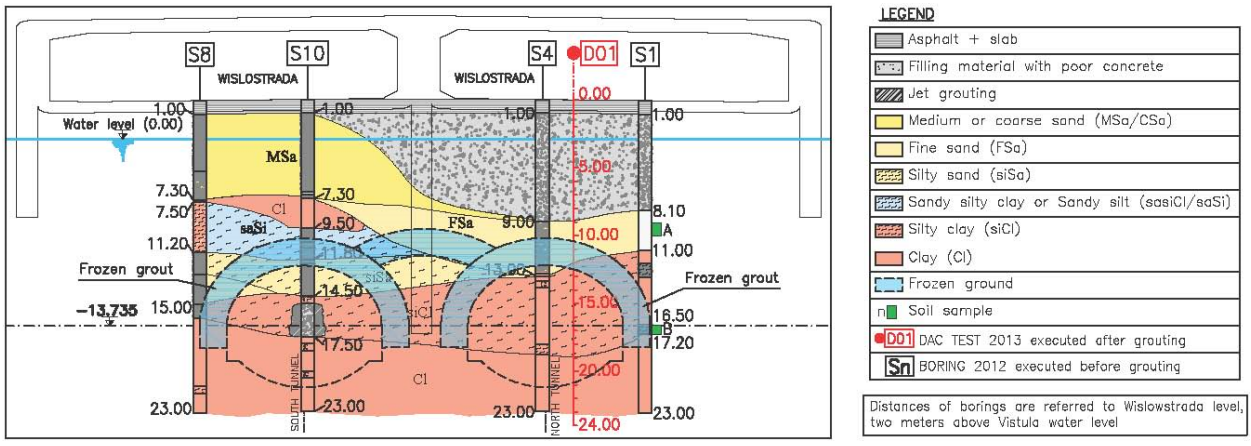


Figure 2: Soil Stratigraphy and Geological Investigation – Section G-G

The tunnels arches have been excavated through the sandy and silty sand layer, whereas almost one-third of the abutments and the inverts are located in the clay. The ground freezing was extended only to the upper sandy-silty layers and only 2 m into the lower clay layer, being this last tight and strong enough to sustain the stress created by the excavation of the tunnels.

GROUND FREEZING METHODS

Frozen soil is a four-phases-mixture comprising mineral grains, ice, water and air. This technology can be applied in nearly all ground conditions regardless of soil permeability and grain size to increase the strength and tightness of the natural ground. Applying ground freezing as a temporary reinforcement measure, only the natural physical characteristics of the soil and the water are used. The impact on the environmental system is very low: groundwater contamination risk due to cement and chemical grouting is dramatically reduced, limited only to drilling and pipe embedment works.
In this project, two different ground freezing technologies were applied:

- Liquid nitrogen method (open system)
- Brine freezing method (closed system)

Liquid nitrogen freezing method

Liquid nitrogen is obtained by air distillation, and it is transported by truck to the site in special tanks, where it is kept at a temperature of -196°C and at a pressure not exceeding 2-3 bars (-196 °C is the state-change temperature of nitrogen under atmospheric pressure). Usually, the liquid nitrogen is stored on site in double-walled storage tanks (under vacuum), where it retains its physical properties until use.
The high cryogenic efficiency of the liquid nitrogen allows quick formation of the frozen structure in only 5-10 days, depending on soil conditions, groundwater temperature, and the distance between pipes, and enables management of scenarios, such as the presence of underground water streams (Figure 3).

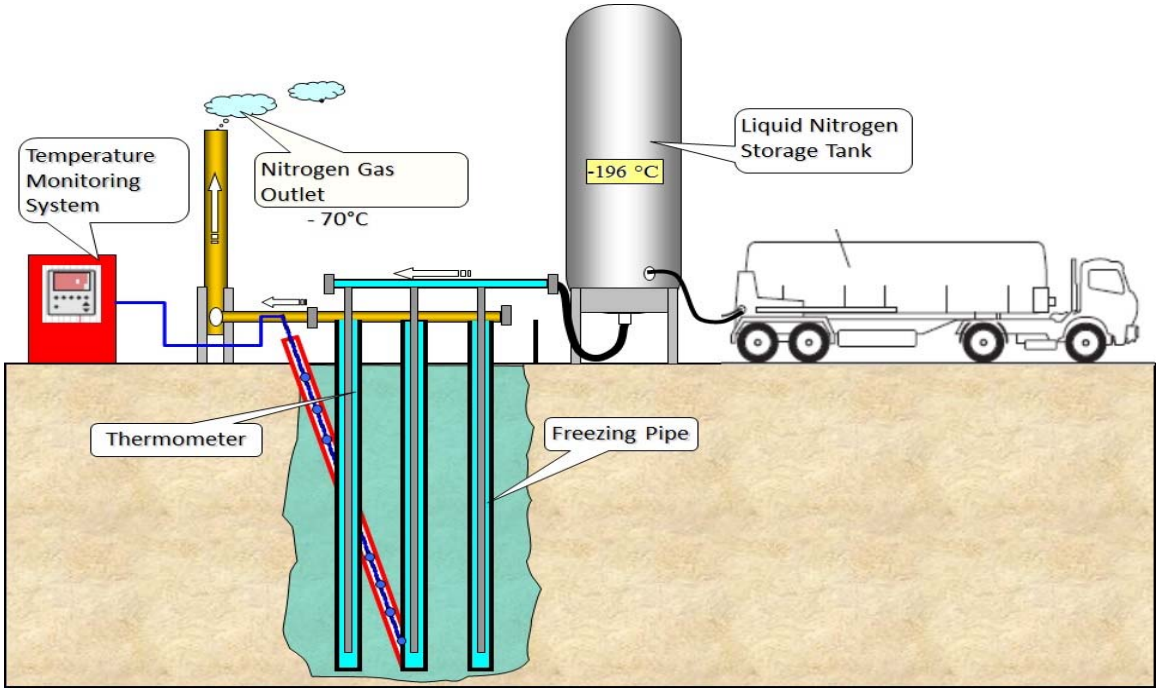


Figure 3: Principle Scheme of the Liquid Nitrogen Freezing System

Brine freezing method

Inside dedicated freeze units (chillers), the brine (a solution of calcium chloride and water) is cooled to a pre-defined temperature and afterwards is pumped through the freezing pipes in a closed circuit and back to the chillers. The primary cooling agent, usually ammonia, circulates inside the freezing plant. The brine is used as a cooling agent that circulates through the freezing pipes (the so called secondary cooling agent). By changing the salt concentration in the solution, different melting points can be achieved. A basic requirement for brine freezing is an absolutely tight circuit (Figure 4).

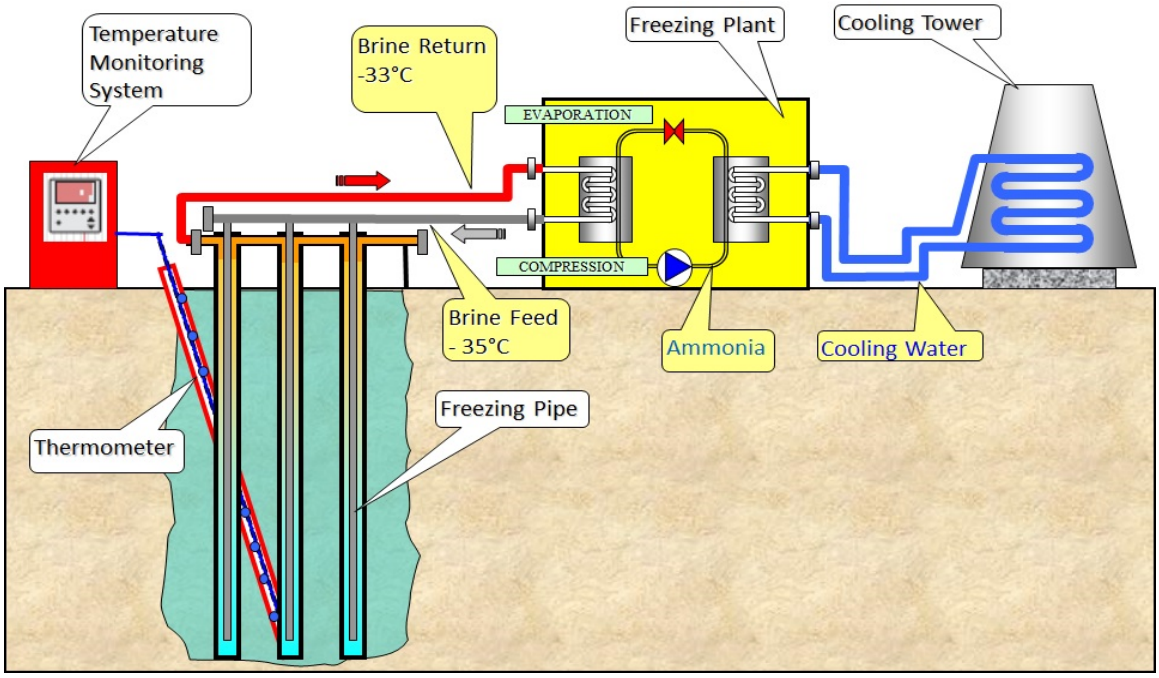


Figure 4: Brine Cooling System

THE PROJECT

The project involves the excavation of the tunnels from each shaft, followed by the demolition of the central DW panels of the Wislostrada tunnel. The ground freezing treatment was used to create a double vertical frozen wall on the sides of this alignment operating from the fast lanes of the Wislostrada, as well as to create a frozen shell surrounding the crown and the sides of each semi-tunnel operating from the two shafts. The works commenced in the Wislostrada Tunnel where due to the safety rules, it was possible only to use the brine method, both for the freezing and for the maintenance stage, and where the sub-vertical drillings were easier to be carried out (Figure 5).

Drillings from the shafts required more time because the pattern of the holes was more complex and the main part of the freezing pipes were horizontal, but the presence of the existing intermediate slab required some sets of inclined holes in order to allow a complete connection between the frozen ground column originated from each pipe. Moreover, the drilling had to be performed against hydrostatic pressure (about 9 m above the tunnel crown) (Figure 6).

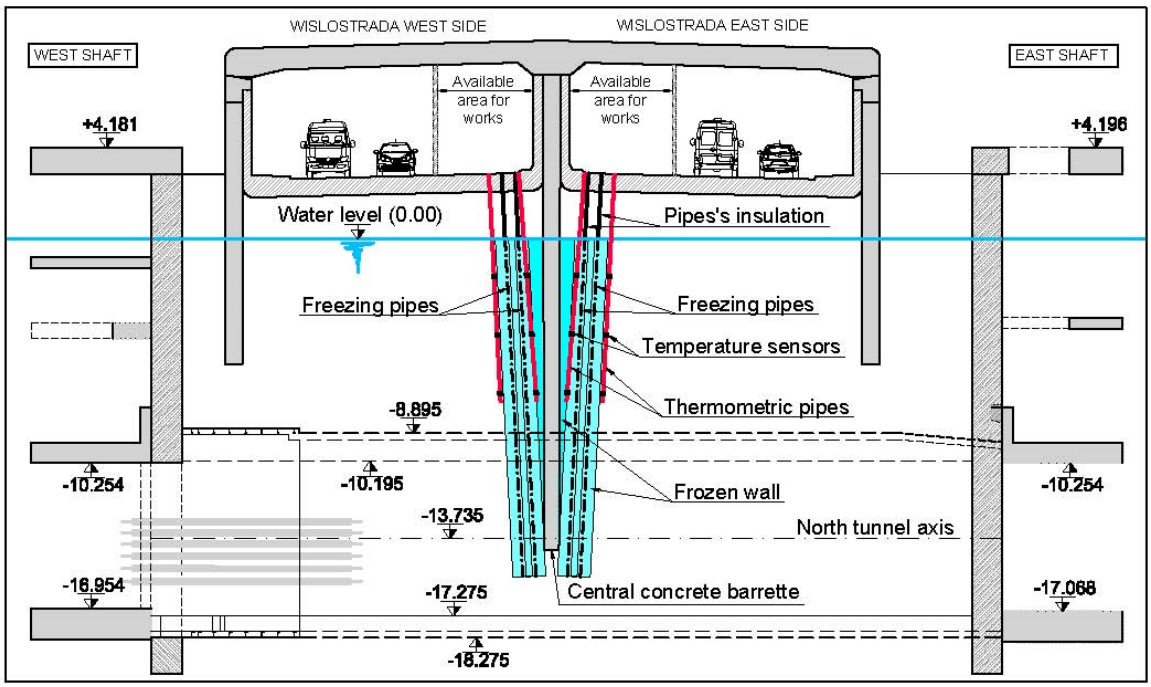


Figure 5: Working Area Wislostrada

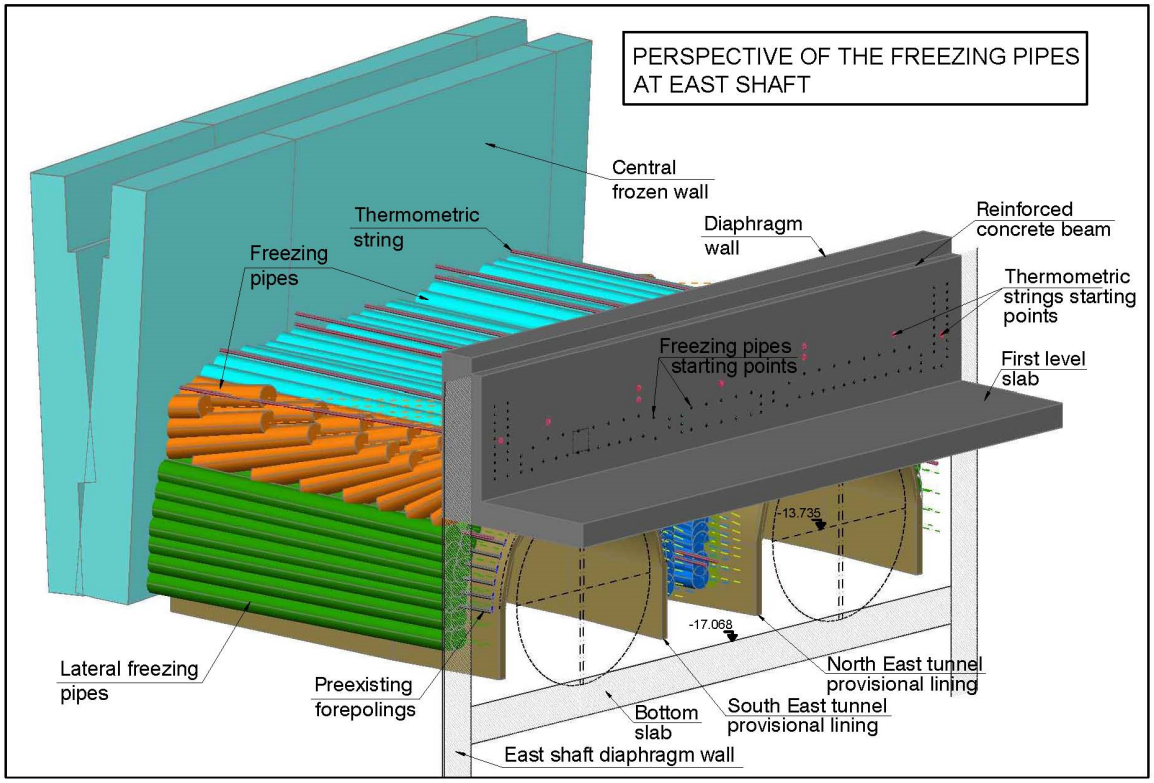


Figure 6: Working Area Shaft

Based on site conditions, a decision was made to freeze the ground using the quicker LN system, and then to proceed with the maintenance using the brine system. The use of the two methods allowed the contractor to synchronize the freezing stage of the wall and of the tunnels, optimizing the costs.
The project envisaged in any zone two lines of pipes in order to obtain a ground frozen wall with a minimum thickness of 1.80 m, where temperature was below or equal to -6°C.

CONSTRUCTION METHOD

The activities started with the drilling of freezing holes. One of the two most important and delicate points of ground freezing works is the precision of the drilling pattern; it has been realized with a very low tolerance, (<1%), in order to have a correct distance between freezing lances. The drilling deviation was expected mainly due to the presence of steel bars and concrete inserts, mostly in the North-West tunnel (the zone of the collapse). During the drilling stage every freezing lance was measured with a laser optical system, called Maxibor; the data were examined in order to check in the design 3D-model the possibility to have a theoretical gap in the frozen body. Finally, it was necessary to install a few additional pipes; the total amount of the latter has been approximately less than 10% of the total amount of pipes foreseen (Figures 7).
The drilling parameters had been recorded in order to check the presence of residual voids (not encountered) and to confirm the geological profile, particularly the upper level of the stiff clay layer in the zone of the invert arches of the tunnels. As a consequence of this, two new freezing lances were added at the base of one of the tunnels side.
In those cases, co-operation between the designer and the drilling company allowed for making quick decision and to avoid time loss in the work program.
The total amount of drilling meter was around 11,100 m, with a length varying between 5 and 19 m and a vertical angle of up to 34°.

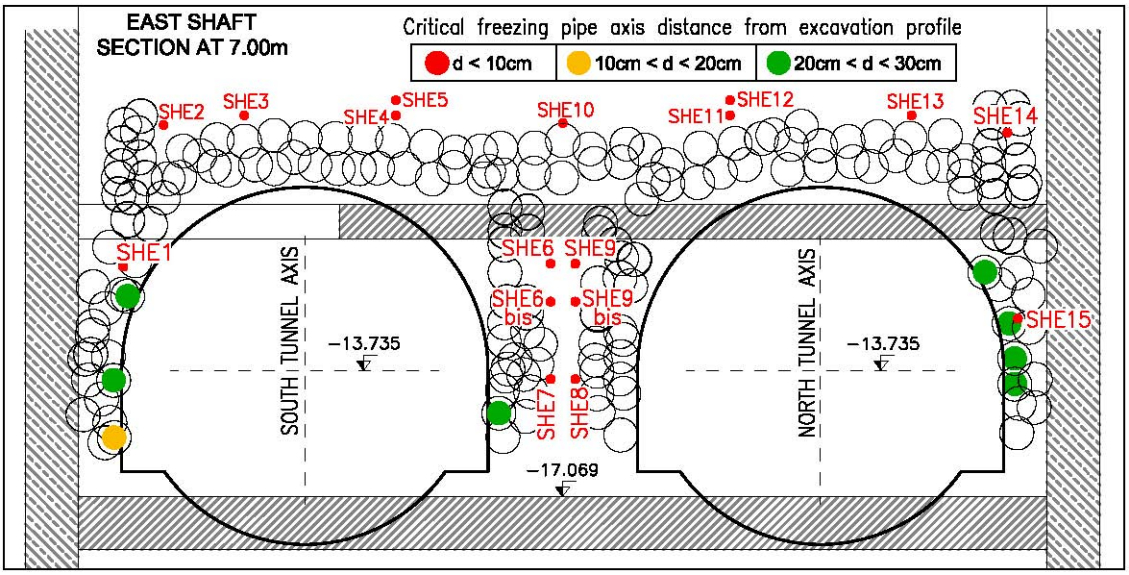


Figure 7: Deviation Freezing Pipes

The second most important point of the ground freezing works was the temperature monitoring system. The control of the ground temperatures was made through direct readings using temperature sensors introduced at different positions into thermometric pipes. These were placed at different sections and distances from the axis of the freezing pipes, in order to verify with the highest possible precision, the thermal gradient of the frozen ground. The data were recorded every hour and transmitted to a central read out unit and

recorded. All data were displayed in graphical and numerical form in a dedicated website for authorized staff (Figure 8).

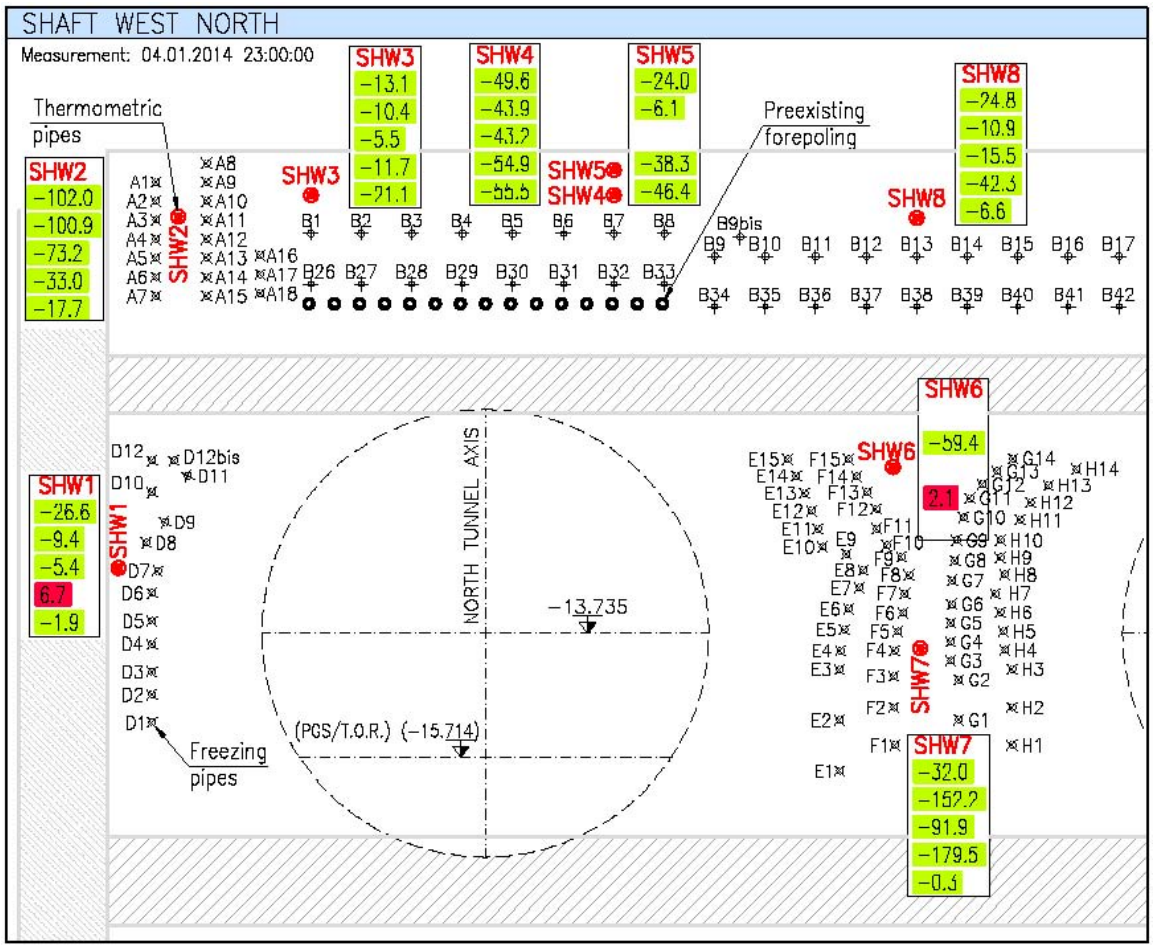


Figure 8: Temperature Monitoring System (Temperature in Degree Celsius)

The freezing stage commenced with the double vertical wall, operating from the Wislostrada with the brine method (Figure 9). It took about 40 days to reach the design thickness. Then, from the shafts, the freezing of each semi-tunnel was performed, starting from the north-west tunnel side. The thickness of the frozen body was reached in an average of 10 days. In the NW tunnel, due to the presence of disturbed soil (lean concrete, steel, former injections), the freezing stage took 15 days with more consumption of LN than the other tunnel (approximately 20%) (Figure 10).

During the freezing stage with LN the soil temperature reached -60 degree Celsius; the thermometric strings were located at a distance between 0.3 and 0.6 m from the closest freezing pipe. Using this data and the correlation between distance and ground temperature, it was possible to estimate that the frozen wall created had a thickness of 1.8 to 2.0 m (Sanger and Sayles 1979).



Figure 9: Brine Circuit

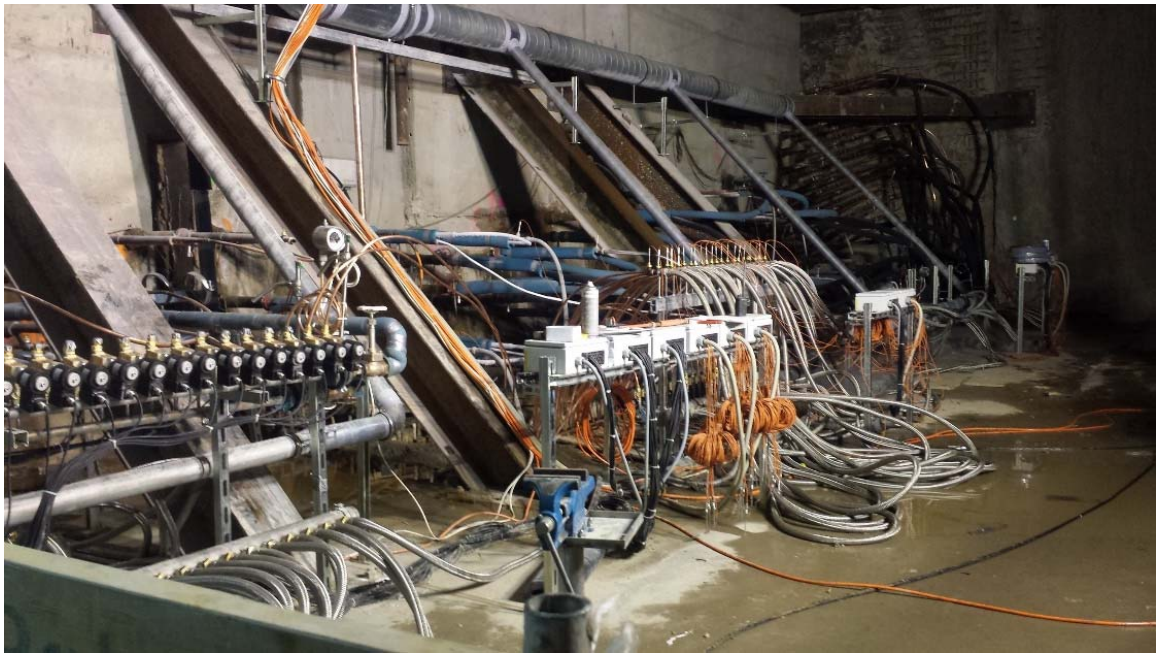


Figure 10: LN Circuit

THE EXCAVATION STAGE

Once the freezing stage with LN was completed, the temperature was maintained during the excavation stage by circulating brine in the same pipes used for the liquid nitrogen. The swap of the circuit took approximately three days for tunnel; the methodology was decided between the designer and the company, to minimize the loss of frozen body volume.

During the maintenance stage with brine, the four semi-tunnel excavations were performed with the traditional method, using a hydraulic hammer and rotary cutting head. The tunnel on the northern side was completed first, followed by the southern tunnel.
Once reached the Wislostrda central DW, the vertical freezing pipes, executed from the Wislostrada Tunnel, were shortened; the cutting position was obtained comparing the detected position of the freezing pipes and the topographically surveyed tunnel excavation profile. The shortening sequence was defined in order to minimize the interruption of the brine circulation into the closed circuit. The freezing groups to be closed were excluded from the circuit and, after the shortening reattached to the main circuit (Figure 11).
Ground temperatures were monitored daily during the excavation activities. Using the brine for maintenance stage, the frozen wall remained stable without significant variations in the average soil temperatures.

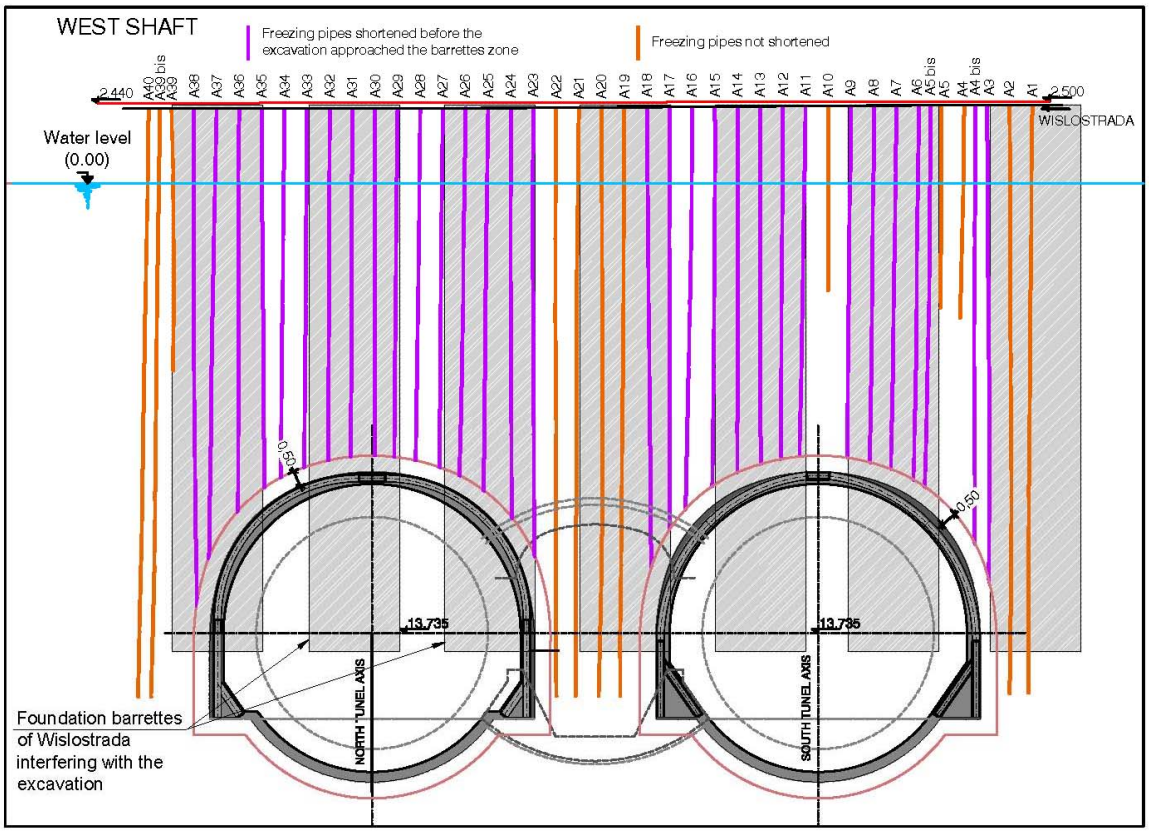


Figure 11: Shortening Freezing Pipes

Monitoring system of Wislostrada structures

A topographic monitoring system installed inside the Wislostrada Tunnel provided information about the displacements of the structure above the frozen tunnels, allowing to calibrate the operative parameter during the freezing process and especially during the maintenance process during, when tunnel excavations, foundation cuts and linings casts were carried out.
After an initial uplift produced both by drilling with cement and by the freezing stages, any relevant settlement during the excavation of the tunnels was not noticed. After four months from the completion of the excavation, the settlements varied from 0.0 mm to 20 mm, depending on the area (Balossi Restelli et al. 2016).

The freezing stage, excavation and, lining cast of each tunnel started gradually and were performed simultaneously. The drilling phase required 2 months. The completion of each tunnel, from freezing to lining, required 3 months. In total, the completion of all works lasted 9.5 months.

CONCLUSIONS

The construction of this underground station using artificial ground freezing as a structural temporary support proved to be the most successful method. The combined method using liquid nitrogen and brine allowed the required thickness of the frozen wall, and maintenance of this ground condition for the duration of the construction activities, to be achieved relatively quickly and cost-effectively.
In economic terms, in case of difficult conditions (i. e. under groundwater level works, in complex urban context), ground freezing can be considered competitive in cost with grouting of fine soils, and even more competitive in very fine soils wherein recourse to injection grouts is required. From an environmental point of view ground freezing can be a valid solution or a valid ground improvement technique as it is considered a non-polluting geotechnical process.
All three tunnels have been excavated on time without any disturbance to the traffic patterns inside the Wislostrada tunnel.
A strict collaboration between the designers and the contractor allowed for the different phases of the work to be completed without time loss or cost increases.
For its dimensions and degree of difficulty, this project can be considered an important achievement in the field of ground freezing techniques, particularly given the very high density area.

REFERENCES

Sanger F. J., Sayles F. H. 1979. Thermal and rheological computations for artificial frozen ground construction. *Eng. Geol*. 13: 311-337

Balossi Restelli A. 1995. Il congelamento del terreno può risolvere situazioni difficili di scavo sotto battente di falda. Rivista Italiana di Geotecnica 3: 179-199

Balossi Restelli A., Cavagna B., Pettinaroli A. 2011. Metropolitana di Napoli – Linea 1 – Il trattamento di congelamento di pozzo Garibaldi. XXIV CNG AGI Napoli. Vol. 2 : 325-333

Mira Cattò F., Roberti P. 2014. The mixed freezed of Warsaw. Tunnelling Journal. Oct-Nov. 2014: 43-47

Lombardi A., Capata V., Bizzi F. 2015. Line II of Warsaw Underground: the excavation of tunnel connector (Centrum Nauki Kopernik station) under existing Wislostrada tunnel. XVI ECSMGE Sep.2015

Bringiotti M., De Angelis F., Piangatelli M.A. 2016. Conventional Excavation of Connecting Tunnels in C13 Metro Station (Poland - Warsaw – Line 2). WTC San Francisco. Paper n. 1309

Balossi Restelli A., Pettinaroli A., Rovetto E. 2016. Combined ground freezing application for the excavation of connection tunnels for Centrum Nauki Kopernik Station - Warsaw Underground Line II WTC San Francisco. Paper n. 1310

Geotechnical Engineering Research Laboratory
One University Avenue
Lowell, Massachusetts 01854
Tel: (978) 934-2277 Fax: (978) 934-3046
e-mail: Samuel_Paikowsky@uml.edu
web site: http://www.uml.edu/research_labs/Geotechnical_Engineering/
DEPARTMENT OF CIVIL AND
ENVIRONMENTAL ENGINEERING

Samuel G. Paikowsky, Sc.D
Professor

Dynamic Load Testing of Drilled Deep Foundations

By Prof. Samuel G. Paikowsky; University of Massachusetts Lowell and GeoDynamica, Inc. USA

Invited Keynote Paper and Presentation at the
Swiss Geotechnic Annual Meeting,
2 May 2013,
Fribourg, Switzerland

Dynamic load testing of drilled deep foundations

By Prof. Samuel G. Paikowsky; University of Massachusetts and GeoDynamica, Inc. USA

Abstract

Due to the way drilled deep foundations are being constructed, their structural integrity and geotechnical capacity are highly variable. Drop weight systems are increasingly being used to dynamically test the capacity and integrity of drilled deep foundations. Conventional pile driving hammers are often either inadequate or not economical to test these foundations and drop weight systems have therefore been developed to allow for dynamic testing.

The advantages of the tests include high mobility, short testing time, low cost relative to static load tests (allowing multiple tests at a single site), and integrity/construction quality evaluation concurrent with capacity determination. The dynamic testing method for drilled deep foundations encounter several difficulties including: the need for a pre-testing analysis for matching pile, soil and testing system, adequate mass and drop height to reflect the mobilized capacity without structural damage, test interpretations for irregularly shaped and/or non-uniform piles, need for reliable dynamic measurements depending on the impact and the distance between the impact and the measuring point, and limited knowledge about the accuracy of the predictions.

The principles of the tests are presented using simplified models and demonstrated via a case history. Drop weight systems are reviewed. Dynamic measurement principles are explained and the construction and testing quality effects are outlined and demonstrated via numerical modeling and case histories. A comparison of dynamic and static tests is presented via a database, case histories and finally a short review of relevant codes is provided.

1 Introduction

Traditional static axial load test is performed by a slow application of a force produced against independent reaction, imitating structural loading. It is the most reliable method to determine the pile's performance as commonly required under typical service conditions. The major limitations of this testing are: (i) high cost associated with set-up, test duration, interpretation and construction delays, and (ii) inability to obtain information about the pile-soil interaction along the pile without additional testing means (e.g. tell tales, strain gauges, etc.). These limitations are acute when high capacity foundations are involved.

In place constructed deep foundations, or drilled deep foundations (known as drilled shafts, bored piles, cast in place piles, caissons, piers, auger cast piles, continuous flight auger piles, etc.) are commonly used worldwide where they are more suitable or cost effective than driven piles and/or alternatively for carrying large loads, replacing pile groups. A variety of construction methods and installation equipment are available (e.g. O'Neill and Reese, 1999, Brown et al., 2010). Due to the nature of their construction, however, limited quality control is possible and the structural integrity and the geotechnical capacity of these foundations remain highly variable and uncertain. The quality of the foundation depends upon the construction method (Camp et al., 2002, Paikowsky et al., 2004a, Paikowsky et al., 2004c), the subsurface conditions, the quality of the materials (grout, cement, concrete, slurry, etc.), and the quality of the contractor (i.e. workmanship). As such, the use of drilled deep foundations confronts the limitations of the traditional static load tests.

Alternative methods to the standard static load testing have been developed in two avenues:

(i) Static loading by methods that either do not require independent, external reaction for load application (e.g. Osterberg cells – Osterberg, 1989), or short duration, pseudo-static loading procedures (e.g. Static-Cyclic Testing; Paikowsky et al., 1999), and,

(ii) Dynamic testing in which the pile is exposed to dynamic effects i.e., a varying stress with time is generated at the top of the pile through the impact of a mass or its combination with explosion.

The dynamic testing methods include the generation of low and high strain waves as well as impacts that produce short and long relative wavelengths. The methods that produce a relatively long wavelength (e.g. Statnamics, Bermingham and Janes, 1990) are most appropriately termed kinetic testing (Holeyman, 1992). These testing methods encounter difficulties in wave resolution with depth, and hence in interpretation of test results based on wave mechanics, as explained below. The traditional impact tests in which a falling mass

strikes the pile top (drop weight systems) become, therefore, an attractive testing solution due to physics principles and economical advantages. As a result, drop weight systems are increasingly being used to dynamically test the capacity of drilled deep foundations. Conventional pile driving hammers are often inadequate to test these deep foundation types since they typically cannot deliver enough energy to mobilize the ultimate bearing capacity, and the size and location of the foundation member can present problems in equipment mobilization as well as adequately delivering the energy from the ram to the pile. Simple drop weight systems have therefore been developed to overcome the limitations of conventional hammers and allow for cost effective dynamic testing of drilled deep foundations.

The present paper reviews the principles behind the tests, present the testing systems, the testing methods mechanism and interpretation methods, their accuracy and provides recommendations for their use.

2 Principles

2.1 Overview

The following section outlines the basic methodology for understanding the underlying principles of the dynamic testing methods. This leads to the testing categorization as well as the description and the analyses of the tests themselves.

2.2 Impact analysis

A realistic analysis of a mass impacting a fixed end rod was discussed by several authors with the final solution given by Boussinesq (1883) (see Timoshenko and Goodier, 1934). The following section is based on Paikowsky (1982) in which a use of the analysis was made. Figure 1 presents the stress propagation in a fixed end bar struck by a moving mass, M.

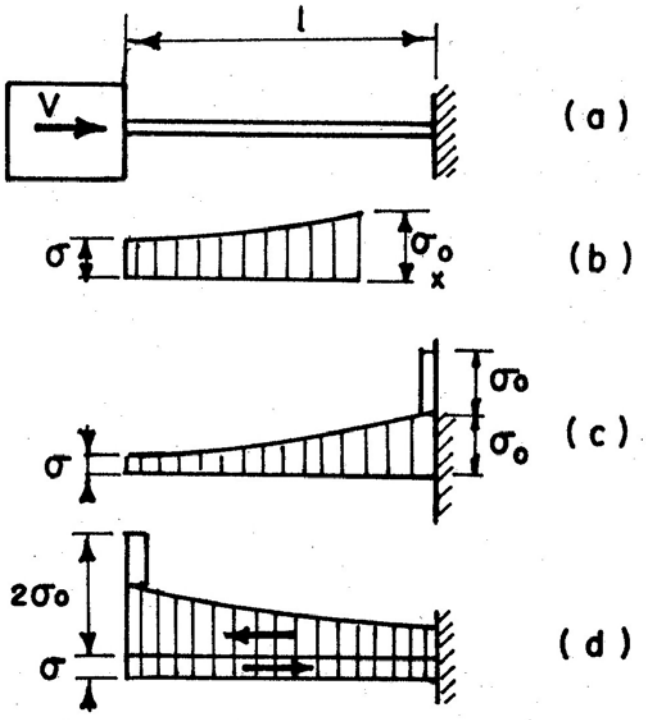


Figure 1: Stress Propagation in a Fixed End Bar Struck by a Moving Mass (after Timoshenko and Goodier, 1934).

In a relatively simple analysis based on the conservation of the momentum and the relationship between force and velocity under elastic wave propagation, one can derive the following relations: (for development details see Timoshenko and Goodier, 1934)

$$\sigma_o = v_o \sqrt{E\rho} \tag{1}$$

$$s_o = \sigma_o e^{-\left(\frac{2\alpha t}{T}\right)} \tag{2}$$

$$s_1(t) = s_o + \sigma_o e^{-2\alpha\left[\left(t/T\right)-1\right]}\left[1 + 4\alpha\left(1 - t/T\right)\right] \tag{3}$$

for which:

σ_o	=	the front stress of the compressive wave pulse
v_o	=	impact velocity of the striking mass, M
E, ρ	=	modulus of elasticity and mass density of the pile
S_o	=	the compressive wave at time interval $0 < t < T$
T	=	stress pulse travel time to tip and back $T = 2l/c$
l	=	Pile length
c	=	speed of wave propagation in the pile
α	=	M_p/M ratio of mass of pile to impacting mass
s_1	=	the compressive wave at time $T < t < 2T$

A graphical representation of the functions S_o and S_1 for various values of α (the ratio between the mass of the rod/pile to the mass of the impacting body) is presented in Figure 2. The relationship of Figure 2 suggests that with the decreasing of the size of the hammer (impacting mass) relative to the pile, a sharper pulse of a shorter duration is achieved. For hammers twice the mass of the pile the produced stress wavelength is significantly longer than the time required for the wave to travel down and up the pile. On the other hand, hammers weighing about one quarter of the weight of the pile (approximately 185kN for 1m diameter, 40m long shaft) produce a shorter impact than the time required for the traveling wave to reflect from the tip.

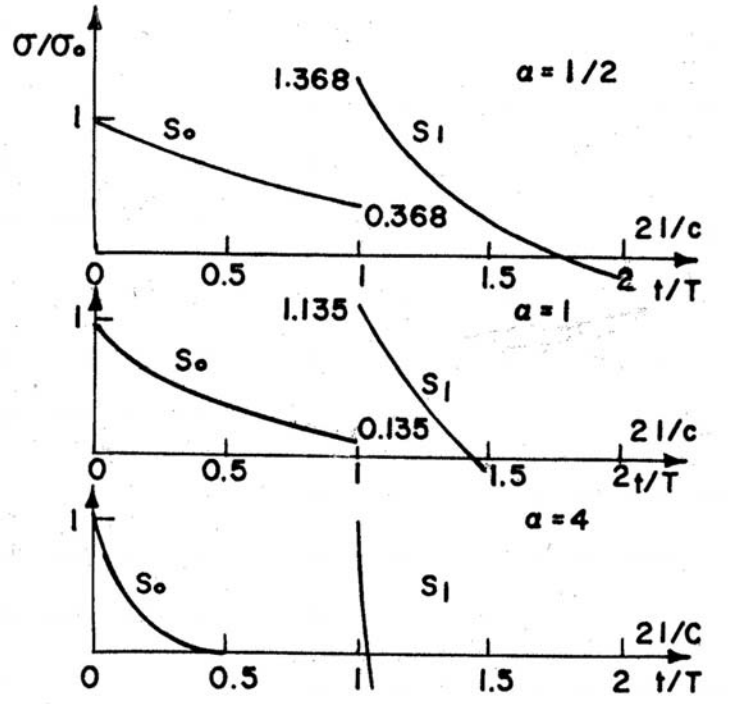


Figure 2: Stress Wave Magnitude and Duration (Graphical Representation of Functions So and S1) as a Function of the Ratio Between the Mass of the Pile to the Mass of the Striking Body.

The model and relationship of Figures 1 and 2 and equations 1 to 3 can be directly applied to impact driving. Further details of impact representation can be obtained via numerical modeling (e.g. Smith 1960), but it is easier in the framework of generic application of bodies in contact (as in this paper) to resort to a simplified relations based on frequencies. The following review was assisted mostly by Holeyman (1992), with appropriate referencing to other relevant publications.

When external mass, M, interacts under impact velocity, v_i, with the head of an half infinite long pile, the physical system and its mechanical representation can be described as shown in Figure 3 (Parola, 1970 and Van Kotten, 1977), or alternatively by a Kelvin-Voight model as described by Irvine (1986). The system includes the impacting mass, the cushioning element in the impact, and the representation of the pile as a dashpot with a damping factor equal to the pile impedance, suitable for short waves dynamic events.

This representation allows, however, for easy development of conceptual analytical relationships between the impacting mass size and velocity, the cushioning element, and the pile's impedance in the shape of non-dimensional force pulses in the pile.

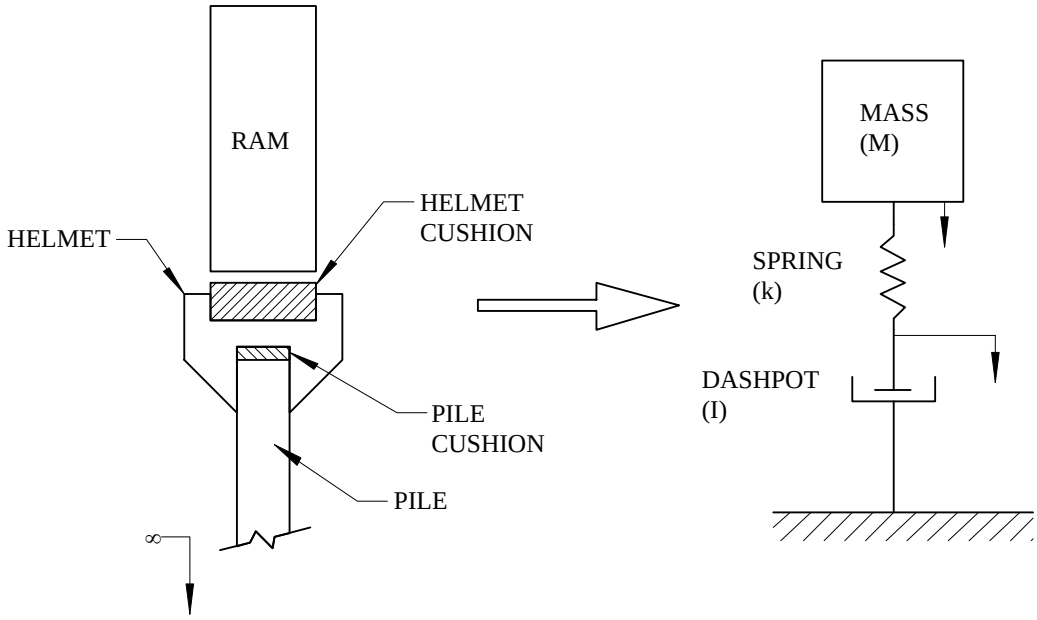


Figure 3: Physical and Mechanical Representation of a Mass Impacting Infinite Long Pile.

In developing the graphs shown in Figure 4, the following relationship has been used:

	M, v_o	=	mass and velocity of impacting body
	k	=	equivalent spring coefficient of cushioning element
	I	=	pile impedance
where	I	=	ρcA
	ρ, A	=	the pile's specific mass and cross-section
	c	=	one dimensional longitudinal wave speed of the pile's material

where

$$c = \sqrt{\frac{E}{\rho}} \tag{4}$$

E = the pile's material Young's modulus

The force pulse in the pile as presented in Figure 4 is normalized in relation to the pile's impedance and impact velocity. The developed pulses are calculated as a function of the natural frequency, ω_n, for different ratios between the cushioning element and the pile's stiffness:

$$\omega_n = \sqrt{\frac{k}{m}} \quad , \quad \gamma = \frac{k}{2I} \quad , \quad \frac{\omega_n}{\alpha} = 2I\sqrt{kM} \tag{5}$$

The relationships in Figure 4 clearly demonstrate the effect of the cushioning element in relation to the pile's stiffness on the time length of the force pulse developed in the pile, and the magnitude of that force as the function of the impact velocity.

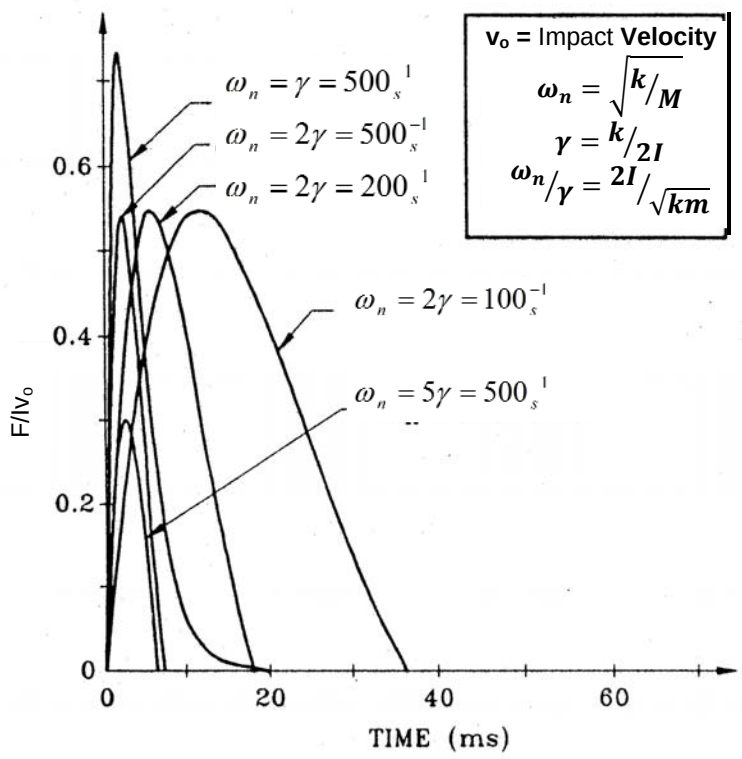


Figure 4: Non-Dimensional Force Pulses in a Pile as a Function of Time and the Ratio of Cushioning Element to Pile Stiffness (Holeyman, 1992, see also Parola, 1970).

The non-dimensional peak amplitude F_{max}/Iv_o decreases as $2I/\sqrt{kM}$ increases, whereas the duration of the impact decreases proportionally with $\sqrt{k/M}$. For example, in dynamic pile driving of direct impact of steel over steel, a very sharp, short duration pulse force (on the order of 5 milliseconds) will develop in the pile. The pulse wavelength will increase when introducing cushion in the system, and further increased when using a system like Statnamic all the way to systems of coiled springs under a falling mass, as the tests conducted by "Dynatest" (Gonin et al., 1984) or Fundex (Schellingerhout and Revoort, 1996), resulting in a wave length of over 400 milliseconds. For waves of very long duration, the representation of the pile in Figure 3 needs to be complemented with a spring in parallel to the dashpot that acts practically alone under static loading (see modeling by Irvine, 1986).

2.3 Relative wavelength and pulse propagation

While Figure 4 provides the relationship between the testing mechanism and the developed wave length, one must examine the relationship between the produced wave length and the ability to analyze the pile-soil system. Such a measure can be done through the relationship of time as presented in Figure 2, or the relationship of distance between the wavelength and the pile length, introducing the relative wavelength Λ.

$$\Lambda = \text{Length of the force pulse / double length of the pile (2L)} \qquad (6)$$

The relationship between pile acceleration, force duration, and relative wavelength (which represents the sharpness and duration of the force pulse) for different pile tests is presented in Figure 5. To understand a relative wavelength, one needs to follow the propagation of a force pulse through a pile realizing the importance of the pulse sharpness and its length relative to the pile's length.

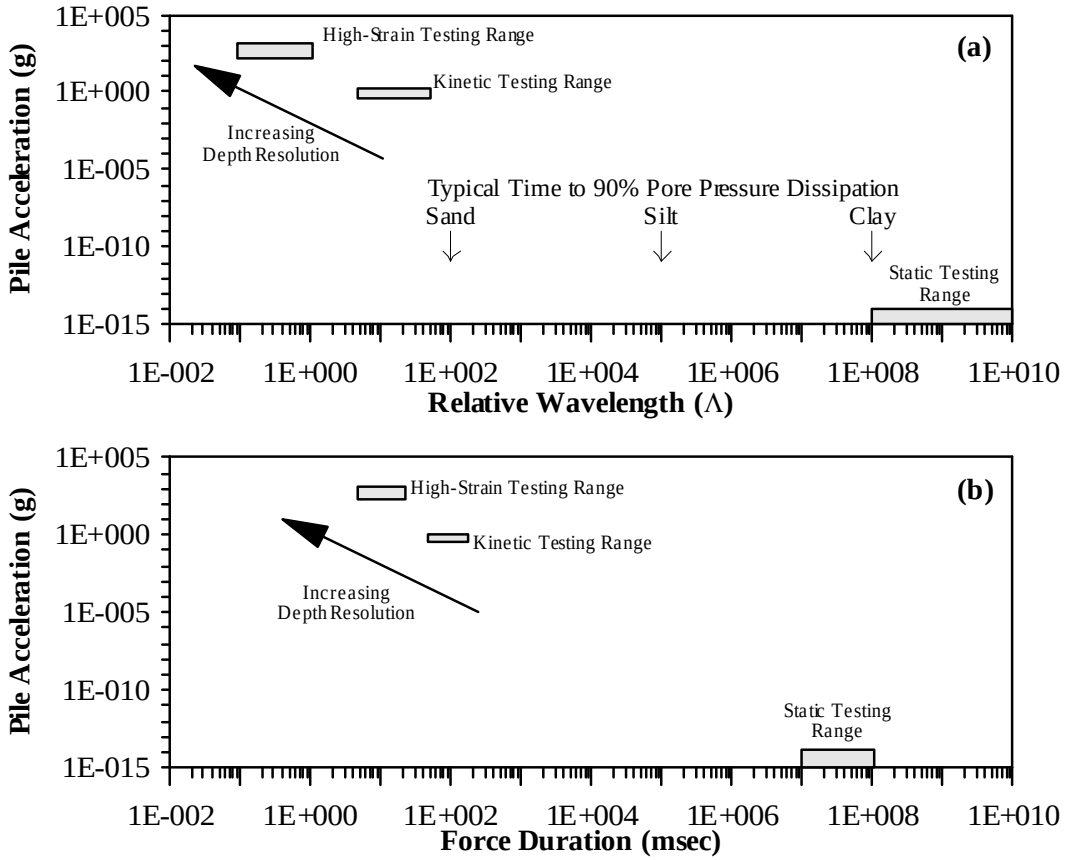


Figure 5: Typical load testing values for pile A acceleration vs. (a) relative wavelength, and (b) force duration (after Holeyman, 1992).

When a compressive force pulse propagates down the pile, it will be reflected whenever there is a change in the pile impedance (e.g. change in cross-section) or as a result of external forces (i.e. friction), generating two waves; a compressive wave up and a tension wave down, which combines with the initial pulse. Upon reaching the pile toe (under easy or normal driving conditions, say less than 8 BPI or 3 blows per 1cm) the resulting downward compressive wave is reflected upward and reversed (compression becomes tension) with a compressive offset corresponding to the mobilized toe resistance. On its way up toward the pile head, the wave interacts again with (and activates) the shaft resistance, and impedance changes, arriving back to the pile top after time t = 2l/c in which l is the pile's length and c speed of wave propagation. This depiction of wave mechanism results in the understanding that:

(i) A shorter pulse duration enables higher resolution of the propagating waves and the combined reflections,
(ii) The number and complexity of the waves depends on the changes of the cross-section of the pile, and
(iii) The reflecting wave is affected by the interaction of the pile with the soil (shaft and end resistances) allowing the interpretation of the soil's resistance along the shaft.

2.4 Pile testing in light of pulse duration and relative wavelength

Following the above, one can examine the different dynamic testing in light of the produced relative wavelength and possible interpretation. Integrity testing that utilizes reflection techniques (see, for example, review by low strain, short duration pulse that is typically characterized by a relative wave length of 0.1, which provides for maximum depth resolution. Dynamic testing during driving is typically characterized by a relative wavelength of 1, associated with force duration of 5 to 20 milliseconds. These relations allow for depth resolution for typical piles while providing high strain testing. Further enhancement of the depth resolution is possible with additional internal measurement near the pile's tip (e.g. Smart Pile System, Frederick, 1996, or McVay et al., 2004). Dynamic Fast Penetration (or Kinetic Testing) such as Statnamic (Bermingham and Janes, 1990), as well as Dynatest or Fundex, are characterized by a relative wave length Λ of 10 or higher and, therefore, do not allow for depth resolution. The produced pulse duration is about 50 to 200 millisec-

onds (about an order of magnitude larger than that of impact dynamic testing), and practically the front of the wave's reflection from the tip arrives back to the top before the main portion of the wave propagates through the pile.

Although these tests resort to inertial actions on masses to generate their extended force pulse, they can be referred to as "Kinetic Tests" or "Dynamic Fast Penetration" as the inertial forces within the pile are small compared to the force being applied, and as a result of their high relative wave length, the interpretation of these tests cannot make use of the wave equation form of analysis, hence, different from tests which can be categorized as Dynamic Wave Action tests (e.g. Drop Weight). This fact does not affect the ability to determine the total capacity/resistance of shafts from kinetic tests using other techniques or diminishes their distinctive advantages such as mobility and the ability to produce high-energy impacts to mobilize the resistance of very high capacity shafts.

The above discussion lend to the categorization of pile testing based on the nature of the loading and it's duration relative to the pile itself. The relative wave length (Λ) explains the relationship between the loading, the transfer of the loading in the pile, the importance of dynamic effects, and the ability to analyze the pile-soil interaction as a result of measurements recorded at the pile's top. Table 1 outlines the different tests based on this categorization and their relevant method of analysis.

Table 1. Typical Key Attributes of Different Types of Pile Tests (Holeyman, 1992).

Attributes	Integrity Testing	High-Strain Dynamic Testing	Kinetic Testing	Static Testing
Mass of Hammer	0.5 - 5kg	2,000 - 10,000 kg	2,000 - 5,000 kg	N/A
Pile Peak Strain	2 - 10 μstr	500 - 1,000 μstr	1,000 μstr	1,000 μstr
Pile Peak Velocity	10 - 40 mm/s	2,000 - 4,000 mm/s	500 mm/s	10^{-3} mm/s
Peak Force	2 - 20 kN	2,000 - 10,000 kN	2,000 - 10,000 kN	2,000 - 10,000 kN
Force Duration	0.5 - 2 ms	5 - 20 ms	50 - 200ms	10^{7} ms
Pile Acceleration	50 g	500 g	0.5 - 1 g	10^{-14} g
Pile Displacement	0.01 mm	10 - 30 mm	50 mm	>20 mm
Relative Wave Length	0.1	<1.0	>10	10^{8}

A comprehensive testing program illustrating the above concept was carried out on a test pile cluster at a bridge reconstruction site in Newbury, Massachusetts. The research at the site was conducted by the Geotechnical Engineering Research Laboratory at the University of Massachusetts Lowell, guided by the author as part of a long-term research sponsored by the Massachusetts Highway Department (see e.g. Paikowsky and Chen, 1998, and Paikowsky and Hajduk, 1999).

Figure 6 presents magnitudes and durations of load measurements during some of the testing conducted on a 14-inch (36cm) square, 80 foot (24m) long pre-stressed, pre-cast concrete pile. The pile was instrumented and subjected to various testing over a long period of time; relevant information is provided by Paikowsky and Hajduk (2004), Hajduk et al. (2000), and Hajduk et al. (1998). The data in Figure 6 demonstrates the principles previously discussed. The driving system produced an impact of about 5 milliseconds in wave length, the Statnamic test produced a wave length of about 60 milliseconds, a Static-Cyclic load test was carried out at about 15 minutes a cycle while a short duration static testing was about 8 hours. A slow maintained load test that was carried out at the site was not included in Figure 6, as it adversely affected the time scale. The data in Figure 6 clearly demonstrates the different time ranges phenomena associated with the different tests, and its ramifications will be further discussed in the following sections.

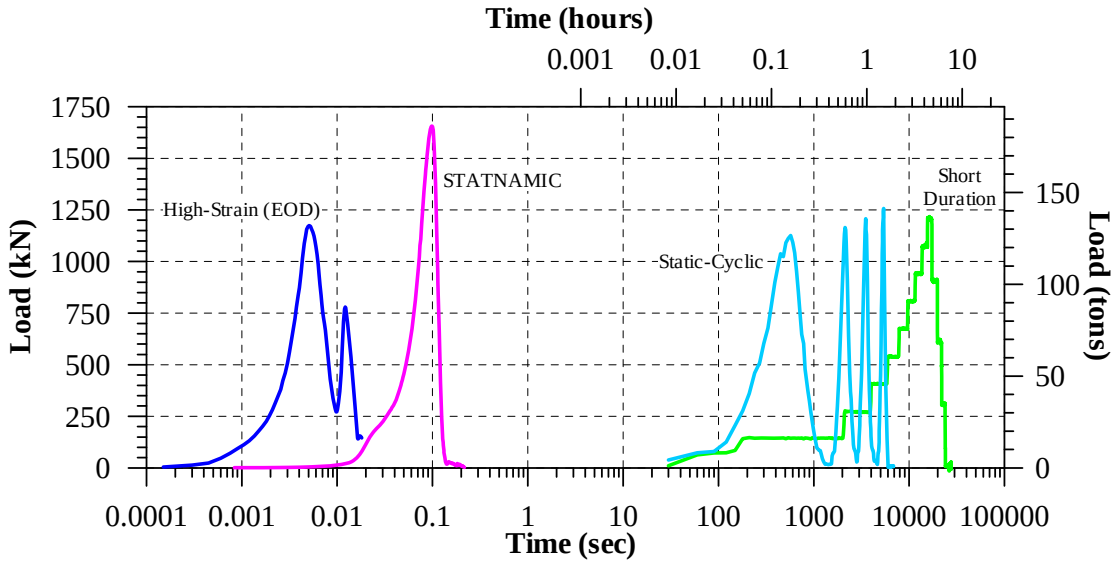


Figure 6: Typical Loading Durations for Various Tests Performed on Test Pile #3 by the Geotechnical Engineering Research Laboratory of the University of Massachusetts Lowell, at the Newbury Test Site.

2.5 Dynamic measurements during pile driving and their analyses

The above presented approach explains how different analyses when applied to kinetic tests, can provide reasonable predictions for capacity, but they cannot handle well, the pile structure (integrity), or soil-structure interaction (load distribution). The use of impact tests and stress wave analysis becomes, therefore, attractive as construction quality is of major interest in the testing of drilled deep foundations.

Dynamic analyses of piles are methods that predict pile capacity based on the pile behavior during driving. Evaluation of static capacity from pile driving is based upon the concept that the driving operation induces failure in the pile-soil system; in other words, a very fast load test is carried out under each blow. There are basically two common methods of estimating the ultimate capacity of piles on the basis of dynamic driving resistance: pile driving formulae (i.e., dynamic equations) and Wave Equation (W.E.) analysis.

The Wave Equation (W.E.) describes the phenomenon of stress propagation in a pile during driving and is being solved for assumed boundary conditions of hammer impact (simulated) and soil resistance. Its modern utilization was proposed by Smith (1960). Dynamic measurements during pile driving or high strain dynamic load tests (see ASTM D4945-12) are carried out by measuring strain and acceleration via reusable transducers in a process first established by Goble et al. (1975).

Post-driving signal matching analyses utilize the measured force signal (calculated from strain readings) and the measured velocity signal (integrated with time from acceleration readings) obtained near the pile top during driving (further discussion is presented in section 4.1). These analyses model the pile-soil system, in a continuous or discrete form. The velocity signal is used as a boundary condition at the point of measurement while varying the parameters describing the soil resistance in order to solve the wave equation and match the calculated and measured force signals.

Iterations are performed by changing the soil model variables for each pile element in contact with the soil until the best match between the force signals (calculated and measured) is obtained. The results of these analyses are assumed to represent the actual distribution of the ultimate static capacity along the pile. This procedure was first suggested by Goble et al. (1970), utilizing the computer program CAPWAP. Similar analyses were developed by others e.g. see Paikowsky, 1982 and Paikowsky and Whitman, 1990, utilizing the program code TEPWAP, and Middendorp and van Weel, 1986, using TNOWAVE.

3 The drop weight system

3.1 Overview

High strain dynamic wave action testing can be applied to any pile type not necessarily during driving. The application of dynamic testing specifically to in-place constructed deep foundations is done by dropping a weight on the pile top, producing a dynamic stress-wave through an impact. The test results are then being analyzed using the conventional dynamic methods of analysis though often those are restricted by the special conditions of the in place constructed piles and the drop weight testing. The first use of high strain dynamic testing of in-place constructed foundations was made in 1975 on a project in Charleston, West Virginia (Goble, et al., 1993).

Drop weight systems are commonly used to dynamically test cast-in-place piles; i.e., drilled shafts, and caissons. These tests are especially important for high capacity piles (say design load over 1.0MN) for which static load test is either very expensive or physically difficult to conduct (e.g., over water). Conventional pile driving hammers are inadequate to test these deep foundation types since (i) they typically cannot deliver enough energy to mobilize the ultimate bearing capacity, (ii) the size and location of the foundation member can present problems in adequately delivering the energy from the ram to the pile, and (iii) they are expensive to use. Simple drop weight systems have therefore been developed that overcome the limitations of conventional hammers and allow for a relatively inexpensive dynamic testing of these deep foundations.

A typical drop weight system consists of four components: a frame and/or a guide for the drop weight (ram), the ram, a trip mechanism to release the ram, and a striker plate with or without a cushion. Strain gages and accelerometers are placed along the pile top to obtain stresswave measurements utilizing available PDA's (Pile Driving Analyzers). The advantages and disadvantages of the system are listed below.

3.1.1 Advantages

The advantages when compared to static load testing methods are similar to those of standard dynamic pile testing:

a. Rapid testing time.
b. The ability to deliver high energy to test high capacity and physically large deep foundations.
c. The ability to use transducers and data acquisition systems for monitoring driven piles (such as the Pile Driving Analyzer of Pile Dynamics and TNO Foundation Pile Diagnostic System).
d. The test provides a means to conduct integrity testing concurrent with capacity determination, which is particularly important for cast in-place foundations.
e. Low test cost relative to standard static load test.
f. Current techniques of analysis include field methods (such as the Case Method (Goble et al., 1975) and the Energy Approach (Paikowsky, 1982, Paikowsky et al., 1994, Paikowsky et al., 2004a)) and signal matching e.g. CAPWAP (Rausche, 1970).

3.1.2 Disadvantages

a. The selected mass and drop height must be of sufficient energy to mobilize the resistance of a deep foundation shaft in order to obtain adequate capacity measurements.
b. The installation process of in-place constructed deep foundations can cause irregularities in pile geometry (shape) and homogeneity that can dramatically affect current measurement techniques and analysis methods.
c. For increased quality of the obtained force measurements, the gauges need to be away from the impact and as high as possible above the ground. This results in the need to create either "extensions" of cast in- place shafts or excavations around the shaft, and the use of multiple gauge systems.
d. Several limited studies have been conducted comparing dynamic and static measurements of cast in-place deep foundations (Rausche and Seidel, 1984, Jianren and Sihong, 1992, Townsend et al., 1991). A comprehensive comparison study, incorporating significant number of case histories and other relevant information (such as installation records), is not yet available. A relatively large scale study was reported by Paikowsky et al., 2004a, and Paikowsky et al., 2004b.

3.2 Review of drop weight systems

3.2.1 General

The testing entails the impact of a mass with the pile top. As such, large variation of possibilities exist ranging from a non-guided drop of a mass by a crane to a well designed guided system of varying ram weight and stroke, including a driving system (capblock, striking plate, cushion) at the pile's top. Naturally these systems are locally developed and at times are site specific. Paikowsky et al. (2004a) present a summary of various available systems and the following section presents one system as an example.

3.2.2 GeoDynamica, Inc. Israeli System

A system developed by GeoDynamica, Inc. to test drilled shafts in Israel is presented in Figure 7. This device is similar in principle to other drop weight systems presently in use with the distinction of modularity in ram weight. The Israeli Drop Weight Impact Device uses modular weights that can be arranged into ram weight combinations of 20, 40, 50, 70, or 90kN and has an adjustable drop height of up to 4 meters thereby allowing for potential energy of up to 360kN•m. Typically, a pile cushion is used below the striking plate to even pile impact stresses across the pile's top. Additional long ram was developed for the production of short duration waves and better integrity capabilities.



Figure 7: GeoDynamica, Inc. drop weight device: (a) general view of the impact device, and (b) hammer stroked to roughly 1m

3.2.3 Summary

A wide range of drop weight systems is available to provide an impact. In addition to the geometrical features of the system, namely guiding system, ram mass, and dropping height (i.e. energy), the system's effective-

ness is greatly affected by the quality of the impact. A detailed impact Finite Element Method (FEM) analysis was carried out (Paikowsky et al., 2004a), able to model the significance of each parameter and its influence on the recorded dynamic values, this analysis is presented in section 5.

4 Dynamic measurements of impacted drilled deep foundations

4.1 Dynamic measurements

Typical dynamic measurements include the attachment of a pair of accelerometers and a pair of strain gauges to the pile (ASTM D4945-12). The acceleration (a_{cc}) is integrated with time (equation 7) to provide the velocity signal at the point of measurements with time (v(t)) and the strain (ε_t) is measured between two fixed points (typically 76.2mm (3 inches) apart) allowing to calculate the force signal with time (F(t)) at the point of measurement (equation 8). This calculation assumes uniformity of strain ((ε_t)), and hence stresses across the pile's section, knowledge of the cross sectional area (A_p), and the pile's material modulus of elasticity, E_p.

$$v(t) = \int_0^t a_{cc}(t)dt \tag{7}$$

$$F(t) = \varepsilon(t) \bullet A_p \bullet E_p \tag{8}$$

4.2 Difficulties associated with the impact of a drilled shaft

Four fundamental sources of difficulties are associated with the dynamic measurements of drilled shafts:

a. Sources related to construction
b. Sources related to the ram's impact
c. Sources related to the point of measurement
d. Sources related to the shaft's resistance

Table 2 presents a summary of sources for difficulties, their effect, and possible remedy. These sources of difficulties affect the aforementioned assumptions made for conducting and analyzing dynamic force measurements. For example, construction procedures affecting the top of the drilled shaft, cause irregular geometrical shape, non-homogeneous cross-section, and often non-uniform concrete. All of these factors affect the calculated forces. The stresses can be assumed as uniform when measured some distance away from the impact location. Non-uniform impact, in particular impact at one point of contact (rotated ram), will cause uneven stresses across the shaft at a large distance from the point of impact. The force measurements remain, therefore, problematic under such conditions. Additional difficulty, more common with the impact of drilled shafts than driven piles, is the high frictional resistance that develops close to the ground surface. This condition creates early large signal reflections upwards that invalidate the proportionality of the force and velocity measurements, hence, do not allow independent assessment of the measurements, and often create difficulties in signal match analyses. The uneven impact stress distribution and early reflections both call for (i) the use of multiple gauges around the shafts' perimeter, and (ii) the establishment of a measurement point at a cross-section further from the pile top and ground surface as much as possible. This last requirement typically contradicts the normal mode of shafts design and construction, and requires either a shaft extension beyond the ground elevation or excavation next to the shaft (see Figure 7). The construction and use of shaft extension in a steel sleeve greatly improve the ability to collect good dynamic data. However, the procedure is not free of construction difficulties as summarized in a document typically provided to contractors by Geo-Dynamica, Inc. and presented in Table 3.

Table 2: Sources for possible difficulties of dynamic measurements on drilled shafts

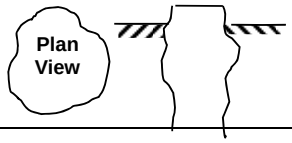
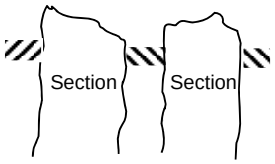
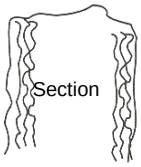
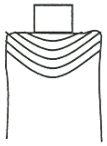
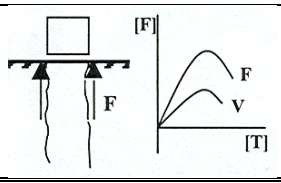
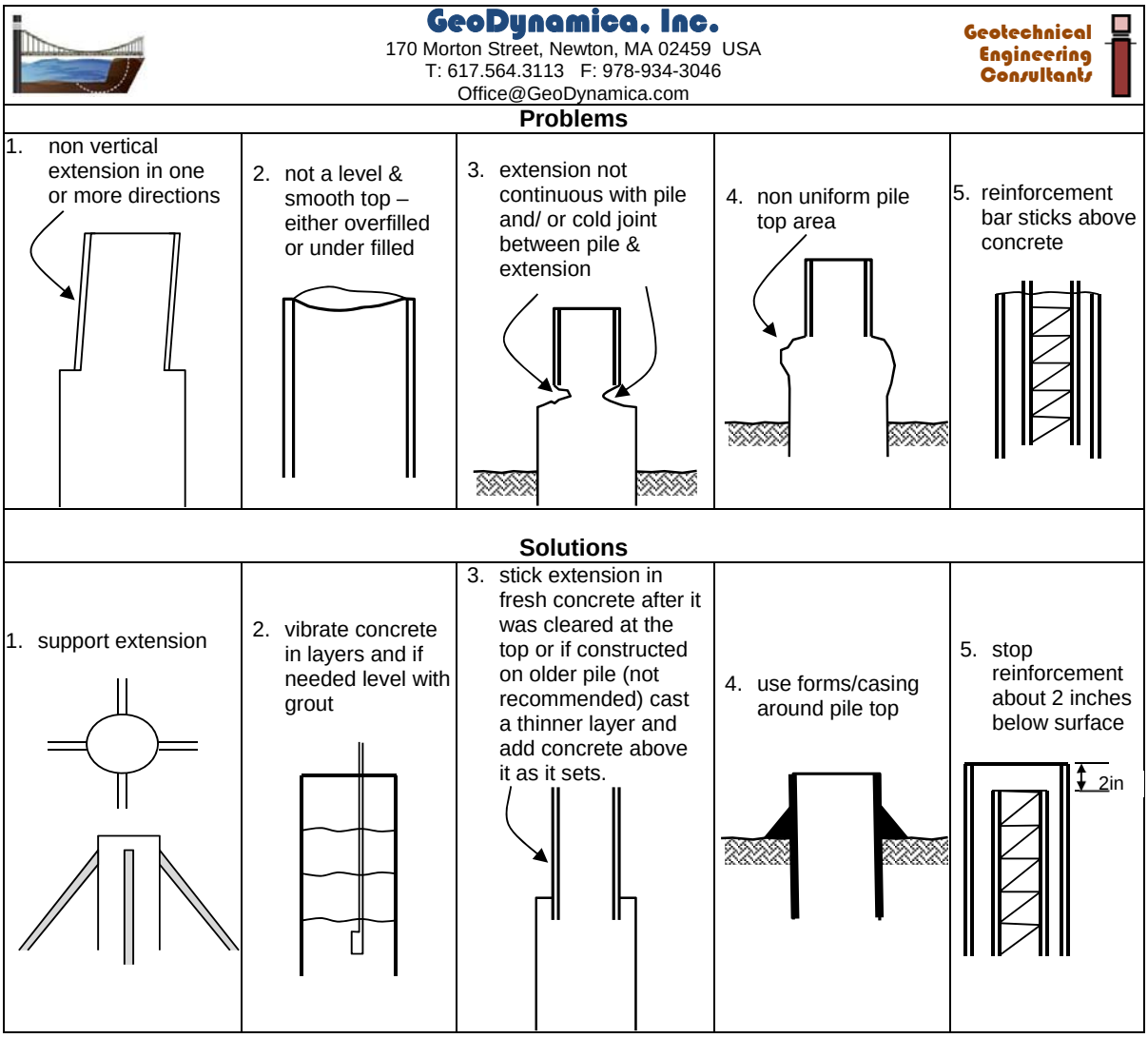
Case	Description	Comment	Figure	Effect	Possible Remedy
1	Non-uniform Cross-section	Mostly dry or slurry construction		• Unknown area for force calculations • Wave reflections and analysis of unknown geometry	• Use of a casing at the top part of the shaft
2	Uneven shaft surface	All type of construction		• Uneven impact results with uneven stress distribution and hence misleading force calculations	• Careful leveling of the shaft top with above ground extension • Multiple gauges (4) located 2-3 diameters below impact • Additional acceleration measurements on the ram
3	Poor quality concrete in the exterior sections	Mostly slurry construction		• Inaccurate force measurements as force calculations based on typical modulus do not reflect actual gauge location conditions	• Use of caissing and concrete quality control at the end of construction (e.g. placing concrete until clear concrete appears at the top)
4	Uneven Ram impact	• Poor or no guiding system • Uneven shaft surface		• Uneven stress distribution, see 2	• Use of a cushion • Use of a guiding system for the ram • Placing gauges as suggested in 2
5	Small Section ram	Shaft area larger than ram's		• Uneven stress distribution, see 2	• Use of a cushion • Use of a striking plate • Placing gauges as suggested in 2
6	High friction at the top of the shaft	Placement of concrete against rock or granular dense soil		Non proportionality between force and velocity due to early reflections does not allow verification of data quality and difficulties in analysis	• Placing gauges as suggested in 2 • Careful signal matching analysis

Table 3: Possible problems to be aware of and avoid, and their possible solutions during construction of a pile extension for dynamic testing



4.3 Case histories

4.3.1 Uneven impact

Five tests were conducted on drilled shafts for researching and optimizing the effect of rock-socket depth on the drilled shaft performance in a given site (GTR, 1997). Shaft A was 60cm in diameter and 13m long, including a 2 m rock socket. A 2m extension was built above ground surface, and 4 pairs of gauges were used around the pile. Drop weight system similar to the one shown in Figure 7, was used to apply impact, and a 75mm thick plywood disk was used as a cushion. Figure 8 presents the individual four force and velocity signals that were recorded for blow no. 3. The numbers next to the individual gauge readings refer to the full scale of the graph (in kN). Blow no. 3 was the result of a 90.7kN ram with a 1.5m stroke. The information presented in Figure 8 suggests the following:

a. The accelerometers readings and calculated velocities were practically identical for all four instruments, unaffected by the ram or the drilled shaft.
b. Uneven forces were calculated at the different points of measurements around the shaft in spite of the advanced guided impact device, the cushion, and the distance between the impact to the point of measurements (about 3 pile diameters).
c. A “symmetric” uneven force impact was recorded for blow 3, such that gauges diagonally to each other recorded similar forces, namely F1 and F3 recorded similar force, as did F2 and F4.

d. The use of multiple points of measurement allowed, however, to obtain reliable and consistent data that were used for a signal match analysis. An average of all gauges was used as the representative force and velocity signals for impact number 3 as presented in Figure 9.
e. Figure 10 presents the summary of the signal match analysis (CAPWAP) for impacts no. 3. A good match was obtained between the measured and calculated forces for both analyzed impacts.
f. Figure 9 clearly shows the smaller peak velocity measurements (presented in force units when multiplying the velocity by the pile impedance) compared to the force measurements. These behaviors are a result of a high friction between the soil and the pile at the upper portion of the pile close to the ground surface. Verification for this observation is obtained from the signal match analyses presented in Figure 10, showing a force distribution along the pile with high frictional resistance forces close to the ground surface.

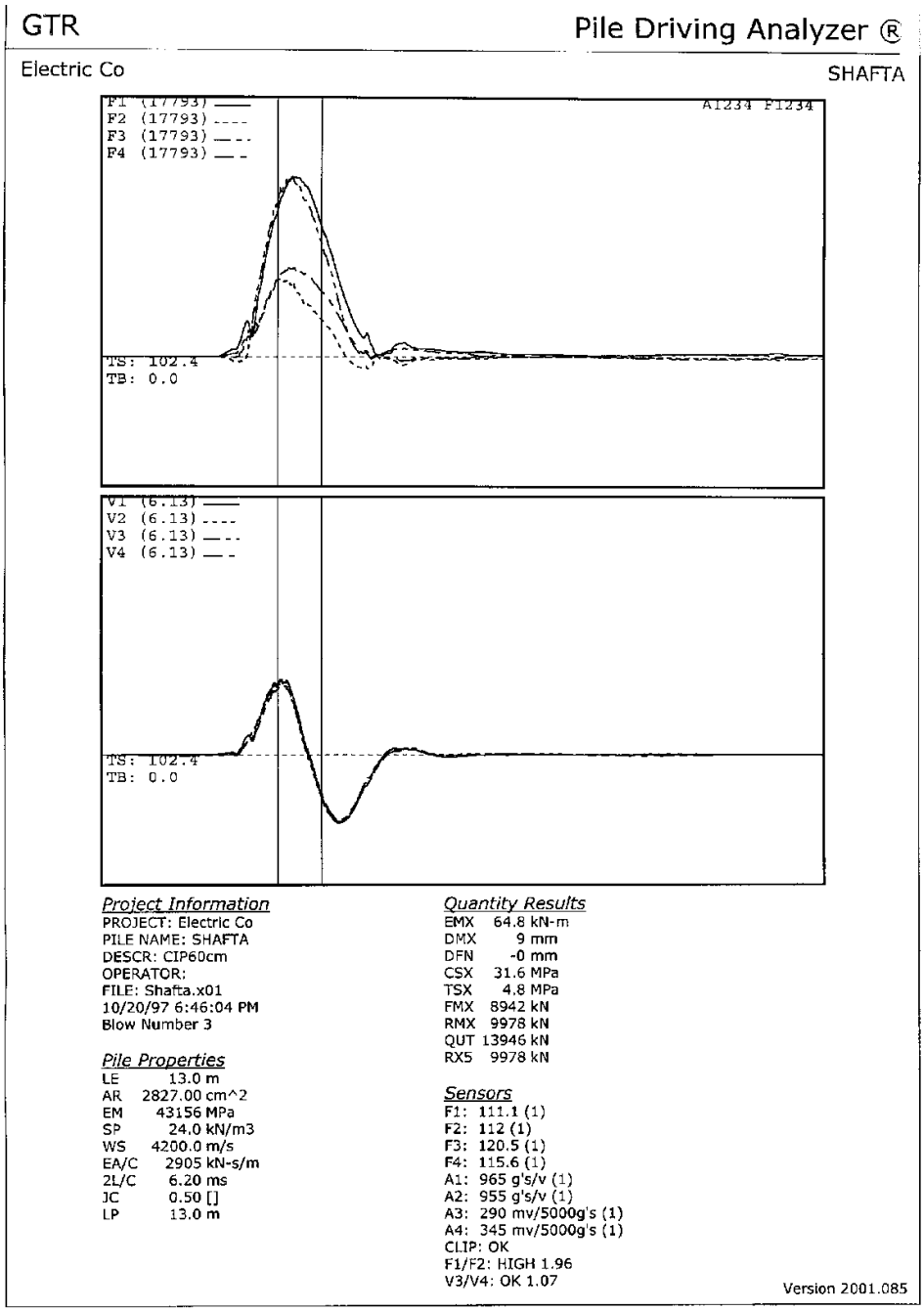


Figure 8: Individual force and velocity records of four strain and acceleration gauges used during impact no. 3 on shaft-A (GTR, 1997)

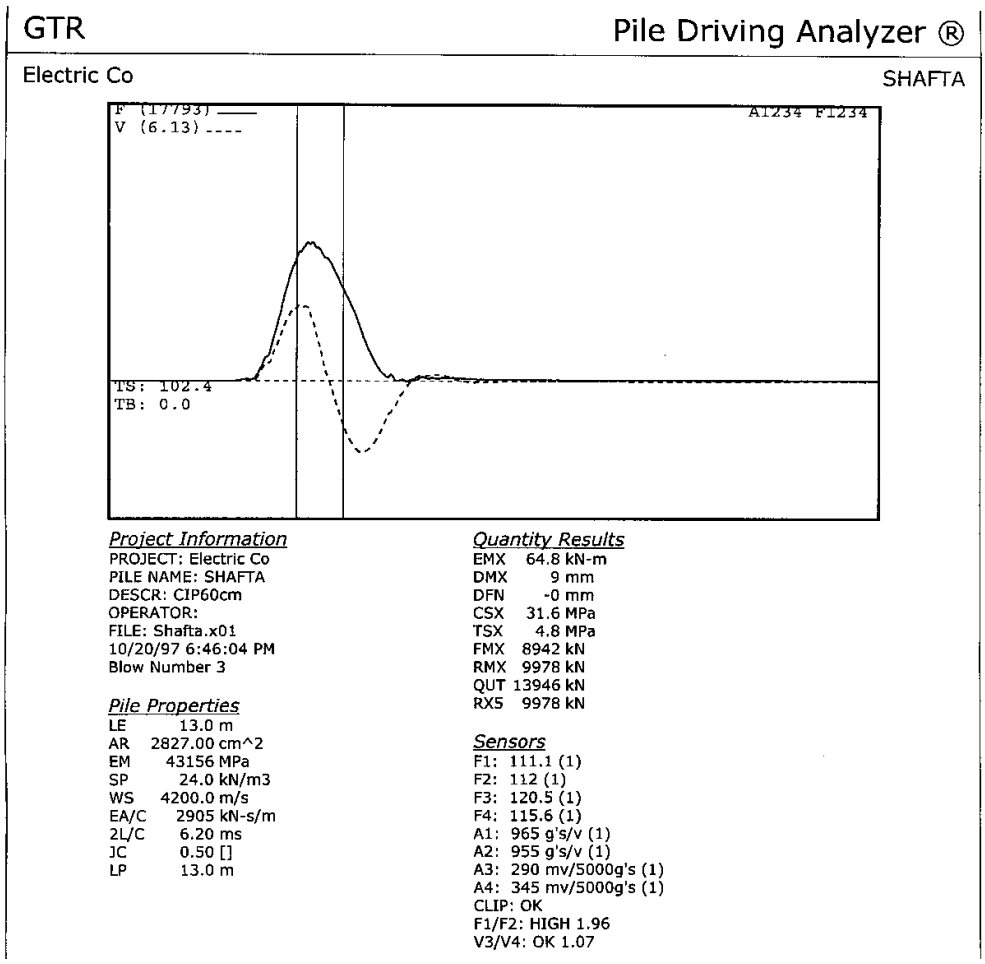


Figure 9: Average force and velocity measurements for impact no. 3 on shaft-A (GTR, 1997)

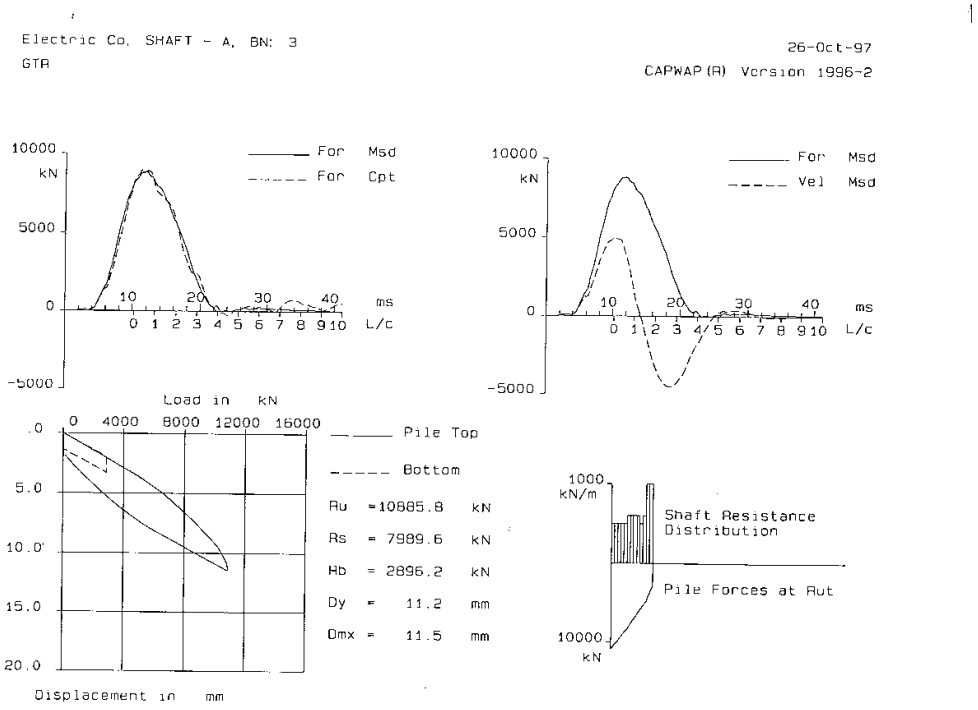


Figure 10: Signal match analysis (CAPWAP) results for impact no. 3 on shaft-A (GTR, 1997)

4.3.2 Defected connection between extension and pile

The dynamic load tests were carried out in January 2012 for a shopping mall and a high-rise complex project in Kefar Sabba, Israel. The tests were carried out on 100cm diameter, 24m depth shafts, constructed by the slurry method in a soil profile consisting mostly of sand or silty sand layers. The signal matching analysis results for the dynamic records are presented in Figure 11. A large mismatch between the force and velocity records (shown in upper right side of Figure 11) suggests a decrease in pile impedance. The impedance analysis had suggested a significantly reduced section at the top part of the pile (small image marked by "pile" in Figure 11) and no resistance at the upper part of the pile. Figure 12a presents a photograph of shaft A during testing. Following the analysis, the concrete pad built around the pile and shown in Figure 12a, was removed and the soil around the shaft was excavated, revealing a significantly compromised pile top shown in Figures 12b and 12c. Unwashed bentonite slurry mixed with the concrete resulted with poor quality mix of no significant strength in a large section of that shaft. One can conclude from the presented case history that accurate measurement, while affected by the construction quality, if analyzed correctly, serve well to identify those defects.

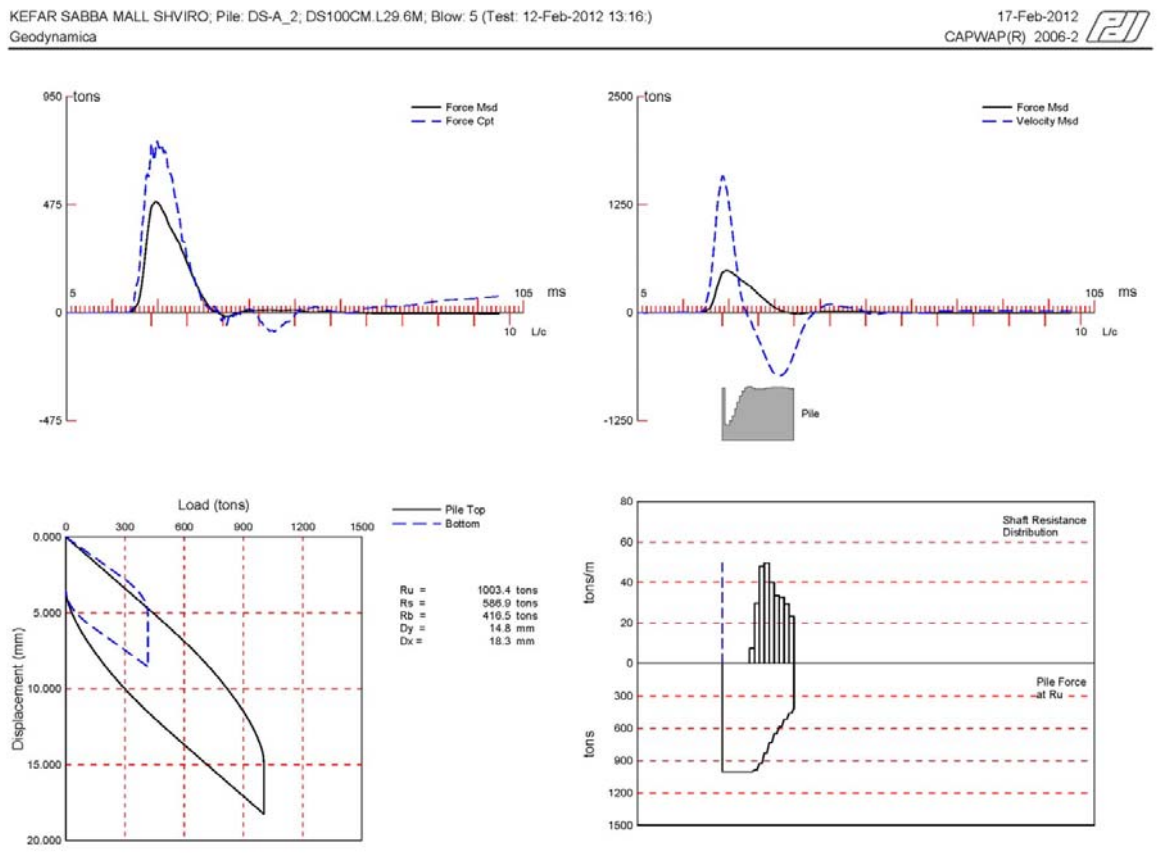


Figure 11: Signal matching analysis (CAPWAP) results for shaft A blow 5 (Geodynamica, 2012).



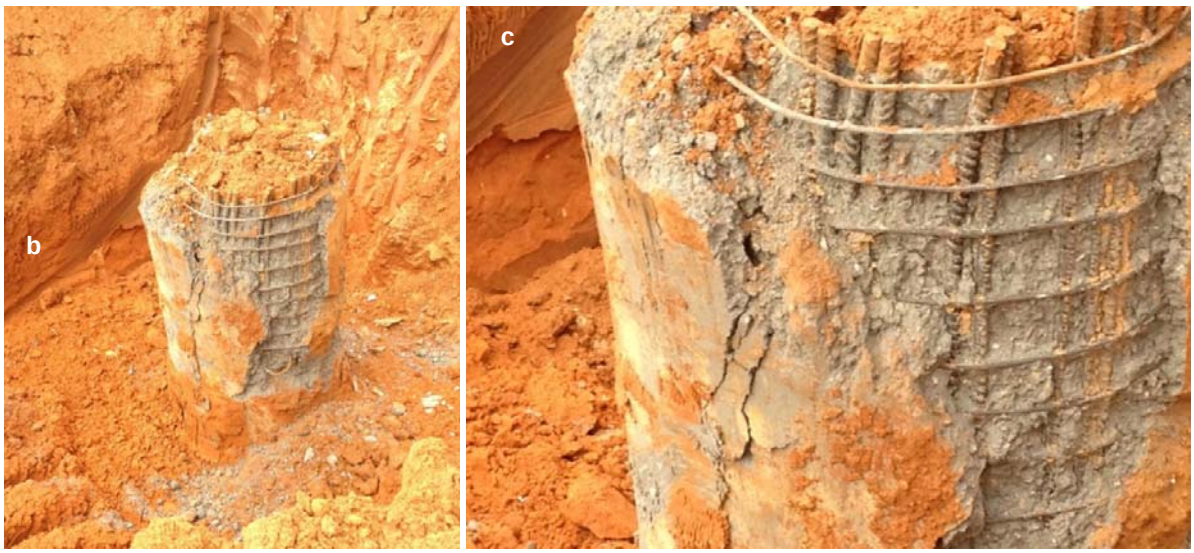


Figure 12: (a) Dynamic load testing of shaft A and the shaft's condition below ground as found during excavations after analysis, (b) general view, and (c) close-up view (Geodynamica, 2012).

5 Investigation of the affecting factors using numerical simulation of a ram impact with a drilled shaft

5.1 Overview

LS-DYNA is an advanced software program for dynamic Finite Element Method (FEM) Analysis developed by Livermore Software Technology Corporation. LS-DYNA is commonly used by the automotive industry for impact analysis and hence serves as an ideal tool for investigating the impact of a ram with a concrete pile. The ultimate goal of modeling such impact is to determine the stress wave distribution across and along the pile as a function of time after impact for different controlling parameters such as the ratio of ram diameter to pile diameter, the drop height, impact angle, and the use of a plywood cushion. The models under investigation were created using the HyperMesh pre-processor and exported in LS-DYNA explicit finite element analysis code format. Post-processing was completed using LS-DYNA Post.

The analysis was carried out in two stages; first, a broad investigation into the aforementioned factors using a relatively simpler modeling, e.g. not modeling the striking plate and the cushion as detached units. In the second stage, a detailed analysis was carried out focusing on what was found to be the most important factor in the first stage, i.e. the uneven impact of the ram. This analysis was examining the stresses across the pile at the surface and at different distances below the pile's top as well as the effect of a softer cushion on the uneven impact. The presented results mainly focus on this stage.

5.2 Analysis procedure

5.2.1 Overview

A 3-D half-symmetry baseline model was initially generated. The baseline model consists of four components, a steel ram, a steel striker plate, a plywood cushion and a 40m long concrete pile. The diameter of the pile and the ram is 1m. A schematic of the model is shown in Figure 13. The analysis simulates a 2m drop of the ram by prescribing an initial velocity for the ram, locating it 0.1m above the striker plate. Table 4 summarizes the major parameters of the baseline model, which was then altered for each subsequent analysis case.

Table 4: Summary of attributes for modeled ram.

Ram Diameter	Ram Length	Ram Drop Height	Ram Mass	Energy	Impact Angle
1.0m	1.6667m	2.0m	1.0276 E+04 kg	2.016 E+5 J	0°

5.2.2 Model geometry and constraints

Figure 14 shows an isometric view of the entire system, with an enlarged view of the region of interest. The different shades (colors in original) in Figure 14 represent the different components, from top down; the ram is shown in red, the striker plate in green, the plywood cushion in blue and the concrete pile in yellow. Figures 15 and 16 show the top view of the pile and ram respectively.

The node and element summary for the baseline model is provided in Table 5. Linear elastic material properties were used for each component in the model and they are listed in Table 6, whereas dimensions for the components are listed in Table 7

To generate the baseline half-symmetry model, constraints were added along the flat portion of each component in the modeled ram-pile system. Essentially, this edge was placed on rollers. The rollers allowed motion in the y-direction from the impact and in the x-direction due to the Poisson effect. Translation and rotation was not allowed in the z-direction along the centerline edge due to symmetry.

The pile's tip was modeled so that the pile could not translate in the y-direction (vertical). In addition, all rotational degrees of freedom were constrained. Again, schematically, this set of boundary conditions is analogous to placing the pile on top of rollers.

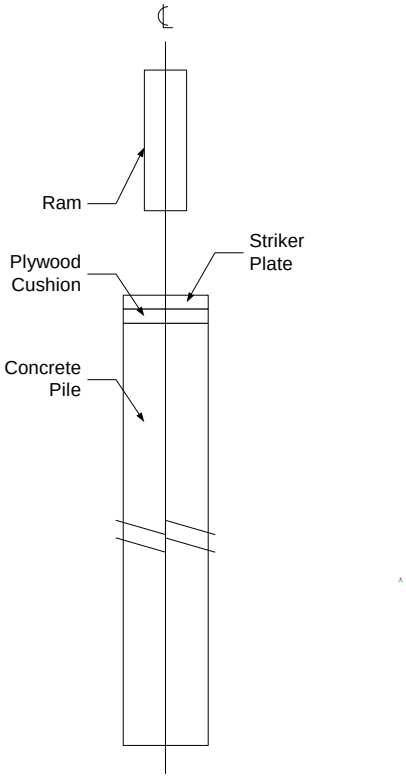


Figure 13: Schematic of Pile and Impact System in LSDYNA Modeling.

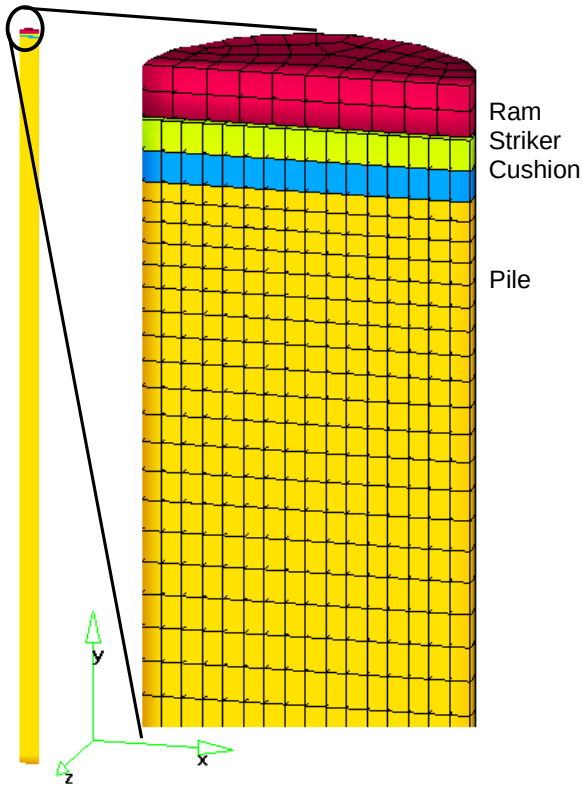


Figure 14: Isometric View of Pile and Ram.

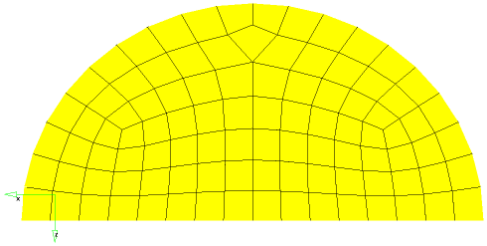


Figure 15: Top View of Pile.

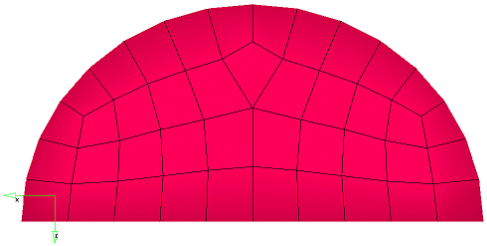


Figure 16: Top View of Ram.

Table 5: Baseline Model FEM Details.

3-D Half-Symmetry Model	
Number of Nodes	9,500
Number of Elements	7,728
Type of Element	8-node solid

Table 6: Material Properties.

Component	Density (kg/m^3)	Elastic Modulus (Pa)	Poisson's Ratio
Striker Plate (steel)	7.850 E+03	2.00 E+11	0.30
Pile (concrete)	2.380 E+03	2.55 E+10	0.15
Cushion (plywood)	4.830 E+02	2.00 E+06	0.30
Ram (steel)	7.850 E+03	2.00 E+11	0.30

Table 7: Component Geometry for Baseline Model

Component	Diameter (m)	Length (m)
Striker Plate	1.00	0.100
Pile	1.00	40.000
Cushion	1.00	0.100
Ram	1.00	0.167

5.3 Parametric studies

5.3.1 General

Parametric studies were designed to study the effects of ram diameter, drop height and impact angle on the developed and propagating stress wave. The altered models were generated directly from the baseline model and are discussed in more detail in the paragraphs that follow.

5.3.2 Models generated to study the effect of drop height

The baseline model was altered to account for a variation in drop height. This change was incorporated into the baseline model by altering the impact velocity. Table 8 shows the parameters that were altered to generate the models for the drop height study.

Table 8: Drop Height and Corresponding Impact Velocity.

Drop Height (m)	Impact Velocity (m/s)
0.5	3.1006
1.0	4.4072
1.5	5.4068
2.0 (baseline)	6.2485
2.5	6.9895

5.3.3 Models generated to study the effect of ram diameter

When altering the ram diameter, it was necessary to keep the amount of energy of the impact equal to that in the baseline model. For the simplicity of the initial analysis stage, the density of the ram was altered so that the weight of the ram would be kept constant in each of these studies while the volume changed due to the changes in the ram's diameter. Table 9 shows the values that were altered to generate models with different ram diameters.

Table 9: Ram Diameter and Corresponding Density.

Ram Diameter (m)	Density (kg/m^3)
0.2	1.9430 E+07
0.6	2.1588 E+05
1.0 (baseline)	7.8500 E+03
1.5	3.4541 E+04

5.3.4 Models generated to study the effect of an offset (uneven) impact

To examine the instance when the ram may not impact the striker plate squarely and the effect of this type of occurrence on the propagating wave, models were generated from the baseline model with a ram diameter of 1m and the ram impacting the striker plate at 3 offsets. To produce the offset, the elements that compose the ram were rotated about a point on the outer edge as shown in Figure 17. Then two other sets of models were generated with a 0.6m diameter ram and a 1.5m diameter ram impacting the striker plate at offset angles (Table 10).

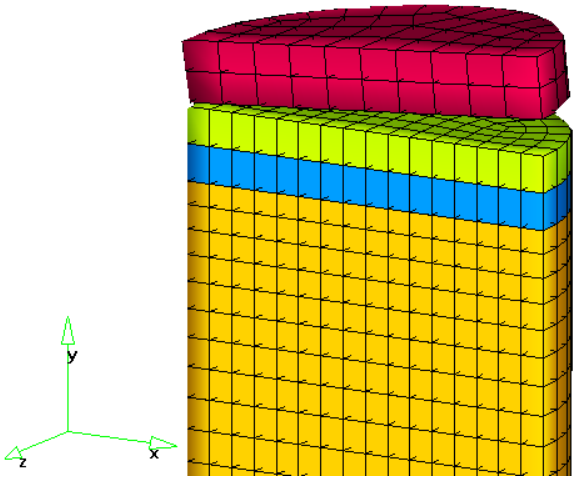


Figure 17: Isometric View of System with a Rotated Ram for an Offset (Uneven) Impact.

Table 10: Ram Modeling with Varied Impact Angle.

Ram Diameter (m)	Ram Impact Angle (degrees)
1.0 (baseline)	0 (baseline)
	1
	5
	10
0.6	0
	1
	5
1.5	0
	1
	5

5.4 Format for results presentation

5.4.1 Stress propagation images

A series of screen captures was generated showing the propagation of the stress wave through the concrete pile. The first image in each series shows the pile in the unstressed state. The second image shows the pile at the time step when impact first occurs. The seven following images depict the stress at equal intervals until approximately 0.005s. It was insured that the plots would show states of stress for the pile exceeding the time of wave travel to pile tip and back. These images were observed and analyzed aiding in the following presentation.

5.4.2 Detailed force and velocity

Sets of stress/force and velocity/force plots have also been generated which show the results for each FE model. The first figure in the set shows stress versus time and the equivalent force (for the local stress multiplied by the cross-section area) at three different distances from the center of the pile, (Figure 18a). The second figure in the set shows the change in velocity (as velocity on one axis and multiplied by the impedance to be expressed in force units in the other axis) versus time for the same locations. It is important to examine the stress distribution at a distance from the top of the pile because following St. Venant principle; the stress wave is expected to become uniform across the pile at some distance away from the impact. Traditionally this distance is believed to be at twice the value of the diameter, or 2m for the analyzed case. Two additional distances, above and below 2m (1m and 3m) were also chosen for this analysis to provide additional values for comparison with the stress developed at the impacted surface. The detailed stresses and velocities were therefore presented at four positions along the length of the pile, making it 12 points all together, (three locations at four cross sections).

5.5 Results of the initial analyses

5.5.1 Overview

The preliminary results include detailed stresses/forces and velocity plots for three cases; the baseline case, a 0.2m ram diameter, and the baseline for an uneven impact (tilted ram). The analyses explored the stress and velocity variations for each case, and their influence on the traditional dynamic measurements. In transferring from stress to force, one should note that the local calculated stress was multiplied by the pile's cross sectional area, hence only under uniform stress distribution the force is correctly calculated. The term Equivalent Force is used to describe the values of the forces obtained this way. While detailed results are presented by Paikowsky et al. (2004b) and Paikowsky et al. (2004a), the meaning of the results, and their operational conclusions are summarized in the following section.

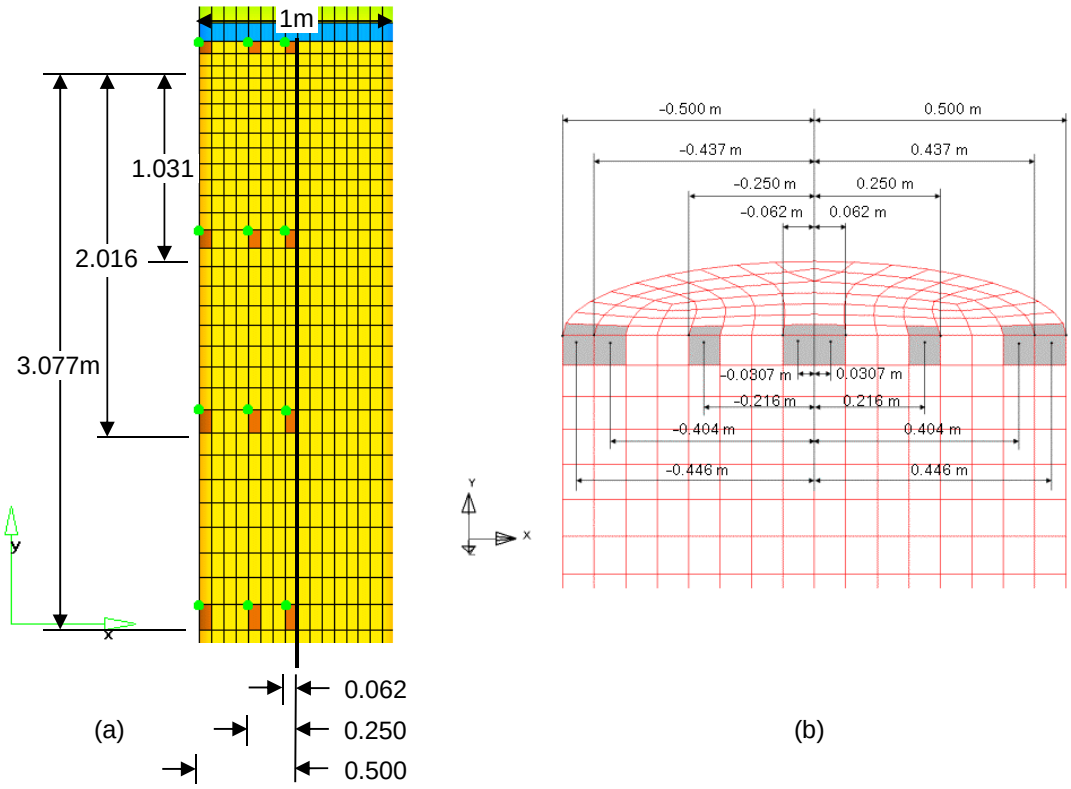


Figure 18: (a) Depiction of Nodes and Elements on the Concrete Pile Chosen for the Detailed Presentation of the Results (b) Depiction of Nodes Chosen for Calculating Velocity and Elements Chosen for Calculating Normal Stress for the Non-symmetric (Uneven impact) Analysis.

5.5.2 Discussion of results

The baseline model analysis suggests that assuming a perfectly even impact over a soft cushion with a round ram (equal to the pile's diameter), results as expected with almost a perfectly even stress wave across the pile section. The match between the velocity multiplied by the impedance and the force calculated based on the local stress, reaffirms the results of an evenly distributed stress wave that continues to propagate in this way along the pile. Detailed examination show that some stress unevenness exists at the top of the pile (close to the impacted surface) to be further investigated in the following section. This relatively small stress unevenness does not affect the velocity, and completely disappears within a distance of one diameter away from the pile's surface.

The smaller diameter ram creates a high stress concentration at the zone of impact such that a very high stress exists under the center of the ram, diminishing in magnitude towards a zone outside the impact area. In all cases, however, the velocity remains mostly unaffected and the uneven stress becomes mostly uniform within one pile diameter. The creation of a high stress short duration wave using such ram can be beneficial for integrity analysis purpose allowing sharp reflection of waves from zones of low quality and/or discontinuity.

A relatively slight uneven impact creates a large stress variation between one side of the shaft to the other. In spite of a sizeable soft cushion, these uneven stresses continue to exist until three diameters away from the impact surface. In all cases uniform velocity exists across the pile in all sections indicating the reliability of these measurements when available.

Operational conclusions:

1. Pile velocity can easily be measured by one or two accelerometers, as uniform velocities exist throughout the pile surfaces and at locations down the exposed shaft.
2. The use of a ram smaller in diameter relative to the shaft it is impacting upon, creates a high stress short duration wave, which can be beneficial for defect detection even under conditions in which the shaft capacity is not fully mobilized.

3. Most significant stress variations exist under uneven impacts when the ram is not parallel to the impacted shaft. This commonly occurring condition takes place due to uneven shaft top surface, non-vertical pile, and in almost all impact systems having difficulties in producing a ram that is perfectly aligned with the shaft's axis. The large variation in stresses exists in the analyzed model in spite of a sizeable soft cushion and, hence, calls for the following actions:
    a. The use of a sizeable cushion when testing drilled shafts. This conclusion affects the energy of the required system as a thicker and softer cushion translates to a higher loss of energy, requiring a larger impact system.
    b. Multiple force point measurements around the shaft.
    c. Measuring dynamic forces at a distance as large as possible away from the impact, in the case of uneven impact this distance can be three pile diameters and more.

5.6 Analysis of uneven impact

5.6.1 Overview

As the most significant effect on the uniformity of the stress distribution seem to originate from an uneven impact due to a tilted ram, this case was examined in detail in comparison to the baseline.

5.6.2 Model geometry, constraints, and material properties

The details of the analyzed driving system (ram) are summarized in Table 11. The segmental modeling was changed by having the striking plate and the cushion (refer to Figures 14 and 17) modeled as free standing bodies (i.e. can separate from each other). The surfaces between the striking plate and the cushion and between the cushion and the pile were modeled using the contact formulation as used between the ram and the striking plate. The material properties used are those presented in Table 6 only differing by the selected wood modulus of 7.0E+09Pa being a more realistic value in relation to the soft cushion used in the initial stage of the analysis.

Table 11: Summary of Attributes for Modeled Ram.

Ram Diameter	Ram Length	Ram Drop Height	Ram Mass	Energy	Impact Angle
1.0m	1.6667m	2.0m	1.0276 E+04 kg	2.016 E+5 J	0°
1.0m	1.6667m	2.0m	1.0276 E+04 kg	2.016 E+5 J	1^o

5.6.3 Baseline model results

The stress and velocity with time at eight points across the pile's surface (refer to Figure 18b) are presented in Figures 19 and 20, with further details on a smaller time scale presented in Figures 21 and 22. A complementary graph presents the stresses as a function of the location at the pile's surface for various times, and is presented in Figure 23. The obtained results suggest large variation in contact stress across the impact location with velocities overall similar at each point.

To obtain a better feel for this variation, isometric 3-D images were prepared, detailing the contact stresses at the pile's surface with time and are presented in Figure 24 (a to l). The obtained images show high stresses around the external rim of the contact between the ram, striking plate, wood and the pile's top.

Figure 25 (a to l) describes the normal stresses across the pile at a location 1.0m (0.5 diameter) below the surface, for various times of the stress passing along the pile. The obtained images clearly show a well-distributed stress across the pile's section. It should be noted that the stress is uniform and what seem to be a stress increase at the circumference is only a result of the isometric presentation of the data. Additional presentation of the stress at the depth of 2m (1 diameter from the surface had shown similar results shifted only in time.

5.6.4 Uneven impact (tilted ram)

The stress and velocity with time at eight points across the pile's surface (see Figure 18) are presented in Figures 26 and 27 with further details on a smaller time scale presented in Figures 28 and 29 respectively.

A complementary graph describes the stress as a function of the location at the pile's surface for various times, and is presented in Figure 30. The obtained results suggest a very large variation in the normal stresses and velocities across the surface of the pile and moreover this variation seem to last for a significant time length in relation to the time required for the stress wave to travel to the pile's tip and back (see Figure 26). A detailed investigation is, therefore, required in order to assess the significance of an inclined impact, even though such an incline is considered in most cases very small (1°).

Isometric 3-D images of the normal stress at the pile's surface with time are presented in Figure 31 (a to k). The images clearly show a stress concentration at the point of initial contact between the ram-striking plate-wood and pile. This concentration remains high throughout the time of impact

Figure 32 describes the normal stresses across the pile at a location 1.0m (1 diameter) below the surface, for various times of the stress passing along the pile. Within the distance of half a diameter, the sharp stress peaks that appear at the surface are muted but a large variation exists between the stresses at one side of the cross-section to the other.

Figure 33 describes the normal stresses across the pile at a location 2.0m (2 diameter) below the surface, for various times of the stress passing along the pile. The stresses remain markedly uneven across the section throughout the passing of the wave.

Further attempts to elucidate the changes in the normal stress distribution across the pile at a large distance from the surface are presented in Figure 34 and 35 for distances of 3m and 4m (3 and 4 diameters) from the pile top, respectively. Both figures show a more evenly stress distribution with increase in the distance from the impact, but even at four diameters away from the pile top the stresses seem to be highly uneven across the pile.

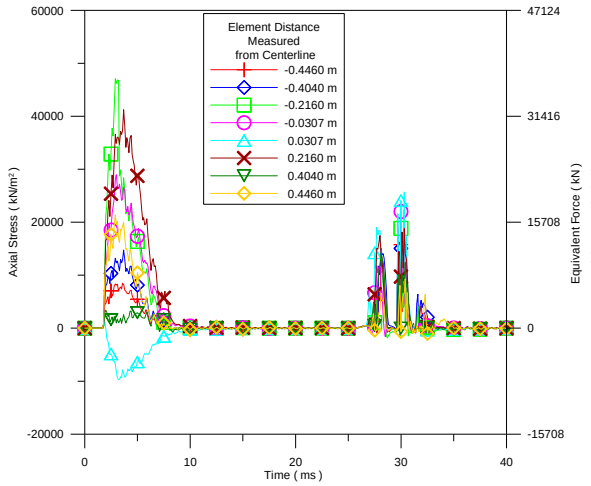


Figure 19: Calculated Normal Stress for Elements on Concrete Surface in FE Model with Ram Diameter = 1.0m and Tilt angle = 0° for Time = 0ms – 40ms.

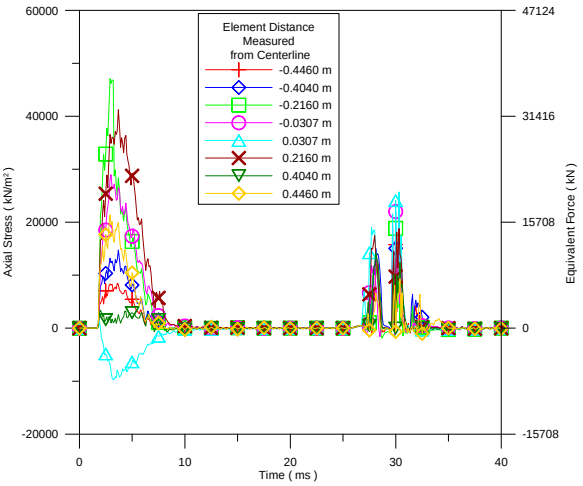


Figure 20: Calculated Velocity for Nodes on Concrete Surface in FE Model with Ram Diameter = 1.0m and Tilt Angle =0° for Time = 0ms – 40ms.

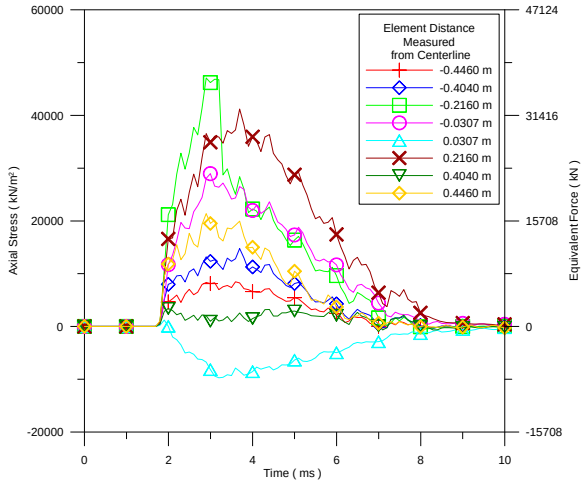


Figure 21: Calculated Normal Stress for Elements on Concrete Surface in FE Model with Ram Diameter = 1.0m and Tilt Angle =0° for Time = 0ms – 10ms.

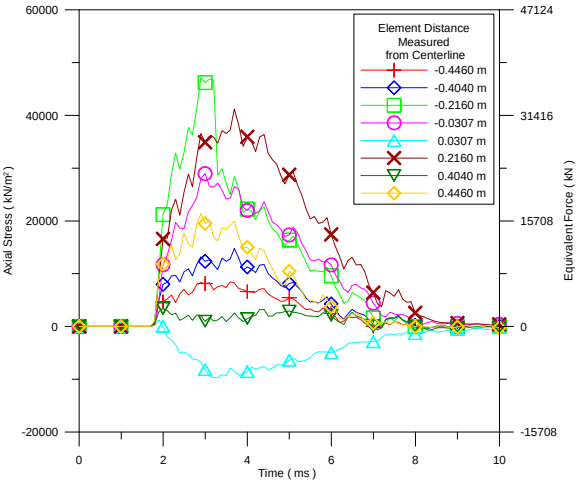


Figure 22: Calculated Velocity for Nodes on Concrete Surface in FE Model with Ram Diameter = 1.0m and Tilt Angle =0° for Time = 0ms – 10ms

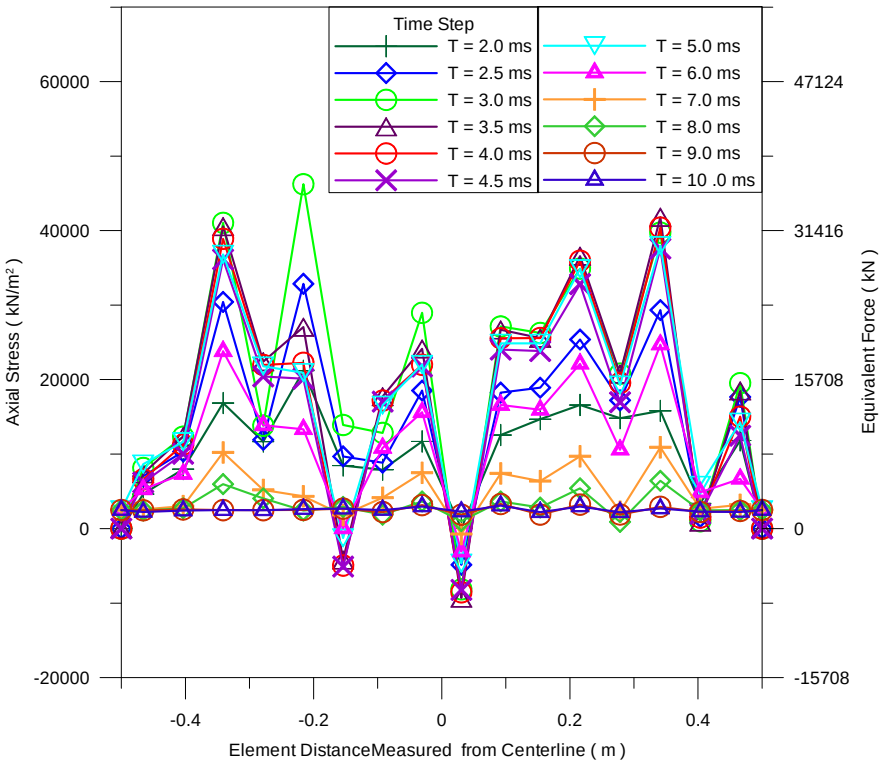


Figure 23: Calculated Normal Stress for Elements on Concrete Surface in FE Model with Ram Diameter = 1.0m and Tilt Angle =0° for d = -0.5 to 0.5m.

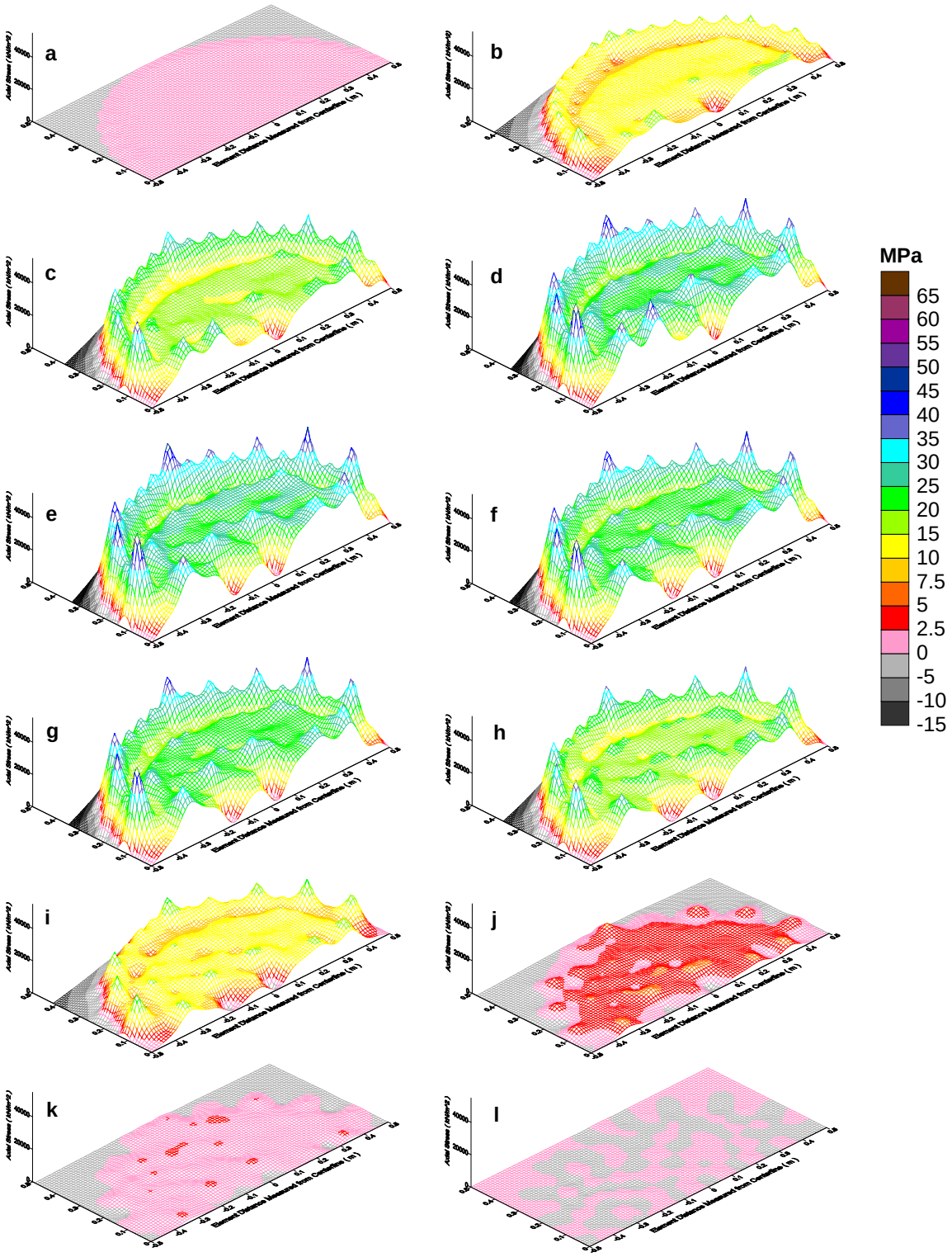


Figure 24: Calculated Normal Stress for Elements on the Concrete Surface in the FE Model with Ram Diameter = 1.0m and Tilt Angle = 0° for Time equal to; (a) 1.8ms, (b) 2.0ms, (c) 2.5ms, (d) 3.0ms, (e) 3.5ms, (f) 4.0ms (g) 4.5ms, (h) 5.0ms, (i) 6.0ms, (j) 7.0ms, (k) 8.0ms, and (l) 9.0ms.

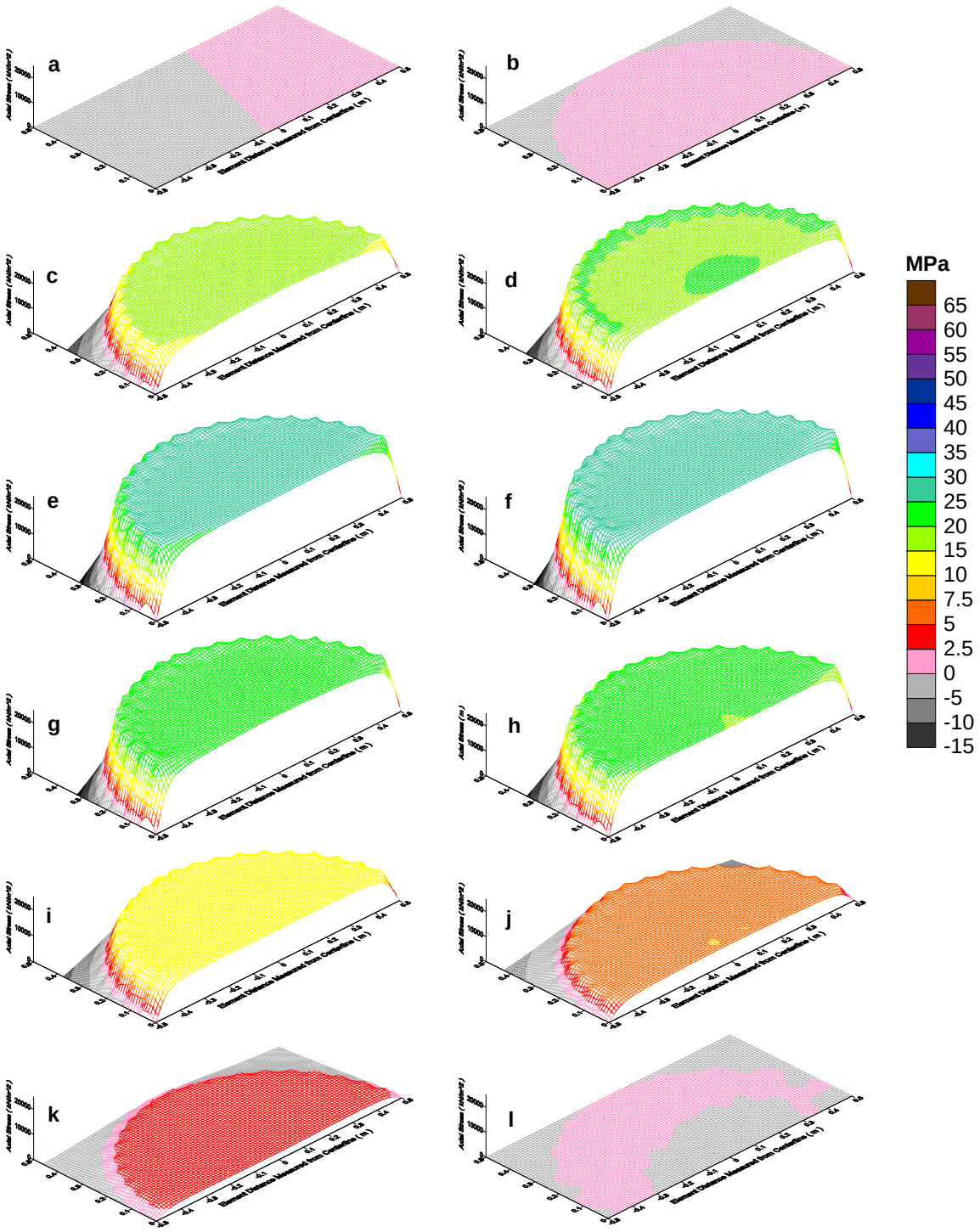


Figure 25: Calculated Normal Stress for Elements 1m Below the Concrete Surface in the FE Model with Ram Diameter = 1.0m and Tilt Angle = 0° for Time equal to; (a) 1.8ms, (b) 2.0ms, (c) 2.5ms, (d) 3.0ms, (e) 3.5ms, (f) 4.0ms (g) 4.5ms, (h) 5.0ms, (i) 6.0ms, (j) 7.0ms, (k) 8.0ms, and (l) 9.0ms.

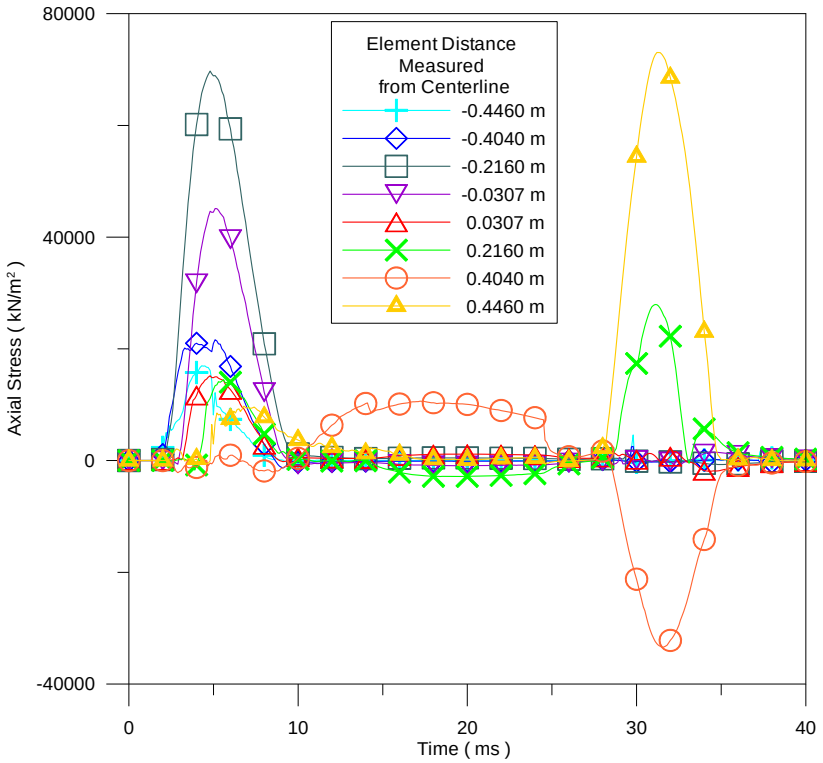


Figure 26: Calculated Normal Stress for Elements on the Concrete Surface in the FE Model with Ram Diameter = 1.0m and Tilt Angle = 1° for Time = 0ms – 40ms.

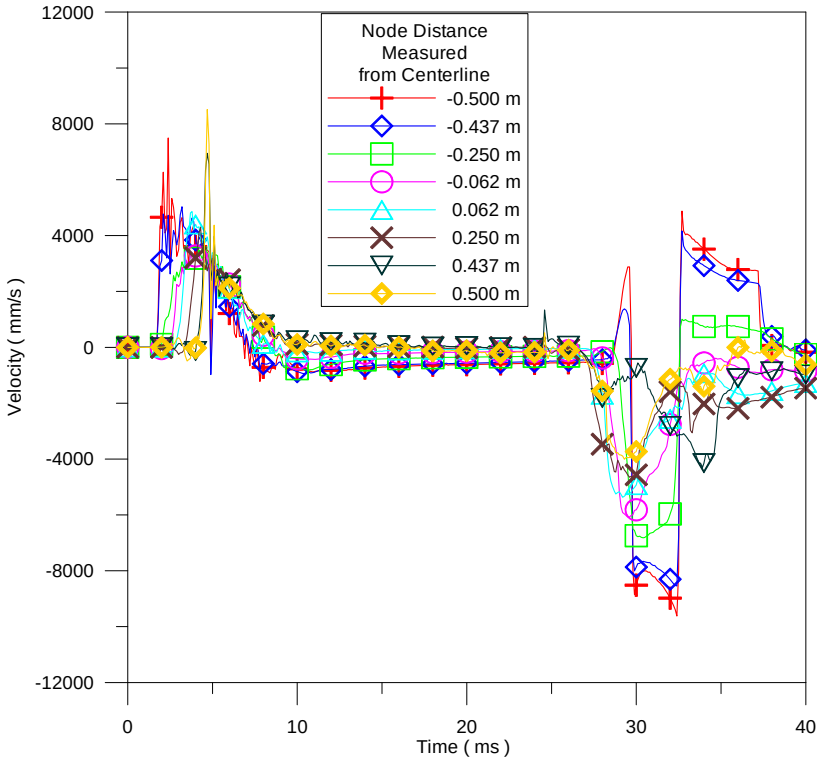


Figure 27: Calculated Velocity for Nodes on the Concrete Surface in the FE Model with Ram Diameter = 1.0m and Tilt Angle = 1° for Time = 0ms – 40ms.

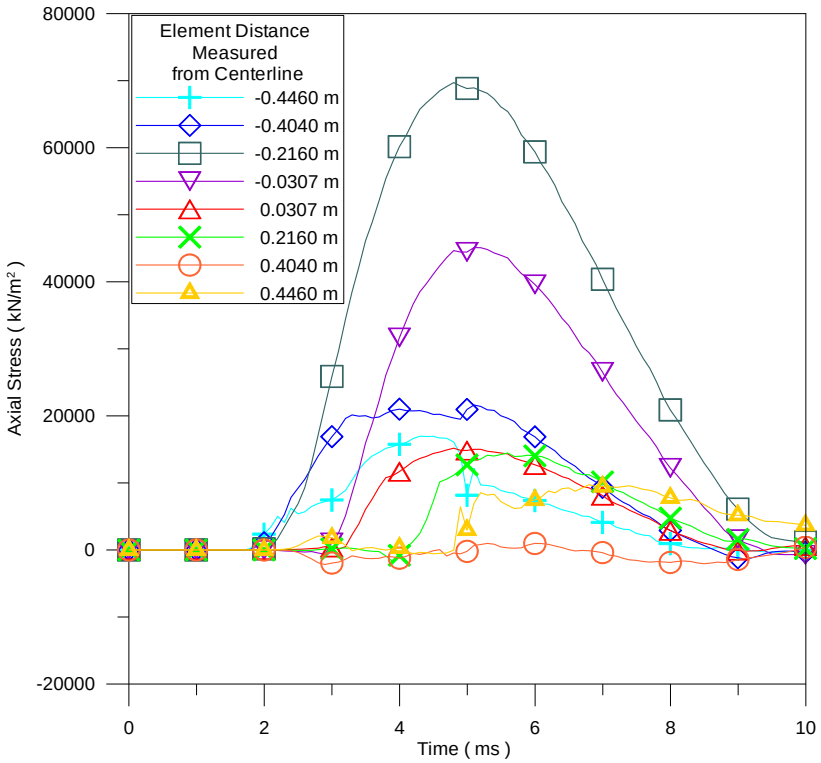


Figure 28: Calculated Normal Stress for Elements on the Concrete Surface in the FE Model with Ram Diameter = 1.0m and Tilt Angle = 1° for Time = 0ms – 10ms.

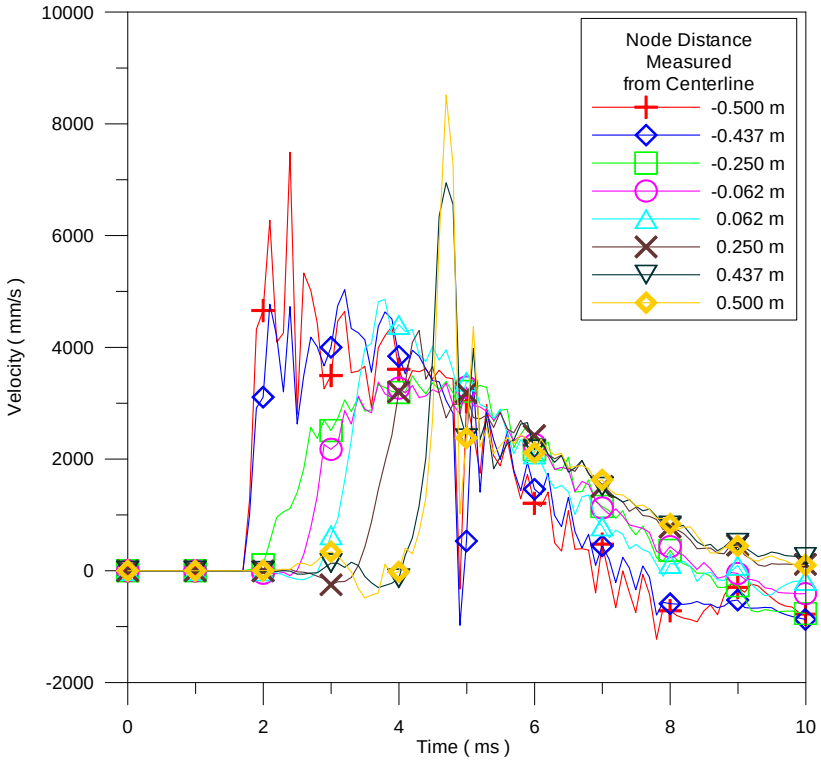


Figure 29: Calculated Velocity for Nodes on the Concrete Surface in the FE Model with Ram Diameter = 1.0m and Tilt Angle = 1° for Time = 0ms – 10ms.

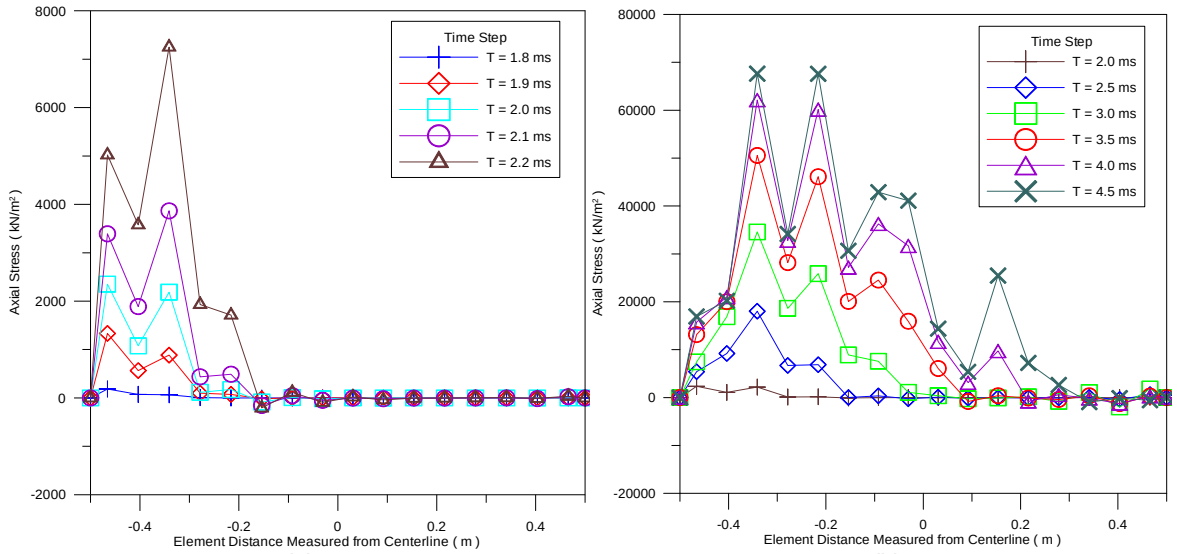


Figure 30: Calculated Normal Stress for Elements on the Concrete Surface in the FE Model with Ram Diameter = 1.0m and Tilt Angle = 1° for d = -0.5 to 0.5m and time equal to (a) 1.8 to 2.2ms, and (b) 2.0 to 4.5ms.

5.6.5 The use of soft cushion to mitigate uneven impact (tilted ram)

The analyzed cases presented in the previous section suggest a troublesome situation in which a ram impact in a small inclination will result with uneven stress distribution across a shaft for a large distance (over four diameters) away from the surface of the shaft. In an attempt to examine mitigating solution, an analysis has been carried out for which the cushion was assumed to be two order of magnitude "softer" than the realistic value used in the original analysis ($E=7x10^7$Pa vs. $7x10^9$Pa). The results of this analysis, describing the normal stress distribution across the shaft at a distance 2m (two diameters) away from the shaft's surface are depicted in Figure 36.

The obtained results clearly show improved stress distribution across the shaft in comparison with the one with a more realistic "harder" cushion presented in Figure 33. However, the duration of the stress wave had significantly increased (in time) and decreased in magnitude. So while an improvement is made in the distribution of the stress, its quality for analysis in signal match or in amount of energy arriving to the shaft had significantly diminished.

Figure 37 illustrates the difference between the two cases. The average force across the shaft's section at the surface, 1m and 2m below the surface are plotted against time for the two cushions discussed above. The "softer" cushion is clearly seen to reduce the peak average force/stress by about half while doubling the wave duration.

5.7 Intermediate conclusions

The advanced modeling of an impact between a ram and a drilled shaft as presented in this section, leads to the following conclusions:

1. Realistic impact analysis is obtained using the FEM analysis LS-DYNA
2. An even impact of a ram with a drilled shaft results with various local stress concentrations at the surface. These variations become irrelevant within a short distance of 0.5m (half a diameter) from the shaft's top.
3. A relatively small tilt in the ram (1°) during impact, results with significant uneven stress distribution across the shaft's surface and away at a relatively large distance (four diameters) along the pile's shaft.
4. The use of a soft cushion mitigates the problem of a large stress variation across the shaft, but diminishes significantly in the quality of the stress wave for use in signal match analysis and reduces the energy transfer to the shaft.

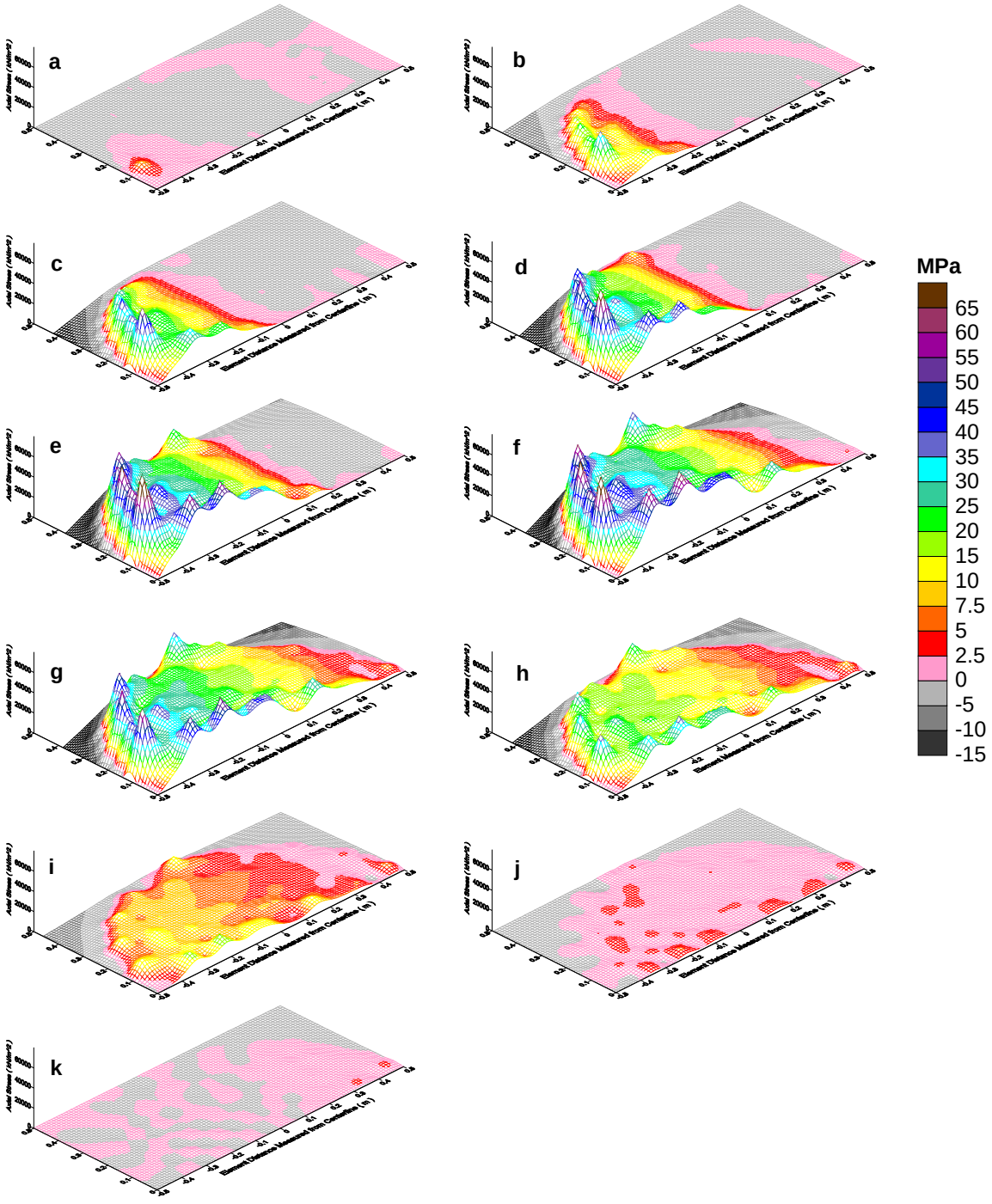


Figure 31: Calculated Normal Stress for Elements on Concrete Surface in FE Model with Ram Diameter = 1.0m and Tilt Angle = 1° for Time equal to; (a) 2.0ms, (b) 2.5ms, (c) 3.0ms, (d) 3.5ms, (e) 4.0ms, (f) 5.0ms (g) 6.0ms, (h) 7.0ms, (i) 8.0ms, (j) 9.0ms, and (k) 10.0ms.

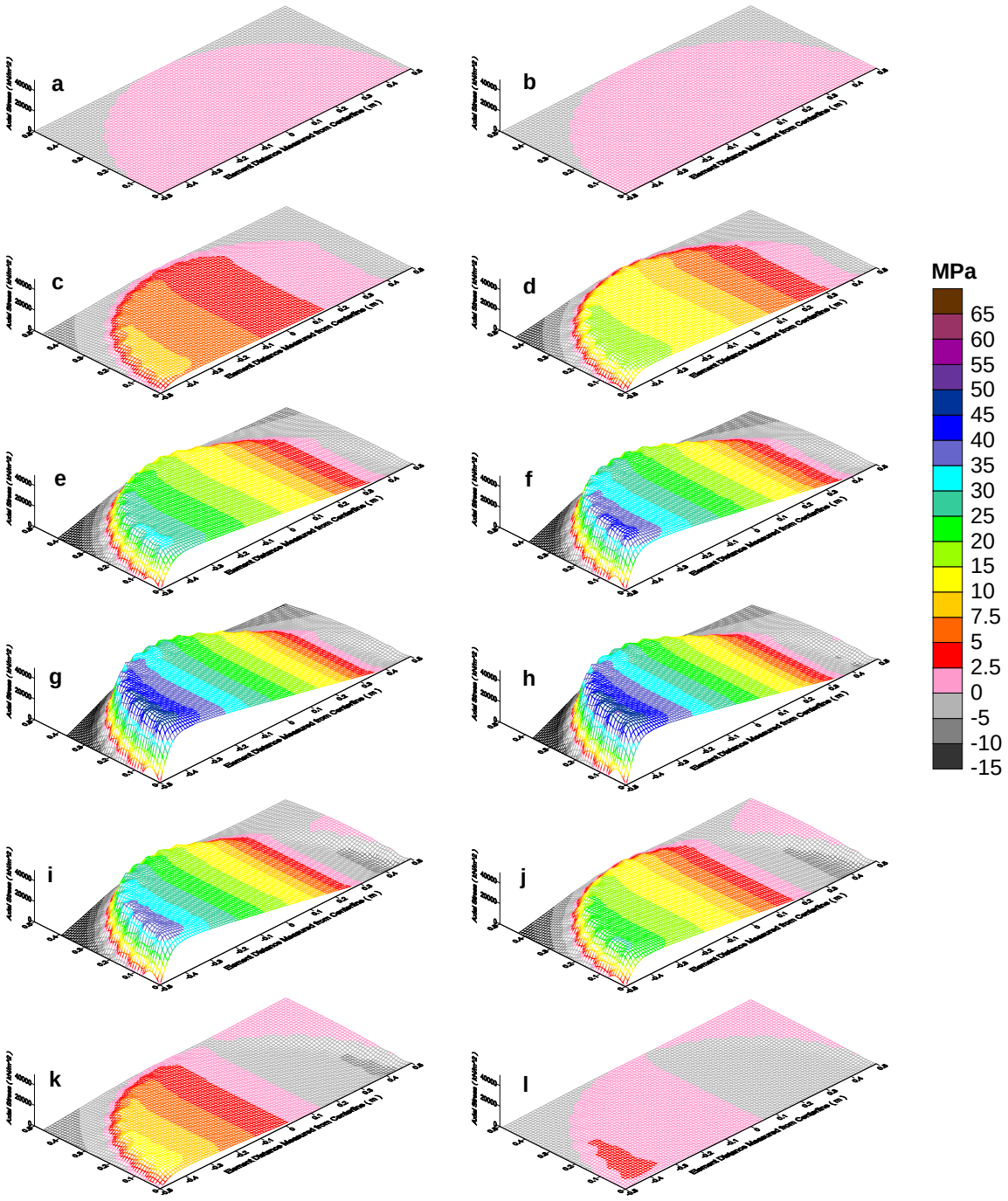


Figure 32: Calculated Normal Stress for Elements 1m Below Concrete Surface in FE Model with Ram Diameter = 1.0m and Tilt Angle = 1° for Time equal to; (a) 2.0ms, (b) 2.5ms, (c) 3.0ms, (d) 3.5ms, (e) 4.0ms, (f) 4.5ms, (g) 5.0ms (h) 6.0ms, (i) 7.0ms, (j) 8.0ms, (k) 9.0ms, and (l) 10.0ms.

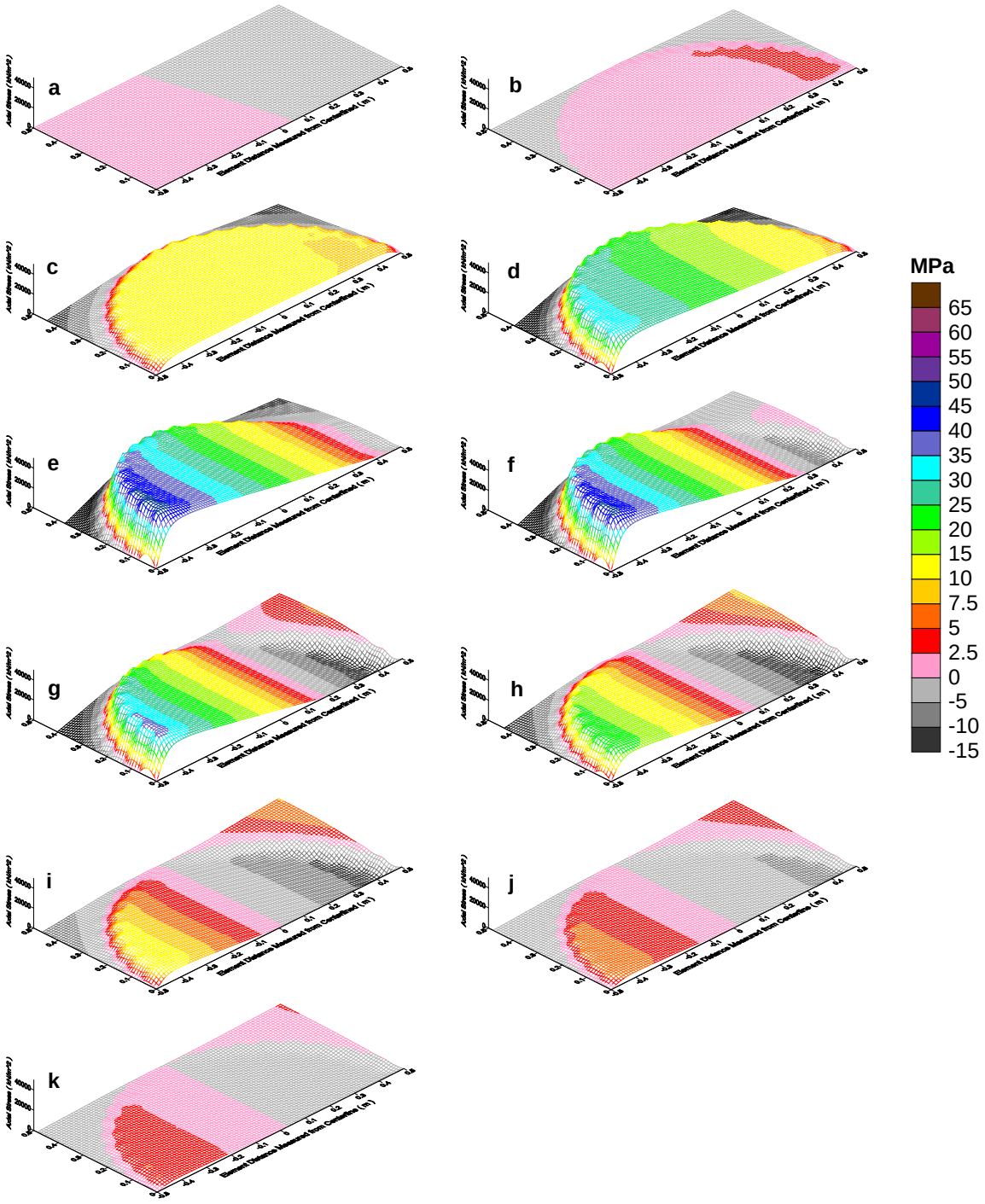


Figure 33: Calculated Normal Stress for Elements 2m Below the Concrete Surface in the FE Model with Ram Diameter = 1.0m and Tilt Angle = 1° for Time equal to; (a) 2.0ms, (b) 3.0ms, (c) 4.0ms, (d) 5.0ms, (e) 6.0ms, (f) 7.0ms, (g) 8.0ms, (h) 9.0ms, (i) 10.0ms, (j) 11.0ms, and (k) 12.0ms.

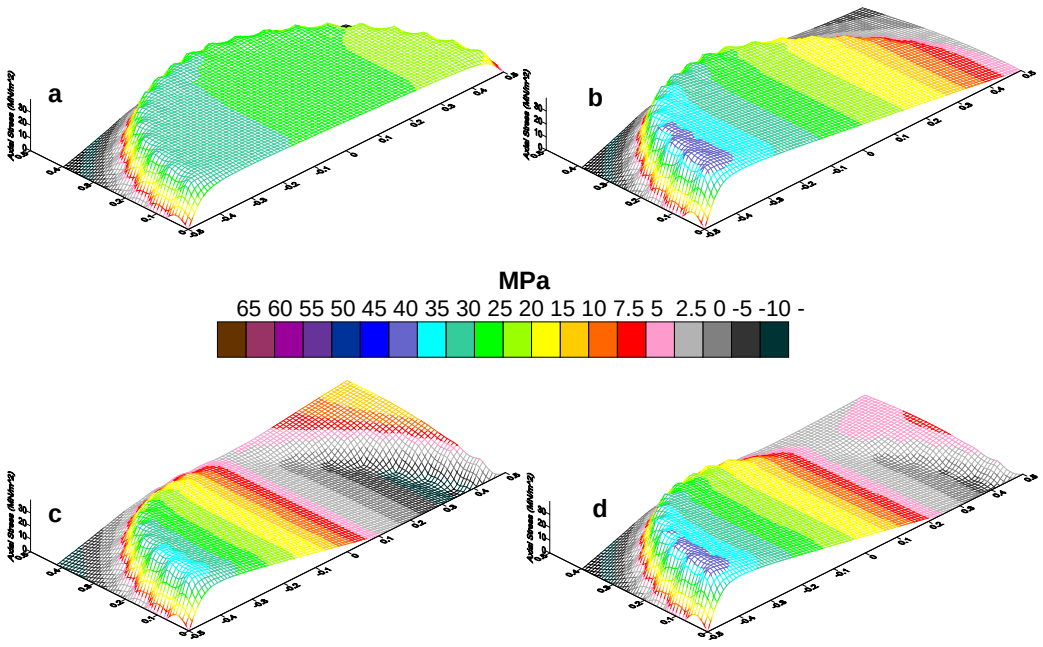


Figure 34: Calculated Normal Stress for Elements 3m Below the Concrete Surface in the FE Model with Ram Diameter = 1.0m and Tilt Angle = 1° for Time Equal to (a) 6.0ms, (b) 7.0ms, (c) 8.0ms, and (d) 9.0ms.

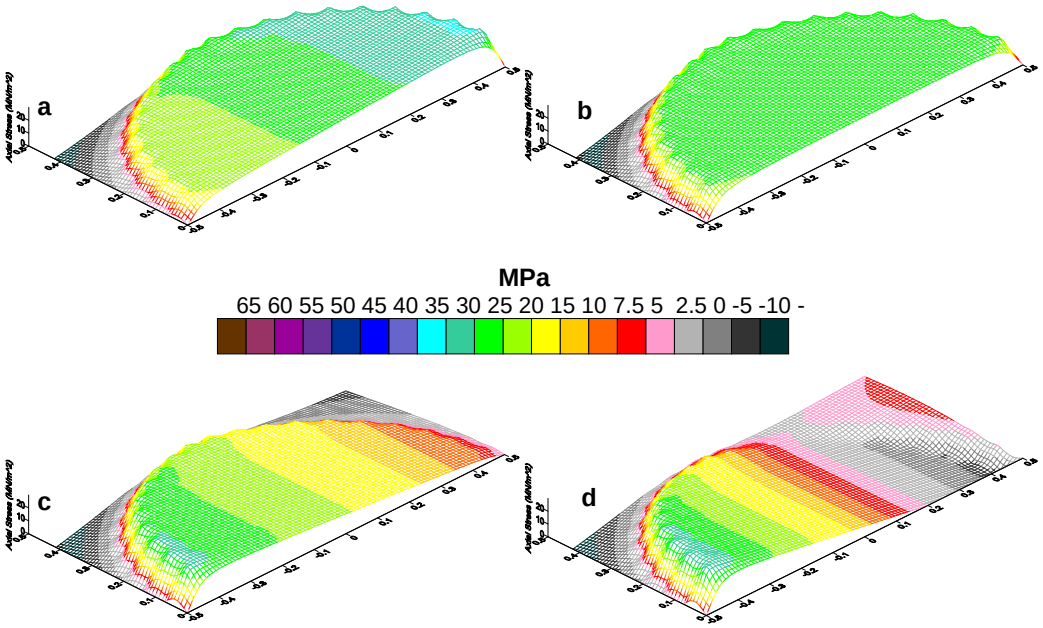


Figure 35: Calculated Normal Stress for Elements 4m Below the Concrete Surface in the FE Model with Ram Diameter = 1.0m and Tilt Angle = 1° for Time Equal to (a) 6.0ms, (b) 7.0ms, (c) 8.0ms and (d) 9.0ms.

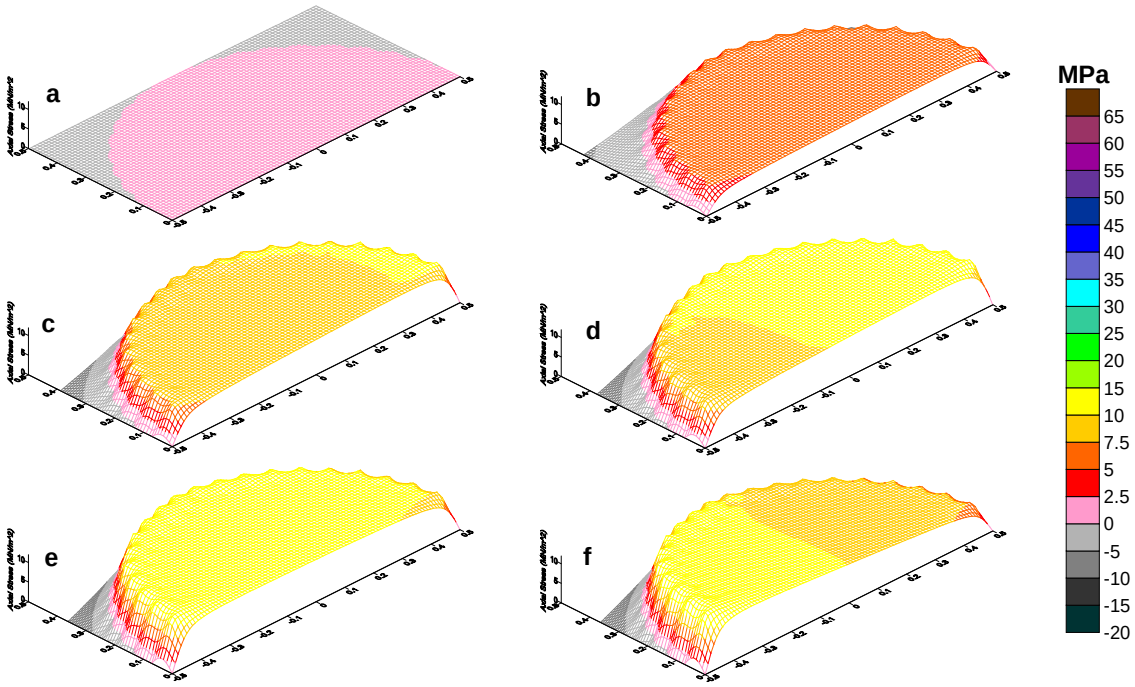


Figure 36: Calculated Normal Stress for Elements 2m Below the concrete Surface in the FE Model with Ram Diameter = 1.0m and Tilt Angle = 1° with a Soft Cushion for Time Equal to (a) 3ms, (b) 6ms, (c) 8ms, (d) 10ms, (e) 12ms, and (f) 14ms.

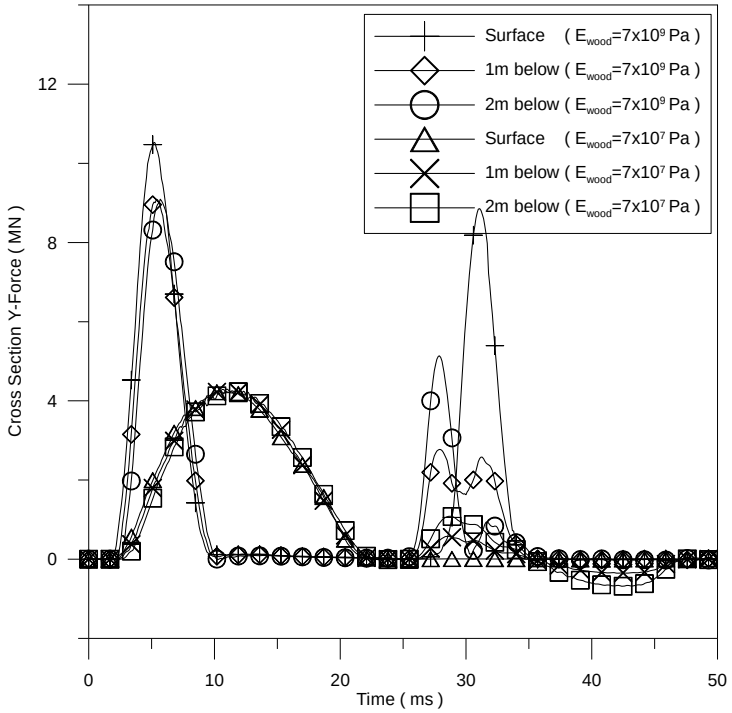


Figure 37: Average Forces with Time Across the Shaft at the Top (Surface) and One and Two Diameters Below the Surface (1m, 2m Respectively) for Representative and "Soft" Wood Cushions.

6 The accuracy of dynamic load testing of drilled foundations

6.1 Overview

The performance of an analysis and/or a testing method can be examined when compared to a reference (benchmark) measurement. The results of a static load test serve as such reference for capacity evaluation of deep foundations. The key stages of using static load capacity predictions for the evaluation of other test results are:

a. Evaluation of the static testing methods and the establishment of a nominal strength.
b. Development of a database that compares the examined method and/or analysis to the established strength.

The next section is based primarily on relevant findings of Paikowsky (2004a), followed by a database specifically developed for the current study.

6.2 Deep foundations nominal strength

6.2.1 General

The definition of the failure load being the ultimate static capacity, given static load test results (load-displacement relations), is not unique. The use of the term reference static capacity for comparison (a value that may include judgment) is more appropriate than nominal strength. The static load test results depend on the load testing procedures and the applied interpretation method, often being subjective.

6.2.2 Databases

Three major databases were developed by Paikowsky et al. (2004a) for the statistical evaluation of design and construction methods of driven piles and drilled shafts. The drilled shaft database consists of 256 cases, the driven pile static analysis database consists of 338 cases, and the driven pile dynamic analysis database PD/LT2000 contains information related to 210 piles that have been statically load tested to failure and dynamically monitored during driving and/or restrike (403 analyzed measurements), Paikowsky and Stenersen (2000).

6.2.3 Failure criterion for statically loaded driven piles

Past work related to driven piles (Paikowsky et al. 1994) have resorted to a “representative” static pile capacity based on the assessment of five interpretation methods; Davisson’s Criterion (Davisson, 1972), Shape of Curve (similar to the procedure proposed by Butler and Hoy, 1977), Limiting Total Settlement to 25.4 mm and to 0.1B (Terzaghi, 1942), and the DeBeer log-log method (DeBeer, 1970). A single representative capacity value was then calculated for the analyzed case as the average of the methods considered relevant (i.e. provided reasonable value). In order to do so, a statistical analysis was then carried out by determining the mean and standard deviations of the ratio of the representative pile capacity to the method being evaluated. Details of the analyses and their results are presented by Paikowsky and Stenersen (2000). Figure 38 shows the histogram and calculated distributions (normal and lognormal) for Davisson’s failure criterion in which k_{SD} is the bias, i.e. the ratio of the representative static capacity to that defined by Davisson’s failure criterion. Davisson’s criterion was found to perform the best overall and was therefore chosen as the single method to be used when analyzing load-displacement curves of driven piles. The method provides an objective failure criterion and was also found to perform well for piles exceeding a diameter of 610mm (examined through 30 pile cases). The data presented in Figure 38 demonstrates, however, that: (i) though small, a bias exists in the representative static capacity used as a reference for the evaluation of predictive methods for capacity evaluation of driven piles, and (ii) this bias (and other considerations) needs to be accounted for when evaluating statistically the performance of a method in comparison with field static load tests.

6.2.4 Load test procedure for statically loaded driven piles

An additional factor to examine is the influence of the static load testing procedure (loading rate within the ‘static’ range) on the designated pile capacity. This influence was examined in two ways. Two detailed case histories from a research site in Newburyport, Massachusetts, were evaluated. A pipe and pre-stressed concrete heavily instrumented friction piles were tested over a lengthy period of time at a bridge reconstruction site. Both piles were tested using three types of static load testing procedures: slow maintained (testing duration of about 45 hrs), short duration (testing duration of about 6-8 hrs), and static cyclic (testing duration of about 15 min.). Details about the piles and the testing are presented by Paikowsky and Hajduk (1999, 2004)

and Paikowsky et al. (1999). The interpretation of the load-displacement relationships in both cases suggested that the 'static' load-test type had an insignificant influence on the pile capacity, (referring to a failure criterion irrespective of the displacement). The effect of the test type was further investigated utilizing a database containing information related to 75 piles tested under slow maintained and static-cyclic load testing procedures. In the static-cyclic procedure, the piles were loaded to failure using a high loading rate and then unloaded. The process was repeated for four cycles. The testing procedure and its interpretation method are presented by Paikowsky et al. (1999). A comparison between the pile capacity based on Davisson's failure criterion for the slow maintained tests and the static-cyclic capacity is presented in Figure 39. The obtained relations and the associated statistical information suggest that there is no significant influence on the static pile capacity based on the applied static load rate. The static cyclic load test results were also compared to the representative static pile capacity (based on the aforementioned five methods) resulting in a mean K_{SC} of 1.023 and a standard deviation of 0.057.

These evaluations led to the conclusions that Davisson's pile failure criterion can be used as a method to determine the reference pile capacity for driven piles irrespective of the pile's diameter and the static load-testing procedure.

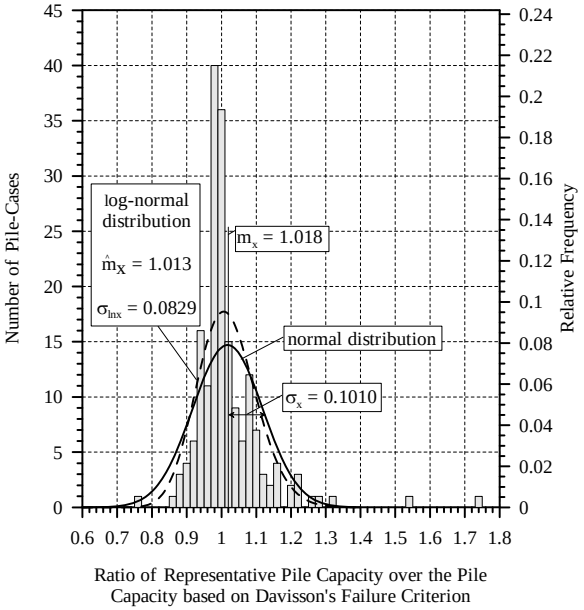


Figure 38: Histogram and frequency distributions of KSD for 186 PD/LT2000 pile-cases in all types of soils. (Paikowsky and Stenersen 2000).

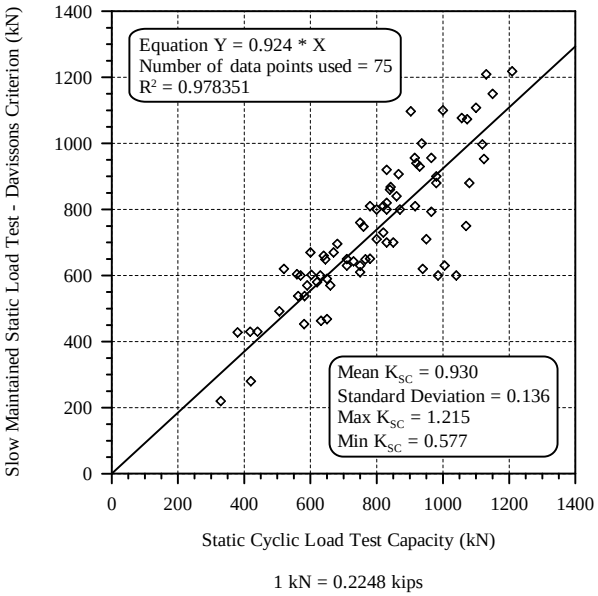


Figure 39: Comparison between pile capacity based on Davisson's criterion for slow maintained load tests and static cyclic load test capacity for 75 piles, (Paikowsky et al., 1999).

6.2.5 Failure criterion for statically loaded drilled shafts

Static load tests of small to medium capacity drilled shafts (say up to 5 MN) are similar to that of driven piles. It is common, however, to design and build high capacity drilled shafts (10 MN and more) often as an alternative to a large group of small capacity driven piles (e.g. in the Northeast region of the USA). As part of the presented project, the static load-test results of drilled shafts were gathered for the drop weight database. These tests were examined utilizing the failure criteria previously described for driven piles, and the FHWA criterion for drilled shafts (O'Neil and Reese, 1999). This criterion establishes the failure load as that associated with a displacement of five percent of the diameter of the shaft (0.05B), if plunging of the shaft cannot be achieved. The results of this study are presented in Table 12, suggesting that the use of the FHWA criterion provides a reliable and a simple failure interpretation for statically loaded drilled shafts.

Table 12: Evaluation of Failure Criteria for Statically Loaded Drilled Shafts

Statistics for the Ratio between Drilled Shaft Capacity of Different Interpretation Methods and the Representative Capacity											
Davisson			**DeBeer**			**Shape of Curve**			**FHWA**		
#	m_x	σ_x	#	m_x	σ_x	#	m_x	σ_x	#	m_x	σ_x
47	0.862	0.17	39	0.908	0.11	36	0.956	0.09	39	0.999	0.13

- no. of cases m_x=mean bias σ_x=standard deviation loads 0.85 to 20 MN
diameter 0.3 to 1.5m length 5.3 to 58.5m

6.3 Database for drop weight load tests

6.3.1 General

The DW/LT 2000 Database has been built up focusing on the research of drilled shafts pile testing using the drop weight system. A concentrated effort was made to obtain case histories where both, static load tests and dynamic measurements of the drop weight system are available. Two hundred and fifty-four (254) cases were identified as potentially viable for the drop weight system analysis. While 167 cases were analyzed for dynamic measurements, only 68 piles were analyzed for static and dynamic capacities of which only 39 cases of the statically loaded drilled shafts met the FHWA failure criterion. The databases were separated and renamed therefore as DW2000 for all cases and DW/LT 2000 for the cases containing static and dynamic data. The results of the databases analyses are presented and discussed in the following sections. These analyses allow us to examine the requirements of the drop weight driving system and carrying out a significant analysis of the method's accuracy.

6.3.2 Drilled shafts static capacity

Database DW/LT 2000 (Paikowsky et al., 2004b) summarizes all the cases for which details of static load test results (load-displacement relations) could be obtained along with dynamic measurements and signal matching capacity predictions. A total of 68 cases were gathered out of which 44 cases were for drilled shafts in which the load test was carried out to failure and 24 cases are for shafts for which failure was not obtained. As not all 44 shafts satisfy all failure criteria, or they are irregular (e.g. CFA shaft) some are excluded from the various analyses. It should be noted that at times even if clear failure was not obtained, the test was carried out to satisfy one of the failure criteria. The number of cases therefore does not match between one interpretation analysis to the other.

Static Capacity The shafts for which the load-test was not carried out to failure were analyzed for load-test extrapolation based on the procedure proposed by Paikowsky and Tolosko (1999). All cases were analyzed using Davisson's failure Criterion (Davisson, 1972), DeBeer's Criterion (DeBeer, 1970), shape of curve similar to the method proposed by Butler and Hoy (1977) and the FHWA drilled shafts capacity criterion (absolute displacement equal to 5% of the shaft's diameter). Details of the methods are provided by Paikowsky et al. (1994) and Paikowsky and Tolosko (1999). A representative capacity value is achieved by averaging the "acceptable" capacities of the different methods. The following section presents the results relevant to the drop weight performance in relation to the representative and FHWA failure criteria only. Figures 40 and 41 differ by the static load test interpretation methods, being the representative and FHWA capacities, respectively. Table 13 summarizes the various analyses conducted relevant to DW/LT2000, including extrapolated load-displacement relations from non-failed load tests and the application of the Davisson's failure criterion to drilled shafts.

6.3.3 Static shaft capacity vs. drop weight dynamic predictions

Figures 40 and 41 present the relationships between the predicted capacity based on dynamic measurements and signal matching analysis (CAPWAP) vs. static capacity. The presented data and the statistical analysis of Table 13 suggest the following:

a. The dynamic prediction for the cases in which the drilled shafts were loaded statically to failure are very accurate with overall prediction ratio varying between 0.85 to 1.05 and coefficient of variations between 0.12 to 0.19 with very small over prediction, (on the unsafe side). These cases are limited to a maximum shaft capacity of 17MN.

b. The predictions are particularly impressive when referring to the 'adopted' static failure criterion, i.e. the FHWA method (0.05B) for which the bias for the 39 analyzed cases is 1.05 and the standard deviation is 0.12, hence having a COV of 0.114.
c. The cases for which extrapolation was required, result in substantially overall less accurate prediction and a high scatter. These included however five drilled shaft cases in the capacity range of 20 to 33MN and most likely dynamic loading, which could not mobilize the shaft's capacity.
d. The obtained results are promising regarding the accuracy of the method and need to be further evaluated in relation to the accuracy of the dynamic predictions as obtained for driven piles and static analysis predictions for drilled shafts.

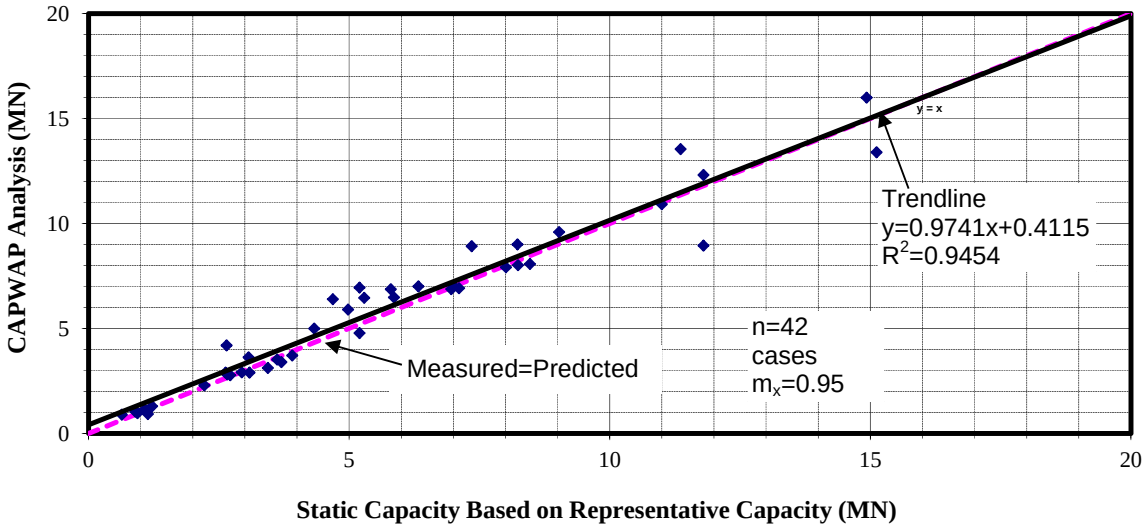


Figure 40: Drilled shaft static load test to failure results (representative capacity) vs. drop weight CAPWAP analysis.

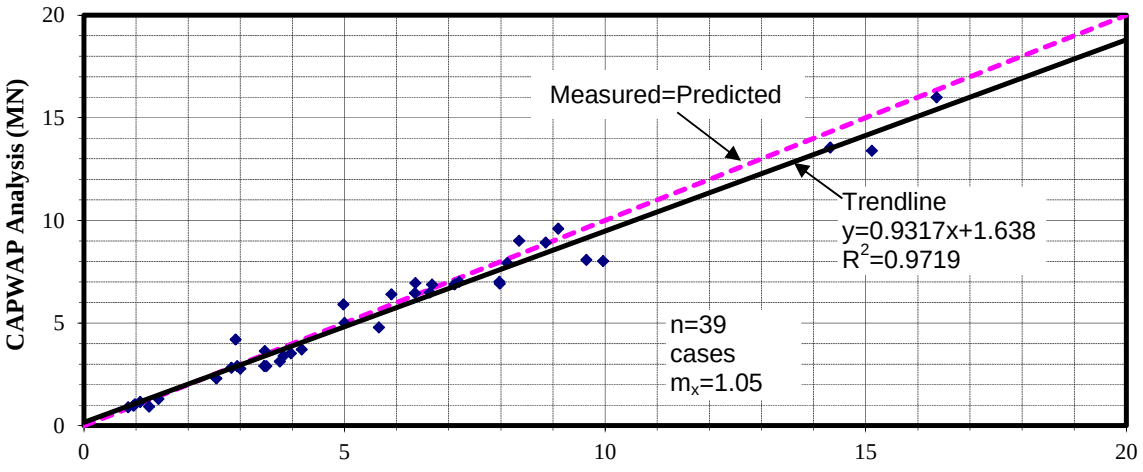


Figure 41: Drilled Shaft Static Load Test to Failure Results (FHWA Failure Criterion) vs. Drop Weight CAPWAP Analysis

Table 13: Statistical Summary of Drop-Weight Dynamic Analysis Predictions For Drilled Shafts

Data Type	Static Failure Criterion											
	Representative				Davisson				FHWA			
	#	m_x	σ_x	Figure	#	m_x	σ_x	Figure	#	m_x	σ_x	Figure
Tests to Failure	42	0.95	0.13	82	39	0.85	0.19	83	39	1.05	0.12	84
Failure from L.T. Extrapolation	22	1.55	0.63	85	21	1.46	0.64	86	20	1.71	0.73	87

- no. of analyzed cases, m_x – Mean (bias) of the static capacity over the dynamic predictions, σ_x – Standard deviation

6.3.4 Evaluation of the drop weight testing results

Overview The obtained results are backed by a good size database, and hence, affirms the performance of the drop weight system. As the method of data acquisition and analysis is similar to that used for dynamic testing of driven piles, an assessment of the results is achieved via comparison to statistical analyses for driven piles. A perspective is also gained by examining the accuracy of static analysis methods commonly used in the design of drilled shafts.

Static Capacity vs. Dynamic Predictions for Driven Piles Time of driving, driving resistance, and area ratio proved to be controlling parameters for the dynamic method's performance for driven piles (Paikowsky et al., 2004a, Paikowsky and Stenersen, 2000). Table 14 present the data relevant to the drilled shafts dynamic analyses. By and large, the dynamic impact of drilled shafts is not associated with large soil displacements and often is accompanied by what could be termed for driven piles as 'refusal' --high driving resistance. The relevant cases are therefore the signal matching (CAPWAP) analyses of driven piles during restrike (marked by BOR in Table 14). For these cases, very little effect was found to the driving resistance (blow count) and overall the signal matching technique of the dynamic measurements was proven as a very accurate method. The results presented in Table 13 for the tests to failure should therefore be compared to the results presented in Table 14 for the BOR cases. As Table 14 refers to static analysis that was defined by Davisson's failure criterion, a direct comparison can be done with the relevant analysis in Table 13. Overall, a fairly reasonable accuracy was obtained in both databases, COV= 0.224 for the drilled shafts and COV = 0.339 for the driven piles. While the bias of the driven piles suggests a small under prediction (1.158) the bias of the drilled shafts suggest an over prediction (0.85).

Static Capacity vs. Static Analysis Predictions for Drilled Shafts Paikowsky et al. (2004a) examined the performance of the drilled shaft's static analysis methods depending on the soil type, design method, and construction method. The static analysis methods predicted the drilled shafts capacities in mean bias ratios varying between 0.83 to 2.27 (measured over predicted) with coefficients of variation varying between 0.25 to 0.74. Table 15 presents a statistical summary of the FHWA drilled shaft design method (Reese and O'Neill, 1988) when applied to drilled shafts in sand, clay, mixed soil and rock (IGM method see O'Neill et al., 1996, O'Neill and Reese, 1999) for varied construction methods. The overall results suggest that the static analyses are by and large over predictive (on the unsafe side) except when the drilled shafts are constructed in clay, and overall the uncertainty of the prediction is high compared to the drop weight testing performance.

Intermediate Conclusions A very high accuracy in prediction was obtained using the drop weight system for drilled shafts. The data related to the driven piles affirms the statistical analysis that was obtained for the drilled shafts when related to cases of restriked piles and relatively small displacements. While it is expected that the drop weight tests under the examined conditions would result with predictions more accurate than static analyses, the accuracy presented in the results of Table 13 remain surprisingly good. One possibility is the lack of knowledge regarding 'class A' predictions for which the dynamic analyses were carried out without the knowledge of the static load-test results. The conclusion regarding the effectiveness and high accuracy of the method remains overall with the emphasized need for additional data of high quality testing.

Table 14: Statistical Summary of the Dynamic Methods for Capacity Prediction of Driven Piles (Paikowsky and Stenersen, 2000)

Method		Time of Driving	No. of Cases	Mean m_x	Standard Deviation	COV
Dynamic Measurements	CAPWAP	General	377	1.368	0.620	0.453
		EOD	125	1.626	0.797	0.490
		EOD - AR < 350 & Bl. Ct. < 16 BP10cm	37	2.589	2.385	0.921
		BOR	162	1.158	0.393	0.339
	Energy Approach	General	371	0.894	0.367	0.411
		EOD	128	1.084	0.431	0.398
		EOD - AR < 350 & Bl. Ct. < 16 BP10cm	39	1.431	0.727	0.508
		BOR	153	0.785	0.290	0.369

m_x = mean (bias) of the static capacity (Davisson) over the dynamic prediction

Table 15: A Statistical Summary of the Performance of the FHWA Drilled Shaft Static Analysis Method (Based on Paikowsky et al., 2004a)

Soil Type	No. of Cases	Mean m_x	COV
Sand	32	1.71	0.60
Clay	53	0.90	0.47
Mixed	44	1.19	0.30
Rock*	46	1.23	0.41

*refers to the IGM design method, m_s=mean (bias of the static capacity (FHWA method) over the static prediction

6.4 Ram requirements

Guidelines for ram requirements in a drop system can now be evaluated based on actual performance. Figure 42 presents the relationship between the accuracy of the prediction (ratio of static capacity over dynamic) versus ram weight over the static capacity (Figure 42a utilizing the representative capacity and 42b utilizing the FHWA failure criterion) for all cases. The overall trend of the data suggests that when the ram's weight is below 1% of the capacity there is mostly under prediction, as apparently the capacity could not have been mobilized. In an attempt to further shed light on the observed behavior, the pile cases were categorized according to end bearing piles and friction piles both for cases in which the load test was carried out to failure and extrapolated cases. This categorization was based on two examinations (i) shape of curve (general failure was assumed to be related to friction piles) and (ii) soil type at the tip. Examination of the data in Figure 42 (a and b) based on this categorization suggests the following conclusions:

a. End bearing shafts most likely require larger ram to capacity ratio for possible mobilization of the capacity. A ratio of over 1.5% seems as appropriate.
b. The capacity of shafts utilizing mostly friction resistance can be mobilized with ram weight of over 1% of the expected capacity.
c. It is reasonable to assume that the extrapolated cases were such that both static and dynamic testing did not succeed to mobilize the capacity.
d. More data are required to affirm the above conclusions.

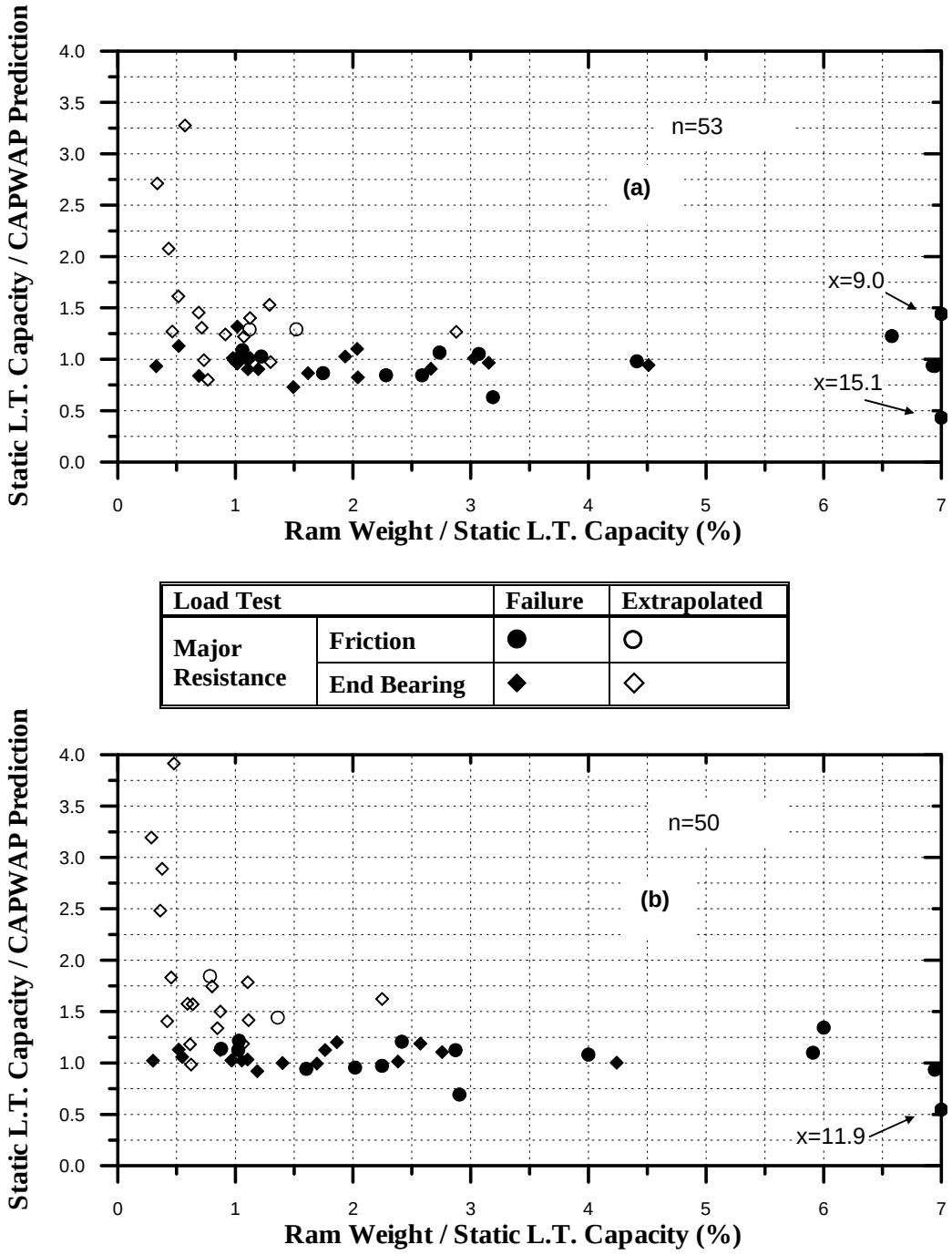


Figure 42: Static L.T. Capacity Over CAPWAP Prediction vs. Ram Weight Over Static L.T. Capacity; (a) Using the Representative Static Capacity, (b) Using the FHWA Failure Criterion.

7 Existing codes and guidelines

7.1 Overview

ASTM D4945-12 “Standard Test Method for High-Strain Dynamic Testing of Deep Foundations” is the worldwide reference for dynamic testing of deep foundations. This standard refers to deep foundations being defined generically as both, driven and cast-in-place piles. The standard includes drop weight systems in parallel to conventional pile driving hammers and, hence, although originally written for driven piles, is equally applicable to drilled shafts. In reference to an impact device, the standard includes the following: *“The device used to apply the impact force should provide sufficient energy to cause pile penetration during the impact event adequate to mobilize the desired capacity, generally producing a maximum impact force of the same order of magnitude or greater than the ultimate pile capacity (static plus dynamic).”* While being popular worldwide, very limited references are available to the use of the drop weight method in codes and regulations directly applied to the method. One such code is the Chinese specifications for high strain dynamic testing. Paikowsky et al. (2004b) present a translation of the Chinese code. The following section refers to the relevant parts related to the drop weight system specifications of size and shape as previously discussed

7.2 Chinese codes

The drop weight system is the main method authorized for capacity evaluation in the Chinese national and some of the provincial codes for high strain dynamic testing of piles. There are two reasons that can explain this issue; (i) cast-in-place piles are commonly used in China as they are more cost effective than driven piles, and (ii) pile capacities based on dynamic test results are permitted to be used only after a significant set-up period following the end of driving. For example, the duration required for piles driven in sands (!) is 7 to 14 days for the Chinese and Shanghai codes, respectively. As a result, drop weight becomes an economical alternative to a costly crane and pile driving hammer mobilization.
The significance of the Chinese code in relation to the drop weight systems is summarized as following:

a. The code fully recognizes the drop weight system with the major parts being applicable for both tests (dynamic tests on driven piles and cast-in-place piles).
b. The tests are recognized also for pile/shaft integrity purpose.
c. Some provisions refer specifically to cast-in-place shafts (e.g. 5.1.2.3, 5.1.3.3, 5.1.4.2, 6.1.6, 7.1.2.2 and 7.3.1.3 in JGJ106-97 referring to Paikowsky et al., 2004b).
d. The set-up duration between the end of driving and dynamic/drop-weight testing is prescribed clearly based on soil type
e. The drop weight system used for high strain pile dynamic testing requires providing sufficient energy with ensured impact eccentricity. No detailed drop weight system specifications, (such as hammer type, trip mechanism and frame), are provided except the requirement that the hammer weight and shape need to stand by general requirements as given in the following two examples:

Chinese Code (Specification for High Strain Dynamic Testing of Piles, JGJ106-97, section 4.0.3): The hammer should be a homogeneous mass with a symmetric shape, preferably made of steel. The bottom of the hammer should be smooth. For a free falling ram, the weight of the ram need to be greater than 1% of the estimated bearing capacity of the pile.

Shanghai Foundation design code (DGJ-11-1999, section 14.5.3): The hammer is required to assure 2mm set (net settlement) under a single blow and the ram weight should be between 0.8% to ~1.5% of the estimated bearing capacity of the pile.

7.3 European codes

7.3.1 The German code

The German annex to EuroCode7 (EC7), DIN 1054:2010-12 refers to three conditions of dynamic pile testing without differentiation between driven and drilled deep foundations. The conditions are: (1) no static load testing is available, (2) with static load testing at the same site where the dynamic testing is being carried out, and (3) with static load testing on a similar pile in similar soil conditions at a different site. The safety calculations are quite complex and different parameters affect the ability to compare between the static and dynamic testing. In order to simplify the comparison, the typical testing conditions were assured, i.e. single static load test and up to four dynamic load tests while the average of the tests controls. Under these assumptions, if a static and dynamic test were carried out at the same site, the resistance will be 100% of the determined allowed load. When dynamic test is carried out while a static load test is available from another site,

the resistance will be 93%, and if only dynamic tests are carried out, the resistance will be 80%. This ratio continues to increase as the number of tested piles increases.

7.3.2 The Swiss code

The Schweizer Norm SIA267:2012 Bauwesen is interesting as (a) it represents the approach of a relatively small country not affiliated directly with central block like the European Union or USA, and (b) the use of dynamic tests is relatively new. The Swiss code's requirement of expertise in conducting and interpreting dynamic measurements is of utmost importance and seldom if anytime put in this way in any other code. More so, the use of the results depending on the experience of the one performing the tests and the availability of a static load test with the range being between 0.8 for a dynamic test and 1.0 to static test.

8 Recent case history – dynamic vs. static load tests

8.1 Static load tests

Two static load tests and 14 dynamic load tests were carried out at six different bridge locations along a 28km railroad track between Netivot and Beer-Sheva, Israel. The static load tests were performed on 70cm diameter piles, 20m long at bridges A4 and A5 locations. Both tests were carried out to 850 tonnes. The associated pile top displacement of about 8mm, the small tip displacements, and stabilized creep under the measured load suggests the loads to be lower than the ultimate capacities. Extrapolation of the tests results based on a procedure developed and quantified by Paikowsky and Tolosko (1999) shows pile capacities of 1050 and 1250 tonnes for piles A5 and A4, respectively. Figures 43 and 44 present the measured and extrapolated pile top load displacement relations.

8.2 Dynamic load tests

The dynamic load tests carried out on the same piles confirmed the above presented results. The dynamic test on pile A5 was carried out mobilizing the full geotechnical capacity of the pile and resulted with 1022 tonnes. The dynamic test on pile A4 was limited by structural difficulties (between the extension and the pile) and was carried out to a maximum load of 1062 tonnes. The load-displacement relation of both tests matches remarkably well. Figures 45 and 46 present the aforementioned static load test results in comparison with the load-displacement relations developed from the analyses of the dynamic tests. Table 16 summarizes the static and dynamic load test results.

The static load test results were further confirmed by comparison to the pre-test load-displacement simulation suggesting that the measured pile response during the test matches well the expected upper safe zone of possible design. In that regard, it was noticed that the lowest pre-test expected possible pile response was in line with the original pile design values of the bridges. Following the confirmation of the dynamic tests, the additional 12 dynamic tests provided detailed pile capacity evaluations and could be directly applied to safe bridge pile capacity redesign with a recommended Factor of Safety between 2.0 (e.g. utilizing the Israeli Code or UBC - Unified Building Code) to 2.25 (utilizing AASHTO Standard Specifications).

In summary, in spite of difficult site and construction conditions, the static and dynamic tests were extremely successful, providing reliable and consistent values for pile redesign.

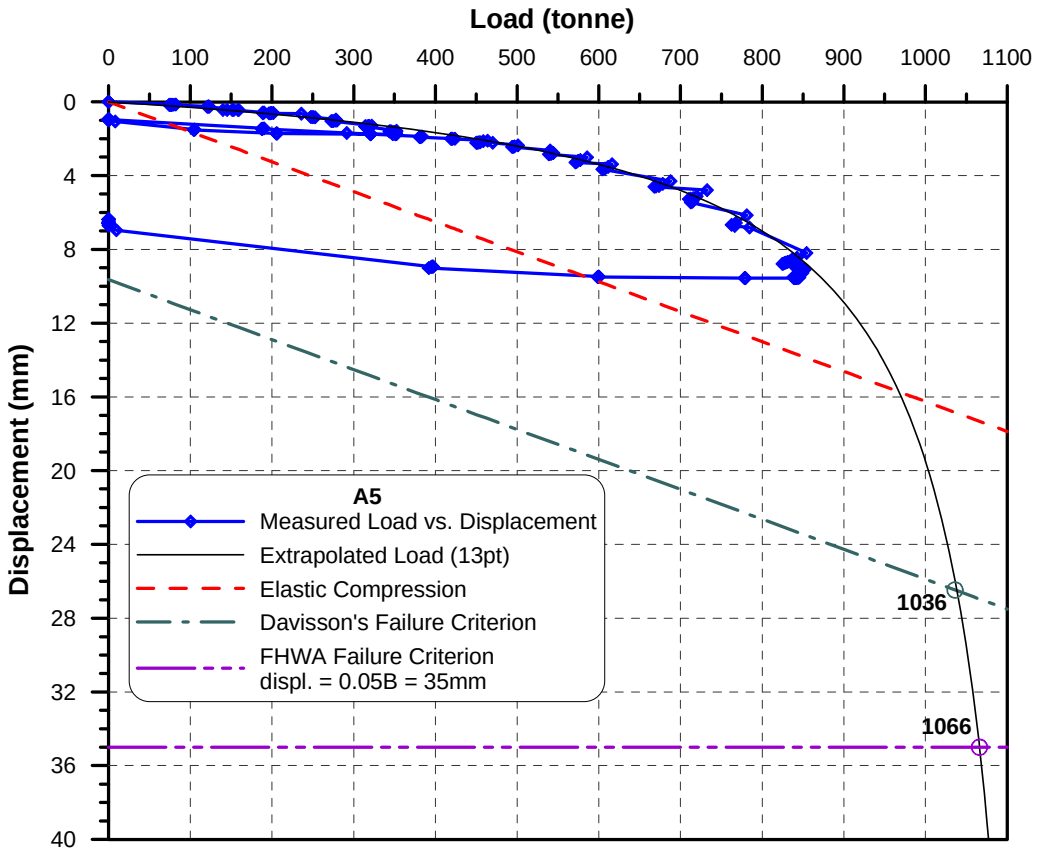


Figure 43: Compression load test A5 along with extrapolated load-displacement relations to failure, Netivot – Beer-Sheva, Israel (GeoDynamica, 2013).

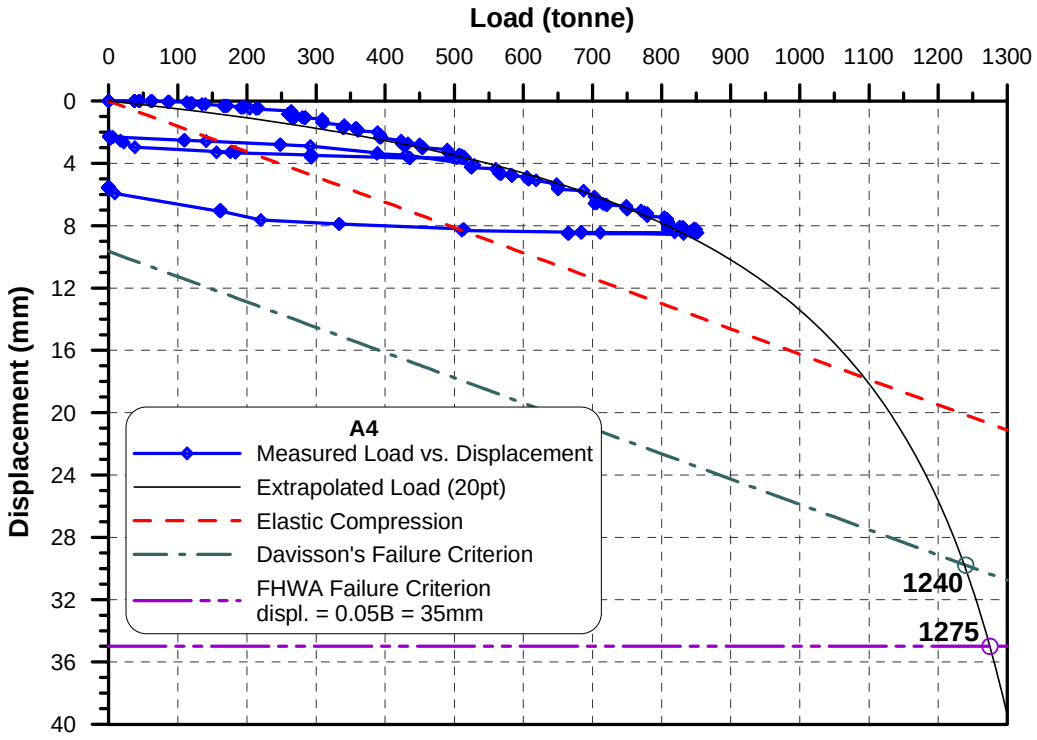


Figure 44: Compression load test A4 along with extrapolated load-displacement relations to failure, Netivot – Beer Sheva, Israel (GeoDynamica 2013).

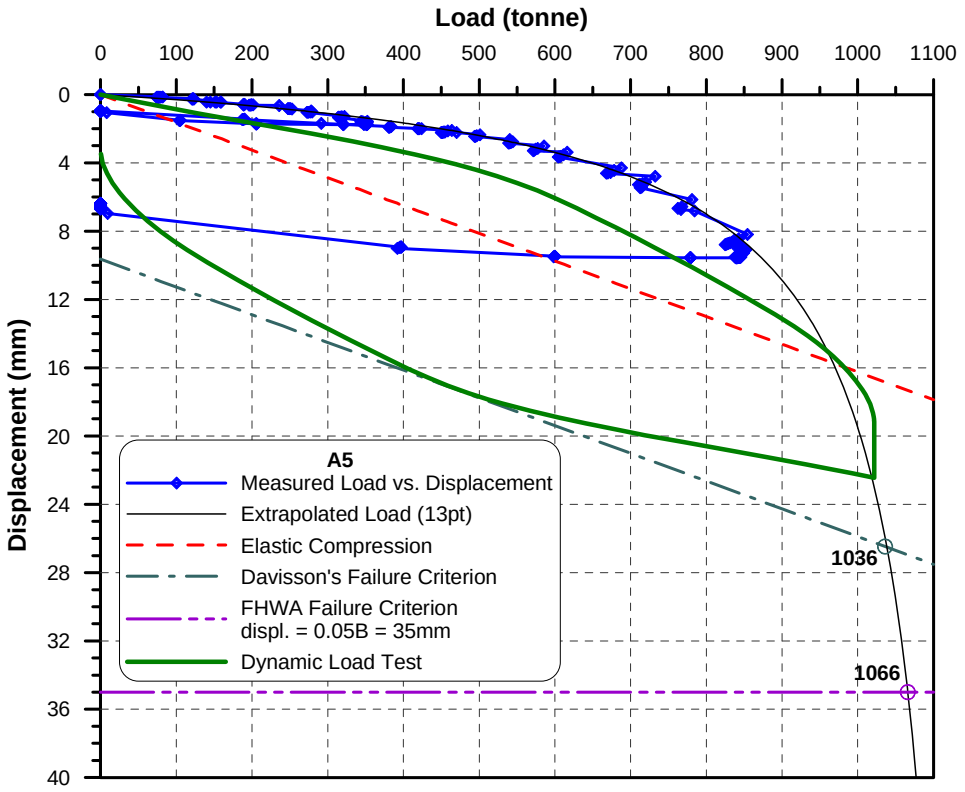


Figure 45: Pile top load-displacement relations obtained during static load test on pile A5-2 and its extrapolation beyond the maximum applied load in comparison with a static load test simulation obtained from signal matching analysis of dynamic load test on the same pile (GeoDynamica 2013).

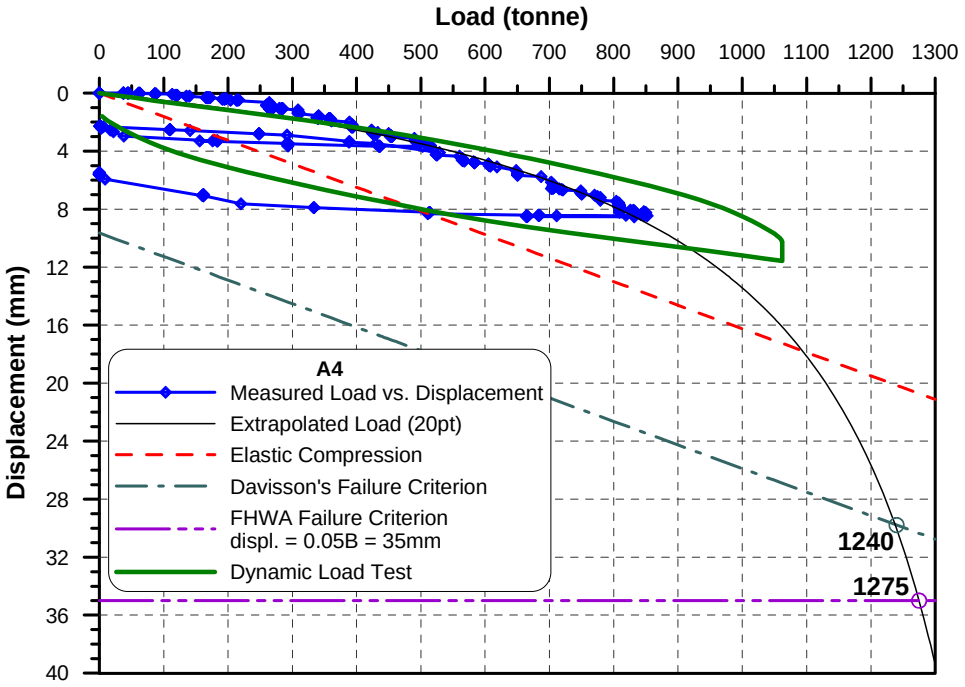


Figure 46: Pile top load-displacement relations obtained during static load test on pile A4-2 and its extrapolation beyond the maximum applied load in comparison with a static load test simulation obtained from signal matching analysis of limited dynamic load test on the same pile (GeoDynamica 2013).

Table 16: Summary of Static and Dynamic Load test Results in Bridge A4 and A5 Locations (GeoDynamica 2013)

Pile	Maximum Static Load Application[1]		Dynamic Load Test[2]		Extrapolated Static Failure[1]		Design Load[1]		Factor of Safety[1]
	Load (tonnes)	Settlement (mm)	Load (tonnes)	Settlement (mm)	Load (tonnes)	Settlement (mm)	Load (tonnes)	Settlement (mm)	
A4	850	8.5	1062[3]	11.3	1250	30.0	425	3.0	3.0
A5	855	9.5	1022	22.0	1050	30.0	425	3.0	2.5

Notes:
1. Data relates to static tests on November 14 and December 12, 2012.
2. Data relates to dynamic testing on the same piles carried out on December 18, 19, and 20, 2012.
3. Maximum mobilized resistance short of ultimate capacity.

9 Summary, conclusions and recommendations

1. The construction methods of drilled deep foundations allow for limited quality control, and hence the structural integrity and the geotechnical capacity are highly variable and uncertain.
2. Dynamic testing is an attractive alternative solution for static load-testing of drilled deep foundations. These need however, to provide wave resolution with depth in order to enable meaningful integrity and soil-pile interaction interpretation based on wave mechanics.
3. The preferable stress wave for drilled foundations dynamic testing for the purpose of integrity and resistance distribution consists of high stress peak short duration signal with a small as possible relative wavelength ($\Lambda<1$). These are obtained by high velocity impact of a longer and narrower ram.
4. The preferable stress wave for dynamic testing for the purpose of maximum capacity mobilization with limiting stress levels consists of lower stress peak and larger signal duration and, hence, a larger wavelength. These are obtained by low velocity heavy rams' impact.
5. Drop-weight systems consist of simple mechanical elements allowing dropping a weight on the top of a deep foundation. Various drop weight set-ups exist with systems of choice encompassing modular weights, variable drop height and better control of ram alignment.
6. Dynamic measurements consist of acceleration and strain measurements on the circumference of the deep foundation element. The calculation of the force signal from the strain measurement assumes the knowledge of the drilled shaft's modulus and cross section as well as uniform stress distribution.
7. Sources for possible difficulties of dynamic measurements on drilled deep foundations include:
    a. Construction problems – non-uniform cross-section, uneven shaft surface and poor quality of concrete in the exterior sections.
    b. Testing problems – low energy and/or low velocity impact, uneven ram impact.
    c. Reaction problems – the development of high friction at the top part of the shaft.
8. The problems associated with the quality and geometry of the foundation can be controlled by the appropriate construction of the shaft's top. The construction of a vertical, uniform and level head shaft extension (possibly in a sleeve) of two-diameter long can also be achieved by an excavation around the shaft.
9. Even ram impact on a striking plate and a cushion creates a symmetric, non-uniform contact stresses at the surface. These stresses become however uniform within a short distance of about one radius from the pile's top. Uneven impacts due to a tilted ram (even with a small inclination of 1°) creates uneven stress wave at the surface that remains uneven at a great distance (of over four diameters) from the pile's top. The use of a soft cushion system attains a more uniform stress distribution with the price of energy loss and a signal of smaller peak stress and higher duration. This difficulty in dynamic measurements can only be solved with the attachment of multi strain gauges (minimum four) around the perimeter at a distance of at least two-diameters from the shaft's top. The use of a ram of a smaller diameter than the shaft itself creates uneven stresses at the surface that become uniform across the shaft within a short distance from the shaft's top (within one diameter).
10. High reaction forces (friction) close to the shaft's top create early reflection waves, which invalidate the proportionality between the measurements of force and velocity (multiplied by the shaft's impedance). This creates two problems: (a) inability to examine independently the force measurements affected by many sources of difficulties, and (b) the need to conduct a very careful signal matching analysis.

11. The ram weight should be larger than 1% of the expected mobilized capacity in the case of frictional shafts or shafts for which more than 2mm permanent set (under the analyzed blow) can be achieved. For end bearing shafts, the ram weight should be larger than 1.5% of the expected mobilized capacity.
12. Drop weight tests to failure (either structural or geotechnical) are best conducted by applying multiple impacts with a gradual increase of the impact energy (height and/or weight). Three to five impacts were experienced to be adequate with the higher number relevant to initial tests in a specific project and the lower number applied to subsequent tests under similar conditions.
13. The comparison between capacity predictions of drilled deep foundations based on dynamic measurements and signal matching analysis and static load tests had resulted in excellent agreement. The ratio of measured to calculated capacity (based on the FHWA failure criterion) was found to be 1.05±0.12 (1 S.D.) for 39 cases. This ratio can be compared to that obtained for driven piles in restrike analyzed by signal matching analysis. For 162 piles, this ratio was found to be 1.16±0.39 (1 S.D.). Both ratios well exceed the typical accuracy of static analyses of drilled shafts, which varies between 0.90 to 1.71 and coefficients of variation between 0.30 to 0.60.

10 Acknowledgement

Most of the presented research was sponsored by the American Association of State Highway and Transportation Officials (AASHTO) under project NCHRP 21-08 conducted by the author and awarded to Geosciences Testing and Research, Inc. (GTR) of North Chelmsford, Massachusetts. At the time, the author was the president of GTR and currently is with GeoDynamica, Inc. of Newton, Massachusetts. The opinions and conclusions expressed or implied in this paper are those of the research agency and not necessarily those of the Transportation Research Board (TRB), the National Research Council (NRC), the Federal Highway Administration (FHWA) or AASHTO.

The collection and analysis of database DW/LT2000 was conducted under a contract with the Geotechnical Engineering Research Laboratory of the University of Massachusetts Lowell by the graduate students Mr. Frank Li, and Ms. Erin Griffin. Mr. Li is also acknowledged for his contributions to data collected from tests carried out in China as well as the translation of Chinese codes. Mr. Timothy Mustone, Ms. Jennifer Gorczyca and in particular Ms. Ching-Pei Liang of the Mechanical Engineering department at the University of Massachusetts Lowell performed the FEM analysis LS DYNA under the direction of Professor James Sherwood and the author. The help and dedication of Ms. Mary Canniff in the preparation of this manuscript is appreciated. The Swiss Geotechnical Society and Mr. Laurent Pitteloud of Gruner are acknowledged for their invitation and support of the presentation.

11 References

[1] ASTM D4945-12, (2012). "Standard Test Method for High-Strain Dynamic Testing of Deep Foundations," Annual Book of Standards, Section Four Construction. ASTM, Vol. 04.08, West Conshohocken, PA.

[2] Bermingham, P. and Janes, M. (1990). "Statnamic test. An innovative method for testing deep foundations", Proceedings of the Annual Conference and the First Biennial Environmental Speciality Conference, May 16-18, Hamilton, Ontario, Canada, vol. 2, part 2, Canadian Society for Civil Engineering, Montreal, Quebec, Canada, p. 590.

[3] Boussinesq, J. (1883). Compt. Rend. vol. 114, p. 1465, by Flamant, Paris.

[4] Brown, D.A., Turner, J.P., and Castelli, R.J. (2010). "Drilled Shafts: Construction Procedures and LRFD Design Methods NHI Course No. 132014, Geotechnical Engineering Circular No. 10", FHWA Report no. FHWA-NHI-10-016, Washington, DC, pp.970.

[5] Butler, H.D., and Hoy, H.E. (1977). Users Manual for the Texas Quick-Load Method for Foundation Load Testing. FHWA Office of Development, Washington, DC, Report No. FHWA-IP-77-8, pp.59.

[6] Camp, W.M., Brown, D.A., and Mayne, P.W. (2002). "Construction Method Effects on Axial Drilled Shaft Performance", ASCE Geotechnical Special Publication, no. 116, vol. I, pp. 193-208.

[7] Chernauskas, L.R. and Paikowsky, S.G. (1999). "Deep Foundation Integrity Testing Techniques and Case Histories", Civil Engineering Practice, Journal of the BSCE section/ASCE, Spring/Summer 1999, pp. 39-56.

[8] DeBeer, E.E. (1970). “Proefondervindellijke bijdrage tot de studie van het grandsdraagvermogen van zand onder funderinger op staal.” English version, Geotechnique, Vol. 20 No. 4, pp. 387-411.

[9] Davisson, M.T. (1972). “High Capacity Piles,” Proceedings, Soil Mechanics Lecture Series on Innovations in Foundation Construction. ASCE, Illinois Section, Chicago, IL, March 22, pp. 81-112.

[10] DIN 1054:2012-12. (2012). *Subsoil - Verification of the safety of earthworks and foundations - Supplementary rules to DIN EN 1997-1*, German Anex to Eurocode7, Bueth-Verlag, Berlin.

[11] Frederick, L. (1996). SMARTPILE System Promotional Material, Frederick Engineering, Whippany, New Jersey.

[12] GeoDynamica, Inc. (2012). “Dynamic Pile Test Report”, final project report for Kefar Sabba Mall and High-Rise Foundation Testing, February 2012.

[13] Goble, G.G., Likins, G., and Rausche, F. (1970). Dynamic Studies on the Bearing Capacity of Piles Phase III, Report No. 48, Division of Solid Mechanics, Structures and Mechanical Design, Case Western Reserve University.

[14] Goble, G.G., Likins, G., and Rausche, F. (1975). Bearing Capacity of Piles from Dynamic Measurements – Final Report, Case Western Reserve University, Cleveland, Ohio, ODOT Report No. Ohio-DOT-05-75.

[15] Goble, G.G., Rausche, F., and Likins, G. (1993). “Dynamic Capacity Testing of Drilled Shafts”, Foundation Drilling, ADSC Foundation Drilling, Dallas, Texas, September/October.

[16] Gonin, H., Coelus, G., and Leonard, M.S.M. (1984). "Theory and performance of a new dynamic method of pile testing", Proceedings, Second International Conference on the Application of Stress-Wave Theory to Piles, G. Holm, H. Bredenberg, and C-J. Gravare eds, Stockholm, Sweden, May 27-30, A.A. Balkema, Rotterdam the Netherlands, pp. 403-410.

[17] GTR (1997) "Dynamic Pile Testing Report - Israel Electric Company, Haifa, Israel", Final Report, Project 97.118, Geosciences Testing and Research, North Chelmsford, Massachusetts.

[18] Hajduk, E., Paikowsky, S., Holscher, P., and Barends, F. (2000). Accelerations of a Driven Pile and the Surrounding Soil. Proceedings, 6th International Conference on the Applications of Stress-Wave Theory to Piles, September 11-13, 2000. Sãn Paulo City, Brazil, Balkema, Rotterdam-the Netherlands, pp. 541-548.

[19] Hajduk, E.L., Paikowsky, S.P., Mullins, A.G., Ealy, C.D., Lewis, C. and Hourani, N.M. (1998). “The Behavior of Piles in Clay during Statnamic and Different Static Load Testing Procedures”, Proceedings, 2nd International Statnamic Seminar, Tokyo, Japan, October 28-30.

[20] Holeyman, A.E. (1992). "Technology of Pile Dynamic Testing", Proceedings, Fourth International Conference on the Application of Stress-Wave Theory to Piles, F.B.J. Barends ed., The Hague, the Netherlands, September 21-24, Balkema, Rotterdam the Netherlands, pp.195-215.

[21] Hussein, M., Robinson, B., and Likins, G. (2004). “Applications of a Simplified Dynamic Load Testing Method for Cast-In-Place Piles”, GeoSupport 2004 Drilled Shafts, Micropiling, Deep Mixing, Remedial Methods, and Specialty Foundation Systems, J.P. Turner and P.W. Mayne eds., ASCE Geotechnical Special Publication No. 124, pp. 110-121.

[22] Irvine, M. (1986). Structural Dynamics, for Practicing Engineers, Allen & Unwin, Ltd., London.

[23] Jianren, D., and Shihong, Z. (1992). "The appraisal of results from PDA high strain dynamic tests on large and long drilled piles." Proceedings, Fourth International Conference on the Application of Stress-Wave Theory to Piles, F.B.J. Barends ed., The Hague, the Netherlands, September 21-24, Balkema, Rotterdam the Netherlands, pp.271-278.

[24] McVay, M.C., Putcha, S., Consolazio, G., and Alvarez, V. (2004) “Development of a Wireless Monitoring System for Pile Driving”, presentation at the 83rd Annual TRB Meeting, January 11-15, TRB, Washington, DC, paper ID 04-3478, 19pgs.

[25] Middendorp, P., and van Weel, P.J. (1986). “Application of Characteristic Stress Wave Method in Offshore Practice.” Proceedings, 3rd International Conference on Numerical Methods in Offshore Piling. Nantes, France, May 21-22, Editions Technip, Paris.

[26] Osterberg, J. (1989). "New device for load testing driven piles and drilled shafts separates friction and end bearing." Proceedings, Third International Conference on Piling and Deep Foundations, J. Mitchell and J. Burland eds, London, Deep Foundations Institute, New Jersey, pp. 421- 427.

[27] O’Neill and Reese. (1999). Drilled Shafts: Construction Procedures and Design Methods, Volume II Chapters 9-19, Appendices. U.S. DOT, FHWA, Washington, DC.

[28] O’Neill, M., Townsend, F., Hassan, K., Buller, A., and Chang, P. (1996). Load Transfer for Drilled Shafts in Intermediate Geomaterials, FHWA-RD-95-172, FHWA.

[29] Paikowsky, S.G. (1982). Use of Dynamic Measurements to Predict Pile Capacity Under Local Conditions. M.Sc. Thesis, Department of Civil Engineering, Technion-Israel Institute of Technology.

[30] Paikowsky, S.G. with contributions by Birgission G., McVay M., Nguyen T., Kuo C., Baecher G., Ayyub B., Stenerson K., O'Mally K., Chernauskas L., and O'Neill M. (2004a). "Load and Resistance Factor Design (LRFD) for Deep Foundations", NCHRP Report 507, National Cooperative Highway Research Program report for Project NCHRP 24-17, pp. 134 (not including Appendices).

[31] Paikowsky, S.G. with contributions by Brown, D.A., Shi, L., Operstein, L., Mullins, G., Li, Z., Gorczyca, J.L., and Chernauskas, L. (2004b). "Innovative Load Testing Systems", Final Research Report submitted to the National Cooperative Highway Research Program on Project NCHRP 21-08.

[32] Paikowsky S.G., and Chen Y.L. (1998). "Field and Laboratory Study of the Physical Characteristics and Engineering Parameters of the Subsurface in the Newbury Bridge Site". Research Report submitted to the Massachusetts Highway Department, January.

[33] Paikowsky, S.G., and Chernauskas, L.R. (2003). "Review of Deep Foundations Integrity Testing - Methods And Case Histories" 2003 BSCES-Geo-Institute Deep Foundation Seminar, Boston November 15, p1-p.30.

[34] Paikowsky, S.G., and Hajduk, E.L. (1999). "Design and Construction of an Instrumented Test Pile Cluster", Research Report submitted to the Massachusetts Highway Department, Geotechnical Research Laboratory, University of Massachusetts-Lowell, Lowell, Massachusetts.

[35] Paikowsky, S.G., and Hajduk, E.L. (2004). "Design and Construction of Three Instrumented Test Piles to Examine Time Dependent Pile Capacity Gain", to be published in ASTM Geotechnical Testing Journal, November 2004.

[36] Paikowsky, S.G., Klar, I., and Chernauskas, L.R. (2004c). "Performance Evaluation of CFA vs. Bentonite Slurry Drilled Shafts Utilizing Drop Weight Testing", ASCE Geotechnical Special Publication no. 124, Geo-Support 2004: Drilled Shafts, Micropiling, Deep Mixing, Remedial Methods, and Specialty Foundation Systems, eds. J.P. Turner and P.W. Mayne, Orlando, Florida, January 29-31, 2004, pp. 637-652.

[37] Paikowsky, S.G., Operstein, V., and Bachand, M. (1999). Express Method of Pile Testing by Static-Cyclic Load. Research Report submitted to the Massachusetts Highway Department, Geotechnical Research Laboratory, University of Massachusetts-Lowell, Lowell, Massachusetts.

[38] Paikowsky, S.G., Regan, J.E., and McDonnell, J.J. (1994). A Simplified Field Method for Capacity Evaluation of Driven Piles. Final Report Publication No. FHWA-RD-94-042, FHWA, Washington, DC, pp.313.

[39] Paikowsky, S.G., and Stenersen, K.L. (2000). "The Performance of the Dynamic Methods, their Controlling Parameters and Deep Foundation Specifications", Key-Note lecture, Proceedings of the 6th International Conference on the Application of Stress-Wave Theory to Piles, S. Niyama and J. Beim eds, September 11-13, São Paulo, Brazil, Balkema, Rotterdam-the Netherlands, pp. 281-304.

[40] Paikowsky, S.G. and Tolosko, T.A. (1999). *Extrapolation of Pile Capacity from Non-failed Load Test*, FHWA publication number FHWA-RD-99-170, December 1999, 169pp (HNR publication).

[41] Paikowsky, S.G., and Whitman, R.V. (1990). "The Effects of Plugging on Pile Performance and Design", Canadian Geotechnical Journal, August, Vol. 27, No. 4, pp. 429-440.

[42] Parola, J. F. (1970). Mechanics of Impact Pile Driving, Ph.D. Dissertation, University of Illinois at Urbana-Champaign, 252 pp.

[43] Rausche, F. (1970). "Soil Response from Dynamic Analysis and Measurements on Piles", Ph.D. Dissertation, Division of Solid Mechanics, Structures and Mechanical Design, Case Institute of Technology (Case Western Reserve University), Cleveland, Ohio.

[44] Rausche, F., and Seidel, J. (1984). "Design and performance of dynamic tests of large diameter drilled shafts", Proceedings, Second International Conference on the Application of Stress-Wave Theory to Piles, G. Holm, H. Bredenberg, and C-J. Gravare eds, Stockholm, Sweden, May 27-30, A.A. Balkema, Rotterdam the Netherlands, pp. 9-16.

[45] Reese, L. C., and O'Neill M. W. (1988). Drilled Shaft: Construction Procedures and Design Methods. FHWA-HI-88-042, FHWA.

[46] Schellingerhout, A.J.G., and Revoort, E. (1996). "Pseudo Static Load Tester", Proceedings, Fifth International Conference on the Application of Stress-Wave Theory to Piles, F.C. Townsend, M. Hussein, and M. McVay eds, Orlando, Florida, September 11-13, pp. 1031-1037.

[47] Schweizer Norm SIA 267:2012 Bauwesen. (2012). Swiss Geotechnical Code, 2012 (German).

[48] Smith, E.A.L. (1960). "Pile-Driving Analysis by the Wave Equation", Journal of Soil Mechanics and Foundations. American Society of Civil Engineers, August 1960, pp. 35-61.

[49] Terzaghi, K. (1942). "Discussions of the Progress Report of the Committee on the Bearing Value of Pile Foundations," Proceedings, ASCE, Vol. 68, pp. 311-323.

[50] Timonshenko, S.P., and Goodier, J.N. (1934). Theory of Elasticity, McGraw -Hill Book Company, Inc., New York.

[51] Townsend, F., Theos, J.F., Sheilds, M.D. (1991). "Dynamic Load Testing of Drilled Shaft - Final Report." University of Florida, Department of Civil Engineering, Gainesville, Florida.
[52] Van Kotten, (1977). Dynamic Pile Testing. Inst. TNO for Building Materials and Building Structures, Report, January, the Netherlands.

Author:

Samuel G. Paikowsky
Professor, Geotechnical Engineering Research Laboratory, Civil & Environ. Engineering Dept., University of Massachusetts Lowell, USA, Samuel_Paikowsky@uml.edu
President, GeoDynamica, Inc., Newton, MA USA, Sam@GeoDynamica.com

IMPLANT FOUNDATIONS – PRESS-IN PILING METHOD FOR URBAN CONSTRUCTION

Tsunenobu Nozaki: General Manager, Giken Ltd.
1-3-28 Ariake, Koto-ku, Tokyo, 135-0063 Japan
Tel: +81(0)3-3528-1633
E-mail: nozaki@giken.com
Key Words: *Press-in Method, sheet pile, embedded retaining wall, noise and vibration-free*

Abstracts

Basically, the "Press-in Piling Method" was invented to eliminate construction nuisances, such as noise and vibration which have been serious unsolved problems for advancing societies over a long time. In the construction industry, piling works have been a major cause of noise and vibration, because most piling methods utilize dynamic load to install piles into the ground. The secret of the Press-in Piling Method is to utilize static loading to install pre-formed piles rather than dynamic load. The piles are hydraulically gripped and jacked into the ground by the special piling rig known as the "Silent Piler". Therefore, the piles can form a robust and firm foundation, which is another advantage of the Press-in Piling Method.

The Press-in Piling Mechanism and Implant Foundations

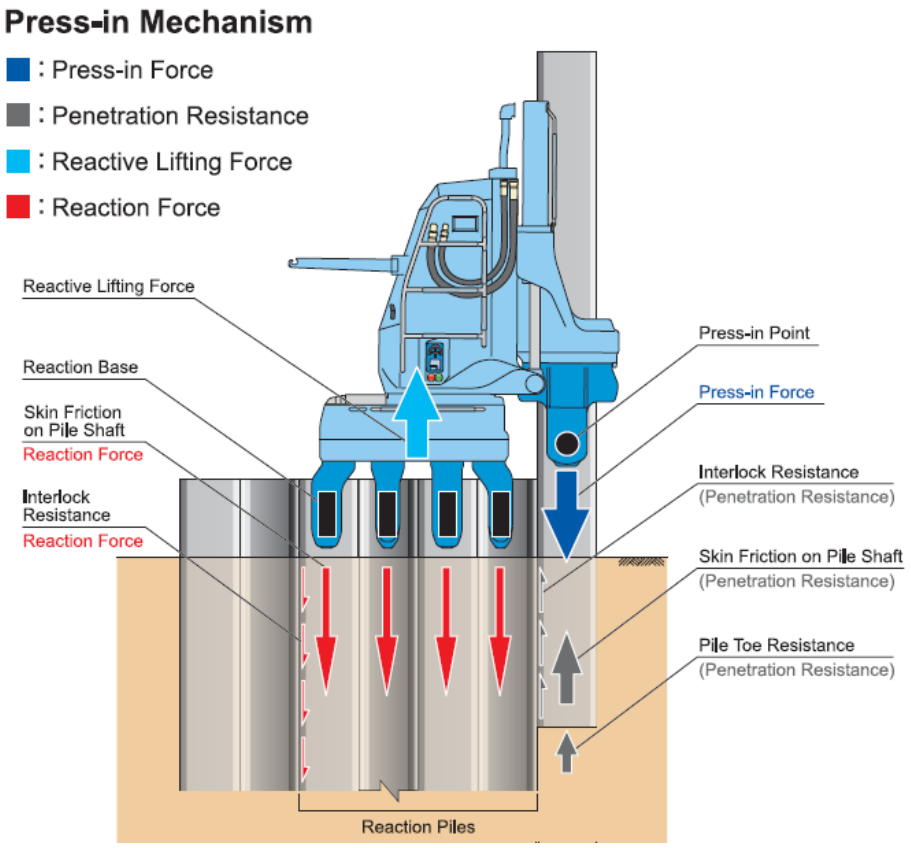


Figure 1: Press-in Piling Mechanism

The basis of the Press-in Piling Method is simple. The Pres-in Piling Machine installs a preformed displacement pile into the ground by static jacking force. The reaction for the Press-in Force is generated by gripping previously installed piles, which are called “Reaction Piles”. Due to this, the Press-in Piling Machine can produce a powerful piling force whilst only requiring minimal machine size.

With the Press-in Piling Method, as piles are pressed into the ground, they are incorporated with the surrounding soils, which provides a large bearing capacity and passive horizontal resistance. These embedded foundations which are firmly anchored into the ground are known as “Implant Foundations”. Being embedded into the ground, the foundations are resilient and maintain their serviceability even in the worst credible design conditions.

Noise Level of the Press-in Method

In British Standard, BS5228, acceptable noise limit is specified as 70dB in urban areas as represented by the red dashed line in the following graph. (Figure 2)

The Press-in Piling Method installs preformed piles with static load, and the only noise source is an engine driven power unit. Therefore, the noise from the Press-in Method is a “steady noise”, whilst other dynamic piling methods generate “highly impulsive noise”, which is less acceptable than steady noise. Furthermore, the noise level of the Press-in Piling Method is much lower than those of the dynamic piling methods and almost never exceeds the noise limit of 70dB.

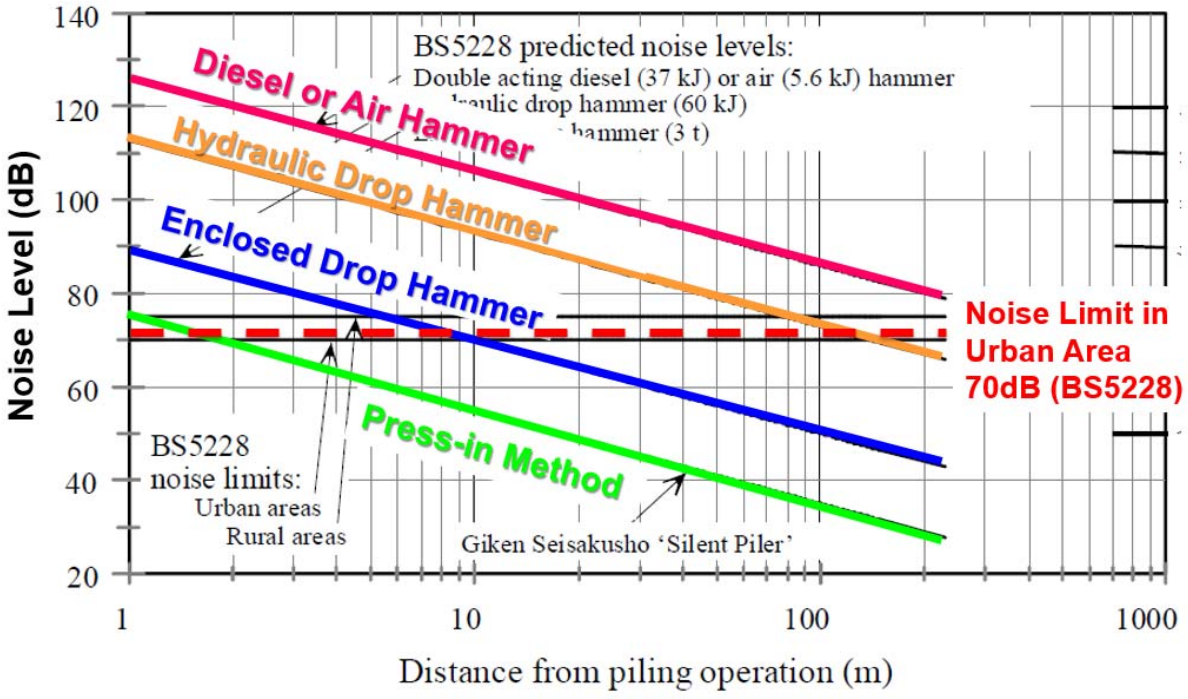


Figure 2: Typical Noise Level of Various Piling Methods

Vibration Level of the Press-in Method

Vibration can cause disturbance to processes and activities in neighbouring buildings, and in certain circumstances can cause or contribute to building damage. Also, vibration can be the cause of serious disturbance and inconvenience to anyone exposed to it. Under Eurocode 3, peak particle velocity at 5mm/s is the maximum acceptable level in residential areas.

The Press-in Piling Method is a hydraulic jack-in method for the installation of preformed piles. Hence, the Press-in Piling Method does not generate vibration greater than 5mm/s, whilst other dynamic piling methods could not achieve this vibration level at close quarters.

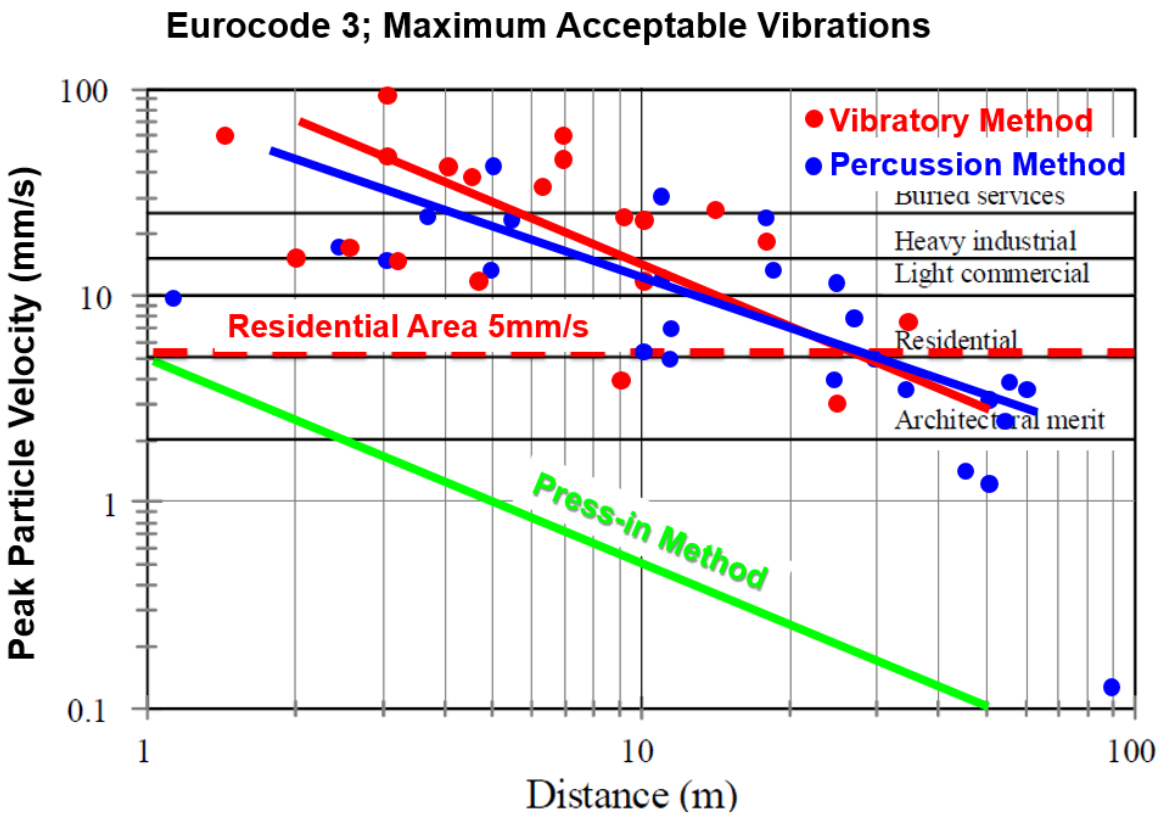


Figure 3: Typical Vibration Level of Various Piling Methods

Ground Displacement

Due to the avoidance of dynamic loading during pile installation, the Press-in Piling Method can minimise ground displacement, which relates to the pile installation. The main factor in ground displacement in Press-in Piling is a down drag force due to the pile installation. However, this Press-in Piling Method minimises the down drag force with a push and pull procedure. The frequency of the push and pull procedure is determined by the soil conditions and type of piles.

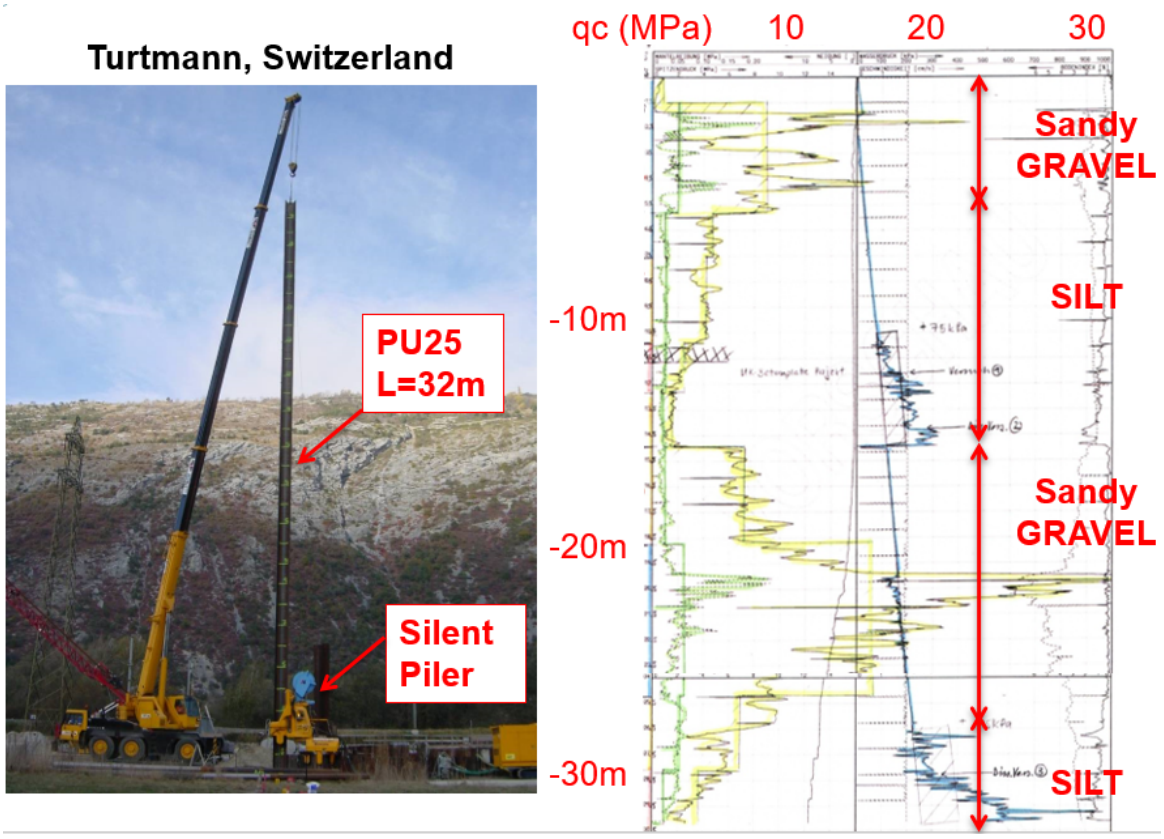


Figure 4: Pile Installation and Soil Conditions (CPT Test Results)

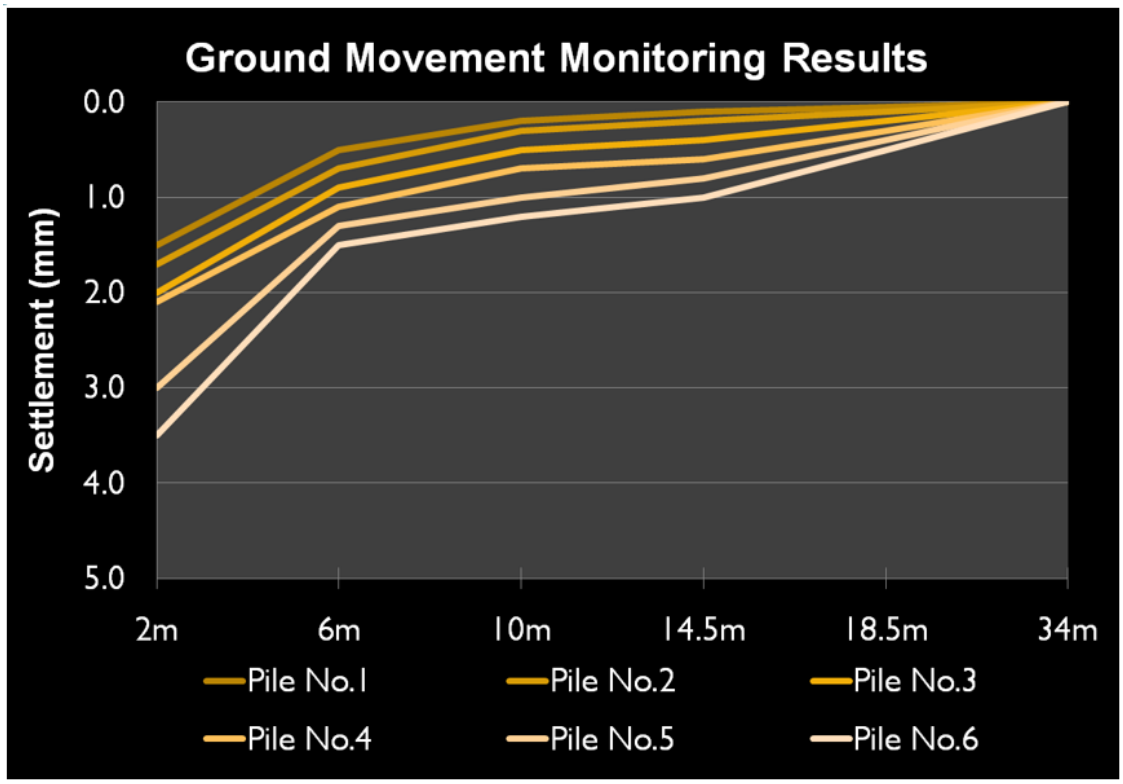
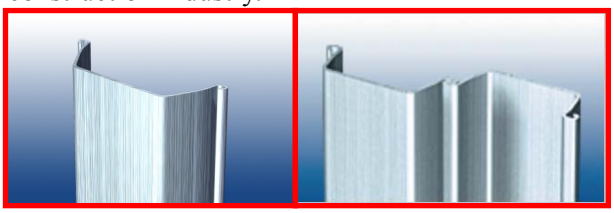


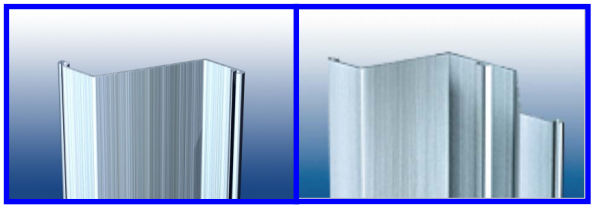
Figure 5: Ground Settlement vs Distance from Pile Installation

Applicable Pile Profile

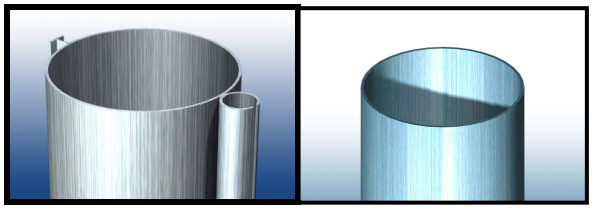
The Press-in Method is applicable to most of the steel piles available on global market i.e. U sheet pile in single form and pair, Z sheet pile, also in single and pair and Tubular Pile as described in Figure 2. Wall thickness of those piles can be 0.3m to 2.5m and moment of inertia of the wall ranges up to about nine million biquadratic cm per meter, which can deliver similar elastic modulus EI (kNm^2/m) to 2.0m thick diaphragm walls and can be utilised for extremely deep excavations required in today's construction industry.



U Sheet Pile



Z Sheet Pile



Tubular Pile

Figure 6: Applicable Pile Profile for Press-in Method

Applicable Pile Depth and Ground Conditions

There are four penetration modes available for the Press-in Method depending on pile depth and ground conditions, which enables piles to be installed into a range of ground conditions, from very loose/ soft ground to very hard ground such as peat in a bog and less weathered rock.

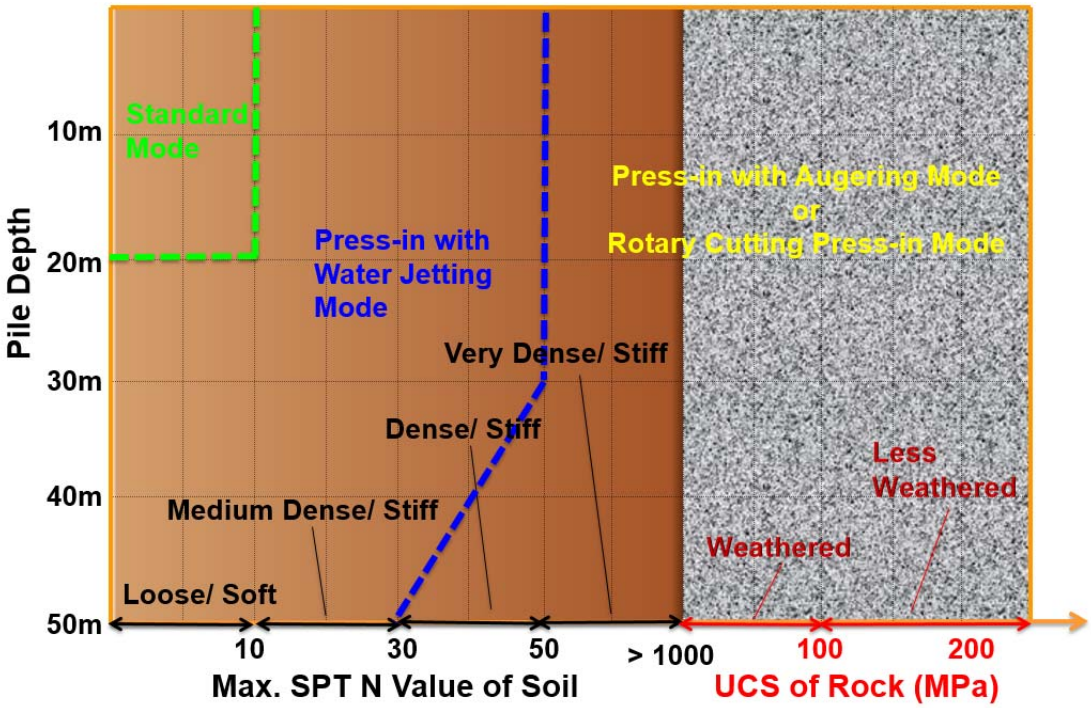


Figure 7 Applicable Pile Depth and Ground Conditions (Steel Tubular Pile)

Various Pile Penetration Modes

- Standard Mode installs a pile vertically by static jacking force alone and is applicable to loose/ soft ground conditions.

- Press-in with Water Jetting Mode uses auxiliary water jetting system in addition to the Standard Mode and is applicable to from medium to very dense/ stiff ground conditions.

  During the operation, high pressure water jetting prevents generation of the pressure bulb by temporarily and locally loosening granular soil and/or softening cohesive soil. Simultaneously, the returning water lubricates the pile surface and the interior of the interlocks, reducing their friction. Both the water pressure and the water flow can be regulated in accordance with the density/ stiffness of the ground to minimise ground movement. Typical water flow rates are shown in the table below:-

Ground Condition	Water Pressure	Water Volume
Medium Dense/ Stiff	2.5-5MPa	50-100L per minute
Dense/ Stiff	5-10MPa	100-200L per minute
Very Dense/ Stiff	10-15MPa	200-350L per minute

Table 1: Typical Flow Rate of Water Jetting

- Press-in with Augering Mode installs a pile with simultaneous augering and can be applied to significantly hard ground such as cobble or boulder mixed ground, and rock. Gripping the auger casing along with a set of press-in piles, hard soil just below the pile toe is loosened by the auger. Effective reduction of toe resistance allows the pile to be installed with minimum ground disturbance and spoil from the augering.

- Rotary Cutting Press-in Mode - rotary jacking - is a newly-developed approach that is a combination of axial penetration and twisting of the pile. This mode is only applicable to a steel tubular pile. The tubular pile with drilling bits on its toe can be installed by the Press-in Piling Machine into significantly harder ground such as less weathered rock.



Figure 8: Various Penetration Methods

Drivability and Applicable Length of Pile

During the pile installation, the Press-in force is directly transmitted to the pile and generates internal stress of the pile. During the process, the stress level needs to be maintained lower than the allowable stress level and the applicable axial press-in force is governed by elastic section modulus and steel grade of the pile. The general guidelines of the applicable pile length for Press-in Method are described below.

Profile / Pile Form / Method	U-Profile	Z-Profile
Single Pile / Standard	L = { Z (cm^3/m) / 100 } × 0.65, ≤ 25 m	L = { Z (cm^3/m) / 100 } × 0.45, ≤ 20 m
Single Pile / Augering	L = { Z (cm^3/m) / 100 } × 0.85, ≤ 25 m	L = { Z (cm^3/m) / 100 } × 0.50, ≤ 20 m
Double Pile / Standard	L = { Z (cm^3/m) / 100 } × 0.70, ≤ 25 m	L = { Z (cm^3/m) / 100 } × 0.65, ≤ 25 m
Double Pile / Augering	——	L = { Z (cm^3/m) / 100 } × 0.85, ≤ 25 m

Z: Elastic Section Modulus (cm3/m)

Table 2: Applicable Pile Length

Pile length / Area	0 ~ 15 m	15 ~ 25 m	25 m ~
Europe (EN10248)	S270GP	S355GP	S460GP
USA (ASTM)	A328	A572Gr.50	A572Gr.65
Japan (JIS)	SY295	SY390	-

Table 3: Recommended Steel Grade

Implant Foundation - Resilient Embedded Foundation by Press-in Piling Method

Implant Foundation is a permanent structural foundation which consists of pre-formed structural elements (mostly, prefabricated piles described in Figure 6) and installed into the ground using the Press-in Piling Method. As structural elements, various pre-formed piles and even composite piles are used to form embedded permanent foundations by combining with steel and RC etc. Whilst traditional footing foundations require “cut and cover processes”, the Implant Foundations can directly be embedded into the ground in one-step, and the area of the construction activities can be minimised and are neither affected by the variations in water level nor any seasonal restrictions. Hence, the total construction period and cost can be remarkably reduced. Also, during the installation stage, horizontal and vertical load capacities are monitored by the Press-in Machine, which ensures the serviceability of the structure.

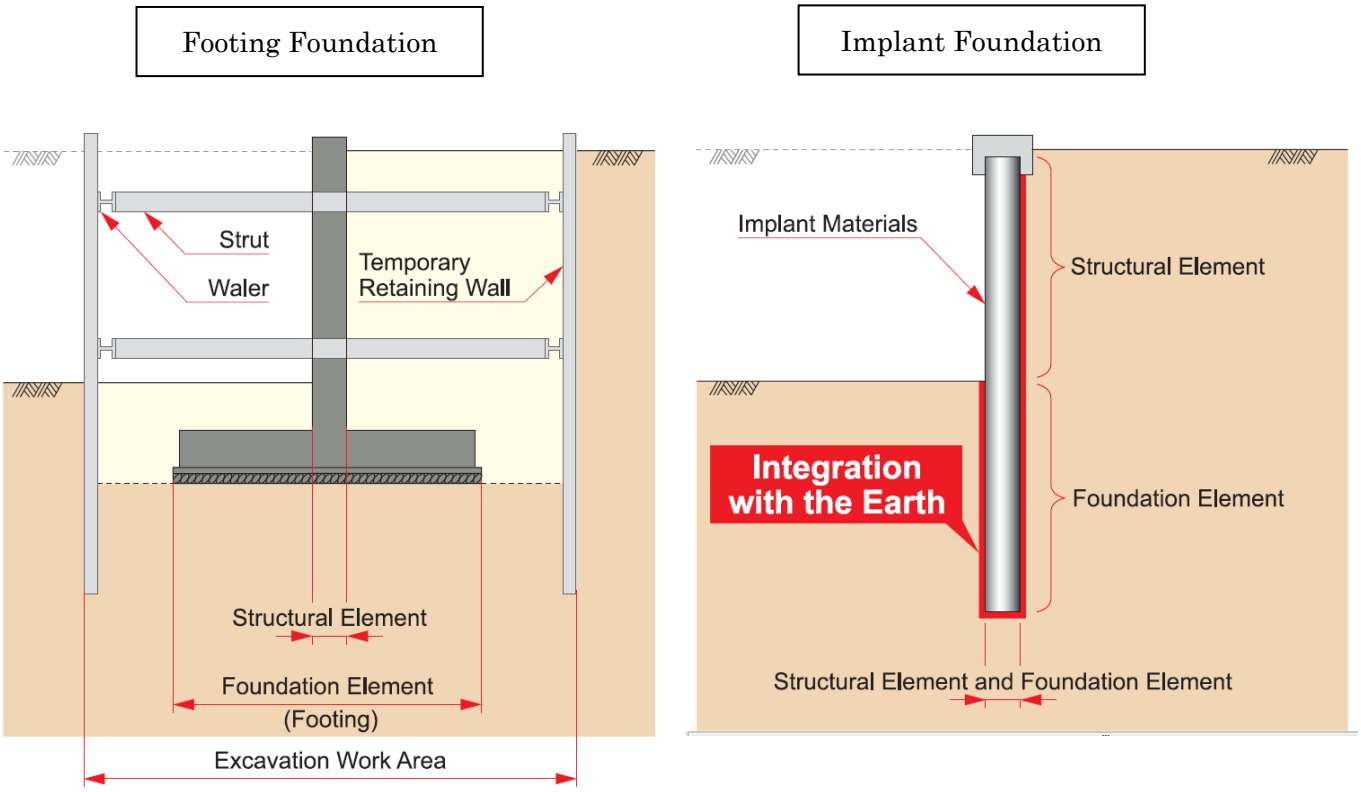


Figure 9: General Cross Section of "Footing Foundation" and "Implant Foundation"

Case Studies

- U Sheet Piles for Basement Wall



Figure 10: Post Installation



Figure 11: Completed Basement

- Z Sheet Piles for Road Retaining Wall



Figure 12: Pile Installation



Figure 13: Completion

- Tubular Piles for Train Station Box



Figure 14: Pile Installation



Figure 15: Post Excavation

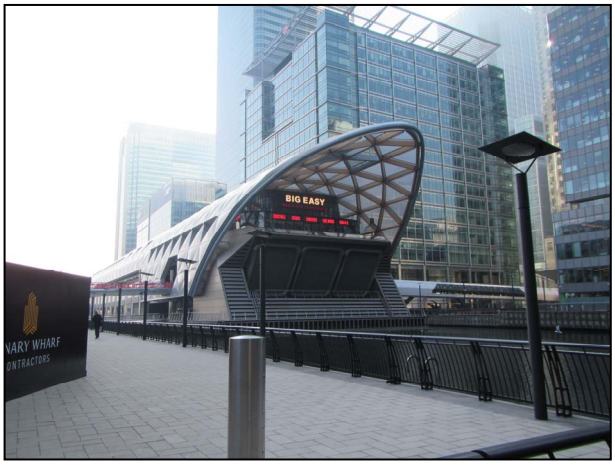


Figure 16: Completion

Summary

The Press-in Piling Method is firstly recognized as an “environmentally friendly piling method”, because it virtually eliminates construction nuisances, such as noise, vibration and ground displacement. In addition, the method can be used in difficult ground conditions e.g. extremely soft ground or extremely hard ground, in which traditional piling methods are not generally considered.

Also, most of the preformed piles available on the global market are applicable to the Pres-in Method. Therefore, the Press-in Method can construct from shallow to deep foundations with a variety of piles depending on the situation. These embedded foundations are also known as “Implant Foundations” because they are robust and resilient against dynamic loads, compared to footing type gravity foundations.

BEHAVIOR OF A PILED RAFT IN DRY COHESIONLESS SOIL SUBJECTED TO LATERAL LOADING

Srijit Bandyopadhyay, Scientific Officer, Bhabha Atomic Research Center, Mumbai, Maharashtra, India, 02225593548, srijit15@gmail.com
Raj Banerjee, Scientific Officer, Bhabha Atomic Research Center, Mumbai, Maharashtra, India, 02225593548, banerjeeraj1990@rediffmail.com
Aniruddha Sengupta, Professor, Indian Institute of Technology, Kharagpur, West Bengal, India, 03222283454, sengupta@civil.iitkgp.ernet.in
G.R.Reddy, Outstanding Scientist, Bhabha Atomic Research Center, Mumbai, Maharashtra, India, 02225595181, rssred@barc.gov.in

ABSTRACT

The objective of the present endeavor is to compare the performance of a pile raft system in foundation sand subjected to lateral loads. To study the behavior of pile raft system in sand a laboratory test was conducted on small scale model foundation system. The raft and pile was modeled by square concrete foundation of 250 mm x 250 mm x 15 mm in length, breadth and thickness and 25mm diameter and 250mm long circular pile located at the center of the raft. The system was tested under static lateral loads of 6.25N, 12.5N, 18.75N and 25 N respectively resting on dry Kasai River sand. A vertical surcharge pressure of 1.5kPa (10 kg) was applied on top of the model raft for each case. The results of the model tests have been simulated by a general purpose 3-D finite element software and the model has been validated with experimental results. The moments of the pile obtained from the model tests and those predicted by the numerical analyses for all the lateral loads matches reasonably well. For matching the trend of bending moments obtained from experiments, validation with theoretical results have been done with the help of Matlock and Reese (1960) approach for a single value of lateral loading. Moreover, a parametric study has been conducted with 5mX5mX0.3m raft size with 0.5m diameter and 5 meter long pile with increasing number of piles namely 2, 5 and 9 respectively to study the response in terms of moment and lateral deformation under available earthquake loadings, like Loma Prieta (1989) and Darfield Christchurch (2010). Bending moments of piles and load deformation curves for lateral loading have been studied for each case in which it is observed that the bending moments of pile significantly reduces (around 4 times) as the number of pile is increased to two, but it decreases to a nearly constant value (it saturates) as the number of pile is increased to five and nine. Moreover, the lateral deformation of piled raft system drastically reduces (around 2.4 times) for two pile system, and it saturates to a constant value with five and nine pile system. All these results indicate the constancy of stiffness irrespective of the number of piles in the piled raft.

Keywords: Pile raft system; Small scale model test.

INTRODUCTION

Pile foundation is being used in the practice for many years to transmit the superstructure load to the competent foundation at a depth. Structures like high rise buildings, bridges, chimneys, nuclear power reactors and offshore jetties/rigs are generally subjected to heavy lateral load due to wind forces, water forces, earthquake forces, etc. Shallow foundations are not good in carrying high lateral loads and under those circumstances pile foundation is utilized. Pile foundations are also called for when the superstructure loads need to be transmitted to a competent soil located at a depth, the soil layers immediately beneath the ground level being weak. Besides above reasons, piles are also used to increase the compaction and the

shear strengths of a soil. Lots of work has been published on the vertical as well as the lateral load capacity of a single pile in sand. The most notable work on this topic is done by Matlock (1970), Matlock and Reese (1960), Meyer and Reese (1979), Reese (1977), Reese and Junius (1977), Poulos (1971), and Brom (1964a; 1964b).

The use of a pile raft foundation has become more popular in the recent years, as the combined action of the raft and the piles can increase the bearing capacity, reduce settlement, and the piles can be arranged to reduce the differential movement of the raft. The pile raft foundation is a geotechnical composite construction consisting of three elements- piles, raft and soil. When a raft foundation alone doesn't satisfy the design requirements, as in the case of a heavy structure like a nuclear reactor located in a marshy coastal area, it may be possible to enhance the performance of the raft by the addition of piles. The use of a limited number of piles may improve the ultimate load capacity, the settlement and differential settlement of the raft and the required thickness of the raft (Poulos 2001). Balakumar et al. (2013) have outlined a simple analytical procedure and effectiveness of pressure-meter tests in predicting pile raft behavior which can be utilized in detailed design of such system. Katzenbach et al. (2005) have given an overview of the theoretical and the practical development of pile raft foundation and its use in reduction of settlement in high rise buildings. Butterfield and Banerjee (1971) analysed pile-soil-cap interaction using Mindlin's equation for interaction and found the load sharing between piles and cap. They found that the load sharing by pile cap ranges from 20% to 60% depending on pile spacing. Poulos (1994) presented an approximate numerical analysis of pile raft interaction. The raft was modeled as a thin plate and piles as interacting springs. The settlement thus predicted were in agreement with the centrifuge tests and full scale tests on the pile raft. Nguyen et al. (2013) have proposed a design method for vertically loaded piled raft considering interaction effects. A centrifuge test on piled raft in sand and Plaxis 3D analysis of the same were presented in this connection. Bourgeois et al. (2012) have also performed settlement analysis of vertically loaded piled raft by means of a multiphase model accounting for soil-pile interaction. Ibrahim (2013) has used Plaxis 3D to evaluate the effect of piles in reducing settlement and contribution of raft in increasing load carrying capacity. Franke (1991) demonstrated with the help of instrumentation of four buildings that a pile raft reduces settlement by about 50% as compared to a raft only.

In a pile raft foundation, the contribution of the piles as well as the raft is taken into account. The conventional pile design philosophy is that the piles carry all the loads and no contribution is made by the raft to the ultimate load capacity. But in a pile raft system, piles are only located to reduce the total settlement and a significant portion of total load is carried by the raft contrary to the conventional design. Placing piles under the raft strategically and of course in a limited number will enhance the ultimate load capacity of the foundation and decrease both the settlement and the differential settlement.

EXPERIMENTAL SETUP

The parametric studies with scaled models can be used to augment areas where case histories and/or prototype tests provide only sparse data. In the present study, experiments were performed on small scale models rather than on the actual prototype. Small scale physical model of pile-raft system was constructed and tested under static lateral loads. The raft and pile was modeled by square concrete foundation of 250 mm x 250 mm x 15 mm in length, breadth and thickness and 25mm diameter and 250mm long circular pile located at the center of the raft. In the model raft, a square steel wire mesh (chicken mesh) of 3mm square openings has been used as the reinforcement. The steel wires are of 1mm in diameter. In the first case, the raft was resting on a single 25mm diameter and 250mm long circular pile located at the center of the raft. The reinforcement cages of the piles was prepared using the same steel wire mesh with 3mm openings. The reinforcements of the pile was prepared by winding up the chicken mesh on a steel rod of diameter 15mm. The pile reinforcements were attached to the mesh reinforcement of the raft maintaining a 50mm lap length in all directions. Figure 1 shows the reinforcement details for the case of a raft with a single pile.

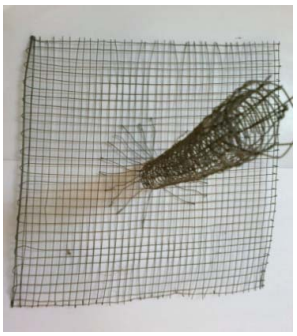


Fig. 1. Reinforcement details for raft/piled raft

The pile along with the raft are casted monolithically using M10 grade concrete. A design mix of 1:3:6 of ordinary Portland cement, fine sand and the coarse aggregate was utilized for the purpose. The coarse aggregate size was so chosen that the mix can pass through the steel reinforcement mesh of the raft and the pile. After the casting, the models are soaked in water and allowed to cure for more than 28 days. Figure 2 shows the model raft with a single pile.

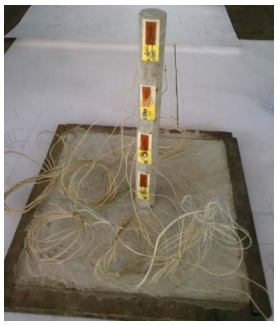


Fig. 2. Model single piled raft

Strain gauges were attached along the length of each pile so that strains along the piles can be measured during the lateral load tests. The moments and shear forces along the piles are then back calculated from the strain gauge data gathered during the tests.

TEST SETUP

The laboratory model tests of the small scale pile raft were conducted in a 1m x 1m x 1m (length x breadth x height) rigid plexi-glass box with top open. The plexi-glass sheets are 16mm thick and glued to each other as well as fixed with steel angles. The box were filled almost up to the top (a 30mm gap between the top of the box and the top of the sand layer is maintained) with the dry sand maintaining a uniform density of 1600 kg/m^3 (unit weight = 15.7kN/m^3). Before inserting the raft and the pile in the sand at the middle of the tank, the sand around the pile location was moistened by adding water from the top. A hand tool (a steel pipe) was utilized to drill a vertical hole of slightly bigger in size than the pile. The pile attached to the bottom of a raft was then inserted into the drilled hole until the raft was resting on top of the sand surface. A vertical surcharge pressure of 1.5kPa (10 kg) was applied on top of the model raft for each case. A horizontally mounted screw type plunger was used to apply lateral load to the raft sitting on top of the sand layer. The lateral load applied to the raft was measured by a proving ring attached to the tip of the plunger and one edge of the raft. The horizontal displacement of the raft was measured by a dial gauge attached between the opposite edge of the raft and the test chamber. Figure 3 shows a top view of the test setup utilized in this study.



Fig. 3. Top view of the test setup

Tests were conducted 24 hours after the installation, so that the moist sand around the piles dries up completely and fill up the gap, if any, around the piles. During a test, lateral load applied to the raft, the strains along the length of the piles were measured by strain indicators. From the strain gauge values, the curvature of the pile was calculated. From the curvature equation, the moments along the piles were calculated using the well-known relationship for a beam,

$$M = \frac{EI}{r} \quad [1]$$

Where, E is the elastic modulus of the pile, I is the moment of inertia of the pile and r is the radius of curvature of the pile given by ε/y. ε is the strain gauge readings and y is the distance of the extreme fiber from the neutral axis.

SOIL PROPERTIES

The foundation soil used in this study was a local uniform grained sand (Kasai River sand). The grain size distribution of the sand is shown in Fig. 4.

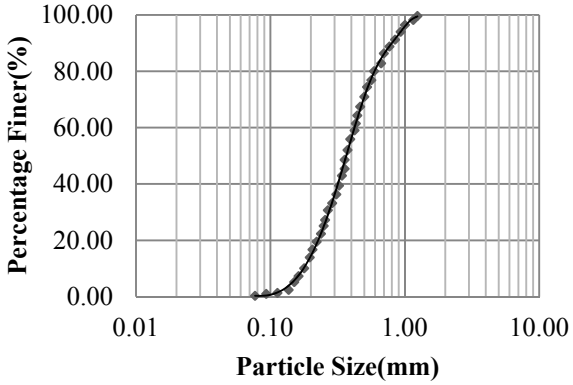


Fig. 4. Grain Size Distribution of Kasai river sand

It was classified as poorly graded sand (SP), according to the Unified Soil Classification System (USCS). The specific gravity of the sand was 2.72. In all the model tests, the bulk unit weight of the sand was maintained at 15.7kN/m^3 and a relative density D_r of 67 %. The effective cohesion (c') and the effective angle of friction (φ') obtained from tri-axial tests were 0.0 kPa and 32^o respectively. The elastic moduli of

the soil have been found from the stress-strain data. Table 1 shows all the material properties of the foundation sand.

Table 1. Geotechnical parameters of the soil

Parameters	Value
Mass density(kg/m^3)	1600
Cohesion(Pa) (c$'$)	0
Angle of internal friction, φ$'$	32^o
Modulus of elasticity, E (MPa)	10.00
Poisson's ratio, ν	0.3

NUMERICAL STUDY

The present study involves modeling in general purpose 3D finite element software of the piled raft foundations tested in laboratory. Soils are modeled with 18060 numbers three dimensional 8 nodded brick element. Non-linear behavior of soil is simulated as Mohr-Coulomb failure criteria. In combined piled raft system piled are model as a combination of beam element and 3D solid element, and raft is a model as a shell element. Pile is modeled by120 numbers of 3D brick elements with 187 nodes and 10 number of 3D beam elements with 11 nodes. 3D brick element is provided inside the pile perimeter which has zero stiffness. At the center of the 3D pile beam elements are placed. Beam element node is connected with all the node of 3D brick element in the same level with multi point constrains (MPC). Here node of beam element is considered as a master node and nodes of the brick elements are considered as the slave element. So, all the active degree of freedom of the slave node is governed by the master node. Actual pile stiffness is incorporated into the beam element. In this way each pile section behaves as a disc element where rotation is allowed in the condition that disc remain always perpendicular along the beam axis, stretching cannot occur. Interactions between soil and pile surfaces are governed by coulomb friction criteria. Surface separations are allowed between soil pile interfaces. Horizontal deformation of soil side boundaries are restricted but vertical deformations are allowed, and at the bottom of the soil both vertical and horizontal deformations are restricted. Total numerical analysis is performed in two steps, in first steps, gravity loads are applied into the soil model and equilibrium achieved. Then in next step lateral load are applied in raft edge as performed in the experiments. Bending moments of piles are measured in the analysis. Finite element modelling of soil is shown in Fig. 5.

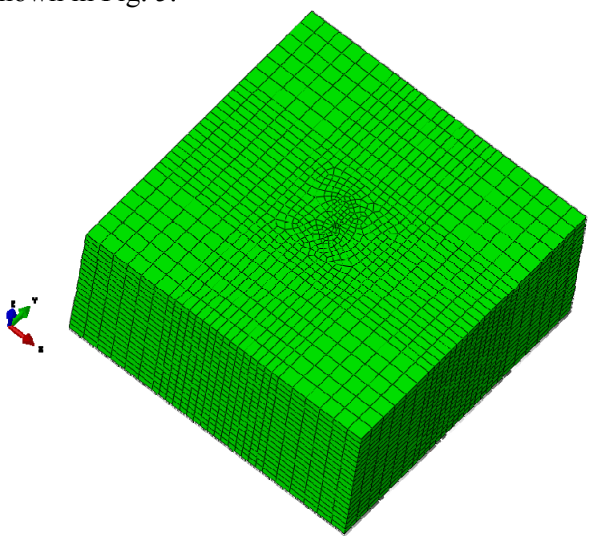


Fig. 5. Finite element modeling of soil

VALIDATION OF THE PILE RAFT MODEL

All the laboratory model tests are performed on small scale and the results of the model tests are compared with the results of the corresponding numerical analysis done in general purpose 3-D finite element software. For the case of raft supported on a single pile, the bending moments in the pile are presented in Fig. 6 for lateral loading of 6.25, 12.50, 18.75 and 25.00 N applied at the level of the raft.

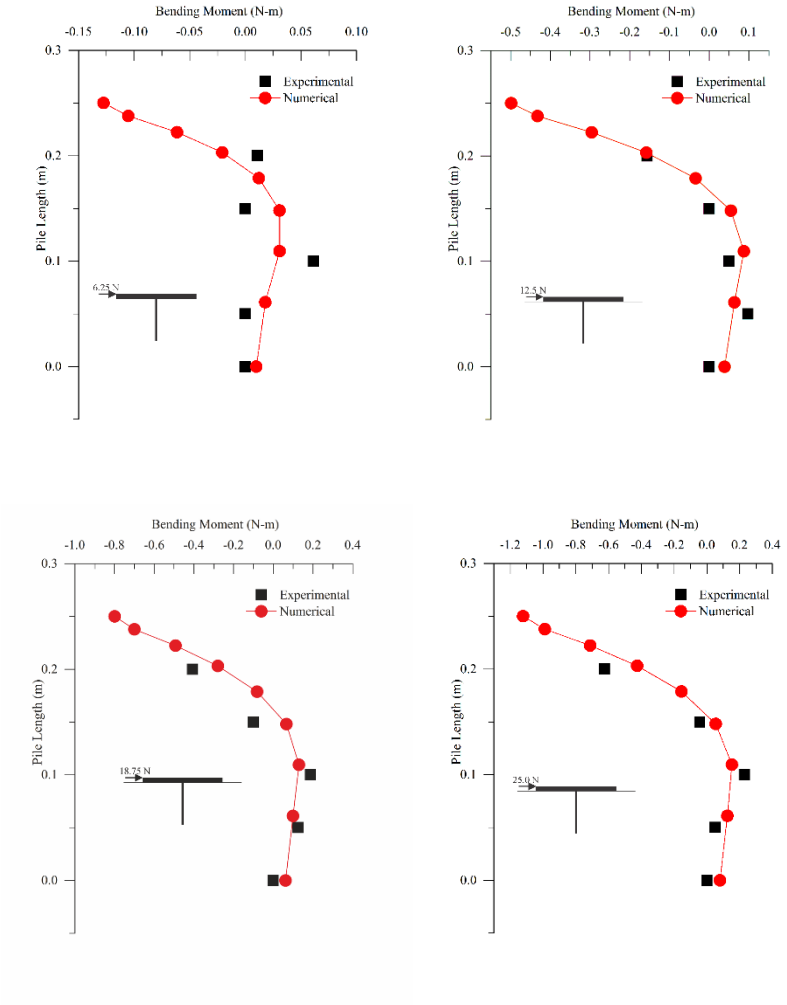


Fig. 6. Bending moment of pile for four values of lateral loading

The moments on the pile increases with the increase in the lateral load applied to the raft. It is interesting to note that the moments of the pile obtained from the model tests and those predicted by the numerical analyses for all the lateral loads are matching reasonably well with the discrepancies within the limits of acceptance. These discrepancies can probably be attributed to some extent to an inability to describe numerically the stress history arising from the sand placement techniques.

Matlock and Reese (1960) developed general solutions for laterally loaded piles supported by an elastic medium. According to them, the expressions are developed for bending moment in pile, for validating the observations found from experiments. Figure 7 shows the comparison of bending moments obtained from experiment, numerical and theoretical studies by Matlock and Reese (1960) for a lateral load of 18.75N. From this figure, it is observed that there is a significant deviation of results in the initial portion, beyond which the differences are within the limits of tolerance. This may be attributed to the fact that the approach

taken by Matlock and Reese (1960) considers the soil to be an elastic medium which is not in case of experiment and numerical analysis and hence the deviation.

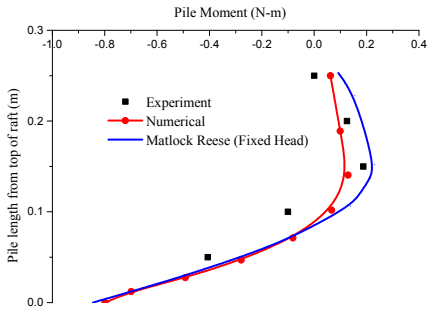


Fig. 7. Comparison of bending moment of pile from experiment, numerical and theoretical approach for lateral loading of 18.75N.

PARAMETRIC STUDY

A parametric study has been performed to investigate the behavior of piled raft subjected to seismically induced horizontal loading. Four different pile configurations underneath the raft are analyzed in this study namely: Category 1 (1 pile raft system), Category 2 (2 pile raft system), Category 3 (5 pile raft system) and Category 4 (9 pile raft system) for a raft of 5 m x 5 m x 0.3 m in length, breadth and thickness and circular pile of 0.5 m diameter and 5.0 m in length subjected to a surcharge load of 30kPa as shown in Fig. 8. Seismically induced load is replaced with equivalent static horizontal load, equal to seismic coefficient times the vertical load on top of the raft. In the present study two earthquakes namely Loma Prieta (18/10/1989, Mw=7.1, N0W component) and Darfield Christchurch (09/03/2010, Mw=7.1, S73W component) motions are selected with PGA of 0.344g and 0.495g and the corresponding lateral loads are calculated to be 250 kN and 350 kN for two earthquakes respectively.

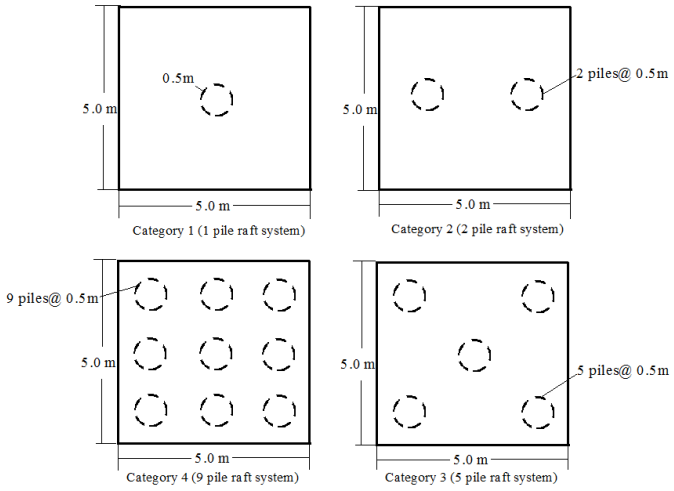


Fig. 8. Different configurations of pile beneath the raft

The pile raft material is chosen to be concrete of M 30 grade for the above comparison. The parameters which are studied from the present analysis are a) Bending moment of pile in piled raft, b) Variation of maximum bending moment of piles with lateral loads and, c) Variation of lateral load deformation curve for piled raft with number of piles. The bending moment diagram for the center pile of all the pile raft arrangements for lateral load of 250 kN are compared in Fig. 9.

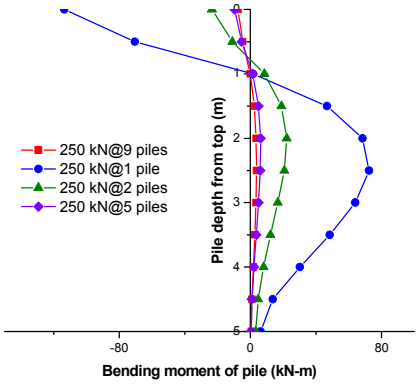


Fig. 9. Bending moment of center pile for different pile configurations

It is observed that the bending moments of pile significantly reduces as the number of pile is increased to two, but it decreases to a nearly constant value (or it saturates) as the number of pile is increased to five and nine, which gives us an indication of the constancy of stiffness irrespective of the number of piles. Moreover the individual pile section reduces although the number of piles is increased which is economically viable and feasible.

Figure 10 shows the effect of pile configuration on maximum bending moment, in which it is seen that by increasing the number of piles the maximum moment reduces, but there is a significant drop in moment (around 4 times) by increasing the number of pile(s) from one to two.

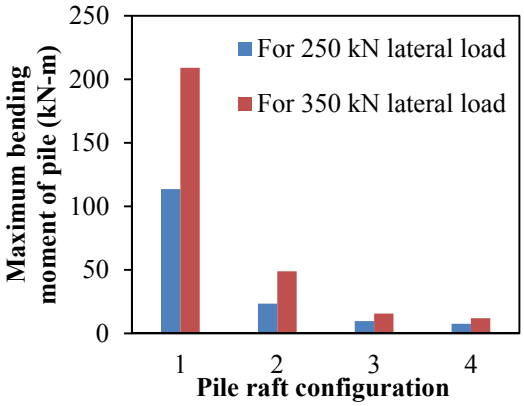


Fig. 10. Variation of the maximum bending moment of pile with its configuration

The load deformation curve for piled raft with increasing number of piles is shown in Fig. 11. From the figure it is observed that there is a reduction in horizontal deformation (around 2.4 times) with increase in pile numbers from one to two in piled raft system, but there is a contradiction in the load deformation curve for five and nine pile raft system in which the result comes out to be opposite than what is to be expected, although the final deformation is less than that for one and two piled raft system.

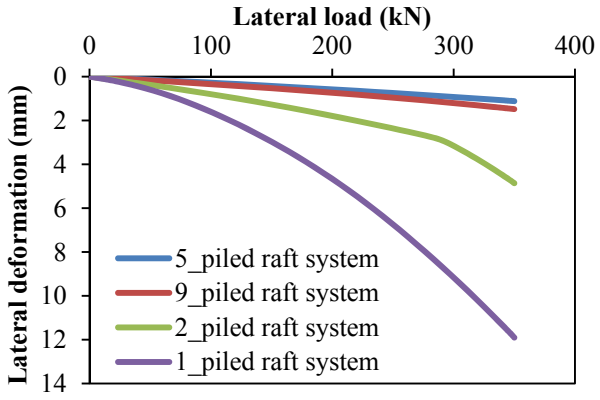


Fig. 11. Lateral load deformation curve for piled raft

CONCLUSIONS

From the above study it is concluded that the combined piled raft system can act as a horizontal deformation reducers of the structure, very minimum number of piles can reduce horizontal displacement of piled raft system. In parametric studies it is also discussed that bending moment of pile decreased with increase of pile(s) in pile raft system, which may govern in pile design. A saturation point is also observed which indicates that the increase in pile(s) may not be effective in improving the performance of piled raft system.

REFERENCES

Balakumar, V., Oh, E., Bolton, M., Balasubramaniam, A. S., 2013. A Design Method For Piled Raft Foundations. Proceedings of the 18th International Conference on Soil Mechanics and Geotechnical Engineering, Paris, pp. 2671-2674.

Bourgeois, E., de Buhan, P., Hassen, G., 2012. Settlement analysis of piled-raft foundations by means of a multiphase model accounting for soil-pile interactions. Computers and Geotechnics, 46(4) 26-38.

Broms, B., 1964. Lateral resistance of piles in cohesionless soils. J. Soil Mech. Found. Div., ASCE, 89(3) 123-157.

Broms, B., 1964. The lateral resistance of piles in cohesive soils. J. Soil Mech. Found. Div., ASCE, 90(2) 27-63.

Wiesner, T. J. and Brown, P. T., 1980. Laboratory Tests on Model Piled Raft Foundations. J. Geot. Engg. Div., ASCE, 106(7) 767-783.

Butterfield, R. and Banerjee, P.K., 1971. The problem of pile group and pile cap interaction. Geotechnique, 21(2), 135-142.

Franke, E., 1991. Measurements beneath piled rafts. Keynote lecture to ENPC Conference on Deep Foundation, Paris.

Iai, S., 1989. Similitude for shaking table tests on soil-structure-fluid model in 1g gravitational field. *Soils and Foundations*, 29(1) 105–118.

Ibrahim, A.M., 2013. Pile raft foundation with piles act as settlement reducer. Resources and geotechnical engineering, Vol. 10, InstitutfürGeotechnic Gustav-Zeuner-Straße 1, 09596 Freiberg.

Katzenbach, R., Bachmann, G., Boled-Mekasha, G., Ramm, H., 2005. Combined pile raft foundations (CPRF): an appropriate solution for the foundations of high-rise buildings. Slovak J. of Civil Engg., 3 19-29.

Matlock, H., 1970. Correlations for design of laterally loaded piles in soft clay. 2nd Annual Offshore Tech. Conf., Houston, Texas, Vol. 1, pp. 577-588.

Matlock, H. and Reese, L.C., 1960. Generalized solutions for laterally loaded piles. Journal of Soil Mechanics & Foundations Division, ASCE, 86(4) 63-91.
Meyer, B.J. and Reese, L.C.,1979. Analysis of single piles under lateral loading. Report No. FHWA/TX-79/38, Texas State Department of Highways and Public Transportation, Transportation Planning Div., Austin, Texas, USA.
Nguyen, D.D.C., Jo, S.B., Kim, D S., 2013. Design method of piled-raft foundations under vertical load considering interaction effects. Computers and Geotechnics, 47 16-27.
Poulos, H.G., 1971. Behavior of laterally loaded piles: I- single piles. J. Soil Mech. Found. Div., ASCE, 97(5) 711-731.
Poulos, H. G., 2001. Piled raft foundations: design and applications. Geotechnique, 2 95-113.
Poulos, H.G., 1994. An approximate numerical analysis of pile-raft interaction. Intl. J. Num. Anal. Methods in Geomech., 18 73-92.
Ramu, M., Prabhu Raja, V., Thyla, P.R., 2011. Development of structural similitude and scaling laws for elastic models. *KSCE Journal of Civil Engineering*, 17(1) 139-144.
Reese, L.C., 1977. Laterally loaded piles: program documentation." J. Geot. Engg. Div., ASCE, 103(4), 287-305.
Reese, L.C. and Junius, D.A., 1977. Drilled shaft design and construction manual. US Dept. of Transportation, FHA, USA, Vol. 2.

DESIGN & INSTALLATION OF OFFSHORE DRIVEN PILES – A GULF OF THAILAND REGIONAL PERSPECTIVE

Kaushik Mukherjee, Group Technical Solutions, PETRONAS, Malaysia, Tel.: +60166955115,
E-mail: *kaushik.mj@petronas.com.my*

ABSTRACT

Malaysian offshore and surrounding region are favorable to the installation of driven piles. During the design phase, pile driveability analysis plays a major role in pile make-up design to suit and selection of the feasible hammer, besides defining acceptance criteria to ensure a certain level of confidence of its fitness for purpose. The accuracy level of driveability analyses depends substantially on the selection of its parameters that best represent the in-situ scenario. The most uncertain of the parameters are those related to the soil model. It is noted in various projects in the region, that the consideration of suitable soil resistance to driving, coupled with soil dynamic parameters, significantly affects driving sequence planning, design, material, hammer selection and most importantly pile acceptance criteria. This is particularly relevant for a region that contains predominantly clayey subsoil resulting in large diameter, long friction piles susceptible to driving disturbances and slow strength recovery. Various researchers suggested suitable dynamic parameters and soil resistance during driving calibrated to specific regions. Regional experience suggests a set of soil degradation and parameters to suit the different stages of driving which is corroborated by pile monitoring records during continuous and delayed driving scenarios. The most sensitive amongst all dynamic soil parameters is the skin damping in clay. Smith's wave theory approach considers a conservative assumption in selecting the parameters in absence of site-specific data, while a different approach may be adopted based on consistency of the clay for a site where the geotechnical parameters are well defined. This paper summarizes some independent studies on the effects of variations in dynamic parameters and resistance at different stages of driving and suitability of choices of different pile make-up and hammers for an optimum design. Similar experiences, coupled with simulation studies and back-analyses of available driving records suggest a reasonable judgment for the region.

Keywords: driven piles, driveability, dynamic parameters, skin damping

INTRODUCTION

Fixed structures are generally supported in the in-place condition on a pile foundation those may either be driven or drilled & grouted piles depending on the subsoil. The piles may be driven inside the jacket legs or drilled through individual skirts normally grouped in clusters at the base of each leg. The types of subsoil dealt with in the Peninsular Malaysia and Gulf of Thailand surrounding region are conducive to the installation of driven piles only. The design of an offshore pile is fundamentally the optimization of pile length, size and make-up those are suitable to the requirement and supply. An interactive effort combining aspects related to geotechnical, structural and constructability are required to converge into a feasible, safe and economic solution. Other than the checking of the installation feasibility using a set of hammers in a given environment, driveability analysis is also used to define acceptance criteria for a majority of the offshore piles. Unlike short and end bearing piles in sand/soft rock, the piles in clayey subsoil regime often could not be rested on a dense strata where it could be met by a definite set criteria. Usually a measurement of blow counts determined and defined by driveability analyses forms the acceptance criteria to ensure a certain level of confidence of its fitness for the purpose coupled with an optimum penetration. While softness and uncertainty of the soil strata at target penetration may be resulted in possible overdrive, an unusual delay or the presence of an unidentified cemented layer or a boulder may cause early refusal or underdrive scenario. Hence, accuracy of the investigation, driveabilty study as well as the precautionary measures to avoid delays during driving are of equal importance.

The is-situ representative parameters are generally extracted from geotechnical investigation report coupled with dynamic parameters attuned to previous experience or measurements available for the region. The parameters related to selected hammers are generally supplied by the manufacturer. The most uncertain of the parameters are those related to soil model [static & dynamic]. The complicated system of hammer-pile-soil interaction and its solution through wave equation analogy forms the basis of driveablity analysis. The strength parameters of the subsoil are used to develop the soil resistance to driving [SRD] in much the same way as it is done to calculate the static capacity. Apart from the method suggested by ISO 19902 [2007] or API RP 2A [2000], the methods suggested by several other authors, e.g., Toolan and Fox [1977], Alm and Hamre [1998], Stevens [1982] etc. are also used to develop SRD calibrated for soils in different geographical regions. In a dynamically driven condition, the clayey subsoil undergo temporary reduction in the shear strength partly due to remoulding and development of undrained condition within the smear or slip zone surrounding the pile. Phenomenon like 'friction fatigue' also responsible for a reduced shear strength of long pile but normally treated as long term effect particularly in clayey subsoil and is generally taken care of in the ultimate capacity design. Some of the methods developed later to calculate SRD in cohesionless strata take this into account.

The dynamic soil parameters are needed to define soil viscous-damping effect and elastic deformation or quake. Friction piles are usually longer in a site that predominantly consists of clayey subsoil. Hence, it is obvious that the driveability analyses would be sensitive to these parameters. Roussel [1979] and many other researchers indicated that the damping parameters vary widely with the consistency of the clay. The public domain softwares generally recommend that the resistance due to viscous-damping is calculated according to Smith's original approach and includes a few proposed damping models similar to those originally proposed by Smith. However, since there are no direct links between Smith's model and standard geotechnical soil test parameters, several investigators of the dynamic behavior of piling have expressed concern that the current approach is unreliable for either previously untested soil conditions or certain extreme conditions (e.g., very high or very low velocities) for which no experience base exists (Rausche, Goble, Likins 1992).

This paper mainly focuses on the effects of variations in soil model parameters and resistance at different stages of driving and suitability of choices of different pile make-up and hammers for an optimum design in the regional subsoil strata coupled with earlier experiences, simulation studies and back-analyses of available driving records.

THEORETICAL BACKGROUND

Impact Formulation & Hammer Selection

Pile driving formulations gained its popularity for it's simplistic approach and are still widely in use for driving piles to the design capacity. A large number of such formulae available in practice, e.g., Janbu, Hiley or Engineering News Record [ENR] are used worldwide. Mostly these are site specific and have their own limitations or uncertainties need to be compensated by using appropriate safety factor. Smith's [1960] approach of application of one dimensional wave propagation theory to understand the complicated driveability phenomenon was probably the first rationalized solution to the problem. With the advent of microcomputers, this approach gained substantial popularity over the time. Similar wave propagation approach were also adopted by few researchers to develop pile driving formulae to manage pile driving in specific cases [Uto et. al., 1992; Weele and Schellingerhout, 1994; Chen et. al., 1997].

Initial Impact: The hammer-pile-soil interaction can be depicted by a simple model as shown in Figure 1. The interaction problem could be separated into two steps: (1) the interaction between pile and hammer and (2) the penetration of the pile into the ground due to the impact generated by the hammer or dynamic pile-soil interaction. It is difficult to set up an accurate model for the interaction of pile and hammer because of the complexity of the driving equipment. Chen et. al. [2003] explored the fundamental solution provided by Clough and Penzien (1975) to solve the primary problem of hammer impact [Step (1)]. The pile driving system is modeled by three basic elements: a relatively rigid ram, a linear spring (pile anvil/cushion) and an elastic pile.

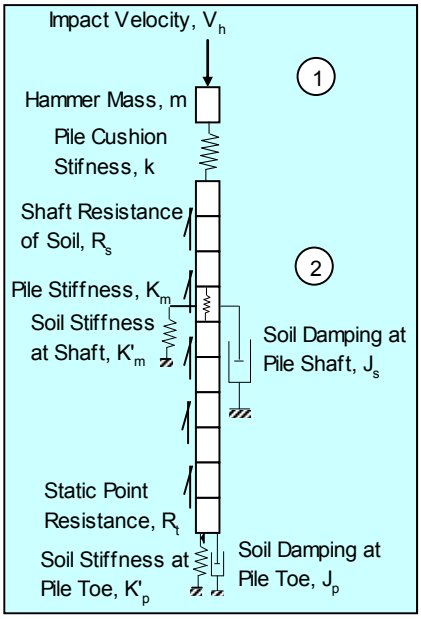


Figure 1 Generic Pile Driving Model

The solution yields the impact force induced at the pile top during the first wave passage, as expressed by the Equation 1.

$$F_t := \left[\frac{k \cdot V_h}{\omega_d} \cdot \left(e^{-\xi \cdot \omega \cdot t}\right)\right] \cdot \sin\left(\omega_d \cdot t\right) \quad \text{for} \quad 0 \le \omega_d \cdot t \le \pi \tag{1}$$

Where,

$$\omega := \sqrt{\frac{k}{m}}, \quad \omega_d := \omega \cdot \sqrt{1 - \xi^2} \quad \text{and} \quad \xi := \frac{k_1 \cdot c}{2 \cdot \omega \cdot E \cdot A}$$

'k' is the combined stiffness of the hammer and pile top cushion/anvil assembly, 'm' is the hammer mass, 'ω' is the system natural frequency, 'ω_d' is the damped frequency, 'ξ' is the damping ratio of the system, 'E' and 'A' are the elastic modulus and cross-sectional area of the pile material and 'c' is the wave velocity. 'V_h' is ram impact velocity, obtained from the kinetic hammer energy (E_t) generally mentioned by hammer manufacturers [usually maintained around 5-6m/s for hydraulic hammers],

$$V_h := \sqrt{\frac{2 \cdot ef \cdot E_t}{m}}$$

Where 'e_f' is the hammer efficiency describes the percentage of maximum hammer energy transferred to the pile and soil or the ratio of the kinetic energy available to do work on the driving system. This depends on various factors, e.g., losses due to friction, misalignment, low stroke, pre-ignition etc. which are different for different types of hammer. Usually, for hydraulic hammers the maximum operating efficiency may reach as high as 95% whereas for the steam hammers this would reach up to a maximum of 67-70%. In original Smith's model, the solution iteration starts from this ram impact velocity and impact forces are calculated numerically in each time step.

The solution plot of Equation (1) takes the shape of a damped sinusoid that shows the variation of impact force with time [Fig. 2(a)]. Figure 2(b) shows the truncated first half plot of the sinusoid that shows the generated impact on the pile. This plot is characterized by three distinct parameters describing the shape: the peak impact force 'F_o', duration 'to' and loading period 't_l' [Figure 2(b)]:

$$F_o := \left[\frac{k \cdot V_h}{\omega_d} \cdot \left(e^{-\xi \cdot \omega \cdot t_1}\right)\right] \cdot \sin\left(\omega_d \cdot t_1\right) \qquad t_o := \frac{\pi}{\omega_d} \qquad t_{.1} := \frac{1}{\omega_{.d}} \cdot \tan^{-1}\left(\frac{\omega_{.d}}{\omega \cdot \xi}\right)$$

Hammer Selection: This analytical calculation is particularly important for the primary selection of the hammer. The drop weight and height has definitive influence on the impact peak force (F_o) and impact duration (t_o) which in turn influences the penetration efficiency of the hammer pile system. The lightweight piles could be driven faster and efficient but this is only true for shorter piles with light loading. For longer piles driven through stiffer media, pile stiffness plays an important role in carrying large forces down into the ground. Following quick rules may be exercised while selecting a hammer:

- The Greater the mass of the hammer larger the impact peak force and longer the impact duration [Fig. 2(c) & 2(f)]
- Greater dropheight keeping the same hammer mass may also produce the higher peak force but could not increase the impact duration [Fig. 2(e)]
- Greater stiffness of the hammer cushion assembly could also increase the peak force but would vary the impact duration as well [Fig. 2(d)]
- The optimum hammer should have higher peak force and longer impact duration to overcome soil resistance and achieve deeper penetration, however, pile top overstressing should be avoided
- It is advisable to use larger hammer with low dropheight rather than smaller hammer with higher dropheight
- Because of continuous blow, cushion gets stiffer as the driving progresses and this rapidly increases the peak force and decrease the impact duration [Fig. 2(d)]. The train of excessive peak force reduces driving efficiency and tends to damage the pile top.

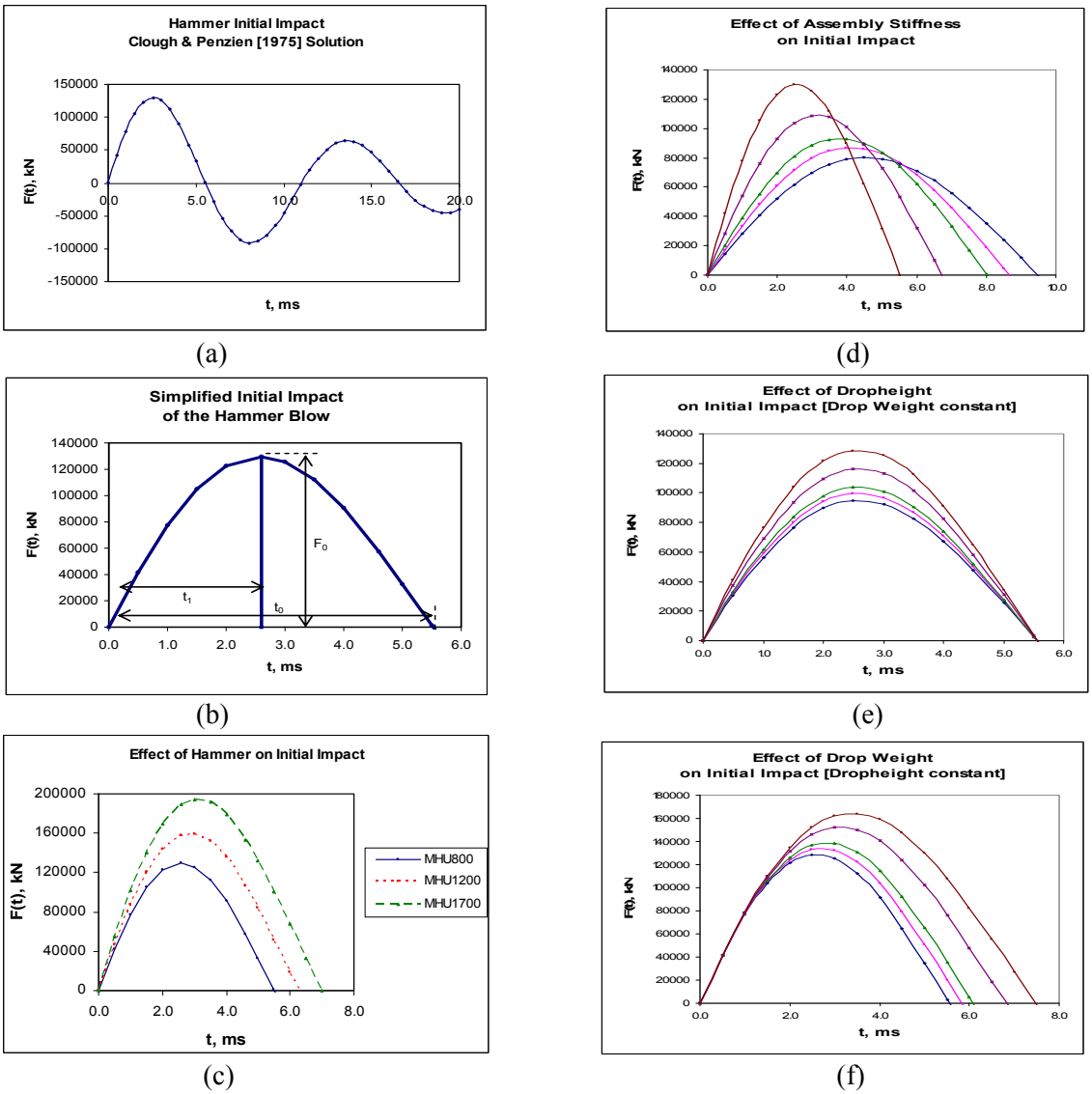


Figure 2 Study on Initial Impact Force

Soil Mechanics Principles

Second step of the driveability analysis is the penetration of the pile in the ground with the effect of initial hammer impact [Figure 1]. In the Smith's model of driveability, the analysis is an integrated approach that consists of time step solution of one dimensional wave equation until the generated wave velocity fully expended and/or displacement convergence achieved. The soil resistance is modeled with both dynamic and static components. The idealistic static soil model devised by Smith is depicted in Figure 3. The static resistance is displacement dependent and is defined by an ultimate strength [R_u] and a "quake" value [Q]. The dynamic resistance depends on the relative motion between the pile and the soil in the slip zone [shaft friction] and pile tip.

The quake represents elastic or temporary soil compression, and is inversely related to soil stiffness. Typical quake values are in the 2 to 5 mm range; soils with high rebound have considerably higher end bearing quake values, sometimes in excess of 25 mm. Idealistically, the soil would enter the plastic zone beyond this quake displacement and would undergo plastic displacement or permanent set 's' as indicated in Figure 3, before entering into the elastic rebound [equal to Q] or unloading stage.

The speed of pile penetration into the ground depends on pile soil interaction. Some piles penetrate faster than the others in the same soil strata while the same pile would behave differently in different subsoil. Ground offers more resistance to rapidly moving piles than the slowly moving ones. This entails the necessity of introducing velocity dependent viscous damping parameters into the system. The probable impact of viscous damping effect on soil resistance model is shown in Figure 3 by dotted lines. Because of dynamic movement this resistance is instantaneous in nature and does not affect the static capacity of the pile as a whole. The soil damping parameters affect both the frictional and toe movement of the pile and at times have substantial effect on overall driveability results.

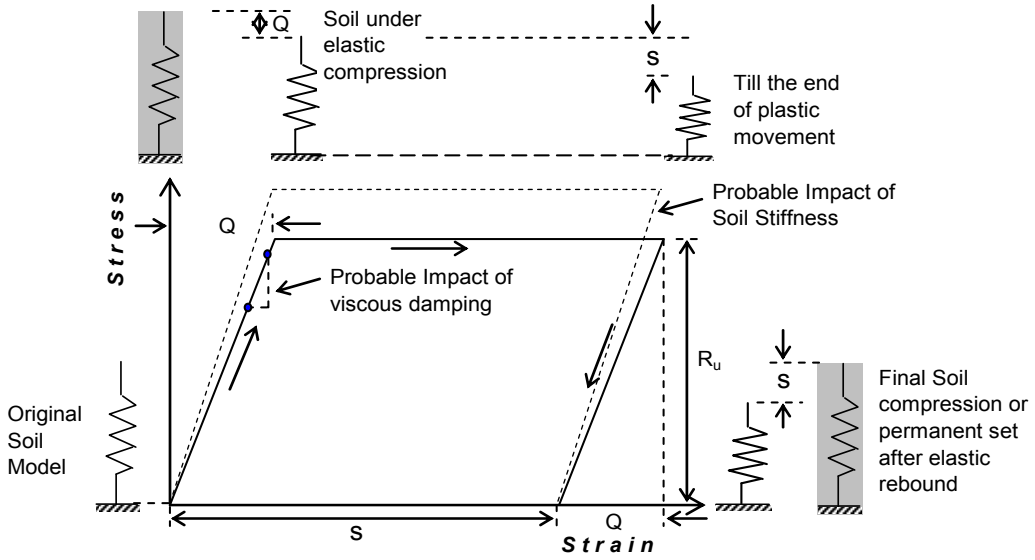


Figure 3 Depiction of Smith's Soil Model

Soil Resistance to Driving [SRD] Overview

There are several methods to calculate SRD. The methods commonly in use to determine resistance to driving are meant for North Sea sands and clays. These methods are generally extended to use in other regions worldwide. Sometimes methods those are meant for axial capacity design, e.g., API/ISO or UWA method, are also modified to calculate SRDs. For Gulf of Thailand [GoT] and regional clay, generally API based method is common. Some of the common methods are:

- API/ISO Method
- Toolan & Fox Method

- Steven's Method
- Semple & Gemeinhardt
- Alm & Hamre
- UWA-05 Method
- Heerema [Proprietary Methods]

A range of resistance is usually determined to provide upper and lower bound to the expected response of the soils. An upper bound profile would be expected to provide the most pessimistic hammer blowcount behavior. If the measured response is less than the lower bound limit, then the assumptions made to determine the soil parameters might need to be examined and pile capacity, which also depends on the assumed soil parameters, might then be modified [typical CAPWAP type of analysis].

The behavior of the pile during driving may be as a plugged or un-plugged response. The size of the pile may have a significant effect on the response. Whereas, smaller diameter pipes, such as conductors, may respond in a plugged response, larger piles will behave as unplugged (cored). Quite often the minimum of the calculated response is assumed, as in the Toolan & Fox method. However, some of the methods (e.g. Stevens) recommend the use of plugged behavior based on back-analysis.

Table 1. Soil Damping Factors Proposed by Various Researchers

	Skin Damping, Js sec/m	Toe Damping, Jp sec/m	Comments
Smith (1960)	0.16	0.49	All Soils
Lowery et al (1969)	0.01 - 0.16 0.11 0.33	0.33 - 0.43 0.33 0.98	Lab tests - Granular Soil Best Correlation - Sand Best Correlation - Clay
Forehand & Reese (1964)	0.16 0.00	0.16 - 0.65 1.64 - 3.28	Sand, Gravel
Poulos & Davis (1980)	0.23	0.66	Sand & Clay
Coyle et al	0.16 0.66	0.49 0.03	Sand Clay
Lowery	0.33	0.49	Silt
GRLWEAP Manual	0.16 0.65 0.33 - 0.49	0.33 - 0.65 0.033 - 3.28 0.33 - 1.64	Sand Clay Silt
McCleland Memo	0.49 0.16 - 0.65	0.49 0.16	Sand Js = f(Su) for Clay
Bowles (1977)	0.1 - 0.23 0.43 - 1.08	0.33 - 0.65 1.31 - 3.28	Sand Clay
De Ruiter (1979)	0.16 0.66	0.49 0.03	Sand & Silt Clay
Heerema (1980)	0.16 0.66	0.49	Sand Clay
Beake & Sutcliffe	0.66	1.15	Carbonate Rock
Stevens (1982)	0.26 0.10	0.49 0.49	Using own method of SRD assessment (Sand & Clay)
D'Appolonia	0.16 0.16 0.33 0.33	0.33 0.49 0.49 0.49	Gravel Sand Silty Sand & Clay Calcareous Sand
Northern Field, Malaysia	0.16 0.30	0.49 0.49	Sand Clay
Chermingat, Malaysia	0.20	0.50	Clay
Briaud & Tucker (1984)	0.16	0.49	Granular
Dolwin et al	0.52	0.20	Experiment & theory
Sutton et al	0.66	0.03	Clay
Tagaya & Heerema (1979)	0.49 - 0.65	0.49	Calcareous Clay
Van Luipen (1979)	0.66	0.36	Clay, some Sand
Semple et al (1981)	0.66	0.16	Clay
Roussel (1979)	0.1 - 0.36 0.23 0.26	0.49 - 0.66 0.49 0.49	Clay Silt Sand

Note: This is a collection of data available from different sources. The authenticity of all data presented here is not completely verified by the author.

Modelling of Dynamic Behavior of Soil

The Smith's soil model as depicted in Figure 3 does not include the effect of time, i.e., the speed of pile penetration into the ground and the relative velocity of the pile with respect to surrounding soil. Smith dealt with this problem by introducing a damping factor 'J' to cater for this viscous damping effect. Thus the part of the actual energy transmitted to the soil caters for the losses incurred by the dashpot. Idealistically, the total resistance offered by the soil would be,

$$R_t = R_s [1+J.v] \quad (2)$$

where, R_t is the total resistance, R_s is the static part of the resistance, 'v' is the relative velocity of the pile and 'J' is the Smith's damping parameter. The parameter 'J' is denoted by J_s or J_p depending on the location on the pile, i.e., damping offered by soil at the side [skin] or toe. It should be noted that in static condition R_t will be equal to R_s only. The second part of the Equation 2 [R_s.J.v] is the instantaneous dynamic resistance offered by the soil. It is obvious that the direction of this force will depend on soil compression or extension and hence, the sign of this force should follow the sign of the velocity.

Later on, several researchers through their limited laboratory tests opined that these damping parameters generally do not vary linearly with the pile velocity. Researchers like Gibson & Coyle (1968) and Heerema (1979) proposed an exponential law applied to the velocity to calculate this dynamic resistance expressed in the form of, $R_d = R_s.J.v^n$, for which 'n' depends on soil type and may be assumed as 0.18 for clay and 0.2 for sand. Goble and Rausche (1976) proposed a damping factor J_c [= $J.R_u/Z$] which is much similar to Smith's viscous damping but it takes the effect of pile impedance [Z] in addition to soil ultimate resistance [R_u]. A review of the soil damping parameters [J_s & J_p] to be used for different subsoil conditions proposed by various researches/consultants is presented in Table 1 above.

REGIONAL CASE STUDIES

Four case studies have been adopted to establish the effect of skin damping parameter on the driveability of offshore steel tube pile driven through the clay dominated subsoil strata typically observed in the Gulf. For the first case [Site A] the pile outer diameter was in the range of 1.5m to 2.35m penetrating upto 135m with varying wall thicknesses to suit the hammer-pile system from the point of view of stress optimization and equipment availability. Standard hydraulic hammer has been used to drive the pile with variable efficiency increasing with depth. The soil stratum generally consists of predominantly clay layers [with intermittent silts] and sands at deeper zone. The second case study [Site B] is presented for comparison where the soil data is not predominantly clay. It is rather mix up with intermittent silt and sand layers and the driven pile outer diameter was 2.1m driven to a target penetration 126m with similar hydraulic hammer. The soil stratum generally consists of alternate layers of clay and sands. The third case study [Site C] was a new design and conditions are very similar to the Site A location. The soil stratum generally consists of predominantly clay layers and with sands at deeper zone. Site D is a new joint-venture project between Thailand and Malaysia. The site also consists predominantly of clayey subsoil. Figure 4 shows the location of the study fields in the Gulf of Thailand. The soil strata have been schematically depicted in the corresponding driveability study curves later.

The soil resistance to driving (SRD) is calculated using a similar procedure to that of the axial capacity calculations following API 21st Edition method. The driving resistance is determined either as a plugged condition or as an unplugged condition. The SRD is generally chosen as the unplugged condition resistances with a check for the plugged condition as ultimate set-up. It has been assumed that with the usage of a thick and slant driving shoe, the effect of internal skin friction will be minimal and chances of plug formation will be much less even in case of a full soil set-up condition. However, both the effect of external skin friction along with annular and fully plugged end bearing cases has been considered in our present driveability study.

When a pile is driven in clay, there is a temporary reduction in the shear strength partly due to remoulding and development of an undrained condition. This remoulded and undrained condition is

usually catered for by using set-up factors on the estimated SRD in the clay layers. For sand and silt layers, drained condition prevailed and hence, there is no reduction considered [capacities are the same as static conditions]. The remoulded shear strengths are generally assumed in the ranges from 20% to 60% of the design shear strength for the clays in the Gulf area based on available experience. Stoppages in pile driving generally result in the regaining of strength in clay layers [thixotropism] and hence the restart resistance is higher than the SRD for continuous driving. The gain in strength is generally time dependent and hence longer delays generally result in a higher restart resistance. The following values are used for the prediction of the restart resistances:

(1) Short Delays (up to 8 hours) – 50% gain in strength [SRD shifts from 30% to 60% Skin friction] &
(2) Long Delays (up to 24 hours) – 100% gain in strength [SRD shifts to 100% Skin friction]

For delays beyond 24 hours, the shear strength will be assumed to be equal to static shear strength.

Three sets of the following SRD have been used in the pile driveability analyses in the Case Studies to ensure all driving conditions are covered:

(1) Continuous driving: 30% [20-40%] skin friction resistance in Clay (external) – API Unplugged case.
(2) Re-start after short delay: 60% skin friction resistance in Clay (external) – API Unplugged case.
(3) Re-start after long delay set-up: 100% skin friction - Full Set-up Condition, API Fully Plugged case.



Figure 4 Approximate Case Study Locations

In Case Study B, continuous driving scenario, SRD with 20% skin friction resistance in clay has been used. In Case Study C, a range of skin friction variation taken into account in preliminary design of pile make-up and driveabilty.

Remoulding due to driving disturbance and time dependent strength recovery may be best represented by a typical time rate of recovery curves those are developed based on regional experience. An empirical procedure based on experiments in Gulf of Mexico clays that include effect of pile diameter and wall thickness on the rate of consolidation and setup has been discussed in Bogard & Matlock [1990].

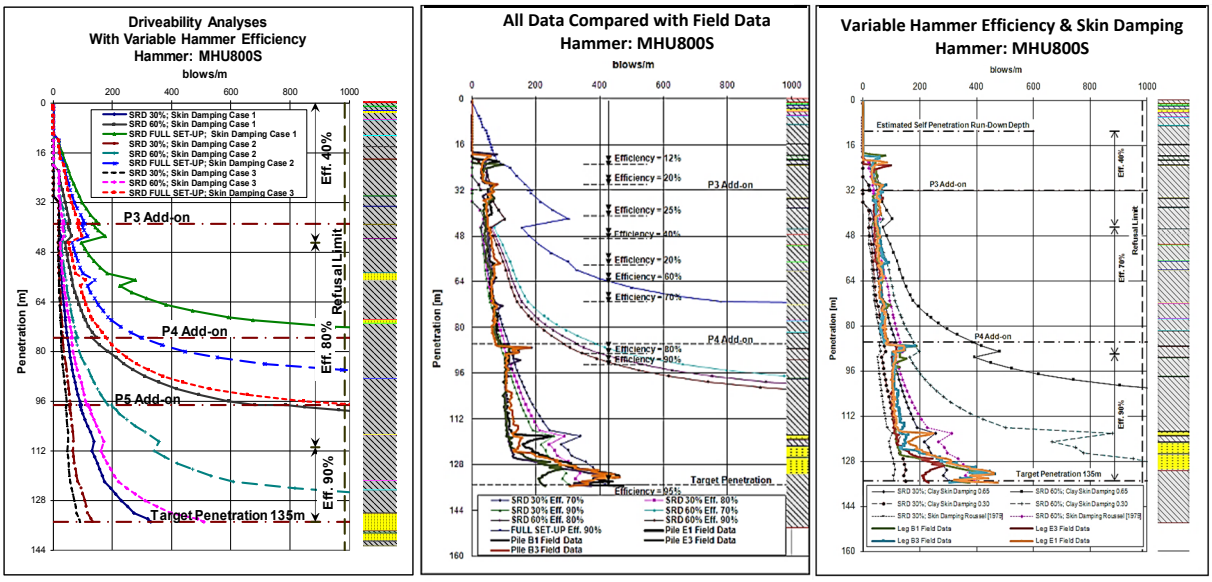
The soil resistances as discussed above are modeled in wave equation analysis with both dynamic and static resistance wave equation parameters. The static resistance component is displacement dependent and is defined by an ultimate strength [R_u] and a quake [Q] or temporary soil compression usually related to soil stiffness. The dynamic component is velocity dependent and known as viscous-damping

parameters which apparently increases the instantaneous soil resistance [Fig. 3]. Generally, the soil damping factors and quakes are taken based on typical values recommended by researchers. Both the skin and toe quake values are considered as 2.5mm and the toe damping factors taken as 0.5s/m for both sand and clayey subsoil. In a site dominated by clayey subsoil, the most sensitive parameters would be skin damping factors. Roussel [1979] suggested that the skin damping in clay is a function of its strength parameters [consistency] and he proposed a range of this parameter based on his experiments [Table 1]. To study the sensitivity of this parameter, three cases have been considered in the analysis [Site A]:

Case 1 : Clay skin damping parameter taken as constant 0.65s/m
Case 2 : Clay skin damping parameter taken as constant 0.30s/m
Case 3 : Clay skin damping parameter taken as suggested by Roussel [1979]

Results and Observations

A set of driveability analyses have been performed for the study combining three sets of SRDs and different skin damping parameters and the blow-count results are plotted in Figure 7 [Site A]. Generally, the dynamic soil parameters, i.e., soil damping coefficient and quake should be taken based on the best-fit values recommended by earlier experience. The wave-equation analyses are quite sensitive to these parameters, particularly the skin-damping parameters in clay [Figure 5(a)]. Actual in-situ values of the parameters may vary widely depending on the type of subsoil in different stratum and consistency. Figure 5(a) also indicates the penetration at which the different add-ons are spliced. Because of the welding delay, the restrike blow-counts are likely to increase at this penetration as the SRD would increase from 30% to 60% skin-friction case or beyond up to full set-up. Hence, the welding delay should be minimized as much as possible to avoid prolonged hard driving or refusal in the worst case scenario. The hammer efficiency controls at different depths indicated in Figure 5(a) are principally to avoid an excessive run-down at the initial stage and overstressing of the pile material.

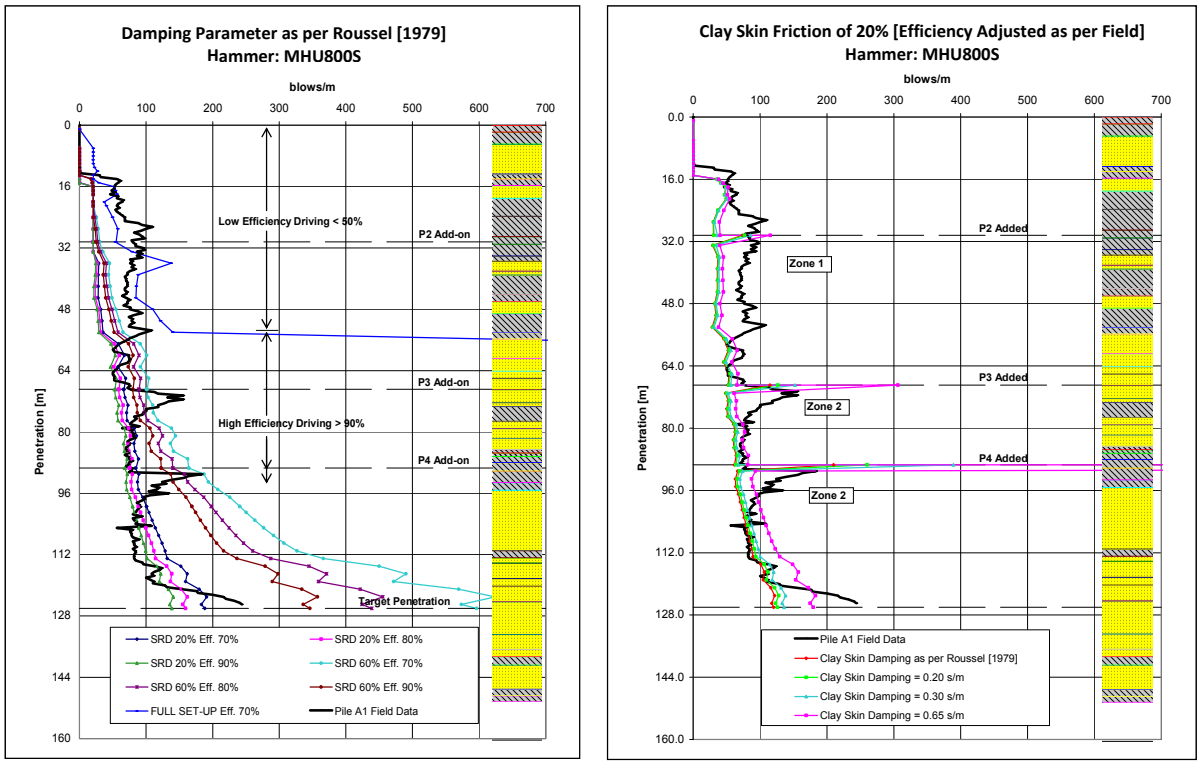


(a) **(b)** **(c)**

Figure 5 Case Study Site A: (a) Effect of Skin Damping on Driveability Blow-Count; (b) Comparison of Field Data Single Efficiency & Damping; (c) Comparison of Field Data Variable Efficiency& Damping

Figure 5(b) and 5(c) incorporates the actual field driving record of the same piles plotted along with the predicted or analyzed driveability blow-count results for comparison. The blow-count and resulting soil resistances are monitored at site. The results clearly indicate the sensitivity of skin damping in a clay dominated site. If we consider that the remoulded skin frictions are predicted reasonably well to simulate different situations, the sensitivity of the results are quite evident from Figure 5(c) where plots showing variable skin damping scenario. It is evident that a skin damping in clay closer to 0.3sec/m or those suggested by Roussel [1979] are more realistic.

Figure 6(a) & 6(b) shown here are from the Case Study B in the same region when the subsoil layers are not predominantly clay but more interspersed with intermittent silt and sand layers. Because of the presence of the sand layers in between and towards the deeper strata, the effects of clay skin damping parameters may not be so prominent in driveability prediction. Nevertheless, from the actual field data it could be observed that with the similar efficiency control the actual blow-count is quite closer to that predicted using a skin damping similar to that suggested by Roussel [1979] particularly at a deeper strata [Fig. 6(a)]. The result also showed that the assumed SRD variation of 20-30% skin friction of clay in case of continuous driving and 60% for delayed driving holds good for the region [Efficiency adjusted analyses; Fig. 6(c)]. A better comparison of SRD could be evaluated by collecting instrumented pile monitoring data that can be obtained during pile driving and subsequent back-analyses.

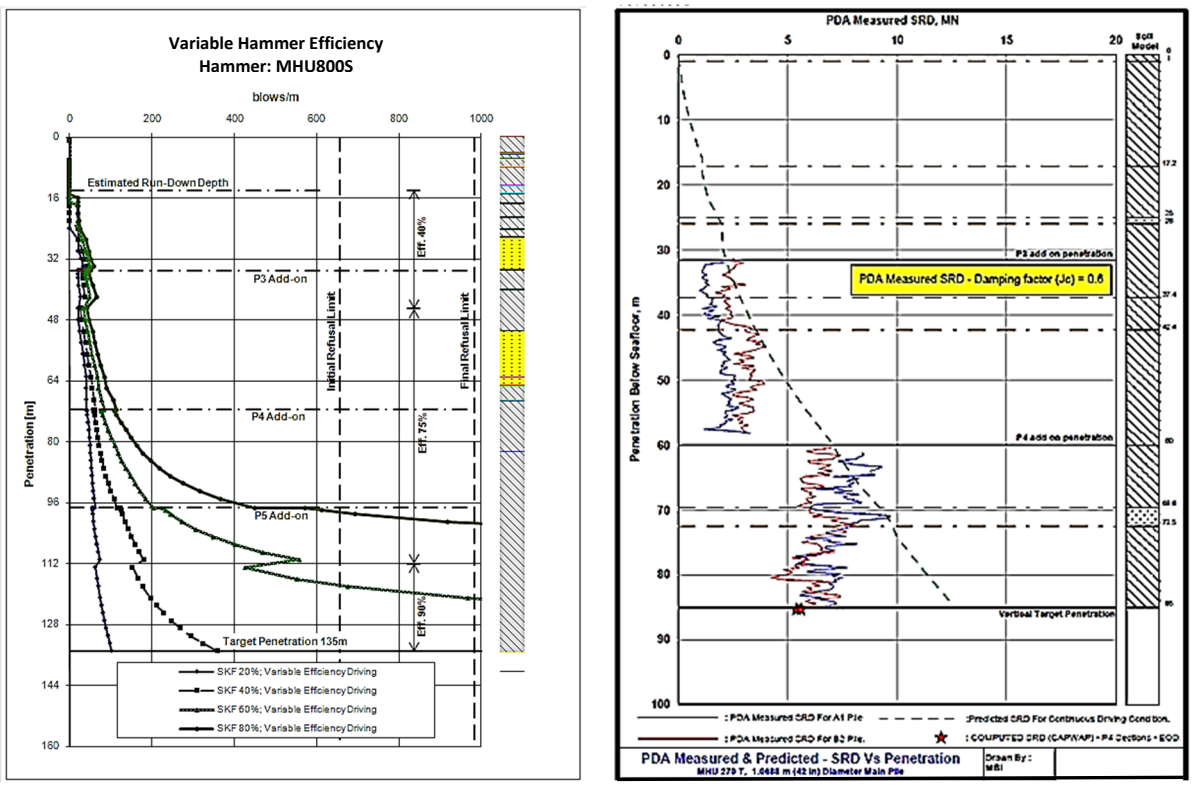


(a) **(b)**

Figure 6 Case Study Site B: (a) Comparison of Predicted & Observed Blow-count; (b) Comparison of Observed & Predicted Blow-count with Skin Damping Variation;

A third Case Study [Site C] is included here is taken from new project from the same region. Only preliminary analyses done based on the available soil data. No field data available for this project. Figure 7(a) shows the predicted blow count for several cases of efficiency controlled driving. Following the previous experience, similar SRD controls and only Roussel [1979] damping parameters are used in the driveability analyses and predictions with different remoulded skin friction in clay for continuous and delayed driving scenario. This should cover the predicted soil resistance during driving and the blow-counts with certain level of confidence and its fitness for the purpose. Figure 7(b) presents the PDA back-analysed SRD at Site D measured from the field monitoring data. The measured SRD has been reduced to 18-20%. This corroborates the actual remoulding effect in clay during driving.

It is to be noted that all the hammers used in these case studies are high efficiency hydraulic hammers. The efficiency control measures are adopted [by adjusting hammer strokes] in practice to avoid any pile damage due to overstressing and/or potential excessive rundown in soft subsoil layers.



(a) **(b)**

Figure 7 Case Study Site C & D: (a) Predicted Blow-count - Efficiency Controlled [Site C]; (b) PDA Measured & Predicted – SRD vs Penetration [Site D];

CONCLUSIONS

On the basis of previous discussions and the case studies, the following conclusions can be drawn with regards to driveability studies conducted on offshore driven piles in the regional [GoT] subsoil.

1. Optimum Hammer Selection - necessary from the point of view of efficient, economic as well as safe driving. Selection criteria should be 'Low Drop Height vs Damage Avoidance'.
2. Analysis Accuracy - driveability prediction is largely dependent on the accurate simulation/representation of the in-situ soil parameters [both static & dynamic] used to analyze the pile-soil interaction problem.
3. Driveability Prediction in Clay - Standard API RP 2A or ISO19902 method with degraded clay skin friction variation between 20-60% [of maximum static friction] to calculate lower and upper bound SRDs [with a maximum upper bound of 80% in some conservative cases] are found to produce a reasonable prediction for subsoil strata in the Gulf of Thailand region. Skin friction in sand is not normally degraded while determining SRD.
4. Clay Skin Damping – Generally, depends On Relative Soil-pile Velocity. There is Non-linear Variation with Velocity which is not well predicted through laboratory test level.
5. Driveability In Regional Clay - For sites dominated by clayey subsoil, the driveability prediction, subsequent acceptance criteria and selection of pile material and hammers are quite sensitive to skin-damping parameters in clay. The careful selection of these parameters should be based on regional experience. For a site with well-defined soil conditions, a constant clay skin-damping parameter value between 0.2-0.3sec/m is found to be suitable for the Gulf of Thailand region. The dynamic parameters based on the clay consistency such as proposed by Roussel [1979] may also be used with caution. For sand dominated sites, as the skin-damping parameter for granular soil is generally lower, the driveability analyses are not so sensitive to damping parameters

Reference List

Alm, T. and Hamre, L., 1998, Soil Model for Driveability Predictions, Offshore Technology Conference, Houston, Paper No. OTC 8835, May, 1998.

API RP 2A, 21st Edition, 2000, Recommended Practice for Planning, Designing and Constructing Fixed Offshore Platforms – Working Stress Design, American Petroleum Institute.

Bogard, J.D. & Matlock, H., 1990, Application of Model Pile Tests to Axial Pile Design, Proceedings, 22nd Annual Offshore Technology Conference, Houston, Texas, Vol. 3, pp. 271-278.

Bowles, J.E., Foundation Analysis and Design, McGraw Hill, 1977

Briaud, J.L. and Tucker, L.M., Coefficient of Variation for In Situ Tests in Sand, ASCE Symposium on Probabilistic Characterization of Soil Properties, Atlanta, April 1984.

Chen, R.P. and Chen, Y.M., 2000, Theoretical Study on Effect of Pile Shaft Resistance on Rebound During Pile Driving, Proceedings of the 6th International Conference on the Application of Stress-wave Theory to Piles, Brazil, pp 29-34.

Chen, R.P., Wang, S.F., Chen, Y.M., 2003, Study on Pile Driveability with One dimensional Wave Propagation Theory, Journal of Zhejiang University Science, V.4, No.6, pp 683-693, Nov.-Dec., 2003.

Clough and Penzien, 1975, Dynamics of Structures, McGraw-Hill, Inc., New York.

Chen, Y.M., Chen R.P., Wu, S.M. and Van Weele, A.F., 1997, Determining Static Resistance of Pile Toe during Driving with Acceleration of Pile Top, Chinese Journal of Geotechnical Engineering, 19(6):16-21.

Coyle, H.M. & Gibson, G.C., 1970. Empirical damping constants for sands and clays, Journal of Soil Mechanics and Foundation, ASCE, Vol 96, No. SM3, pp 949-965.

de Ruiter, J. and Beringer, F., 1979, Pile Foundations for Large North Sea Structures, Marine Geotechnology, 3, No. 3, pp. 267-314.

Forehand, P.W. & Reese, J.L., 1964, Prediction of pile capacity by the wave equation, Journal of Soil Mechanics and Foundations. ASCE, March 1964, No. SM2, pp 1-25.

Gibson, G.C. and Coyle, H.M., 1968, Soil Damping Constants Related to Common Soil Properties in Sands and Clays, Research Report No. 125-1, Texas Transportation Institute, Texas A & M University.

Goble, G.G., Rausche, F., 1976, Wave Equation Analysis of Pile Driving – Program Manuals, Department of Transportation, Report No. FHWA IP-76-14-3.

GRLWEAP, Wave Equation Analysis of Pile Driving, GRL Engineers, Inc., 2005.

Health & Safety Executive (2001), "A study of pile fatigue during driving and in-service and of pile tip integrity", HSE Books, Sudbury, Offshore Technology Report, 2001/018.

Heerema, E.P., 1979, Relationships between Wall Friction, Displacement Velocity, and Horizontal Stress in Clay and in Sand, for Pile Driveability Analysis, Ground Engineering, Vol. 12, No. 1.

Heerema, E.P., 1980, Predicting pile driveability: Heather as an illustration of the "friction fatigue" theory, Ground Engineering, 13, 15-37.

ISO19902:2007, Petroleum and Natural Gas Industries – Fixed Steel Offshore Structures.

Lehane, B.M., Jardine, R.J., Bond, A.J., & Frank, R. (1993), Mechanisms of Shaft Friction in Sand From Instrumented Pile Tests, Journal of Geotechnical Engineering, 119(1), 19-35.

Lehane, B.M., Schneider, J.A. & Xu, X., (2005), The UWA-05 Method for Prediction of Axial Capacity of Driven Piles in Sand, Proceedings of the International Symposium on Frontiers in Offshore Geomechanics, Perth, Australia, 683-690.

Lehane, B.M., Schneider, J.A. & Xu, X., (2007), Development of UWA-05 Design Method for Open and Closed Ended Driven Piles in Siliceous Sand, Contemporary Issues in Deep Foundations, ASCE GSP 158, 1-10.

Lowery, L.L., T. J. Hirsch, T. C. Edwards, H. M. Coyle & C. H. Samson, Jr., 1969, Pile Driving Analysis State of the Art, TTI Research Report No. 3313 (Final).

Mukherjee, K., Nagaraju, N., 2012, Installation of Offshore Driven Piles – Regional Experience, MOSS 2012, NUS Singapore, Proceedings, Research Publishing, 271-289.

Poulos, H. G. and Davis, E. H., 1980, Pile Foundation Analysis and Design, John Wiley and Sons.

Randolph, M.F., 2003, Science and Empiricism in Pile Foundation Design, Geotechnique, 53(10), 847-875.

Randolph, Mark, Cassidy, M., Gourvenec, S., Erbrich, C. (2005), "Challenges of Offshore Geotechnical Engineering", Osaka 2005.

Rausche, F., Goble, G.G., Likins, G., 1992, Investigation of Dynamic Soil Resistance on Piles Using GRLWEAP, Application of Stress-Wave Theory to Piles, F.B.J. Barends (ed.), Balkema, Rotterdam, ISBN 90 5410 0826, pp 137-142.

Roussel, H.J., 1979, Pile Driving Analysis of Large-Diameter, High-Capacity Offshore Pipe Piles, PhD Thesis, Department of Civil Engineering, Tulane University, New Orleans, Louisiana.

Schneider & Harmon, 2010, Analyzing Driveability of Open Ended Piles in Very Dense Sands, DFI Journal, Vol. 4, No. 1 August 2010.

Semple, R.M. and Gemeinhardt, J.P., 1981, Stress History Approach to Analysis of Soil Resistance to Pile Driving, OTC, Houston, Vol. 1 pp 165-172, 1981, Balkema.

Smith, E.A.L., 1960, Pile Driving Analysis by the Wave Equation, Journal of the Soil Mechanics and Foundations Division, Transaction of ASCE, Paper No. 3306, Vol. 127, 1962, Part I, pp 1145-1193.

Stevens, R.M. and Wiltsie, A.W. and Turton, H.T., 1982, Evaluating Pile Driveability for Hard Clays, Very Dense Sand and Rock, Offshore Technical Conference, 1982, OTC Paper No. 4205.

Tagaya, K., Heerema, E. P., Uchino, T., and Kusaka, T., 1979, Pile driveability test on actual offshore platform in calcareous clay for Qatar NGL offshore project, OTC 3440. Proceedings,11th Annual Offshore Technology Conference. Vol. 2, p. 713–16.

Toolan, F.E. and Fox, D.A., 1977, Geotechnical Planning of Piled Foundations for Offshore Platforms, Proceedings of Institution of Civil Engineers Part I, May 1977, Paper No. 7996.

Uto, K., Fuyuki, M. and Omar, H., 1992, New Development of Pile Driving Management System. Proceedings of 4th International Conference on the Application of Stress Wave Theory to Piles, The Hague, pp 351-356.

Van Luipen, P. and Jonker, G., 1979, Post Analysis of Full-scale Pile Driving Test, Proceedings of International Conference on Numerical Methods in Offshore Piling, ICE, London, pp 43-52.

Weele, A.F. and Schellingerhout, A.F.G., 1994, Efficient Driving of Precast Concrete Piles, Proceedings of Conference Development in Geotechnical Engineering, Bangkok, pp 1-8.

CONSTRUCTION INDUCED VIBRATION DURING SHEET PILE AND PILE DRIVING IN DEEP EXCAVATION

Ambarish Ghosh, Professor of Civil Engineering, IIEST Shibpur, INDIA, +91 9831286527, ambarish@civil.iiests.ac.in
SubhaprasadChakraborty, Post Graduate Student, IIEST Shibpur, INDIA, +91 9476246613, subhaprasad50@gmail.com

ABSTRACT

Construction of basement floors has become necessary to meet the requirement of parking in office and residential complexes and in hospitals for radiotherapy treatment. Important projects coming up in Kolkata are mostly in closer proximity of residential buildings, office buildings and historical monuments. Sheet piling is mostly used as temporary shoring system during construction. Deep excavation in urban environment creates great problem related to construction induced vibration due to driving of sheet piles for basement, pile driving etc. which raises the chances of damage of adjacent buildings and nearby structures. Vibratory sheet-pile driving is the most common method of sheet pile installation. The knowledge of induced vibration due to this phenomenon is still very deficient. This paper presents the analysis of measured vibration data collected from different sites of Kolkata with varying soil profile. Typical two case studies of sheet pile and pile driving has been presented and the vibration values are analysed. The responses of the vibration are reported in terms of peak particle velocities (PPV). To evaluate the effects of vibration due to pile driving two aspects have been considered: the effect of the energy entering the ground from the pile and the effect of the soil condition.

KEYWORDS: deep excavation, construction induced vibration, peak particle velocity.

INTRODUCTION

In urban areas infrastructure development projects are mainly located adjacent to existing structures like residential buildings, offices and historical structures. The construction work of such project influences the surrounding environment as well as human perception (Wiss 1981). During the construction of basement for residential complexes and hospitals sheet piling is mostly used as temporary shoring system or as to support the earth mass. The vibration induced due to driving of piles and sheet piles have been presented herein. Deep excavation projects close to existing structures increase the concern of environmental impact. For this reason the vibration assessment and prediction has become a subject of great interest. It is important to develop a site specific model for predicting the ground vibration resulting from pile and sheet pile driving at the construction sites. The developed model gives the efficacy to guide the engineer to select the construction methodology ensuring the safety of the surrounding structure. The model developed here is site specific and the parameters that has been used are dependent on the soil condition and the energy source.

WAVE PROPAGATION MECHANISM

Man-made vibration are the vibration which are generated by human activities. The waves associated with man-made vibration propagates through ground and interact with the nearby structures. It may disturb the people occupying the structure and in extreme cases the serviceability and integrity of the structure might be threatened (Svinkin 1996).The vibratory driving of pile generates ground vibration, when the ground is subjected to vibratory excitation from a vibration source, propagation of waves occurs away from the source(Athanasopoulos, G. A. and Pelekis, P. C. 2000). Vertically polarized shear waves are generated at the skin of the piles and it propagates outwards having the shape of a cone, along a cylindrical surface.

The displacement of soil volume at the tip of the pile also generates both compressional P-waves and shear S-waves and it propagate outward as a spherical wave front(Athanasopoulos, G. A., and Pelekis, P. C., 2000). When the P-waves and S-waves are superimposed at the ground surface a part of it is converted to surface Rayleigh waves and one part is reflected back to the ground. The R-waves propagate along the surface of the ground and consist of both horizontal and vertical components. The amplitude of the surface wave decay with the distance and the waves generated due to the reaction of body waves is close to the pile driving point.
The amplitude of vibration diminishes with distance from the source. The attenuation is mainly due to two factors (1) Expansion of wave-front (Geometrical Damping) (2) Dissipation of energy within the soil itself (Material Damping). The rate of geometrical attenuation is mainly dependent upon the type of wave and the shape of the associated wave-front.

PEAK PARTICLE VELOCITY

The ground vibrations are mainly quantified in terms of peak particle velocity which is defined as the vector sum of maximum velocity components of vibration.

$$\text{PPV} = \sqrt{V_{x,max}^2 + V_{y,max}^2 + V_{z,max}^2}$$

PPV is mainly a measure of damage potential of vibration. The velocities generally does not damagestructure; it is the resulting dynamic strain that are of concern. Human distress is linked to acceleration level. PPV parameters are very easy to measure and it co-relates well with the measured effect of ground vibrations and therefore very good indicator of damage potential.

VIBRATION PREDICTION MODEL

Square root scaled distance

$$V = k\left(\frac{r}{\sqrt{Q}}\right)^{-n}$$

V = Peak Particle Velocity (mm/s)
Q = Energy source (Joule)
D = distance (m)
k = site constant
n = site exponent
The square root scaled distance is most commonly used and is based on the observation that the energy is distributed in a long cylindrical surface of wave front, therefore the diameter of the cylindrical surface is proportional to the square root of the energy applied(Massarsch, K. R. and Fellenius, B.H. 2008). However, it can be considered that as the cylinder length shortens in relation to the diameter, the wave approaches a spherical shape, in that case the diameter is proportional to the cube root of the energy source. In energy decay terms, the decay may depend on what waveform the energy is dissipated in. It has been noted earlier that at some sites the surface waves predominate. At other sites, the energy is dissipated mainly through body waves. It may well be stated that at different sites with different wave front configurations, different types of vibrational waves are generated which becomes a more complex function than the square root or cube root or the general equation.

CASE STUDY OF CONSTRUCTION INDUCED VIBRATION

Case study I-

In a site near Alipore 16.0 m long sheet piles (U-section) has been driven for the temporary support of the sides of deep excavation of basement by braced sheet pile walls. The driving of sheet piles has

beenaccomplished by Hydraulic Vibratory Hammer (25HIA) of maximum frequency of 1600 rpm with necessary power pack. Monitoring of ground vibrations has been carried out with vibrometer using vibration sensor which has been positioned in such a way so as to measure the particle velocity in both horizontal and vertical direction. In man-made ground vibration measurement, it has been found convenient to describe the intensity of shaking by the peak value of particle velocity. The reason for this choice is the well established correlation between particles velocities and observed cosmetic cracking, which has been established theoretically by the fact that the strain induced in the ground during vibration is proportional to the particle velocity.





Fig. 1. Vibratory driving of sheet pile in a site near Alipore and the measurement of PPV

Field Observation

The ground vibrations has been presented in terms of PPV (mm/s) which has been measured at different horizontal distances and perpendicular distances. PPV values at different penetration depth of the pile and at different floors of nearby buildings has been also recorded. Each component of PPV measured has been named as horizontal, and vertical.

Table I. Variation of PPV with different distance and different depth of driving

DISTANCE (m)	2.0	3.0	3.3	3.5	5.0	6.7	8.2	9.7	12.0
DEPTH(m)	**PEAK PARTICLE VELOCITY(mm/s)**								
0.0	5.2	7.4	8.1	6.5	4.1	3.9	4.2	1.7	1.9
3.0	6.5	8.0	5.6	4.8	4.2	2.1	2.7	2.8	1.3
6.0	3.4	4.0	5.2	3.5	3.0	2.6	1.3	1.2	1.1
9.0	8.4	3.6	1.6	2.9	0.4	3.2	1.1	0.7	2.6
12.0	4.1	2.8	3.9	2.4	1.0	3.5	1.2	1.3	2.1

Soil condition of the site

The soil exploration at the test site revealsthe followings:
Stratum-I: varying between depth from 0.00 m to 4.80 m, heterogeneous fill material.
Stratum-II: varying between depth from 4.80 m to 15.00 m, soft to medium/deep grey/stiff steel grey/dark grey/brownish grey clayey silt with traces of brick pieces & black spots.
Stratum-III: varying between depth from 15.00 m to 22.65 m, soft to medium deep grey/stiff to very stiff steel grey/yellowish/brownish grey clayey silt with black/rusty spots.
The depth of sheet pile driving in this project is about 16.0 m.

Analysis of the vibration data

The values k and n as obtained from the analysis for different depths has been presented in table 2. The values of PPV have been plotted against the square root of scaled distance. It has been revealed from the analysis that soil type and energy source govern the constants of the proposed regression models. Different researchers have proposed different model but the scale distance model considers both of these parameters i.e., soil type and energy source and gives satisfactory results. Figs. 2 – 4 present the typical ground PPV vs scaled distance as obtained based on field observations.

Fig.2. Variation of PPV with scaled distance (at ground level)

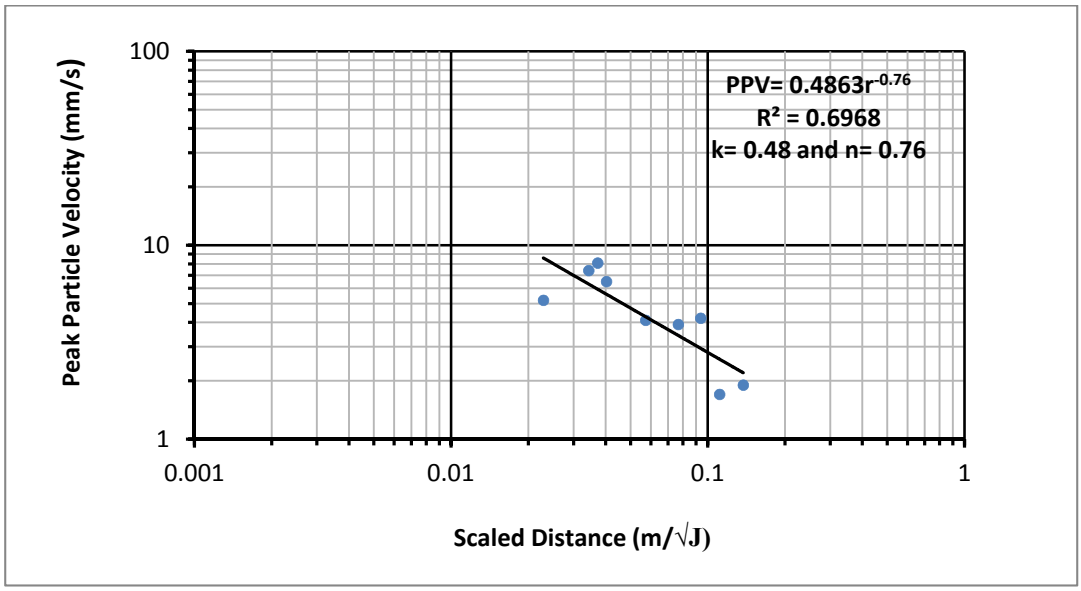


Fig. 3. Variation of PPV with scaled distance (at 3m depth)

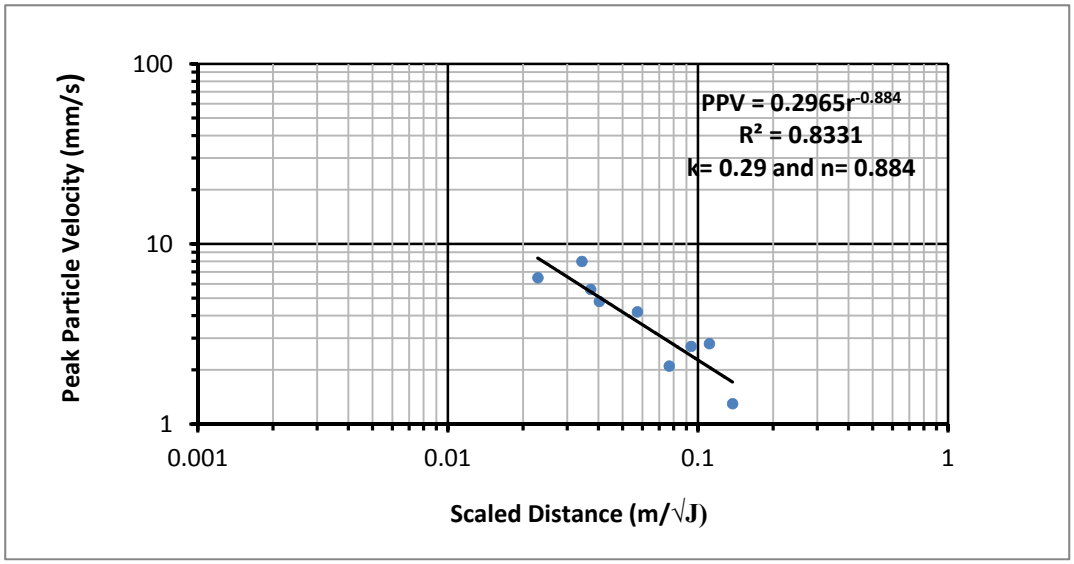
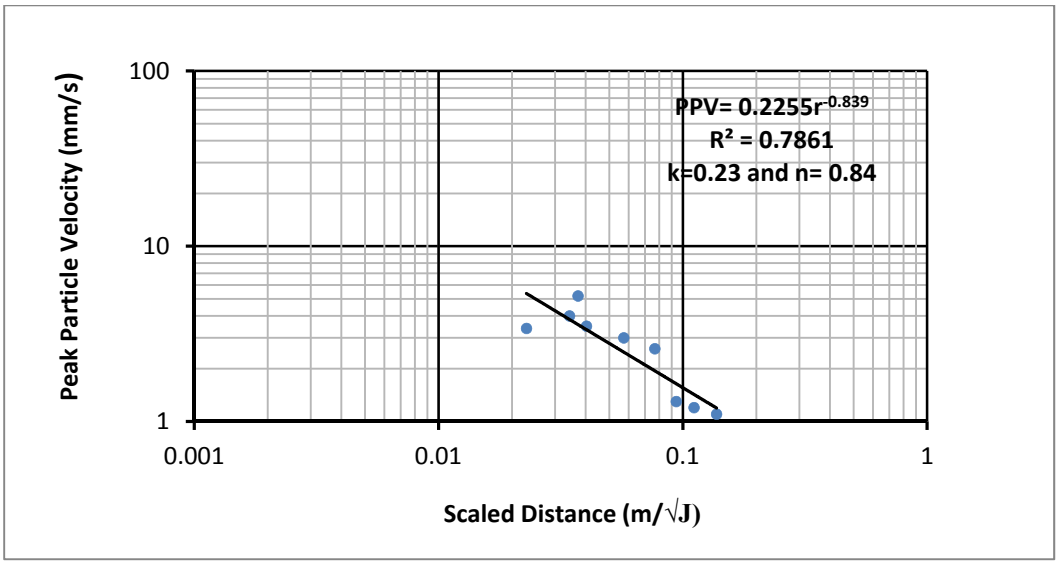


Fig.4. Variation of PPV with scaled distance (at 6m depth)



Similarly for other depths, the site constant k and the site exponent n has been calculated and presented in Table. 2. with varying soil type.

Table. 2.Variation of k and n value with soil type

Depth	Soil Type	k	n
0.0 m	Filled up soil consists of brownish grey silty fine sand with brick bats.	0.48	0.76
3.0 m	Filled up soil consists of brownish grey silty fine sand with brick bats	0.30	0.88
6.0 m	Soft deep grey silty clay/clayey silt	0.23	0.83
9.0 m	Soft to medium deep grey clayey silt with decomposed wood & organic matter	0.28	0.77
12.0 m	Soft to medium deep grey clayey silt with decomposed wood & organic matter	0.28	0.70

Case study II-

In a site near Esplanade 16.0 m long pile casing has been driven for the foundation of a G+16 storied building. The driving of piles has been accomplished by Vibratory Hammer (FAV 416L) of maximum frequency of 1600 rpm with necessary power pack. Monitoring of ground vibrations has been done with vibrometer using vibration sensor that has been positioned in such a way so as to measure the particle velocity in both horizontal and vertical direction. During driving of piles, generation of vertically polarized body shear waves took place along the skin of the pile and their wave front propagated outward along a cylindrical surface. On the other hand at the tip, the displacement of the volume of soil generated body waves which when encounter at the ground surface has been converted partly to surface wave and partly reflected back to the ground.



Fig.5. Vibratory driving of pile casing in a site near Esplanade

Field observation

The ground vibrations has been presented in terms of PPV (mm/s) which has been measured at different horizontal distances and perpendicular distances. PPV values at different penetration depth of the pile and at different floors of nearby buildings has been also recorded. Each component of PPV has been measured namely horizontal, and vertical.

Table 3. Variation of PPV with different distance and different depth of driving

DISTANCE (m)	3.0	6.0	9.0	10.0	12.0
DEPTH(m)	**PEAK PARTICLE VELOCITY(mm/s)**				
3.0	12.8	8.2	5.2	4.2	2.1
6.0	7.0	3.7	3.8	3.1	1.8
8.0	4.3	4.6	3.2	2.2	1.4
10.0	4.6	3.8	3.0	2.1	1.5
12.0	2.6	2.1	1.9	1.5	1.1

Field condition

The soil exploration at the test site revealsthe followings:

Stratum - I: varying between the depths from 0.0 m to 2.0 m, heterogeneous fill material.

Stratum - II: varying between the depths from 2.0 m to 7.0 m, soft to medium to stiff brownish grey to grey silty clay.

Stratum - III: varying between the depths from 7.0 m to 14.7 m, soft to medium stiff dark grey to grey silty clay. The depth of pile casing driving in this project is about 12m. The ground water table was located at about 1.2 m depth below the ground surface.

Analysis of the vibration data

The values k and n as obtained from the analysis for different depths has been presented in table 4. The values of PPV have been plotted against the square root of scaled distance. It is revealed from the analysis that soil type and energy source govern the constants of the proposed regression models. Different researchers have proposed different model but the scale distance model consider both these parameters i.e., soil type and energy source and gives satisfactory results. Figs. 6 – 8 present the typical ground PPV vs scaled distance as obtained based on field observations.

Fig.6. Variation of PPV with scaled distance (at 3m depth)

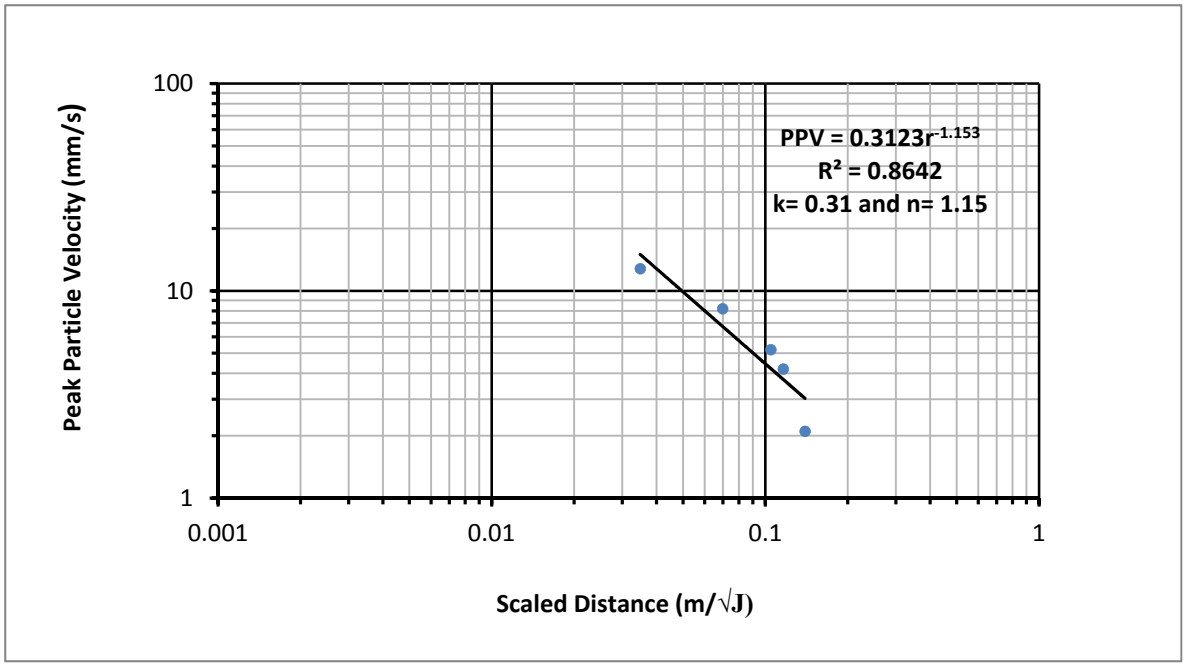


Fig.7. Variation of PPV with scaled distance (at 6m depth)

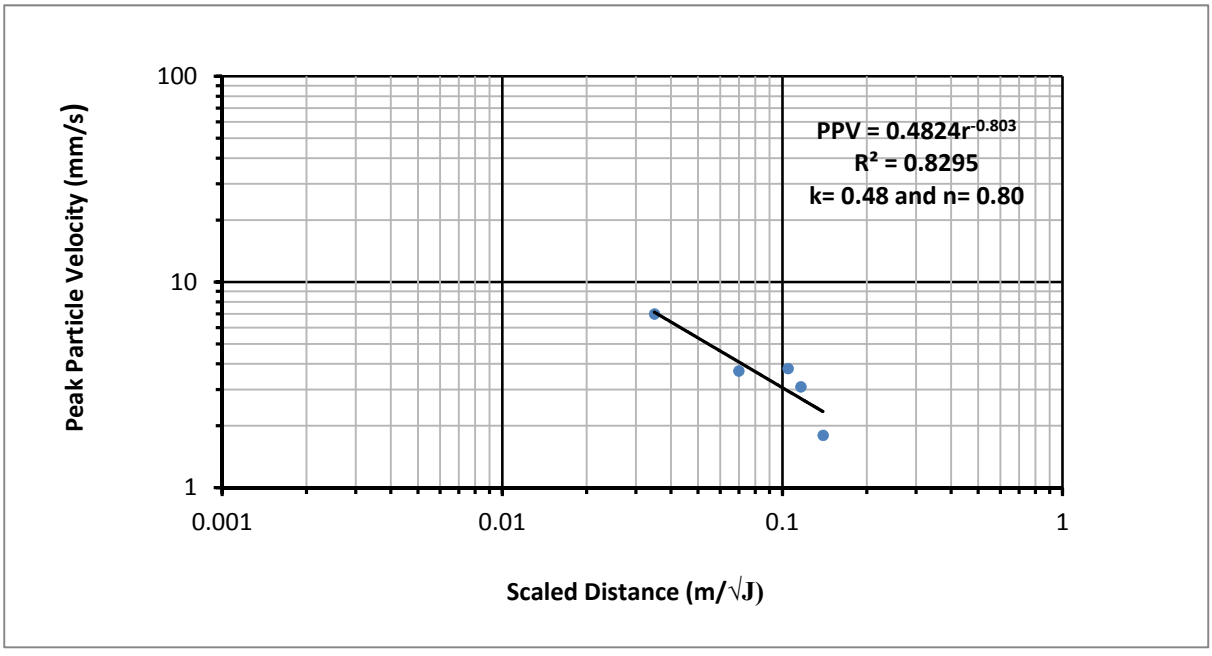
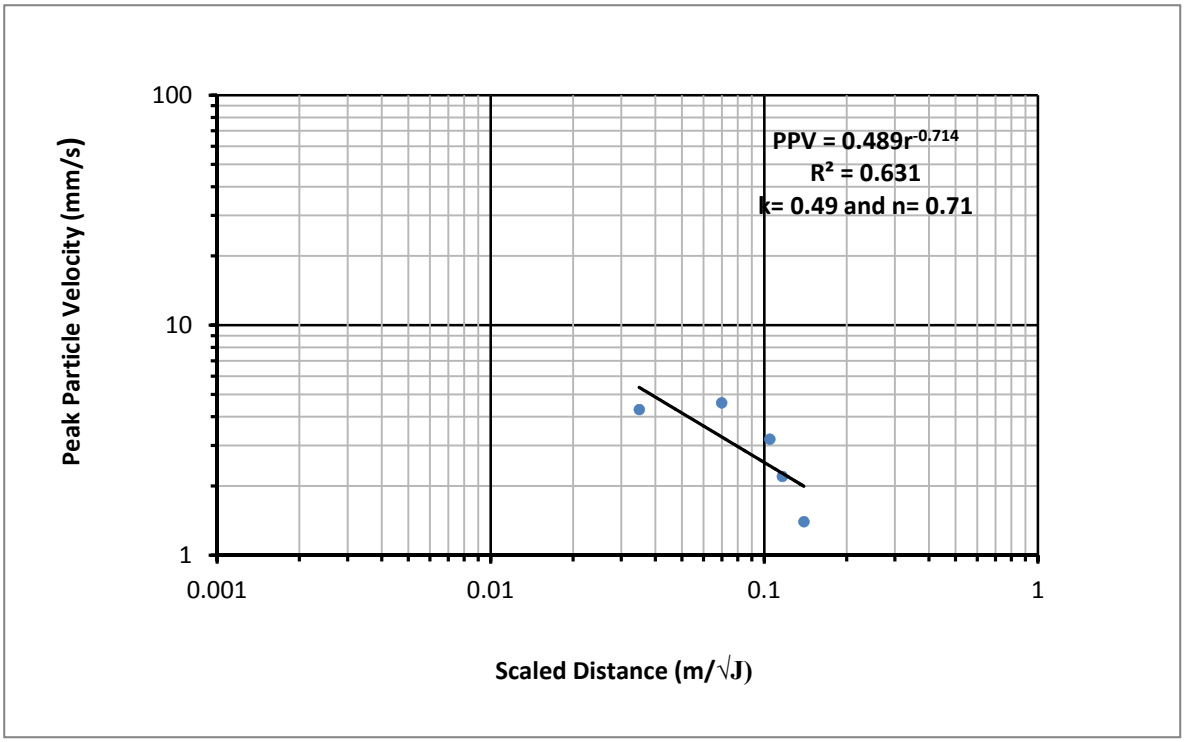


Fig.8. Variation of PPV with scaled distance (at 8m depth)



Similarly for other depth the site constant k and site exponent n is calculated and tabulated which is dependent on the soil condition and the energy source.

Table 4.Variation of k and n value with soil type

Depth	Soil Type	k	n
3.0 m	Heterogeneous fill material	0.31	1.15
6.0 m	Soft to medium brownish grey silty clay	0.48	0.82
8.0 m	Soft to medium brownish grey silty clay	0.48	0.71
10.0 m	Soft dark grey silty clay	0.45	0.72
12.0 m	Soft dark grey silty clay	0.47	0.60

For the Esplanade site the site constant and site exponent values has beenobtained through regression analysis and the variation of this value with soil profile is shown in the above table.
This values help to predict the peak particle velocities considering the soil type and energy generated by the vibratory hammer. It will help to select the construction methodology keepingthese vibration velocities within the limit.
Different researchers have proposed different values of k and n. Wiss (1981) stated that an n lies between 1.0 and 2.0 with a relatively common value of 1.5 and k is 1. According to Attewell et al. (1992) a best fit line from measurements of ground vibrations from both impact and vibratory pile driving give k = 0.76 and n = 0.87. They have given these values which is same for all type of soil.But considering this two cases it can be concluded that the k, n values are site specific and varying with the soil profile.

COMPARISON OF PROPOSED MODEL WITH OTHER PREDICTION MODEL

Different researchers have proposed different models for prediction of the ground vibration in terms of peak particle velocity. They have given different values of k and n considering soil type. Values of k, n given by different researchers has been presented in table.5.

Table 5.Summary of values of parameters used in different prediction models

Researchers	Parameters	
	n (site constant)	k (site exponent)
Attewel and Farmer (1973)	1.00	1.50
Whyley and Sarsby (1992)	1.00	0.25 (Soft or loose soil) 0.75 (Stiff or medium dense soil) 1.50 (Very stiff or very dense soil)
Attewell et al. (1998)	0.87	0.76
CEN standard (1998)	1.00	0.50 (Soft cohesive soil) 0.75 (Stiff cohesive soil) 1.00 (Very Stiff cohesive soil)
Arcelor Mittal (2008)	1.00	Impact Driving 0.50 (Soft cohesive soil, loose granular media, loose fill and organic soil) 0.75 (Stiff cohesive soils, medium dense granular media, medium compacted fill) 1.00 (Very Stiff cohesive soil, dense granular media, rock fill with large obstructions) Vibratory Driving 0.70 (All soil conditions)

CONCLUSION

Two case studieshave been presented in this paper to highlightthe influence of major factors controlling the construction induced vibrations. The parameters like vibratory source, the soil condition of the site, and the distance from the source have been considered.Two different case studies one illustrating the driving of sheet piles and the other for driving of pile casing has been presented herein. From the analysis of the field data, the following conclusions may be drawn:

From the case Study- I, it has been observed that for soft to stiff silty clay in Alipore region the k value is ranging from 0.25 to 0.30 and range of n value is 0.70 to 0.85. In case Study II for pile casing driving the site constant and exponent values obtained are 0.30 to 0.45 and 0.65 to 0.85.For these two sites the k and values obtained for silty clay soil nearly the same.

It can be concluded from the study that the developed site specific model is efficient to predict the construction induced vibration for the specific site and also used for adaptation of the suitable mitigation strategy.

REFERENCE LIST

Athanasopoulos, G. A., and Pelekis, P. C., (2000), "Ground vibrations from sheetpile driving in urban environment: measurements, analysis and effects on buildings and occupants". JournalofSoil Dynamics and Earthquake Engineering, 19, 371-387.

Attewell, P.B., and Farmer, I.W., (1973) "Attenuation of ground vibrations from pile driving."Ground Engineering 3(7): 26-29.

Attewell, P.B. Selby., A.R. and O Donnell, L. (1992) "Estimation of ground vibration from driven piling based on statistical analyses of recorded data." Geotechnical and Geological Engineering 10(1992): 41-59.

Massarsch, K.R., and Fellenius, B.H., (2008) "Ground Vibrations Induced by Impact Pile Driving."In Proceedings of the sixth International Conference on Case Histories in Geotechnical Engineering

Svinkin, M.R., (1996). Overcoming soil uncertainty in prediction of construction and industrial vibrations.Proceedings of Uncertainty in the Geologic Environment: From theory to Practice, GeotechnicalSpecial Publication. No. 58, Vol. 2, pp. 1178-1194, Madison: ASCE.

Svinkin, M.R., (2008). Soil and Structure Vibrations from Construction and Industrial Sources, the 6th International Conference on Case Histories in Geotechnical Engineering. Arlington, Virginia.

Wiss, J. F., (1981), "Construction Vibrations: State of the Art," Journal of the Geotechnical Division, ASCE, 107(2), 167-181.

DETERMINATION OF COEFFICIENT OF MODULUS OF SUB-GRADE REACTION FOR FREE HEAD SHORT PILE

Sumit Kumar Biswas, Assistant Professor, Civil Engineering, Jadavpur University, Kolkata, West Bengal, India, 9831943818, sumiturdr1@rediffmail.com
Sibapriya Mukherjee, Professor, Civil Engineering, Jadavpur University, Kolkata, West Bengal, India, 9874304637, sibapmukh@yahoo.co.in
Moyukh De, Assistant Engineer, PHED, Govt. of West Bengal, India, 9231718278,123sherlock@gmail.com

ABSTRACT

The piles often are also subjected to lateral (horizontal) forces and moments. In fact, there are some structures where the primary function of piles is to transfer lateral loads to the ground. Proper analysis of laterally loaded piles is very important to the geotechnical and civil engineering profession.In the present investigation an experimental study has been carried out with free head short model cast iron hollow piles of outer diameter of 24 mm and *L/d* ratios of 8, 10, and 15. The experimental results have been supplemented by numerical techniques using PLAXIS-3D Foundation version 2.1 software. The results have been found to agree reasonably well with the experimental results. Further finite difference approach has been adoptedto reduce the computational time and to calculate the coefficient of modulus of sub-grade reaction (η_h) from the load- deflection data obtained from PLAXIS output at different pile depths. The parametric study has been extended for the non-dimensional form defined as flexibility ratio (F.R.), ($FR = \frac{\eta_h L^5}{E_p I_p}$ where η_h, *L*, E_p and I_p are the coefficient of modulus of sub-grade reaction, the embedded length of model pile, elastic modulus of pile material and the moment of inertia of model pile about the central axis respectively).The variation of coefficient of horizontal modulus of sub-grade reaction (η_h) has been studied with respect to the following parameters for homogeneous soil system: relative density and*L/d* ratio. It has been found that the logarithm of flexibility ratio increases with increase inrelative density and increase in*L/d* Ratio. The values of η_h obtained by the proposed method have been, found to be close to the numerical results.As output of this research, graphs have been generated in respect of different parametric variations to gain an insight into behavior of piles under lateral load for short piles.

Keywords: model pile, relative density, *L/d* ratio, free head, PLAXIS-3D, Coefficient of modulus of horizontal subgradereaction.

INTRODUCTION

In civil engineering practice piles are subjected to a wide variety of loading conditions due to earthquake, wind, sea wave and the like. Thus it is understood that response of pile under lateral loading has a great importance in analysis and design of piles. Many approaches have been made by various researchers so far. Elastic analysis has been extended to piles (Davisson and Gill 1963) and subsequently design charts for prediction of lateral response of piles using theoretical and experimental studies have been created (Broms 1965). Reese et al. (1974) proposed criteria for cohesionless soils for analyzing the behavior of piles under static and cyclic loading. In the present decade, many remarkable studies have already been furnished by the distinguished investigators. Maheshwari et al. (2011) has developed a finite-element code in MATLAB to model three-dimensional soil-pile-structure systems.Kim and Jeong (2011) investigated the load distribution and deflection of large diameter piles by lateral load transfer method (*p-y* curve). Dynamic response characteristics of reinforced concrete group piles with embedded pile-cap condition in the field under varying levels of coupled harmonic excitations have been investigated by Biswas et al. (2013).An efficient analytical approach using the finite element (FE) method has been

proposed by Chatterjee et al. (2015) to calculate the bending moment and deflection response of a single pile under the influence of lateral and axial compressive loading simultaneously during an earthquake, in both saturated and dry homogenous soil, and in a typical layered soil.
The present study brings out the behavior of laterally loaded short pile with variation of relative density and *L/d*ratioin homogeneous sand medium. This study involves one new method of determination of η_h without using or without generating p-y curve. In that sense this approach is helpful in profession.
In the present investigation an experimental study has been carried out with model cast iron hollow piles of diameter 24 mm (O.D.), *L/d* ratios of 8, 10 and 15 in homogeneous soil. Subsequently the experimental results have been supplemented by adopting numerical techniques. The analysis has been done using PLAXIS-3D Foundation version 2.1 software. Further in order to find out the failure load or ultimate load of the piles the load displacement curves have been plotted and by using the conventional failure criterion (like Meyerhof's method (1981), double tangent method and empirical method by Reese (1960) the failure load has been evaluated. It has been seen that the empirical method (Reese 1960) of finding the failure load to provide better results in finding the failure loads than the other conventional methods. The variation of failure load has been studied with respect to the following parameters for homogeneous soil system:
1. Relative density (33%, 42%, 62%, 67%, 74% and 90%),
2. *L/d* ratio (8, 10 and 15) i.e. with embedded length of 192mm, 240 mm and 360 mm respectively,
The figures within the parenthesis indicate the values of the parameters considered in this study.
In this paper an attempt has been made to formulate an expression to find the value of coefficient of modulus of sub-grade reaction (η_h) depending on soil pile parameters embedded in homogenous soil of known relative density.

LONG PILE AND SHORT PILE CRITERIA

A pile based on its behavior during loading has been classified as long and short piles. It is done using a constant known as stiffness factor (R or T).For cohesionless soil stiffness factor, T is used. It depends on flexural rigidity of pile, EI and the coefficient of modulus of sub-grade reaction, η_h which is given by a specific relation as mentioned by Mukherjee et al. (2013). Moreover, as mentioned by Mukherjee et al. (2013) in this respect, model cast iron piles with *L/d* ratio 8 and 10 can be classified as short piles whereas the model cast iron piles with *L/d* ratios of 15 can be classified as piles lying between long and short regions.

FAILURE LOAD CRITERION

The failure load criteria considered in the study are similar to the failure load criteria considered by Biswas et al, (2012).
To find the failure or ultimate load initially three conventional techniques have been employed

1. Double tangent Method
2. Meyerhof's Method (1981)
3. Empirical Method: Reese and Matlok (1960) gave an empirical method to calculate the horizontal pile head deflection corresponding to the ultimate soil resistance of the pile.

It has been observed that the empirical method has furnished very consistent results compared to the other two methods. Thus this method has been used for both experimental and numerical analysis.The failure load or ultimate load for the present study is considered to be load causing deflection of pile head equal to 0.0354 inch or 0.9 mm (this ultimate deflection accounts about 3.75% of the pile diameter).

MODEL PILE AND FOUNDATION MEDIUM

The model pile and the foundation medium considered in the experimental and numerical study are taken according to those considered by Biswas et al. (2012) in their model pile experiments.

Model Pile

Hollow cast iron model piles of outer diameter 24mm and thickness of 2.4 mm with lengths of 192mm, 240 mm and 360 mm (to achieve desired *L/d* ratios of 8, 10 and 15respectively), have been considered. The material properties of the cast iron considered in the modeling is given below:

Table1. Properties of Cast Iron (Biswas et al. 2012)

Properties	Value	Properties	Value
Density of Cast Iron	9.23×10-8kN/mm^3	Shear Modulus (τ_p)	27130.424 MPa.
Young's Modulus (E_p)	66307.55 MPa.	Poisson Ratio (μ_s)	0.222

Foundation Medium

In this study sand has been considered as a foundation medium. The properties of sand (dry density, void ratio, φ, young's modulus and poisons ratio), as considered is shown in figure 1, figure 2and table 2 respectively.

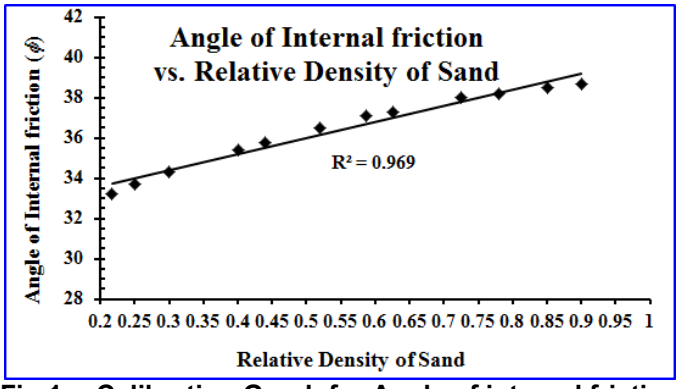


Fig.1. Calibration Graph for Angle of internal friction vs. Relative density (after Biswas et al. 2012)

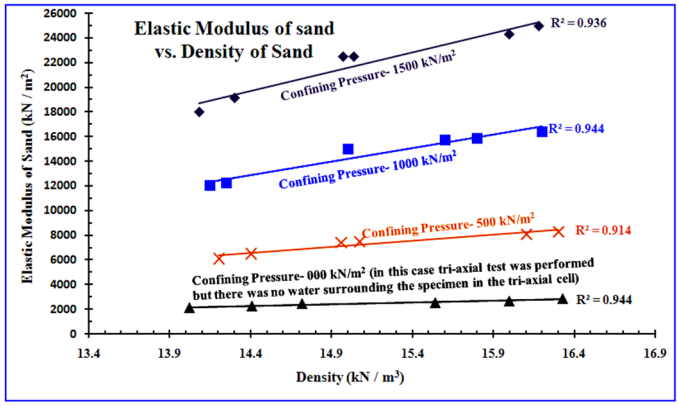


Fig. 2. Elastic modulus of sand vs. density with respect to different confining pressure (after Biswas et al. 2012)

Table2. Properties of Sand (Biswas et al. 2012)

Properties of Sand prepared for model test		Properties of Sand prepared for model test	
Maximum Dry Density (γ_{dmax})	1.70 gm/cc	Void Ratio (loosest) e_{max}	0.992
Minimum Dry Density (γ_{dmin})	1.37 gm/cc	Void Ratio (densest) e_{min}	0.605
Specific Gravity (G_s)	2.696	Poisons Ratio (μ)	0.20

EXPERIMENTAL STUDY

The model pile and the foundation medium considered in the model tests are taken according to those considered by Biswas et al, (2012) in their model pile experiments.
Following results have been obtained from the experiments with model piles as already mentioned.

Table 3. Model pile experiments showing the failure load obtained from lab experiments

L/d ratio	Relative density of sand	Test ultimate load ($\times 10^{-2}$kN)	L/d ratio	Relative density of sand	Test ultimate load ($\times 10^{-2}$kN)
8	33%	4	10	67%	7.5
8	42%	4.9	10	74%	7.8
8	62%	5.5	10	90%	8.1
8	67%	5.8	15	33%	6
8	74%	6.1	15	42%	7
8	90%	6.5	15	62%	7.6
10	33%	5.9	15	67%	8.0
10	42%	6.75	15	74%	8.2
10	62%	7.4	15	90%	8.5

NUMERICAL STUDY

The numerical study has been carried out by PLAXIS 3D finite element software by which numerical finite element models are generated simulating respective test conditions.
The method followed to perform the numerical study are alike to the method followed by Mukherjee et al. (2013) to carry out the numerical study in their analysis.

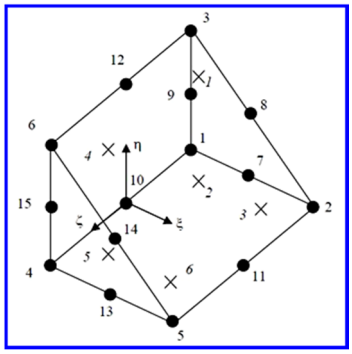


Fig. 3. Distribution of nodes (•) and stress points (×) in a 15 – node wedge element

The whole soil continuum has been divided into a number of 15-noded wedge elements to form the 3D finite element mesh. The 15-noded elements (figure 3) have been constructed with 8-noded quadrilaterals in vertical direction and 6-noded triangles in horizontal direction. Consequently interface elements have been modeled as 16-node (consisting of eight pairs of nodes) interface elements. The depth of soil continuum has been taken as 1.7 times the length of the pile (Kim and Jeong 2011) for numerical modeling. These dimensions have been considered adequate to eliminate the boundary effects on the performance of pile.
To model the behaviour of soil surrounding the pile, Mohr-Coulomb failure criteria have been used. This elasto-plastic model depends on the soil parameters, friction angle "φ′" and cohesion intercept "c′". Young's modulus "E′", change in elastic modulus with depth "$E_{increment}$" and Poisson's ratio "ν′". These parameters helped to obtain stress-strain behaviour of the soil.
From the analysis of PLAXIS 3D models the variation of moments with respect to the depth of pile and the displacement profile of the pile for gradual increment of horizontal load are obtained in each case of

analysis. On these results the finite difference approach is further infused to obtain horizontal modulus of sub-grade reaction (η_h). The process has been illustrated as follows:

The pile has been divided into number of nodes (n) having the node to node length of 'h' units; and the boundary conditions used in this study [Poulos and Davis (1980)] are briefly outlined below.

(1) For long floating free head pile the value of end moments that is M_1 (moment at extreme top of the pile) and M_{n+1} (moment at extreme bottom end of the pile) will be equal to zero.

(2) It is known that the soil induced stress in cohesionless soil medium varies with the depth as the node '1' is situated at the ground level so it can be assumed that the soil reaction per unit length of the pile at node '1' will be negligible, so $w_1=0$ (as no overburden is present).

Another boundary condition incorporated in the present analysis is furnished below:

(3) For pile under consideration at the pile head shear force at the node '1' will be equal to the horizontal load acting on it.

In case of a laterally loaded pile (like a transversely loaded beam), applying finite difference technique over the relationship between moment 'M' and load 'w' (i.e. $[(d^2M)/ (dx^2) = -w]$), the coefficient of modulus of subgrade reaction 'k_h' having units of force/length^3 at a node 'n' can be obtained in the following way (where "h" is the incremental depth between two successive nodes along the pile):

$$k_h = \frac{(M_{n+1} - 2M_n + M_{n-1})}{dyh^2} \quad (1)$$

The coefficient of horizontal sub-grade reaction 'k_h' has been obtained from equation 1 through a computer program developed for the purpose which has been coded in C++ programming language to attain at the value of k_h. The value of $k_h$has been calculated for each incremental load up to the assumed fixity point (Chin et al. 2009). The fixity point has been calculated for each incremental load corresponding to a depth where horizontal deflection has beenfound to be negligible.

It has been observed that the values of k_h obtained from finite difference calculations have been found in close proximity (at a variation of 10%) with those obtained indirectly from PLAXIS 3D.

From output of the PLAXIS 3D, the failure load has been calculated for the pile horizontal head deflection equal to 0.9mm. The experimental as well as the PLAXIS 3D results are presented in **table**4.

Table4. Failure load of Numerical and Experimental Results

L / d Ratio	Relative density of sand	Test ultimate load ($\times10^{-2}$kN)	PLAXIS ultimate load ($\times10^{-2}$kN)	% Deviation w.r.t. test load
8	33%	4	4.69	-17.25
8	42%	4.9	5.15	-5.10204
8	62%	5.5	5.75	-4.54545
8	67%	5.8	5.88	-1.37931
8	74%	6.1	6.07	0.491803
8	90%	6.5	6.43	1.076923
10	33%	5.9	6.3	-6.77966
10	42%	6.75	6.86	-1.62963
10	62%	7.4	7.58	-2.43243
10	67%	7.5	7.72	-2.93333
10	74%	7.8	7.91	-1.41026
10	90%	8.1	8.27	-2.09877
15	33%	6	6.4	-6.66667
15	42%	7	7.2	-2.85714
15	62%	7.6	8.15	-7.23684
15	67%	8.0	8.27	-3.375
15	74%	8.2	8.39	-2.31707
15	90%	8.5	8.58	-0.94118

The deviation between ultimate loads obtained from the test results and obtained from numerical approaches are small. Hence PLAXIS can be used as a tool for further analysis.
In this respect, the complete flowchart of the program constructed is given here (Figure 4). The program has been made as a 'self -checking' type as it checked the consistency of its input.

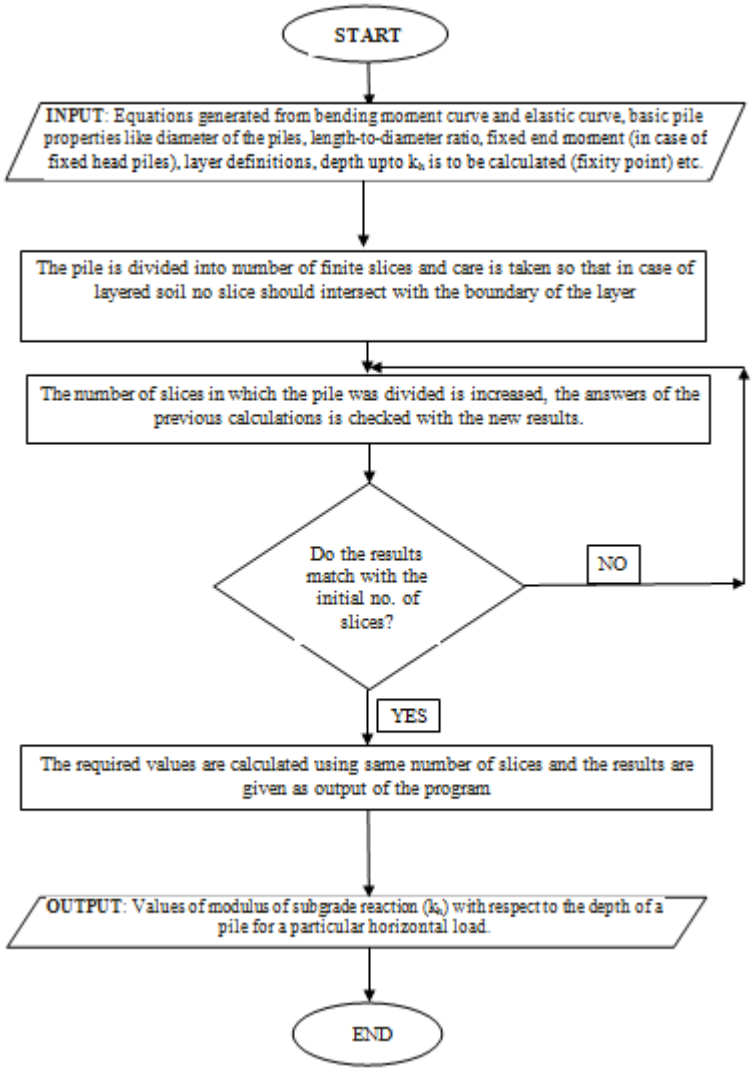


Fig. 4.Flow Chart of the Finite Difference Program

RESULTS AND DISCUSSIONS

Soil Interaction Parameters: k_h and η_h

From the results of PLAXIS 3D model analysis an attempt has been made to study the variation of the soil interaction parameter, (η_h) for the cohesionless soil medium with different soil-pile parameters.
Main soil interaction parameter is the horizontal sub-grade reaction, K (force/length^2), the ratio of K to the diameter or width of pile is known as coefficient of horizontal sub-grade reaction, k_h (force/length^3). Further the product of k_h with the ratio of diameter or width to the depth is known as coefficient of modulus of sub-grade reaction, η_h (force/length^3). So, η_h can be obtained from k_h as:

$$k_h = \eta_h \times \frac{z}{B} \tag{2}$$

Where, z is depth of the pile (length) and B is breadth of the pile or the diameter of the pile (length), which in this case is the pile diameter. Equation 2 has been considered from Poulos and Davis (1980).
In other words, the above equation indicates a linear variation of coefficient of horizontal sub-grade reaction with depth and actually such linear variation of coefficient of horizontal sub-grade reaction with depth is reasonable only for sands and soft clays.

Determination of η_h from k_h vs. Depth Graph

The modulus of horizontal sub-grade reaction, η_h is used as an integral soil interaction parameter in case of cohesionless soil medium as it has a constant value for a specific cohesionless soil medium.
For all cases irrespective of soil and pile conditions using the data obtained from the PLAXIS 3D models and subsequently by the finite difference approach k_h vs. depth graphs have been prepared. After obtaining the graph an average line of variation for values of k_h with respect to depth has been drawn.From each of thevalue of k_h, the concerned value of η_h has been calculated using above equation (2).

Flexibility Ratio: Normalizedform of coefficient of modulus of sub-grade reaction (η_h)
The normalized form of the coefficient of modulus of subgrade reaction (η_h) has been considered in this study as the Flexibility Ratio (F.R.) and is represented as:

$$FR = \frac{\eta_h L^5}{E_p I_p} \text{ (Barber 1953)} \quad (3)$$

Where, L = Length of pile, E_p = Young's modulus of pile (= 6.52E + 07 kN / m^2),
I_p = Moment of inertia of the section of the pile about the central axis (= 1.05E - 08 m^4),
The values of estimated η_h and F. R. (normalized form of coefficient of modulus of sub-grade reaction) are summarized in following table 5.

Table5. Coefficient of modulus of sub-grade reaction, $\eta_h$and F.R. of Numerical Results

L / d ratio	Relative density of sand	PLAXIS ultimate load($\times 10^{-2}$kn)	Estimated η_h (kN/m^3)	Flexibility ratio (F.R.)=($\eta_h L^5$) / ($E_p I_p$)
8	33%	4.69	2553.658	0.973267
8	42%	5.15	3089.256	1.177398
8	62%	5.75	4863.087	1.853452
8	67%	5.88	5246.26	1.999489
8	74%	6.07	5771.484	2.199666
8	90%	6.43	7104.355	2.707659
10	33%	6.3	3962.592	4.608915
10	42%	6.86	5144.12	5.983157
10	62%	7.58	7487.39	8.708629
10	67%	7.72	8016.26	9.32376
10	74%	7.91	8742.38	10.16832
10	90%	8.27	10527.83	12.24498
15	33%	6.4	7394.993	65.31507
15	42%	7.2	7926.94	70.0134
15	62%	8.15	10774.99	95.16834
15	67%	8.27	11732.96	103.6294
15	74%	8.39	12943.69	114.323
15	90%	8.58	13000	114.8204

From table5 it is observed that in case of short piles the value of coefficient of horizontal modulus of sub-grade reaction (η_h) increased with increase in relative density as well as increase in L/ d ratio.

An attempt has been made to examine the variation of flexibility ratio with variation of relative density and variation of L/ d ratio as shown in figure 5 and figure 6 respectively.
Figure 5 and figure 6 show variation of the parameters in their respective logarithmic form because of the large variation in respective values.It has been observed that the value of logarithm of F.R. increases with increase in logarithm of relative density as well as increase in logarithm of length to diameter ratio. This is due to the increase in stiffness of soil and pile parameters respectively.

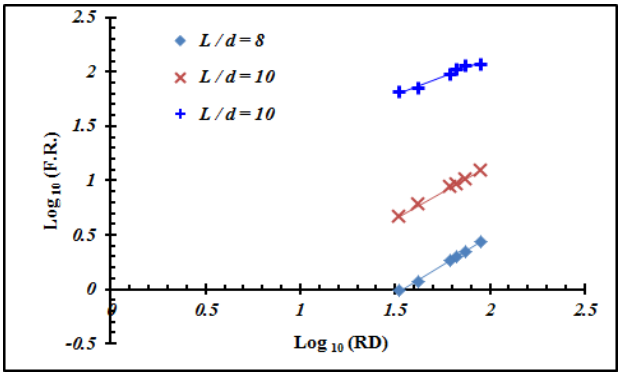


Fig. 5.variation of Log_{10} (F.R.) withvariation of Log_{10} (RD)

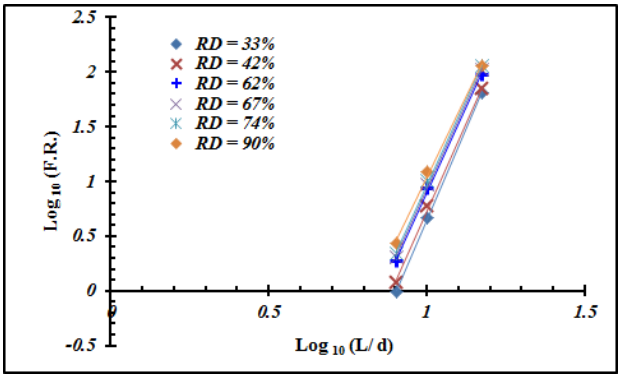


Fig. 6.Variation of Log_{10} (F.R.) withvariation of Log_{10} (L/d)

From equation (3) it may be written, F.R. = K × (η_h) where, K = a constant = L^5/ E_pI_p.
So, F.R. ∞ η_h
From Fig.5 it has been seen that
$Log_{10} \{(\eta_h L^5) / (E_p I_p)\} \propto Log_{10} (RD)$ (4)
Again from Fig. 6, it is noted that:
$$Log_{10} \{(\eta_h L^5) / (E_p I_p)\} \propto Log_{10} \{L/d\} \quad (5)$$
So, combining (1) and (2), it can be written now,
$Log_{10} \{(\eta_h L^5) / (E_p I_p)\} \propto Log_{10} (L/d) \times Log_{10} (RD) \Rightarrow Log_{10} \{(\eta_h L^5) / (E_p I_p)\} \propto Log_{10} [(L/d) + (RD)]$
Cancelling the logarithms on both sides
$$\Rightarrow Log_{10} \{(\eta_h L^5) / (E_p I_p)\} \propto Log_{10} [(L/d) + (RD)] \Rightarrow (\eta_h L^5) / (E_p I_p) \propto [(L/d) + (RD)] \quad (6)$$
As F.R. = $(\eta_h L^5) / (E_p I_p)$,
$$\text{So, F.R.} \propto [(L/d) + (RD)] \Rightarrow \text{F.R.} = K_1 [(L/d) + (RD)] \quad (7)$$
Where 'K_1' is the constant which is dimensionless as F.R. & $[(L/d) + (RD)]$ is also dimensionless.
Thus, K_1= F.R. / $[(L/d) + (RD)]$ (8)
A graph has been plotted between (F.R.) in Log_{10} scale and $[(L/d) + (RD)]$ for different slenderness ratio of 8, 10 and 15 respectively. The slope of the respective curves helps to find out the concerned value of K_1. Logarithmic form has been used here because of the large variation in respective value of "F.R.".
After getting the values of "K_1" from figure 7, subsequently figure 8 has been plotted between $Log_{10}(K_1)$ vs. (L/d + RD) for different slenderness ratio of piles. This plot in figure 8 is a design curve developed for any pile within the parametric range covered.
After the value of 'K_1' has been ascertained, F.R. can be found out using equation (8).

From Equation 8, F.R. =K_1 $[(L/d) + (RD)]$
$\Rightarrow(\eta_h L^5/E_pI_p) = K_1 [(L/d) + (RD)]$
$\Rightarrow \eta_h = (E_pI_p/L^5) K_1 [(L/d) + (RD)]$ (9)

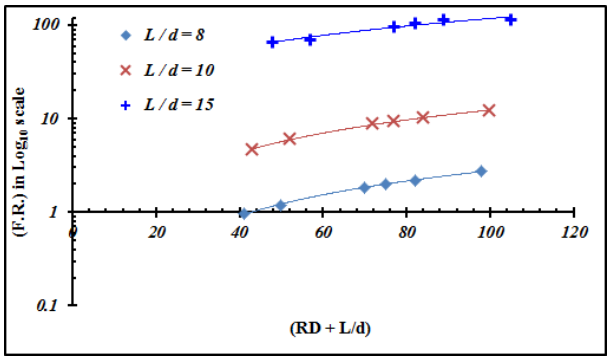


Fig. 7.Graph between F.R. (in $\log_{10}$ scale) vs. summation of relative density and L/d ratio

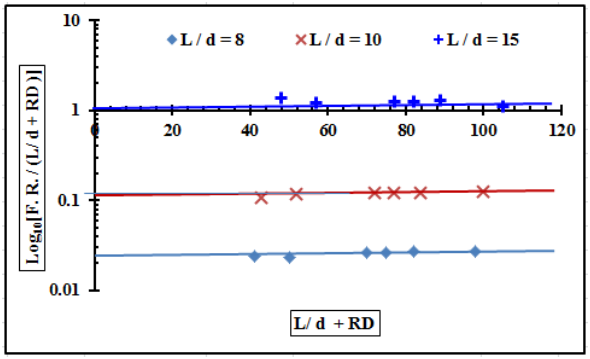


Fig. 8. Graph between "Log_{10}[Flexibility Ratio/ summation of relative density and L/d ratio]" and "summation of relative density and L/d ratio"

Using equation 9, value of η_h can be ascertained for pile of any material having specific slenderness ratio and embedded in homogenous cohesionless soil medium. Further a laboratory test has been performed to ascertain the correctness and accuracy of the above expression by using hollow pile of PVC (Chlorinated) material. The physical properties of the pile, is shown in table 6.

Table6. Properties and specifications of CPVC (Chlorinated PVC) used

Properties and Specification	Value	Properties and Specification	Value
Young's Modulus (E_p)	2900000 KN/m^2	Inner Diameter	0.0266446 m
Thickness	0.0033782 m	Length	0.405m
Outer Diameter	0.033401 m		

For the section of the CPVCpile, I_p = 6.1718E-08 m^4, E_pI_p = 0.1789822 KNm^2
Relative Density of the Foundation Medium used = 53%
From table 6, the Value of slenderness ratio (L/ d) = 405/33.401=12.1254
So the [(L/d) + (RD)] = 53+12.1254=65.1254
Thus from figure 8, the value of Log $_{10}$ K_1 (constant) for L/ d=15, is: 1.18
The value of Log $_{10}$ K_1 (constant) for L/ d =10, is: 0.12
So, for L/d=12.1254the value of $\text{Log}_{10}K_1$ (constant) is = 0.571, So, K_1= 3.720359
Thus from equation 9, $\eta_h = (E_pI_p/L^5)\, K_1\, [(L/d) + (RD)]$
$\Rightarrow \eta_h$=3979.878673KN/m^3.
Subsequently the experimental results obtained from the laboratory experiment has been compared using PLAXIS 3D software which has been found to agree reasonably well thus using the numerical techniques cited above the value of $\eta_h$has been found out to be 4103KN/m^3. Thus as the deviation has beenfound to be within ±5% with those obtained from equation 9, the results are found to be reasonable.

CONCLUSIONS

1. The deviation between ultimate loads obtained from the test results and those obtained from numerical approaches were within an average range of -3.74% (Table 4).
2. Flexibility ratio increases nearly equal to 178%, 166% and 76% with the increase of Relative Density from 33% to 90% for pile having slenderness ratio of 8, 10 and 15 respectively (Fig 5).
3. With the increase of L/d Ratio from 8 , 10 to 15 and for every subsequent relative density of 33%, 42%, 62%, 67%, 74% and 90% the flexibility ratio increases by 67.1%, 59.5%, 51.4%, 51.83%, 51.97% and 42.4% respectively (Fig 6).
4. From the study a design chart has been developed as plot between "Log_{10} [Flexibility Ratio/ summation of relative density and L/d ratio provided]" and "summation of relative density and

L/d ratio" for different L/ d ratios within a specific parametric range. This chart is useful for any pile within the parametric range (relative density up to 90% and slenderness ratio of pile up to 15% respectively).

REFERENCES

Barber, E. S. 1953. Discussion to paper by S. M. Gleser, *Special Technical Publication*, ASTM, Vol.154, pp.96–99

Biswas, S.K. et al. 2012. A Study on Response of Laterally Loaded Piles Embedded in Layered Cohesionless Soil. Proceedings, IGC-2012, Delhi, December 13-15, India.

Biswas, S., Chaudhary, S. S., Manna, B., and Baidya, D. K. 2013. Field Test on Group Piles under Machine Induced Coupled Vibration. International Journal of Geoengineering Case Histories, Vol.3, Issue 1, pp.10-23.

Broms, B. B. 1965. Design of Laterally Loaded Piles.Journal of the Soil Mechanics and Foundations Division, ASCE, Vol. 91, No.3, pp.79-99.

Chatterjee, K., Choudhury, D., and Poulos, H.G. 2015.Seismic analysis of laterally loaded pile under influence of vertical loading using finite element method, Computers and Geotechnics, Elsevier, UK, Vol. 67, pp. 172-186.

Chin, Ir. Tan Yean, Ir. Sew, Gue See and Chung, Ir. Fong Chew, 2009. Interpretation of Subgrade Reaction from Lateral Load Tests on Spun Piles in Soft Ground G&P, *Geotechnics Sdn*. Bhd. Kuala Lumpur, Malaysia. pp. 1-21.

Davisson, M.T. and Gill, H.L. 1963. Laterally loaded piles in layered soil system. Journal of Soil Mechanics Foundation Division, ASCE, Vol. 89, No. 3, pp.63-94.

Kim, Y. and Jeong, S. 2011. Analysis of soil resistance on laterally loaded piles based on 3D soil–pile interaction, *Computers and Geotechnics,* Vol. 38, No. 2, pp. 248–257

Maheshwari, B. K., and Sarkar, R. 2011. Seismic behavior of soil-pile structure interaction in liquefiable soils: Parametric study, International Journal of Geomechanics, ASCE, Vol. 11, No.4, pp. 335–347.

Meyerhof, G. G., Mathur, S. K. and Valsangkar, A. J. 1981. Lateral resistance and deflection of rigid wall and piles in layered soils. Canadian Geotechnical Journal, Vol. 18, No. 2, pp.159-170.

Mukherjee, S. et al. 2013. Comparative study between the behavior of long and short laterally loaded single pile. Proceedings, Pile 2013, Bandung, June 02-14, Indonesia.

Poulos, H.G. and Davis, E.H. 1980. Pile Foundation Analysis and Design, *John Wiley and Sons*, New York, p. 593

Reese, L. C. and Matlock, H. 1960.Generalised solutions for laterally-loaded piles. Journal of the Soil Mechanics and Foundations Division, ASCE,Vol. 86, No. SM3, pp. 63-91.

Reese, L. C., Cox, W. R, and Koop, F. D. 1974. Analysis of laterally loaded piles in sand. Proceedings, 6th Annual Offshore Technology Conference, Houston, paper OTC 2080, pp. 473–483.

DESIGN OF PILE FOUNDATION FOR TALL RAILWAY BRIDGES IN NORTH-EAST INDIA

Sumantra Sengupta
Chief Manager (Design), STUP Consultants Pvt. Ltd., Kolkata, WB, India
Ph: 9433728977
sumantra.sengupta@stupmail.com

ABSTRACT

Northeast Frontier Railway (NF Railway) intends to connect Imphal, the capital of Manipur (bordering Myanmar) with Assam by railway link. They have planned a 125km long railway line that passes through steep rolling hills of Patkai region, eastern trail of Himalaya, and as a result large number of tunnels and bridges need to be designed. While the high mountains are penetrated by tunnel, the deep gorges between the mountain ridges are connected by tall bridges. The tallest of such bridges connects a gorge at about 140m above its bed level with an overall length about 700m at rail level. In all, five such bridges with tall piers are now under construction. With extensive study on possible alternate arrangement of the bridges considering the effect of high seismicity of the area, moderately to highly weathered siltstone/ sandstone as ground bed material, slope of the hills etc it was decided that bridge will be founded on 1.5m diameter bored cast in situ piles with length varying from 20m to 30m depending on the location. The substructures are RCC hollow pier and superstructures are steel open web through type girder of 103.5m span. Considering absence of any major construction work in the vicinity, it was decided that prior to design work, Site-specific spectrum study will be carried out and design will be carried out considering the varying stiffness of the tall piers, each of different height. Interesting results were obtained regarding behavior of piles under lateral loads generated by high seismic conditions. The paper discusses in detail the design of Pile foundations and the effect of bed material along the steep slope on which the piles are being constructed.

Key Words: Pile in rock on hill slope, Bearing capacity of pile in weathered sandstone/ siltstone, High seismic zone, Site specific spectrum

INTRODUCTION

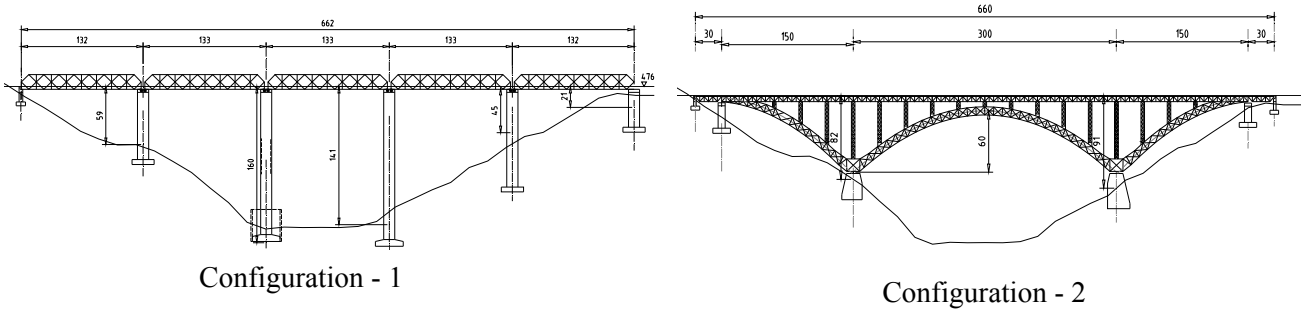
Indian Railway has undertaken the construction work of connecting the North-Eastern states of India through railway line. The major stretches of the area passes through hilly terrain and as a result the line passes through tunnels and bridges in succession. The tall mountains are being penetrated with tunnels and immediate after deep gorges are crossed with high level bridges. The entire area is under high seismically active zone. The bed material below the ground level of the sloped hill is 4 to 10 meter of mixed soil of sand, gravel, pebbles etc underlain by moderately to highly weathered sandstone, siltstone at the higher level and moderately weathered sandstone, siltstone at lower level. Considering all the aspects like constructability, maintainability, geological and geotechnical aspect, seismicity, stability, safety, functional aspect and cost it was finally decided that the bridges will be simply supported structure with open web through type steel superstructure of maximum span 103.5m and hollow cylindrical discretely varying RCC substructure with 1.5m diameter group of piles as foundation. The paper discusses on the design aspect of the pile foundation in the rocky strata in the hill slope. The codes and standards that have been followed for design are IRS (Indian Railway Standard), IS (Indian Standard), IRC (Indian Road Congress), AREMA (American Railway Engineering and Maintenance-of-way Association), UIC (International Union of Railway) provisions.

BRIDGE CONFIGURATION

Different options of bridge configuration were studied initially and finally zeroed down to two different forms. One is simply supported or continuous superstructure with vertical substructures and the other type is arch configuration as shown in **Fig. 1**.

It was found that the continuous bridge option is not desirable due to uncertain differential settlement of the foundation that can overstress the members. The arch options of the bridge were found not suitable in view of the unstable characteristics of the geological formation and possibility of ground movement. Moreover the lateral deflection of the deck at its mid span is extremely high in wind and seismic case. As such arch bridge option or any long span bridge option is viable only if multiple track provision is there requiring wide deck.

As the region is under high seismic zone, light superstructure was preferred so that less force is drawn to the foundation during seismic and thus only steel superstructure has been considered for alternate bridge configuration study. Difficult terrain and problem of concrete construction at the high level also tilted the preference towards steel. Simply supported open web through type steel superstructure of maximum span length 103.5m has been considered. For substructure RCC hollow pier and steel trestle was considered for alternate study. From deflection criteria under wind load it was found that steel trestle pier exhibits horizontal deflection much higher than the recommended deflection at the top of pier which is L/1500. As a result RCC hollow cylindrical pier with discretely varying thickness was considered as a final option.



Configuration - 1

Configuration - 2

Fig. 1: Alternate bridge configurations



Fig. 2: Site of the tallest bridge

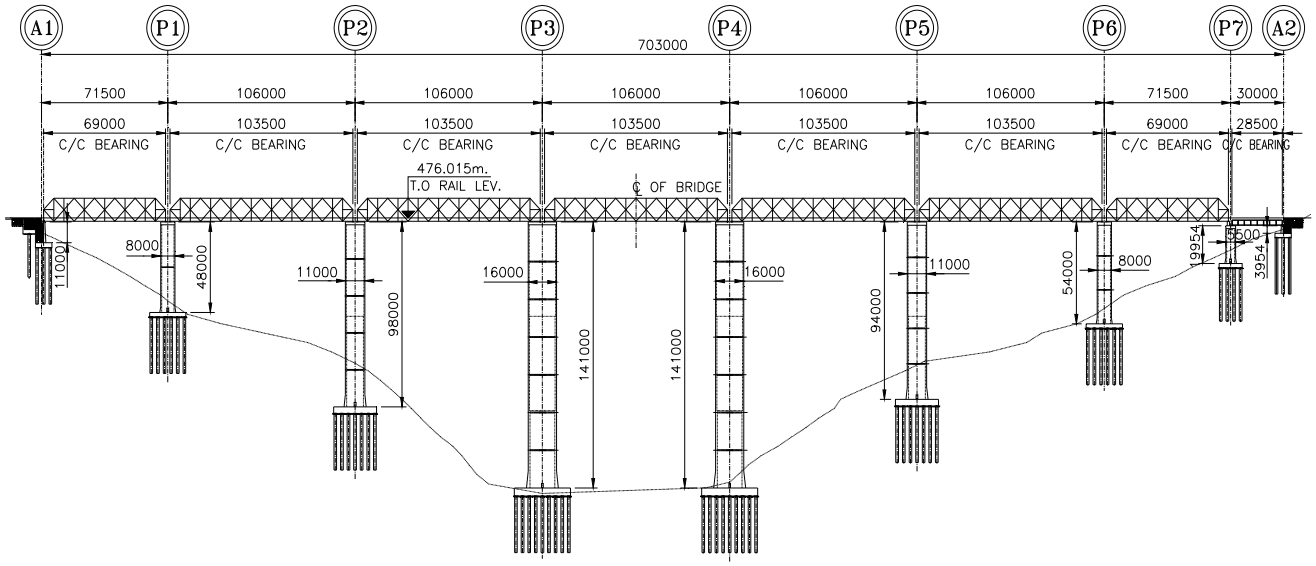


Fig. 3: Elevation of the tallest bridge

In the **Fig, 2** and **Fig. 3** the site of the tallest bridge and the final configuration of the bridge are shown.

GEOLOGICAL ASPECTS OF THE AREA

In general the area where the bridges are located comprises mainly two geological units, namely Tertiary Sedimentary rocks and Quarternary sediments. The general Geological Succession of the study area is as shown in **Table 1**:

Table 1. Geological succession of the Study area

Age	Group	Lithological Description
Quarternary	Older and Younger Alluvium	Dark grey to black clay, silt and sand deposits with gravels, pebbles, boulders, etc.
Late Cretaceous to Eocene	Disang	Dark grey, splintery shale interbedded with sandy shale and siltstone.

The quarternary deposits essentially comprise of alternating sequence of gravels, silty clay and sand etc. The flanks of this valley exposes mainly Disang Group of rock of late Cretaceous to Eocene in age and are composed of mainly splintery shale, well laminated, inter-bedded with siltstone which forms continuous ridge encompassing the entire valley areas. In general bed sloping towards hill is less stable and the stability depends on the angle of inclination. Slopes inclined against the direction of dip of the sedimentary beds are not likely to be affected by rock slips and, as a consequence, such slopes are generally stable. **Figure 4** exhibits the stability of the slope with respect to the dipping plane direction. In general it has been found that in the valleys along the bridge the hill slopes are either inclined against the

direction of bedding dip of the rock formation as shown in the **Fig. 5** or in horizontal direction as shown in the **Fig. 6** causing the slopes stable.

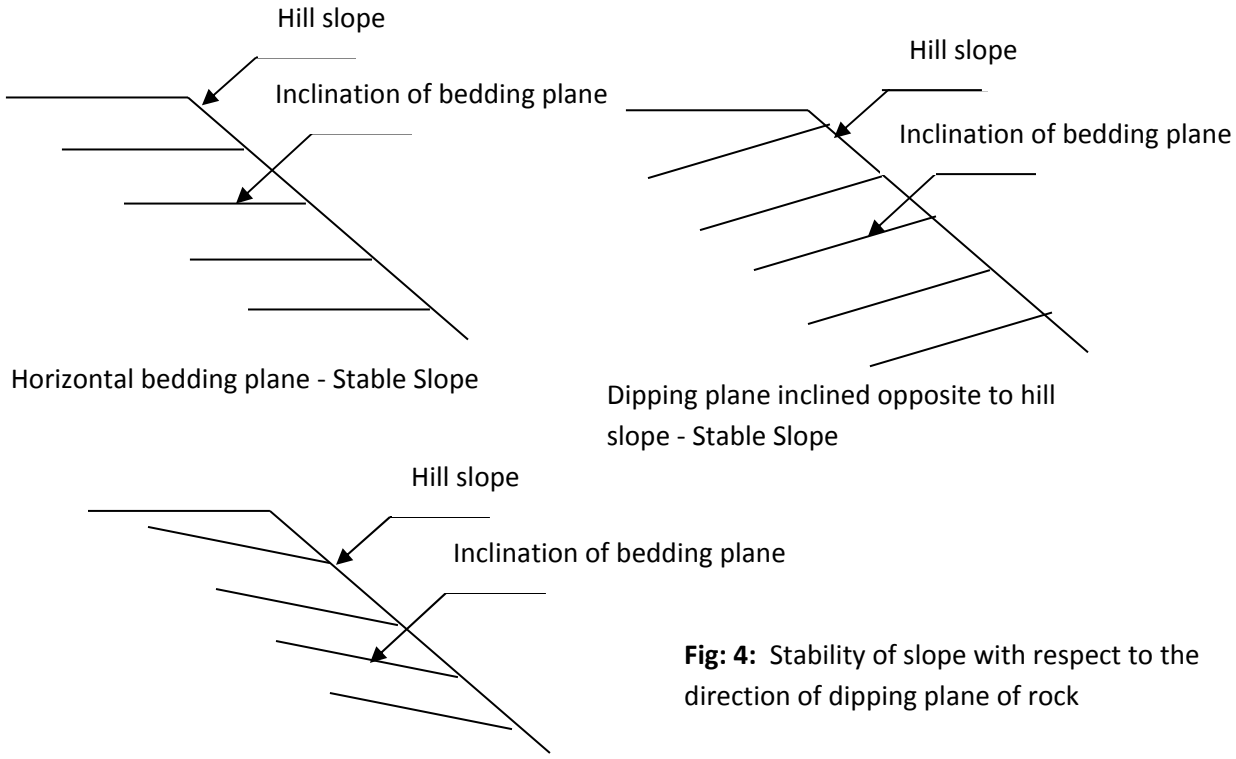


Fig: 4: Stability of slope with respect to the direction of dipping plane of rock



Fig. 5: Splintery shale, well laminated siltstone dipping towards hill



Fig. 6: Excavated profile shows the horizontal dipping plane of rock

GEOTECHNICAL ASPECTS OF THE SITES

Geotechnical study has been undertaken by making soil exploration under every foundation location. Due to the high seismicity of the area and the very tall piers, the foundation sizes in plan are large and thus it was found that more than one bore hole location is preferable for soil exploration at tall pier locations. Four numbers of borehole locations has been thus proposed at such locations.



Fig. 7 : Rock core sample

In general it has been found that for all the bridge locations the top 4 to 10 m depth is comprised of stiff clayey silty sand with mix of gravels and below this level there is moderately to highly weathered shale/ sandstone. Refusal has been encountered in the standard penetration test at the shale/ sandstone layer. From the geotechnical investigation report, it was found that in most of the cases core recovery was found up to 50% but RQD was almost nil.

Figure 7 shows the sample of the rock obtained during boring. The general soil profile up to 40m depth from the ground is shown in **Table 2**.

Table 2: General Profile of bed material

Sl.No.	Description of the bed material	Depth (m)	Average SPT value	RQD	Unconfined compressive strength (MPa)
1	Silty clay / clayey silt with varying percentage of sand / sandy silty clay / clayey silty sand / silty sand / sand with kankars, gravels, nodules, boulders pieces etc.	4	20		
2	Gravels, pebbles and boulders of siltstone / shale	6	100		
3	Highly weathered shale / sandy shale / siltstone	10	150-300	Nil	5-7 MPa
4	Moderately weathered / slightly weathered / fresh shale / sandy shale / siltstone	20	300-600	Nil	7-20 MPa

DESIGN OF FOUNDATION

Open foundation, well foundation and pile foundation are the alternative options of foundation. From strength criteria open foundation is a viable option but from slope stability aspect it cannot be a dependable foundation option as was found from stability analysis. Well foundation is difficult to sink in rocky strata. Pile foundation has been found to be better option under present case as the majority of the substructures are located on the sloped hill for which slope stability of the foundation is a guiding factor. Secondly as the area is under high seismically active zone large lateral force is generated at the base of the substructure and to ascertain the stability of the structure pile foundation is found to be the most preferred option.

Governing criterion for length of pile

The length of pile foundation has been guided from the following criteria:
1) Depth required from vertical load capacity of pile,
2) Depth required from horizontal load carrying criteria and the effect of flexible pile consideration and
3) As the piles are located on hill slope the length of pile is governed by slope failure criteria ie it should penetrate the potential failure surface.

In the present case there is another criterion for selecting length of pile evolved from the tension capacity of pile. As the IRS foundation code does not permit skin friction component in pile vertical load capacity in seismic zone, only the self weight of the single pile has been considered as tension capacity and thus the length of pile has been governed at few cases from this criterion.

Bearing capacity of weathered siltstone/ sandstone

For the bearing capacity of pile foundation in weathered sandstone/ siltstone IRC 78: 2014, IS 2911 (Part1/ Section 2): 2010 and IS 14593: 1998 have been followed. There are three different methods given in IS 14593. The method considering the shear strength parameter Cu given in IS 14593 which is applicable specifically for weathered sand stone/ siltstone are same as the general method given in IRC and IS 2911 and the same has been considered in the present design calculation. The formula is as shown below.

$Qu = Cu.Nc.\pi D^2/4 + \alpha.Cs.\pi.D.Ls$ where Qu is ultimate pile vertical load capacity, Cu is shear parameter at end bearing level, Cs is shear parameter along socket length, Nc = 9, $\alpha = 0.9$, D is pile diameter and Ls is the socket length.

The SPT value of the rock at shallow depth from 10m to 20m varies between 150 and 350 where as at greater depth beyond 20m it varies between 350 and 600. RQD of the samples were virtually nil as the rock is highly fragmented. The unconfined compressive strength of the undisturbed samples under 24 hours soaking condition exhibits values between 5 to 7 PMA at depth up to 20m and 7 to 20 at higher depth. Shear parameter Cu from unconfined compressive strength thus gives minimum value of 2.5 MPa (Half of unconfined compressive strength).

The shear parameter values from the correlation between SPT and Cu as given in the IRC 78: 2014 and IS 2911 (Part 1/ Section 2): 2010 in tabular form have also been examined. While IRC restricts the SPT value up to 300 and corresponding shear parameter value Cu up to 3.3 MPa, IS 2911 considers the SPT value up to 600 and recommends the corresponding shear parameter Cu in higher range. In general IS gives higher value of Cu and for the present study values given in IRC has been adopted. From the above correlation between SPT and Cu it has been found that the shear strength parameter at higher level of rock strata ranges between 1 to 1.5 MPa whereas at lower level it varies between 2 to 3 MPa. The field SPT values have been considered while choosing the shear parameter from the correlation table as no correction is necessary for SPT in rock. Shear parameter obtained from SPT gives more realistic value in comparison to the value from unconfined compressive strength as SPT values are better representative of the strength of the in situ bed material which includes the contribution of the effect dipping of the bed. However it was found that the two sets of values of shear parameter are almost comparable.

From the above criteria the vertical load capacity of the pile has been found about 1200t from end bearing component and 400 t from skin friction component. The factor of safety against end bearing has been considered as 3 and for skin friction as 6. The diameter and length of pile has been considered as 1500mm and 30m respectively. **Table 3** shows the strength of bed material and vertical load capacity of pile from shear parameter corresponding to field SPT value. In general SPT value has been found very high and as such wherever from initial blows it has been found more than 100 by doing extrapolation, test has been stopped. From the bore log data, doing extrapolation, the tentative value of SPT in lower side has been estimated and has been furnished in the table.

Table 3: Strength of bed material and pile vertical load capacity

SPT at lower depth	SPT at higher depth	Cu at lower depth (MPa)	Cu at higher depth (MPa)	Ultimate end bearing capacity (T)	Ultimate Skin friction capacity (T)	Safe end bearing capacity (F.S. = 3) (T)	Safe skin friction capacity (F.S. = 6) (T)
150-350	350-600	1.5	2.5	3600	2400	1200	400

An alternate calculation of bearing capacity of pile has also been done considering the bed material as granular soil with equivalent shear parameter ϕ (angle of internal friction) as 36 degree. The end bearing capacity from this consideration varies with the overburden pressure and accordingly the value increases with length of pile.

From the above two considerations the end bearing component of the 1500mm diameter pile has been found as 600t with 15m length, 800t with 20m length and 1200t with 30m length. As the generalized soil profile for all the bridges under present case is almost identical, this load capacity of pile is valid for all the bridges. Maximum design load in pile occurs under seismic load condition and the value is 675t. Considering permissible increase in bearing capacity in seismic case this load can be reduced with factor 1.25 and the corresponding normalized load reduced to 540t.

Governing criteria of number and length of piles in each foundation

The number pile under each pier location has been guided from either horizontal load capacity or from vertical load capacity of the pile. In general it has been found that with uniform diameter of piles for all piers, for shorter pier the number has been guided from horizontal load capacity and for taller piers it has been guided from vertical load capacity. Accordingly varying number of 1.5m diameter of pile in square grid has been provided at each foundation location.

The required length of pile has been found 15m from vertical load capacity as discussed above. From horizontal load carrying capacity the minimum length was found 20m. The substructures which are standing on the hill slope the piles haven been considered to penetrate the potential failure surface and accordingly the length of pile was found 30m. In general the foundations on the horizontal plane have 22m length of pile and foundations on the hill slope have 30m length of pile. **Table 4** shows the length of pile provided at different substructure location of the tallest bridge and corresponding governing criteria.

Table 4: Summary of length of the pile of the tallest bridge and corresponding governing criteria

Location	Length of pile	Governing criterion
A1	20	Horizontal load carrying criterion and long elastic pile behaviour
P1/ P2/ P5/ P6	30	Slope stability
P3/ P4	22	Horizontal load carrying criterion and long elastic pile behaviour
P7	30	Slope stability/ Tension capacity of pile
A2	30	Slope stability

CONSTRUCTION OF PILE

Piles construction is being done using rotary drilling machine. Proper care is being taken to maintain the quality of the concrete. Liner is being provided up to a suitable depth where rock strata is being started. Both Routine load test and Initial load test have been performed on the pile to ascertain the capacity of the pile. It was found that the test result conforms to the design results. **Fig. 8** shows Pile construction is in progress at site.



Fig. 8: Pile construction under progress

SITE SPECIFIC SEISMIC ACCELERATION SPECTRUM

A site specific seismic vulnerability study was undertaken with the help of academic institution Indian Institute of Technology, Kharagpur (IITKgp). In the study the estimates of peak horizontal ground acceleration (PGA) and peak horizontal ground velocity (PGV) for the bridge sites has been made. The study also suggests the design acceleration spectrum to be considered for the seismic design of the bridges. Although penetration resistance or shear wave velocities were generally unavailable, qualitative information from the geotechnical investigation report indicates that the sites are likely to be of National Earthquake Hazard Reduction Program (NEHRP) class A or B. The study is based on earthquakes of magnitude 3.5 or more that occurred between 1762 and 2011 with epicenters within a rectangular area bounded by latitudes and longitudes over a radius of 350 km from the bridge sites. The deterministic approach was followed in assessing the seismic hazard. The required attenuation relationships were developed by first relating felt earthquake intensity to the logarithm of hypo-central distance (in kilometer) and exponent of moment magnitude information and subsequently converting the relationships for estimating PGA and PGV using relationships between felt intensities and instrumental PGA and PGV records developed for data from two recent northeastern Indian earthquakes. The results indicate that for site classes A and B (NEHRP) the maximum PGA for the bridge sites is expected to be 0.31g and the maximum PGV is expected to be 20.81 cm/s without considering topographic amplification. For bridge sites with valley slopes less than 30° without any likelihood of earthquake-related slope instability a

topographic amplification factor of 1.2 on the PGA estimate has been suggested. The finally suggested PGA as per the study is 0.31 x 1.2 = 0.372 which is marginally above the code suggested value 0.36 in the seismic zone V.

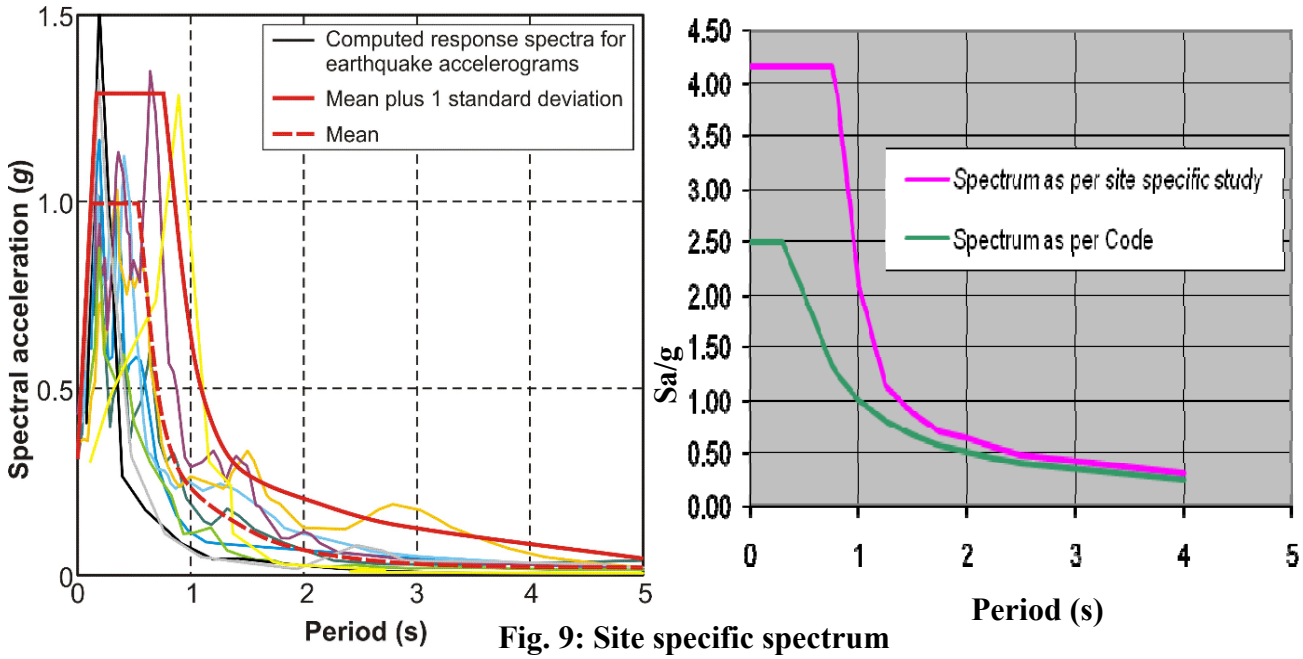


Fig. 9: Site specific spectrum

For estimating the acceleration spectrum, nine free-field accelerograms obtained from www.srongmotioncenter.org and www.knet. bosai.go.jp recorded at hard rock and stiff soil sites during earthquakes with MW between 7.0 and 7.7 with max ground acceleration between 280 cm/sec2 to 315 cm/sec2 and max velocity between 20 m/sec to 30 m/sec which is the present site specific values, the response spectra were computed. The earthquakes used in this assessment were of the strike slip and thrust strike-slip type mechanisms similar to what is expected in the geographic region under consideration.

In the **Fig. 9** all the nine free field accelerograms and their mean and mean plus one standard deviation curve has been plotted. The suggested design acceleration spectrum is the mean plus one standard deviation curve as shown in the red firm line. The above spectrum when compared with the code specific spectrum, as shown in the same Figure, it can be found that the values of the spectral acceleration are at some points more than two times higher.

EFFECT OF SOIL FLEXIBILITY IN DESIGN OF PILE AND IN SEISMIC ANALYSIS

IITK-RDSO guideline

As per IITK-RDSO guideline of seismic design of railway bridges soil flexibility factor need to be considered for the seismic analysis of the bridges. This is particularly important when deep foundation is considered. While the pile is designed with soil flexibility characteristics, due to the wide range of elastic properties of soil the time period of the structure varies. Thus for lower elastic parameter of soil the structure becomes flexible and its deflection reaches higher value. For higher elastic parameter the structure becomes stiffer and it draws more force and undergoes less deflection. Code suggests highest stiffness of soil to get maximum forces in structure and lowest stiffness of soil to get maximum deflection. In the present analysis same recommendation has been followed.

Actual flexibility of soil

The soil parameter in the first 10m depth of soil, ie portion above the rocky strata is having SPT value varying from 20 (at 3 to 4 m below bed level where pile cap bottom rests) to 100 and accordingly this may be classified as dense category of sand as per table 3 of IS 2911 (Part-1/Sec-2):2010. The modulus of sub-grade reaction may be considered as per the soil characteristics furnished in the soil report in the range of 7.5 to 20 MN/cum for granular and normally consolidated clay category for which the soil stiffness factor (T) varies from 4m to 3.3m and corresponding depth of fixity varies from 8.8 m to 7.3m. If soil is considered as preloaded clay category the modulous of sub-grade reaction may be considered as per the soil characteristics furnished in the soil report in the range of 36 to 72 MN/cum. Corresponding soil stiffness factor (R) varies from 5.8m to 4.8m and depth of fixity varies from 11.5m to 9.7m. From the above data it may be judicious to consider the average higher side of the soil stiffness factor as 5 and the depth of fixity 8m to get maximum forces in the structure as stipulated in the code.

Seismic Analysis

Dynamic analysis of the bridge structures by multi modal analysis using the acceleration spectrum suggested in the site specific seismic vulnerability study has been performed. The analysis is done for the whole model of the bridge including all the piers, pile foundation and superstructure. Stick model analysis of each pier has also been performed.

As the structure is comprised of uniform diameter pier with discretely varying thickness, the mass distributions along the height of the piers are non uniform. Moreover the presence of heavy pile cap at the bottom of the piers on group of piles also make the mass distribution extremely non uniform. Due to this non uniformity of mass, in most of the cases the participations of higher modes are also become predominant. It has been found in general that for tall piers the higher modes are predominant and for short piers first fundamental mode is predominant. As a result the gross horizontal seismic coefficient from the modal analysis comes out to be higher than that of for first fundamental mode with 100% mass participation for the tall piers where as for short piers it is found to be the reverse. In the modeling of the structures the piles are provided over a length up to their depth of fixity and at the bottom of piles they are made fixed.

Due to the high seismic spectrum and considerably tall pier heights it has been found that in all the members including substructures and pile foundation the section forces are critical under seismic load case.

Response reduction factor

The value of response reduction factor (R) has been considered as 1 at the junction of pier and pile cap, 1.5 for pile foundation and pier sections, 2.5 for pier cap. For stability of the structure in seismic case, ie while estimating the minimum vertical forces in pile in seismic, R has been considered as 1.5.

Limit state design

The design of the sections has been done considering both the ultimate limit state (ULS) and serviceability limit state (SLS) condition as per the guideline of IRS code. Section sizes and reinforcement have been estimated from ULS condition. As all the sections have become critical for seismic load condition, only stress check has been performed in SLS condition, no crack width check has been done considering it is not required for transient load case. Difference in stress between normal load case and seismic load case are so high that with the above design principle it was found that when crack width was checked for normal load condition it remained well within the permissible value.

Under ULS condition the load factor in seismic load case is much higher for no LL case than the LL case. As a result it was found that all the sections of different units of the substructure and foundation have become critical for no LL condition.

Reinforcement in pile

In general it was found that the reinforcement requirements in the piers vary from 120 to 250 kg/cum. The taller piers require less reinforcement and the shorter piers require higher due to the higher stiffness and relatively higher moment in the shorter pier sections. In case of the pile reinforcement requirement was about 130 kg/cum at pier location and 300 kg/cum at abutment location.

Criteria for thickness of pile cap

Thicknesses of pile caps are determined from the flexural strength requirement. In spite of the high thickness of the pile caps it was found that shear reinforcement could not be avoided and was provided wherever it is necessary. However the spacing of the shear reinforcements was so adjusted so that adequate space can be made available to bind the rods manually. It was found that in order to keep the lateral deflection of the pier with in permissible range higher thickness of the pile caps than what was required from flexural criteria were becoming necessary. Instead of increasing the entire pile cap thickness for this purpose local thickening below the pier base covering the piles directly below pier has been considered in the form of pedestals. Reinforcement requirement in pile caps has been worked out as about 120 kg/cum.

The **Table 5** below gives a comparative chart showing the height of the piers, their sizes and foundation requirement for the seismic behavior of the structures.

SLOPE STABILITY ANALYSIS

Detailed topography survey of the bridge sites over a corridor of 100m in each side of the bridge alignments have been undertaken for finalising the pile cap location and for performing slope stability analysis. It was found that in many cases there are transverse slope of the ground in the foundation locations. The slope stability is most critical in the steepest slope direction and thus for each foundation location steepest slope line is considered for the slope stability analysis as shown in **Fig. 10** and **Fig. 11**.
Slope stability analysis has been performed by Equivalent – Static slope stability analysis using the software STED, widely used for two-dimension stability analysis. The existing slope of the hill side is analysed first. As the slope has remained stable for a considerable period of time over the centuries it is found judicious to consider that the slope remains stable under design earthquake level of force. In order to justify the existing slope stable in the analysis, the value of the angle of internal friction is judged and the same was found more than 45 degree. From this analysis it was ascertained that the friction coefficient being played in the stability aspect of the slope is considerably high. Once the actual status of the stability was ascertained, the analysis is performed once again considering the theoretical angle of internal friction to be used for the further analysis, which is 36 degree with the bridge foundation on the slope. In order to ascertain the stability of the slope as per the above theoretical calculation the length of the piles are suitably modified so that they penetrate through the possible failure surface and make the slope stable.

Table 5: Table showing design details of the substructure and foundation

Height of pier (m)	Outer diameter of the hollow pier (m)	Wall thickness of pier at base (mm)	No. of pile below pier	Size of pile cap (m x m)	Thickness of pile cap (m)
141	16	1000	9 x 9	31.8 x 31.8	4.2
118	15	1000	9 x 9	31.8 x 31.8	4.0

100	12	750	7 x 7	24.3 x 24.3	3.5
80	11	750	7 x 7	24.3 x 24.3	3.0
54	9	500	6 x 6	20.6 x 20.6	2.5
35	5	500	5 x 5	16.8 x 16.8	2.25
20	7.5	500	6 x 6	20.6 x 20.6	2.25
10	6	700	5 x 5	16.8 x 16.8	2.25

In a very recently occurred EQ in the region where the epicenter was only 5km from one specific bridge site no slope failure has been noticed in the vicinity. The magnitude of the EQ was 6.7 and the hypocenter was 55km from the ground. The PGA map given by USGS site as shown in **Fig. 12** shows that near the epicenter the maximum acceleration of the ground was 0.14g. With the above data in hand an analysis has been performed to estimate the shear parameter of the bed material of the ground at the hill slope. As the bridges are under the construction stage steep excavation profile for construction of the pile foundation exists all over the site which didn't fail in the EQ and this suggests that the bed material has high shear parameter. Any angle of internal friction value cannot keep any near vertical slope stable unless there cohesion property exists. It has been found that an equivalent cohesion of about 20 t/m^2 or equivalent angle of internal friction value of 45 degree along with cohesion value of 5 t/m^2 should be the shear parameter value in order to keep the slopes stable. In the present design of the bridges an equivalent angle of internal friction of 36 degree with no cohesion value has been considered which is in the conservative side and imparts adequate safety margin to the structure against stability.

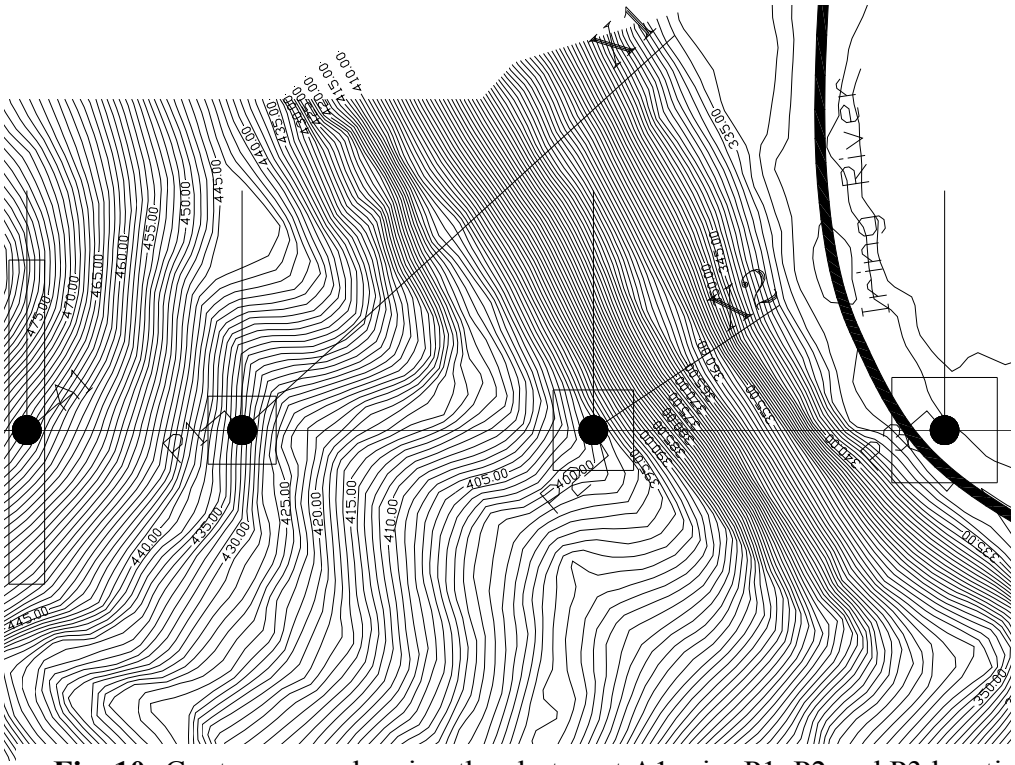


Fig. 10: Contour map showing the abutment A1, pier P1, P2 and P3 location and the steepest slope line A1-P1, P1-X1, P2-X2

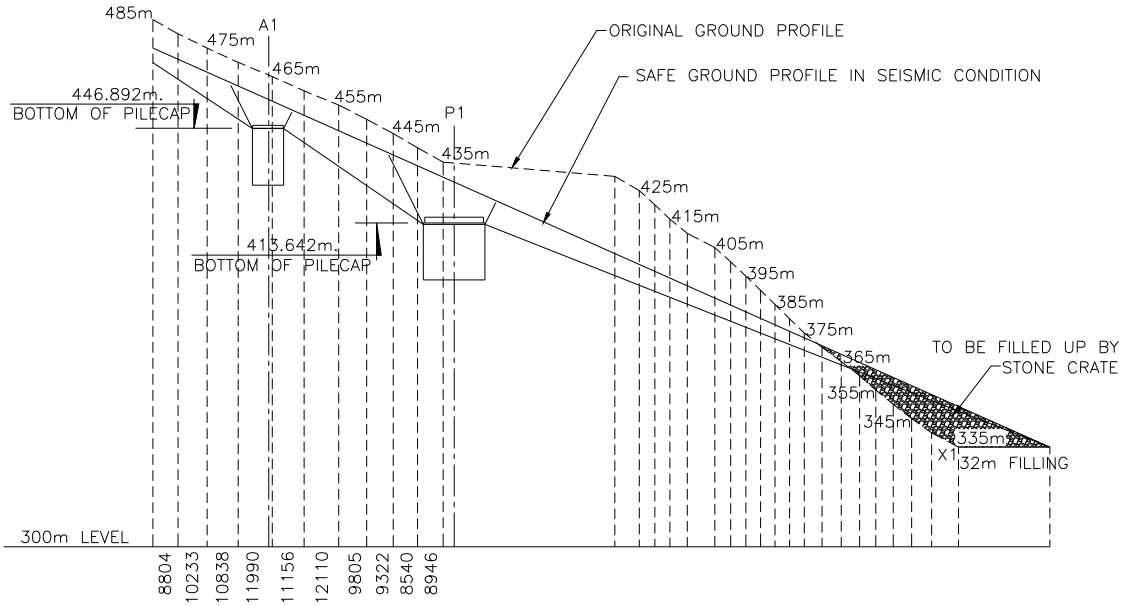


Fig. 11 Section along the steepest slope A1-P1-X1



Fig. 12 USGS record of PGA for recent EQ in Manipur

CONCLUSION

The design of the foundation of the bridges discussed above is critical in many respects. Due to the undulated terrain, tall and varying height of the piers, large length of the bridges, position of the piers on the hill slopes, the presence of severe most earth quake zone and the high response acceleration spectrum of the particular site as obtained from the site specific seismic vulnerability study made the design unique of their own. Pile foundation in sloped hilly terrain with weathered sandstone/ siltstone as bed material and in a high seismically active zone is a preferred option than any other type of foundation like open foundation or well foundation. The shear strength is the most important parameter to ascertain the load capacity of the foundation under such condition and as such it needs very careful examination.

Credits:
Client: Northern Frontier Railways, a wing of Indian Railways
Designer: STUP Consultants Pvt. Ltd., India

INSTRUMENTED PILE LOAD TESTS ON ACIP PILES FOR A REAL ESTATE PROJECT IN KOLKATA-A-CASE STUDY

Er. Krishnendu Mandal , Chief Executive, Mythcon, India+91-9903022389
Email: krishnendu.man@gmail.com

For a multi-story building project in Kolkata, a pile load testing program was conducted to minimize pile performance uncertainty resulting from variable subsurface conditions and to verify the pile load vs. settlement response. The program consisted of performing five (5) instrumented load tests on augured cast-in-place (ACIP) pre-production test piles. Vibrating-wire strain gages and extensometers were installed in the test piles at strategic locations to enable measurements of the load vs. deformation behavior of the test piles. This paper presents a description of site subsurface conditions, test pile installation, instrumentation setup for a maintained load test (MLT), static compression pile load test results , and pile instrumentation result interpretation. Average mobilized unit shaft resistance values are calculated .

Keywords: Maintained static load test, vibrating-wire strain gages, tell-tale extensometer

2.0 INTRODUCTION

The project site is located in Kolkata, near river Ganges, and the proposed development plans consist of constructing six (6)25-story (G+25) towers; see Fig. 1 and Fig. 2 below for approximate site location and proposed development layout, respectively. The buildings were designed to be supported on ACIP piles. A field load test program was implemented to verify sub-surface conditions and pile design. The test program consisted of installing Five (5) instrumented test piles numbered LP1A and B through LP6A and B, and performing static compression load tests on these piles. The piles were instrumented with vibrating-wire strain gauges and extensometers, so that the pile shaft resistance distribution along pile length and the pile toe resistance could be interpreted using direct instrumentation measurements.



Fig. 1: Map of West Bengal

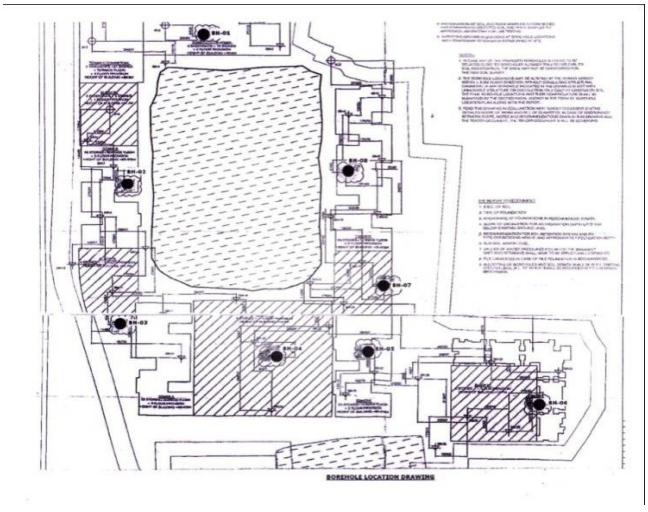


Fig. 2: Project site layout

Figure 3 summarizes site subsurface and groundwater conditions observed in on-site borings. Although shallow groundwater levels were measured in groundwater observation wells throughout the site, the design groundwater level was conservatively considered at the ground surface.

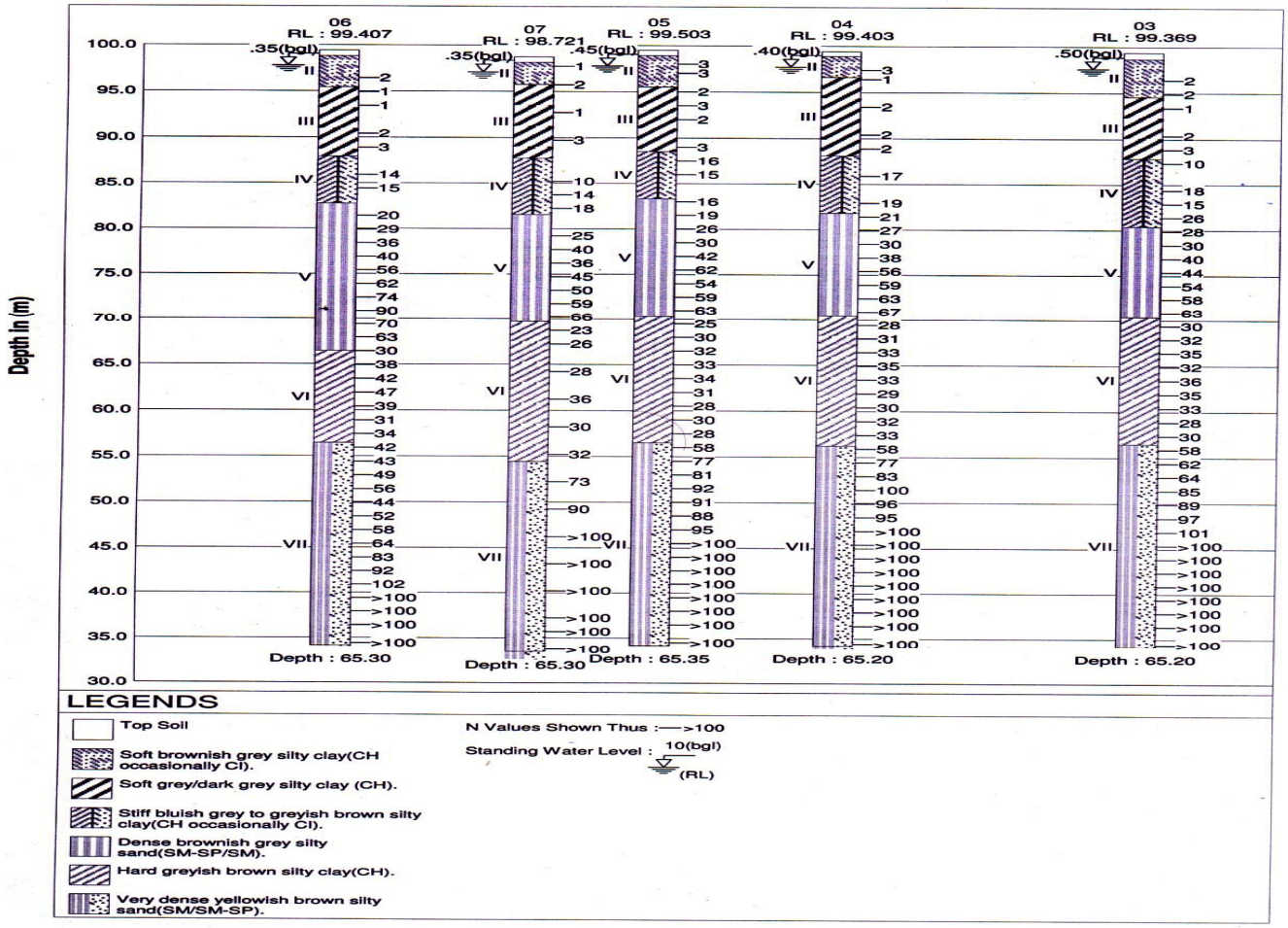


Fig. 3: Soil profile

Stratum	Description of Soil	N value	Shear Parameters	
			C (kPa)	Φ°
I 0.60	Top Soil	-	-	-
II 2.80	Soft brownish grey silty clay(CH occasionally CI).	2	25	-
III 8.00	Soft grey/dark grey silty clay (CH).	2	20	-
IV 6.50	Stiff bluish grey to greyish brown silty clay(CH)	15	65	-
V 11.90	Dense brownish grey silty sand(SM-SP/SM).	40	-	32*
VI 13.70	Hard greyish brown silty clay(CH).	32	200	-
VII 22.35	Very dense yellowish brown silty sand(SM/SM-SP).	75	-	34*

Average Standing Water Level (m) : BGL – 0.45, RL. – 98.93

Generalized Soil Profile

3. LOAD TEST PROGRAM DESCRIPTION

3.1 Pile structural properties

The instrumented test piles LP1A, LP2B, LP5B, LP6A, and LP6B were all augured cast-in-place (ACIP) reinforced concrete piles having structural properties summarized in Table-1.

Table 1 : Structural properties of the piles

Test Pile No	Pile dia (mm)	Pile length (m)	Main reinforcement	Circular links	Concrete grade
LP1A	600	35m	T16	T8	M30
LP2B	750	35m	T20	T8	M30
LP5B	600	24m	T16	T8	M30
LP6A	500	24m	T16	T8	M30
LP6B	500	24m	T16	T8	M30



Fig. 4: Kentledge (concrete blocks as dead load) of the pile load test

3.2Piles instrumentation

For the 24 meter long, 500 mm and 600 mm dia test piles, each pile had 2 extensometers at 12m and 24m, 6 vibrating-wire strain gages at 3 levels (2 strain gages at each level are shown in Fig. 5), and a data readout unit for monitoring the output results.

For the 35 meter long, 600 mm, and 750mm dia piles, each pile had 2 extensometers at 17.5m and 35 m, 6 vibrating-wire strain gages at 3 levels (2strain gages at each level are shown on Fig. 5), and a data readout unit for monitoring the output results.

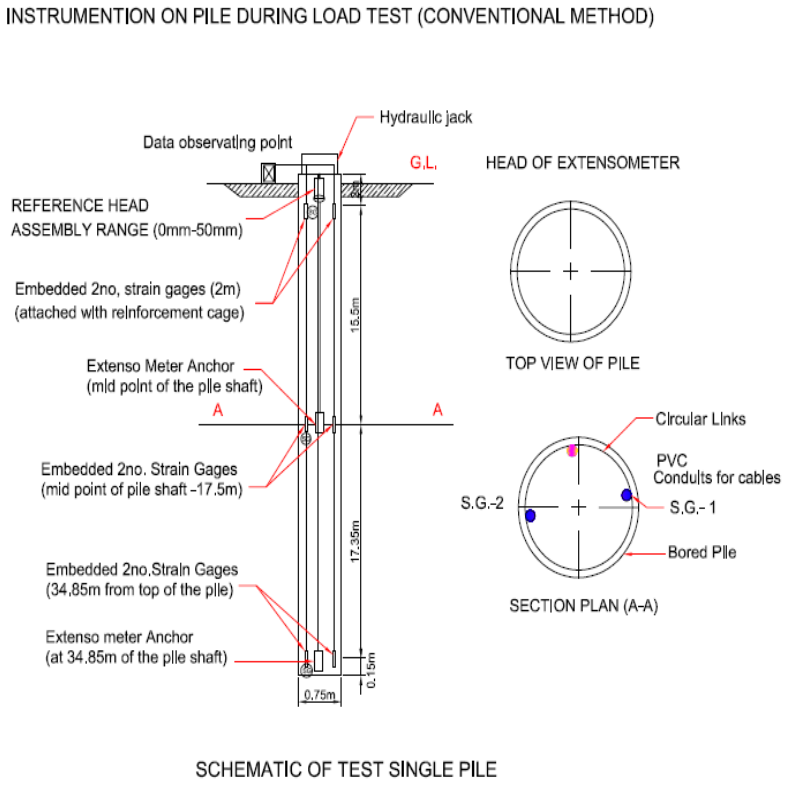


Fig. 5: Schematic of test pile



Fig. 6: Bottom portion of rebar cage with sensors

3.3. Measurement Principles

Vibrating wire strain gages

Vibrating-wire strain gages are recommended over other types of strain gauges to measure strains at discrete locations along a pile. Vibrating-wire strain gages (embedment type) are connected directly to the pile rebars .Inside the strain gauge, the change in the frequency of a pre-stressed inductive energized steel wire is measured as a function of change in deformation. This change in frequency is then related to the change in concrete strain. Fig.7 shows a schematic of a vibrating-wire strain gauge and a photograph showing strain gauge placement inside a pile. For a dependable measurement, it is necessary to fully embed the strain gauges and to place them at strategic locations that are representative of strain variations along the pile. The strain gages are relatively insensitive to environmental and mechanical influences and are generally stable and robust in the long run.

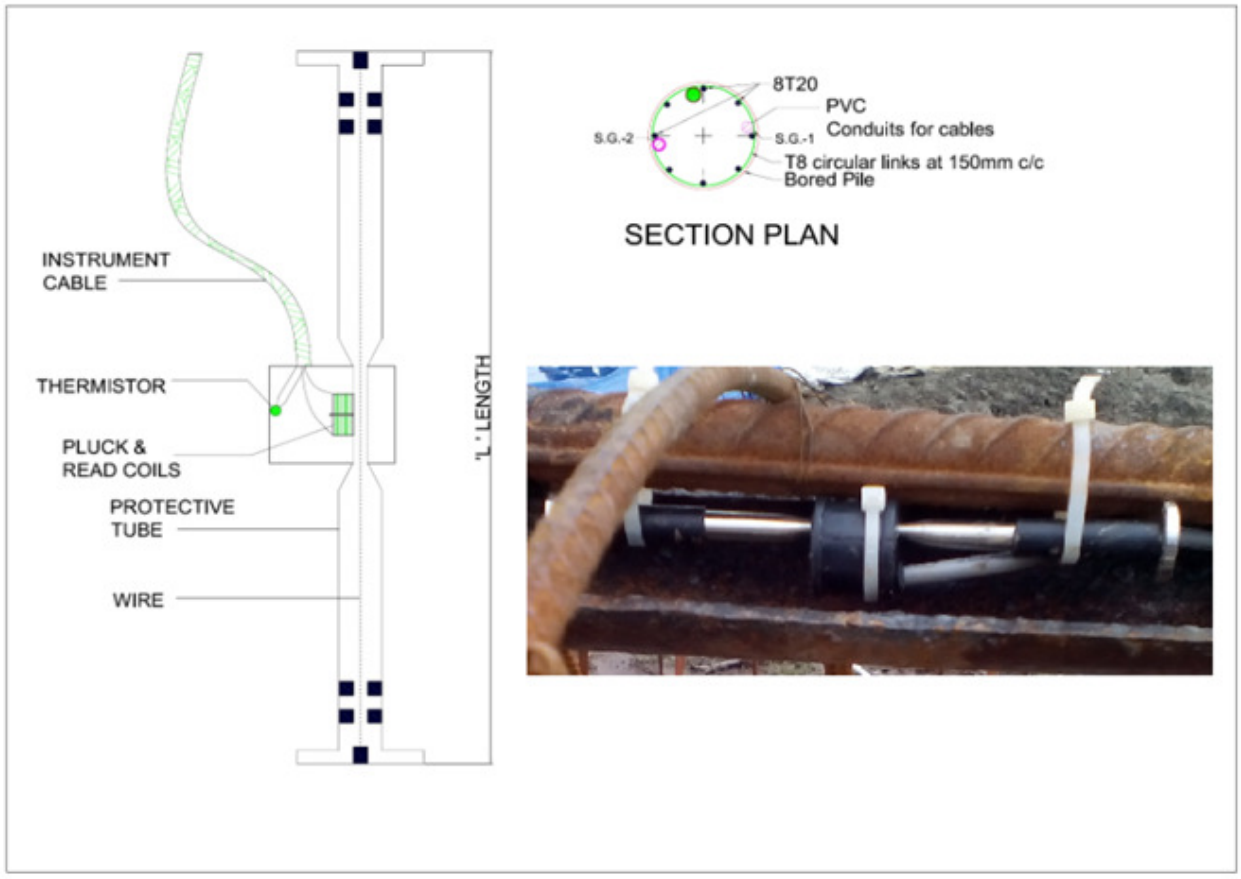


Fig. 7: Vibrating-wire strain gage schematic and strain gauge installation procedure.

3.4. Execution of the test

Pile compression load tests were performed in general accordance with the requirements of Indian Standard 2911(Part4, 2013) and the piles were loaded per the following loading schedule:

Table 2: Test Load Sequence

LP1A (Dia-600mm) load (kN)	**LP2B** (Dia-750mm) load (kN)	**LP5B** (Dia-600mm) load (kN)	**LP6A** (Dia-500mm) load (kN)	**LP6B** (Dia-500mm) load (kN)
502.6	502.6	251.3	251.3	251.3
753.9	1130.85	628.25	502.6	502.6
1005.2	1759.1	879.55	753.9	753.9
1507.8	2261.7	1256.5	1005.2	1005.2
1759.1	2889.95	1507.8	1256.5	1256.5
2010.4	3392.55	1759.1	1507.8	1507.8
2513	4020.8	2136.05	1759.1	1759.1
2764.3	4523.4	2387.35	2010.4	2010.4
3266.9	5151.65	2764.3	2261.7	2261.7
3518.2	5779.9	3015.6	2513	2513
3769.5	6408.15	3392.55	2764.3	2764.3
4020.8	----	---	2889.95	2889.95

4. EVALUATION AND ANALYSIS OF THE MEASUREMENTS

Assuming pile strain is the same in pile concrete and steel at a given cross-section, and using known and reasonably assumed pile cross-sectional properties (steel and concrete areas and elasticity moduli), the pile strain at each strain gauge level was converted into pile load at that level. Based on these loads and strain gauge locations, mobilized shaft and end-bearing resistance values were computed.

Loads transferred (P_{ave}) at strain each gauge level was calculated as follows:
$P_{ave}=\epsilon(E_cA_c + E_sA_s)$

Where,
ϵ = Average change in global strain gage readings
A_c= Cross-sectional area of concrete.
E_c=Concrete modulus.
A_s=Cross-sectional area of steel reinforcement bars.
E_s= Young's modulus of elasticity in steel=200kN/mm^2

For the test piles, the concrete modulus , E_c, was taken (**5000 x$\sqrt{}$fck) as** per the Indian Standard Code.

The resulting calculated pile shaft and toe load distributions are given in Table 3.

Table 3: Mobilized unit shaft friction and end bearing

Pile No	Load reading, (kN)	Total shaft resistance (kN)	Base resistance (kN)	Mobilized unit shaft resistance, f_s(kN/m^2)		Mobilized unit end bearing resistance, kN/m^2
				SG1 to SG2	SG2 to SG3	
LP1A	4020.8	3849.75	171.05	24.84	95.66	604.89
LP2B	6408.15	6075.43	332.72	72.17	84.57	753.03
LP5B	3392.55	3354.62	37.93	29.99	125.03	134.13
LP6A	2889.95	2735.14	154.81	41.72	104.97	788.34
LP6B	2889.95	2849.49	40.46	57.08	95.67	206.03

A typical pile top load vs. settlement plot is presented in Fig.8 and a typical pile top load vs. micro-strain plot is presented in Fig.9. In addition, typical mobilized unit shaft friction vs. pile top settlement and typical micro-strain vs. strain gauge depth plots are presented in Fig.10 and Fig.11, respectively. A typical pile depth vs. unit shaft friction plot is presented in Fig.12. Finally, a typical load distribution curve for the strain gauge locations is presented in Fig.13.

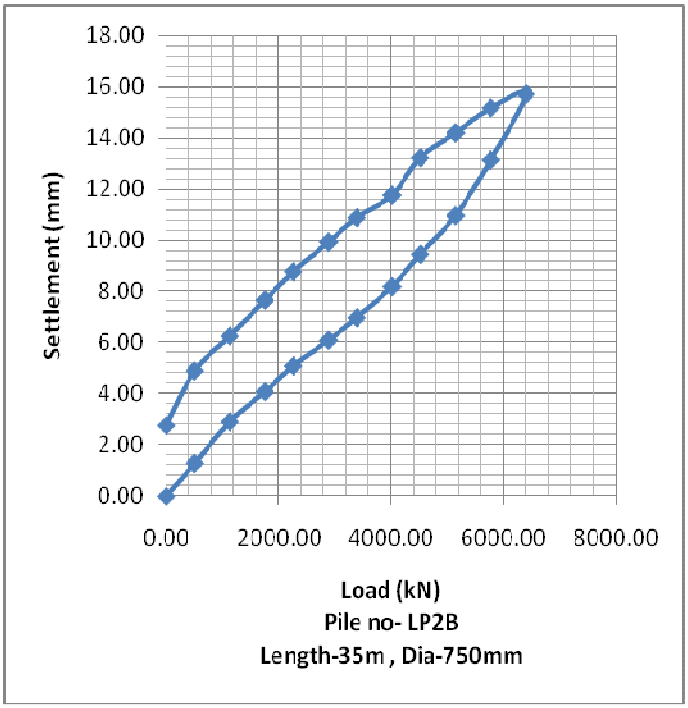


Fig. 8 : Top load (kN) vs top settlement (mm) curves of LP2B

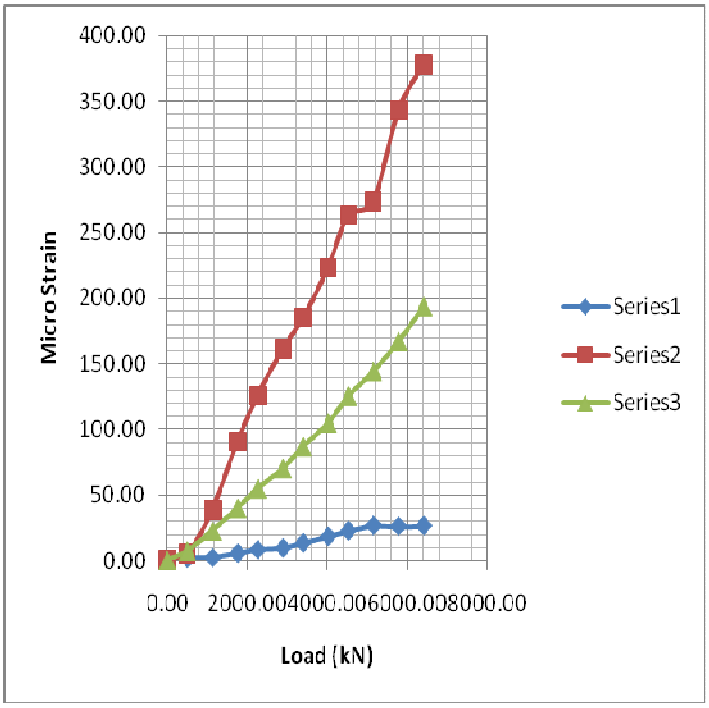


Fig. 9: Top load (kN) vs micro strain curves LP2B

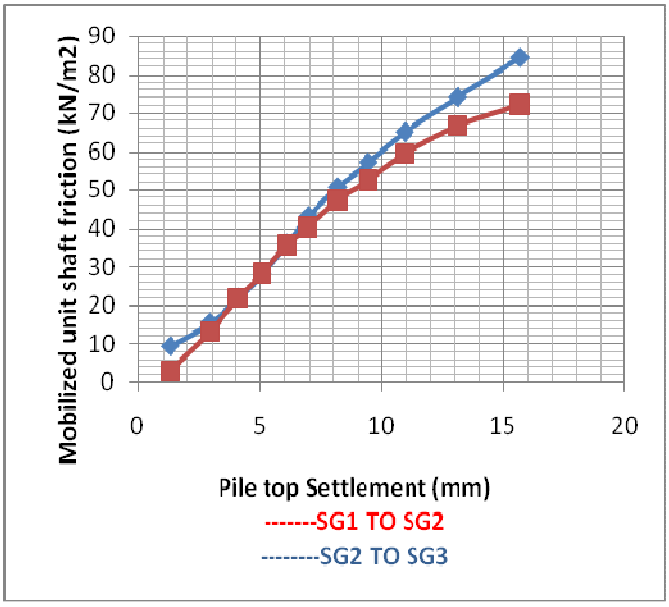


Fig.10 : Mobilized unit shaft friction vs pile top settlement of LP2B

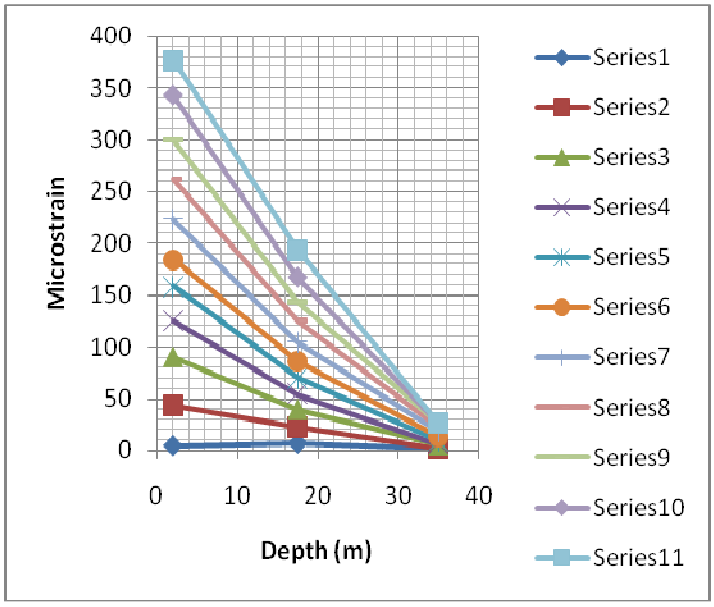
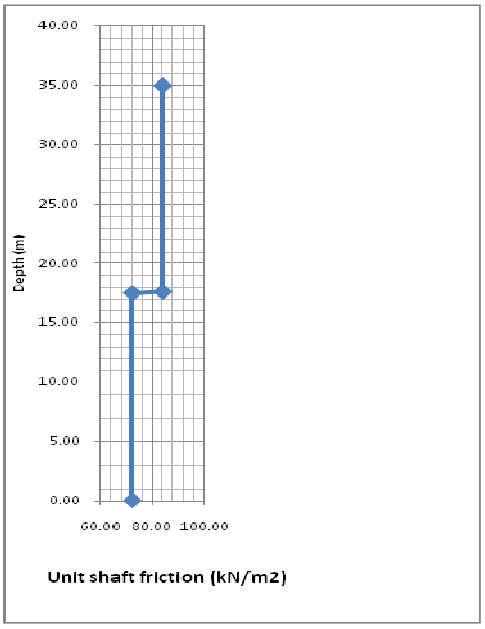


Fig.11: Strain distribution of pile during load test of LP2B



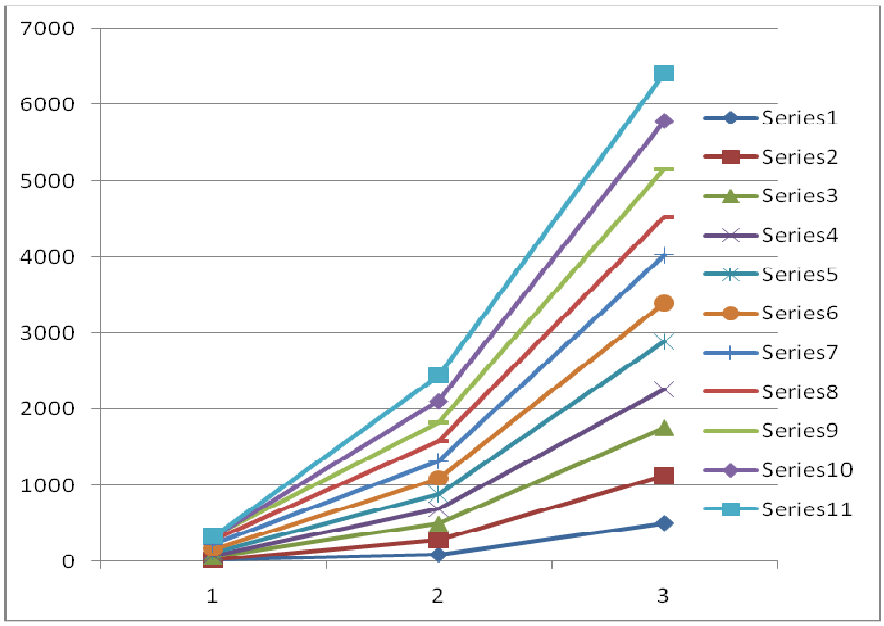


Fig.12: Unit shaft friction vs. depth of LP2B

Fig.13: Load distribution curve computed from VW strain gages of LP2B

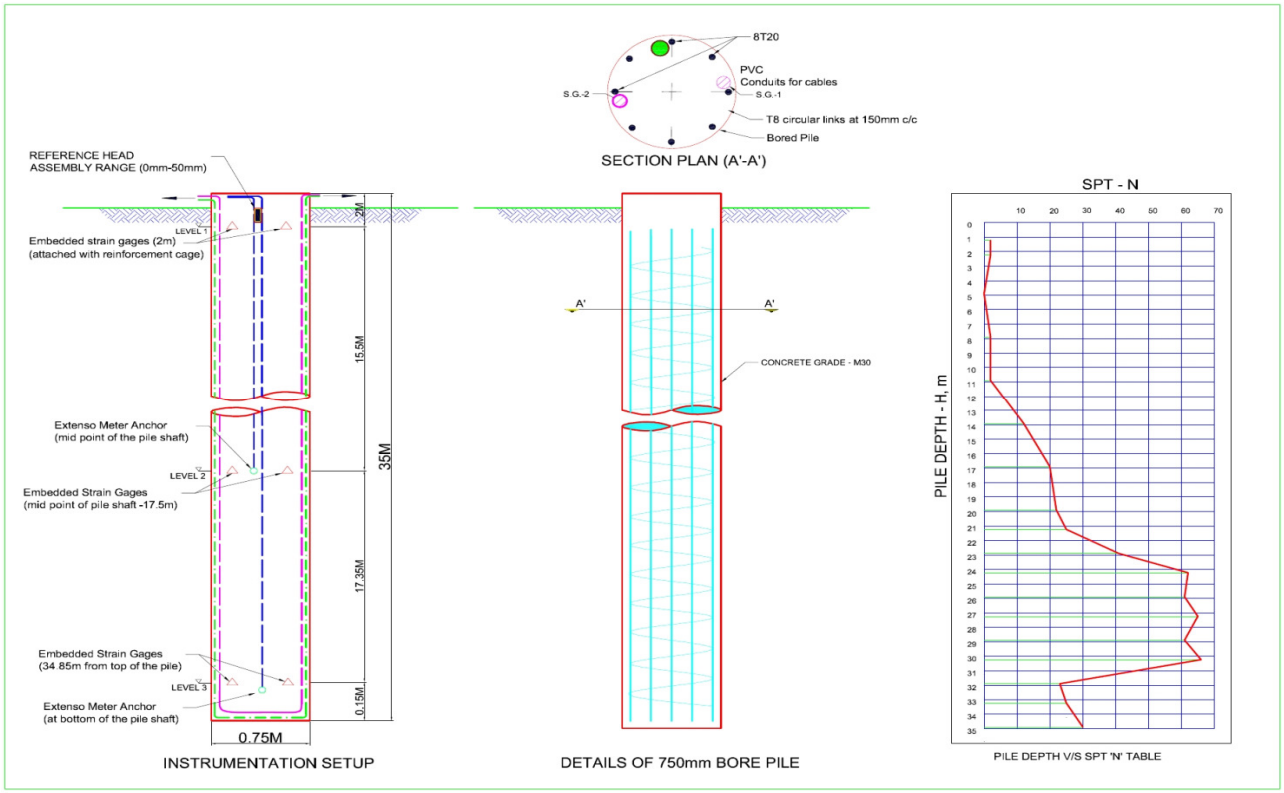


Fig.14: Typical instrumentation setup, test pile detail, and SPT-N value

5.0 CONCLUSIONS

The author has the following conclusions based on the above-described load test program and subsequent data interpretation work:-

1. For all test piles, mobilized toe resistance was insignificant. The mobilized toe resistance values ranged from about 0.53% to about 6.21% of the applied top load.
2. Soft toe conditions were observed. Therefore it was recommended that the pile toe resistance should be utilized only after proper pile base cleaning and confirming firm base conditions.
   Variation of pile shaft diameter and conditions can affect shaft load distribution. For example, for bulged sections, load transfer may occur through direct bearing below the bulged shaft.
3. Also, at such sections, the concrete cross sectional area is larger than the average area assumed in pile design, which should be accounted for in pile load distribution calculations. Therefore, good quality construction records are very important for reliable and accurate interpretation of instrumentation data.

6.0 REFERENCES

Fellenius, B.H, 2001. From strain measurements to load in an instrumented pile. Geotechnical news Magazine ,Vol.19,No 1pgs.35-38.

Fellenius, B.H. Determining the true distribution of load in instrumented piles. American Society of Civil Engineers , ASCE , International Deep Foundation Congress "Down to Earth Technology". Orlando, Florida, February 14-16, 2002,Vol.2, pp. 1455-1470

Sellers J.B , 1995. Pile load test instrumentation, Instrumentation in Geotechnical Engineering , Proceeding of Geotechnical Division of the Hong Kong Institute of Civil Engineers. Pgs 23-33.

Interpreting Strain Measurements from Load Tests in Bored Piles
Jack Hayes, Load Test Inc., Gainesville, Florida, USA
Tony Simmonds, Geokon Inc., Lebanon, New Hampshire, USA

Samuel G. Paikowsky & Edward L. Hajdak. Design and construction of three instrumented test piles to examine time dependent pile capacity gain. (Geotechnical Testing Journal, Vol.27, No.6; Paper ID GTJ12191)

Jorj Osterberg (1999) "Value Engineering-A Great Concept. Why Isn't It used More Frequently ?" Ohio River Soil Seminar,1999.

H.M. Abdul Aziz bin K.M Hanifah and Lee Sieng Kai "Innovation in Instrumented Test Piles in Malaysia: Application of Global Strain Extensometer (GloStrExt) Method Bored Piles. JURUTERA, October 2005

Thomas H. Hanna "Foundation Instrumentation ; Series on Rock and Soil Mechanics" 1973.

LATERAL LOAD TEST ON PILES WITH LARGE FREE STAND

Chandramohan P.V. Author, Navayuga Engineering Company Ltd, Hyderabad, India, +91 9849011789, pvcmohan@gmail.com

ABSTRACT

In ports, piled berths are designed and constructed for berthing of ships with a finite draught. Piles in a bridge foundation also have a large free stand above scoured level. The piles of these structures have to withstand large horizontal forces imparted by the impact of the approaching vessels or due to longitudinal and transverse action in a bridge. It is also imperative that these piles have to project out of the dredged / scoured bed. These piles are normally designed as slender compression members subjected to bending also. They are subjected to vertical load tests for assessing the soil resistance. Lateral load tests, as a rule, are also stipulated. IS and IRC codes stipulate a deflection criteria for lateral load test to arrive at the capacity. These tests are usually conducted on a working pile by jacking out two piles. At the time of the test, pile will be free headed. But in service, piles are fixed head. There is a large difference in deflections between a fixed head and a free headed pile. Besides, a free headed pile will be subjected to a much higher bending moment than the fixed head one. This will put the working test pile under risk of breaking during the test. The problem is analyzed with case studies.

Key words: lateral load test, free stand, movement, moment

INTRODUCTION

Vertical capacity of piles is assessed by static formulae. This formula is based on the soil properties obtained from random soil exploration and laboratory and in-situ testing. Since soil is not a homogeneous medium, properties can vary. The design parameters taken for computations may be different from the ones at the interface of the pile with the soil. The best way is to find out is by a load test. The code IRC:78-2014 has rightly stated that initial load test is part of the design process. This is true with the vertical load test. But there are certain problems with the purpose and inference of the lateral load test. In both the tests the criteria for acceptance is the quantum of movement of the point of application of the load. In the former, the movement is vertical and depends more on the compression of the soil than the compressive strain in concrete. But in the latter, this movement is partly on account of the flexural rigidity of the pile and partly due to the horizontal compressibility of the soil. The role of rigidity of the pile is more when compressibility of the soil is higher. Lateral load test is done by jacking one pile against another because it is difficult to get an independent horizontal reaction. Please see Fig.1 Photo.



Fig 1 Lateral load test set up photo

This means that the test is invariably done on a working pile. In the actual service life of the pile, it will be with a cap and will be structurally restrained from rotation at the top. But load test is done in a free head condition where the head is free to rotate. There is a difference in the deflections. Deflection of a free head pile at the head of the pile is several times that of a fixed head pile. The Bending moment induced on the pile also will be much more in a free head pile. Theoretically one may be able to find out the deflection of a free head pile and regulate the load test. Also, one can observe the dial gauge readings. But the bending moment is invisible. Even the failure occurs much below the ground level and will not be visible. The magnitude of the moment will be much higher in the case of piles with a sizable free stand. This is usually the case with piles under a jetty for deep draughted vessels or a bridge with scour. We are now talking about a fracture in a working pile without it being noticed. The result is a structure will be erected on top of it.

PROBLEMS INVLOVED

Lateral load test ends up testing the structural strength and stiffness of the pile section, especially for piles with a large free stand. The problems are enumerated below.

1. Any load test on pile is conducted to ascertain or assess the soil resistance to the load on the pile. Normally structural capacity of the pile as a column is designed to be more than the soil resistance. But wherever, piles are projecting above bed level as in the case of berths in a port and pier supports of a bridge, the unsupported length of the member could be a critical factor in the structural strength. It is not the intention to load test the structural strength of any member. If that was so, then beams and slabs should be load tested. For piles, a short portion could be subjected to bending to find out the moment it can withstand.
2. When a lateral load is applied to the pile with a free stand over the soil, it invariably results in inducing a sizeable bending moment on the pile. This increases with the free stand. So, the structural stability of the pile is at stake much before any soil failure.
3. It is not possible to apply the load at the dredged level in a berth or scour level in a bridge.
4. Almost all the piles in the above structures are fixed head type. This cannot be simulated in a lateral load test. The result is that the pile will be subjected to higher deflection and bending moment than in actual service. The deflection is observed during the load test. If the load test is terminated at the stipulated maximum deflection, the load applied will be negligible. So the pile will have very low capacity. On the

other hand, bending moment being induced in the pile during a test is invisible and cannot be felt until the pile breaks.

5. When the pile is pushed to one side, the horizontal sub-grade reaction of the soil will try to resist the force. This will reduce the moment from that of an equivalent cantilever. This is represented in the calculations by a reduction factor. This factor increases slightly with the free stand of the pile above the soil. It must be remembered that for larger free stand, the lever arm of the sub-grade reaction will become very small and its contribution to reduction in the moment will not be considerable.

6. Many of the lateral load tests on piles are conducted in the ports. Engineers in ports are aware about this problem. Recently, a berth was constructed in a Port. This difficulty was faced there. Lateral load tests were dispensed with for the construction of the next berth. If the site engineers who faced this problem give a feed back to the designers, repetition of the problem could be avoided.

7. Nowadays, it so happens, that some consultants do the design of berths. They are not aware of the intricacies of lateral load testing of piles with a large free stand. During the preparation of the tender documents lateral load tests are also added. Contractors also do not bother about them during tendering. Later on this becomes a contractual obligation.

8. In order to restrain the pile heads from rotation, the pile cap has to rigid enough. This means that the stiffness of the cap should be much higher than that of the piles. In the usual case, this will be true as the section of pile cap is rectangular and that of the piles is circular. Besides, spacing of piles is very small compared to its unsupported length. The I/L value of cap will be much higher. IRC code has mentioned that if the thickness of the cap is one and a half times the diameter of the pile, it could be taken as rigid. This is found to be true in computations as well. Another factor is that if there are only two piles in a group, piles could be fixed in one direction and free headed in the other. In the case of a bridge the heavy super and substructure also ascertain fixity. In a jetty, the piles are tied in all directions.

EXAMPLE LOAD CASES

Case 1: Cut Off Is At Ground Level

Please refer to Fig 2. A pile of 1000 mm diameter is installed into the soil. The soil is medium sand with N=20 and is submerged. The material of the pile is concrete of M40 grade. The cut off is at ground level. A lateral (horizontal) load of 100 kN is applied at the ground level on the pile. As per IS 2911 Part 1, Sec 2:210 Appendix C,

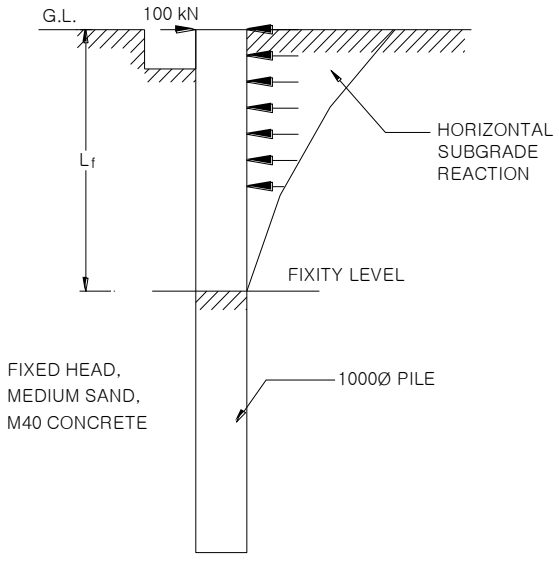


Fig. 2 Cut off at Ground level

$$T = \sqrt[5]{\frac{EI}{\eta_h}} \qquad [1]$$

Where, $E = 5000\sqrt{f_{ck}} = 5000\sqrt{40} = 31623MPa$

$I = \frac{\pi d^4}{64} = \frac{\pi 1^4}{64} = 0.04909m^4 = 4.909x10^{10}mm^4$

η_h = 2840kN/m3 (0.00284N/mm^3) (from Table 3 of Appendix C)

$$T = \sqrt[5]{\frac{31623x4.909x10^{10}}{0.00284}} = 3528 \text{ mm} \qquad [2]$$

In this particular case, since there is no free stand of the pile, $L_1 = 0$, so $L_1/T = 0$. From Fig 4 of the Appendix C, $L_f / T = 2.2$.

L_f = 2.2x3528 = 7762 mm

Deflection at the load point of the pile $Y = \frac{Q(L_1 + L_f)^3}{12EI}$ (For fixed head) [3]

Where Q is the load in Newton

$$Y = \frac{100000x(0 + 7762)^3}{12x31623x4.909x10^{10}} = 2.510mm \qquad [4]$$

Now, proceed to calculate the moment on the pile.

The fixed head moment of the equivalent cantilever, $M_F = \frac{Q(L_1 + L_2)}{2}$ (for fixed head) [5]

$$M_F = \frac{100000(0 + 7762)}{2x10^6} = 388.1kNm \qquad [6]$$

Since the Subgrade reaction from the soil will be resisting this moment, there will be a reduction in this moment. This is effected by a factor to be obtained from the graph in Fig 3 of Appendix C. In this case this comes to 0.82, m = 0.82. The actual moment on the pile works out to 388.1x0.82 = **318.2 kNm.**

Deflected shapes of free and fixed head piles are given in Fig. 3.

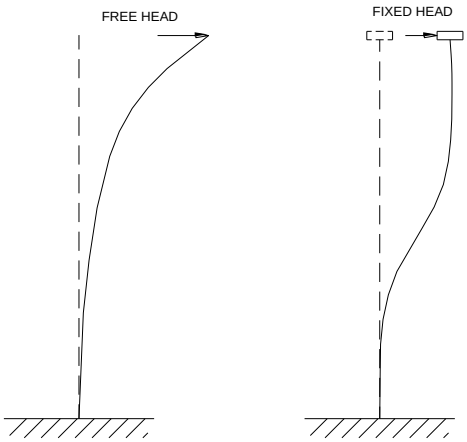


Fig. 3 Deflection of free and fixed head

According to IS 2911 Part 4; the lateral capacity of the pile is the load when the deflection reaches 5mm or 50% of the load corresponding to 12mm deflection. Here, the deflection at the cut off level is only 2.51 mm. The pile has a capacity in excess of 100kN. The moment is only 318.2 kNm. The load is 100 kN. Structural capacity of the member is not a subject here. Here again there is an additional point. The above calculations are for a pile with a fixed head i.e., rotation at the pile head is restricted. When, the load is applied by a jack, the pile will have a free head, i.e., rotation at the head will be a maximum. Pure structural moment in this case will be much more than that of a pile with a fixed head. But reduction coefficients in the case of free head condition are slightly different. Putting in the changed coefficient, 0.41 in this case, the actual moment on the pile during test will come to **318.2 kNm.** The coefficients are 0.82 and 0.41. This applies more drastically to the deflection. Deflection for a free head cantilever will be 4 times that of the fixed head. (This is as per the formula given in the IS, but coefficients are different). So during the test, in this particular case, the deflection will be 10.04mm. Lateral load capacity of the pile is covered by the lower of two stipulations. One is the load at which the final displacement is 50% of the 12mm. The other is the load at which the final deflection reaches 5mm. If the load test were done in fixed head condition, then these criteria are satisfied and the capacity will be retained as 100kN. But as the test is done in free head condition, the capacity has to be arrived at. This becomes the load at 5mm movement ie, 49.792kN in place of 100kN. If this is known, correction for the condition of the head of the pile could be made in the movement and inference on the test could be arrived at accordingly. However significance of the method is more pronounced with large free stand.

Bureau of Indian standards is aware about this problem and suggested that lateral load test is done between group of piles or under sustained vertical load. Both are not practical.

The above computations were made based on the expressions given in IS 2911. But in recent times, the simple analysis given in IS 2911 is hardly followed in the analysis of pile foundations. The analysis is carried out by non-linear methods using sophisticated software. Springs representing the subgrade reaction of the soil are simulated around the pile. In this paper, for the sake of comparison, the subgrade reaction is taken the same as was used in the IS formula. Analysis was done using a computer program. Movement at the top of the pile came to 5.779mm. This was 2.51mm in computations with IS formula. The value is more than double. The bending moment comes to 341.9kNm. During test for free head condition, movement at the top will be 11.676mm, with a maximum moment of 238.8kNm. This means that the lateral load capacity of the pile will vary with the type of analysis.

Case 2: Pile Projecting 20m Above Ground Level

Often there is a feeling that the stipulations in the IS have been framed for piles under buildings which normally do not project above the ground. The revision of the standard in 2013 has stipulated that the deflection should be governed by that at the scour/mud level for off-shore piles. Load would be applied at the head and deflection at the scour level could be computed.

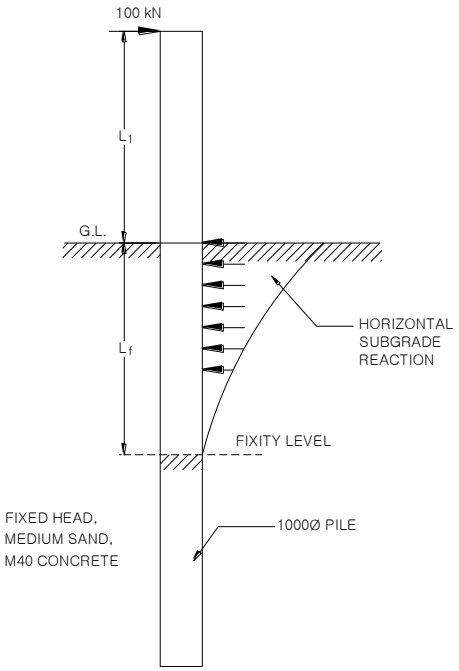


Fig. 4 Cut off above ground level

Please see Fig. 4. No change is made except that the pile is projecting above the ground level by 20m and the load of 100 kN is applied at the head of the pile. This is the general case in a berth where there is deep draught at the berthing face or in the case of a bridge with scour. In the case in fig 4, L_1 = 20000 mm. T depends on the sectional and material properties of the member and deformation properties of the soil medium. This does not change.

L_1 becomes 20m or 20000 mm.

L_1 /T = 20000/3528 = 5.669

From Fig 4 of the Appendix C, L_f / T = 1.86

L_f = 1.86x3528 = 6562 mm

$L_1 + L_f$ = 20000 + 6562. = 26562 mm. Deflection at scour level is found out as below.

Deflection at the scour level, $$Y = \frac{Q}{EI}\left[\frac{{L_f}^3}{3} + \frac{{L_f}^2 L_1}{2} - \frac{{L_f}^2 (L_f + L_1)}{4}\right] \quad [7]$$

$$Y = \frac{100000}{31623x4.909x10^{10}}\left[\frac{6562^3}{3} + \frac{6562^2\, x20000}{2} - \frac{6562^2\, x(6562 + 20000)}{4}\right] = 15.386mm \quad [8]$$

$$M_F = \frac{100000x26562}{2x10^6} = 1328.1kNm \quad [9]$$

The reduction factor in this case also, comes to 0.95.
Moment on the member = 1328x0.95 = **1261.6 kNm**

Due to the lack of a fixity at the head during test, the observed deflection will be 33.805mm. The lateral capacity as per load test will become 32.50kN. Moment on the pile during test will be 2152kNm. (The reduction factor here is 0.81) This moment is nearly 71% more than the fixed head moment in service. This will certainly endanger the working pile. It is needless to say that the former will result in relative under capacity of the pile while the latter will structurally damage it. But as per IRC, applying a deflection criterion of 1% of the diameter of the pile, lateral pile capacity will be 29.581kN. Piles in both jetties and bridges are ones with large free stand. But in a jetty the pile will have a lateral capacity of 14.791kN while the same pile in a bridge will have a capacity of 29.581kN. This works out to double.

Now, like in case 1, computations are carried out by non-linear method using soil springs. Results are summarized in table 2. The assumption is, as earlier, pile will be fixed head in service but test is done in free head condition. Please see that lateral capacity of the same pile varies with the method of computation. Capacity as per IS criterion (5mm deflection at mud line) obtained by IS formula came out as 14.791kN while that as per non-linear analysis came to 11.15kN. The same using IRC criterion was arrived at as 29.581 and 22.3kN respectively. Apart from capacities, please note that during test the moment on the pile is 2072kNm against a service moment of 789kNm as per non-linear analysis. This means a working pile will be put to danger.

Table 2. Free stand of pile = 20m

	Non-linear method					IS formula	
	Movement at head (mm)	Movement at bed (mm)	Max moment (kNm)	Capacity as IS (kN)	Capacity as IRC (kN)	Capacity as IS (kN)	Capacity as IRC (kN)
Free head (test)	475.778	44.833	2072	11.15	22.3	14.791	29.581
Fixed head (service)	122.126	22.476	789				

The assumption is, as earlier, pile will be fixed head in service but test is done in free head condition.
All the computations point out that the computed moment during lateral load test is much more than the design service moment on the pile. In fact, the author became aware about this problem early enough and avoided breaking of the piles by stopping the test at the point of allowable moment. Later on approach to the later load test had been with extreme caution.

VARIATION OF PARAMETERS WITH FREE STAMD

There is a substantial difference between the movement at the bed and movement at the pile head. The increase in difference is hyperbolic with the amount of free stand. A graph was plotted with the results obtained from non-linear analysis. Please see Fig. 5 below.

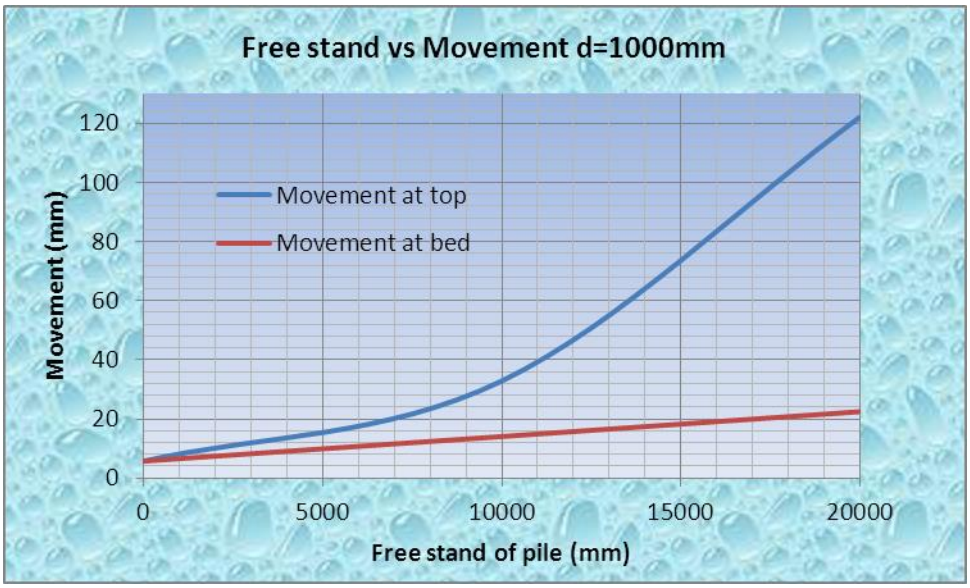


Fig. 5 Variation of Movement at top and bed with free stand

There is sizable difference in the bending moments on the pile in fixed head condition (service) and free head condition (test). Please see how this varies with the free stand in Fig. 6. It is evident that during tests the pile is subjected to higher moments than that during service endangering the structure.

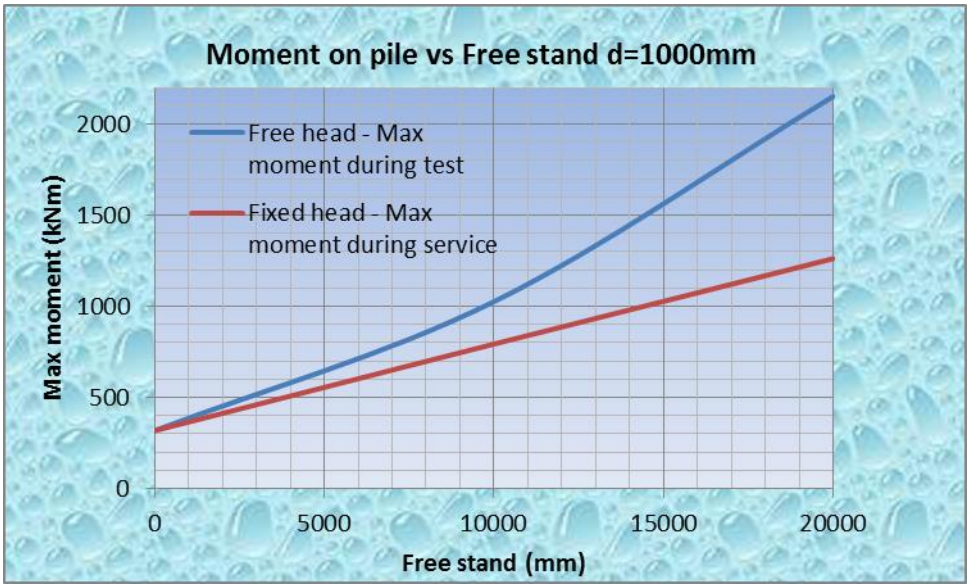


Fig. 6 Variation in moment with free stand with rotation restraint at top

Since lateral load capacities are arrived at based on a deflection criterion, the capacities of piles will vary substantially. Location of the deflection is also important. The Indian Standard and Indian Road Congress hase taken deflection at the head of pile and at the bed respectively for arriving at lateral capacities. This has resulted in wide difference in capacities. Please see Fig. 7.

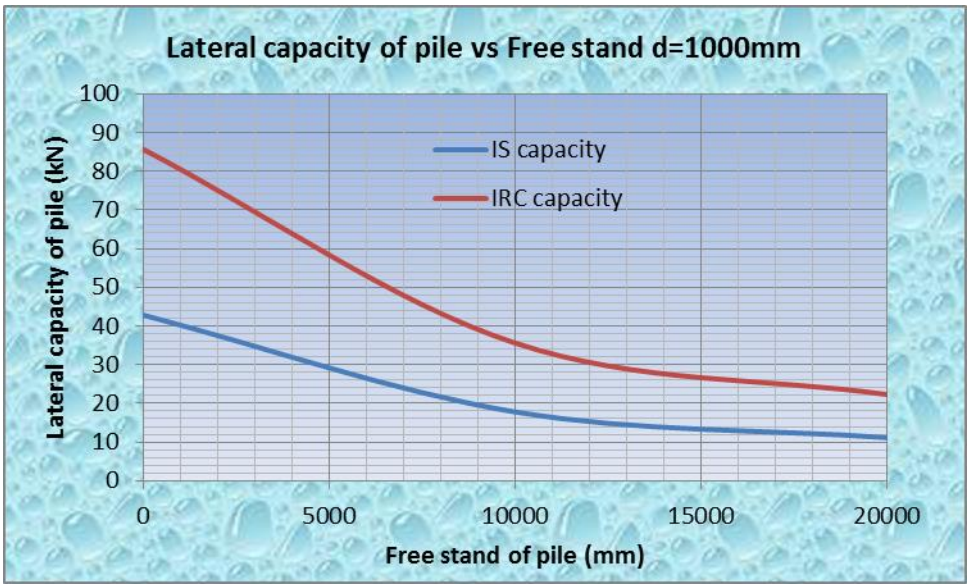


Fig. 7 Difference in IS & IRC capacities with free stand

INEFFECTIVENESS OF THE TEST

1. From the calculations above, it can be seen that lateral load tests on, piles with a sizeable free stand, do not yield any valuable data. It is ironical that sometimes people go into the lateral load test by the letter, not the spirit and stipulate that a casing of a larger diameter is first installed to reach below the dredged / scour level. Boring is done up to the proposed dredged level and the pile is separately installed inside this annular casing. Sometimes, stipulation is to the extent that two such piles should be installed and lateral load test should be carried out butting one pile against the other. All this is meticulously stipulated to remove any lateral soil support to simulate the actual conditions! If this item is operated, as it will be, the whole paraphernalia becomes a national waste. It is not important whether the contractor does it at a profit or loss. Regardless of that, the nation stands to lose its much-needed resources.
2. The Indian Standard for concrete stipulates certain serviceability criteria for structures. This has been done to prevent excessive deflections from impairing the use of the structure for general purposes. Sometimes, it is applied to the berth structure by letter. It should be remembered that primarily a berth has to withstand the berthing force induced by the berthing vessel. Berthing energy is transmitted through fenders. Fenders convert the kinetic energy into strain energy and pass on a reaction force to the structure. It is in the interest of the structure that this reaction force is kept to a minimum. As the very term indicates, fenders are able to store the energy from the deflection it undergoes. A classic example is the flexible dolphins for deep draughted vessels. A cluster of steel piles will act as dolphin cum fender by virtue of their deflection. The steel piles absorb the berthing energy by way of its own deflection. A combination of rubber fender and steel piles is also employed to absorb the impact. The principle is to utilize the large deflections. RCC piles may not deflect as much as steel or wooden piles. But it is all the more important to utilize the deflections to reduce the reaction force on the structure. The energy stored in a system is equal to $P\delta/2$ where, P is the force and δ is the deflection. It is needless to say that in berthing structures, resilience is the catch word. It is counter productive to make the structure stiff. This will increase the berthing force on the structure.
3. A pile is vertically loaded at the top in service. The test is simulated in the same manner. But on a pile with free stand there are horizontal loads acting on the body of the pile below the head. Current, seismic and wave forces are examples. This is to say that apart from the structural risk, correct loading is not simulated in a lateral load test. IRC:78 stipulates that lateral load test is to be done only for normal load condition which means loads due to temperature, wind and seismicity are excluded.

CONCLUSION

Piles are versatile foundation structures, which help in transferring the load from the superstructure to the deep soil below. It can resist vertical, horizontal and inclined loads. Design and construction of piles require systematic subsoil data collection. But due to the uncertainties involved, much emphasis is placed on actual load testing to ascertain the capacity. Indian Standards have also made certain specifications. One such specification is on the lateral load testing of piles. There is tendency to follow the printed specifications without understanding their spirit and context. Lateral load testing is usually done for piles in a berthing structure, which are subjected to large horizontal forces. It is a coincidence that these piles have large free stand from the bed. Carrying out lateral load tests on such piles involves a great risk especially as the test will be conducted on a working pile. Lateral load tests on such piles do not yield any useful data and so becomes wastage of the much needed national resources.

REFERENCES

1.IS 2911 (Part 1/Sec 2) : 2010 Design and construction of pile foundations – code of practice Part 1 Concrete piles Section 2 Bored cast in-situ concrete piles Bureau of Indian Standards 2010

2. IS 2911 (Part 4): 2013 Design and construction of pile foundations – code of practice Part 4 Load test on Piles Bureau of Indian Standards 2013

3. IRC:78 Standard Specifications and code of practice for road bridges Section VII Foundation and substructure Indian Road Congress 2014

DIAPHRAGM WALLS FOR INFRASTRUCTURE PROJECTS HOW TO DEAL WITH COMPLEX DEMANDS?

Franz-Werner Gerressen, BAUER Maschinen GmbH, Schrobenhausen, Germany, Franz-Werner.Gerressen@bauer.de
Manfred Schoepf, BAUER Maschinen, Schrobenhausen, Germany, Manfred.Schoepf@bauer.de

ABSTRACT

Diaphragm walls are known as underground structural elements commonly used as retention systems for excavation pits and shafts and permanent foundation walls or elements. It can be anticipated that, with the increasing trend of utilizing more and more underground space to accommodate environmental considerations and urban/suburban development, there will be an increasing requirement for diaphragm walling in even more complex conditions. Complex and/or challenging conditions in terms of ground conditions have a major impact in regards of choosing the right tools for excavation purpose. Complex conditions in terms of space limitations, especially for inner city job sites, require specifically adapted solutions for slurry, spoil, reinforcement and concrete handling and the related logistic to ensure smooth production. Furthermore, one focus will be given to the QA/QC topics of the production process. Real time installation control, data transfer and reporting systems become more and more important ensuring the five dimensions of a jobsite. Therefore, the paper will describe the construction method and the sequence of activities required for the construction of diaphragm wall systems with the focus on the cutter technology. It will describe also the main equipment which will be needed to execute these works under the various conditions

Keywords: Diaphragm wall, Trench Cutter, Rock

INTRODUCTION

Diaphragm walls are known as underground structural elements commonly used as retention systems for excavation pits and shafts and permanent foundation walls or elements.
It can be anticipated that, with the increasing trend of utilizing more and more underground space to accommodate environmental considerations and urban/suburban development, there will be an increasing requirement for diaphragm wall usage in even more difficult conditions.
Of course diaphragm wall can also be used as deep groundwater barriers (Cut-Off-Walls). This market has shown that the demand for these types of walls is reaching more and more difficult soil conditions or required depths which are surpassing the current standard. The trench cutter is the most important tool for performing this work.

The trench cutter itself is a reverse circulation excavation tool. It consists of a heavy steel frame with two drive gears attached to its bottom end, which rotates in opposite direction around horizontal axis. Cutter wheels are mounted onto the drive gears. As they rotate, the soil beneath the cutter is continuously being broken up, removed, mixed with the bentonite slurry in the trench and moved towards the opening of the pump suction box. The slurry loaded with soil and rock particles is pumped by a centrifugal pump which is located right above the cutter wheels, up through a hose system up to a desanding plant where the slurry is cleaned and returned into the trench.
The torque of the cutter wheels combined with the weight of the cutter is strong enough to cut into hard soils, crush stones to a certain grade and to overcut into the concrete of adjacent panels.
Depending on the soil type, different types of cutter wheel configurations and teeth can be deployed, ranging from aggressive teeth for cutting fine-grained soil to percussive teeth for crushing boulders. Changing the cutter wheels to suit different types of rock can be readily accomplished as well. Experiences exist for being able to cut rock with strength up to 250 MPa.

THE WORKING PRINCIPLE

Working sequence

The typical working sequence for the construction of a diaphragm wall as shown in figure 1 comprises the following key steps:

- Site preparation,
- Guide wall construction
- Trench pre-excavation
- Panel excavation
- Panel cleaning (desanding)
- Reinforcement installation (for retaining walls)
- Concreting

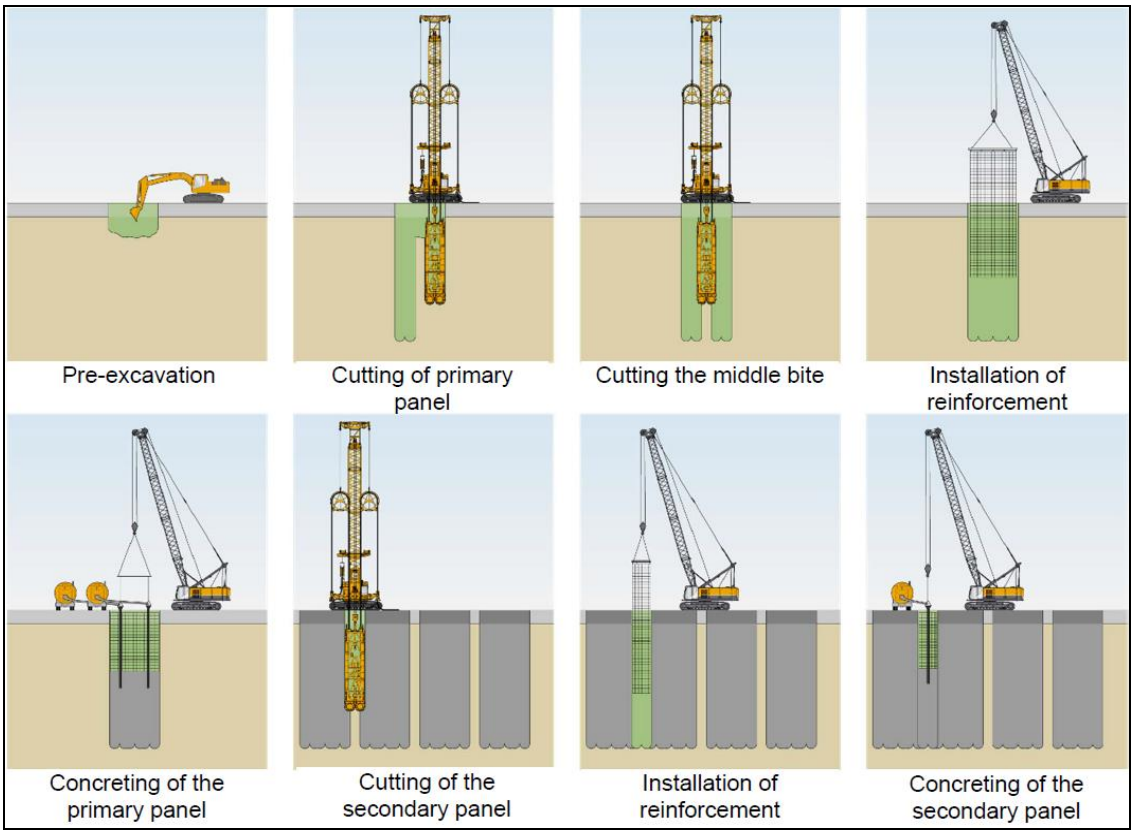


Figure 1: Construction process, exemplary for Diaphragm wall process

COMPLEX DEMANDS AND THE FACTORS OF INFLUENCE ON PERFORMANCE

There are a number of influencing factors which have an impact on the cutting performance. Besides the influence of the geological conditions and therefore the choice of required tooling, there are also other factors related to suitable equipment, e.g. for limited space. Besides that, also the operating staff can have a huge impact (Figure 2).

The estimation of these parameters and characteristics for a specific job site might have a major impact in the cost structure of a job. It can also bear a high risk of increased costs. Therefore, accurate prediction would be highly desirable.

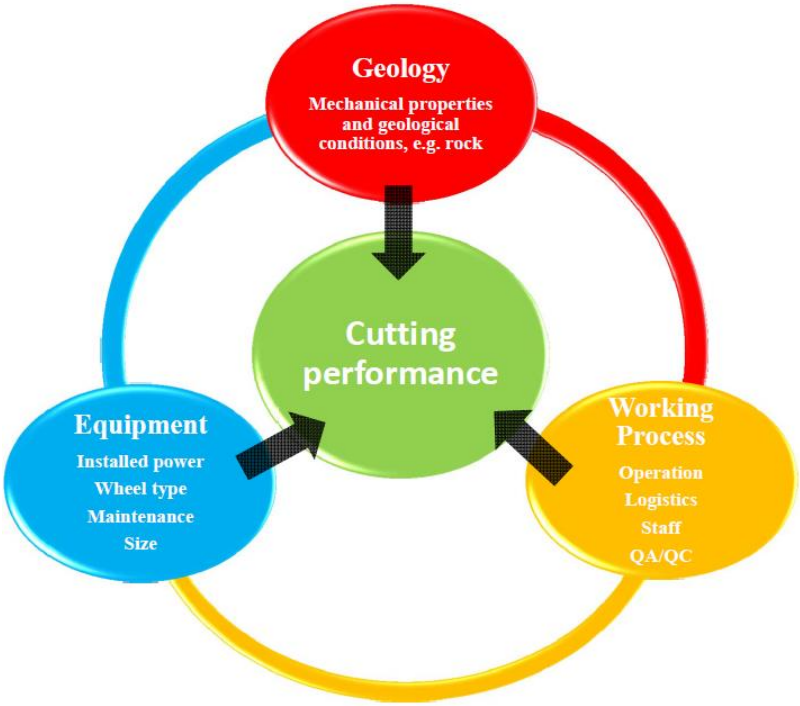


Figure 2: Conceptual overview of the main parameter influencing the cutting performance

Looking deeper into detail, furthermore we will have a focus on the complexity of space limitation, geology and quality control.

Complexity of space limitations

Space limitations require intelligent solutions, ensuring the ability for installing the diaphragm wall without major impact to the productivity.

Height restriction

Working under restricted height requires development of special equipment. Actual developments allow a height restriction for so called “low headroom cutter” of approx. 6.m (Figure 3).



Figure 3: Low headroom cutter

Space restrictions for storage area

For the installation of a diaphragm wall, slurry is required to ensure stability of the excavated trench. In case of the cutter technology, the slurry acts as well as transport medium for the loosened soil.

The needed slurry volume is quite substantial, and the storage volume is normally separated in several areas:

- Swelling basin for hydrating freshly mixed bentonite slurry
- Concrete bentonite basin - buffer for exchanging slurry prior to concreting
- Working bentonite basin - for slurry circulation during excavation
- Waste bentonite basin

The storage unit can be made up of a series of ponds excavated in the ground, steel tanks (Figure 4) stacked parallel or on top of one other or, if space is at a premium, a series of silos (Figure 5). The layout can have different configurations to best suit the geometry of the site but it is important, in order to guarantee continuity in the work that the total capacity of the storage by unit is at least 3 times the volume of one panel trench.
In the design of storage capacity, consideration should be given to the local geology. If there are indications of the presence of formations that could lead to a sudden loss of bentonite during excavation and that could thereby compromise the stability of the trench. The size of the storage basins should take into account a surplus supply that needs to be used in these emergency situations.



Figure 4: Bentonite storage in tanks


Figure 5: Desanding plant and bentonite storage in silos

Space restrictions for logistic of slurry and spoil handling

During the excavation of the trench, two main tasks have to be fulfilled. At first, slurry needs to be transported to the trench to ensure trench stability during excavation. Second, the excavated material needs to be disposed.
At this point, we have to distinguish the two common excavation methods, the use of a grab and the use of the cutter.

The use of the grab requires a high logistic effort for handling the disposal, as the grab will typically load the excavated material directly at the trench into a truck (Figure 6). This requires access and working space for the truck, which might be complicate in inner city sites with limited space. In addition, the loading process typically will generate also some pollution on the working platform. Compared to that, the cutting process will require less space for the handling of the excavated material, as the loosened soil will be transported via a second slurry line to a slurry treatment plant, which can be positioned e.g. some

hundred meter away. The closed bentonite slurry circulation (Figure 7) therefore causes only low-level pollution during the construction process. Due to the removal of solid particles from the support fluid in the slurry treatment plant, the excavated material can also simply be moved off site and disposed.



Figure 6: Loading process for grab

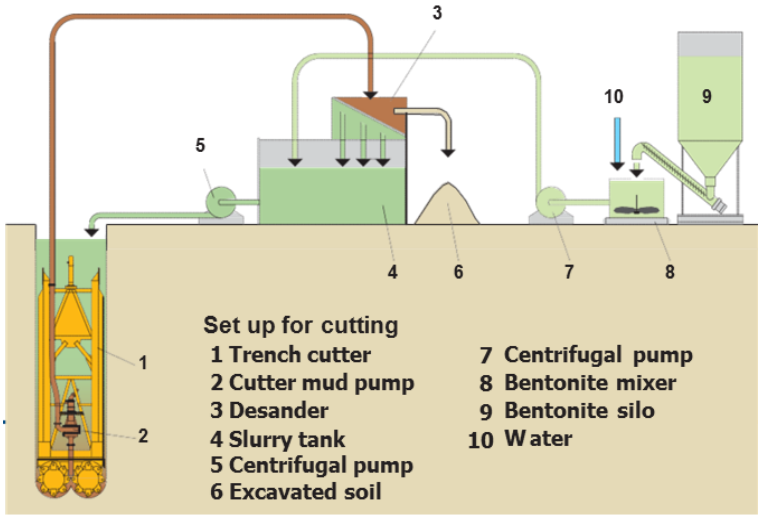


Figure 7: Slurry circuit

The two slurry lines for the cutter process, the so called conveying unit, is made up of a series of pumps, pipes, valves and controls designed to facilitate conveying bentonite to and from the trench. In the design of the conveying unit account must be taken the high volume of flow of bentonite to and from the trench. It can be as high as 500 m^3/h.

Complexity of ground conditions

Ground conditions are as they are. That means, whatever will be found, one has to deal with it. An extensive investigation program is mandatory to be best prepared for the job. Investment in ground investigation is worth the money, as it will safe lots of costs in the execution. Ground conditions will influence the stability of the trench and of course the performance of the excavation itself. Therefore, well known ground conditions allow to choose the most suitable working procedure and execution technique.

One of the biggest challenges for the installation of a diaphragm wall is the existence of rock in the ground. But what is rock all about? Looking at rock characteristics, one can find e.g. a definition, that “A rock mass is usually made up of the rock material or rock substance and the discontinuities”. The presence of these discontinuities and the effects of weathering have significant influence on the mechanical properties and behaviour of a rock mass. These characteristics can also have major impact to the achievable performance of rock cutting. Unfortunately, all relevant data is often not available for evaluation and estimation. The most commonly available rock property found in the geotechnical reports is the UCS Value. But there are more related characteristics, e.g. abrasiveness, which would be of high importance. At this stage it must also be mentioned, that the categorization of various properties can differ from each other depending on the region in the world, which makes it even more difficult to give a definitive overall guideline.

The estimation of these parameters and characteristics for a specific rock type might have a major impact in the cost structure of a job. It can also bear a high risk of increased costs. Therefore again, accurate prediction would be highly desirable.

It must be said that the number of influencing factors is nearly endless. A lot of variables, with various importance, also interact during the construction process. Some of these factors are measurable, but not provided on a regular base. This leads to a situation, were reliable performance estimation is nearly impossible. Nevertheless, everybody expects to get the best possible estimation, however a guarantee can never be given.

Therefore, based on experiences made on over 100 projects, a performance estimate chart has been developed to provide a better approach to these kinds of jobsites.
As already stated, due to the availability of relevant data, the chart just shows generalized performance data based on experienced gained on these projects. Utilizing at least one factor as a guide, the most commonly provided information is the unconfined compressive strength UCS. Therefore, the performance is displayed as a function of the UCS values Figure 8).

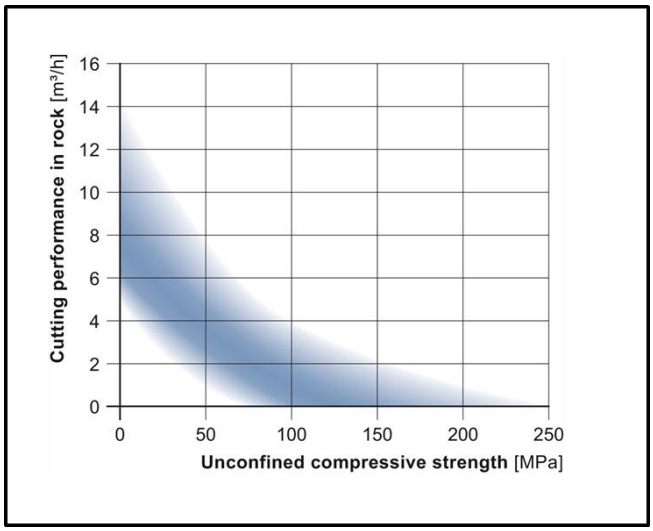


Figure 8: Performance estimation chart

As the diagram is based on experiences gained from a limited number of completed projects, these values represent no legally binding assurance or warranty for future projects. The final selection has to be made by the end-user, based on the type and weight of the cutter, the type of cutter wheels (Figure 9) and above all on the detailed knowledge of ground conditions as described before.

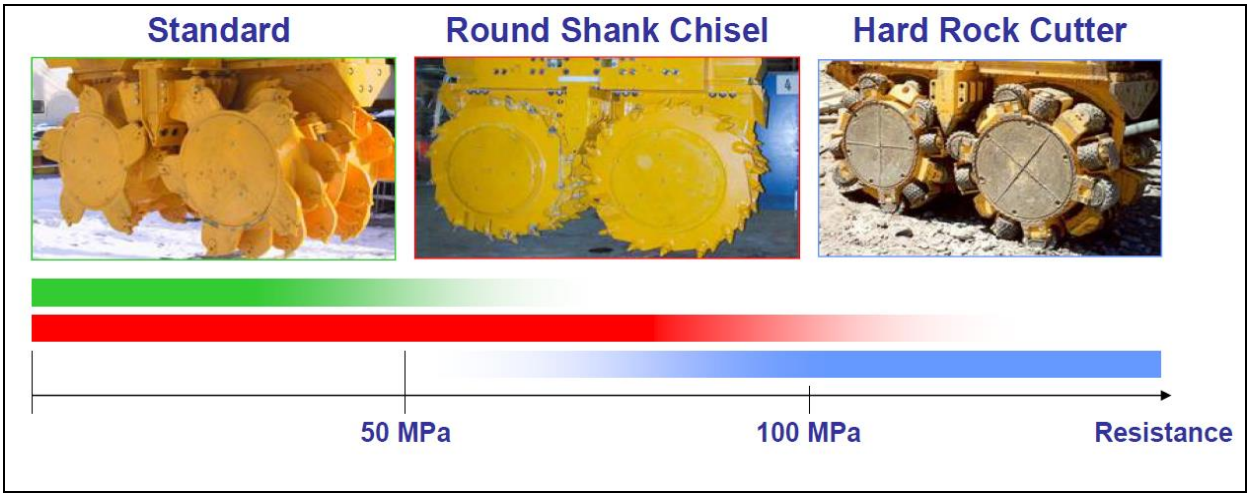


Figure 9: Type of cutter wheels

Complexity of QA/QC

Quality assurance and quality control starts already prior to the start of the excavation process. The first step in terms of QA therefore is the installation of a guide wall.

Guide wall

Guide Walls need to be constructed prior to the diaphragm wall to provide:

- Guidance to ensure the correct alignment of the pre-excavation.
- Stability of the upper trench that could be affected by the vertical surcharge induced by the Cutter and other heavy jobsite traffic adjacent to the trench.
- Protection against instability of the uppermost layers of soil caused by washing and fluctuating levels of bentonite slurry during excavation.
- Prevent collapse of the top of the trench due to equipment loads close to the trench.
- Support for the vertical loads imposed by the reinforcement cages that are suspended off the top of the guide wall.
-

The guide walls are normally constructed as a cast-in-situ reinforced concrete unit. Figure 10 shows exemplary dimensions, which have to be verified according to the actual site conditions.

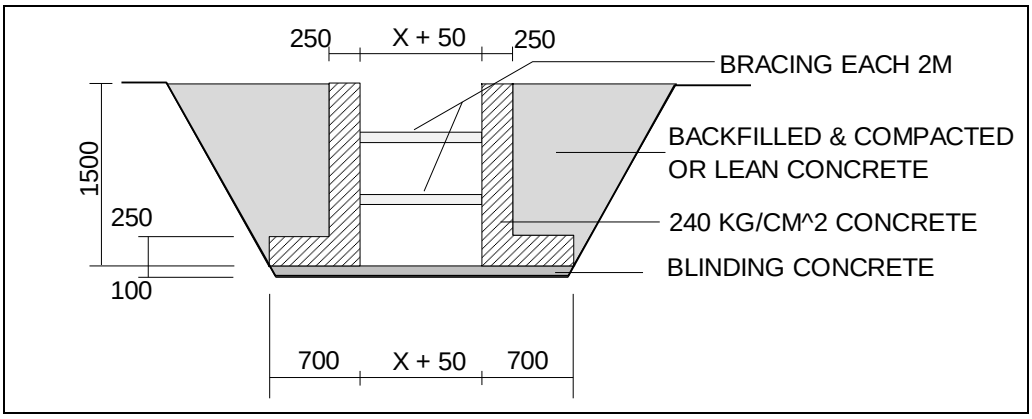


Figure 10: Typical guide wall section

Support Slurry

The trench support slurry is typically a mixture of bentonite, polymer or a combination of both with water. Admixtures such as soda may also be included in the mix design to prevent, for example, cement contamination or flocculation due to salinity of water. The slurry mix design will be finalized on site following the results obtained from trial mixes, in order to fulfil the main duty of the support slurry, to guarantee the trench stability and avoid collapse of the trench.

A typical bentonite concentration will be 30 - 40 kg of dry bentonite per 1 m^3 of slurry. Dry bentonite or Polymer powder is stored on site. After mixing it thoroughly with water, it is pumped to a hydration tank where the slurry is kept in motion and aerated for 12 hours. This process is necessary for the bentonite to fully develop its properties of viscosity and thixotropy. Using colloidal mixer may reduce the hydration time to a minimum.

It is then pumped to the main storage tanks for use. During the excavation process the fluid may become diluted or contaminated, it is important therefore that its properties be checked at regular intervals to ensure consistency in its quality.

The source and properties of the bentonite or polymer to be used shall be provided in the form of supplier certificates. The certificates will be submitted prior to the commencement of the works for approval.
The properties of the bentonite should be checked at regular intervals at the trench to ensure consistent quality of the slurry. For checking the quality of the slurry the following equipment shall be used:

- Marsh funnel
- Mud balance
- Sand content measuring kit
- Filter Press
- Fann Viscometer (or similar)

The following table lists a range of properties of typical bentonite slurry. The values are empirical and can be used unless different values are given in the project specifications.

Property to be measured	**Test method and apparatus**	**API RPI3 Section**	**Recommended values**	
			slurry pumped to the trench	**slurry in the trench prior to concreting**
Density	Mud balance	1	< 1.30 g/ml	< 1.15 g/ml
Viscosity	Marsh cone	2	30 - 70 seconds	< 90 seconds
Sand content	Sand screen set	4	unlimited (high content is advantageous in permeable layers)	< 5 %
pH	Electrical pH meter range pH 7 to 14	-	9.5 to 12	9.5 to 12

Table 1: Typical bentonite properties

Prior to the concreting process it is essential to adjust the slurry properties to ensure proper concreting. Using a trench cutter, it is common practice to use the trench cutter itself to replace or recycle the trench slurry. The machine is kept just off the bottom of the trench and its centrifugal pump is used to pump the slurry to the treatment plant. Alternatively a heavy duty submersible pump may be lowered to the bottom of the trench in lieu of the cutter.

Controlling the excavation process

The B-Tronic system developed by BAUER Maschinen is an integrated system for controlling all cutter operations and visualizing actual operating parameters in real-time on a large interactive touch-screen monitor. The following operating parameters are displayed (Figure 11):

- Actual cutter depth
- Speed of rotation and hydraulic oil pressure of each cutter gearbox
- Speed of rotation and hydraulic oil pressure of mud pump Delivery volume of mud pump
- Crowd pressure of cutter teeth Penetration rate
- Inclination of trench cutter and computed deviations in x- and y-axes (digital and graphic)
- Internal gearbox pressure Gearbox temperature
- Residual pull on crowd winch (surcharge)

Of highest importance is the inclination control of the tool in the trench. The information as displayed in real time on the screen assists the operator in maintaining the verticality of the trench excavation, but does not show the final alignment of trench. Therefore, after finishing the excavation, the use of an independent measuring device like an ultrasonic measurement is recommended.

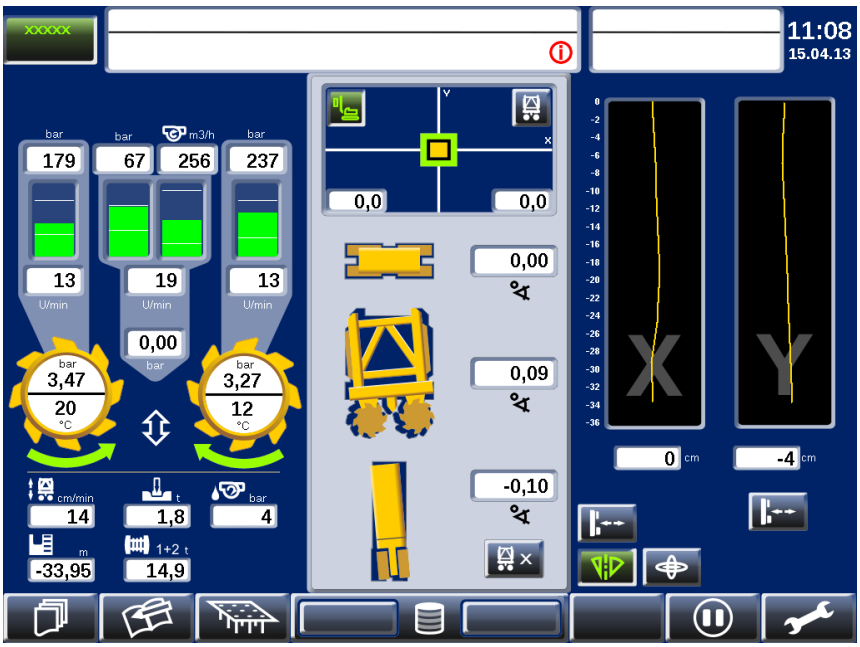


Figure 11: B-Tronic screen

In addition to these basic operational data, general machine operating parameters (e.g. engine data) are also acquired and monitored. The display of current machine operating states and error messages is a valuable aid for targeted and effective fault finding by service personnel on site, but also by specialists based at the offices, as data can be transferred real time via internet connection. This does not only allow the control of equipment and installation process including relevant reporting, it also allows comparing "virtual reality" and "reality", hence planned and actual execution, which enables the project manager to control not only the schedule, but also the use of budget.

Ultrasonic Measurement (Koden Measurement)

As an independent measuring device, the ultrasonic measurement is frequently used for verticality measurements of bore holes as well as for diaphragm wall trenches.

The use of ultrasound technology allows measurements to be taken in water or bentonite slurry. The density of the slurry must not exceed 1.15 g/cm³. The deviation of the trench from the perpendicular and any surface cavities in the trench surface are measured. The ultrasonic measurement probe is suspended vertically by a cable and lowered into the trench to be surveyed. Simultaneously, orthogonal waves are continuously emitted by the device and reflected from the walls. The reflected waves are registered by measurement sensors. The distances, calculated as a function of wave speed and reflection time, are presented in graphic form. The printout shows the distance between the probe and the wall in function of depth.



Figure 11: Koden device and measurement log

CONCLUSION

The diaphragm walling technique has become a universal, standard system for solving many foundation engineering problems. The design of new equipment features made it possible for designers to specify challenging projects, even in complex conditions in terms of space and/or ground conditions. Wall depth of 150 m can be reached with the introduction of hose and pipe handling systems. Gear boxes with high torque and shock absorbers in combination with new cutting teeth design allow penetration of rock. Electronic controls and steering facilities ensure vertical tolerance of 0.3 %. Real time installation control, data transfer and reporting systems become more and more important and will serve also future demand ensuring the five dimensions of a jobsite.

REFERENCES

NZ GEOTECHNICAL SOCIETY INC, December 2005
FIELD DESCRIPTION OF SOIL AND ROCK, GUIDELINE FOR THE FIELD CLASSIFICATION AND DESCRIPTION OF SOIL AND ROCK FOR ENGINEERING PURPOSES

Manfred Schöpf, December 2009, Diaphragm wall technique, Principles, Systems and Equipment, Mexico

DEEP FOUNDATIONS: STUDY ON EFFECT OF DRILLING FLUIDS ON CONCRETE INTEGRITY

Sri Ram Ramankutty[1]; Alberto Carmona Rosell[2]

[1]Technical Team Leader, GEO – Ground Engineering Operations Malaysia Sdn. Bhd., Kuala Lumpur, Malaysia, +(6)0327145724, sriram.ramankutty@geosoil.com

[2]Technical Consultant, GEO – Ground Engineering Operations Ltd., Madrid, Spain, +(34)912773179, alberto.carmona@geosoil.com

ABSTRACT The installation of Bored Piles and Diaphragm Wall under slurry using tremie raises quality concerns on the integrity of concrete. It is vital to understand the effects on concrete integrity during concrete pouring process. This paper intends to unveil to what extent the compressive strength of the concrete pour is affected in contact with drilling fluid still. Another important angle of analysis proves whether the inclusion of solids particles of un-hydrated fluid could have impact on the concrete compressive strength. The testing comparing the response of concrete compressive strength when drilling fluid is included into the concrete mix altering the water/cement ratio by 5%, 20% and 30%. Comparative results are analysed between two different hydrated slurries namely sodium activated Bentonite and 3rd generation synthetic polymer.

Keywords: Bentonite, PolyMud®, concrete-slurry intermix

1. INTRODUCTION

Soil stabilization is the base for a successful deep foundation execution. The G3 System Slurry developed by Ground Engineering Operations (GEO), with its third generation polymer, namely PolyMud®, is an innovative and unique alternative to the mineral based slurries for soil stabilization, enhancing the quality and integrity of the underground foundation structures. It optimises the production rate of work progress and cost as well. At the same time, PolyMud® slurry is proven to be environmentally friendly.

Guaranteeing the maximum quality of the foundation elements according to the initial design is one of the most important objectives and a concern for the foundations contractors. In order to fulfil the project expectations in this aspect, any incident that could compromise the designed concrete integrity and capacity must be avoided.

GEO, has carry out its own research regarding effects on the concrete compression results if drilling fluid intermixes with fresh concrete while pouring. To shed light in this regard, GEO, in collaboration with CML (Concrete Materials Laboratory) Sdn. Bhd., carried out empiric tests that analyse this particular event from different perspectives, bringing up the corresponding results that will be studied and commented in this article.

The scope of this research is divided in two main goals:

- To evaluate if the compressive strength of the concrete is affected when concrete is in contact or partially contains drilling fluid in its composition.
- To evaluate if the compressive strength of the concrete is affected by the ratio of water/cement.

2. OBJECTIVE

Lab tests were carried out to prove effects on the concrete compressive characteristics if alterations were made in the composition of the concrete design mix. This composition alteration refers to the drilling fluid; those were PolyMud®, and Bentonite (GTC 4). In order to make a fair comparison, a control mix sample which batched according to the actual concrete mix design was also prepared and tested.

These tests replicate the actual scenario on field where the excavations were filled with stabilizing fluid before concrete is being poured. There are chances for the fresh concrete to be intermixed with the slurry, thus affecting the compressive strength of the concrete. This study is demonstrated through concrete cube tests to evaluate the changes in the concrete compressive strength when fresh concrete is intermixed with stabilization fluid.

Two different protocols were executed, with four different percentages in volume of drilling fluid in the mix (0% or control mix, 5%, 20% and 30%).

The purpose of mixing different percentages in volume of the drilling fluid with the concrete is to quantify their impact in the concrete's resistance.

In order to determine the effects on the concrete properties occurred, all samples were tested for compression resistance after 7 and 28 days of concrete hardening and results were collected for analysis and interpretation.

3. TEST METHODOLOGY

3.1 Materials used

The products involved in this test have been concrete, PolyMud® and Bentonite drilling fluids, with the following further specifications in the mix design:

3.2 Concrete

Table 1. Concrete Mix Design

SUMMARY CONCRETE MIX DESIGN			
Feature	***Value/Type***	***Unit***	***Observations***
Characteristic Strength	40	N/mm^2	At 28 days
Margin	8	N/mm^2	
Target Mean Strength	48	N/mm^2	
Summary			
Batch for one cubic metre of concrete	Value	Unit	Observations
Design Concrete Density	2355	kg	
Cementitious	465	kg	
Water	160	kg	
Fine Aggregate	780	kg	
Coarse Aggregate	950	kg	
Admixture	1400	ml	D45
	3950	ml	ADVA181

3.3 PolyMud® drilling fluid

Table 2. Parameters of Polymer drilling fluid

PolyMud® drilling fluid		
Feature	***Value/Type***	***Unit***
Water	1	m^3
PolyMud	1	kg
Mixing Time (under Air Agitation)	2	hours
Viscosity	50-60	seconds
Density	1.00	g/cm^3
pH	11	

3.4 Bentonite drilling fluid (GTC 4)

Table 3. Parameters of Bentonite drilling fluid

Bentonite drilling fluid		
Feature	***Value/Type***	***Unit***
Water	1	m^3
Sodium Bentonite	50	kg
Maturing Time	24	hours
Viscosity	34-42	seconds
Density	1.02 – 1.04	g/cm^3
pH	9	

3.5 Test Protocols

Two different protocols (Protocol 1 and Protocol 2) were carried out in order to evaluate the changes in concrete's compressive capacity when intermix with drilling fluids during pouring under different considerations.

Parallel to both protocols sample preparation, a control mix sample batched according to the design mix was also prepared in order to take it as a reference when load tests were executed.

3.6 Nomenclature in Tests

For data recording purposes, the different mixes and tests were named as follows:

- **TM1**: Control mix test specimens (concrete batched according to design mix)
- **TM2**: Test specimens with inclusion of PolyMud® drilling fluid
- **TM3**: Test specimens with inclusion of Bentonite drilling fluid
- **Test 1**: Compression test for TM1, TM2 and TM3 (7 and 28 days).

TM2 and TM3 will have **5%** of its water volume from the concrete mix design being replaced with **5%** of drilling fluid volume respectively.

- **Test 2**: Compression test for TM1, TM2 and TM3 (7 and 28 days).

TM2 and TM3 will have **20%** of its water volume from the concrete mix design being replaced with **20%** of drilling fluid volume respectively.

- **Test 3**: Compression test for TM1, TM2 and TM3 (7 and 28 days).

TM2 and TM3 will have **30%** of its water volume from the concrete mix design being replaced with **30%** of drilling fluid volume respectively.

- **Test 4**: Compression test for TM1, TM2 and TM3 (7 and 28 days).

TM2 and TM3 will include additional **5%** volume of water by respective drilling fluid.

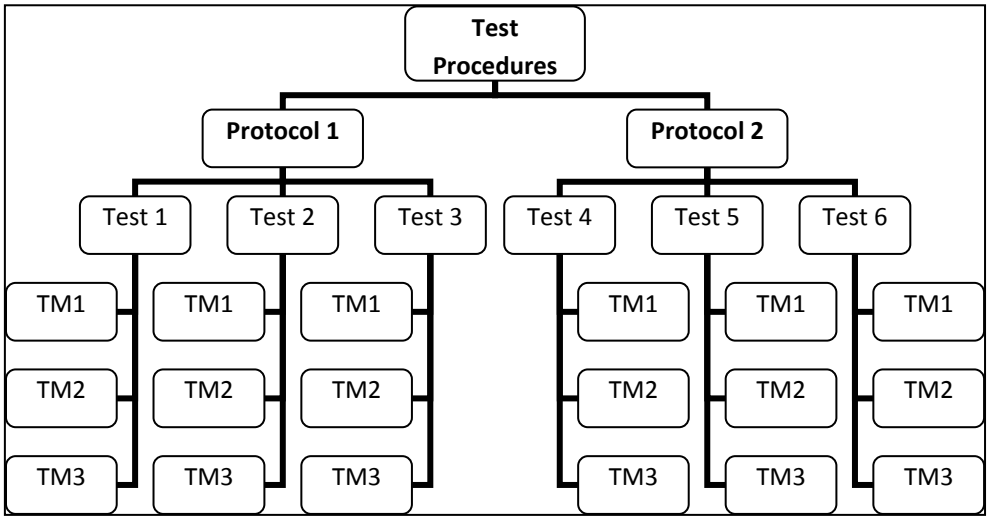
- **Test 5**: Compression test for TM1, TM2 and TM3 (7 and 28 days).

TM2 and TM3 will include additional **20%** volume of water by respective drilling fluid.

- **Test 6**: Compression test for TM1, TM2 and TM3 (7 and 28 days).

TM2 and TM3 will include additional **30%** volume of water by respective drilling fluid.

Chart 1. Test and sample grouping



3.7 PROTOCOL 1

3.7.1 General Description

All samples (except TM1) for Test 1, Test 2 and Test 3 were prepared according to Protocol 1. This includes sample preparation by removing certain amount of water (by percentage) from the concrete design mix and replacing it with same amount of drilling fluid.

Eighteen standard compression tests were conducted according to procedures specified in BS EN 12390-3:2002 (Excluding Cylinder Testing).

3.7.2 Test samples preparation

A volume of 0.3m^3 of concrete was mixed for every batch according to the design mix. Concrete slump is measured and recorded for each batches.

For TM1 (control mix), the concrete was batched according to the design mix and concrete cubes with the dimension of 150mm x 150mm x150mm were produced.

3.7.3 PolyMud® drilling fluid

1 kg of PolyMud® was mixed in 1m^3 of water in a tank and left for 2 hours continuously under air agitation to enhance the hydration process, until fluid parameters shown in Table 2 were achieved.

For TM2, there batches of concrete mix were batched according to the design mix leaving 5%, 20% or 30% of water volume and replacing them with PolyMud® drilling fluid respectively. 6 concrete cubes with dimension of 150mm x 150mm x150mm were produced for each batch.

3.7.4 Bentonite drilling fluid (GTC 4)

50kg sodium activated Bentonite were mixed in 1m^3 of bentonite mixer, being left maturing for 24 hours, until the slurry reached parameters specified in Table 3.

For TM3, there batches of concrete mix were batched according to the design mix leaving 5%, 20% or 30% of water volume and replacing them with Bentonite drilling fluid respectively. 6 concrete cubes with dimension of 150mm x 150mm x150mm were produced for each batch.

Figure 1a. Preparation of TM2 mix **Figure 1b. Preparation of TM3 mix**





3.8 PROTOCOL 2

3.8.1 General Description

In this protocol, certain amount of drilling fluid (in percentage of water volume from the design mix) was added into the fresh concrete that had been batched according to the design mix. Test 4, Test 5 and Test 6 had been prepared according to Protocol 2.

Eighteen (18) standard compression tests were conducted according to procedures specified in BS EN 12390-3:2002 (Excluding Cylinder Testing).

3.8.2 Test samples preparation

The PolyMud® and Bentonite drilling fluid was prepared in the same procedure as Protocol 1.

For TM1 (control mix), the concrete was batched according to the design mix and concrete cubes with the dimension of 150mm x 150mm x150mm were produced.

For TM2, three batches of concrete mix were batched according to the design mix. Once the concrete was homogenously mixed in the mixer, PolyMud® drilling fluid was added into the fresh concrete with an equivalent amount of 5%, 20% or 30% of water volume. 6 concrete cubes with dimension of 150mm x 150mm x150mm were produced for each batch.

For TM3, three batches of concrete mix were batched according to the design mix. Once the concrete was homogenously mixed in the mixer, Bentonite drilling fluid was added into the fresh concrete with an equivalent amount of 5%, 20% or 30% of water volume. 6 concrete cubes with dimension of 150mm x 150mm x150mm were produced for each batch.

Concrete slump is measured and recorded.

4. COMPRESSIVE STRENGTH TESTING

4.1 Cubes

After preparing the corresponding concrete cube samples following the protocols described, the concrete is poured into the tightly fixed steel mould. The top surface of these cube samples were made even and smooth for accurate results in the compression strength test. After 24 hours these moulds are opened carefully and test cube samples are placed in a curing tank filled with water.

The cube samples have all the same sizes, cube shaped 150mm of width, length and height, cube weight ranging 8 ± 0.2kg and density 2340-2370 kg/m^3.

Figure 2a and 2b. Test 2 TM2 concrete collection and test cubes preparation





For each Test, 18 cubes were made, 6 for each type of mix (TM1, TM2 and TM3). Out of the 6 cubes group, 3 were tested at 7 days and the remaining 3 at 28days as shown in Table 4.

Table 4. Test cube samples

Test Number	% of additive used (TM2 & TM3)	Additive Replacing water volume	Additive added to water volume	TM1 cubes tested at 7days	TM1 cubes tested at 28days	TM2 cubes tested at 7days	TM2 cubes tested at 28days	TM3 cubes tested at 7days	TM3 cubes tested at 28days	Total cubes tested
1	5	✓		3	3	3	3	3	3	18
2	20	✓		3	3	3	3	3	3	18
3	30	✓		3	3	3	3	3	3	18
4	5		✓	3	3	3	3	3	3	18
5	20		✓	3	3	3	3	3	3	18
6	30		✓	3	3	3	3	3	3	18

5. TEST

After 7 and 28 days curing, the concrete cube samples are tested in a standard compression testing machine, as shown in Picture 5.

Load was applied gradually at a rate of 140 kg/cm^2 per minute until the cube sample fails. Compressive strength of concrete cube samples as described in the formula below.

$$\textit{Compressive strength } (N/mm^2), \quad = \quad \frac{W_f}{A_p} \qquad [1]$$

where,
W_f = Ultimate load in N
A_p = Plan area of cube sample in mm^2

The test results of each test protocols are collected and recorded. The concrete design mix was catered for characteristic strength of 40 N/mm^2 at 28days. The mean target strength is set for 48 N/mm^2.

Figure 3a and 3b. Cube compression test



6. RESULTS

The cube compression tests results both Protocol 1 and Protocol 2 for 7days and 28days curing process are shown in the Table 5 and Table 6 below:

Table 5. Results of Protocol 1

	Test Number	% of Slurry replacing water in concrete mix	Average Compressive strength (MPa)		Sample Type	Remarks
			7 days	28 days		
PROTOCOL 1	1	0%	49.9	67.4	TM1	Control Mix
		5%	47.8	56.2	TM2	PolyMud®
			51.1	70.8	TM3	Bentonite
	2	0%	44.3	60.8	TM1	Control Mix
		20%	45.3	60.7	TM2	PolyMud®
			44.9	62.3	TM3	Bentonite
	3	0%	40.5	51.9	TM1	Control Mix
		30%	44.6	60	TM2	PolyMud®
			37.9	59.3	TM3	Bentonite

Table 6. Results of Protocol 2

	Test Number	% of Slurry added to water in concrete mix	Compressive strength (MPa)		Sample Type	Remarks
			7 days	28 days		
PROTOCOL 2	4	0%	38.7	58.5	TM1	Control Mix
		5%	35.3	53.7	TM2	PolyMud®
			35.6	53.8	TM3	Bentonite
	5	0%	37.1	50.1	TM1	Control Mix
		20%	29.8	47.8	TM2	PolyMud®
			30.8	50.4	TM3	Bentonite
	6	0%	32.9	49.2	TM1	Control Mix
		30%	25.3	41.1	TM2	PolyMud®
			25.2	40.4	TM3	Bentonite

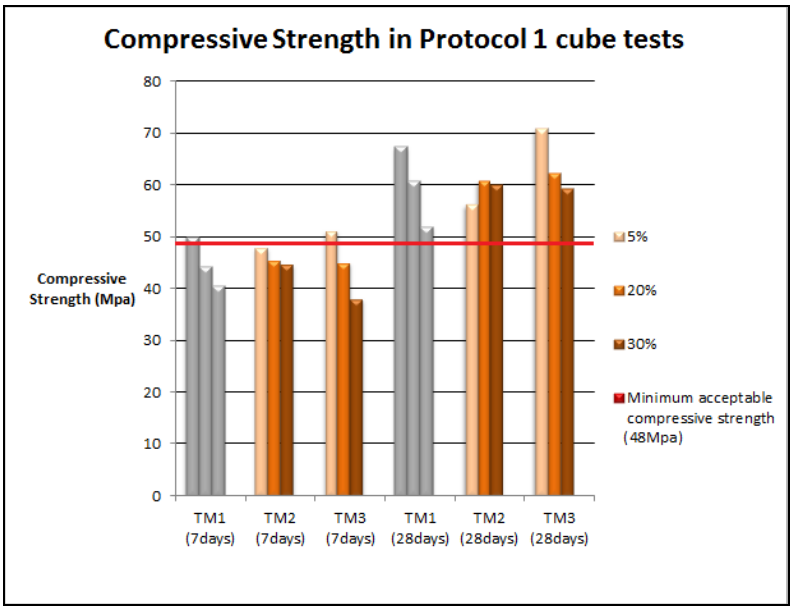
7. ANALYSIS

Based in the lab tests carried out above and the results obtained, the following conclusions can be drawn.

7.1 Protocol 1

Results of the compressive strength tests showed a consistent compressive strength development for the control mix (TM1) and the samples mixed with PolyMud® (TM2) and bentonite (TM3) slurries, for both 7 and 28 days tests.

Graph 1. Cube compressive strength according to Protocol 1



The Graph 1 above, shows all the samples widely accomplished to resist over the target mean strength at 28 days, set on 48MPa (40MPa Compressive strength + 8MPa Margin). This suggested that the inclusion of drilling fluid either PolyMud® or Bentonite even with the maximum amount of 30%, did not affects the characteristic strength of the concrete.

However, the results also show that the increase in percentage of Bentonite drilling fluid into concrete mix lowers the compressive strength gradually. This phenomenon most likely occurs as more foreign particles (Bentonite clay particles) available in the concrete fresh mix that affects the concrete cube compression strength.

It was interesting to understand that synthetic based PolyMud® did not have any significant effects on the concrete cube compression strength even at 30% of its inclusion. This shows that PolyMud® itself do not contain any element that weekend the concrete compression strength.

7.2 Protocol 2

Results of the cube compressive strength for Protocol 2 shows what is predicted. With the fact that drilling fluid either PolyMud® or Bentonite being added into the concrete lab mix, the design water/cement (w/c) ratio is being altered. Therefore, the cube compressive strength was decreased corresponding to the percentage of drilling fluid addition. Graph 2 below shows the relation between w/c ratios to the concrete compressive strength.

Graph 2. Relation between w/c ratio and Concrete Compressive Strength. Source: *"28 days strength of concrete in 15 minutes", Kaushal Kishore, Materials Engineer, www.engineeringcivil.com*

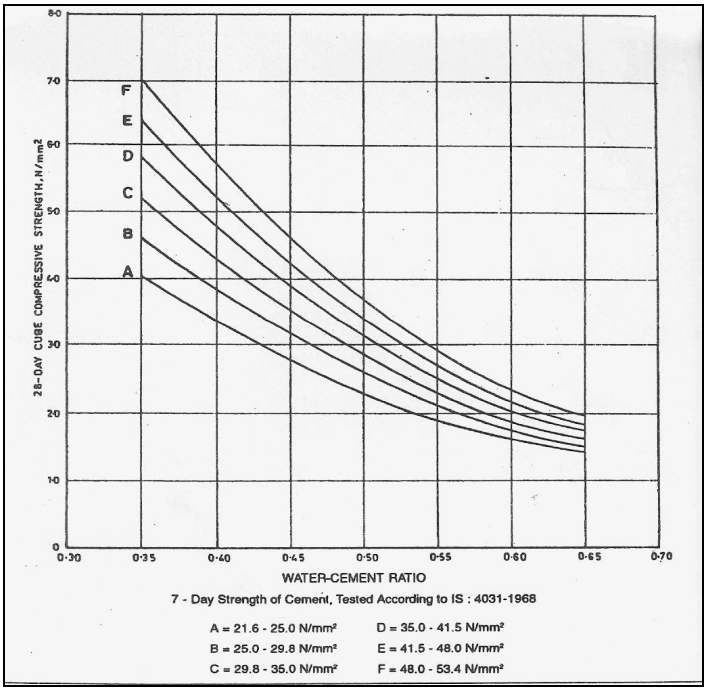
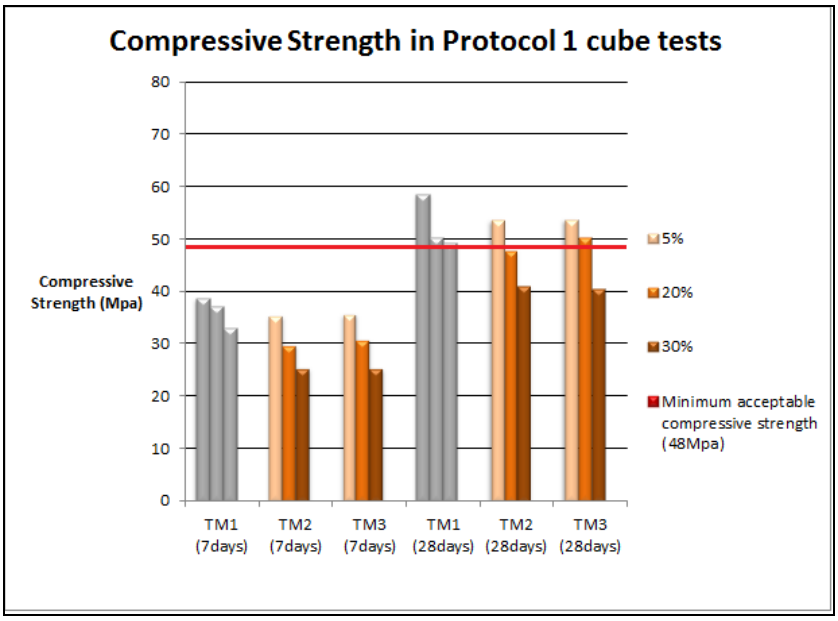


Table 7. W/C Ratio calculated for Protocol 2

Concrete mix with addition of drilling fluid (in %)	**W/C Ratio**
0% (Original Design Mix)	0.34
5%	0.36
20%	0.41
30%	0.44

Results for Protocol 2 were compared in the Graph 3 below.

Graph 3. Cube compressive strength according to Protocol 2



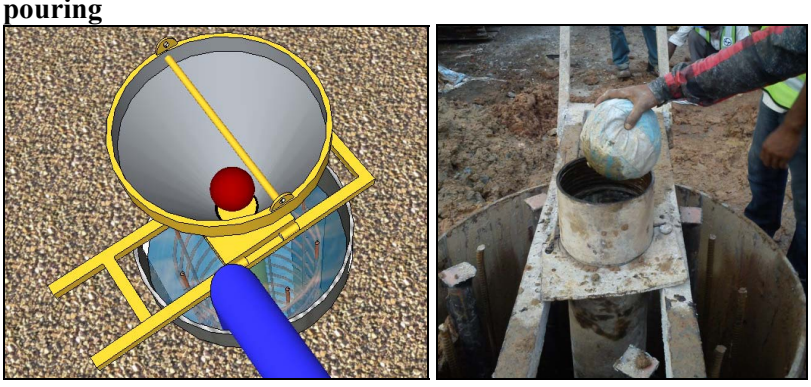
The samples containing additional 5% and 20% volume of drilling fluid accomplished to resist over or the target mean strength at 28 days, set on 48MPa

Test samples containing additional 30% of volume drilling fluid be it either PolyMud® of Bentonite in the mix failed the test hardly achieving values between 40 - 41 MPa of compressive strength at 28days, below the targeted mean strength. This is because the original w/c ratio has been altered due to introduction of foreign fluid into the concrete mix composition.

It is important to note in here, that any increase in intermix above 20% between concrete and drilling fluid, be it PolyMud® or Bentonite, affects the concrete compressive strength. This is very critical during concrete pouring process using tremie method for bored piles and diaphragm walls.

Important measures has to be taken to avoid intermixes of fresh concrete and drilling fluid to happen while pouring concrete such as placing concrete interface. Concrete interface has to be placed at the mouth of the tremie, so that the first concrete that is being discharge into do not have significant contact with the drilling fluid as shown in Picture 4a and 4b. Plastic ball is widely used as concrete separator due to its buoyancy.

Figure 4a and 4b: Inclusion of a concrete-slurry interface in the tremie pipe before concrete pouring



8. CONCLUSIONS

A maximum inclusion of at least 30% of foreign material, be it Bentonite or PolyMud® powder into the concrete mix, does not affect the compressive strength of the concrete itself.

If volume of water in w/c ratio is increased by 20% or more with drilling fluid (either Bentonite or PolyMud® slurry), the concrete's compressive strength is reduced. There is no significant impact in the concrete compressive strength if drilling fluid was added into the concrete mix up to 20% of water volume provided the mixture is homogenous. However, in the event of localized concentration of drilling fluid in the concrete mixture, may contribute to significant reduction in the concrete compressive strength. This has to be avoided during construction phase.

While Bentonite drilling fluid is being used widely for its specific swelling properties that forms permanent 'cake' along the excavation wall to provide greater stability, the quality of the concrete which is in contact with the slurry is exposed to compressive strength defects. PolyMud® slurry on the other hand, promotes the same stability achievements with unlikely affects the foundation element integrity when in contact with fresh concrete. Temporary 'membrane' which is formed along the excavation wall is also eliminated while concreting leaving a strong bond between the structure and the soil formation.

Further research is needed to understand about bonding strength between reinforcement steel bar and concrete when the reinforcement steel bar is in submerged in drilling fluid for a certain period of time.

Another interesting topic that requires further studies would be about development of skin friction between concrete pile and soil formation using Bentonite and PolyMud® drilling fluid.

REFERENCES

1. British Standard Institution. BS EN 12390:2002. *Testing Hardened Concrete – Part 3.* BSI, London, 2002.

2. British Standard Institution. BS 8004:1986. *Code of Practice for Foundations – (Formerly CP 2004).* Code of Practice. BSI, London, 1998.

3. European Standard. EN 1536:2010 (E*). Execution of Special Geotechnical Work – Bored Piles.*

4. Kaushal Kishore, Materials Engineer, *"28 days strength of concrete in 15 minutes"* www.engineeringcivil.com

DEEP EXCAVATION WITH WELL POINT DEWATERING IN SOFT SOIL

Dr. Mihir B. Roy, Consulting Geotechnical and Industrial Foundation Engineer, Kolkata, West Bengal, India. Cell: +91 94322 24629, Email: "roymihir@yahoo.com"

ABSTRACT

Coal transported by rail for Thermal Power Plant in Haldia, West Bengal, India, was to be received and stored in Coal Complex comprising of Wagon Tippler, Track Hopper, Junction Houses and network of horizontal and inclined tunnels. The site was very soft with high ground water level. Deep excavation and dewatering posed great difficulty. Original plan was to drive about 1000 m of steel sheet pile and well sinking which had major impact on cost and time. High ground water was identified as the main problem. Controlling water level and maintaining it would allow open excavation over major areas. Scheme for lowering aquifer with one and two-stage well-point dewatering system was developed following basic principles of groundwater and seepage. Arrangements of wells, installation and pumping were worked out in detail. Water levels could be lowered below bottom levels of excavation. Design of sheet pile was modified under lowered ground water condition. Overall length and depth of sheet pile were reduced drastically. Open excavation was possible in segments over major areas. The scheme was highly successful in smooth and fast progress of underground works. The works were completed safely months ahead of schedule time and with significant saving in cost.

KEYWORDS: soft soil, high groundwater, deep excavation, well point dewatering, steel sheet pile, cost saving

INTRODUCTION

The Coal Receiving Complex of thermal power plant comprised of 250 m long 8 m deep Track Hopper (TH), 12 m deep Wagon Tippler (WT) with provision for addition of another Wagon Tippler. Track center lines of TH and WT were very close. Coal unloading facilities were connected with a network of underground tunnels and Transfer Points (TP) upto Pent House (PH). The facilities were optimized in a compact layout within about 400 m x 120 m area. Initially excavation for TH was started adopting side slope of (1 V : 1.5 H) with 2 m wide berm and dewatering by in-pit sump and pump. When depth of excavation reached about 5-6 m, failure occurred over a long stretch as shown in Figs. 1a - 1b photos. Further work was stopped to develop scheme for carrying out deep excavation and civil works safely.



Fig. 1a: Failure in Excavation for Track Hopper



Fig. 1b: Closer view of Slope Failure

Objectives of the new scheme were to (a) optimize depth and maximize extent of open excavation, (b) minimize overall length and depth of sheet pile by (c) lowering and maintaining ground water level below bottom of excavation during construction period of 3-4 months,

A comprehensive scheme for lowering aquifer by one and two-stage well point dewatering system, maximizing extent of open excavation, restricting braced steel sheet pile protection only for WT was developed. To ensure control and safety of excavation and civil works, stretch of excavated area was limited, construction was planned to start from TH and progress longitudinally ending in PH. Depending upon depths of excavation, one and two stage well point dewatering systems were designed. Site activities were planned, materials procured in advance and works progressed in planned sequence. All underground civil works were completed safely and satisfactorily without any interruption.

DESIGN APPROACH

Targets of design revision were : (a) optimization of profile (side slope, berm width) of excavation, (b) reduction in length and depth of braced sheet pile protection, (c) reduction of lateral thrust on struts, (d) control on ingress of ground water and (e) prevention of heave at bottom of excavation.

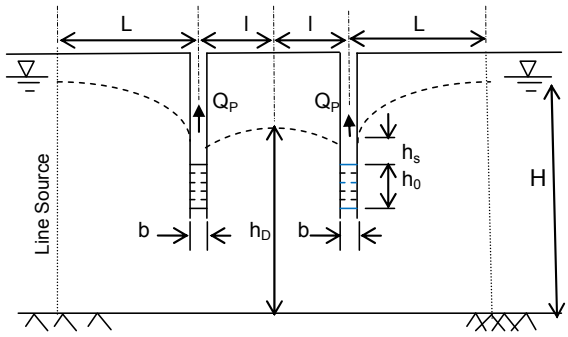
The project site was located in soft sub-soil of Bengal Delta Basin. Subsoil upto 9 m was very soft to soft (SPT N = 2–4) followed by medium dense silty sand (N= 15-29) upto 22 m depth and groundwater encountered within 1.0 m below surface. The design objectives can be met only if ground water level can be lowered sufficiently below bottom of excavation and maintained. Hydraulic parameters of sub-soil were determined by conducting one pumping-out test.

Depths of excavation for TH, WT and tunnels ranged from 8.0 to 12.0 m. For safe excavation and civil works, water level had to be lowered and maintained at least 1.0 m below lowest excavation level. Accordingly, highest point of lowered phreatic surface should be 9.0 and 13.0 m below GL respectively for TH and WT which could be possible only by well point dewatering system.

WELL-POINT DEWATERING

First step in design of dewatering by well point system is to collect realistic hydraulic parameters of water bearing strata. Representative data on hydraulic conductivity, yield versus draw-down, phreatic surface can be evaluated by conducting pumping out test. One pump-out test was carried out near the tippler building. Both main and observation wells of 150 and 100 mm diameter respectively were 23.5 m deep. After completion of boring, 150 mm diameter PVC casing pipe was placed upto 18.0 m depth followed by 5.50 m long strainer. Observation wells were located at 5.0 m and 10.0 m away from main well. To prevent chocking, boreholes were shrouded with graded filter media. Main well was washed and surging was done for smooth flow. Elevations of natural and variable water heads were measured before and during test. Stable condition was attained after pumping for about 3 hours at discharge rate of 3.56 m^3/day at drawdown of 7.06 m. Values of specific capacity and hydraulic conductivity were 3.338 m^2/day and 1.1 x 10^{-4} cm/second respectively. Radius of influence was 39.4 m.

Design of well point dewatering system was based on classical approach of '*Gravity Flow to Partially Penetrating Wells*' midway between and parallel to '*Two line Sources*' (Fig. 2). Spacing of wells was calculated following principle of flow to '*infinite line of partially penetrating wells from an infinite line source of seepage*' (Fig. 3). Design of well point system to finalize location of wells, levels, diameter and depth of strainer, lowered phreatic line were based on results of field pump-out test.



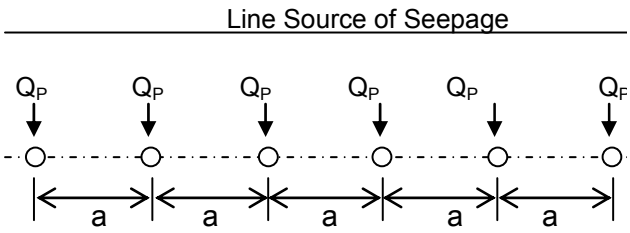


Fig. 2: Gravity Flow to Partially Penetrating Wells Fig. 3: Flow to Wells from Infinite Line Source

Theoretical analysis revealed water level can be lowered by about 5.5 m by well points. In order to lower water level to (-) 13 m, two-stage system preceded by general excavation of about 3 m at surface was required. The first stage well points could lower water level (WL) to (-) 8.5 m followed by second stage wells to lower upto (-) 14.0 m so that depth water line (phreatic surface) is kept at least 1.5 m below bottom of excavation for WT. Accordingly, single stage well point was considered for TH, tunnels and two-stage for WT, TPs. Final scheme for dewatering and excavation consisted of following activities.

i) General excavation from NGL upto 2.2 to 3.0 m depth.

ii) Well diameter : 50 mm, Depth of well = 9 m, (Standpipe = 6 m and strainer length = 3 m).

iii) First (upper) stage wells for construction of TH and tunnels:
Spacing = 3.5 m, Discharge = 1.5 m^3/well/day, Lowering of WL = (-) 8.5 m.
No. of wells for 72 m stretch of excavation at upper level = 38 for both sides.
Estimated discharge of water = 57 m^3/day

iv) Second (lower) stage wells for construction of WT & TPs:
Spacing = 2.5 m, Discharge = 1.3 m^3/well/day, Lowering of WL = (-) 14.0 m.
No. of wells for 51 m stretch of excavation at lower level = 38 for both sides.
Estimated discharge of water = 50 m^3/day.

Initially of discharge of water was high, gradually tapered off with time and progress of work but increased during rains. Therefore, pumps and piping were planned for 30% additional capacity. Final arrangements of excavation showing two-stage well points, profile of excavation and lowered phreatic lines for both stages are shown in Fig. 4a. Arrangements of wells at both levels are shown in Fig. 4b.

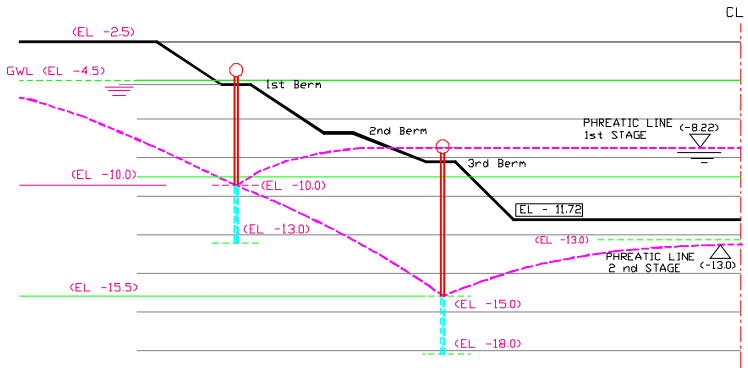


Fig. 4a : Profile of Excavation, Well points and Phreatic Surface

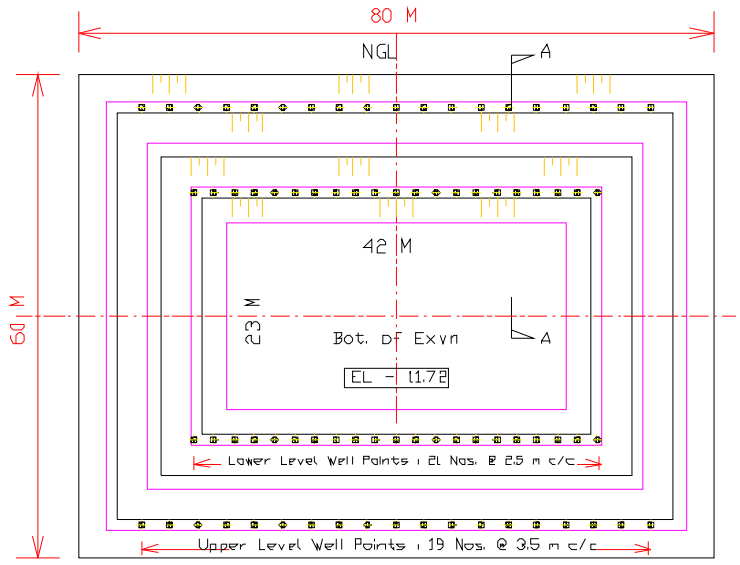


Fig. 4b : Excavation Plan, Arrangement of Wells

INSTALLATION AND OPERATION OF WELLS

a) Stage-1 wells were installed after excavation to upto 1st berm at (-) 4.22 m level.
b) Pumping out continued till stable condition reached, further excavation continued to third berm level.
c) Stage-2 wells were installed at third berm at (-) 8.22 m level and pumping continued till stable condition reached.
d) Excavation for TH, tunnels and WT continued upto required depths as per profile shown in Fig. 4b.
e) To maintain water level at desired depth, rate and duration of pumping from wells at both levels had to be adjusted depending on site condition.

DESIGN OF STEEL SHEET PILE

As cost and time of about 1000 m long steel sheet pile wall was prohibitive, it called for critical review and optimization on length and depth. Software based design of sheet pile submitted by the supplier adopted 19 m long sheet piles with struts only at single level. This resulted in axial load of 466 KN/m requiring heavy structural member for bracing and strut. The design was revised considering 2.4 m excavation at surface and 14 m long sheet piles but struts were provided at three levels and total axial load was 402 KN/m. The design was not acceptable as struts at three levels will pose serious obstruction for excavation, placement of struts and civil works. It was then decided to analyze sheet pile wall system following basic principles of '*braced single-wall cofferdam*'. Design considerations included (a) ground water level lowered at least to 13 m below ground and maintained, (b) to reduce length of sheet pile, general excavation carried out upto 3 m and (c) struts only at two designated levels. Design of sheet piles and load on struts are commonly estimated upto deepest level of excavation. But with progress of construction, bottom level struts are removed in sequence and redistribution of loads on upper level struts is often missed. Sometimes the situation could be critical. Therefore, struts need to be designed for the maximum load during full cycle of excavation and backfilling. In this project, analysis was carried out to estimate enhancement of load on upper level strut after removal of bottom strut.

Sheet pile protection was redesigned on above lines which resulted in following improvements.

a) Length of sheet pile reduced from 19 m to 12 m.
b) Maximum axial loads on first and second level struts were 90 and 306 KN/m respectively at full excavation and 240 KN/m in upper strut after removal of bottom strut as construction progress.
c) Coverage length of sheet pile reduced drastically from about 1000 to 190 m only.

Designed sheet pile system is shown in Fig. 5 and results of different sheet pile designs and savings are furnished in Table 1.

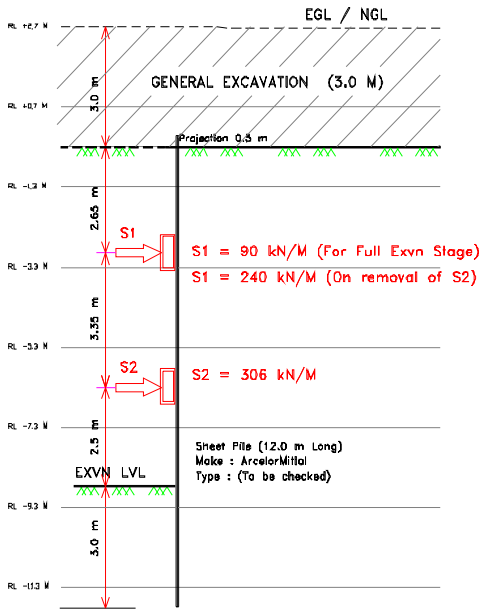


Table 1. Summary of Sheet Pile Designs

DESCRIPTION	TRIAL – 1	TRIAL - 2	TRIAL-3	TRIAL-4 ##
NO. OF STRUTS	**1**	**3**	**3**	**2**
DEPTH OF SHEET PILE	19.0 m	14.0 m	15.0 m	**12.0 m**
LOAD ON STRUTS	466 kN/m	391 kN/m	523 kN/m	**396 kN/m**
WT. OF SHEET PILE /100 m	246.7 T	207.1 T	220.8 T	**176.6 T**
COST (Crores) PER 100 m **	2.47	2.07	2.21	1.77
DEPTH OF SHEET PILE REDUCED FROM **17.4 M TO 12.0 M** ##				**30%**
REDUCTION IN TOTAL LOAD ON STRUTS				**12.5%**
REDUCTION IN WEIGHT OF SHEET PILE				**31%**
REMARKS	NOT USED	NOT USED	NOT USED	**ADOPTED**

GENERAL EXCAVATION UPTO 3 m; ** COST OF SHEET PILE @ RS. 1,00,000 / MT

Fig. 5 : Final Design of Sheet Pile

OPEN EXCAVATION

Failure of slope during excavation for track hopper (Fig. 1a and 1b photo) called for studies on causes of failure and develop remedial measures. Profile of excavation for track hopper was re-analyzed under following considerations : (a) Maximum depth of excavation of 8.0 m, (b) ground water level lowered by well point system and (c) seismic coefficient of 0.02. In order to ensure safety in the event of failure of well point system, minimum stability factor was also determined considering water level at 1.0 m below surface. Multiple trial slip surfaces were analyzed following Bishop's method of slices to evaluate minimum factor of safety under following cases : (a) dry condition, (b) water level at 1 .0 m below surface and (c) earthquake forces. Minimum factor of safety were evaluated using commercial software and minimum factor of safety for above three cases are presented in Table 2.

Table 2 : Summary of Results of Stability Analysis

Sl. No.	Failure Mode	Min. Factor of Safety
a	Dry slope	1.43
b	Water at 1 m below	1.00
c	Effect of earthquake	0.97

It is observed that minimum factor of safety for optimum slope is 1.0 and is considered safe under short term consideration. Although under earthquake, it is slightly less but probability of occurrence is remote. Moreover, when excavation reaches bottom level, the parabolic phreatic surface meets ground water line at least 8 m away from slope edge and as such is on conservative side. Accordingly the proposed profile is safe under all circumstance.

Profile of open excavation upto 8 m depth was optimized considering water level lowered by single stage well point system. Side slopes were revised from 1.0 V : 1.5 H to 1.0 V : 1.25 H (Fig. 6) resulting in about 20% saving in volume of excavation. Typical arrangement of well points is shown in Fig. 7 photo.

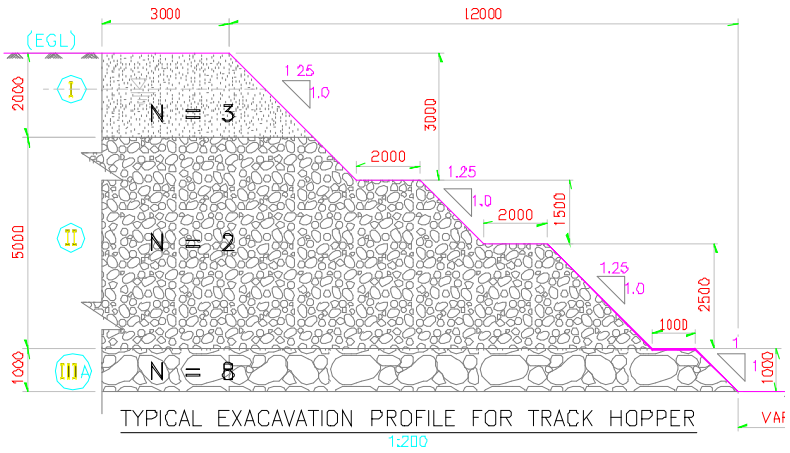




Fig. 6 : Typical Profile of Open Excavation

Fig. 7 : Arrangement of Well Points

Hazards of deep excavation and dewatering were brought under control by well point system. Excavation and civil construction progressed nicely as shown in Fig. 8a and 8b photos.





Fig. 8a : Single-Stage Well Point System

Fig. 8b: Two-Stage Well Point System

SUMMARY AND CONCLUSIONS

Coal transported by rail for a thermal power plant in Haldia was to be unloaded in Wagon Tippler and Track Hopper. Depths of excavation varied from 8 to 12 m. The site being located in Bengal Delta basin, sub-soil upto 22 m depth was very soft to soft and ground water was close to surface. At initial stage, open excavation caused large scale slope failure forcing stoppage of work. High ground water level was identified as the root cause and had to be brought under control. Scheme for lowering aquifer by installing one and two stage well point system was designed and implemented at site. Performance of the scheme was highly satisfactory as excavation upto 12 m depth and civil works spreading over 400 m x 120 m area were completed in about 4 months time without a single interruption. Not only that, lowering aquifer helped in reducing length of and depth of protection by sheet pile down to 20% from original plans. The project site which initially was un-manageable was transformed into 'construction-friendly' by adopting site-specific solutions. The scheme helped save huge cost and under-ground works were completed nearly two months ahead of schedule.

It is concluded that thorough study on sub-soil and ground water conditions is important before starting deep excavation in soft soil with high ground water environment. Seepage and ingress of water play significant role and can be brought under control by adopting simpler methods. It is also emphasized that fairly accurate estimates of seepage flow can be worked out in-house following classical approaches like 'Gravity Flow to Partially Penetrating Wells' midway between and parallel to 'Two Line Sources' available in standard text books. Similarly, standard method of sheet pile design following 'Braced Single-Wall Cofferdam' yielded improved solutions. The analysis should be based on site-specific data on geotechnical and hydraulic parameters. It is pointed out that, success of well point system and sheet pile wall depend on quality of procurement, implementation, operation, routine inspection and maintenance.

In last few years, various software packages are available for solving such problems and are used widely. However, the designer should judiciously assess pros and cones of the package before use. It is necessary to know basics of the software namely analytical model used in analysis, data input format and units, boundary conditions and limitations before using them. It is important to assess and verify the software generated output before accepting them for application.

ACKNOWLEDGEMENT

Success of deep excavation with massive dewatering was attributed to collective cooperation, involvement, support and sincere efforts of all concerned. Level of confidence, full support and cooperation received from site engineers and owner is acknowledged with gratitude. Co-operation of the civil contractor towards implementation of the scheme ensuring compliance of design is acknowledged.

BASEMENT EXCAVATION: COST EFFECTIVE RETENTION SYSTEM FOR A MULTI STOREYED STRUCTURE

Madan Kumar Annam, Technical Manager, Keller India, madankumar@kellerindia.com
Hari Krishna Y, Director, Keller India, yhari@kellerindia.com

ABSTRACT

Basement construction is one of the challenging geotechnical concerns in the urban environment. Several types of retention systems are practiced to support the earth which is suitable for restricted access, rapid mobilization, fast excavation and cost-effective designs. A thorough understanding of geotechnical engineering as well as the structural mechanics is important for the earth retention systems. This paper discusses a project with various types of foundation solutions including monitoring of deflections during excavation stage of a retention system.

A multi storeyed residential building (3B+Stilt+18F) in Chennai having structure foot print area of 1500 m^2 has to be constructed on large diameter pile foundations and also to support the proposed basement excavation. Ground water table was encountered at about 6m below the existing ground level (EGL). In order to support heavy structural loads, large diameter bored cast-in-situ piles were chosen and installed. Further, complete retention system was economically designed and built, which includes installation of Contiguous Bored Piles (CBP) in combination of vertical grout columns behind CBP wall to seal the gap between the CB Piles, installation of inclined ground anchors, construction of capping beam, stressing and locking of installed ground anchors. A detailed monitoring program was in place and continuous monitoring of wall deflections is being measured at the time of publishing this paper. This paper describes the design and construction aspects adopted for foundation and retention system including the monitoring results during excavation stage of the project.

Keywords: Pile foundations, Retention system, CBP system, Inclined Ground Anchors, Grout Columns, Basement Excavation, Monitoring of lateral deflection

INTRODUCTION

In general, stage wise open excavation will be opted for basement construction where plenty of space is available. Due to urbanization and restricted space, open excavation became a difficult task nowadays. To overcome this problem, suitable retention system need to be selected to retain the soil mass. Selection of suitable retention system for multi-level basement excavation is a great challenge in geotechnical industry, especially when the proposed site is located within the minimum set back distance from the existing structures. This in turn calls for the advanced and innovative methods of retention system.

Several earth retention systems such as Diaphragm Walls, Secant Pile Walls, CBP system, Soldier Pile Walls, Sheet Piles, Deep Soil Mixing (block walls) etc. with or without inclined ground anchors are being practiced worldwide. Considering the advantages and disadvantages of the available retention systems in practice locally and keeping in view of present site conditions, the developer has chosen CBP system with inclined ground anchors so that all foundation related works of the project will be handled in a single package. The main advantage of such packaged solution will ease the coordination between design consultants and foundation contractor resulting in faster construction of foundation works which in turn reflect savings in time and cost.

PROJECT AND SOIL CONDITIONS

The project involved heavy structural loads and 168m long retention system for an excavation depth of about 10m below the finished ground level. The site is excavated up to a depth of 2.8m in order to clear

the debris of existing old building and to ensure proper working environment. The subsoil consists of silty clay and clayey sand, underlain by siltstone up to the explored depth of 30m below the EGL.

FOUNDATION SOLUTIONS

The subsoil at final excavation level is not sound enough to carry the heavy structural loads. It was anticipated by the structural designers that vertical column loads of 150 T to 350 T would be acting on piles. After critical analysis of the soil conditions, bored piles of 600mm, 750mm and 900mm diameters were proposed with 3m socketing into the competent strata (siltstone). Hydraulic rotary rigs were used to install bored piles as shown in Fig. 1. Routine pile load test results are presented in Fig. 2.



Fig. 1. Load test performance at site (900mm dia. bored pile)

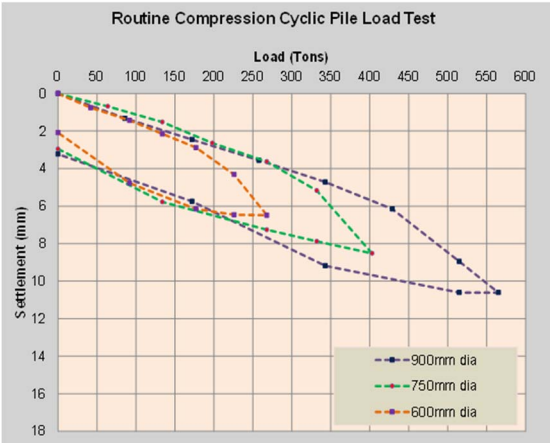


Fig. 2. Results of Routine compression pile load test

COMPLETE RETENTION SYSTEM

Based on the project requirements, deep excavation of 7.4m from the present ground level requires a stable retention system to retain the soil. CBP wall with single level inclined ground anchor plus grouting behind the CBP wall system was critically analyzed and designed. Conceptual sketch is shown in Fig. 3.

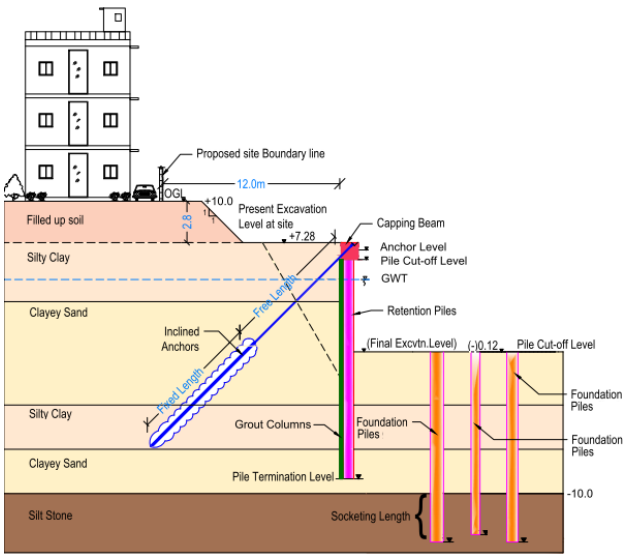


Fig. 3. Packaged solution for deep excavation

Analysis and Design of Retention System

Finite element software Plaxis 2D was used to carryout overall stability of the retention system for various stages of construction. Plaxis model is shown in Fig. 4 and maximum bending moment and deflection at final excavation is shown in Fig. 5.

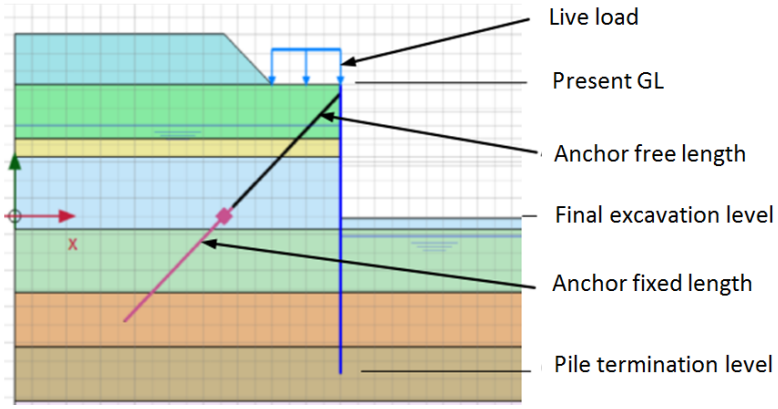


Fig. 4. Critical C/s of Retention system developed in Plaxis 2D model

Sequence of Construction of Retention System

Stage 1: Installation of CB piles along the perimeter of retention line
Stage 2: Installation of grout columns behind the CB piles
Stage 3: Installation of inclined ground anchors
Stage 4: Construction of capping beam
Stage 5: Stressing of inclined ground anchors
Stage 6: Earthwork excavation up to the required level

Brief description of each stage of construction is explained in the following sections.

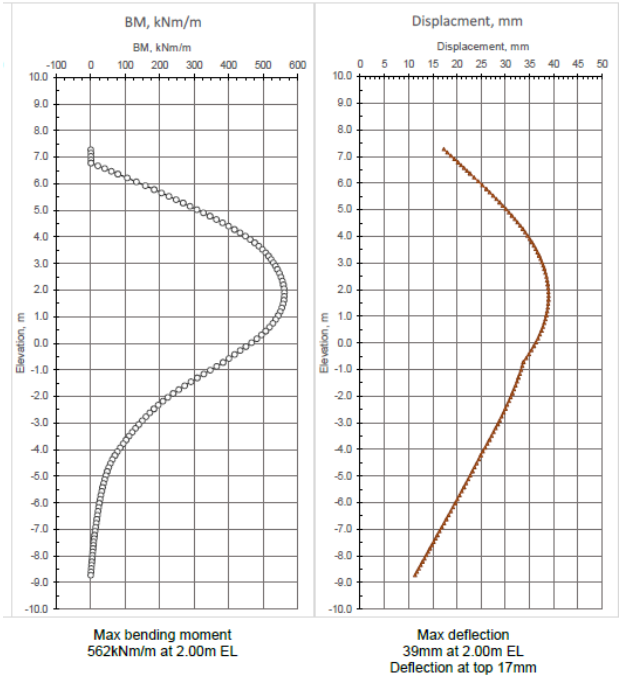


Fig. 5. Bending Moment and deflection at final excavation

Vertical grout columns were installed behind the retention piles to control the erosion of soil due to seepage of water during the excavation. Seepage cannot be fully controlled by installation of grout columns; however, dewatering need to be done by controlling the extent of drawdown limiting within the project boundary. Typical arrangement of grout columns is shown in Fig. 6.

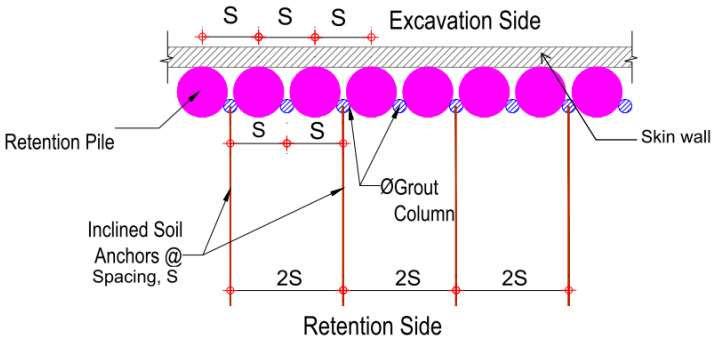


Fig. 6. Concept of Grout column behind retention piles

After installation of CB piles, excavation was carried out to about 0.5m below the proposed anchor level for installation of ground anchors. Inclined ground anchors were designed and installed to cater required lateral earth pressures and typical installation is shown in Fig. 7. The retention piles were chipped off up to the cut off level and cleaned for further construction process. Capping beam was built after installation of 100mm diameter sleeve through which anchor strands were allowed for stressing (refer Fig. 8). Each anchor was stressed to assess the performance of the design load and locked at locking loads. The key plates were welded to the base plate for safety considerations. Final excavation was done after completion of stressing. Present site condition is shown in Fig. 9.



Fig. 7. Installation of Anchors at site



Fig. 8: Cage fabrication and capping beam after concreting



Fig. 9: View of final excavation depth

MONITORING OF DEFLECTIONS

Continuous monitoring of deflections is important to understand the behaviour of retention system during excavation. In order to check the post construction performance of the retaining system, local bench marks were established for better control of observations. Several monitoring points were established covering the entire retention line and various heights as illustrated in Fig. 10. Deflection monitoring was carried out using sophisticated Total Station instrument under the guidance of a Geotechnical Expert. Frequency of the monitoring was carried out on daily basis initially and later reduced once the deflection of the wall is stabilized.

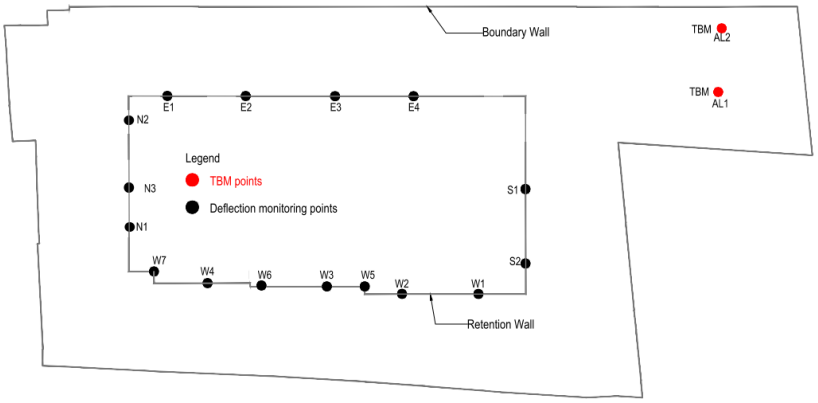


Fig. 10. Monitoring points for lateral deflection

The maximum recorded deflection was about 8mm after full stage of excavation (by end of week 12). Monitoring is being carried out at the time of preparation of this paper. Predicted deflection is about 39mm at final excavation level as per Plaxis analysis. The predicted and observed deflections with respect to excavation levels are shown in Fig. 11. It is inferred from the observed results that the long-term deflections are less than the expected.

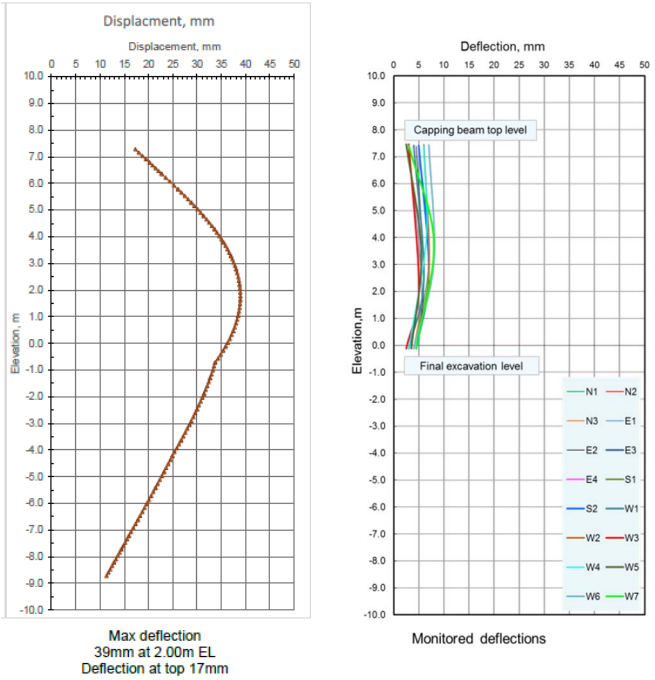


Fig. 11. Results of Predicted and Observed deflections

CONCLUSIONS

Evaluation of project conditions, project needs, methodology of construction and suitable monitoring programs are required for an efficient and optimal solution for any project. Packaged foundation solutions (foundation piles, retention system with inclined ground anchors, grout columns, capping beam, testing and monitoring) offers the most cost effective and speed in the overall construction schedule. This project demonstrated the advantage of packaged solutions under experienced single foundation specialist contractor.

ACKNOWLEDGEMENTS

The authors would like to thank the developer (Mr Ananth Vummidi MD, M/s BBCL) for giving permission to publish this paper. The authors are grateful for the support extended by project site management of M/s BBCL during construction and monitoring periods. The authors would also like to thank the Project Consultants (M/s Buro Engineers and M/s Geotechncial Solutions) who supported in reviewing designs and valuable suggestions. In particular, the authors wish to acknowledge Keller management for their continuous support and encouragement in finalization of this paper. Thanks are also due to Keller India technical and site team for providing photographs and other execution data.

REFERENCES

1. Project soil investigation report, conducted in October 2014.
2. Stability analysis report for retention system using Plaxis 2D
3. Design and Construction of pile foundation – code of practice, IS 2911 Part 1, Section 2: 2000
4. Design and Construction of pile foundation – code of practice, IS 2911 Part 4: 2013
5. BS code for practice for ground anchorages, BS 8081: 1989
6. Guidelines for design of RCC structures, IS 456 2000, SP 16 1980.

A CASE HISTORY – TERMINATION OF PILE IN ROCK BASED ON PENETRATION RESISTANCE FOR A BRIDGE ACROSS RIVER MANDOVI IN GOA

Akshay Sakhuja, EDRC-Special Bridges, L&T Construction, Chennai, akshaysakhuja@lntecc.com
Karthika M S, EDRC-Special Bridges, L&T Construction, Chennai, karthikams@lntecc.com
Vignesh R, EDRC-Special Bridges, L&T Construction, Chennai, rvignesh@lntecc.com

ABSTRACT

The bridge across River Mandovi in Goa is a cable stay bridge structure proposed parallel, along existing bridges for regulation and reduction of vehicular traffic; the entire bridge structure is supported on pile foundation socketed in rock. This paper describes drilling related issue encountered during execution of pile where bed rock varies considerably from factual geotechnical investigation, which in turn affected the productivity of bored piles socketed in rock then chiseling is advocated for rock socketing with limited number of blows based on penetration resistance of rock encountered or equivalent energy principle to increase the productivity and also to avoid excess chiseling which otherwise would have fractured the rock mass below and around the pile tip resulting in increased settlement of pile subjected to design load. Contractor decision on socket length have been taken without compromising either quality or productivity; the paper presents various procedures and the equipment involved for installation of pile in rock along with the conclusion related to termination of pile in rock and also the lessons learned in process.

Keywords: socketing, drilling, penetration

INTRODUCTION

Pile foundations are generally used to transfer heavy loads in deeper bearing stratum if the soil immediately beneath the base of the foundation does not have sufficient capacity. The bridge across River Mandovi, Goa is in its construction phase as a part of the development plan of Goa State Infrastructure Development Corporation Ltd (GSIDC). The project was awarded to M/s. L&T Construction, Heavy Civil Infrastructure; subsequently the geotechnical investigation was awarded to M/s L&T Geostructures.

The client has specified the foundation of the bridge as rock-socketed. Rock socketing is generally done to achieve higher bearing pressure through concrete-rock shear interface which many building codes permit. The design and construction of rock socketed pile foundation entails a detailed analysis and judgement on the superstructure loads, predominant geological conditions as well as ground water levels. The termination of pile is normally based on thumb rule of half to three times the pile diameter into the rock. Quite often the criteria is based on chisel penetration rate (Gandhi,1990) In fact, this is the key factor to consider appropriate and economical depth of embedment of pile into rock stratum which necessitates enormous understanding on the type and quality of rock strata encountered which may significantly influence the selection of suitable rotary rig for pile installation. Such criteria are site specific and also applicable for the set of equipment used for the particular project.

For the present project, it is observed that the quality of rock at main bridge location has shown considerable variation during on-site drilling from what has been reported in the geotechnical investigation report leading to drilling of confirmatory boreholes for achieving more clarification. The rock quality encountered in confirmatory boreholes was better than that provided in the initial data, triggering difficulty in the penetration while drilling deeper. Designers had to revise the depth of embedment of pile based on penetration resistance estimated from on-site chiseling data. This paper deals

with some of the practical problems encountered during the design and construction of pile foundation into hard rock and the feasible solution implemented is described.

PROJECT DETAILS

The project involves construction of extra-dosed bridge across River Mandovi at Panaji including approaches on NH-17 between Pundaliknagar and Merces Junctions which is a 900m four lane bridge with a 550m cable stay portion and approach viaduct spanning 3.20km mainly to facilitate unobstructed flow in Goa. A detailed geotechnical investigation was carried out which comprises of 93 boreholes to recognize the sub-surface stratification including various field and laboratory test results. In more than 60 boreholes it is observed the presence of grade III to grade V chloritic schist rock which is moderately to slightly weathered. Client has recommended rock socketed pile as foundation type and 8mm thick M.S steel liners to provide to all piles below pile cap and up to a depth where SPT N >15.

REGIONAL GEOLOGY OF PROJECT SITE

Geologically the project area comprises rocks of Precambrian age viz. Gneisses, migmatites, granitoids, granites schists, meta–volcanic, Meta greywackes, banded ferruginous quartzite associated with phyllites / argillites, limestones with thin bands of ultramafic complex underlined by the late Cretaceous basalts of Deccan traps overlie on the Goa group of formations i.e. Barcem, Sanvordem, Becholim and Vagheri as mentioned in Table 1.

Table 1: Geological Time scale of project area

Era	Group	Formation	Litho-assemblage
Quaternary			Beach sands of riverine alluvium deposits – marine clay
Pliocene to Pleistocene		Western Ghats Latertization zone	Lateritic Deposits
Late cretaceous to Paleocene	Deccan trap		Basalts with Dykes
Archaean	Goa	Vagheri	Schists
		Bicholim	BIF/Limestones
		Sanvordem	Quartzite/Greywackes
		Barcem	Meta Basalts

PILING WORKS

The project has been bifurcated into three sections viz. northern, marine and southern zones and a total of 405 piles are being constructed of diameter 1.2 and 1.5m in which the former ones are proposed for viaduct and approaches while latter are designed for the cable stay portion of the bridge. The main bridge comes under marine section which comprises of 4 pier locations P29 to P32 with corresponding drilled boreholes be BH-32 to BH-35. The sub-soil at river crossing is stratified into three layers as mentioned below:

- Layer I: Lateritic silty gravel/silty sand.
- Layer II: Hard clayey silt/silty sand.
- Layer III: Weathered chlorite/schist rock.

Corresponding field SPT N value with respect to depth below river bed level is provided in Fig.1 .The scour depth measured from the river bed level varies drastically from 3.55m to 17m. From the figure, it is observed that the non-scourable stratum is available at an average depth of 27m from bed level.

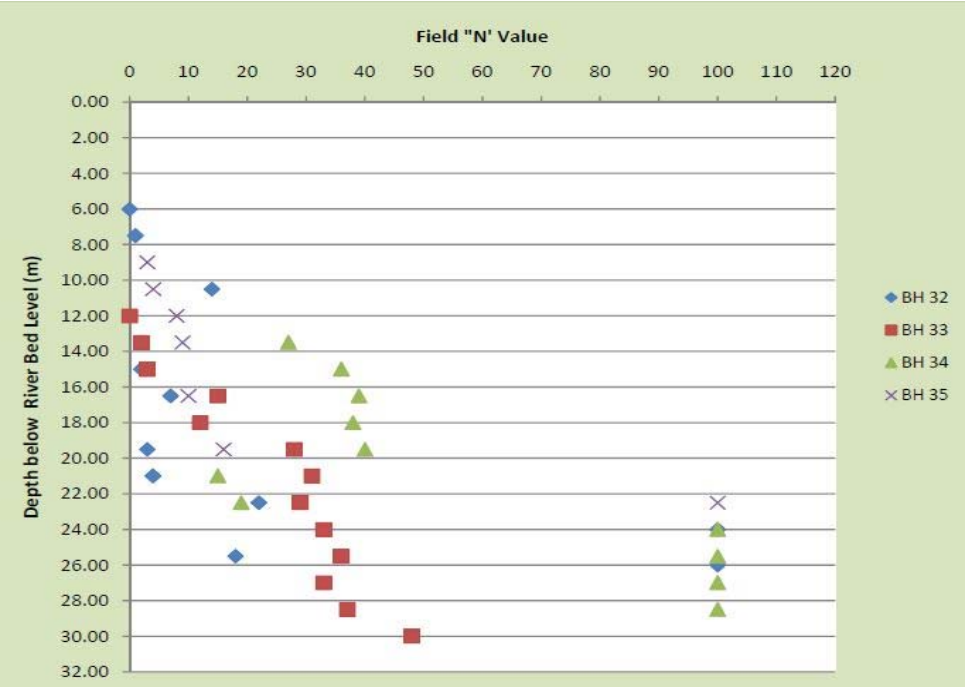


Fig. 1. Variation of field SPT N value with depth

The drilling works is carried out using BG-28 and WINCH. Bauer Hydraulic Piling Rig (BG 28) is a heavy duty rotary drilling rig with high torque capabilities. The piling works is in operation at the river location as shown in Fig. 2.



Fig.2.BG28 in operation, Mandovi, Goa

Issue encountered during piling

During the execution of piling works, it is observed that piling rig could not penetrate through rocky strata at pier 32, L14 pile location for which reference borehole is BH-35 indicating rock top level is (-) 21.13m,RL. Site expressed inability to carry out further rock boring using BG 28 because of kelly bar jam, loss/shear of rock bullets and rock boring time more than 3 days for 2.37m with current rate of penetration 5cm/hour. Very weak to moderately weak grade IV chloritic schist rock extends for a depth of 8.4m below rock top level followed by moderately strong grade III rock with an average UCC strength of 75.6 MPa. The depth of embedment for 1.5m diameter pile into rock is designed as 5.4m since RQD is observed as nil or very less for the top layer of rock. The average penetration rate in rocky strata at various depths is mentioned in the Table 2.

Table 2: Various depths and Penetration rate in rock at Pier 32

Major Bridge Piling Works – P32,L14		Equipment : BG 28		
	Unit of Measurement	**RL = (-) 20.70**	**RL = (-) 21.70**	**RL = (-) 21.37**
Bore Cutting in Rock	**Cm**	**50**	**100**	**30**
Duration	**Hours**	**2.16**	**7.75**	**6.33**
Penetration	**Cm/Hours**	**23**	**13**	**5**

This issue aroused due to the variation in the data provided in the geotechnical investigation report and while proceeding with the same, the driller got stuck as the colossal rig was unable to drill after certain depth. As indicated in above table, the rate of penetration was 5cm/hour at (-) 21.37m, RL which finds very low to achieve the design pile termination point. Furthermore it definitely cause significant delay in project completion as well as damage the drilling rig. The concern was conveyed to the design team for suggestions and providing feasible solution to drill into the rock without deteriorating the quality of the stratum. Initially, the data provided was consisting highly weathered chlorite-quartzite-schist. The core log of the initial investigation is provided in Fig. 3.



Fig. 3. Core box of Initial Investigation at P-32 location

Confirmatory Boreholes

The design team has conveyed to site that present design founding level has been arrived based on the initial borehole investigation and subsequent test results furnished, which were done exactly at the pier location and any change in founding level can be justified only based on additional data through pile boring / drilling records and additional investigations. Henceforth though with shortage of time, two confirmatory boreholes were done at locations near to pier 32. The location plan for confirmatory boreholes is provided in Fig. 4. Confirmatory boreholes (CBH) are done at L15 and L20 pile locations (CBH-1 and CBH-2 accordingly) up to a depth of 32 and 38m respectively. It is observed that the rock quality is better in the confirmatory bore log compared to that of initial investigation data with improved core recovery and rock quality designation values. The core recovery and RQD at L15 pile location is provided in Fig.5. Furthermore the rock type changes from gneiss to amphibolite of moderately to slightly weathered in CBH-1 and metabasalt to chloritic schist of highly to moderately weathered in CBH-2.

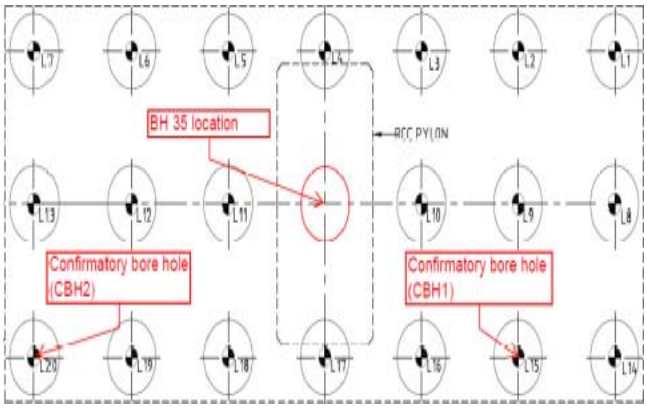


Fig. 4.Location of Confirmatory boreholes

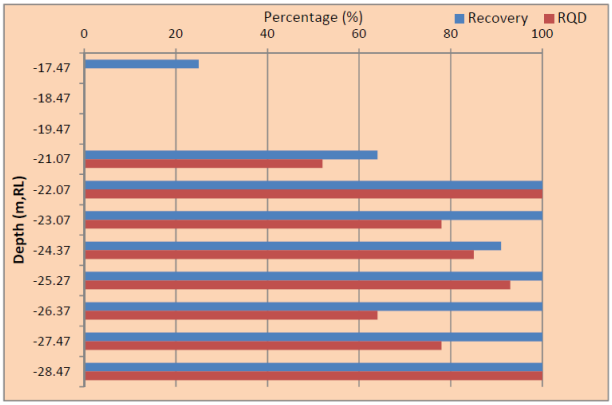


Fig. 5. Core Recovery and RQD (L15)

Core box photographs from the confirmatory bore logs are presented in Fig.6 which indicates good quality rock.



Fig. 6.Core box photographs at P32 location (CBH-1 and CBH-2)

From the confirmatory bore logs, it is noticeable that there is significant variation in rock type as well as quality; and from the laboratory results it is found that the rock available is plutonic basalt rock with

quartz vein intrusion due to high metamorphism. Due to unexpected discrepancy in rock strata encountered, driller could not envisage the penetration rate and the site faced trouble in pile execution leading to delay in the productivity besides increasing the cost and duration of the project.

Recommendation for pile termination

As per the client's requirement, the pile has to be rock socketed up to a minimum depth of embedment of 2.5 times the diameter of pile which was unachievable with BG-28 and the deployment of additional drilling rigs will incur more time and cost for the project. Then negotiating with the site and the clients, the design team headed with the solution of going for the pile penetration resistance concept which is mentioned as per relevant specifications and technical standards, the length of socketing depends proportionally on the quality of rock encountered which can be estimated using concept of Pile Penetration Ratio (PPR).If for basalt, core recovery more than 90%, and RQD >25%, and a pile penetration ratio 225 T-m, ½ times diameter of pile is suitable as depth of embedment (Datey, K. R).

The Pile Penetration ratio (PPR) is an estimate of energy required to advance the pile bore of $1m^2$ cross-sectional area by 1cm. It actually reflects the SPT 'N' value i.e. the chisel energy required to advance which is a function of weight of chisel(W), height of fall(h), number of blows (n), cross-section area of pile (A) and penetration into rock (IRC:78-2014).

PPR corresponding to SPT N values can be calculated as:

$PPR = 63.5 \times 10^{-3} \times 75 \times 10^{-2} \times N / (0.785 \times 5.2^2 \times 10^{-4})$.

The rate of PPR value variation with depth is provided in Fig. 7.

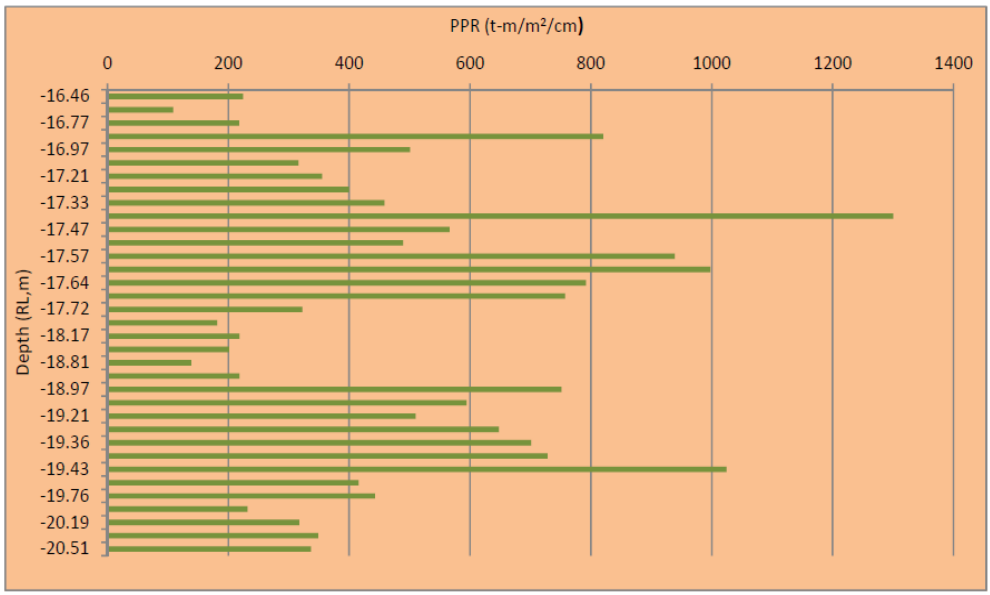


Fig. 7.PPR values for CBH (L15)

From confirmatory bore logs at pier number 32 location, it is evident from Fig.7 that PPR values obtained at various depths are greater than 225 T-m which confirms presence of hard rock suitable for terminating foundation. The concept of PPR has been used as a tool for confirmation of hard strata; henceforth pile design has been revised by the consultant based on confirmatory bore log data with modified pile founding level with a reduced socket depth of 2.5D i.e. 3.75m from an initial depth of socket of 3.6D i.e. 5.4m. It conforms to minimum depth of embedment of 2.5D advocated by client as well as satisfies design requirement of 500 T/m^2.

The pile numeration drawing pertaining to revised depth of embedment into hard rock is presented below in Fig.8.

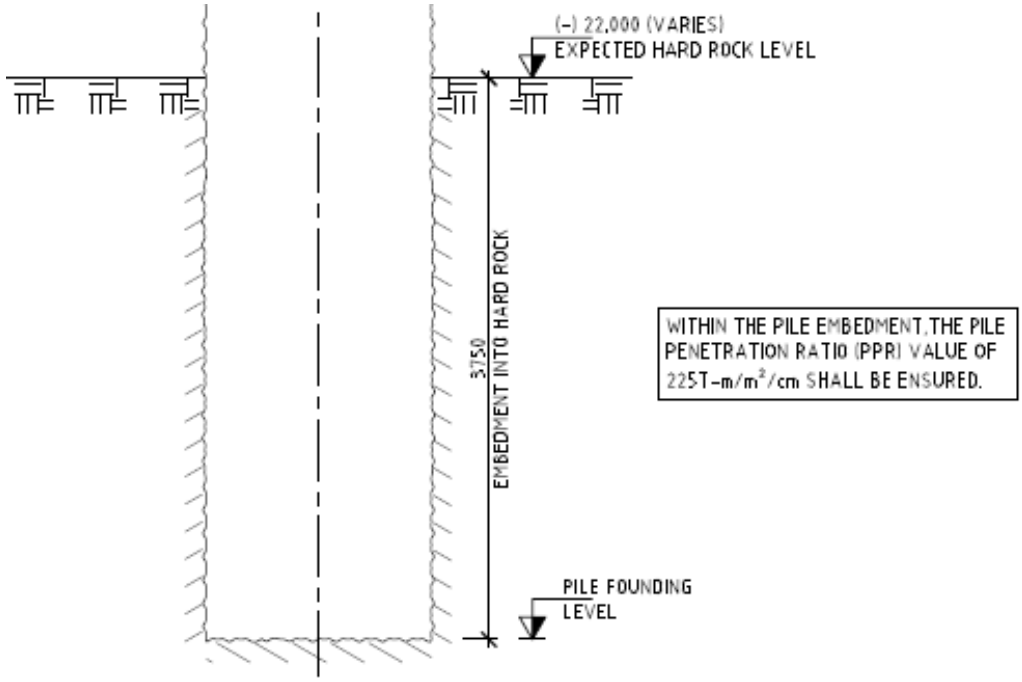


Fig. 8.Pile drawing with revised depth of embedment

CONCLUSION

Comparing the initial investigation data and the confirmatory bore log, it can be clearly seen from Fig. 8 & Fig.9 respectively showing the variation in the core recovery and RQD values; thus indicating that the rock quality in the confirmatory bore logs is better than the previously investigated data.

. **Fig.8.Core recovery comparison for BH-35**

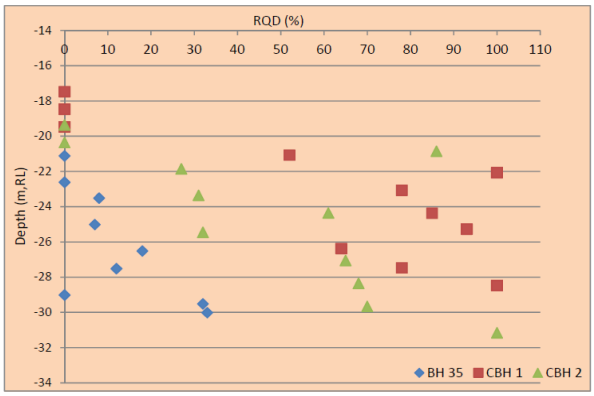
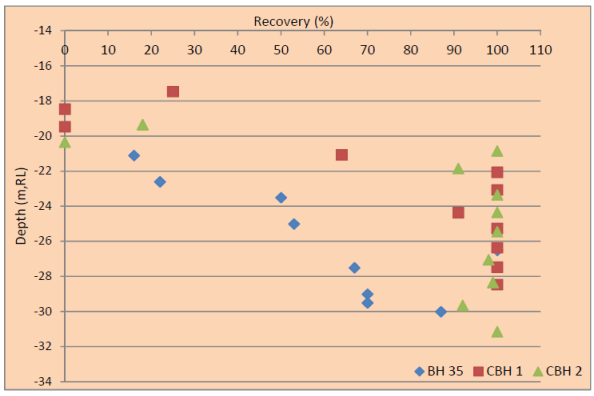


Fig.9.RQD comparison for BH-35



From on-site pile chiseling records, it is found that PPR > 225 t-m/m^2/cm, the strata is considered as hard which is evident from confirmatory boreholes and thus the depth of embedment has been revised by the

consultant by providing a minimum rock socket of 2.5times the diameter of pile; which is found adequate for achieving required axial capacity and the same has been successfully accepted by the client; henceforth implemented out as a measure for rock socketing criteria and pile embedment.

REFERENCE

1. Cole,K.W. and Stroud.M.A. Rock socket piles at Coventry point, Market Way, Coventry.
2. Confirmatory field bore logs furnished by M/s Renuka Consultants.
3. Datey,K.R.,1990.Bored piling in Bombay region. Proceedings, Indian Geotechnical Conference.
4. Gandhi,S.R. Pile design and construction practices in India-A review. Proceedings, Indian Geotechnical Conference, IIT Mumbai.
5. Ganpule,V.T.,1975.Estimating geotechnical capacity of bored cast in situ piles from penetration resistance.
6. Ganpule,V.T. and Gupte,S.M.,2004.Study of theoretical and observed capacities of bored cast in situ piles in Tuff, Braccia and weathered basalt. Proceedings, 5th international conference on case histories in geotechnical engineering.
7. Geotechnical factual soil investigation report furnished by M/s L&T Geostructure.
8. IRC: 78-2014, Standard specifications and code of practice for road bridges, section VII, Foundations and substructures.
9. Sivanarayana, K.V., 2015.Technical note on termination criteria for piles in rocky strata. L&T Infrastructure Engineering Limited,Chennai.
10. Khare,M.G. and Mhaiskar,S.Y.,2010.Pile termination criteria for rock socketed piled in Mumbai-A new approach, Proceedings, Indian geotechnical conference, December 16-18,IGS Mumbai chapter& IIT Mumbai.
11. Maertens ,L. Bored sockets in weathered basalt. Associate professor Catholic University Leuven.
12. Pells,P.J.N.State of practice for design of socketed piles in rock.
13. Srinivasamurthy,B.R. and Pujar,K.L.,2009. Socketing of bored piles in rock. Proceedings, Indian geotechnical conference, Guntur.
14. Tomilson.M.J., 2008.Pile design and construction practice,5th edition.

ANALYTICAL METHOD OF STONE COLUMNS COMPARED WITH AN ANALYSIS AS PER ROWE DILATANCY THEORY

Abhijit Saha, Irrigation & Waterways Department, Government of West Bengal, India, 9433509798, ovijeet@rediffmail.com.

ABSTRACT

Two analytical closed-form elastic-rigid-plastic solution methods to predict the rigid foundation behaviour on stone-column reinforced soil are compared, both of which takes into account the stone material yield within the host soil according to stress-dilatancy theory. These are the mechanistic methods developed by the author (2004, 2005) [*that presently incorporates the dilatancy angle as per Schanz and Vermeer (1996)*] and that developed by Pulko and Majes (2006), that takes into account the column yield as per Rowe dilatancy theory. Since optimal design of stone column necessitates optimum stress concentration on column, which is generally composed of dense gravel with/or without sand, the vertical stress on granular column is often close to its peak strength and the material dilates. To arrive at closed-form analytic solution to this complex soil-stone column interaction problem, some common assumptions like axi-symmetric soil-stone column 'unit-cell', elastic host soil and rigid-plastic Mohr-Coulomb stone column material are combined with equilibrium and kinematic conditions. The results reflect the beneficial effect of dilatancy within the optimal range or techno-economic domain of area-ratio. The settlement predictions are compared with other analytical methods available in literature as well as with measured settlement reduction of stone-column reinforced ground at different subsoil conditions around the globe reported in literature.

Keywords: ground improvement, stone columns, Rowe dilatancy, settlement reduction, stress concentration.

INTRODUCTION

Stone columns or granular piles are frequently used in stabilization of soft clays, silts and loose silty-sands with large amount of fines. The majority of analytical methods assume infinitely wide loaded area with end-bearing columns having constant diameter and spacing that approximate to axi-symmetric conditions, and the approach is known as 'unit-cell concept'. Several analytical solutions are available, and many of them (Aboshi et al; 1979, Balaam & Booker; 1981) are based on elastic approach considering the stone-column and surrounding soil as elastic materials. However, elastic methods give the ratio between the vertical stress in the column to soil (stress concentration factor) approximately equal to the ratio of constrained modulus of both materials. This ratio was found to be considerably higher than measured in the field and it is believed that elastic methods may overestimate the effects of stone columns on settlement reduction (Barksdale & Bachus, 1983). The elastic and elasto-plastic solutions presented by Balaam and Booker (1981, 1985) indicate that the problem can be idealized by assuming that the stone column is in a triaxial state and possibly yielding, such that there is no shear stress at the stone-soil interface and no yielding in the soil. Similar assumptions of stone column to be in a state of limiting equilibrium and under a triaxial stress state are considered in other methods also (Priebe; 1976, Van Impe & De Beer; 1983, Van Impe & Madhav; 1992, Saha & De; 1994, Saha; 2004, 2005, Pulko & Majes; 2006). In majority of the methods it is assumed that under load the stone-column yields at constant volume. However, the last three cases cited consider another parameter; the dilation of stone column. In Van Impe and Madhav's (1992) and author's (2004, 2005) method, the dilation is taken into account through the final value of the volumetric strain of column, whereas Pulko & Majes (2006) considered the stone column as Mohr-Coulomb rigid-plastic; dilating at yield in line with Rowe (1962) dilatancy theory.

All the analytical methods consider stone column deformation along its entire height within the soil-stone column cylindrical 'unit-cell'. However, ***it is unlikely that the whole length of stone column would bulge under a foundation load placed at the upper boundary of the soil-stone column 'unit'.*** It has been found in model as well as in the prototype tests, that under uniaxial compression the column bulges upto a certain length near the upper boundary under vertical load and upon a complex interaction, the composite mass carries higher loads at reduced settlements. This issue is also addressed in the present investigation.

The complex interaction between the properties of intervening soil (E_s, μ_s, c_u) and the installed column (E_c, μ_c, ϕ'_c), dilatancy factor (ω), the magnitude of the external stress level (p_o), the length of column (H) and the geometry of column installation (A_r) have been investigated through development of mechanistic models (Saha, 2005). This study incorporates the dilatancy angle (Ψ) into the analysis. Since the load and geometry are symmetrical in the unit cell, a frictionless boundary at the outer wall with zero shear stress, zero radial displacement, and no water flow has been assumed. These assumptions imply total vertical stress applied on the top of 'unit-cell' remains within the unit, though the distribution of stress between the column and host soil varies with depth. The uniform loading applied on top of unit-cell being analogous to one dimensional (1D) consolidation test, and since the encapsulated column is stiffer than the native soil, concentration of stress occurs in the column with simultaneous reduction of stress in peripheral soil. The results are compared with some existing analytic methods and with published field test results to show that ***dilatancy of granular material has significant effect on settlement reduction and stress concentration.***

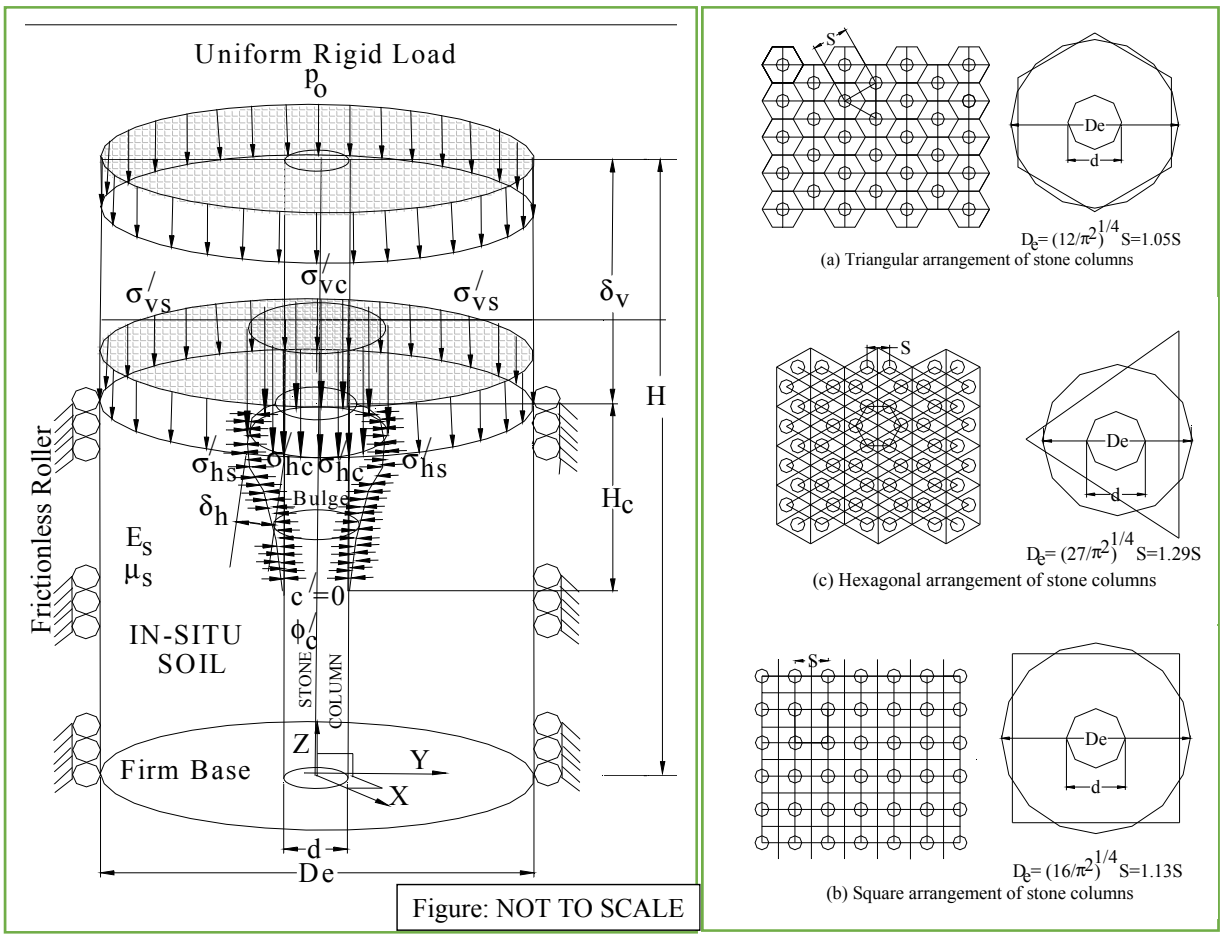


Fig. 1. The axisymmetric 'Unit-Cell' with boundary conditions & stress-deformations

MECHANISTIC MODELLING & PROBLEM FORMULATION

In the proposed mechanistic model, it is considered that the columns are installed in a regular array of triangular, square or hexagonal grid in plan area. Use of "unit-cell" concept has been considered based on some general assumptions and boundary conditions. The tributary area of subsoil encircling each stone column is closely approximated by an equivalent circular area of effective diameter D_e known as domain of influence of each column. For an equilateral triangular pattern arrangement of columns, D_e=1.05S, while for a square pattern, D_e=1.13S and for a hexagonal pattern, D_e=1.29S, where S is the spacing of columns. General assumptions & boundary conditions are: (1) The cylindrical unit-cell surface is frictionless (2) The end bearing of stone column is rigid and non-deformable (3) The ambient sub-soil is elastic (4) The friction between the installed stone column and host soil as well as the self-weight of stone column and in-situ soil are neglected. (5) The stone column is assumed to be in an active state of plastic equilibrium. At a higher stress level, the dilation of column material takes place with consequent lateral compression of soil along critical depth. The free body diagram of unit-cell (Fig.1) defines the problem. The mathematical formulation based on idealized 'unit-cell' has been described (Saha & De, 1994) and mathematical expressions for design parameters were presented in dimensionless form considering dilating stone-column is given by Saha (2004). The stress-deformation equilibrium equations are given below:

Vertical Stress Equilibrium

$$p_o\left(\frac{\pi}{4}\right)D_e^2=\left(\frac{\pi}{4}\right)\left(d+2\delta_h\right)^2\sigma'_{vc}+\left(\frac{\pi}{4}\right)\left(D_e-\overline{d+2\delta_h}\right)^2\sigma'_{vs} \qquad [1]$$

On simplification,

$$\frac{\sigma'_{vs}}{p_o}=\frac{1}{\left(1+\psi\right)^2 A_r n+\left\{1-\sqrt{A_r}\left(1+\psi\right)\right\}^2} \qquad [2]$$

Where, $\psi=2\delta_h/d$ = Diametrical Strain, $A_r = d^2/D_e^2$ = Area Ratio & $n = \sigma'_{vc}/\sigma'_{vs}$ =Stress Concentration Ratio

Deformations and Stresses of Soil & Column

Deformations of intervening subsoil:

$$\delta_v=\frac{H}{E_s}\left(\sigma'_{vs}-2\mu_s\sigma'_{hs}\right) \qquad [3]$$

$$\&\quad \delta_h=\frac{\left(D_e-d\right)}{2E_s}\left\{\sigma'_{hs}-\mu_s\left(\sigma'_{vs}+\sigma'_{hs}\right)\right\} \qquad [4]$$

Limiting equilibrium of stone column material:

$$\sigma'_{vc}=\sigma'_{hc}\tan^2\left(\frac{\pi}{4}+\frac{\varphi'_c}{2}\right)=\sigma'_{hc}\lambda \qquad [5]$$

$$\text{Where,}\quad \lambda=\tan^2\left(\frac{\pi}{4}+\frac{\varphi'_c}{2}\right) \qquad [6]$$

At soil-stone column interface:

$$\sigma'_{hs}=\sigma'_{hc}=\sigma'_h \text{ (say)} \qquad [7]$$

Comparing [2], [6] & [7], one gets,

- NORMALIZED VERTICAL SOIL STRESS

$$\frac{\sigma'_{vs}}{p_o}=\left[\frac{1}{\left\{1-\sqrt{A_r}(1+\psi)\right\}^2+K_o(1+\psi)^2A_r\lambda}\right]\left[1+\psi\left(\frac{E_s}{p_o}\right)\left\{1\Big/\left(\frac{1}{\sqrt{A_r}}-1\right)\right\}\left\{\frac{(1+\psi)^2A_r\lambda}{(1-\mu)}\right\}\right] \quad [8]$$

Where, $K_o = \mu/(1-\mu)$. In a similar fashion as above, it can be shown that,

- NORMALIZED HORIZONTAL SOIL STRESS

$$\frac{\sigma'_{hs}}{p_o}=\left[\frac{1}{\left\{1-\sqrt{A_r}(1+\psi)\right\}^2+K_o(1+\psi)^2A_r\lambda}\right]\left[K_o+\psi\left(\frac{E_s}{p_o}\right)\left\{1\Big/\left(\frac{1}{\sqrt{A_r}}-1\right)\right\}\left\{\frac{\left\{1-\sqrt{A_r}(1+\psi)\right\}^2}{(1-\mu)}\right\}\right] \quad [9]$$

Dividing [9] by [8], one gets,

- SOIL STRESS RATIO

$$k'_s=\frac{\sigma'_{hs}}{\sigma'_{vs}}=\frac{\left[K_o+\psi\left(\frac{E_s}{p_o}\right)\left\{1\Big/\left(\frac{1}{\sqrt{A_r}}-1\right)\right\}\left\{\frac{\left\{1-\sqrt{A_r}(1+\psi)\right\}^2}{(1-\mu)}\right\}\right]}{\left[1-\psi\left(\frac{E_s}{p_o}\right)\left\{1\Big/\left(\frac{1}{\sqrt{A_r}}-1\right)\right\}\left\{\frac{(1+\psi)^2A_r\lambda}{(1-\mu)}\right\}\right]} \quad [10]$$

Observing $n = \sigma'_{vc}/\sigma'_{vs} = \lambda\,\sigma'_{hc}/\sigma'_{vs} = \lambda\,\sigma'_{hc}/\sigma'_{vs} = \lambda k'_s$, we obtain,

- STRESS CONCENTRATION RATIO

$$n=\frac{\sigma'_{vc}}{\sigma'_{vs}}=\lambda\frac{\left[K_o+\psi\left(\frac{E_s}{p_o}\right)\left\{1\Big/\left(\frac{1}{\sqrt{A_r}}-1\right)\right\}\left\{\frac{\left\{1-\sqrt{A_r}(1+\psi)\right\}^2}{(1-\mu)}\right\}\right]}{\left[1-\psi\left(\frac{E_s}{p_o}\right)\left\{1\Big/\left(\frac{1}{\sqrt{A_r}}-1\right)\right\}\left\{\frac{(1+\psi)^2A_r\lambda}{(1-\mu)}\right\}\right]} \quad [11]$$

Dilating Stone Column

Within the framework of above assumptions and boundary conditions, if it is assumed that the column has dilated by a very small magnitude, ϖ fraction of the initial volume along its critical depth and equating the initial and final volumes of stone column,

$$\left(\frac{\pi}{4}\right)d^2H=\left(\frac{\pi}{4}\right)\left\{(d+2\delta_h)^2H_c\right\}(1-\varpi)+\left(\frac{\pi}{4}\right)\left(H-\overline{\delta_v+H_c}\right)d^2 \quad [12]$$

Where, $\varpi = \varepsilon_{vd}$ = Volumetric strain or dilatancy factor of column material along critical depth. On simplification of above equation,

$$\delta_v=H_c\psi\left[\left(2(1-\varpi)+\psi(1-\varpi)-\frac{\varpi}{\psi}\right)\right] \quad [13]$$

Now, as per Schanz & Vermeer (1996), angle of dilatancy (Ψ) can be expressed in terms of the volumetric strain due to column head dilation and vertical strain of the column:

$$\sin\Psi=-\left(\frac{\varepsilon_{vd}}{\varepsilon_z}\right)\Big/\left(2-\frac{\varepsilon_{vd}}{\varepsilon_z}\right)=\frac{\varepsilon_{vd}}{2\varepsilon_z-\varepsilon_{vd}}=\varpi\Big/\left(2\left(\frac{\delta_v}{H}\right)-\varpi\right) \quad [14]$$

Where ε_{vd} & ε_z are volumetric strain & vertical column strains. On transposing,

$$\varpi = -\left[\left\{2.\left(\frac{\delta_v}{H}\right).\sin\Psi\right\}\Big/\left(1-\sin\Psi\right)\right] \qquad [15]$$

Comparing [3] & [4], one gets,

$$\varepsilon_z = \frac{\delta_v}{H} = \frac{1}{E_s}\left\{\sigma'_{vs}\left(1-2\mu K_o\right) - 2E_s\psi p_o \Big/ \left(\frac{1}{\sqrt{A_r}}-1\right)\right\} \qquad [16]$$

On simplification,

$$\frac{\delta_v}{H} = \frac{\left(\frac{p_o}{E_s}\right)\left(\frac{1}{\sqrt{A_r}}-1\right)\left(1-2\mu K_o\right)\left(2(1-\varpi)+\psi(1-\varpi)-\frac{\varpi}{\psi}\right)\left(\frac{H_c}{H}\right)}{(1-\mu)\left\{(1+\psi)^2 A_r K_o\lambda + \left\{1-\sqrt{A_r}(1+\psi)\right\}^2\right\}\left\{\left(2(1-\varpi)+\psi(1-\varpi)-\frac{\varpi}{\psi}\right)\left(\frac{1}{\sqrt{A_r}}-1\right)\left(\frac{H_c}{H}\right)+2K_o\right\}+(1-2\mu K_o)(1+\psi)^2 A_r\lambda} \qquad [17]$$

Putting the value of δ_v & σ'_{vs} from [13] & [8] in [16] & simplifying, we obtain,

- <u>DIAMETRICAL STRAIN IN COLUMN</u>

$$\psi = \left[\frac{\left(\frac{p_o}{E_s}\right)(1-\mu)(1-2\mu K_o)}{\left\{2(1-\varpi)+\psi(1-\varpi)-\frac{\varpi}{\psi}\right\}}\right]\left[\frac{1}{\left\{\left(\frac{H_c}{H}\right)+\frac{2K_o}{\left\{2(1-\varpi)+\psi(1-\varpi)-\frac{\varpi}{\psi}\right\}\left(\frac{1}{\sqrt{A_r}}-1\right)}\right\}\times\left[(1+\psi)^2 A_r K_o\lambda+\left\{1-\sqrt{A_r}(1+\psi)\right\}^2\right]+\frac{(1-2\mu K_o)(1+\psi)^2 A_r\lambda}{\left\{2(1-\varpi)+\psi(1-\varpi)-\frac{\varpi}{\psi}\right\}\left(\frac{1}{\sqrt{A_r}}-1\right)}}\right] \qquad [18]$$

In the above equation, the term $\left\{2(1-\varpi)+\psi(1-\varpi)-\frac{\varpi}{\psi}\right\}$ shall be substituted by

$$\left\{2\left(1+\frac{2.\left(\frac{\delta_v}{H}\right).\sin\Psi}{(1-\sin\Psi)}\right)+\psi\left(1+\frac{2.\left(\frac{\delta_v}{H}\right).\sin\Psi}{(1-\sin\Psi)}\right)+\frac{2.\left(\frac{\delta_v}{H}\right).\sin\Psi}{\psi}\right\}$$

to get the diametrical strain ψ (*the key factor dictating improvement*) in terms of angle of dilation Ψ of stone column material at column head. Now, as ψ appears on both sides of the equation, an iterative procedure is followed to get the value of ψ for different values of μ_s, ϖ (or Ψ), p_o/E_s, H_c/H, ϕ_c' and A_r.

The other parameters, namely, σ'_{vs}/p_o, σ'_{hs}/p_o, k'_s & n spelt above are obtained by substituting the values of ψ for specific values of μ_s, ϖ (or Ψ), p_o/E_s etc. in the respective equations.

Now, the settlement of virgin ground (δ_{vo}) is given by,

$$\delta_{vo} = p_o m_v H = p_o \left\{ \frac{(1+\mu)(1-2\mu)}{E_s(1-\mu)} \right\} H = \left(\frac{p_o}{E_s} \right) \{1 - 2\mu K_o\} H \quad [19]$$

Substituting ψ from [18] to [1] & the resultant expression of δ_v is divided by [19] to get

- SETTLEMENT REDUCTION FACTOR

$$\frac{\delta_v}{\delta_{vo}} = \frac{\left(\frac{1}{\sqrt{A_r}} - 1 \right)(1-\mu)\left(2(1-\varpi) + \psi(1-\varpi) - \frac{\varpi}{\psi} \right)\left(\frac{H_c}{H} \right)}{(1-\mu)\left\{ (1+\psi)^2 A_r K_o \lambda + \left\{ 1 - \sqrt{A_r}(1+\psi) \right\}^2 \right\}\left\{ \left(2(1-\varpi) + \psi(1-\varpi) - \frac{\varpi}{\psi} \right)\left(\frac{1}{\sqrt{A_r}} - 1 \right)\left(\frac{H_c}{H} \right) + 2K_o \right\} + (1-2\mu K_o)(1+\psi)^2 A_r \lambda} \quad [20]$$

COMPARISON WITH AN ANALYSIS AS PER ROWE DILATANCY THEORY

Pulko & Majes (2006) presented an analytical closed-form elastic-rigid-plastic solution which takes into account confined yielding of the stone material within soil stone column unit-cell according to Rowe (1962) stress-dilatancy theory. As per Rowe's (1962) equation:

$$\sin\Psi = \frac{\sin\varphi_c' - \sin\varphi_{cv}'}{1 - \sin\varphi_c' \sin\varphi_{cv}'} \quad [21]$$

Where, ϕ_c' & ϕ_{cv}' are the peak triaxial shear angle and triaxial shear angle at constant volume of stone column material respectively. According to Rowe stress-dilatancy theory,
[5] may be re-written as:

$$\left(\sigma_{vc}'\right) \Big/ \left\{ \sigma_{hc}' \left(1 - \frac{\varepsilon_{vd}}{\varepsilon_z} \right) \right\} = \frac{1 + \sin\varphi_{cv}'}{1 - \sin\varphi_{cv}'} \quad [22]$$

Pulko & Majes (2006) further summarized that as per Bolton (1986):

$$\varphi_c' \approx \varphi_{cv}' + 3I_R \quad [23]$$

Where, the relative dilatancy index I_R is defined as:

$$I_R = D_R (10 - \ln p') - 1 \quad [24]$$

Where, D_R is the relative density & p' the mean effective stress.
And I_R is directly related to the dilatancy angle (Schanz & Vermeer, 1996) as:

$$\sin\Psi = \frac{I_R}{6.7 + I_R} \quad [25]$$

In absence of reliable laboratory data on dilatancy behavior and properties of column material, above relationships may be used for estimation purposes (Pulko & Majes, 2006).

To investigate the complex mechanism of column head dilation on the stresses and displacements, both the proposed methods of Pulko & Majes (2006) and author are programmed and outputs presented below in Fig.2. Different dilatancy percentage of column head (ω = 0.5%, 1%, 1.5% & 2%) were assumed for representative value of peak shear angle (ϕ_c') of column material as 45^0 and Poisson's ratio of 0.30. Further, as the author's study (2004, 2005) considered that the column of height H bulges along the critical column depth (H_c) at its head, the non-dimensional parameter, Critical Height Factor = $h_f = H_c/H$ is also considered.

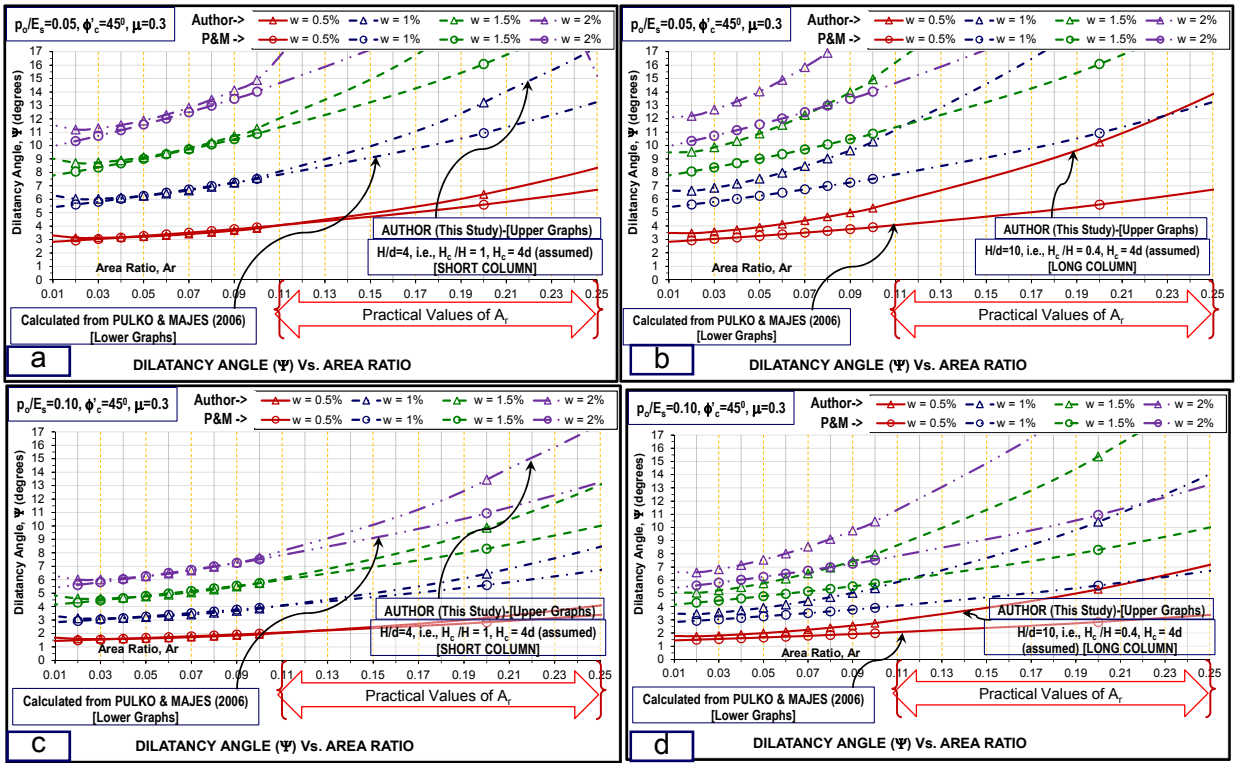


Fig. 2. The effect of area replacement ratio (A_r), upper boundary strain (p_o/E_s) level, column length (H) & dilation percentage of column material on dilation angle at column head.

Replacement ratios A_r upto 25% has been considered in view of the fact that both mathematically by way of mechanistic modelling (Saha, 2005) and from analysis of full-scale load test results reported in literature (Prakash et al, 2005) on rammed stone columns installed in a wide range of alluvial ranging from loose to medium dense sands/silty sands and clayey silt/silty clays with and without fill over them (Saha; 2007, 2010), it has already been proved and reported that the practical domain of A_r for optimal benefit lies within $0.10 \leq A_r \leq 0.25$ (i.e., $2d \leq$ Spacing, $D_e \leq 3d$).

It is found (from Fig. 2a & 2c) that the computed dilatancy angle as per the present method matches excellently with the method as per Rowe dilatancy theory (Pulko & Majes, 2006) at any magnitude of upper boundary strain (p_o/E_s) for area ratio below 0.11 (i.e., D_e=3d), for short columns (h_f=H_c/H=1, where bulging along the entire column depth has been considered). As the area replacement increases, dilatancy angle (Ψ) computed by present method increases marginally within the optimal range of area ratio. For long columns (Fig. 2b & 2d), that is for columns of a length much greater than the critical depth of 4d; as expected, the dilation angle at column head is higher than that of columns bulging along the entire column length for same levels of upper boundary strain (p_o/E_s), that increases non-linearly as area replacement increases, making the unit-cell more stiff with higher column diameter. Further, higher dilation percentage of column head results in higher dilatancy angle (Ψ).

PARAMETRIC STUDY

A parametric study has been carried out by the proposed method and computed values as per Pulko & Majes (2006) equations (as per Rowe dilatancy theory), to investigate the change of area replacement ratio A_r on the effect of dilation on settlement reduction and stress concentration. It is noticed from Fig. 3 that the settlement reduction within the practical range of A_r {i.e., $0.10 \leq A_r \leq 0.25$ (i.e., $2d \leq D_e \leq 3d$)} increases

significantly for the dilation case over the no-dilation case. As the length of column increases, the ground becomes stiffer within a larger unit-cell domain along the column depth resulting in higher settlement reduction.

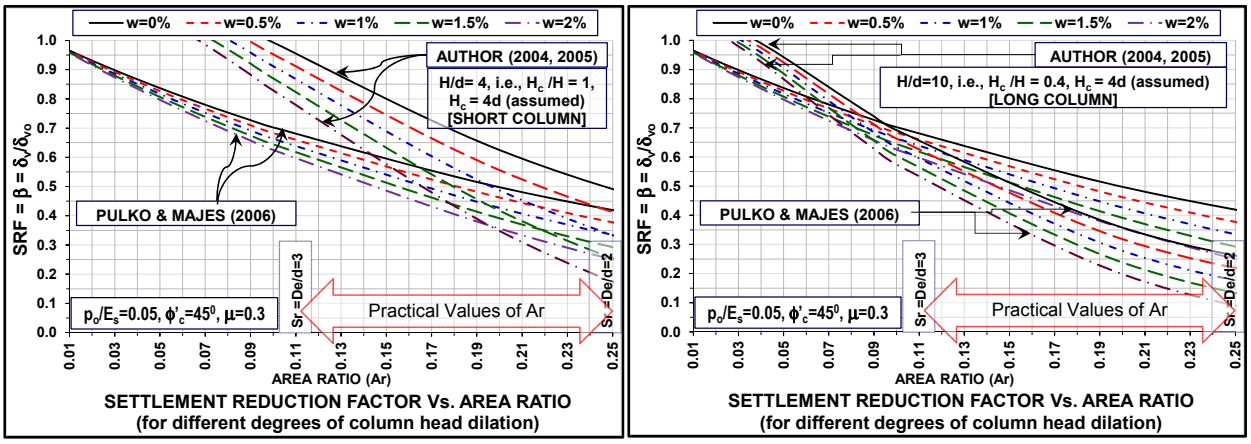


Fig. 3. The effect of area replacement ratio (A_r), column length (H) & dilation percentage of column material at column head on settlement reduction.

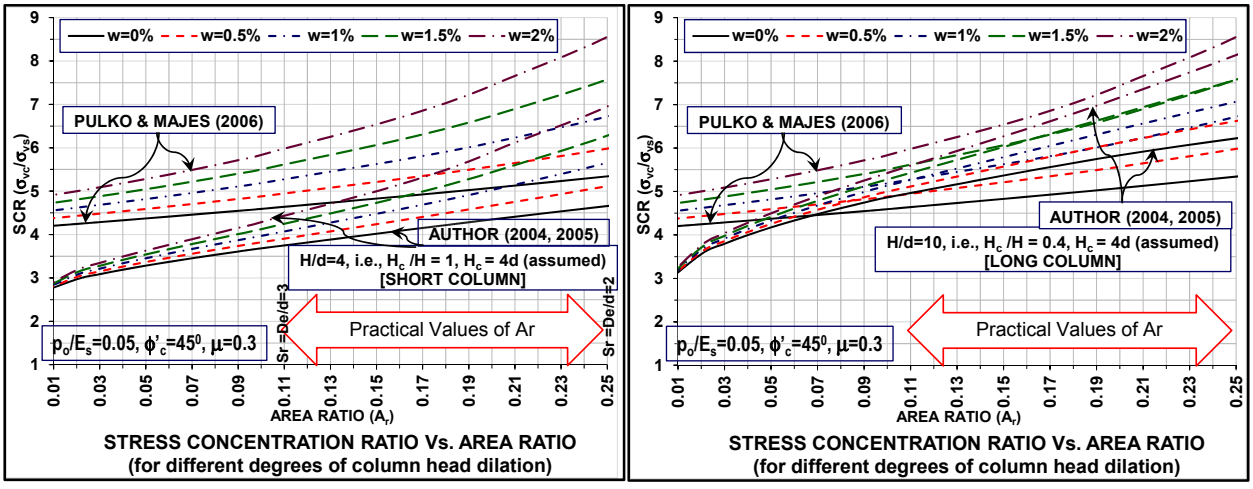


Fig. 4. The effect of area replacement ratio (A_r), column length (H) & dilation percentage of column material at column head on stress concentration ratio (SCR=n=$\sigma'_{vc}/\sigma'_{vs}$).

The effect of area replacement ratio A_r and dilation percentage ω on stress concentration factor (SCR=n) is shown in Fig.4. The importance of dilation of column on stress concentration is clearly evident. Well densified stone-column with high dilation angle Ψ acts stiffer and can absorb higher proportion of external applied stress. ***Within the optimal range of A_r {i.e., $0.10 \le A_r \le 0.25$ (i.e., $2d \le$ Spacing, $D_e \le 3d$)}, stress concentration factors (n) are within the range from 4 to 7 for short columns and from 5 to 8 for long columns***.

COMPARISON WITH OTHER METHODS

Fig. 5 presents a comparison of predictions of settlement reduction factor. The settlement reduction factor (β), by present method is compared with the elastic methods of Aboshi et al (1979), elasto-plastic methods

of Priebe (1976) and Van Impe & De Beer (1981) that takes into account the yield of the stone column at constant volume, finite element method of Balaam & Poulos (1983) and finally by Pulko & Majes (2006) that takes into account the column dilation. Interestingly, within the practical domain of column spacing, the predictions based on the proposed method are higher than those of Priebe, Van Impe & De Beer, Balaam & Poulos, Balaam & Booker, Aboshi et al at lower column spacing. At a higher column spacing of 3d, the predictions match excellently with Balaam & Poulos FEM analysis and Priebe's approaches. Further, it matches excellently with the method as per Rowe dilatancy theory by Pulko & Majes (2006) within the optimal area replacement domain. A further interesting point to note is that the predictions based on the proposed method are in fairly good agreement with the results obtained in actual field tests on soft Bangkok clay by Bergado et al (1987).

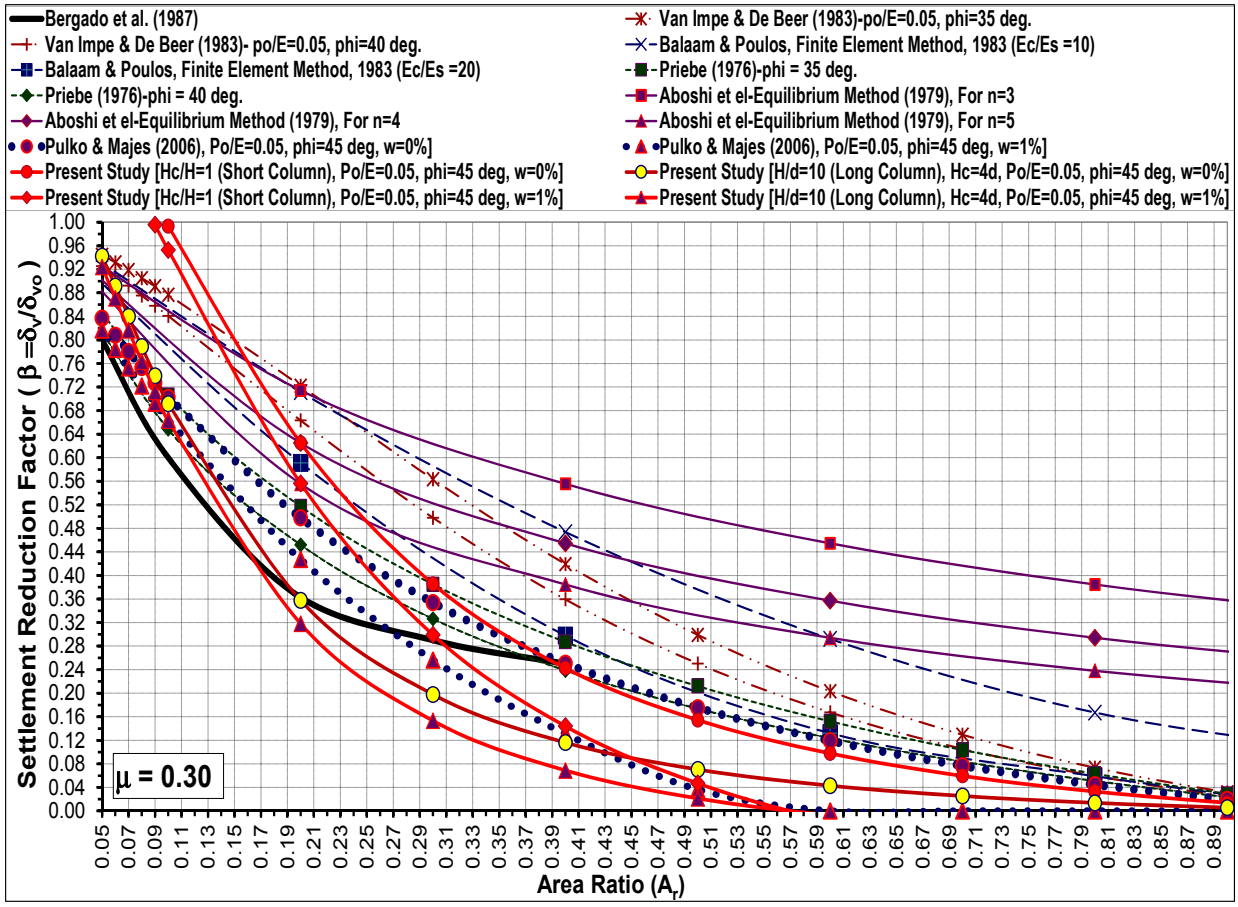


Fig. 5. Comparison of Settlement Reduction Factor (β) as per some analytical methods superimposed on field test results on soft Bangkok clay by Bergado et al (1987).

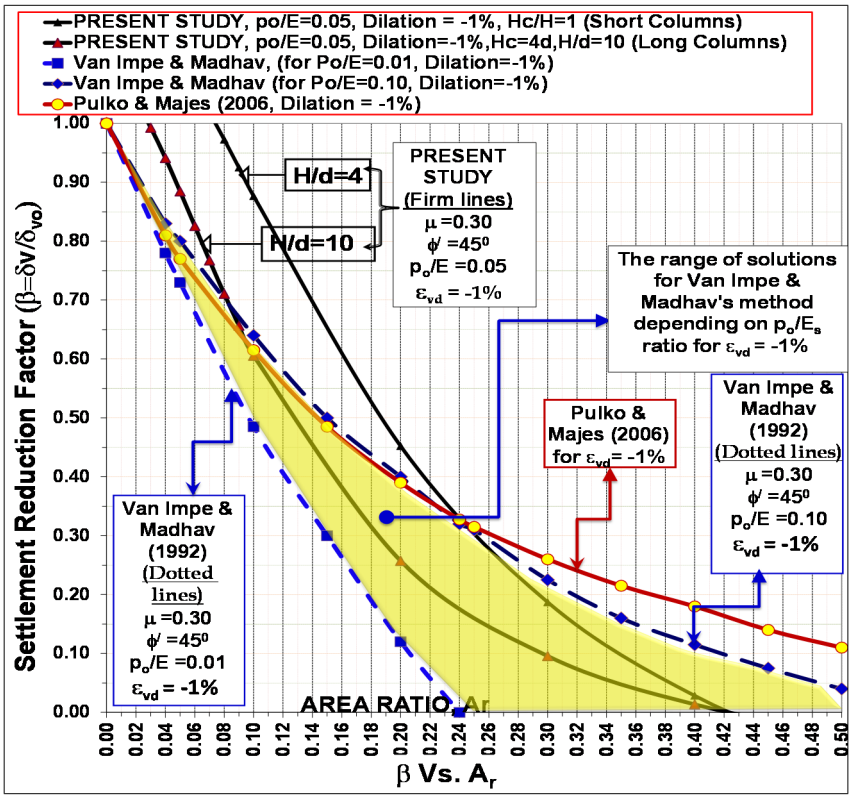


Fig. 6. Comparison of settlement reduction (β) for Dilating Stone Column according to author's study (2004, 2005), Van Impe & Madhav's (1992) method & Pulko & Majes (2006) method.

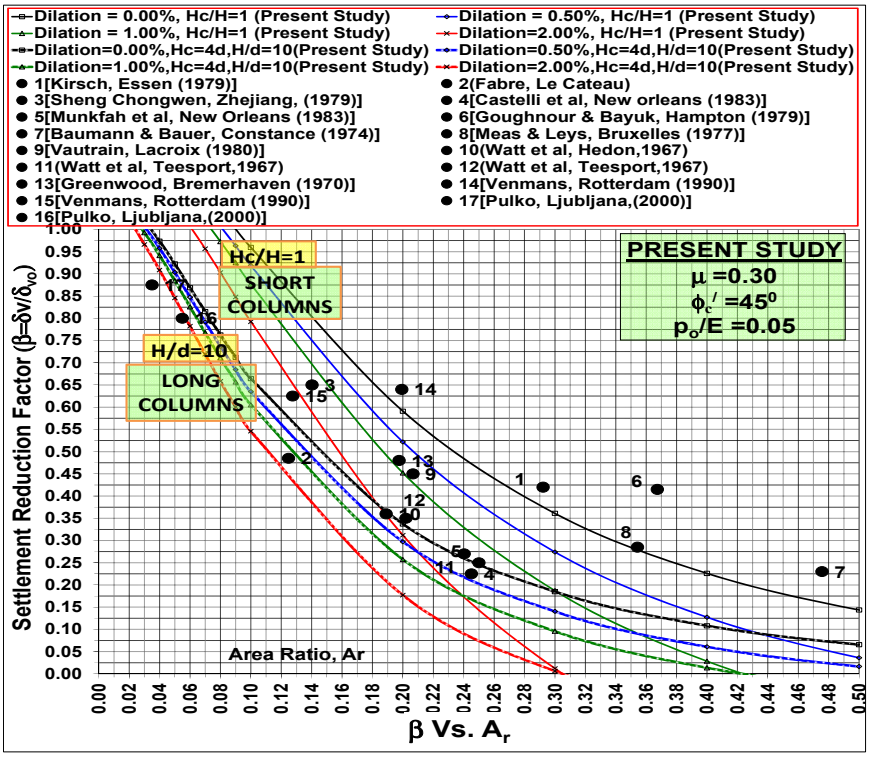


Fig. 7. Settlement Reduction Factors (β) vs. Area Ratio (A_r) for short and long columns [Author's study; 2004, 2005] compared with some field test results.

Fig. 6 presents the comparison of results between the author's (2004, 2005) (for short and long columns), Van Impe & Madhav's (1992) and Pulko & Majes' (2006) method, wherein the dilatancy of granular material is taken into account. Author's and Pulko & Majes method assumes small strains and vertical equilibrium of the un-deformed geometry to simplify the problem and to get the closed form solution instead of nonlinear solution.

COMPARISION WITH FIELD TEST RESULTS

Fig.7 presents a comparison of predictions of settlement reduction factor by the author's model for short and long columns with experimental results obtained in the field under different conditions at various sites reported in literature. The predictions are based on Poisson's ratio, $\mu = 0.30$, upper boundary strain, $p_o/E_s = 0.10$ & peak shear angle of stone column material, $\phi'_c = 45^0$. There is a significant variation in the measured settlement reduction factor for a given area ratio, and the reasons may be attributed to different site conditions, method of column installation and as a direct outcome, on the dilation behavior.

CONCLUSIONS

An analytical method for design of stone-column reinforced foundation is presented. The encapsulated stone-column in ambient subsoil is modelled as a 'unit-cell', wherein the peripheral soil is assumed to behave elastically whereas the rigid-plastic granular column is assumed to behave according to Mohr-Coulomb failure criterion. In addition, the dilation of the column material according to Schanz & Vermeer's (1996) equation is unified within the method. A simple closed-form solution for prediction of the effect of stone-column on the resultant stresses in soil and column are presented. Comparisons with some other existing analytic methods and field test results are done and some parametric study have been presented and discussed. The method is compared with an analysis as per Rowe stress-dilatancy theory. It emerged that the dilatancy of granular material has significant effect on the settlement reduction as well as on stress concentration. It corroborates the fact that densification of column goes a long way to achieve greater initial stiffness that significantly affects the column behaviour at yield and the overall behavioral performance of reinforced ground. It transpires that a very small quantum of dilation of column material could produce significant improvement in settlement reduction.

REFERENCES

Aboshi H., Ichimoto E., Enoki M. & Harada K. (1979). The Composer-A Method to Improve Characteristics of Soft Clay by Inclusion of Large Diameter Sand Columns. Proc. International Conference on Soil Reinforcement: Reinforced Earth & Other Techniques, Paris, France: pp. 211-216.

Balaam, N.P. and Booker J.R. (1981). Analysis of rigid rafts supported by granular piles. International Journal for Numerical and Analytical Methods in Geomechanics, 5, 379-403.

Barksdale, R.D. and Bachus, R.C. (1983). Design and construction of stone columns. Report No. FHWA/RD-83/026, Federal Highway Administration, Office of Engineering and Highway Operations, Research and Development, Washington D.C.

Bergado D.T., Alfaro M.C. & Chai J.C., (1991). The Granular Pile: Its Present State and Future Prospects for Improvement of Soft Bangkok Clay. Geotechnical Engineering, 22:143-175.

Chandra Prakash, Ramakrishna V.V.G.S.T., Sharma A.K. & Rastogi P.C. (2005). Performance of Rammed Stone Column Foundations in Alluvial Soil, Indian Geotechnical Journal, Vol.33, No.3, 227-244.

De P.K. and Saha Abhijit (1991). The Field and Analytical Responses of Stone Columns in Soft Soil. Indian

Geotechnical Conference, Surat, India, Vol. 1, pp. 393-397.

Priebe, H. (1976). Abschätzung des Setzungverhaltens eines durch Stopfverdichtung verbesserten (Estimating settlements in a gravel column consolidated soil), Baugrundes. Die Bautechnik, 5, 160-162.

Pulko, B. & Majes, B. (2006). Analytical method for the analysis of stone-columns according to the Rowe dilatancy theory. Acta Geotechnica Slovenica, 1, 37-45.

Saha Abhijit & De P. K. (1994). Field & Analytical Study of Stone Columns by Non-Linear Strain. Proc. XIII International Conference on Soil Mech. & Foundation Engg., New Delhi, India, 3:pp.1211-1214.

Saha Abhijit (2004). Analysis of Dilating Granular Column in Soil-Stone Column Interaction, Proceedings of Indian Geotechnical Conference, Warangal, India, 2: pp.268-273.

Saha Abhijit (2005). A Study of Behaviour of Stone Columns for Ground Improvement. Ph.D. Thesis, Jadavpur University, India, 197 p.

Saha Abhijit (2006). Analysis of Stone-Column Reinforced Soil by Arching Theory, Proceedings of Indian Geotechnical Conference, Chennai, India, 2: pp.551-554.

Saha Abhijit & Das S.C. (2007). Analytical Study & Back Analysis of Field Response of Stone-Column Reinf. Ground, Proc. 13th Asian Regional Conference on SMGE, Kolkata, India, 1(II):pp.881-884.

Saha Abhijit (2007). Analysis and Design of Stone-Column Reinforced Ground, Proc. of Seminar on Stone Column: Experiences of the Constructors, Kolkata, India, pp.13-65.

Saha Abhijit (2009). Interpretation of field test results on stone column Reinforced alluvials, Proceedings of the National Seminar on Emerging Trends in Ground Improvement, Kolkata, India, pp.5-15.

Saha Abhijit (2010). Limits of Applicability of Stone-Column in Ground Improvement, Proceedings of Indian Geotechnical Conference, Vol.-II (IGC-2010, Geotrentz), Mumbai, pp.591-594.

Saha Abhijit (2011). The time-settlement-load behaviour of stone-column drain-well, Proc. of 14th Asian Regional Conference on Soil Mech. & Geotechnical Engineering, Hong Kong, China, pp.1843-1846.

Schanz, T. and Vermeer, P.A. (1996). Angles of internal friction and dilatancy of sand. Géotechnique, 46(1), 145-151.

Rowe, P.W. (1962). The stress-dilatancy relation for static equilibrium of an assembly of particles in contact. Proceedings of Royal Society, 269A, 500-527.

Van Impe, W. & De Beer, E. (1983). Improvement of Settlement Behaviour of Soft Layers by means of Stone Columns. Proc. 8th Euro. Conf. on Soil Mech. & Fdn. Engg., Helsinki, 1: pp.309-312.

Van Impe, W. & Madhav, M.R. (1992). Analysis and settlement of dilating stone column reinforced soil. Österreichische Ingenieur und Architekten Zeitschrift (ÖIAZ), 137(3), 114-121.

INVESTIGATIONS ON THE DISTRESS TO THE PAVEMENTS/PQC SLAB AROUND MONORAIL PIERS, WADALA, MUMBAI

Sandeep S Nikam, L&T Construction, Powai, Mumbai, India, 9619413437, sandeepnikam@lntecc.com
Sanjay D Patil, L&T Construction, Powai, Mumbai, India, 8286035888, sdpatil@lntecc.com
Unnikrishnan Nair C S, L&T Construction, Powai, Mumbai, India, 9819615015, csunair@lntecc.com
Prabir C Basu, L&T Construction, Powai, Mumbai, India, 9820647061, pcb@lntecc.com

ABSTRACT

Mumbai Metropolitan Region Development Authority (MMRDA) entrusted to implement Monorail Systems in various parts of Mumbai Metropolitan Region (MMR) with the objective to supplement the present transport system in MMR. The stretch of Monorail is starting from Sant Gadge Maharaj Chowk (SGMC) and extending up to Chembur Railway Station, divided into 2 phases. Construction of Phase 1 (Chembur to Wadala Depot) is complete and Phase 2 (Wadala Depot to SGMC) is under construction.

Monorail runs on prestressed girder (guide beam) of span ranging from 20m to 28m supported on pier founded upon group of end bearing piles embedded in rock, pile group ranging from 2-4 piles of diameter 1000mm each.

For the purpose of site characterization, geo-technical investigations were carried out along the alignment of Monorail system as mentioned above. These investigations included field and laboratory tests. The subsurface strata mainly consist of silty sand, gravel, underlain by marine clay extending up to stronger basalt rock with volcanic breccia. Overburden consisting of mainly marine clay ranging from 5.5m to 11m at all locations within the influence zone of settlement.

The existing rigid pavement along of Sion-Koliwada and Anik-Wadala were constructed about 5 years prior to the construction of Monorail piers. Before laying the rigid pavement, to improve the geotechnical strength of subsoil (mainly marine clay), ground improvement using stone columns was undertaken by MMRDA. In light of limited right of way, the Monorail piers have been constructed in the median portion of the road. The line became operational on February 2014, in few months it was noticed that, in the vicinity of the Monorail piers, along Sion-Koliwada link and Anik-Wadala link, the Road Pavement Quality Concrete (PQC) panels adjacent to the Monorail piers started showing distress in form of non-uniform settlement of the concrete panels.

Effect of pile foundation on pavements/PQC slab distress and possible causes of distress were investigated. Initially the distress was thought to be upheaval of monorail pier cap, but further investigations revealed the same to be soil settlement occurring over time. This paper describes the investigation carried out for identifying the cause of this settlement.

Keywords: Monorail, PQC Panels, Marine Clay

INTRODUCTION

Mumbai Metropolitan Region Development Authority (MMRDA) entrusted L&T to implement first monorail in India with the objective to supplement the present transport system in MMR. Total alignment length of monorail is 19.29 km comprising of two phases. Phase I is from Wadala to Chembur (8.92km) and Phase II is from Wadala to SGM Chowk (10.36km). Detailed layout plan of monorail alignment and stations is shown in Fig. 1.

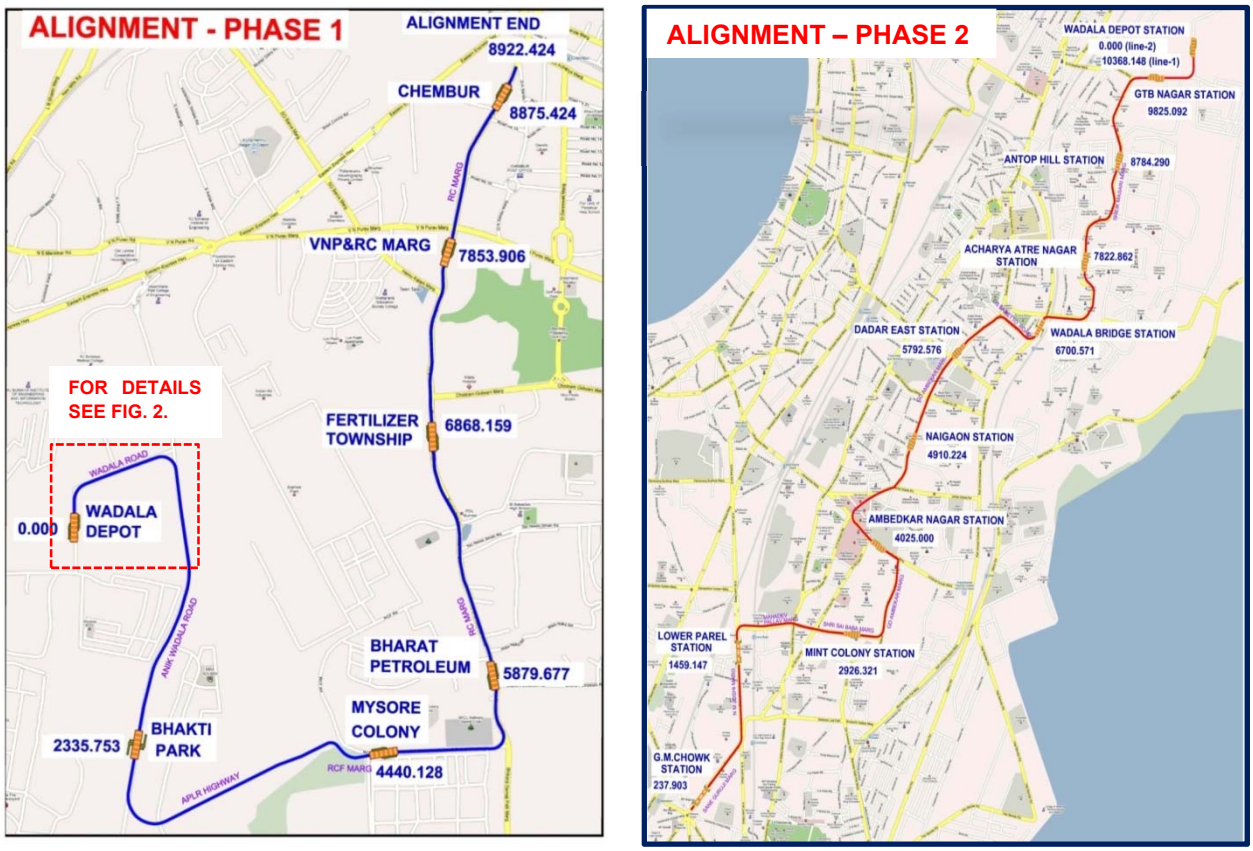


Fig. 1. Layout plan of Phase I and Phase II of Monorail alignment

Cement concrete pavement in front of Wadala Monorail station / Sion-Koliwada road were constructed above the filled up material at these locations (See Fig. 2). Since the sub-soil comprises of marine clay in these roads, stone columns (0.9 m diameter at a spacing of 2.5 m c/c in a triangular pattern) were installed (as per data obtained from MMRDA) before constructing the cement concrete pavement. Construction of monorail piers and cement concrete pavement was carried out almost simultaneously. The thickness of PQC is about 300 mm, below which dry lean concrete (DLC) bed has been provided. Granular sub base (GSB) layer has been provided below DLC and fill soil can be seen below GSB layer. These roads (Sion-Koliwada Connector road and road in front of Wadala Monorail station) are six lane divided carriage way roads with a median in between.

Anik-Wadala Road (North Connector Road) also have pavement composition similar to Sion-Koliwada road. Probably similar ground improvement measures were adopted before constructing the cement concrete pavement. Monorail piers have been constructed in the median portion in this road also.

Presently the cement concrete pavement near the monorail piers in these roads (Sion- Koliwada Connector road and Anik-Wadala Road as well as in front of Wadala Monorail Station) is severely distressed in the form of level displacement (which was thought to be as upheaval) and cracking as shown in Fig. 3 and 4, while the concrete panels away from the piers are intact. The problem of level displacement of slabs near monorail pier and subsequent cracking in such panels can be seen from Wadala Depot to Bhakti Park Monorail Station on Anik-Wadala Road (North Connector road) until the alignment takes a turn towards Mysore Colony Station (See Fig. 1 and 2).

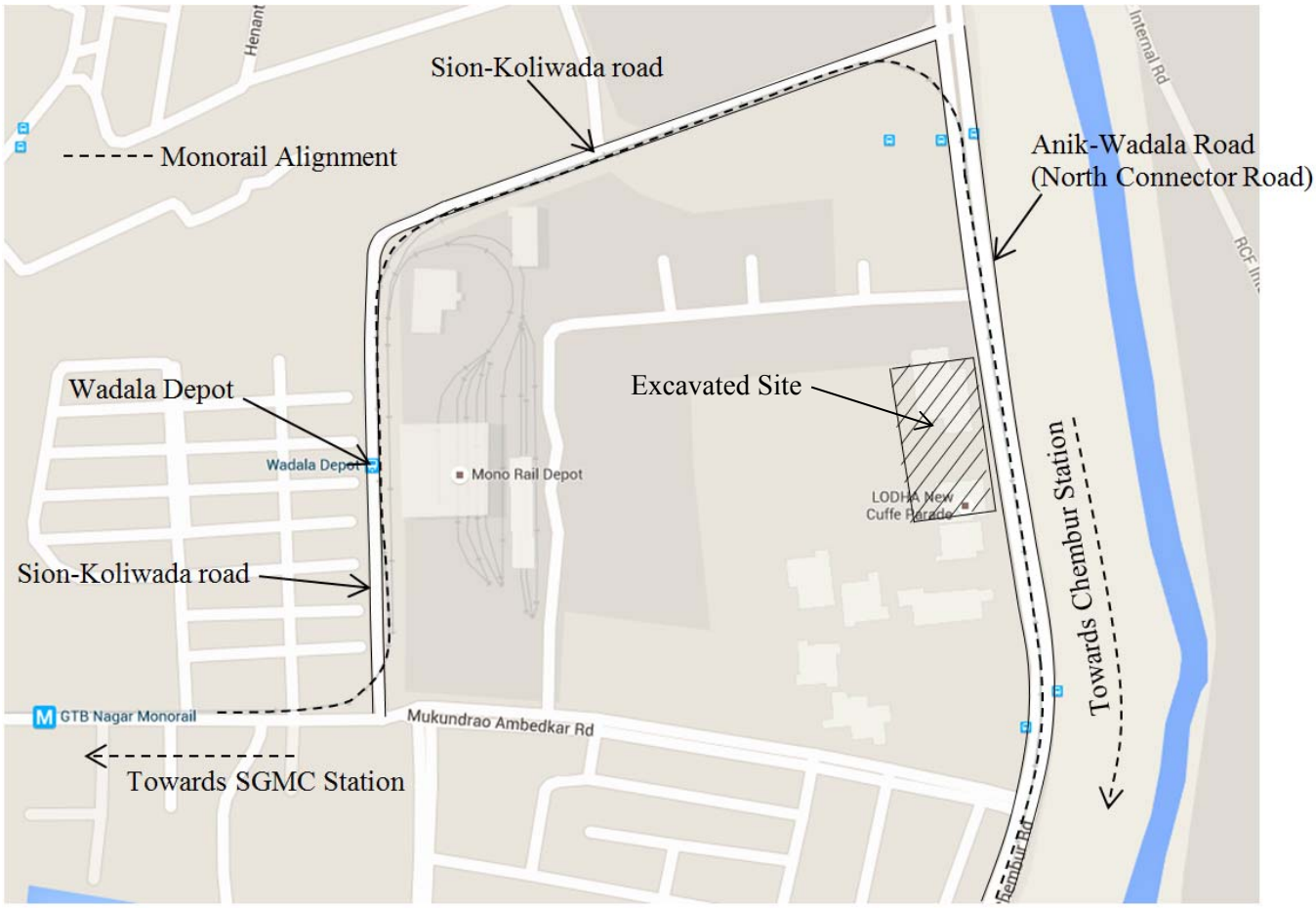


Fig. 2. Layout of Monorail alignment (affected area)



Fig.3. Distress of PQC slabs around-Monorail piers



Fig.4. Cracking of PQC slabs around-Monorail piers

INVESTIGATION ON DISTRESS OF PQC SLAB

A. SOIL INVESTIGATION

The geotechnical investigation was carried out along the proposed alignment at each pier location of Monorail system before the construction of monorail piers to indicate the sub soil and rock stratification. As the part of investigation the geotechnical investigation report was obtained and studied. Summary of sub-surface profile is as described below.

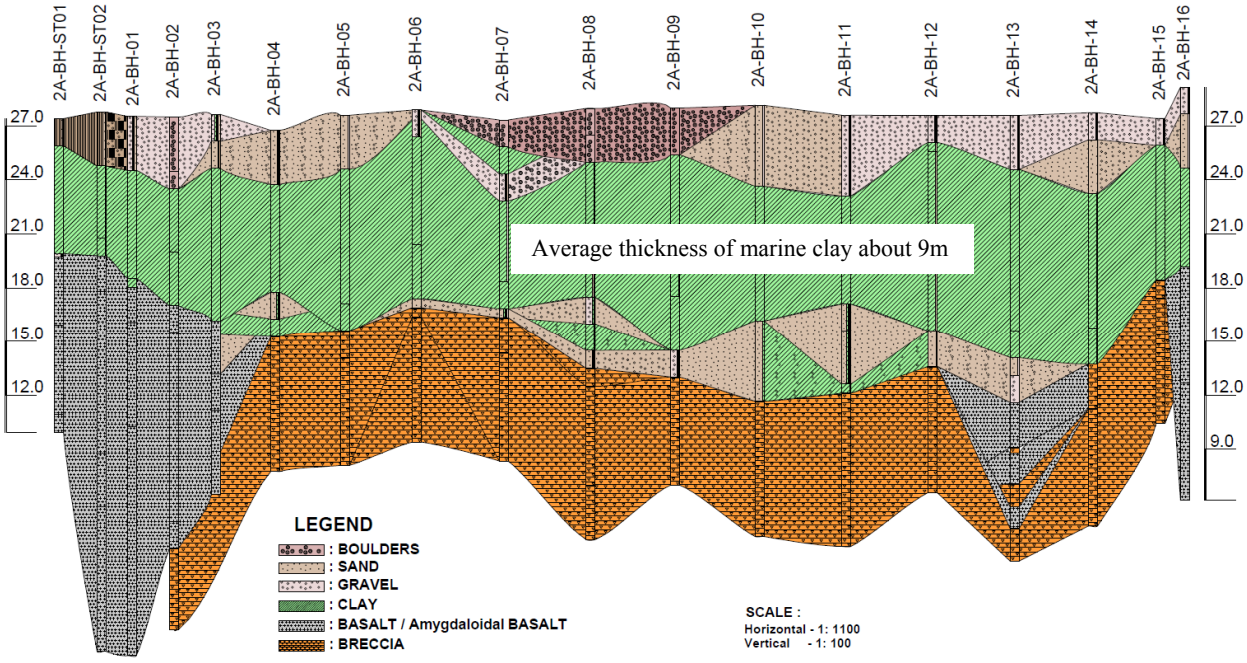


Fig.5. Typical subsurface profile of Sion-Koliwada Connector road

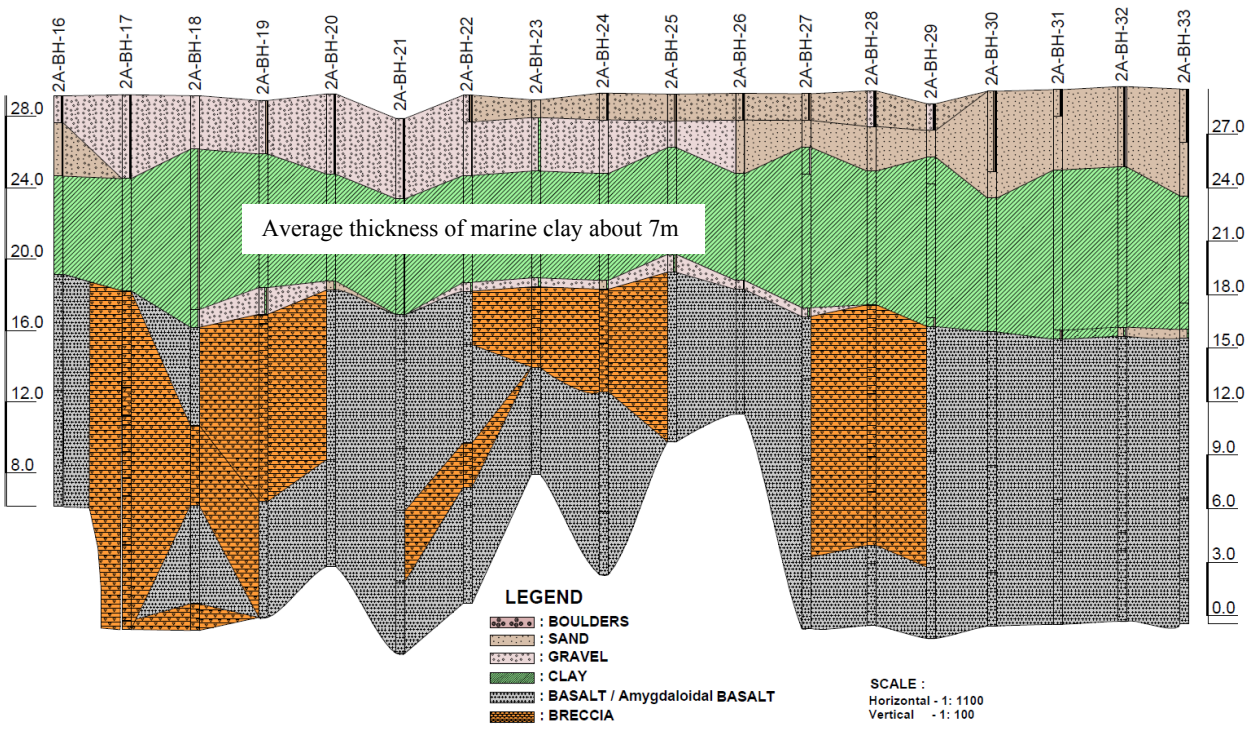


Fig.6. Typical subsurface profile of Anik-Wadala Road

Stratum I - Strata is essentially a fill material, which mainly comprises yellowish brown silty sandy gravel with some traces of PCC and shell fragments. At few locations, layers of cobbles and boulders are also observed; these materials do not retain water and thus, facilitate the percolation of water. The thickness of this stratum varies from 1.5 m to 7.5 m.

The ground water depth varies between 0.5 m to 5.5 m, below EGL.

Stratum II - This stratum consists of a cohesive deposit, which is described as a very soft to soft dark grey/brown CLAY material. At a few locations, traces of organic matter are observed. The thickness of this stratum varies from 5.5 m to 11.0 m, with an average of 8.0 m. SPT N values in this stratum range between 2 -15, with an average of 4. Higher N values in the range between 18 -67 are also observed at a few locations, where the stratum consists of hard brown/stiff dark grey clay.

Stratum III and Stratum IV - Below Stratum II, a combination of Basalt and Breccia is encountered; the details of which are as given below.

Stratum III - This stratum comprises moderately weak, moderately weathered/highly weathered grey/brown Amygdaloidal Basalt. At some locations, a very weak and completely weathered/highly weathered residual soil grey Basalt is also observed. The thickness of this stratum varies from 10.0 m to 22.5 m, with an average of 15.0 m.

Stratum IV - This stratum comprises moderately weak, moderately weathered/highly weathered reddish brown/greenish grey BRECCIA. The thickness of this stratum varies from 6.0 m to 20.5 m, with an average of 10.0 m.

Based on lower N values and higher Atterberg limits as reported in geotechnical investigation report Stratum II can be summarized as soft to very soft marine clay with high plasticity and stratum III and stratum IV can be summarized as moderately strong rock mass.

B. FIELD SURVEY

A topography survey was carried out as a part of investigation on September 2014 and levels were taken from PQC panels just adjacent to monorail piers and PQC panels away from piers (5 m away from pier on either side). These level-readings were compared with original road levels and it was observed that average settlement on Sion-Koliwada road and Anik-wadala was of magnitude 250mm and 110mm respectively as shown in Fig. 7. Observed settlement on Sion-Koliwada road was more compared to settlement on Anik-Wadala road.

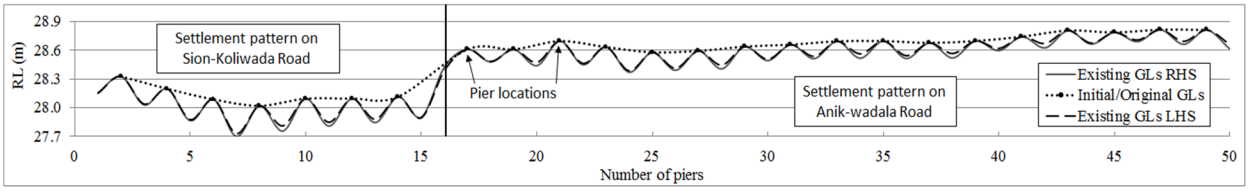


Fig.7. Comparison between existing GL and original GL

It was seen that existing PQC panels at pier locations were dismantled to carry out Monorail piling work and were also properly restored back to match the original road levels (See Fig. 8). Filling of area up to pile cap top was done with crushed sand with proper compaction as shown in Fig. 9.



Fig.8. Restored back PQC panels matching original road level



Fig.9. Crushed sand filled in the gap between casted pile cap and existing ground

During investigation it was noticed that excavation for the laying of a raft foundation was in progress in the neighboring area as shown in Fig. 1 (hatched area), along with dewatering. The objective of dewatering was to lower the ground water level which might have induced an additional effective stress in

the clay layer. Loss of fines due to continuous pumping might have triggered settlement as ground is lost to the voids created by expulsion of soil-water slurry. Consolidation settlement occurs predominantly in fine grained clayey soils that cannot dissipate pore water pressure changes quickly due to low permeability. A recharge system should have been installed, to mitigate settlement of adjacent sites. Fig. 10 shows extent of mass excavation carried out in the neighboring area.

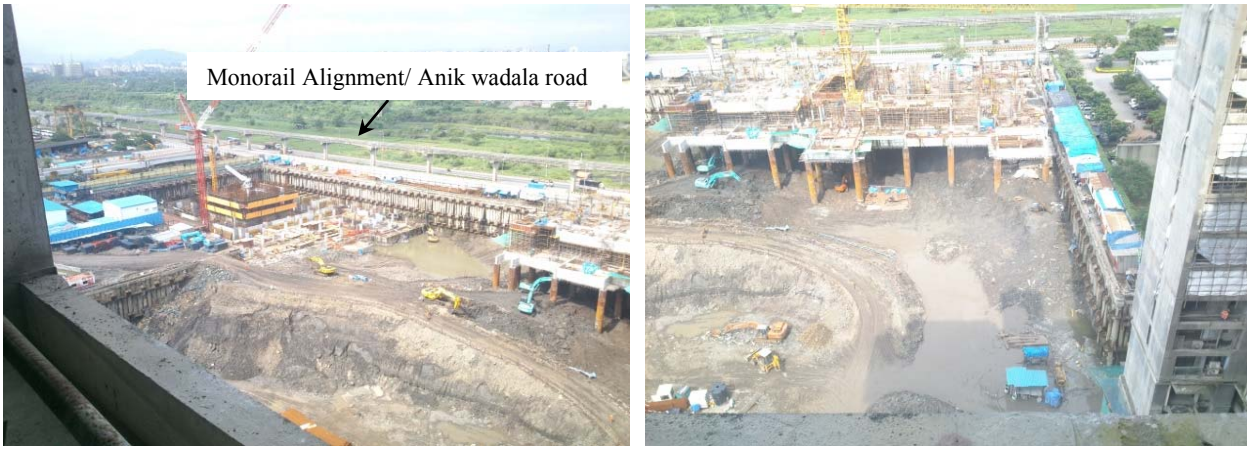


Fig.10. Extent of mass excavation and dewatering in neighboring area

Provision of stone columns below existing pavement might have accelerated the rate of settlement. Stone columns help in reducing the total settlement, but they cannot completely eliminate consolidation settlements which can be seen in Fig. 11 showing distress/settlement around box culvert in neighboring area.



Fig.11. Distress of pavement around box culvert in neighboring area

SUMMARY AND CONCLUSIONS

From above discussion it can be concluded that Monorail structure (Pier, Pile cap and Piles) is intact. Since monorail operations are going on unhindered, this indicates no differential settlement of monorail track. Field survey revealed that soft marine sub-soil found in this stretch has undergone consolidation settlement due to load imposed by fill soil and pavement over time. The monorail piers and pier cap did not settle since they have been founded on piles which rest on hard stratum (Basalt Rock). As a result, PQC slabs which are resting on monorail pier pile caps stayed at their original position while all other slabs away from piers gradually settled.

Another reason of pavement distress can be dewatering in the neighboring area which might have triggered consolidation settlement.

ACKNOWLEDGEMENTS

We are thankful to the L&T Construction and entire monorail site team for making all the relevant data available for this paper. We are thankful to authors of various books / papers / reports listed in the references below. We are also thankful to DFI-India for giving an opportunity and platform to put up this paper.

The views and opinions expressed in this paper are those of the authors and do not necessarily reflect the official interpretation or position of the company

REFERENCES

Gopal, R., and Rao, A., S., R., 2000. Basic and Applied Soil Mechanics, pp. 221-286.

Fugro Geotech Pvt. Ltd., 2009. Soil Investigation Works for Mumbai Monorail Project, 251/09 (R-3).

General Arrangement of Foundation drawings 2A1 to 2A86, Mumbai Monorail Project.

MOBILISED SHEAR STRENGTH ON THE FAILURE SURFACE OF 2D BELLED ANCHOR MODEL PILES UNDER UPLIFT IN COHESIONLESS SOIL

Tanaya Deb, Research scholar, Civil Engg. Deptt., NIT Agartala, Agartala, Tripura, India, ph: 9774187352; E-mail: debtanaya88@gmail.com
Sujit Kumar Pal, Associate Professor, Civil Engg. Deptt., NIT Agartala, Agartala, Tripura, India, ph: 9436582750; E-mail: skpal1963@gmail.com

ABSTRACT

Experimental investigations are carried out on failure pattern around 2D models of belled anchor piles in dry sand bed of density 15.60 kN/m^3 under uplift. The models are having thickness ratio (T_s/T_b) = 0.28, 0.32, 0.38 and 0.46 and total 12 numbers tests are performed on models possessing 45° bell angle and shaft thickness 26 mm. The foundation bed is prepared with alternate dyed and non-dyed sand layers and continued upto reaching embedment ratio of 3, 4 and 5 for each width ratio. The failure points are presented with respect to meridian section of anchor in X-Y coordinate system and the equations formed are of polynomial of degree 3; and R^2 values are near about 1. The developed wedge is implemented as three-dimensional axisymmetrical failure surface around similar 3D models. In the horizontal slice method vertical limit equilibrium is used for calculating weight of wedge and mobilized shear (as per Chattopadhyay and Pise, 1986) on the slip surface of each element. The summation of all elementary forces demonstrates gross uplift capacity. The initial and final failure angles are detected and parametric study is conducted on failure pattern as well as predicted net ultimate uplift capacity. Almost all the analytical data are within ± 10% variations with respect to the experimental results of uplift capacity which shows better correlations.

Keywords: Uplift capacity, belled anchor pile, 2D model, embedment depth ratio, failure surface, and mobilized shear.

INTRODUCTION

Belled or enlarged base anchor piles are attractive and economic alternative to the geotechnical engineers for compressive load bearing capacity as well as tension anchorage. These types of anchors may be useful for foundations erected below ground water table. In light weight structures like radar tower, television tower, power pole and outdoor sign pools imbalance horizontal forces due to wind loads, are more than of those self-weight of those structures. Due to chronic tensile loads most possibly from wind loads and associated imbalanced cable tension, the legs of power transmission tower should be properly designed to be safe against resultant pull-out forces. In belled anchor pile, uplift is influenced by embedment ratio, diameter ratio; so, contributions of these parameters on failure surface influence uplift capacity. Balla (1961) first introduced non-linear failure surface in the pattern of circular arc based on Kotter's equation (1903) and soil friction was assumed to act on slip surface. The predictive mathematical models established by Matsuo (1967), Rao and Kumar (1987), Chattopadhyay and Pise (1986), Saeedy (1987) and Ghaly and Hanna (1994); it was reported that net ultimate uplift capacity was combination of bulk weight of failure wedge and shear resistance along slip surface acting in opposite direction of wedge movement. From the literatures available till date, it reveals that the contribution of mobilised shear and weight of breakout wedge separately, demanding for more clarification depending on the on parameters like embedment ratio, diameter ratio.

FAILURE MECHANISM

During uplift loading, there are changes in the state of stresses within failure wedge of buried soil media. At the preliminary stage of applied uplift load, there is relief of total stress just below the anchor and simultaneously just above the anchor; there is gradual increase of total stress with rise of anchor which continues upto the failure. This phenomenon described by Saeedy (1987) that compression of soil above anchor produced shear stress. With further pulling of anchor, when shear stress level reaches upto shear strength, the shear strength mobilization as well as breakout wedge formation is commenced. Continuous pulling results in gradual formation of cavity below the base of anchor and simultaneously expansion of cavity as well as development of non-linear failure surface upto ground surface. Dialatancy of sand is responsible for locking up of sands within compressed zone help to develop collapsed zone as explained by Rowe and Davis (1982); and higher interlocking among the sand particles within failure zone than rolling and sliding as stated by Ilamparuthi and Muthukrisnaiah (1999). Saeedy (1986) observed that compression of the locked up soil was dependent on state of stress of soil. At the collapse stage, soils around the base undergo plastic flow in downward to fill the voids. In mathematical model, Matsuo (1967) assumed that during uplift of anchor earth pressure within wedge altered from semi-active condition in the vicinity of footing base to passive state in that of ground surface. Failure mechanism was presented by Dickin and Leung (1990) and Nazir et al. (2014) by using semi-cylindrical modelling.

MATERIALS

Sand

The sand used in this study is collected from local market and completely dried by keeping it in oven in temperature of 105 to 110°c, prior to use for all experiments. Sand contains more than 70% of particles within the range of 1.4 to 0.71 mm. The use of dry sand is friendly to control the test condition and the density within the testing tank with dry sand. The physical and engineering properties are determined according to ASTM standards and experimental results are tabulated in "Table 1".

Table 1 Physical properties of sand sample

Physical Properties	Test Results
Medium sand, 2 to 0.425 mm, (%)	91.00
Fine sand, 0.425 to 0.075 mm, (%)	07.95
Silt and clay,(0.075 to 0.002mm, (%)	1.05
Effective grain size, D_{10}, (mm)	0.55
Average grain size, D_{50}, (mm)	0.90
Coefficient of curvature, C_c	1.07
Coefficient of uniformity, C_u	1.73
Unified Soil Classification System	SP
Specific gravity, G_s	2.67
Minimum void ratio, e_{min}	0.63
Maximum void ratio, e_{max}	0.88
Void ratio, at placement density, $e_{exptl.}$	0.71
Minimum dry density, γ_{min} (kN/m^3)	14.20
Maximum dry density, γ_{max} (kN/m^3)	16.50
Placement dry density, $\gamma_{exptl.}$ (kN/m^3)	15.60
Relative density D_r, (%)	64.38

Sand Bed Preparation for 2D Panel Model

For this model study, density of sand deposit is maintained as 15.60 kN/m^3 and achieved by calibrating the height of fall of sand by raining technique (Dickin and Leung, 1992) and the free fall is fixed from the height of 70 cm. In order to check the homogeneity of sand deposit within model tank, four wooden cubes of 80 cc are placed in the corners of tank in different elevation to check the variation in local density. The variation in local density is within ±1% only. The homogeneous sand bed is prepared by laying successive layers of 3 mm thick dyed (red coloured) and 18 mm thick yellowish sand (natural colour). A total thickness of 21 mm sand layer is prepared to facilitate regarding vertical contour and the upper most layers is terminated as per the continuation of either dyed or non-dyed sand.

Experimental Set-up, Test Procedure and Observations

The model tank is 70 cm (Length) × 60 cm (Width) in plan area and 70 cm in depth. The box is made of plaxiglass in four sides supported by steel frame. Vertical mild steel stiffeners are provided in three sides to prevent outward deflection. To have a clear view of developed wedge from outside no stiffeners are provided in front side. A plaxiglass of 12 mm thick is used and it is stiffer enough to undergo any volume change by deflecting outward. The size of the tank is chosen to be free from boundary effects as the maximum failure point at ground surface is within 5 times of the largest bell thickness concerned in the present study.

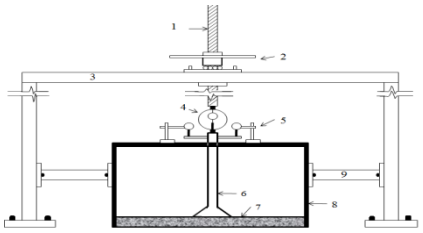
Belled anchor pile is generally characterised by its geometry as bell diameter, shaft diameter, bell height and bell angle. The 2D panel anchors are fabricated from mild steel plates of 1 mm thickness and sufficiently stiffer to undergo negligible deformation compared to soil. The 2D panels are 58±0.5 cm in length and other dimensions are less enough to consider that plain strain condition would prevail. The geometric parameters and their designations are presented in "Table 2". The top of all the 2D anchors are internally threaded to fit proving ring gently and two numbers of horizontally projected wings are welded, located closer to the top of the shaft. These are positioned at 180° to each other and are provided to facilitate the dial gauges to rest on them. The models are installed parallel to the width of the tank.

Table 2 Detailing of 2D panel models and their designations

2D panel designation	T_s (mm)	T_b (mm)	Height of bell (mm)	L/T_b	L (mm)	2D panel designation based on L/T_b
M: 45-0.46	26	56	15	5	280	M: 45-0.46-5
				4	224	M: 45-0.46-4
				3	168	M: 45-0.46-3
M: 45-0.38	26	68	21	5	340	M: 45-0.38-5
				4	272	M: 45-0.38-4
				3	204	M: 45-0.38-3
M: 45-0.33	26	80	27	5	400	M: 45-0.33-5
				4	320	M: 45-0.33-4
				3	240	M: 45-0.33-3
M: 45-0.28	26	92	33	5	460	M: 45-0.28-5
				4	368	M: 45-0.28-4
				3	276	M: 45-0.28-3

The tests are conducted to study failure pattern in around 2D panels. The schematic diagram of loading frame, model inside the tank, position of proving ring, and dial gauges and other accessories are presented in "Fig. 1". At first, a 100 mm thick and compacted sand bed is prepared inside model tank on which the model would rest. A pulling shaft, like a screw jack is connected with model along-with proving ring. Thus the models are suspended freely and vertically on sand bed within

tank with the help of screw jack. Vertical movement of shaft is imposed by manually operated rotating circular wheel fixed with nut and screw arrangement and nut-screw system is supported by ball-bearing system. The sand filling has been continued by rainfall technique upto attainment of desired embedment depth. An arrangement is made in the centre of the panel length with internal threading to hold a tension proving ring of 2.0 kN capacity. A couple of dial gauges of 0.01 mm accuracy are used for measuring corresponding vertical displacements. The dial gauges are fitted with magnetic bases and these bases are resting on couple of bars running over the top of model tank.



1. Long screw, 2.Rotating wheel, 3. reaction frame, 4. Proving ring, 5. Dial gauge in magnetic base, 6. Model anchor, 7. Sand datum, 8. Test tank, 9. Stiffeners

Fig. 1 Schematic diagram of experimental set-up (front view)

A centre-line is marked vertically along the thickness of panel models which are visible from outside of plaxiglass. With the application of tensile load, at first the sand layers around bell base tends to move along model and gradually inclined in horizontal direction with further upward movement; and simultaneously there is a gradual formation of cavity or gap below the anchor. The pulling is continued till the sand particles around the base of models move downward to fill the cavity, though the failure is already indicated by the proving ring. At the collapse stage, from the displaced dyed sand layers horizontal extent of break-out points can be measured by normal scaling. The positions of break-out points remains unaltered even for a further pulling and the region outside of failure surface remains in rest position.

EXPERIMENTAL PROGRAMME

In this study, constant parameters used are bell angle (α), 45°, tank size, sand type and density, installation method, loading arrangement and shaft thickness in 2D panels. To study the failure pattern in cohesionless soil media in both sides of 2D panels having bell angle of 45°, at width ratio (T_s/T_b) = 0.46, 0.38, 0.33 and 0.28, and each model at embedment ratio (L/D_b for 3D model and L/T_b for 2D model) of 3, 4 and 5 have been considered. Total 4×3 = 12 numbers of tests are conducted at placement density 15.60 kN/m^3. In case of 3D models, the same value of the thickness ratio is treated as diameter ratio.

MODEL DESIGNATIONS

The detail designations of 2D panel models are presented in "Table 2". The models are represented with common coding system consisting of three parts. The first, second and third parts represent bell angle, thickness ratio and embedment ratio respectively. For example: a 2D model possessing 45° bell angle, 0.33 thickness ratio at embedment ratio 5 is designated as M: 45-0.33-5 and 'M' stands for the model.

RESULTS AND ANALYSIS

The "Figs. 2 and 3" present the typical pictorial failure surfaces of M: 45-0.46-3 and M: 45-0.28-5 respectively. Due to the symmetricity about vertical axis in 2D panels as well as generated wedge, failure points of any one half of the collapsed wedge along with meridian section of corresponding

models is presented in coordinate axes system. The midpoint of base of model is taken as origin (0, 0), failure points are presented in coordinate system in semi-infinite soil mass are named as 'horizontal extent of failure surface' and 'distance above base' in X-axis and Y-axis respectively. In "Figs. 5 and 8" the symbol 'FS' is indicating failure surface. The equations formed with failure points at vertical contour of 21 mm are finalized to be polynomial of degree 3 and those non-linear equations are presented in "Table 3". These equations may be helpful for full scale foundation size of same ratio in the field, but here the geotechnical properties of in-situ soil are playing a vital role. So, before direct application in field, few tests should be conducted, considering the site conditions.

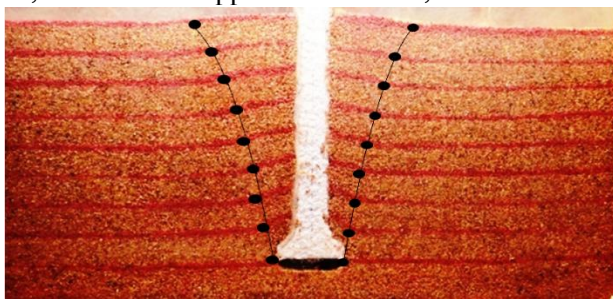


Fig. 2. Pictorial view of failure around model M: 45-0.46-3

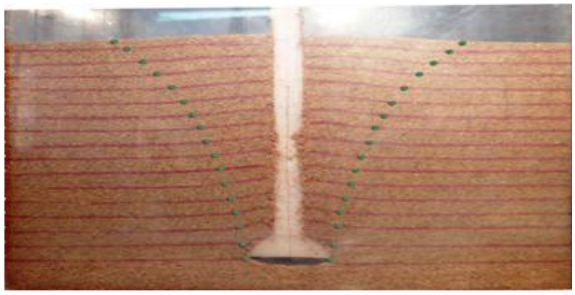


Fig. 3. Pictorial view of failure around model M: 45-0.28-5

It is revealed from "Table 3" that the β_a values for the models are within (ϕ/4+2) to (ϕ/2+3)° and this range is reported by Meyerhof and Adams (1968), Ilamparuthi and Muthukrisnaiah (1999), and Ilamparuthi et al. (2002). The β_f values for models having bell angle 45° are within the range of 36.03 to 59.24°.

Table 3. Polynomial equations of the failure surface

Designation.	**Equation**	**R^2**	$W_{\gamma.anchor}$ (N)	**$Q_{u.Anlyl}$ (N)**	X_{max} (mm)	**β_a** (°)	**B_f** (°)
M:45-0.46-5	$L = 9E-05X^3-0.051X^2 + 9.056X - 219.7$	0.999	2.52	79.56	122	13.74	45.83
M:45-0.46-4	$L = -9E-05X^3-0.019X^2+6.868X - 180.3$	0.998	2.05	40.41	100	16.70	36.03
M:45-0.46-3	$L = 1E-05X^3 - 0.041X^2 + 7.59X - 182.00$	0.999	1.59	28.43	82	10.44	36.87
M:45-0.38-5	$Y = -4E-05X^3 - 0.005X^2 + 5.114X - 164.40$	0.999	3.23	146.83	170	11.85	49.76
M:45-0.38-4	$L = 7E-05X^3 - 0.044X^2 + 8.577X - 251.40$	0.998	2.66	95.70	150	12.41	48.12
M:45-0.38-3	$L = -5E-05X^3 - 0.019X^2 + 6.506X - 200.70$	0.999	2.10	50.38	100	10.20	48.01
M:45-0.33-5	$L = 9E-05X^3 - 0.048X^2 + 9.644X - 315.6$	0.999	4.07	240.19	200	12.35	59.24
M:45-0.33-4	$L = -0.066X^2+10.95X-351.7$	0.998	3.41	152.35	165	16.69	48.01
M:45-0.33-3	$L = 3E-05X^3 - 0.032X^2 + 7.548X - 252.50$	0.998	2.75	85.19	140	17.74	49.40
M:45-0.28-5	$L = -3E-05X^3+ 0.001X^2 + 3.969X - 180.10$	0.999	5.05	382.74	215	10.20	49.69
M:45-0.28-4	$L = 7E-05X^3 - 0.040X^2 + 8.852X-327.50$	0.998	4.29	213.37	180	14.57	53.62
M:45-0.28-3	$L = -0.069X^2 + 11.42X - 396.40$	0.999	3.53	123.72	150	16.17	42.49

ANALYSIS OF FAILURE SURFACES BASED ON HORIZONTAL SLICE METHOD

Failure of soil around belled anchor is a three-dimensional axisymmetrical case. So, the same failure surface as obtained from 2D panel models can be used for three-dimensional axisymmetrical situation and it helps to predict net ultimate uplift capacity. A number of horizontal slices (as truncated cone) are considered having 21mm (Δz) thickness and an inclination angle with vertical for each slice from experimental data is calculated. The thickness of upper most slices are differing on the basis of embedment ratios of corresponding models. Vertical equilibrium of all the elementary forces is considered and finally summed up to produce gross uplift capacity is the of mobilised shear on failure surface of slices opposite to the direction of anchor movement, resultant surcharge on each slice and self-weight of the respective slices. For 2D models, only the thickness is

observed from front elevation, which is useful only to locate the failure pattern; and obviously, in axisymmetry case, the same value of the ratio (thickness ratio) will be treated as diameter ratio. As each slice is using as truncated cone, the variables involving 'X' term would present the term 'radius'. Free body diagram of elemental forces acting on slice wedge is presented in "Fig.4". So, the forces on i^{th} slice are explained below:

Let,

i = Any slice number within the failure wedge;

$K_o = (1-\sin\phi)$, coefficient of earth pressure at rest, as used by Jacky (1944) and Chattopadhyay and Pise (1986);

n = Number of slices within wedge;

β_a and β_f = Initial and final angle making with vertical by failure plane in bottom most and top most failure slice respectively;

β_i = Angle making with vertical in failure plane of i^{th} slice;

Q_i = Gross uplift capacity of i^{th} slice;

$Q_{g,anlyl.}$ = Gross ultimate uplift capacity of failure wedge;

$Q_{u,anlyl.}$ = Net ultimate uplift capacity of failure wedge;

Δz = Thickness of each slice;

x_i = Smaller radius of i^{th} slice at height of z_i from anchor base;

$x_i + \Delta x_i$ = Larger radius of i^{th} slice at the height of $z_i + \Delta z$ from bell base;

Δx_i = Difference between upper and lower radius of i^{th} slice;

z_i = Elevation of i^{th} slice from bell base;

$\Delta L_i = \dfrac{\Delta z}{\cos\beta_i}$ = Lateral dimension of failure plane in i^{th} slice;

W_i = Weight of i^{th} slice wedge;

$W_{\gamma.anchor}$ = Weight of equal volume of soil same as volume of the respective anchors model inside the wedge;

ΔR_i = Resultant normal force on the failure plane of i^{th} slice;

Soil reaction on failure plane, in i^{th} slice, $\Delta F_i = \Delta R_i L_i = \Delta z \gamma \{k\cos\beta_i + \sin\beta_i\} \dfrac{\Delta z}{\cos\beta_i}$;

At the state of limit equilibrium in soil, Mohr-Coulomb failure criteria can be prevailed. Downward acting resultant vertical component of shear resistance for i^{th} slice surface, calculated according to Chattopadhyay and Pise (1986), as follows

$$\Delta T_i \cos\beta_i = 2\Delta z \gamma\pi \{k\cos\beta_i + \sin\beta_i\} \Delta z \tan\phi \left(x_i + \frac{\Delta x_i}{2} \right) \quad \text{..... (i)}$$

Resultant surcharge intensity for i^{th} slice $= \pi q \left\{ (x_i + \Delta x_i)^2 - x_i^2 \right\}$ ..... (ii)

Self-weight of the slice $W_i = \gamma\pi \dfrac{\Delta z}{3} \left\{ x_i^2 + x_i (x_i + \Delta x_i) + (x_i + \Delta x_i)^2 \right\}$; ..... (iii)

Considering vertical equilibrium for all elementary forces of i^{th} slice, gross uplift capacity as follows:

$$Q_{i,.} = 2\Delta z \gamma\pi \{k\cos\beta_i + \sin\beta_i\} \Delta z \tan\phi \left(x_i + \frac{x_i}{2} \right) + \pi q \left\{ (x_i + \Delta x_i)^2 - x_i^2 \right\} + \gamma\pi \frac{\Delta z}{3} \left\{ x_i^2 + (x_i + \Delta x_i)^2 + x_i (x_i + \Delta x_i) \right\}$$

..... (iv)

Gross ultimate uplift capacity for total wedge is found by summing up gross uplift capacities for all the n number of slices,

$$Q_{g,anlyl.} = \sum_{i=1}^{n} Q_{i,} \quad \text{..... (v)}$$

Analytical net ultimate uplift capacity, $Q_{u,anlyl.} = Q_{g,anlyl.} - W_{\gamma.anchor}$ ..... (vi)

From the above analysis, the calculated data of mobilised shear and dead-weight of wedge are mentioned and illustrated in "Discussion" section.

DISCUSSIONS

The effects of different parameters on the failure surface as well as predictive net uplift capacity are discussed below.

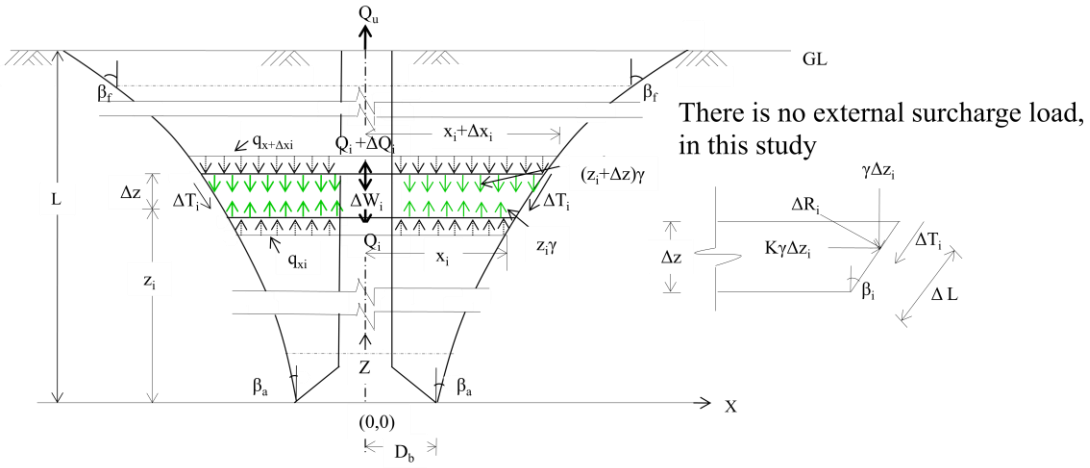


Fig. 4. Free body diagram of slice wedge according to horizontal slice method

Effect of Embedment Ratio on Failure Surface of Model Anchor

For certain thickness of bell (for 2D panel), with the increase in embedment depth, embedment ratio also increases. The plots of distance above base vs. horizontal extent of failure surface at the respective meridian section of the anchors are presented in typical "Fig. 5" for model M: 45-0.33 at embedment ratio of 3, 4 and 5. From the aforementioned figure it is observed that all the curves of failure surface are following similar pattern and extended upto ground surface. Due to the overburden pressure and influence of confinement of soil near to anchor base, failure points are little expanded near about the anchor base. But with increase in height from base level, the failure points are gradually more extended, in horizontal direction and finally become maximum at ground surface. At higher embedment ratio, a failure points generally have a tendency to expand more near about the ground surface and ultimately terminates at higher elevation with maximum expansion at respective ground surface, than those failure surfaces formed at shallow embedment ratio. The similar failure trend was explained by Matsuo (1967).

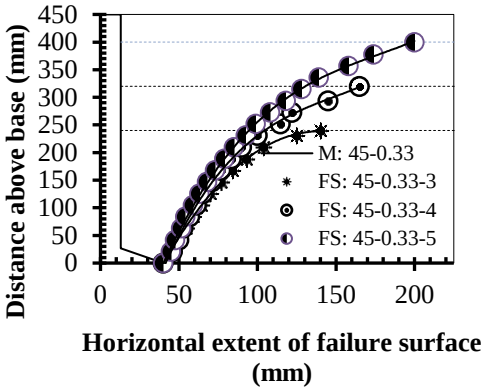


Fig.5. Embedment ratio vs. horizontal extent of failure surface curves of anchor for thickness ratio 0.33 at embedment ratio 3, 4 and 5

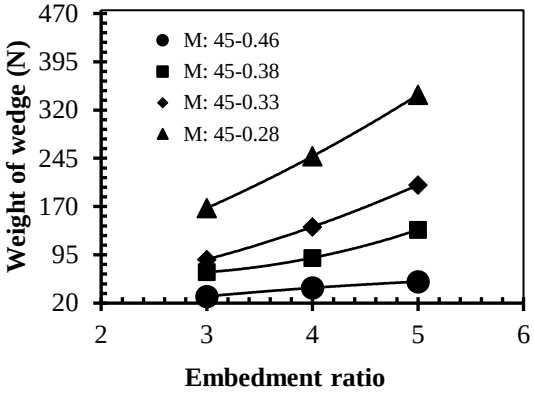


Fig.6. Weight of wedge vs. Embedment ratio curves of anchors for thickness ratio of 0.28, 0.33, 0.38 and 0.28 each at embedment ratio 3, 4 and 5

Effect of Embedment Ratio on Weight of Wedge and Mobilised Shear

For higher embedment ratio larger wedges generated than those developed at lesser embedment ratio as illustrated in "Fig.5" and already discussed in §***Effect of Embedment Ratio on Failure Surface of Model Anchor.*** The "Figs. 6 and 7" reveal that, there is a gradual increase in the values of dead weight of wedge and mobilised shear irrespectively, as embedment ratio increased from 3 to5, for each model having thickness ratio of 0.28, 0.33, 0.38 and 0.28. For example, in case of M: 45-0.46, increase in the value of embedment ratio from 3 to 5, results in enhancement of dead weight of wedge and mobilised shear from 20.11 to 63.48 N and from 8.32 to 16.09 N respectively. The failure mechanism reveals the reason of higher uplift capacity with higher embedment ratio. The calculated values reported in "Table 3" and measured values in "Table 4" explain increase in uplift capacity values because of higher embedment ratio (L/T_s, for 2D and L/D_b, for 3D model). The similar trend of increase in uplift capacity values due to higher embedment ratio was also reported by Dickin and Leung (1990). Ghosh and Bera (2010), Bera and Banerjee (2013), Bera (2014), and Nazir et al. (2014).

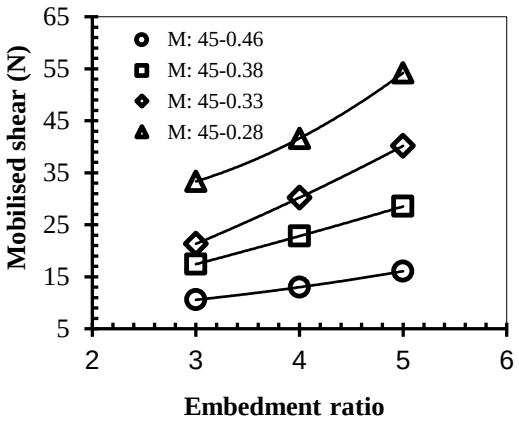


Fig.7. Mobilised shear vs. embedment ratio curves of anchors for thickness ratio 0.28, 0.33, 0.38 and 0.28 each at embedment ratio 3, 4 and 5

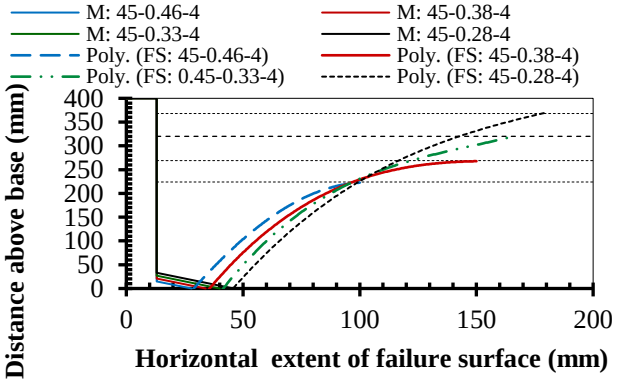


Fig.8 Embedment ratio vs. variation in failure curves of anchor for thickness ratio 0.28, 0.33,0.38 and 0.46 at embedment ratio 4

Effect of Thickness ratio on Failure Surface of Model Anchor

For certain thickness of shaft, with the increase in bell thickness (for 2D panel), thickness ratio decreases. The plots of distance above base vs. horizontal extent of failure surface due to variation in thickness ratio, for certain embedment ratio, at the respective meridian section of the anchors are presented in typical "Fig. 8"; for models M: 45-0.28, M: 45-0.33, M: 45-0.38 and M: 45-0.46 at embedment ratio 4. From the plots it is found that, for a certain value of embedment ratio, with increase in the value of thickness ratio, the depth of soil gradually decreases; hence, the overburden pressure is lesser above the anchor base than those generated for models having smaller values of thickness ratio. For example: in "Fig. 8", the volume of wedge for M: 45-0.46-4 is smallest whereas, for M: 45-0.28-4 is maximum.

Effect of Thickness ratio on Weight of Wedge and Mobilised Shear

For higher thickness ratio smaller wedges generated than those developed at lesser thickness ratio for a specified embedment ratio, as already illustrated in "Fig. 8". The "Figs. 9 and 10" show that, there is a gradual decrease in dead weight of breakout wedge and mobilised shear respectively, for models having diameter ratio 0.28, 0.33, 0.38 and 0.46, irrespective of embedment ratio 3, 4 and 5. For example, in case of models at specified embedment ratio of 4, due to increase in the value of thickness ratio from 0.28 to 0.46, results in decrease in the value of dead weight of wedge and mobilised shear from 178.24 to 28.82 N and from 35.13 to 11.59 N respectively. The failure mechanism explains the reason of lesser uplift capacity with higher thickness ratio at certain embedment ratio. The calculated values reported in "Table 3" and measured values in "Table 4" explain decrease in uplift capacity values due to higher thickness ratio (for 2D model) or diameter ratio (for 3D model). The similar trend of decrease in uplift capacity values because of higher diameter ratio was also reported by Dickin and Leung (1990).

Maximum Extent of Failure Surface at Ground Surface

The maximum horizontal extent of failure surface is located in the ground surface and its value increases with higher embedment ratio, thickness ratio as presented in "Table 3". For example, X_{max} values are increased from 140 to 200 mm for model M: 45-0.33 due to increase in embedment ratio 3 to 5. The similar trend in results were also reported by Ilamparuthi and Dickin (2001).The X_{max} values are also increased with higher thickness ratio for a certain embedment ratio; for example X_{max} values are increased from 82 to 150 mm in model M: 45-0.28 than M: 45-0.46 due to specific embedment ratio of 3.

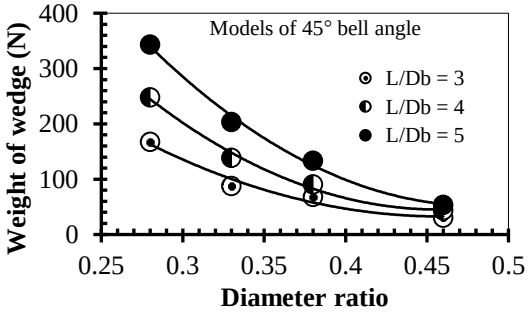


Fig.9. Weight of wedge vs. thickness ratio curves of anchors for embedment ratio 3, 4 and 5.

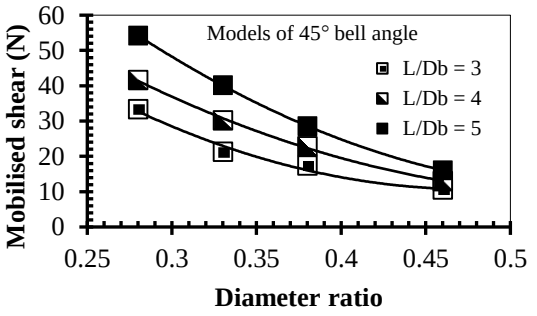


Fig.10. Mobilised shear vs. thickness ratio curves of anchors for embedment ratio 3, 4 and 5.

COMPARISON STUDY

$Q_{u,exptl.}$ represent the measured uplift capacity of the models of same scale and ratio. The $Q_{u,exptl.}$ and $Q_{u,anlyl.}$ values as well as errors (%) on $Q_{u,\ anlyl}$ data with respect to $Q_{u,\ exptl.}$ are presented in "Table 4". Among the 12 numbers of analytical data, almost all are within ± 10% variations with respect to the experimental data of uplift capacity.

Table 4 Experimental ($Q_{u,exptl.}$), analytical data ($Q_{u,anlyl.}$) of net ultimate uplift capacity and errors on experimental ($Q_{u,exptl.}$) data with respect to analytical data ($Q_{u,anlyl}$).

Sl. no	Designation.	$Q_{u, Exptl.}$ (N)	$Q_{u, Anlyl.}$ (N)	prediction Error (%)
1.	M:45-0.46-5	71.56	70.40	-01.62
2.	M:45-0.46-4	47.11	40.42	+14.19
3.	M:45-0.46-3	25.70	28.36	-10.35
4.	M:45-0.38-5	134.35	146.83	-09.29
5.	M:45-0.38-4	93.38	95.72	-02.51
6.	M:45-0.38-3	48.09	50.39	-04.79
7.	M:45-0.33-5	235.75	240.08	-01.84
8.	M:45-0.33-4	154.75	152.43	+01.50
9.	M:45-0.33-3	82.30	85.21	-03.54
10.	M:45-0.28-5	347.56	382.78	-10.13
11.	M:45-0.28-4	234.84	213.39	+09.13
12.	M:45-0.28-3	123.98	123.74	+00.19

PRACTICAL IMPLICATIONS

Here anchor installation technique describes simulates the in-situ bored anchor pile, though it can never be implemented in field. Wenbai et al. (2004) reported the uplift capacity of belled anchor pile in loess enriched with gluing property of calcium.

- A knowledge regarding soil properties in horizontal layers in field and lab modelling of those soil strata as well failure mechanism study using proposed 2D panel models may be helpful for the practicing engineers to evaluate net uplift capacity.
- This study may be a substitute of field test data. If field test data are available, then a net uplift capacity can be predicted within a close range.
- Homogenous frictional soil strata are very rear in field. In case of low lying land, fill is usually done by cohesionless soil. In those cases, the concept of higher wedge formation as well as shear mobilisation may be quite helpful.

SUMMERY AND CONCLUSION

On the basis of experimental investigations and observations, the following significant findings have listed below:

- At higher embedment ratio, larger failure wedge is formed than those formed due to lesser embedment ratio. The larger volume of wedge offers higher mobilised shear and weight of wedge.
- With increasing thickness ratio, for specific bell angle and embedment ratio, smaller breakout wedge is developed; hence lesser mobilised shear as well as wedge weight is obtained.
- The failure terminate at ground surface are generally expanding for higher embedment ratios and thickness ratio.
- Amongst the 12 numbers of data, predicted data are within ± 10% variations with respect to the experimental data of uplift capacity, which shows better correlations.
- Due to uplift of belled anchor, non-linear failure surfaces are observed. The shape can be fitted by polynomial functions.
- As there is a much difference between the initial and final angle of failure wedge. Hence it may be stated that, this failure curve is non-linear.

References

Balla, A. 1961. The resistance to breaking-out of mushroom foundations for pylons. Proceedings of 5th International Conference on Soil Mechanics and Foundation Engineering, Paris, 1 569-576.

Bera, A. K. 2014. Parametric study on uplift capacity of anchor with tie in sand. Korean Society of Civil Engineers, Springer, 18 (4) 1028-1035.

Bera, A. K. and Banerjee, U. 2013. Uplift capacity of model bell shaped anchor embedded in sand. International Journal of Geotechnical Engineering, 7(1) 84-90.

Chottapadhyay, B. C, and Pise, P. J. 1986. Breakout resistance of horizontal anchors in sand."Japanese Society of Soil Mechanics and Foundation Engineering, 26(4), 16-26.
Dickin, E.A., and Leung, C.F. 1990. Performance of piles with enlarged bases subjected to uplift forces. Canadian Geotechnical Journal, 27(5) 546-556.
Dickin, E.A., and Leung, C.F. 1992."The influence of foundation geometry on uplift behaviour of piles with enlarged bases." Canadian Geotechnical Journal, 29(3) 498-505.
Ghaly, A., and Hanna, A., 1994. Ultimate uplift resistance of single vertical anchors." Canadian Geotechnical Journal, 31 661-672.
Ghosh, A., and Bera, A. K. 2010. Effect of geotextile ties on uplift capacity of anchors embedded in sand." Geotechnical Geology Engineering, Springer, 28 567-577.
Ilamparuthi, K., and Muthukrishnaiah, K. 1999. Anchors in sand bed: delineation of rupture surface." Ocean Engineering, Elsevier, 26 1249-1273
Ilamparuthi, K., and Dickin, E.A. 2001. Predictions of the uplift response of model belled piles in geogrid-cell-reinforced sand. Geotextiles and Geomembranes, Elsevier, 19 89-109.
Ilamparuthi, K., Dickin, E.A. and. Muthukrisnaiah, K. (2002). "Experimental investigation of the uplift behavior of circular plate anchors embedded in sand." Canadian Geotechnical Journal, 39 648-664.
Jacky, J. 1944. Coefficient of earth pressure at rest. Journal of the Society of Hungarian Architects and Engineers, 355-358.
Kotter, F. 1903. Die Bestimmung des Drucks an gekru ¨mmten Gleitfla¨chen, eine Aufgabe aus der Lehre vom Erddruck, Sitzungsberichte.
Matsuo, M., 1967. Study of uplift resistance of footing. I." Soils and Foundations, 7(4) 1-37.
Meyerhof, G. G., and Adams, J. I., 1968. The ultimate uplift capacity of foundation. Canadian Geotechnical Journal, 5(4) 225-244.
Nazir, R., Moayedi, H., Pratikso, A., and Mosallanezhad, M. 2014. The uplift load capacity of an enlarged base pier embedded in dry sand. Saudi Society for Geosciences, Springer, DOI: 10.1007/s12517-014-1721-3.
Rao, K. S. S. and Kumar, J. 1994. Vertical uplift capacity of Horizontal anchors." Journal of Geotechnical Engineering, 120(7) 1134-1147.
Rowe, R. K., and Davis, E. H. 1982. "The behaviour of anchor plates in sand." Geotechnique, 32(1) 25-41.
Saeedy, H.S. 1987. Stability of circular vertical earth anchors. Canadian Geotechnical Journal, 24 452-456.
Wenbai, L., Jian, Z., and Mohr. M.T. 2004. Uplift bearing tests and calculations of belled piles in loess of arid regions. Fifth International Conference on Case Histories in Geotechnical Engineering., New York, pp. 13-17.

PULLOUT CAPACITY OF PILE GROUPS IN SAND

S. P. Mukherjee, Professor, Department of Civil Engineering, Jadavpur University, Kolkata, West Bengal, India, 9874304637, sibapriya.mukherjee@gmail.com
Smita Tung, Research Scholar, Department of Civil Engineering, Jadavpur University, Kolkata, West Bengal, India, 9126180244,smita1989smita@gmail.com

ABSTRACT
Piles are generally subjected to uplift in case of under ground and water front structures. Sometimes piles are also to resist uplift loads in transmission towers, dry rock, and so on. Experimental investigations of single piles and pile groups have been carried out using model hollow circular aluminum piles, having 25.4 mm outer diameter and lengths of 600 mm, 750 mm and 900 mm. Pile groups of 2×1 and 2×2 arrangements have been used in the experimental investigations. L/d ratio has been kept equal to 24, 30 and 36 in all the cases. All the single piles and pile groups have been tested under vertical uplift. Spacing between two piles in a group has been varied with respect to pile diameter such that spacing to diameter ratios of pile are 3, 4 and 5 in case of pile groups. An attempt has also been made to analyze those models of single piles and pile groups under vertical uplift by PLAXIS 3D software. Good analogy has been observed between the results of experimental and numerical studies. A parametric study has been carried out to observe the variation of ultimate uplift capacity of pile groups with spacing and depth of embedment. It is observed that for a particular embedment length of pile and a particular group arrangement the ultimate uplift capacity increases with increase of spacing. It is also investigated that for a particular spacing and particular group arrangement, the ultimate uplift capacity increases with increase of embedment depth. Those variations have also been presented with graphs which are generated considering non dimensional forms of parameters. The paper brings out change in pullout capacity of pile groups with spacing and embedment depth of piles.

Keywords: Uplift capacity, Spacing, PLAXIS 3D

1. INTRODUCTION

Prediction of uplift capacity of single piles and especially of pile groups is one of the most interesting areas of research in geotechnical engineering. Pile foundations are frequently used to transmit the superstructure loads to deeper strata if the subsurface soil is of inadequate strength. The worst possible case may be considered to occur when all the piles in a group subjected to uplift. In cohesionless soils, the shaft resistance is an important source of pile capacity under axial loading, especially when the pile is subjected to uplift loading. Poulos and Davis (1980) recommended estimating the uplift capacity of piles as 2/3 of the downward shaft resistance. Later Ramasamy et al. (2004) indicated that the upward shaft resistance is significantly less than the downward shaft resistance. Some studies were conducted on the behavior of a single pile under uplift loads, such as those by Sowa (1970), Vesic (1970), Das and Seeley (1976), Levacher and Sieffert (1984), Rao and Venkatesh (1985), Chattopadhyay and Pise (1986), and Shanker et al. (2007). Das et al. (1976) conducted a model study to test the uplift capacity of single piles and pile groups buried in sand, and they also determined a relationship between the efficiency of a pile group and its spacing. Chattopadhyay and Pise (1986) proposed an analytical method for predicting the uplift capacity of piles embedded in sand and obtained reasonable agreement between experimental and theoretical results. Gaaver (2013) investigated experimentally that an upward displacement of about 1.4–2.5% of the pile diameter is required to attain the net uplift capacity for both single piles and pile groups. The uplift resistance of pile groups depends on the several variables like group size, shape, spacing to diameter ratio of piles, embedment depth to diameter ratio of piles, soil type and its density and soil-pile friction angle.

In present investigation, varying the parameters such as centre to centre spacing to diameter ratio of piles, embedment depth to diameter ratio of piles, a simplified analysis has been studied to predict the uplift capacity of the single pile and group of piles. Laboratory model tests on group of piles were conducted in medium dense sand under axial uplift loads with different centre to centre pile spacing and with varied embedment length to diameter ratio. The experimental values of uplift capacity by model test results were compared with the numerical analyses done by PLAXIS 3D software to check the validity of the developed method of analysis.

2. EXPERIMENTAL STUDY

Model pile and pile groups have been studied to investigate the uplift capacity of pile and pile group embedded in sand through rational approach. The relevant parameters considered for the study were length of embedment, pile spacing for two types of pile groups- 2x1 and 2x2 groups. A constant value of shearing resistance was used throughout the investigation.

2.1 EXPERIMENTAL SET-UP

The experimental tests were performed on model piles in Fig. 1 illustrates the schematic diagram of the test setup. The experimental model was designed by appropriate dimensional analysis.

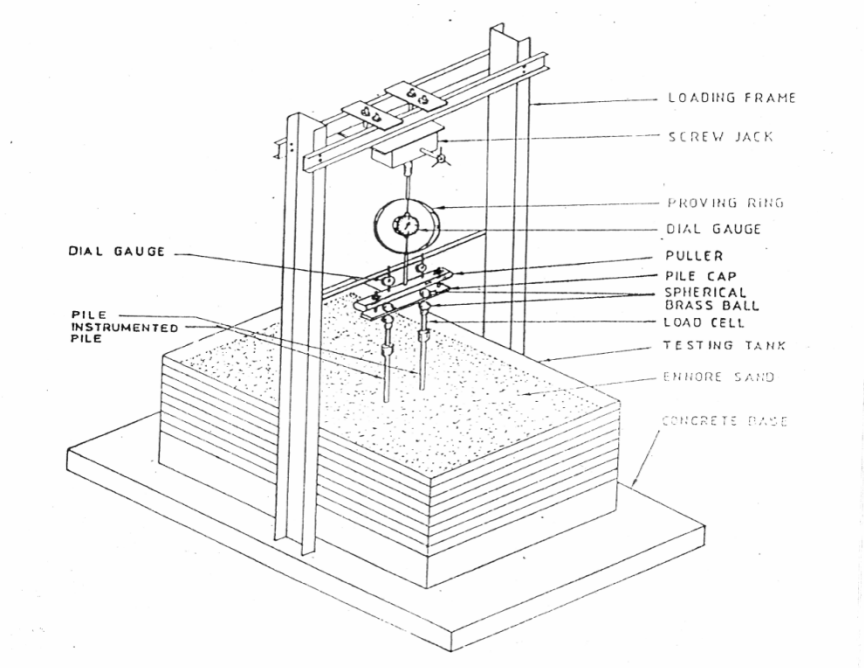


Fig.1. Schematic diagram of the experimental test setup.

2.1. Model Foundation Tank

The size of the foundation tank was fixed as 900 mm×900 mm×1100 mm deep with a view to keep adequate edge distance, avoiding boundary effects and maintaining a 200 mm thick sand cushion at the bottom of the pile.

2.2. Foundation Medium

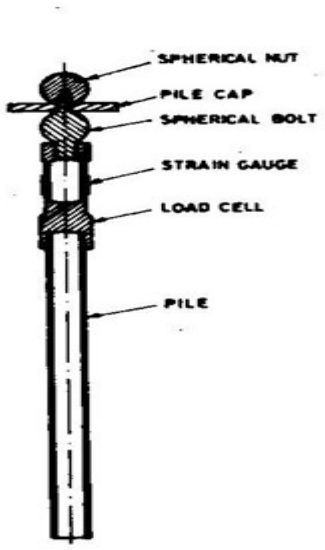
In order to carry out model studies in laboratory, uniform dry Ennore sand, obtained from Tamil Nadu was used as foundation medium for the model study in the present investigation. This sand, when poured by rainfall technique with the help of calibrated hopper with 600 mm free height of fall, yielding densities of 16.2 KN/m^3. The engineering properties of Ennore sand were determined by routine standard test in the laboratory presented in Table 1.

Table 1. Properties of sand medium

Parameter	Value
Specific Gravity, Gs	2.64
Uniformity coefficient, C_u	1.1
Placement density (γ)	16.2 KN/m^3
Relative density (D_r)	88.0%
Modulus of Elasticity (E_{soil})	82.00E+5 N/m^2
Poisson's ratio (ν)	0.3
Angle of shearing resistance (ϕ)	37°
Angle of wall friction (δ)	21°

2.3 Model piles and pile caps

Experimental investigations of single piles and pile groups have been carried out using model hollow circular aluminum piles, having 25.4 mm outer and 21mm inner diameter and lengths of 600 mm, 750 mm and 900 mm. The variation in outer diameter and surface characteristics of the instrumented pile were ignored. All the closed ended single piles and pile groups have been tested under vertical uplift. The pile caps placed 30 mm below soil surface and were modeled of aluminum plates of 10 mm thick. Details of fixing piles with pile cap have been shown in Fig. 2 and pile caps with different configuration of piles have been shown in Fig. 3.



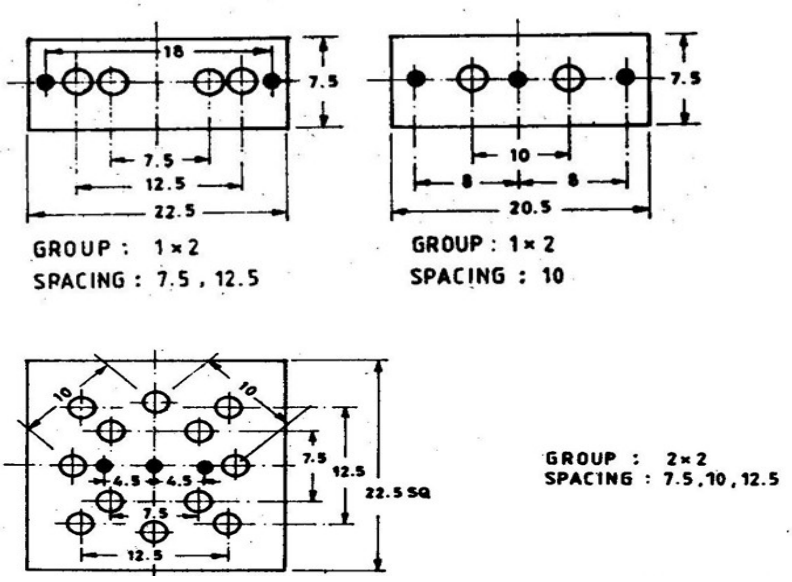


Fig.2. Sketch showing fixing arrangement of pile and pile cap

Fig.3. Sketch of pile caps for different pile group with varying spacing

2.4 Experiment on model pile

In each test, the pile or pile group was suspended centrally and vertically in the empty soil medium through the loading machine and the proving ring arrangement, as shown in Fig. 1. The pile cap with the puller was fixed to the tension proving ring attached to the screw jack. The piles with the load cells fitted at the top were then attached to the pile cap with the help of brass ball (nut), while the threaded head of the load cell passed through the holes. The verticality of the pile and pile group was confirmed by using a plumb bob. Before starting the loading, the pile or pile group verticality was rechecked, and the tilt in the pile cap was also checked using the same water level balance. Then, the uplift load was applied incrementally. A loading frame made of channel section was used for the application of the load through a jack attachment to the frame. The pulling load was applied concentrically on the pile cap, and the average value of displacement readings was considered by dial gauges. Each test was continued till failure occurred indicated by continuous pile movement with no application of uplift load.

2. NUMERICAL ANALYSIS

In order to validate the experimental study for predicting uplift capacity of pile and pile group a three-dimensional numerical analyses have been carried out with the help of PLAXIS 3D software in finite element analysis.

3.1 Finite element meshing

To perform finite element calculation, the soil pile model was discretized into smaller finite number of tetrahedral elements. The basic soil elements of 3D finite element mesh are the 10-noded tetrahedral elements. PLAXIS 3D program (Refernce: Faizi et al.) allows for a fully automatic generation of finite element meshes. In this present study uplift capacity has not been checked for higher embedment ratio, that's why Coulomb failure appears to be more appropriate. Fig. 4 and Fig. 5 represents meshing of pile group of 2×1 and 2×2 for embedment length to diameter ratio *(L/d)* = 24 and centre to centre spacing to diameter ratio*(S/d)* =3.0 respectively.

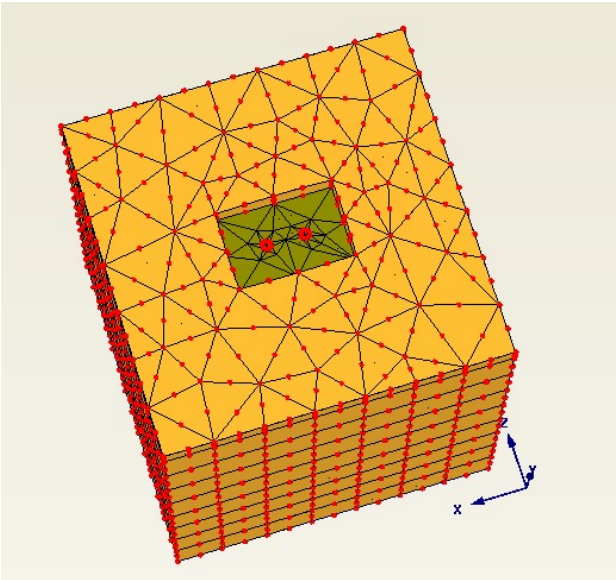


Fig.4. Pile group of 2×1 for *L/d=24* and *S/d=3*

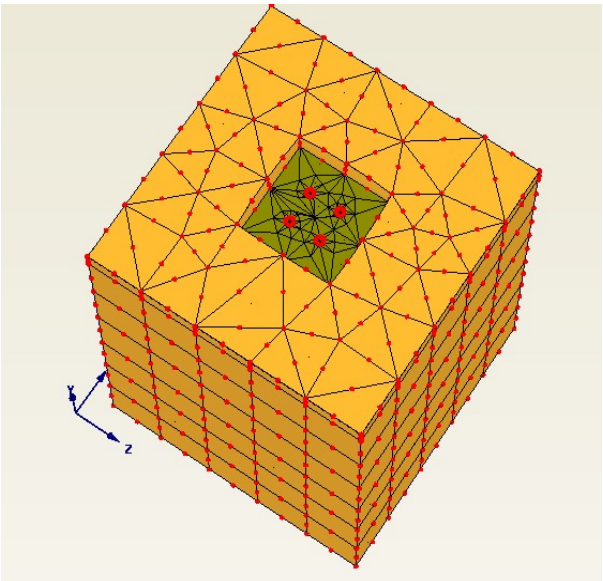


Fig.5. Pile group of 2×2 for *L/d=24* and *S/d=3*

3.2 Material Model

Mohr –Coulomb model is adopted for this finite element analysis as per first approximation of soil behavior. The model involves five parameters, i.e. Young's modulus, E, Poisson's ratio, ν, cohesion, c, internal friction angle, ø, and dilatation angle, ψ. Material nonlinearity has been considered to model the

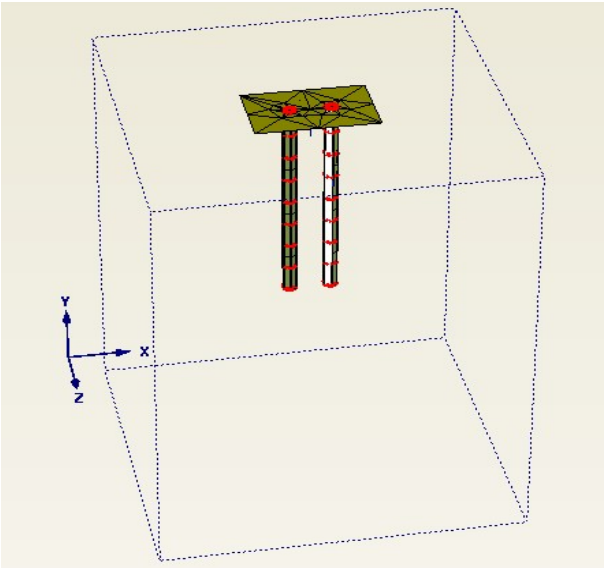
soil using Mohr –Coulomb failure theory and elastic-perfectly plastic behavior of soil. In PLAXIS 3D, for cohesion less sand , it is good to give a nominal cohesion value for numerical stability in finite element calculations otherwise truncation error may occur in numerical computation. Table 1 represents the details of soil medium used in this present numerical analysis.

3.3 Pile model

The piles are modeled as Linear Elastic Model which is governed by Hooke's law of isotropic linear elasticity. The model involves two elastic stiffness parameters, i.e. Young's modulus, E, and Poisson's ratio, ν. The model was drowning sufficiently large so that the boundaries do not influence the numerical results. Fig. 6 and Fig. 7 represent partial geometry of pile group of 2×1 and 2×2 for embedment length to diameter ratio *(L/d)* = 24 and centre to centre spacing to diameter ratio*(S/d)* =3.0 respectively. Table 2 represents the details of pile element in these present numerical analyses.

Table 2. Details of Pile Element

Parameter	Value
Unsaturated unit weight (γ)	27.8 KN/m^3
Modulus of Elasticity (E $_{pile}$)	16.2E+13 N/m^2
Angle of wall friction(δ)	21°
Poisson's ratio(ν)	0.32



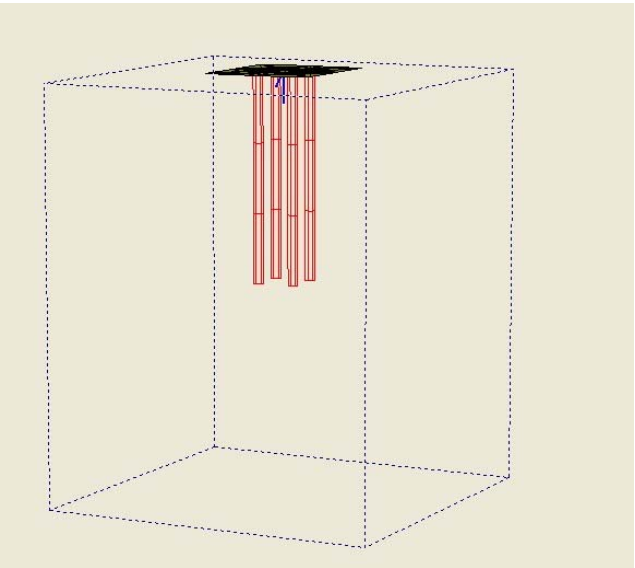


Fig.6. Pile group of 2×1 for *L/d=24* and *S/d=3* **Fig.7. Pile group of 2×2 for *L/d=24* and *S/d=3***

3.4 Constitutive modeling of sand–aluminum interface

Interfaces are to be added to allow for a proper modeling of soil-structure interaction. The stiffness of the embedded interface element does not influence the total elastic stiffness of the pile soil structure. Thus, to simulate interaction between pile elements and surrounding soil, a strength reduction factor (R_{inter}) has been adopted as main interface parameter in embedded interface properties. (Reference: PLAXIS 3D MATERIAL MODEL MANUAL, & Al-Baghdadi, 2015) and the following equation has been considered.

$$\tan(\varphi_i) = R_{inter} \tan(\varphi_{soil}) \quad (1)$$

4. PROGRAM OF EXPERIMENTAL AND NUMERICAL STUDIES

A testing program was designed to evaluate the uplift behavior of single piles and pile groups embedded in cohesion less soil with respect to various parameters, such as embedment depth-to-diameter ratio (*L*/*d*), arrangement of piles in a group and spacing to diameter ratios *(S/d)* ratio. Table 3 describes the different cases of parametric studies carried out in the experimental investigation as well as in numerical analyses by PLAXIS 3D.

Table 3. Program of experimental and numerical study

Test no.	No. of piles	*L/d*	L	*S/d*
1	Single pile	24	60	-
2	Single pile	30	75	-
3	Single pile	36	90	-
4	2×1			3
5	2×1	24	60	4
6	2×1			5
7	2×1			3
8	2×1	30	75	4
9	2×1			5
10	2×1			3
11	2×1	36	90	4
12	2×1			5
13	2×2			3
14	2×2	24	60	4
15	2×2			5
16	2×2			3
17	2×2	30	75	4
18	2×2			5
19	2×2			3
20	2×2	36	90	4
21	2×2			5

5. RESULTS AND DISCUSSION

Test results are grouped in two sets of figures representing the behavior of single piles and pile groups under uplift. During each test the uplift load was increased and corresponding axial movement of the piles and pile group was measured in stages and net uplift load vs. axial movement diagram have been plotted in each test and shown in Fig. 8 to Fig.10 with various size and geometry of the group with varying spacing and embedment length of piles. From these figures, the load movement response of piles and pile groups appears to be non linear in general.

5.1. Axial movement under uplift loading for variation of *(L/d)* ratio

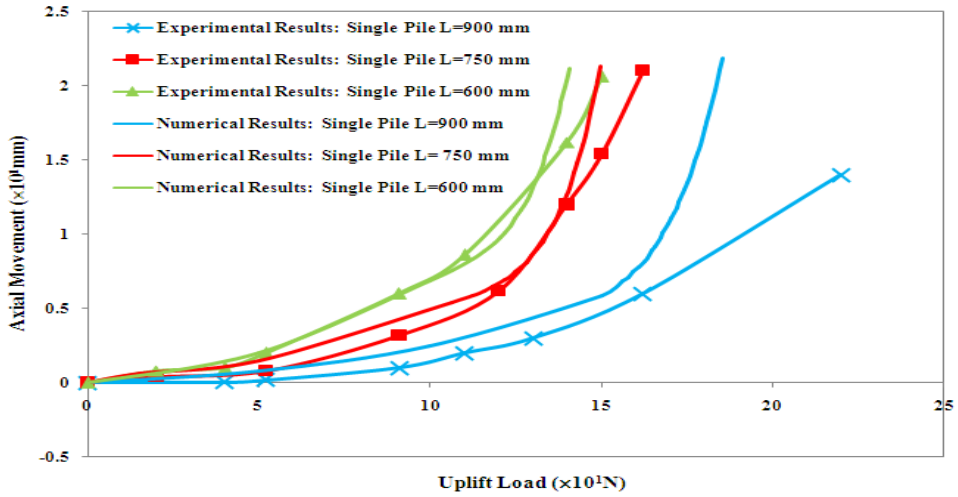


Fig.8. A typical graph showing axial movement vs. uplift load diagram for single pile

The ultimate uplift capacity has been obtained for this investigation by conventional double tangent method as each curve indicated no definite yield point, the last part being continuously curvilinear except for a very short portion at the end. It is observed from Fig. 8 that ultimate uplift load increases with increased embedded length. For single piles, the ultimate uplift capacity increased by approximately 20 to 25% for an increase of embedment ratio 24 to 30 and also from 30 to 36. It is observed that the numerical values overestimate the experimental one by approximately 15-20% only.

5.2. Axial movement under uplift loading for variation of *(S/d)* ratio

It is observed from Fig. 9 that ultimate uplift capacity increases with increased centre to centre spacing for a particular embedded depth. It is also observed that for a particular embedment length of pile and a particular group arrangement the ultimate uplift capacity increases with increase of spacing. No definite trend has been found for variation of axial movement at failure with variation of spacing for a particular embedded depth. The apparent reduction of axial movement corresponding to ultimate uplift load of the groups may also be due to the double tangent method adopted for determining the ultimate uplift load and the correspond the axial movement. In general for pile group the relative movements are found to increase with number of piles. This effect has been noticed in case of relative movements calculated either on the basis of minimum dimension or spacing.

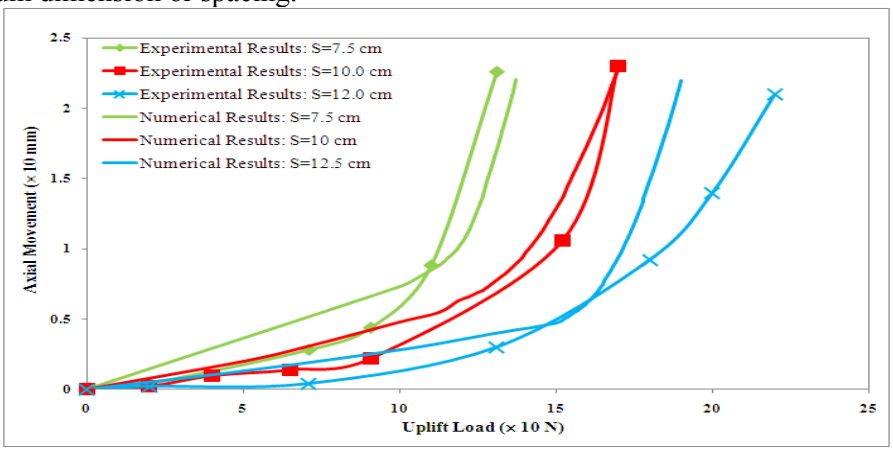


Fig.9. A typical graph showing axial movement vs. uplift load diagram of pile group 2×1

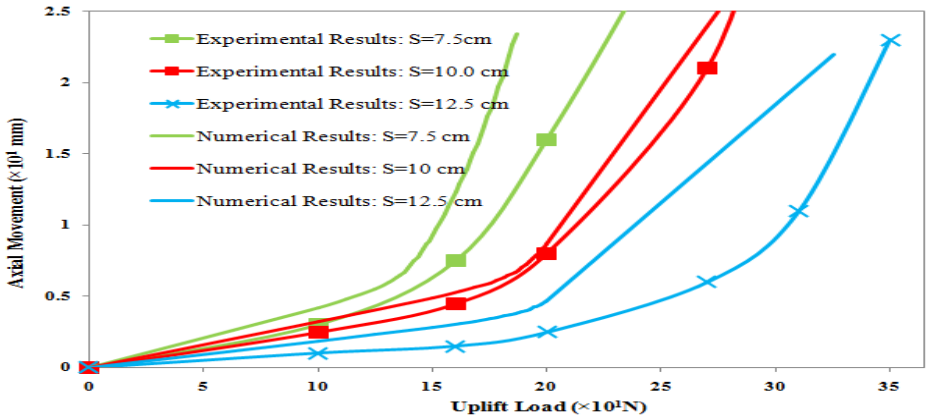


Fig.10. A typical graph showing axial movement vs. uplift load diagram of pile group 2×2

5.3 influence of non dimensional quantity *(S/d)* on normalized form of Uplift load ($P_u / \gamma L A_g$)

In this present investigation the relationship between non dimensional quantities have been studied to generate some design chart for single pile and pile groups under uplift. The ultimate load values obtained from experimental and numerical results have been normalized in the form $P_u / \gamma L A_g$. The variation of non dimensional quantity *(s/d)* with normalized form of uplift capacity $P_u / \gamma L A_g$ has been presented in Fig.11. It is also found that the normalized form of uplift capacity quantity ($P_u / \gamma L A_g$) decreases with increase on number of piles. Such decrease is noticeable in case of square group. It is observed from Fig. 11 that the normalized form of uplift capacity $P_u / \gamma L A_g$ decreases with increased value of *S/d* ratio for a particular group size. The main reason to consider the normalized form of uplift capacity $P_u / \gamma L A_g$ of an embedded pile subjected to uplift, for a fixed s/d ratio is to investigate the effect of pull out capacity against depth of embedment. For a fixed s/d ratio, uplift capacity has been increased with increment of depth of embedment. The plot of dimensionless load factor $P_u / \gamma L A_g$ against s/d ratio is a straight line. A similar trend observes in this design chart in between experimental and numerical investigation indicating minimum differences. A similarity has been observed between the predicted uplift resistances by the proposed method, Meyerhof's (1973) method.

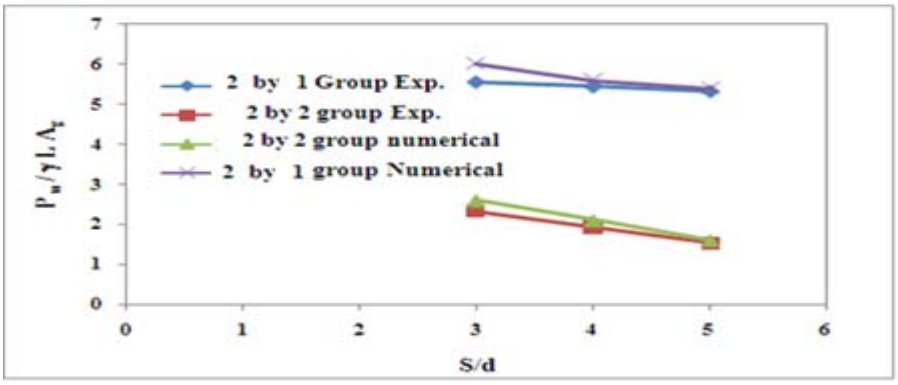


Fig.11. Variation of $P_u / \gamma L A_g$ with *S/d* ratio for pile group of 2×1 and 2×2

5.4 Failure surface

In this present investigation a typical failure surfaces obtained from test as well as numerical analyses have been shown in Fig. 12 to Fig. 14. Failure plane has been determined to the extent i.e. average of distances of breaking point of vermicelli's from the periphery of the pile. It has been observed from the figures that as L/D ratio becomes more than 6, the pattern of failure surface has been appeared as a

concave curvature and they are not found to reach higher levels. The entire failure surface started near about the pile tip with an angle of approximately (45°-φ/2) with the vertical. This indicates that the direction of major principal stress is nearly vertical. The results of the present study to predict the ultimate uplift resistance and failure surface has been compared to analysis of model piles (Chaudhuri & Symons 1983; Das 1983) as well as on driven pile (Vesic 1970), bored piles (Sowa 1970) . On scrutiny of numerical and experimental results are examined it is observed that the failure surface obtained from numerical analysis follows a logarithmic spiral and the trend is similar in case of the experimental results also.

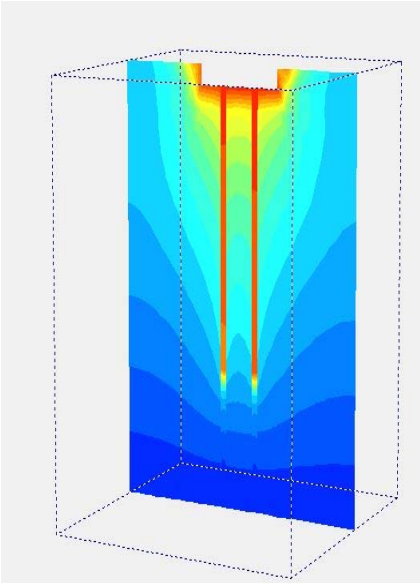


Fig.12. Failure plane contour for Pile group of 2×2 for *L/d=36* and *S/d=5 (By PLAXIS 3D)*

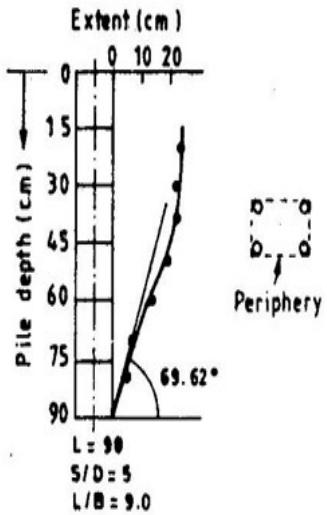


Fig.13. Failure plane of Pile group of 2×2 for *L/d=36* and *S/d=5(Experimental)*

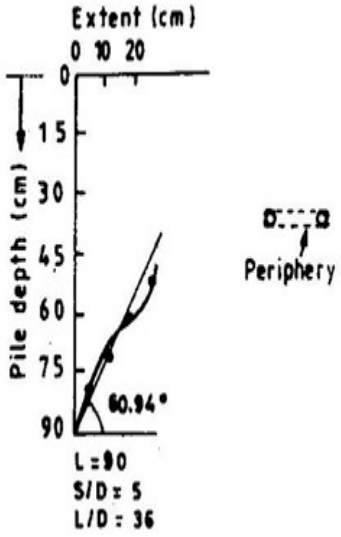


Fig.14. Failure plane of Pile group of 2×1for *L/d=36* and *S/d=5 (Experimental)*

6. CONCLUSIONS

Experiments were conducted on single piles and pile groups containing two and four piles under uplift and numerical studies were also carried out by PLAXIS 3D for the same cases. The test results are presented and discussed in this paper. Based on the foregoing study, the following main conclusions may be drawn:

1. For single piles, the ultimate uplift capacity increased by approximately 20 to 25% for an increase of embedment ratio 24 to 30 and also from 30 to 36.
2. For a particular embedment length of pile and a particular group arrangement the ultimate uplift capacity increases with increase of spacing.
3. For a particular spacing and particular group arrangement, the ultimate uplift capacity increases with increase of embedment depth.
4. Normalized form of uplift capacity $P_u / \gamma L A_g$ decreases with increased value of *S/d* ratio for a particular group size.
5. It is found that the normalized form of uplift capacity quantity ($P_u / \gamma L A_g$) decreases with increase in number of piles.
6. All the failure surfaces started near the pile tip approximately at an angle of (45°-φ/2) with the vertical, indicating that the direction of major principal stress is nearly vertical.and they follow logarithmic spiral

REFERENCES

1. 2. A.S. Vesic, Test on instrumented piles, Ogeechee River site. Journal of Soil Mechanics and Foundations Division, ASCE 96 (2) (1970) 561–584.
2. B.M. Das, G.R. Seeley, J.E. Smith, Uplift capacity of pile groups in sand. Journal of Geotechnical Engineering, ASCE 102 (3) (1976) 282–286.
3. Chattopadhyay, B.C., and Pise, P.J. (1986). Uplift capacity of piles in sand. Journal of Geotechnics Engineering, Vol.112, No.9, pp. 888-904.
4. Chaudhuri, K. P. R., and Symons, M. V. (1983). "Uplift Resistance of Model Single Piles." Proceedings of the Conference on Geotechnical Practice in Offshore Engineering, Sponsored by Geotechnical Engineering Division, ASCE, Austin, Tex., 335-355.
5. D.R. Levacher, J.G. Sieffert, Test of model tension piles. Journal of Geotechnical Engineering, ASCE 110 (12) (1984) 1735–1748.
6. G. Ramasamy, B. Dey, E. Indrawan, Studies of skin friction in piles under tensile and compressive load. Indian Geotechnical Journal, 34 (3) (2004) 276–289.
7. H.G. Poulos, E.H. Davis, Pile Foundations, Analysis and Design. first ed., John Wiley and sons, New York, NY, 1980.
8. Khaled E. Gaaver, Uplift capacity of single piles and pile groups embedded in cohesionless soil. Alexandria Engineering Journal (2013) 52, 365–372
9. K.S. Rao, K.H. Venkatesh, Uplift behavior of short piles in uniform sand. Journal of Soils and Foundations 25 (4) (1985) 1–7.
10. K. Shanker, P.K. Basudhar, N.R. Patra, Uplift capacity of pile groups embedded in sand, prediction and performance. Journal of Soils and Foundations 46 (5) (2007) 633–640.
11. T.A. Al-Baghdadi, M.J. Brown, J.A. Knappett , R. Isikura, Modeling of laterally loaded screw pile with large helical plates in sand. Frontier in offshore Geotechnics III-Meyer (Ed), 2015
12. V.A. Sowa, Pulling capacity of concrete cast in-situ bored piles. Canadian Geotechnical Journal 7 (4) (1970) 482–493.
13. K. Faizi, R. Kalatehjari, R. Nazir, A. S. A. Rashid , Determination of pile failure mechanism under pullout test in loose sand, Journal of central south University, April 2015, Volume 22, Issue 4, pp 1490–1501

NOTATIONS

The following symbols are used in this paper.

φ_i Friction angle of embedded interface

ϕ_{soil} Angle of internal friction of the soil

δ Pile-soil interface friction angle

γ Unit weight of the soil

E_{soil} Modulus of Elasticity of soil

E_{pile} Modulus of Elasticity of pile

Gs Specific Gravity

C_u Uniformity coefficient

D_r Relative density

ν Poisson's ratio

P_u Ultimate uplift capacity of pile

s Centre to centre spacing of the piles

L Embedded length of pile

d Pile diameter

SITE SPECIFIC STUDY FOR FOUNDATION DESIGN OF ISWAR GUPTA BRIDGE

Sankar Kumar Nath, Professor of Geology and Geophysics, IIT Kharagpur, INDIA, +91 9434005953, nath@gg.iitkgp.ernet.in
Ambarish Ghosh, Professor of Civil Engineering, IIEST Shibpur, INDIA, +91 9831286527, ambarish@civil.iiests.ac.in
Tarun Sengupta, General Manager, RITES Limited, Highway Division, Kolkata, INDIA, +91 9433013133, tsgcivil@yahoo.co.in
Sajib Das, Manager, RITES Limited, Highway Division, Kolkata, INDIA, +91 9433145077, sajib_d@yahoo.com
Tanumaya Mitra, Post Graduate Student, IIEST Shibpur, INDIA, +91 9674333976, tanumayamitra@gmail.com
Chitralekha Ghatak, Ph D Scholar, IIT Kharagpur, INDIA, +91 9434202845, ghatak.chitra@gmail.com

ABSTRACT

Currently construction of important structures like bridges, flyovers and high rise buildings in and around Kolkata are in full swing. These structures have mostly pile or well foundations. The design methodology and construction techniques are being employed keeping in view both the safety and economy of the project. The data presented in this investigation have been taken from Geotechnical Investigation report of Component B in connection with construction of Extradosed Cable Stayed Bridge over River Hooghly in Hooghly and Nadia district of West Bengal, India. The investigation site is located within close proximity of Eocene Hinge Zone which is being taken as the principal contributor of Earthquakes in and around Kolkata. Considering the importance of the project detailed and exhaustive geotechnical investigation has been carried out and site specific response spectra have been generated for analysis and design of the bridge.This paper presents site specific response spectra, liquefaction analysis and comparison of lateral load carrying capacity of pile using Winkler approach and IS 2911 guidelines.

Keywords: PGA, Liquefaction, Pile, Design

INTRODUCTION

Pile foundations are used to transfer the load of the super structure through soft soil deposit to deeper bearing stratum by means of skin friction or end bearing or both. Pile foundations are regarded as a safe alternative for supporting structures in seismic areas and have been used for this purpose in non-liquefying as well as liquefying soils. But their design in case of potentially liquefiable soil is quite different from that of non liquefiable soil. In liquefiable soil the progressive buildup of excess pore water pressure will cause stiffness degradation and loss of strength which in turn will induce additional shear force and bending moment in the pile. The mechanism of pile behavior in liquefying soil has been investigated by several investigators in the recent years based on observations of pile performance during earthquakes and studies in the centrifuge and Shake Table tests. Exhaustive geotechnical investigation has been carried out along the proposed alignment of the Extradosed Cable Stayed Bridge i.e., along Baropara, Bansberia ROB, Ishwar Gupta Bridge, Saraswati River to collect disturbed as well as undisturbed soil sample, to develop average soil profile and to determine the design parameters. The proposed project site is very close to Eocene Hinge Zone, which is basically a strike slip fault, capable of generating an earthquake of Mw 6.7. Thus it is evident that the proposed Bridge needs to be designed considering the adverse geo-hydrological condition as well as the earthquake aspects needing special attention following the state-of-the-art technology as guided by relevant codes and published literatures. Considering the soil profile of these locations ground response analysis has been carried out using equivalent linear method to determine the site amplification. Site specific response spectra have been developed for the four zones and zone factors have been determined. The computed zone factors are 0.198g, 0.195g, 0.195g and 0.20g for the four zones respectively, much higher than the zone factor 0.16g, which is for zone III, as stipulated in IS 1893:2002.

Depending upon the Zone factors, liquefaction and cyclic failure analysis have been carried out considering the soil type and plasticity index. Liquefaction and cyclic failure analysis have shown that soil profiles at Bansberia and Saraswati River are susceptible to liquefaction for 4.0 m to 7.0 m and 5.0 m to 8.0 m depth zones, respectively. Lateral load carrying capacity of piles have been determined using Beam on Nonlinear Winkler Foundation approach and codal provisions of IS 2911-2010 and lateral deflection of pile with or without considering liquefaction and compared for both the locations with soil susceptible to liquefaction.

SOIL PROFILE OF FOUR ZONES

Typical soil profiles of the four zones of the present site are illustrated as follows:

Baropara: Typical soil profile of Baropara consists of top surface soil followed by medium stiff, greyish brown clayey silt/sandy silt upto a depth of 5.0 m with SPT value of 5, medium stiff, dark grey clayey silt with decomposed wood upto a depth of 14.0 m with SPT value of 5 to 6 , stiff yellowish brown silty clay with fine sand and black silt kankar upto a depth of 20.0 m with SPT value 8 to 13, dark greyish brown very dense sandy silt upto a depth of 25.0 m with SPT value 12 to 79, hard, brownish grey silty clay/clayey silt upto 34.0 m with SPT value 39 to 55 and Dense, greyish brown sandy clayey silt upto a depth of 40.0 m with SPT value 48 to 100.

Bansberia ROB: Typical soil profile of Bansberia ROB consists of top surface soil followed by medium stiff deep grey silty clay with little fine sand upto a depth of 3.0 m, Loose, greyish brown sandy silt with lump of clay upto 7.0 m with SPT value 5, Medium stiff, deep grey silty clay/clayey silt with decomposed wood upto 16.0 m with SPT value 5 to 9, stiff to very stiff, grey with brown lamination silty clay upto 20.0 m with SPT value 21 to 23, Medium dense, greyish brown silty sand upto 22.0 m with SPT value 28, Very stiff, yellowish brown silty clay with kankar upto 31.0 m with SPT value 18 to 27, and too hard, brown silty clay/clayey silty upto a depth of 40.0 m with SPT value 41 to 48.

Ishwar Gupta Bridge: Typical soil profile of Ishwar Gupta Bridge consists of top surface soil followed by filled up ground comprising cinder, sand upto 4.5 m with SPT value 5 to 8, medium stiff, yellowish brown clayey silt with traces of fine sand upto 8.5 m with SPT value 7, loose to medium dense, dark grey sandy silt upto 11.0 m with SPT value 7 to 11, medium to stiff, brownish grey silty clay/clayey silt with semi decomposed wood upto 18.0 m with SPT value 7 to 9, stiff bluish grey silty clay upto 20.0 m with SPT value 16, very stiff, yellowish brown with grey lamination, clayey silt/silty clay with little fine sand and calcareous nodules upto 34.0 m with SPT value 21 to 27, too hard, brownish grey clayey silt with calcareous nodules upto 38.5 m with SPT value 66 and very stiff deep grey clayey silt/silty clay with traces of fine sand upto 40.0 m.

Saraswati River: Typical soil profile of Saraswati River consists of top surface soil followed by soft/very loose, light brown clayey silt/sandy silt upto 4.0 m with SPT value 2, very loose deep grey silty fine to medium sand/sandy silt upto 9.0 m with SPT value 2, stiff to very stiff, yellowish grey silty clay/clayey silt with little calcareous nodules upto 16.5 m with SPT value 13 to 52, very stiff, yellowish brown clayey silt/silty clay with fine sand, black silt kankars upto 33.0 m with SPT value 15 to 26, and hard to too hard greyish brown clayey silt with some calcareous nodules with intermittent sand pockets upto 40.0 m with SPT value 45 to 54.

Hence, from the soil profile data of the four zones (about 18 number of bore holes were analysed) discussed above, it is evident that both cohesive as well as non plastic, cohesionless soils are present.

SITE SPECIFIC RESPONSE SPECTRA

The city of Kolkata, one of the most urbanized and densely populated regions in the world has developed primarily along the eastern bank of the River Hooghly about 150 km north of the Bay of Bengal. The

major tectonic framework of Eocene Hinge Zone, Main Boundary Thrust (MBT), Main Central Thrust (MCT), Main Frontal Thrust (MFT), Dhubri Fault, Dauki Fault, Oldham Fault, Garhmoyna–Khandaghosh Fault, Jangipur-Gaibandha Fault, Pingla Fault, Debagram-Bogra Fault, Rajmahal Fault, Malda-Kishanganj Fault, Sainthia-Bahmani Fault, Purulia Shear Zone, Tista Lineament, and Purulia Lineament in an around Bengal Basin pose seismic threat to Kolkata and its adjoining region. The response of man-made structures during earthquakes is significantly controlled by two major factors viz. the earthquake ground motion and the local site conditions. A Maximum Earthquake of magnitude Mw 6.7 is predicted in the region with a return period of 475 years with 10% probability of exceedence in 50 years (Maiti et al., 2016) from within an epicentral distance of about 100km which is considered as Design Basis Earthquake (DBE). The input ground acceleration is synthesized using stochastic modeling package EXSIM with the source parameter extracted from the Global Centroid Moment Tensor (GCMT) catalog at engineering bedrock for the large magnitude Far-Field earthquakes viz. 1934 Bihar-Nepal of Mw 8.1, 2015 Nepal-Gorkha Earthquake of Mw 7.9, and moderate magnitude Near-Field earthquakes like 1964 Sagar Island earthquake of magnitude Mw 5.4. In the present study considering the Probabilistic Seismic hazard analysis of the region DBE generated Design spectra has been used as it covers nearly all the expected response spectra of ground motions from multiple sources based on the cumulative risk for all significant seismic sources (Lew & Neim 1996). Stochastic approach provides expedient methods of synthesizing strong ground motion and is modeled with Gaussian noise using a spectrum that is either empirical or physical representing the earthquake source (Nath et al., 2008). The representative time history as simulated for these earthquakes at Bansberia, Hooghly is presented in Figure 1. The surface geology and soil condition at a site have significant effects on the level of ground shaking which necessitates site response analysis through a 1-D sediment column by performing nonlinear analysis through DEEPSOIL (Hashash et al., 2011) at four project sites viz. Bansberia, Baropara Jn., Iswar Gupta Bridge and Saraswati River as presented in Figure 2. The design response spectra defined as a smoothened plot of maximum acceleration asa function of frequency or time-period of vibration for 5% damping ratio for earthquake excitations at the base of a single degree of freedom system. They are useful in analyzing the performance of structures under earthquake loading. The procedure for the development of design response spectra as given by Indian Building code (IBC, 2006) anchors the spectral shape to the peak ground acceleration (i.e. zero period spectral acceleration or effective peak ground acceleration). In the present study, the Design response spectra have been generated using PSA at 1.0 sec and 0.2 sec with 10% probability of exceedence in 50 years for the selected site at surface levels as presented in Figure 3.

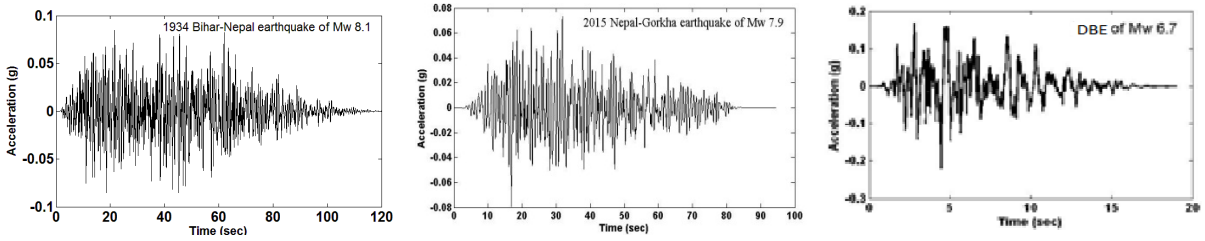


Fig.1. Representative acceleration time history for 1934 Bihar-Nepal, 2015 Nepal-Gorkha earthquake and Design Based Earthquake for Eocene Hinge Zone at bedrock level at Bansberia, Hooghly.

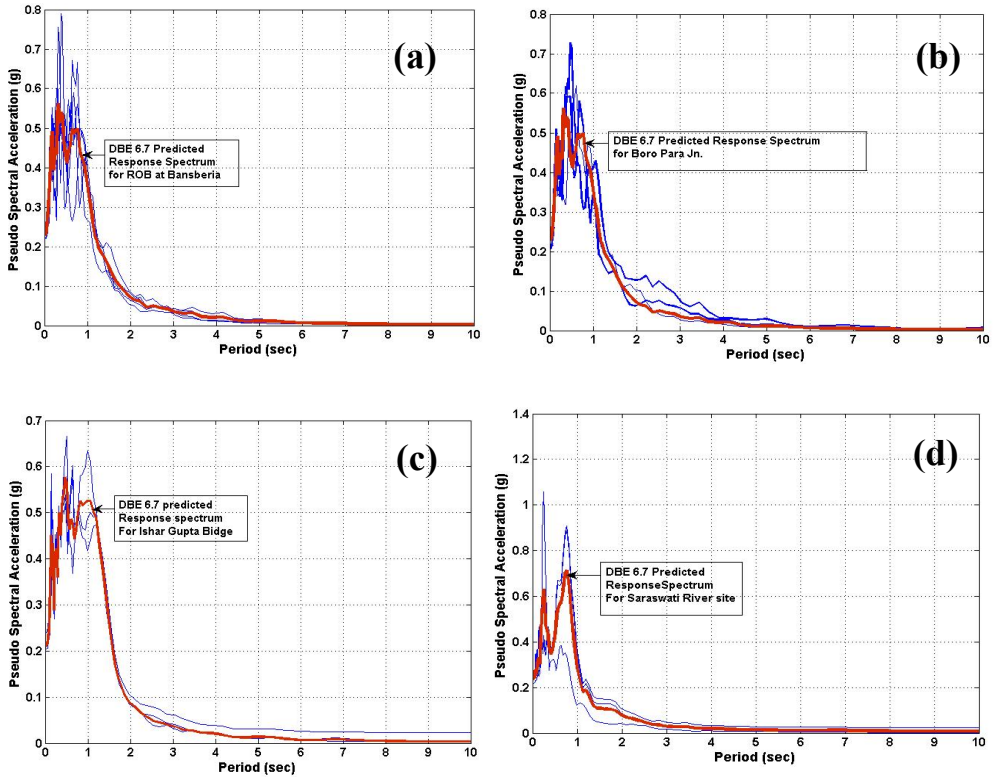


Fig. 2. Representative Design Based Earthquake based Response Spectrum at (a) Bansberia, (b) Baro Para Jn (c) Iswar Gupta Bridge, (d) Saraswati River

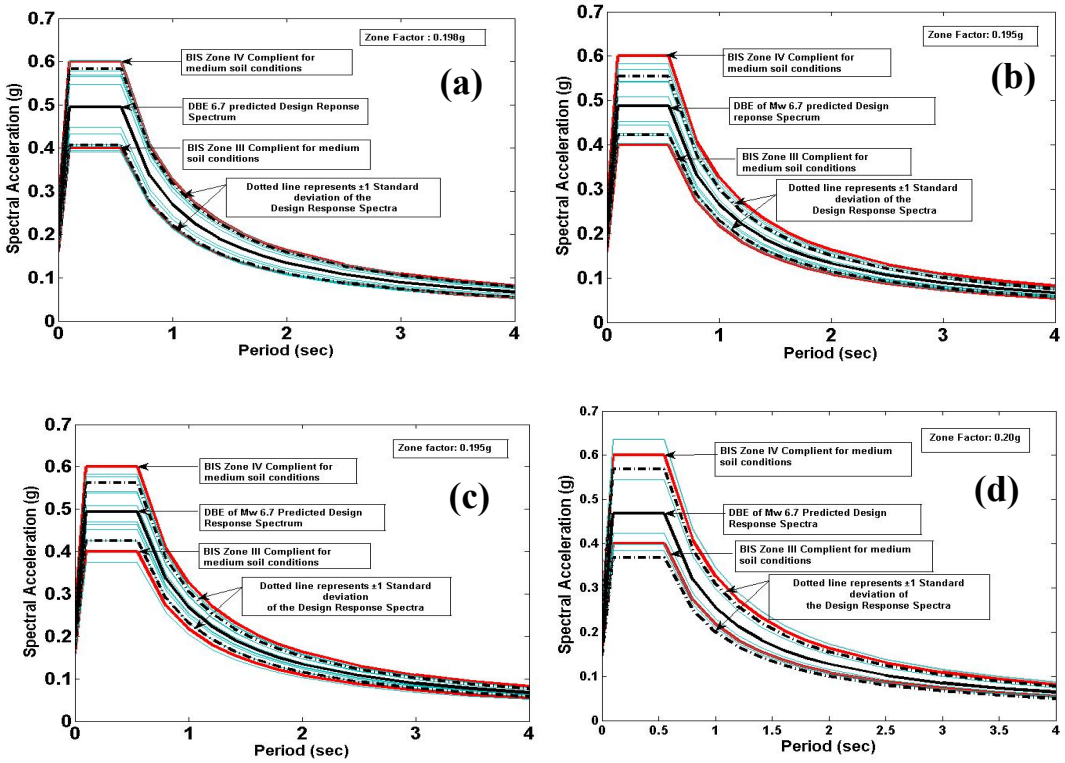


Fig. 3. Representative Design Based Earthquake based Design Response Spectrum at (a) Bansberia, (b) BaroPara Jn., (c)Iswar Gupta Bridge, (d) Saraswati River

LIQUEFACTION AND CYCLIC FAILURE ANALYSIS

Liquefaction is a major hazard during earthquakes. For carrying out any important civil engineering project in moderate to highly active seismic region, liquefaction analysis is imperative. After carrying out liquefaction analysis, if the existing soil is found to be potentially liquefiable, then various mitigation strategy can be applied or the deep foundation system has to be designed considering the zone of liquefaction. A number of investigations have been reported correlating the liquefaction potential of a site with in situ tests. Boulanger and Idriss (2006) recommended that, for practical purposes, fine-grained soils can be expected to exhibit clay like behavior if they have PI≥7 and sand like behavior if PI<7. The most used methods for determining liquefiability are the in-situ Standard Penetration Test (SPT) and Cone Penetration Test (CPT). Of these, the SPT presents a dynamic load to the soil while CPT a continuous push, therefore, the SPT should be more likely to pick out a liquefiable soil. For soils that behave more fundamentally like sands (PI<7), the cyclic strengths may be more appropriately estimated within the framework of existing standard penetration test (SPT) and cone penetration test (CPT) based liquefaction correlations. For soils that behave more fundamentally like clays (PI≥7), the cyclic and monotonic undrained shear strengths are closely related and show relatively unique stress-history-normalized behaviors. Their cyclic strengths can be estimated based on in-situ testing, laboratory testing, and empirical correlations.

Standard Penetration Test (SPT) Based Liquefaction Triggering Procedure

The original work for SPT was by Seed and Idriss (1971), and perhaps the most up-to-date version was presented by Idriss and Boulanger (2014). The method works by estimating the expected resistance of the soil, the "cyclic resistance ratio" or CRR, and the expected load on the soil, the "cyclic stress ratio" or CSR. The ratio between these is the factor of safety against liquefaction. Recommended criteria for SPT based evaluation of liquefaction resistance are largely incorporated with the Cyclic Stress Ratio versus $(N_1)_{60}$. The value of $(N_1)_{60}$ is the corrected SPT blowcount that can be calculated using the following Equation

$$(N_1)_{60} = N_m C_N C_E C_B C_R C_S$$

Where, N_m is the measured penetration resistance, C_N is the factor to normalized N_m to a common reference effective overburden stress (100 kPa), C_E, C_B, C_R, and C_S are the correction for hammer energy ratio, borehole diameter, rod length, and sample with or without liners, respectively.
$(N_1)_{60cs} = (N_1)_{60} + \Delta(N_1)_{60}$, where $\Delta(N_1)_{60}$is a function of Fines Content of soil.
Based on this method for a given earthquake magnitude (valid for < 7.5) the factor of safetyagainst liquefaction can be determined (Youd and Idriss 2001), where the CRR is a function of $(N_1)_{60cs}$.

Cyclic Failure of Cohesive Soil

Fine grained soils such as silts, clayey silts and sands with fines and silty clay soils were considered non-liquefiable in the past. But the observations following the Haicheng (1975) and Tangshan (1976) earthquakes indicate that many cohesive soils had liquefied. The experience during Aadapazari and the Koceli (1999) earthquakes indicates that soils with PI more than 7 may also be prone to liquefaction. The soils with PI=18 have been found susceptible to liquefaction during the 2007 earthquake in Iran. Cyclic softening is a term used to describe liquefaction-like behavior in clays. It involves cyclic pore pressure induced softening and strength loss. However, peak pore pressure ratios in clays are typically smaller than those in sands, and accordingly the characteristics of the cyclic stress–strain responses differ.
For clean non-plastic saturated silts, the behavior under cyclic loading and nature of generation and buildup of pore-pressure should be expected to be about the same as that for clean sands. If, however a small fraction of highly plastic material is added to non-plastic silt, one of two things may happen:

1. The rate of buildup of pore water pressure may increase because the addition of clay fraction will reduce the hydraulic conductivity of the soil, which may lead to higher pore water pressures.
2. Plasticity of clay fraction will impart some cohesion to the soil which may increase the resistance of the soil to liquefaction.

Boulanger and Idriss (2004, 2007) have recommended guidelines for estimation of the CSR and CRR for cohesive soil to evaluate the cyclic failure of cohesive soils. In this method, the CRR of soil can be determined empirically based on Undrained shear strength profile of soil.

TYPICAL LIQUEFACTION AND CYCLIC FAILURE ANALYSIS OF FOUR ZONES

Liquefaction analysis has been carried out for cohesionless soils exhibiting sand like behavior (i.e. PI<7) using SPT based framework and cyclic failure or cyclic softening analysis has been carried out for cohesive, plastic soils exhibiting clay like behavior (i.e. $PI \geq 7$). Four zones were investigated for determining the probable extent of liquefaction and cyclic softening. Plasticity Index of soil has been used as the criteria, whether to use SPT based framework or Undrained shear strength based framework for Liquefaction and/or Cyclic failure analysis. Factor of Safety value against depth for proposed sites has been depicted in Figure 4 and susceptibility criteria checks have been shown in Figure 5-8.

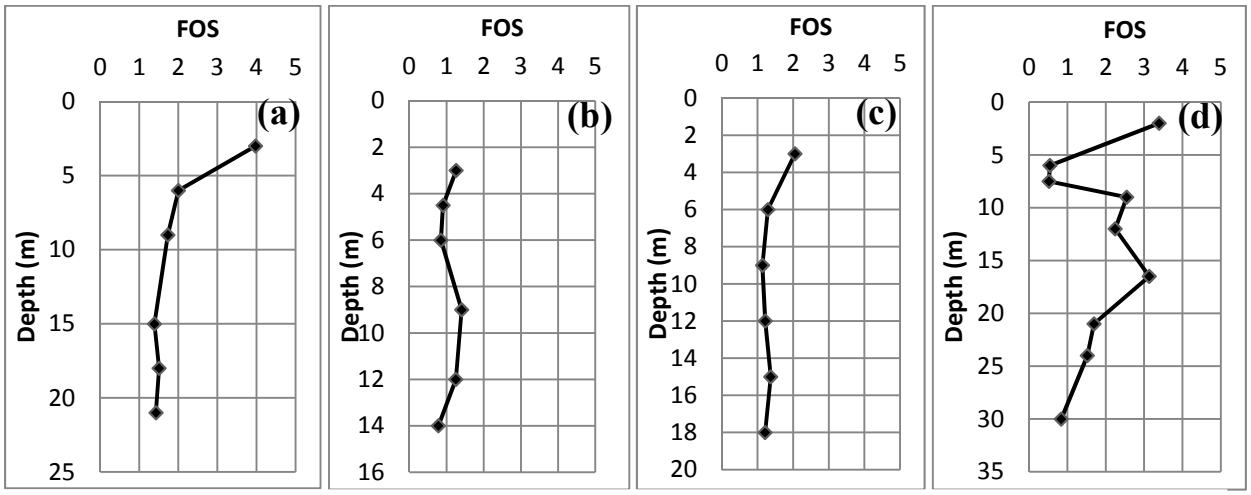


Fig. 4. Factor of safety vs Depth – (a) Baropara, (b) Bansberia ROB, (c) Ishwar Gupta Bridge, (d) Saraswati River

From the liquefaction and cyclic failure analysis, it has been found from Figure 4 (a-d) that the Bore holes located in Baropara and Ishwar Gupta Bridge are not susceptible to liquefaction and cyclic softening as indicated in Figure 4a, 4c, 5 and 7 respectively. But for Bansberia ROB, factor of safety value against liquefaction at a depth range of 4 m to 7 m is less than 1 as depicted in Figure 4b, indicating liquefiable condition at this depth. The FOS value at depth 14 m is also less than 1 but susceptibility criteria at this depth shows that Plasticity Index of soil is 22%, outside the liquefaction susceptibility criteria as per Bray and Sancio (2006) as presented in Figure 6. For Saraswati River, the FOS is less than 1 for a depth range of 5 m to 8 m as shown in Figure 4d, indicating liquefiable condition because of the presence of very loose silty sand as presented in Figure 8.

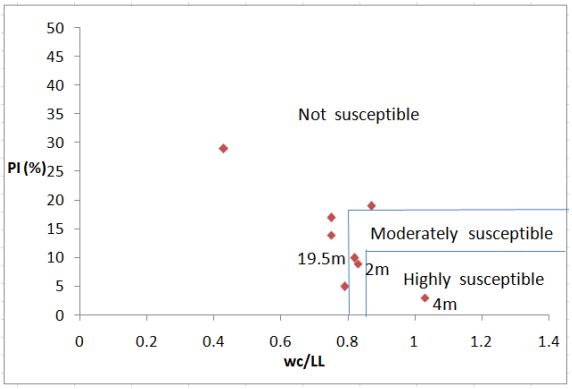


Fig. 5.Susceptibility Criteria Check – Baropara

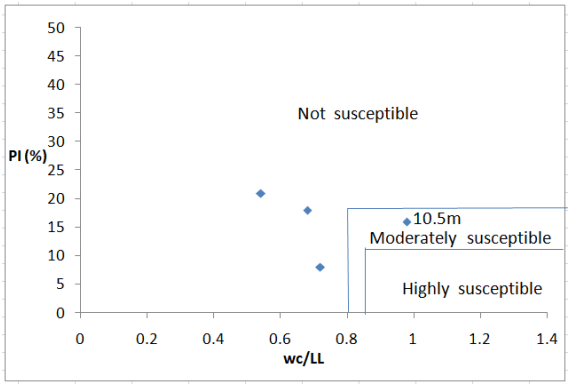


Fig. 6.Susceptibility Criteria Check – Bansberia ROB

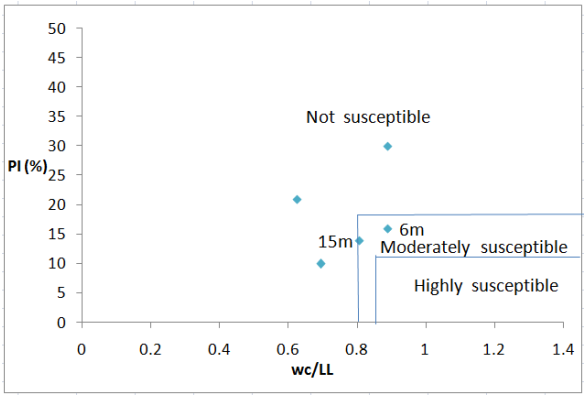


Fig. 7.Susceptibility Criteria Check – Ishwar Gupta Bridge

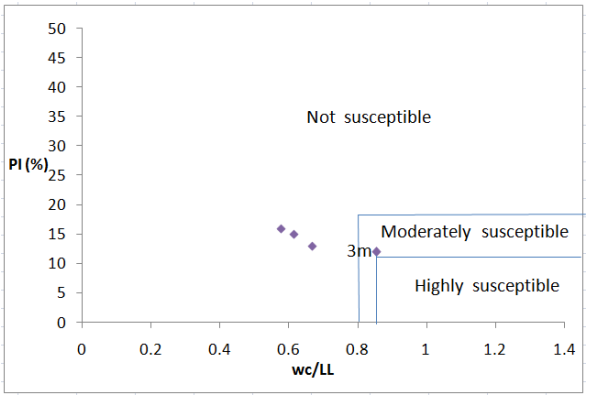


Fig. 8.Susceptibility Criteria Check – Saraswati River

LATERAL LOAD CARRYING CAPACITY OF PILE

Any bridge pier may be subjected to lateral load due to Wind load, Braking of vehicles, Earthquake load, Centrifugal force acting at curves etc. Ultimately the load will be transferred to the soil by means of pile foundation. Hence, determination of lateral load carrying capacity of piles is very much important for design of pile foundation.

Methods Adopted for Determining Lateral Load Carrying Capacity of Pile

Attempt has been made to determine the Lateral load carrying capacity of piles using Winkler Model i.e. by replacing the soil surrounding the pile by a series of non linear Winkler springs and by using IS 2911-2010. Suitable subgrade modulus has been determined for each spring as shown in Figure 9.



Fig. 9. Winkler Model of Laterally Loaded Pile without considering Liquefaction

Description of Model with Boundary Conditions

The soil has been assumed to be equivalent to an infinite number of elastic springs. This assumption is sometimes referred to as the Winkler foundation. The elastic constant of these assumed springs is referred to as the coefficient of subgrade reaction, k. The pile has been taken as a beam element. The base of the pile is fixed in the horizontal and vertical directions i.e. at the bottom of the pile, hinged support has been used, whereas at the top end fixed support has been used with release in X direction (in the direction of applied load).

Calculation for Modulus of Subgrade Reaction- Spring Values

Modulus of Subgrade Elasticity for clay has been determined by using, Es = 150 C_u (J.E. Bowles, 1997), where Cu is the undrained cohesion value and for clayey sand, Es = 300 (N+6); N is the observed SPT blow count and Modulus of subgrade reaction Ks = $\frac{E_s}{B(1-\mu^2)}$,where, μ is the Poisson's ratio and B is the width of footing, in this case diameter of pile.While determining the lateral load carrying capacity of pile using IS 2911-2010, the modulus of subgrade reaction values have been determined using Table 3 and Table 4 of IS 2911-2010 (Part I/Sec 2).

Lateral Deflection and Lateral Load Carrying Capacity of Piles (Without Considering Liquefaction for Bansberia ROB and Saraswati River)

Lateral deflection of pile has been determined by applying a concentrated horizontal load at the top of the pile (i.e. at the cut-off level, which is 3.0 m below E.G.L.) and the corresponding deflection value at the top has been measured. The load value corresponding to a deflection equals 1% diameter of pile has been taken as the lateral load carrying capacity of the pile. Lateral deflections of piles are presented in Figures 10-13 and lateral load carrying capacity of the piles has been shown in Table 1.

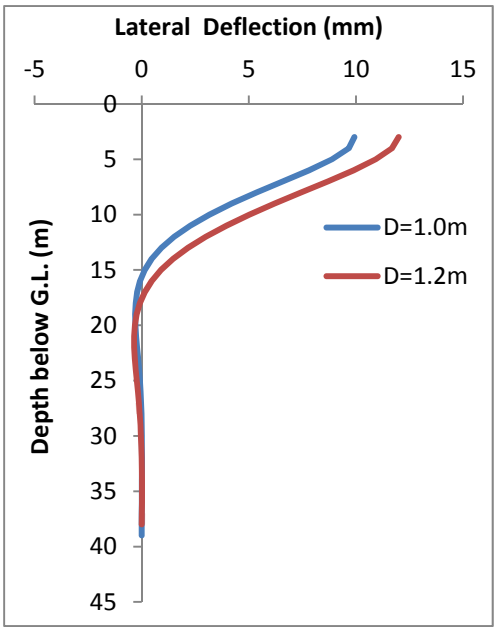


Fig. 10. Pile Deflection vs Depth for Baropara (Lateral Load=255 kN for D=1.0 m and 380 kN for D=1.2 m)

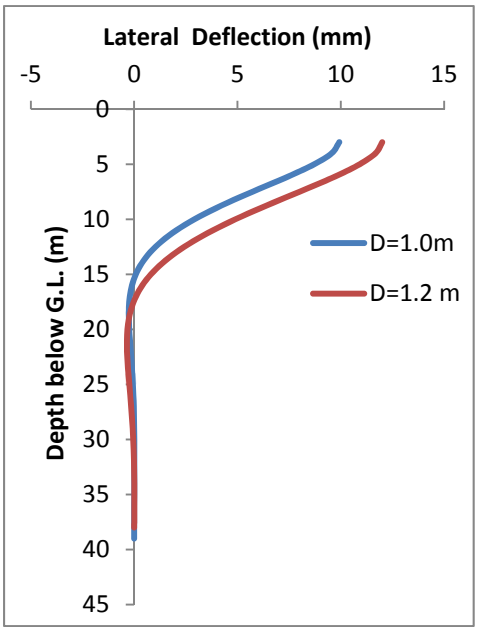


Fig. 11. Pile Deflection vs Depth for Bansberia ROB (Lateral Load=262 kN for D=1.0 m and 392 kN for D=1.2 m)

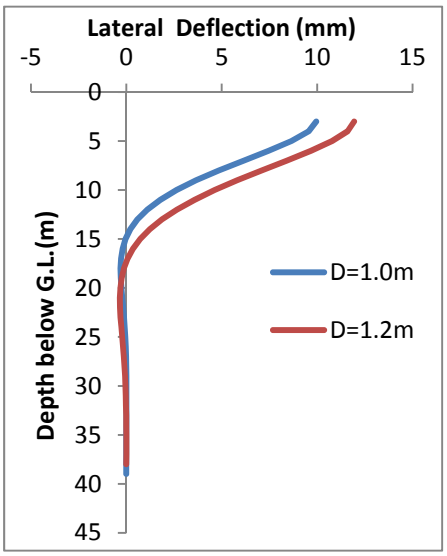


Fig. 12. Pile Deflection vs Depth Ishwar Gupta Bridge (Lateral Load=295 kN for D=1.0 m and 442 kN for D=1.2 m)

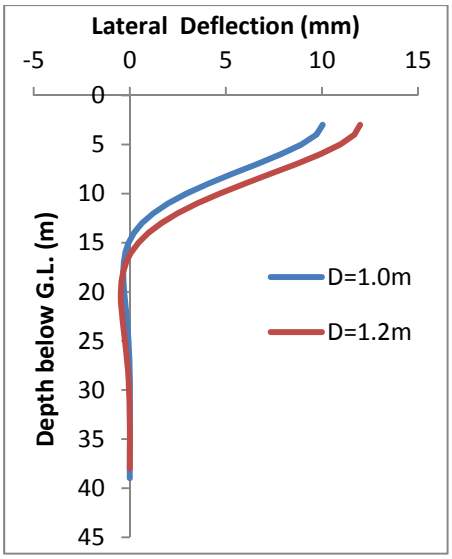


Fig. 13. Pile Deflection vs Depth Saraswati River (Lateral Load=262 kN for D=1.0 m and 393 kN for D=1.2 m)

Table 1. Comparison of Lateral Load Carrying capacity of pile using Winkler Model and IS 2911-2010 for allowable deflection equal to 1% pile diameter at the top of pile (ignoring liquefaction depth for Bansberia and Saraswati River)

Location	Pile Diameter	Embedded length	Lateral load for allowable deflection of 1% pile diameter Using Winkler Model	Lateral load for allowable deflection of 1% pile diameter Using IS 2911,2010 (Part 1/sec 2)
Baropara	1.0 m	36 m	255 kN	178kN
Bansberia ROB			262 kN	116kN
Ishwar Gupta Bridge			295 kN	193kN
Saraswati River			262 kN	76kN
Baropara	1.2 m	36 m	380 kN	251 kN
Bansberia ROB			392 kN	186kN
Ishwar Gupta Bridge			442 kN	278kN
Saraswati River			393 kN	122kN

Lateral Deflection and Lateral Load Carrying Capacity of Piles (Considering Liquefaction for Bansberia ROB and Saraswati River)

For Bansberia ROB and Saraswati River, soil is liquefiable for a depth of 4 m to 7 m and 5 m to 8 m, respectively. Hence, lateral load carrying capacity of pile for these locations have been determined using codal provision of IS 2911-2010 as shown in Figure 15 and Figure 16 respectively, which says that the lateral resistance of soil susceptible to liquefaction should be ignored. So, while determining the lateral load carrying capacity of pile in these two locations, the stiffness values of springs within the zone of liquefaction have been assumed as zero as depicted in Figure 14. Comparison of Lateral Load Carrying capacity of pile using Winkler Model for allowable deflection equal to 1% pile diameter at the top of pile for these two locations (ignoring and considering liquefaction) has been presented in Table 2.



Fig. 14. Winkler Model of Laterally Loaded Pile considering Liquefaction

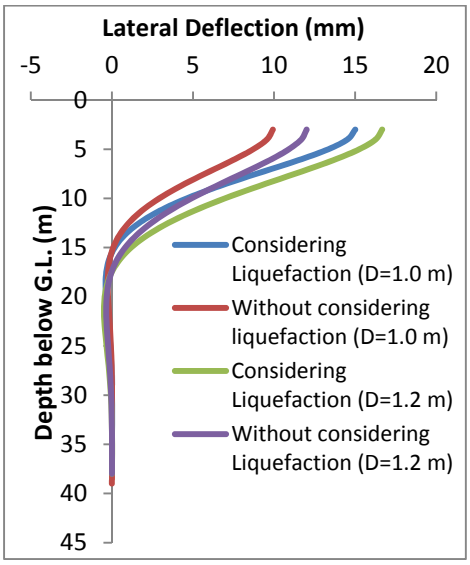


Fig. 15. Pile Deflection vs Depth for Bansberia ROB (Lateral Load=262 kN for D=1.0 m and 392 kN for D=1.2 m)

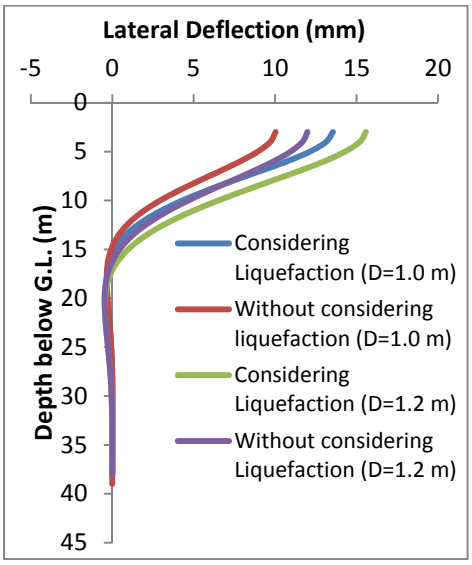


Fig. 16. Pile Deflection vs Depth for Saraswati River (Lateral Load=262 kN for D=1.0 m and 393 kN for D=1.2 m)

Table 2. Comparison of Lateral Load Carrying capacity of pile using Winkler Model for allowable deflection equal to 1% pile diameter at the top of pile (Considering and Ignoring Liquefaction depth)

Location	Pile Diameter	Embedded Length	Lateral Load without considering liquefaction	Lateral Load considering liquefaction
Bansberia ROB	1.0 m	36.0 m	262 kN	175 kN
	1.2 m		392 kN	282 kN
Saraswati River	1.0 m		262 kN	192 kN
	1.2 m		393 kN	305 kN

SUMMARY AND CONCLUSION

In this paper an effort has been made to develop site specific response spectra for four zones along the proposed alignment of the proposed cable stayed bridge considering seismicity of the region and

importance of the project. From the site specific response spectra generated, it is evident that the site specific zone factors came out to be much higher than the zone factor value of 0.16 for zone III as indicated in IS 1893-2002.The zone factors came out to be 0.198g, 0.195g, 0.195g and 0.20g for the four zones, i.e. Bansberia, Baropara, Ishwar Gupta Bridge and Saraswati river, respectively. From Liquefaction and cyclic failure analysis carried out using site specific zone factors, it has been observed that the soil profile of Bansberia and Saraswati River are susceptible to liquefaction for a depth range of 4.0 m to 7.0 m and 5.0 m to 8.0 m, respectively, because of the presence of loose to very loose silty sand. Comparison of lateral load carrying capacity of piles using Beam on non linear Winkler Foundation (BNWF) approach and IS 2911-2010 (part I/sec 2) has been carried out for these four zones. From the comparison it has been found that the lateral load carrying capacity of pile considering Winkler approach is much higher than the values obtained using IS 2911-2010 (Part I/Sec 2). For Bansberia ROB and Saraswati River, lateral load carrying capacity of pile has been determined considering both liquefiable and non liquefiable conditions. For Bansberia ROB, lateral load carrying capacity of pile got reduced to 175 kN from 262 kN and to 282 kN from 392 kN, for 1.0 m and 1.2 m of pile diameter, respectively, and for Saraswati River, capacity got reduced to 192 kN and 305 kN from 262 kN and 393 kN, for 1.0 m and 1.2 m diameter pile, respectively, when liquefaction depth was taken into account. Hence, engineering judgement has to be used carefully while finalizing the final lateral load carrying capacity of the piles.

REFERENCES

Boulanger, R. W., and Idriss, I. M. (2004). "Evaluating the potential for liquefaction or cyclic failure of silts and clays." *Rep. UCD/CGM-04/01*, Center for Geotech. Modeling, Univ. of Calif., Davis, Calif.

Boulanger, R. W. and Idriss, I. M. (2006) "Liquefaction susceptibility criteria for silts and clays," Journal of Geotechnical and Geoenviromental Engineering, ASCE, Vol. 132 No. 11, pp. 1413-1426.

Bowles, J. E. (1997), Foundation Analysis and Design, McGraw Hill Book Co. New York.

Bray, J. D. and Sancio, R. B. (2006). "Assessment of the liquefaction susceptibility of fine-grained soils," Journal of Geotechnical and Geoenvironmental Engineering, ASCE, Vol. 132, No. 9, pp. 1165-1177.

Hashash, Y. M. A., D. R.Groholski, C. A. Phillips, D. Park, and M. Musgrove (2011).DEEPSOIL 5.0, user Manual and Tutorial, University of Illinois, Urbana, IL, USA.

Idriss, I.M and Boulanger, R.W (2014) "CPT And SPT Based Liquefaction Triggering Procedure". Centre for Geotechnical Modelling, University of California at Berkeley,

IS: 2911 Code of Practice for Design and Construction of Pile Foundations.

Lew, M. and F. Naeim (1996). Use of design spectrum-compatible time histories in analysis of structures, 11th world conference on Earthquake engineering, ELSVIER.

Nath, S. K., K. K. S. Thingbaijam, and A. Raj (2008).Earthquake hazard in the northeast India – A seismic microzonation approach with typical case studies from Sikkim Himalaya and Guwahati city, J. Earth.Sys. Sci. 117, 809–831.

Nath, S. K., M. D. Adhikari, S. K. Maiti, N. Devaraj, N. Srivastava and L. D. Mohapatra (2014) Earthquake scenario in West Bengal with emphasis on seismic hazard microzonation of the city of Kolkata, India, Nat. Hazards Earth Syst. Sci. 14, 2549–2575, doi:10.5194/nhess-14-2549-2014, 2014.

Maiti, S. K., S. K.Nath, M. D. Adhikari, N. Srivastava and P.Sengupta (2016), Probabilistic seismic hazard model of West Bengal, J. Earth Engg.doi 10.1080/13632469.2016.1210054.

Youd, T. L. And Idris, I. M. (2001), Liquefaction Resistance of Soils: Summary Report from the 1996 NCEER and 1988 NCEER/NSF Workshops on Evaluation. J. of Geotech. And Geoenv. Engg. Division, ASCE, 127(4), 297-313.

VERTICAL LOAD TEST ON A DRILLED SHAFT INSTALLED IN GLACIALLY DERIVED SEDIMENTS

Ghada S. Ellithy, U.S. Army – Engineer Research and Development Center, Vicksburg, MS, USA, 601.634.7433, ghada.s.ellithy@usace.army.mil
Robert C. Simpson, Loadtest, Atlanta, GA, USA, 800.368.1138,
bob@loadtest.com

ABSTRACT

There are several methods for estimating the axial capacity of drilled shafts installed in coarse-grained soils. Most methods estimate the ultimate capacity for side friction and tip resistance. Design capacity is then calculated by applying a resistance factor to the ultimate capacity. In reality, however, ultimate resistance may not be mobilized except after a significant displacement that is not structurally tolerated in either compression or tension modes.

A full- scale load test is the best way to obtain the load settlement curve for a drilled shaft, especially in soil formations where accurate estimation of soil frictional properties from a field investigation may be difficult. This paper presents the results of a static, axial, compressive bi-directional load test, using the Osterberg method (O-cell test). The test was designed so that the shaft above the O-cell would move up and the shaft below it would move down when loaded. At the start of the test the concrete around the O-cell is fractured generally on a plane near the bottom of the cell.

The test was designed to validate the design capacity of drilled shafts embedded into the Vashon recessional outwash (Qvro), which is a glacially derived sediment consisting of thick deposits of cobbly sand and gravel relatively free of silt and clay found in the Seattle, WA area. The test shaft consisted of a 2.5- feet (0.75 m) diameter drilled shaft. The test shaft was installed to a depth of about 47 feet (14.3 m) into this formation. A maximum load of 437 kips (1.95 MN) was applied during the test, in each direction. The maximum load was attained at upward and downward displacements of less than 0.1 inch (2.5 mm), respectively.

Although the load test did not yield ultimate values, the results are compared to the design assumptions using methods adopted in the FHWA and AASHTO guidelines, which verified the adequacy of the design assumptions. We conclude that more emphasis is needed in the prediction of the service loads and corresponding mobilized displacement that may lead to a more cost effective design. It is also clear that more testing to higher loads could lead to more efficient designs on specific projects and generally as data is added to the local knowledge base.

Keywords: Drilled shafts, Osterberg method, bi-directional load test, glacial sediments, mobilized side friction, mobilized end bearing

INTRODUCTION

Drilled shafts have been widely used as a foundation system for high buildings and towers to support both axial and lateral loads especially in areas where seismic loading is present. Numerous research efforts have been conducted on drilled shafts installed in cohesionless soils consisting of sands and gravels under vertical loads; however, to the knowledge of the authors, there are few published results of load tests in glacially derived deposits. The vertical load test presented in this paper was performed on a drilled shaft embedded into the Vashon recessional outwash (Qvro), which is a glacially derived sediment consisting of thick deposits of cobbly sand and gravel relatively free of silt and clay present in the Seattle, WA area. A variety of load tests have been conducted in the Troutdale formation in and around Portland, Oregon. The

subsurface material, specifically the Troutdale, is very similar to the Ovro. In several cases, ultimate values were obtained.

To improve the design analysis methods for estimating vertical capacity of drilled shafts in these glacial derived deposits, there is a need for additional high quality vertical load test data. The main objectives of this paper are twofold: (1) to present the results of a vertical load test on a fully instrumented 29.5-inch-diameter drilled shaft embedded in glacial derived deposits, and (2) to validate the design assumptions based on existing FHWA and LRFD criterion (O'Neil and Reese 1999) using the compiled vertical load test data presented in this paper.

TEST SITE CONDITIONS

The U.S. Army Corps of Engineers, Seattle District supervised the design and construction of the air traffic control tower (ATCT) in Lakewood, WA (about 40 miles south of Seattle) and its deep foundation system consisting of a pile cap supported on eighteen uncased 47-foot- long drilled shafts. During the design stage, a decision was made to perform a testing program to ensure the adequacy of the design as far as the drilled shaft compression and tension capacity and to gather information for future design in the same subsurface conditions that have few documented field tests. The load test was conducted on a sacrificial test drilled shaft that was constructed in the middle of the ATCT footprint.

The soil borings drilled in the vicinity of the ATCT encountered layers of sands and gravels extended from the ground surface to about 70-feet deep. The upper layers consisted of top soil and man-made fill material that extended to about elevation 300 which is the bottom of the pile cap at 10 feet below the ground surface. Below this elevation, the soil layers consisted of the Vashon recessional outwash (Qvro) deposits that were left by outburst floods and meltwater streams flowing from the margin of the Vashon ice sheet as it wasted and retreated from the Puget Lowland. Qvro deposits in the project area compose the majority of soils encountered.

Qvro typically consists of loose to very dense, poorly graded and well-graded, sandy gravel, sand, and gravelly sand with variable amounts of silt, clay, cobbles, and boulders. Qvro is locally interbedded with fine-grained layers. These layers may be overbank deposits or deposits that accumulated in quiet water depressions within the outwash plain. The soils encountered in the borings generally varied in their relative density from loose to very dense and generally increased with depth; however, loose sands were encountered at lower depths.

CONSTRUCTION OF THE TEST SHAFT AND INSTRUMENTATION

The nominal 29.5-inch- diameter test shaft was excavated dry to a base elevation of about +252.7 feet in the middle of the pile cap footprint. The shaft was drilled by installing a 29.5-inch outer diameter (OD) segmented casing using a rig-mounted rotary tool as the drilling progressed. An auger was used for drilling the shaft, and a clean-out bucket for cleaning the base. After the shaft was approved for concrete placement, the carrying frame with attached bi-directional loading assembly and instrumentation was inserted into the excavation and temporarily supported from the drilling rig. Concrete was then delivered by pump through a 5-inch OD pipe into the base of the shaft until the top of the concrete reached an elevation of 300 ft. The contractor removed the 29.5-inch OD casing in sections as the concreting progressed. The specified concrete strength was 4000 psi, construction of the test shaft was completed on December 03, 2015 and the test was performed on December 11, 2015 where temperature was 46^{o}F on average, cloudy skies and no precipitation. Fig. 1 shows photos during the construction of the test shaft.

The loading assembly consisted of a single 9-inch- diameter O-cell, located 11.0 feet above the shaft base. It was calibrated to 538 kips and then welded closed prior to shipping. Embedded testing instrumentation included the following:

- Paired upper compression telltale casings (nominal ½-inch steel pipe) attached diametrically opposed to the carrying frame, extending from the top of the loading plane to ground level.
- Four Linear Vibrating Wire Displacement Transducers (LVWDTs)) positioned between the lower and upper plates of the loading plane.
- One level of two sister bar vibrating wire strain gages (VWSGs) attached diametrically opposed to the carrying frame below the base of the loading plane. Two levels of two VWSGs attached diametrically opposed to the carrying frame above the top of the loading plane.
- Two lengths of ½-inch steel pipe, extending from the top of the shaft to the top of the bottom plate, to vent the break in the shaft formed by the expansion of the O-cell and to accommodate bottom plate telltales. Fig. 2 shows details of the instrumentation placement and strain gage positions.



Fig. 1 Installation of the loading assembly and concreting the drilled shaft

TEST SET-UP AND PROCEDURES

Test Arrangement

Throughout the load test, key elements of shaft displacement response were monitored using the equipment and instruments detailed below: Top of shaft displacement was monitored using a pair of automated digital survey levels. Upward displacement was measured using ¼-inch telltale rods positioned inside casings and monitored by vibrating wire displacement transducers.

- Downward displacement was measured using ¼-inch telltale rods positioned inside casings and monitored by vibrating wire displacement transducers attached to the top of the shaft.
- Expansion of the loading assembly was measured using four embedded vibrating wire displacement transducers.
- A bourdon pressure gage, vibrating wire pressure transducer and a voltage pressure transducer were used to measure the pressure applied to the O-cell at each load interval.

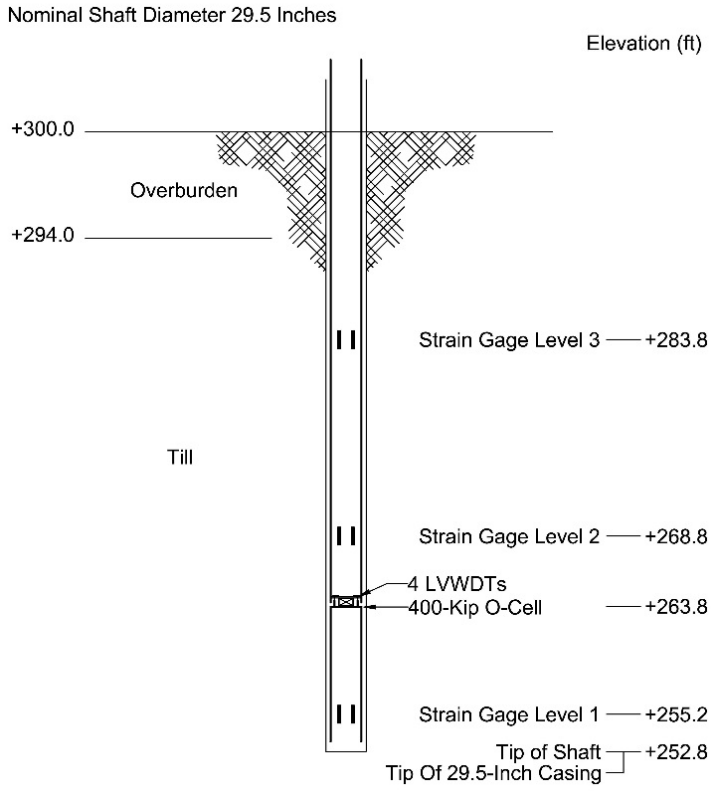


Fig. 2 As- built schematic section of the test shaft

Data Acquisition
All instrumentation were connected through an electronic data logger connected in turn to a laptop computer.

Testing Procedures
Testing was begun by pressurizing the O-cell in order to break the tack welds that hold it closed (for handling and for placement in the shaft) and to form the fracture plane in the concrete surrounding the its base. After the break occurred, the pressure was immediately released and the testing recommenced from zero pressure.

The load increments were applied using the Quick Load Test Method for Individual Piles, ASTM D1143/D1143M – 07 (2013). Each successive load increment was held constant for eight minutes by automatically adjusting the applied pressure. Approximately one minute was used to move between increments. The O-cell was pressurized in 15 nominally equal increments, resulting in a maximum bi-directional load of 437 kips applied to the shaft above and below the loading plane. The loading was halted after increment 1L-15 because the maximum capacity of the loading apparatus had been exceeded. The shaft was then unloaded in five decrements, and the test was concluded.

LOAD TEST RESULTS

General
The loads applied during a bi-directional test act in two opposing directions, counteracted by the resistance of the shaft above and below. It is assumed that no additional upward load is applied until the expansion force exceeds the buoyant weight of the shaft above the loading assembly. Therefore, *net load*, which is defined as gross applied load minus the buoyant weight of the shaft above the loading assembly, is used to determine side shear resistance above it and to construct the equivalent top load displacement curve. For this test, a shaft buoyant weight of 25 kips was calculated.

Upper side shear resistance
The loading assembly applied a maximum upward *net load* of 412 kips to the upper side shear at load interval 1L-15. At this loading, the upward displacement of the top of the O-cell was 0.090 inches (Fig. 3).

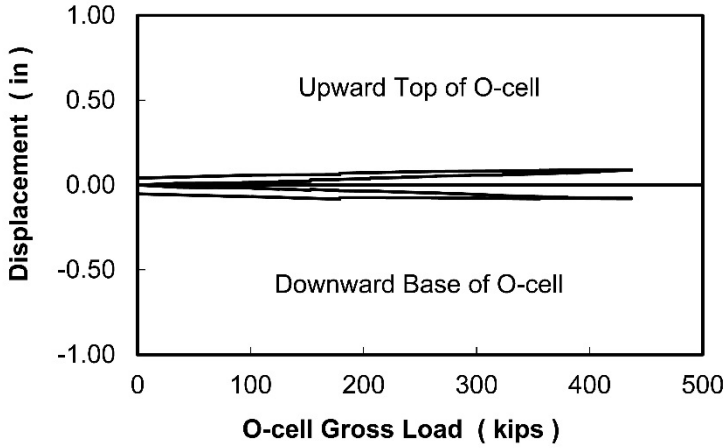


Fig. 3 Load vs. displacement plot

Combined end bearing and lower side shear resistance
The loading assembly applied a maximum downward load of 437 kips at last load interval. At this loading, the average downward displacement was 0.080 inches (Fig 3). The load resisted by side shear in the 2.5-foot shaft section below the Level 1 strain gages is subtracted to determine the maximum applied end bearing load of 101 kips. The unit end bearing at the base of the shaft is calculated to be 21.2 ksf (Fig. 4).
Strain gage analysis
Using the ACI formula ($E_c=0.033 \times \gamma_c^{1.5} \times \sqrt{f'_c}$) , the area of reinforcing steel and nominal shaft diameter, provided an average shaft stiffness (AE) of 3,050,000 kips along the length of the shaft. The stiffness allows loads to be calculated at the various strain gage elevations. The load distribution curves for each load increment, based on the applied load and computed strain gage loads, are presented in Fig. 5. T-Z curves are presented in Fig. 6.

Equivalent top load-displacement
Fig. 7 presents the equivalent compression top load (ECTL) curve. The curve is generated by Loadtest (2007), assuming the load is applied at the top of shaft (+300.0 ft.). A combined side shear and end-bearing resistance of 849 kips was mobilized during the test. The plotted ECTL curve includes the additional elastic compression of a top-loaded shaft.

Equivalent tension top load-displacement

Fig. 7 also presents the equivalent tension top load (ETTL) curve. The curve is generated by Loadtest (2007), assuming the load is applied at top of shaft (+300.0 ft.) but also assuming that the end bearing resistance is zero. The plotted ETTL curve includes the additional elastic compression of a tension top-loaded shaft.

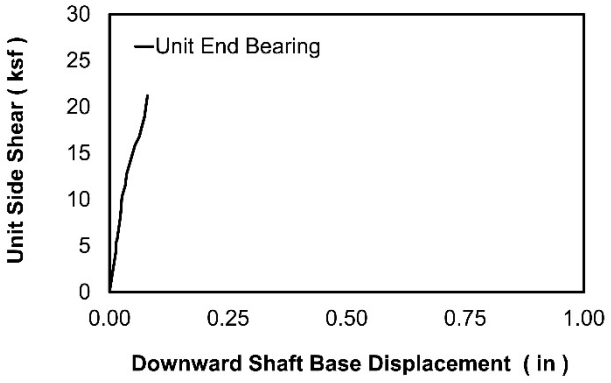


Fig. 4 Mobilized unit end bearing

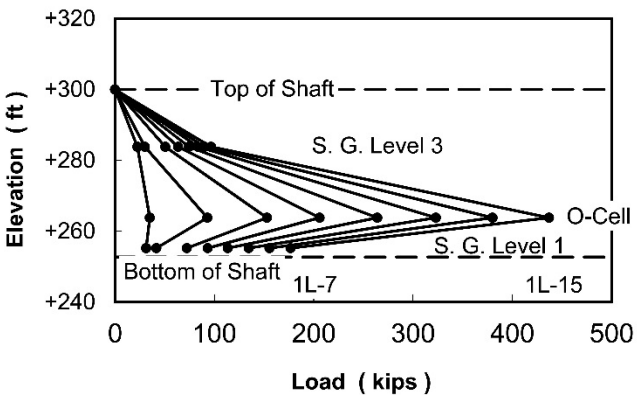
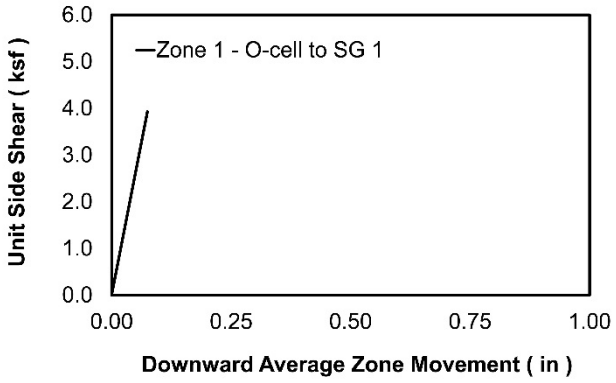


Fig. 5 Strain Gage load distribution



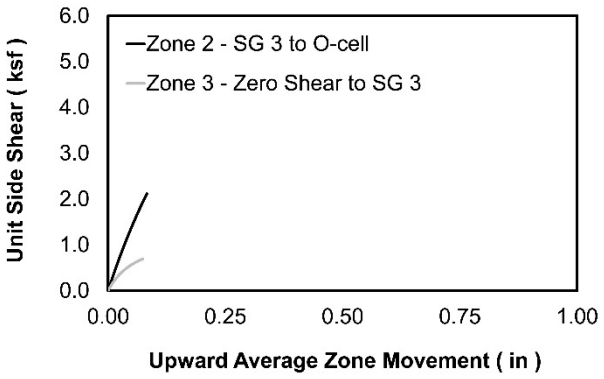


Fig. 6 a) Mobilized downward net unit side shear, b) Mobilized upward net unit side shear

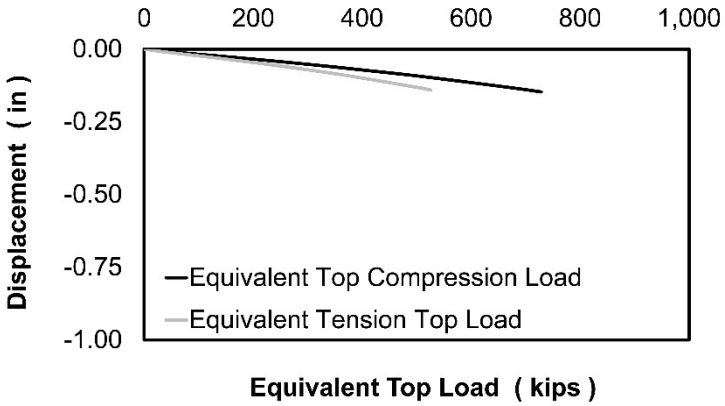


Fig. 7 Equivalent top load-displacement

DESIGN ASSUMPTIONS

During design, the axial resistance of the drilled shafts was evaluated in accordance with the USACE EM 1110-1-1905 and FHWA IF-99-025 adopting limit state design approach per AASHTO (2010), which allows for performance factors to be applied to different resistance components; side friction and base resistance. The Allowable Strength Design (ASD) method as specified in the IBC code could be used as well by considering the factored strength limit resistance to be the value to be used for allowable design capacity including side and tip resistances.

Axial resistance analyses were performed originally for cast-in-place, uncased reinforced concrete 24-inch-diameter drilled shafts based on side friction resistance and base resistance for service settlement limits of 0.5 and 1.0 inch, and for strength limit based on ultimate side friction resistance and ultimate base resistance. It was decided that the drilled shaft base be founded at least 5 feet below the dense to very dense sandy gravel layer at or below elevation 270 feet. For design, some conservative assumptions were made to account for variability of the subsurface conditions and the possibility of presence of loose sand seams, also considered a shallow potential water table at about elevations 282 feet.

Due to construction constraints related to drilling temp casings in gravelly material with cobbles, the built-in diameter of the drilled shafts was changed to 29.5 inch, and a decision was made not to change the embedment depth into the Qvro deposits. Different approaches for drilled shafts resistance are based on empirical factors derived from in-situ test. While many field load tests have been performed on drilled shafts in clays, fewer have been performed on drilled shafts in sands and gravels which initiated this study to compare field load test results with the design assumptions.

Side Resistance

The FHWA design method, O'Neill and Reese (1999), assumes that the drilled shaft resistance in cohesionless soils is independent of the soil friction angle or the *SPT* blow count where the friction angle approaches a common value due to high shearing strains in the sand caused by stress relief during drilling. The method uses a load transfer coefficient β. The nominal axial unit side resistance, q_s in ksf is calculated using the β-method as follows:

$$q_s = \beta\sigma_v' \qquad \text{Eq. 1}$$

where σ_v' is the vertical effective stress at soil layer mid-depth in ksf and is a dimensionless load transfer coefficient. For $N_{60} \geq 15$, $\beta = 1.5–0.135\ (z)^{0.5}$ in sands, and $\beta = 2.0 – 0.06(z)^{0.75}$ in gravels, where; z is the depth below ground at soil layer mid-depth in feet, and N_{60} is the corrected (for hammer efficiency only) average SPT blow count in the design zone in blows/ft. For $N_{60} < 15$, $\beta = N_{60} * (1.5\text{-}0.135(z)^{0.5}/15$ in sands and gravels. β has a min value of of 0.25 and a max value of 1.2 in sands and 1.8 in gravels. The O'Neill and Reese (1999) method recommends q_s be limited to 4 ksf. The above design calculations were used for both compressive and tension capacity estimates; however, AASHTO LRFD (2010) recommends a lower resistance factor that results in tension capacity of about 0.8 of the side friction portion of the compressive capacity.

Tip Resistance

Using the FHWA design method, the nominal unit tip resistance, q_p. in ksf is calculated using Eq. 2:

$$q_p = 1.2N_{60} \qquad \text{Eq. 2}$$

The O'Neill and Reese (1999) method recommends q_p be limited to 60 ksf unless greater values can be justified through load test data. If SPT-N60 blow counts are greater than 50, but limited to 100, which was the case in Qvro layers at the base / tip of the drilled shaft, tip resistance in ksf can be calculated using Eq.3:

$$q_p = 0.59\left[N_{60}\left(\frac{P_a}{\sigma_v'}\right)\right]^{0.8}\sigma_v' \qquad \text{Eq. 3}$$

where P_a is atmospheric pressure = 2.12 ksf. Eq 3. Was checked for calculating the unit tip resistance, however, the difference was not significant and the value was estimated at 60 ksf.

Settlement

Figs. 8.a and 8.b show the normalized load-displacement curves in side resistance and in end bearing, respectively, in cohesionless soils. Fig. 8 was used to compute the drilled shaft resistance for service limit

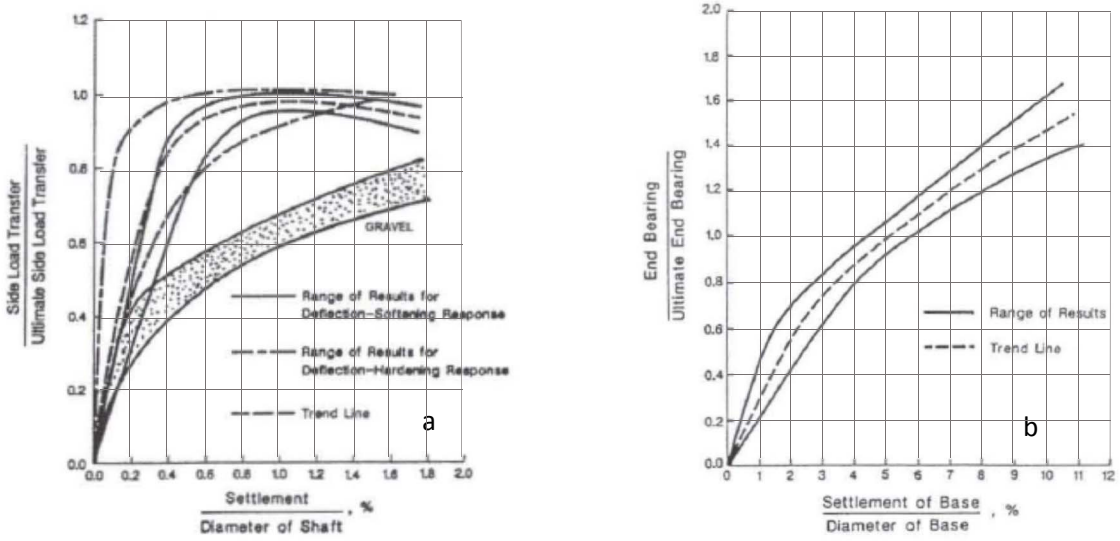


Fig. 8 Normalized load transfer versus settlement in cohesionless soils; a) side resistance, b) end bearing (from O'Neill and Reese, 1999)

state movement values of 0.5 and 1.0 inch using trend curves. Fig. 8.a shows that the skin friction is typically fully mobilized at displacements of 0.2% to 1% of the shaft diameter depending on the nature of deflection response and whether it is a deflection-softening or deflection-hardening. Fig. 8.b shows that settlement due to end bearing loading often does not exhibit a break point or well defined failure, and that end bearing resistance continues to increase as the settlement increases beyond 5% of the base diameter which is typical when end bearing is fully mobilized for drilled shafts in cohesive soils.

COMPARISON BETWEEN LOAD TEST RESULTS AND DESIGN VALUES

The curves in Fig. 8 were used for the purpose of validating design assumptions with load test results. The drilled shaft axial capacity was recalculated for a 29.5- inch- diameter size and presented as plots with depth of mobilized resistance at 0.1- inch settlement using the upper, lower, and trend curves. The ultimate resistance was also added for comparison as shown in Fig. 9.

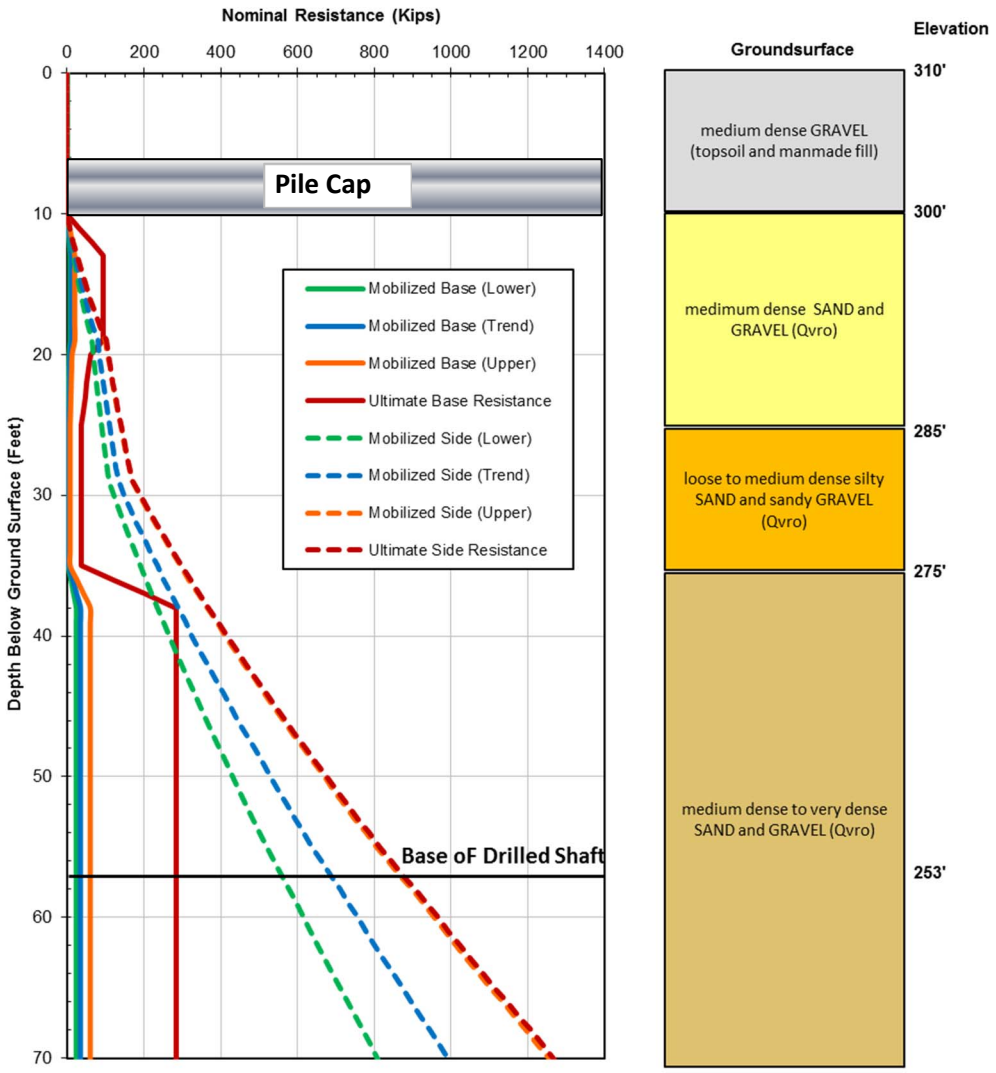


Fig. 9 Estimated ultimate and mobilized axial resistance at 0.1 inch of 29.5 inch diameter drilled shaft

Due to a late construction decision to increase the shaft diameter to 29.5 inch from the proposed design size of 24 inch, the shaft capacity increased but the test capacity did not. Partly as a result of this and as a result of greater than expected resistances, the ultimate capacity of the shaft could not be reached.

Fig. 7 shows that about 550 kips were mobilized as an equivalent top compressive load at a settlement of 0.1 inch or 0.34% normalized settlement. This value matches the lower mobilized side friction for the embedded shaft length per the FHWA method as shown in Fig. 9. Other point values on the load-displacement curve suggest that the Qvro exhibits a deflection-hardening response. At about 0.5% of normalized settlement, the mobilized unit side friction reaches a value of 3.9 ksf (Fig. 6.a) close to the max allowed of 4 ksf. This suggests that for such deposits, a max unit side friction could be increased by about 20% and a value of 5 ksf could be used. Fig. 7 shows about 400 kips were mobilized as an equivalent top tension load at a settlement of 0.1 inch. This value compared to corresponding compressive load mobilized at the same displacement is about 70%, which may suggest that resistance factor for tension loads in such deposits should be lowered to 70% instead of 80% of the compressive loads.

Fig. 4 shows a mobilized unit end bearing of about 21 ksf or 0.35 normalized end bearing capacity at a displacement of less than 0.1 inch. This value corresponds to a mobilized end bearing load of about 100 kips, which is higher than the upper bound shown on Fig. 9 of about 60 kips. This result suggests that the upper bound curve of mobilized end bearing should be steeper at lower displacements allowing for higher mobilized end bearing. Load testing in similar deposits need to be conducted at higher loads to examine the mobilized end bearing at 5% normalized displacement and compare the corresponding unit end bearing to the currently accepted 60 ksf.

SUMMARY AND CONCLUSIONS

The results of the bi-directional, static, compressive, axial load test were presented. A comparison was made between the unit end bearing pressure and unit side friction used in the design and the ones calculated from the load testing for Vashon recessional outwash layers (Qvro). The data presented in this paper show that the mobilized side friction at the site for the Qvro exhibited a deflection-hardening response and that ultimate unit skin friction could be increased to 5 ksf. Measured equivalent top load in tension suggests that resistance factors for tension loads in similar deposits should be in the range of 70% instead of 80% of the compressive loads. The mobilized end bearing exceeded the assumed values based on the FHWA design method by about 65%, which allows for increasing the ultimate design values taking into consideration the serviceability requirements of the structure. Ultimate end bearing mobilized at 5% normalized displacement needs to be further examined by a higher capacity load testing.

REFERENCES

American Association of State Highway and Transportation Officials (AASHTO). 2010. LRFD Bridge Design Specifications.

American Society for Testing and Materials (ASTM). 2013. Standard Test Methods for Deep Foundations Under Static Axial Compressive Load D1143/D1143M-07.

Loadtest USA. 2007. Construction of the Equivalent Top Load-Displacement Curve, Appendix C.

O'Neill, M.W., and Reese, L.C. 1999. Drilled Shafts: Construction Procedures and Design Methods. Publication No. FHWA-IF-99-025, Federal Highway Administration, Washington, D.C.

U.S. Army Corps of Engineers. 1992. Bearing Capacity of Soils, Engineering Manual EM 1110-1-1905.

SETTLEMENT REDUCING AUGER CAST-IN-PLACE PILES BELOW A MAT FOUNDATION OF A 41-STORY STRUCTURE

Swaminathan Srinivasan, P.E., M.ASCE, Terracon Consultants, Inc., Olathe, KS, USA, (949) 864-2068, vasan.srinivasan@terracon.com
Aaron J. Muck, P.E., M.ASCE, Terracon Consultants, Inc., Cincinnati, OH, USA, (513) 612-9051, aaron.muck@terracon.com

ABSTRACT

When an opportunity arises to combine state-of-the-art concepts with advanced modeling tools, engineers need to take what they know and apply forward thinking to geotechnical solutions to promote the state-of-practice. Such an opportunity was seized during the design and construction of the Great American Tower in Cincinnati, Ohio. The forty-one story Great American Tower at Queen City Square – currently the tallest building in Cincinnati – has not only changed the downtown skyline, it is also contributing to the advancement of the state-of-the-art use of auger cast-in-place (ACIP) piles as settlement reducers. Predicted settlements of a traditional mat foundation were excessive, and the costs and construction time associated with traditional ACIP piles extending to bedrock were not preferred. A mat supported on a limited number of ACIP piles, with the piles primarily acting as settlement reducers, was evaluated as the preferred foundation type.

Promoting the unique soil-structure interaction of the foundation system with confidence required the use of sophisticated numerical modeling tools. Traditional standard penetration test boring data (SPT) was initially used to develop a numerical analysis of the soil-structure interaction using FLAC 3D software. The model was further modified with cone penetration (CPT) and pressuremeter testing (PMT), along with actual load test results on several ACIP pile elements of varying lengths, but all tipping above bedrock. Through a combined design team effort, and detailed numerical modeling analysis, ACIP piles were recommended for reducing mat foundation settlement. Instrumentation during and post-construction confirmed design assumptions and predictions. Integrating sound geotechnical concepts, and using advanced geotechnical analysis and design methods, traditional mat and ACIP pile foundations were successfully integrated into a unique foundation support system.

Keywords: ACIP pile, mat, instrumentation, soil-structure interaction

INTRODUCTION

The Great American Tower at Queen City Square in Cincinnati, Ohio is located within a region dissected by historical geologic deviances associated with the meander of the Ohio River and glacial progression/recession. Combining a challenging geology, with the development of a high-rise office building afforded the design team an opportunity to combine state-of-the-art soil-structure interaction concepts and method with traditional geotechnical engineering concepts. Such a combination required a variety of field tests, collaboration with the design team and owner, and geotechnical-structural modeling during the design phase. During construction, in addition to materials testing and observation, a variety of instrumentation systems were employed. Together, the data was used to corroborate the design model and make adjustments during construction and further substantiate design assumptions following construction.

Predicted settlements of a traditional foundation types exceeded tolerable settlement due to a variably thick zone of moderately to highly compressible lakebed soils across the footprint. Typically, auger cast-in-place (ACIP) piles tipping on bedrock would be assumed for structure support; however, the estimated 1,200+ ACIP piles were unaccommodating to the project completion timeline and owner's budget.

As a result, advanced numerical modeling tools were used to combine traditional mat foundation and ACIP pile systems, which resulted in a mat foundation being supported by a limited number of "settlement reducing" ACIP piles. A design approach that used ACIP piles to "stiffen" the mat foundation and act as settlement reducers was recommended. The approach significantly reduced the number of ACIP piles needed as compared to the traditional foundation supported on piles extending to bedrock.

Three-dimensional numerical analysis software was used to model the soil-structure interaction of the mat, piles, and subsurface materials. The available tools allowed the geotechnical designer to model different soil types and groundwater conditions, consider interaction between the structural elements and surrounding geo-materials, and simulate construction, including pre- and post- loading conditions. In combination with numerous discussions and consulting between the projects design team member and the owner, a total of 281 ACIP piles located at specific locations below the mat foundation were designed to reduce mat foundation settlement and target mat stresses to within tolerable limits. The project used advanced geotechnical analysis and design to combine traditional foundation types into a unique "soil-structure" interaction centered foundation system.

This paper briefly outlines the design steps, analyses, and methodology used in the development of the ACIP pile settlement reducer/mat foundation system, and focuses on the use of sophisticated geotechnical instrumentation to support the design assumptions and predicted response. Project information, along with an overview of the general subsurface and geologic conditions at the project site is also provided.

PROJECT INFORMATION

The Great American Tower at Queen City Square consists of an office tower and a parking garage generally located northeast of the intersection of 3rd and Sycamore Streets in downtown Cincinnati, Ohio. The 203-meter (665-foot) tall structure provides roughly 92,903 square meters (1,000,000 square ft) of office space with views of panoramic views of both downtown and the Ohio riverfront. Generally located within the southern third of the site, the tower footprint measures about 46 meters (150 ft) north/south by about 67 meters (220 ft) east/west. A parking garage area, along with a promenade with retail and restaurant space occupies the northern two-thirds of the project area. The footprint of the garage measures about 76 meters (250 feet) north/south by about 37 meters (120 ft) east/west. Overall, the project includes approximately 1,858 square meters (20,000 square ft) of retail space and 2,350 parking spaces. Project construction began in 2008 was fully open for occupancy less than three years later. The completed tower along with the Cincinnati skyline is shown in Fig. 1 below.



Fig. 1. Cincinnati, Ohio skyline with Great American Tower to the far right.

HISTORICAL BACKGROUND

Establishing the geo-structural model used in the analyses of the foundation system for the Great American Tower considered both historical and recent developments at the site. The most recent prior development

included a seven to nine story above-grade parking garage, with three to four stories below grade. The brick and concrete masonry garage was constructed in 1968 and was founded on spread footing foundations. The structure, including foundations and below grade walls, were completely demolished and removed prior to construction of the new tower and garage.

The subject tower structure is the second phase of the overall development at the square. East of the tower location, the first phase was completed in 2002. Design requirements for the overall complex included "linking" the two structures at two different floors. Foundation support for the first phase construction consists of 457-mm (18-inch) diameter, approximately 15 to 18 m (50 to 60 ft) long ACIP piles bearing on/within the interbedded shale and limestone bedrock over 30 m (100 ft) below existing site grades. In comparison, the mat subgrade elevation of the tower structure is about 2 m (6.5 ft) above the lowest level elevation in the first phase construction.

GEOLOGIC CONDITIONS

The unique geology and depositional history at the tower site was considered in the foundation model. The project site maps within the Cincinnati Basin, which generally consists of granular glacial outwash and earlier water-deposited lakebed material. The deeper lakebed soils were deposited within lakes created by advancing ice sheets, which dammed the northward flowing deep stage river. These lower deposits were later covered by granular outwash materials consisting mainly of sands and gravels, with varying amounts of silt. The outwash was subsequently eroded during various glacial periods to varying degrees. Glacial terraces exist along portions of the river such as downtown Cincinnati where substantial depths of outwash exist. The glacial outwash typically reduces in thickness in closer proximity to the Ohio River and is nearly absent across the project site.

Lakebed deposits (i.e., lakebed bottom sediments) consist essentially of clays and silts, but with occasional sand layers. Lakebed soils are characterized by a gray to dark gray color, but sometimes brown in the upper oxidized zone. The lakebed soils typically occur as silty clay, lean clay, and occasionally plastic to fat clays at the project site. The lakebed soils have a varved appearance due to the presence of thin layers, lenses, or partings of silt and sand. Lakebed soils are usually low to moderate in strength, but can be very stiff in the lower profile due to effects of overconsolidation. The lakebed soils below the site exhibit a moderate to high compressibility, with moderate to high moisture contents and occasional organics.

The underlying bedrock at the project site maps as Ordovician Age interbedded shale and limestone of the Kope Member. Based on the bedrock elevation at the site, the bedrock falls within the Economy Member of the Latonia Formation. The bedrock is classified as "shale-rich", with the shale component making up about 75 percent of the formation and limestone making up the remaining approximate 25 percent.

SITE SUBSURFACE CONDITIONS

Terracon Consultants, Inc. has performed numerous geotechnical studies between 1968 and 2008 in downtown Cincinnati and multiple studies within the limits of the Great American Tower complex. In total, nearly fifty Standard Penetration Test (SPT) borings were performed at the site, as well as Cone Penetrometer Testing (CPT) and Pressuremeter Testing (PMT).

The subsurface profile was subdivided into seven major strata based on material type, geology, and engineering characteristics. Existing fill was encountered below the ground surface at the majority of the test borings in the project area. The existing fill was underlain by a relatively thick granular zone, which was divided into "upper sands", "fine sands", and "lower sands" based on consistency and gravel content. The predominant and governing material underlying the site consists of Lakebed soils. Compressible Lakebed soils were encountered below the granular zones. A relatively thin and variable transitional zone

of cohesive and/or granular soils was encountered below the lakebed and prior to encountering bedrock. Bedrock was encountered at depths of approximately 27 to 43 m (90 to 140 ft) below existing grades. A cross-section of the expected subsurface profile across the Great American Tower footprint is shown in Fig. 2.

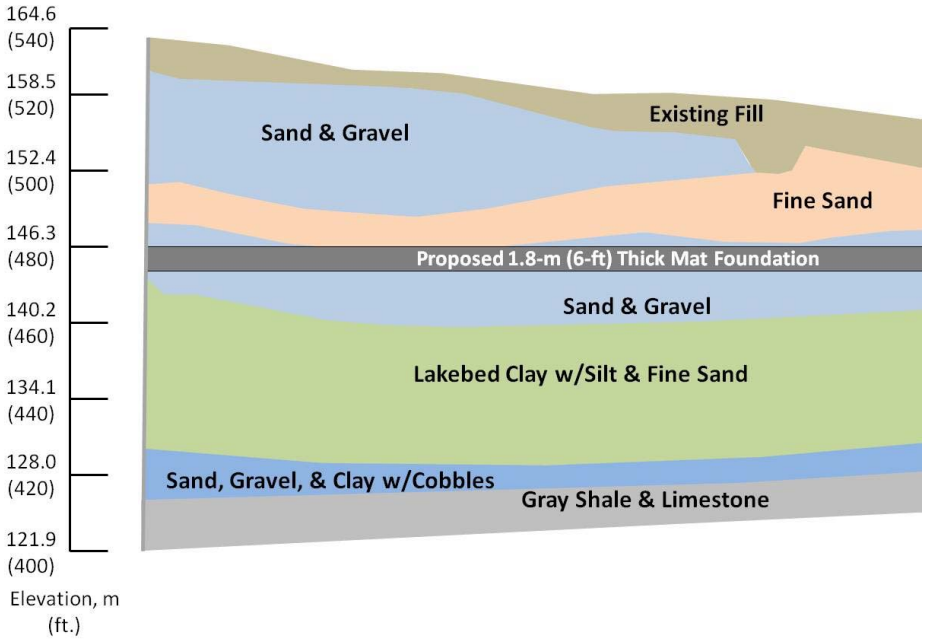


Fig. 2. Generalized Subsurface Profile

Existing fill was encountered at the majority of the test borings drilled across the project area. The fill was encountered up to about 6.1 m (20 ft) below grade, and was variable in thickness and content. Layers of sands and gravel were generally medium dense to dense and had a maximum thickness of about 10.7 m (35 ft) in the northern and mid-portions of the site (parking garage area); however, was minimal or even absent in the southern portion of the site (office tower area). An approximate 1.5 to 6.1 m (5 to 20-ft) zone of predominantly fine sandy soils were encountered below the upper coarser zone in the proposed parking garage area and below the existing fill in the tower area. This layer was generally encountered uniformly across the project area. The thickness of this layer was up to 6.1 m (20 ft) and extended to depths of about 13.7 to 22.9 m (45 to 75 ft) below existing grades at the site.

Glacial lakebed material was encountered in all of the test borings and generally extended to a maximum depth of about 36.6 m (120 ft) below existing grade. This layer was ranged from about 9 to 15 m (30 to 50 ft) thick and consisted of lean clays, fat clays, clayey silts, and sandy lean clays. A “transitional layer”, encountered just above the bedrock, varied from sandy lean clays to sands, and sands and gravels, with gravel and rock fragments. The thickness of this zone ranged between about 1.5 and 7.6 m (5 and 25 ft). Interbedded shale (about 75 to 80 percent of the bedrock matrix) and limestone (about 20 to 25 percent of the bedrock matrix) bedrock within the project area was generally encountered at depths of about 27 to 43 m (90 to 140 ft) below existing grade, or between about elevations 130 and 124 m (426 and 406 ft).

Based on observations in the boreholes and piezometer data, the groundwater table is at about elevation 143 m (470 ft) near the south end of the site (area of the office tower) and rises to about elevation 145 m (475 ft) to the north (area of parking garage). Based on review of the groundwater data, there does not appear to be a significant change in the groundwater table below the project site when the river stage

changes. However, this reaction to river stage was considered in our evaluation, since water levels at the site likely depend on the height of river stage and duration of elevated or flood stages.

The published normal pool elevation of the Ohio River in the project area is elevation 139 m (455 ft). The 10-year and 100-year flood levels are presently at elevations 148 and 152 m, respectively (elevations 487 and 498 ft, respectively). The recorded maximum flooding occurred in 1937 where the river reached elevation 155 m (elevation 510 ft) or slightly over 9.5 m (31.5 ft) above the mat foundation subgrade elevation.

FOUNDATION SYSTEM SELECTION

Several foundation options were evaluated based on the anticipated high structural loads, load distribution, and total/differential settlement limitations. The relatively thick compressible lakebed soils as shallow as 3 m (10 ft) below the proposed lowest level elevation was also of concern. Shallow spread footings were not considered feasible for support of the office tower. Large footing sizes [over 6.1 m (20 ft wide)] would be needed and predicted settlements were well in excess of tolerable limits.

Driven steel H-piles or pipe piles driven to a practical refusal on bedrock were also considered. Pile lengths ranging between about 12 and 24 m (40 and 80 ft) were estimated. Cost and the urban setting (vibration risks) made driven piles a less attractive option.

Both straight shaft drilled piers and ACIP piles socketed into bedrock were also considered as viable foundation alternatives. Pier/pile element lengths were estimated to be about 24 m (80 ft) or more, and would require penetration of granular zones below the groundwater table. Caving of the drilled pier during construction and tremie methods for concrete placement were anticipated. The drilled piers were cost prohibitive and the construction schedule would be negatively impacted.

Using FLAC 3D, analyses showed that a traditional mat foundation alone would result in unacceptable settlements. A mat supported on piles extending to bedrock would result in significant cost and construction duration. Therefore, a “piled mat foundation system” consisting of a mat supported by an optimal (limited) number of deep foundation elements was selected. Deep foundation elements (ACIP piles) primarily serve as settlement reducers. This is not a structurally pile-supported mat, but rather the primary purpose of the piles is to reduce total and differential settlement.

DESIGN METHODOLOGY

The design methodology for use of the ACIP piles to “stiffen” the mat foundation and act as settlement reducers considers terminating the piles in the transitional zone above the bedrock. The pile locations were selected based on detailed analyses to maximize the benefits of settlement reduction while reducing the total number of piles needed. The mat foundation and ACIP pile elements were modeled using the numerical modeling program – FLAC 3D.

The primary concern with the soil subgrade supported mat foundation is the magnitude and distribution of total and differential settlements. Settlement across the mat due to the building loads will be non-uniform and must be accurately estimated in order to ensure that the tolerable limits are not exceeded. The specified maximum differential settlement, between the center core and the edge of the mat was 25 mm (1 in). Differential settlement between adjacent columns was limited to 12 mm (1/2 in).

Settlement is influenced by multiple factors consisting of the complex and heterogeneous subsurface profile and variable thickness of each layer across the site. Therefore, even if load conditions are symmetric, settlements will not be symmetric. Construction sequence also required consideration since a specific soil

layer will respond differently to an imposed load if it experiences different stress paths. For example, ground settlement will be different if a soil stratum is experiencing a direct loading, compared to when the soil stratum is experiencing an unloading (removal of existing structure) and reloading (new construction). The loading sequence, variability of subsoil conditions, and non-symmetrical loading, results in a complex stress condition change. The actual distribution of the loads from the superstructure on the mat must be accurately modeled. The pattern of foundation settlement depends not only on the soil and external load conditions, but also on the rigidity of the building structure (i.e., soil-structure interaction). The rigidity of the structure can help "regulate" differential settlement through the interaction between structure and foundation soil. Again, the loads from the superstructure are not symmetrical and their actual distribution on the mat must be accurately modeled.

A 3D numerical modeling program was able to model the mat in adequate detail. The program modeled behavior of the different soils, tracing the construction sequence, accounting for the actual load distribution, and simulating the interaction between the foundation soil, mat foundation and superstructure.

ENGINEERING ANALYSIS

The analysis consisted of three primary steps, or conditions, which influence what is/will be felt by the underlying materials at the site. The three steps include establishing the initial stresses in the soil strata under the weight of overburden soil, simulating the excavation for the mat foundation, and calculating the settlement of the mat under the building load. The three steps are illustrated in Fig. 3.

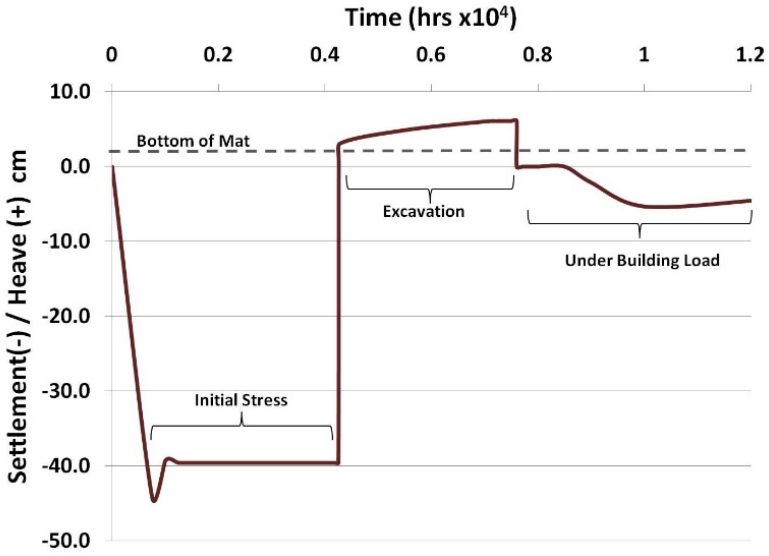


Fig. 3. Foundation Settlement during Construction Sequence

The first step established the initial stresses in the soil strata under the weight of overburden soil. The second step of the analysis simulated excavation for the mat foundation. In this process, the soil in the building area is removed from the surface to the bottom of the mat foundation at elevation of 145.8 m (478.5 ft). During excavation, a shoring system is installed from top to bottom. Therefore, no horizontal movement is allowed in the wall of the excavation. Excavation releases the vertical stress at the bottom of the excavation, therefore the bottom of the excavation "heaves". The third step of the analysis was to calculate the settlement of the mat under the building load. The load distribution and magnitude was provided by the structural engineer. Three foundation options were analyzed, including: the building supported only by a mat foundation; mat foundation with building core affect; mat with limited number of piles for settlement reduction and building core effect.

RESULTS

The estimated maximum settlement of the mat foundation only model was about 25.9 cm (10.2 in) near the center of the mat. The maximum differential settlement was about 17.0 cm (6.7 in) over a distance of about 22.9 m (75 ft). Considering the mat foundation modeled with improved rigidity as a result of the addition of the building core, the maximum settlement was improved by about 13.7 cm (5.4 in) over the mat foundation only model, a reduction of about 50%. The predicted settlements with the rigid building core located at the center of the tower and connected to the mat, resulted in a maximum settlement of about 12.2 cm (4.8 in) and a maximum predicted differential settlement of about 10.7 cm (4.2 in). Even with the core effects, the predicted settlements are not acceptable.

The same analysis was performed with the mat-building core, but with the addition of a limited number of piles. The pile supported mat is a combined foundation, where piles act as settlement reducers and only carry a portion of the load, allowing the mat to settle so that the soil subgrade can carry a portion of the total load. The soil-structure interaction between the mat and soil subgrade along with the piles serve to reduce foundation settlement. An example of the analysis showing the locations of the piles (light hash marks) and the computed mat settlements, and the mat contact pressure distribution with the piles modeled are shown in Fig. 4 and 5, respectively.

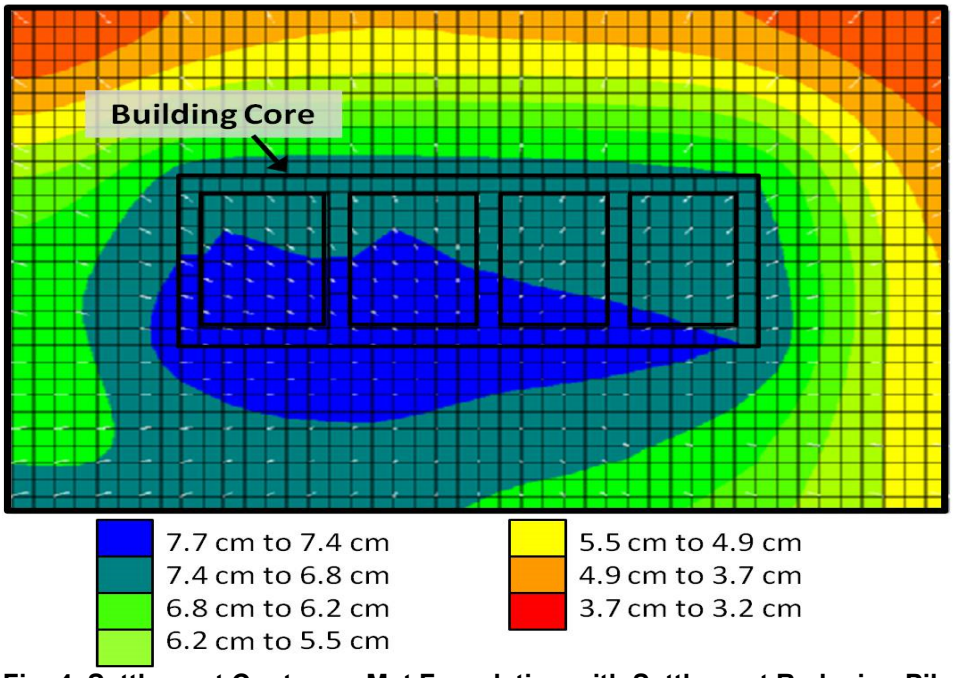


Fig. 4. Settlement Contours- Mat Foundation with Settlement Reducing Piles

The piles are designed to operate at a working load of which significant creep starts to occur, typically 70 to 80% of the ultimate load capacity. Sufficient piles were included to reduce the contact pressure between the mat and soil. The pile locations have also been selected to reduce the differential settlement, rather than to substantially reduce the overall average total settlement. Based on multiple iterations, it was recommended that 281 piles be used, where the piles extend to the lower sand, gravel, and clay with cobble layer above the bedrock.

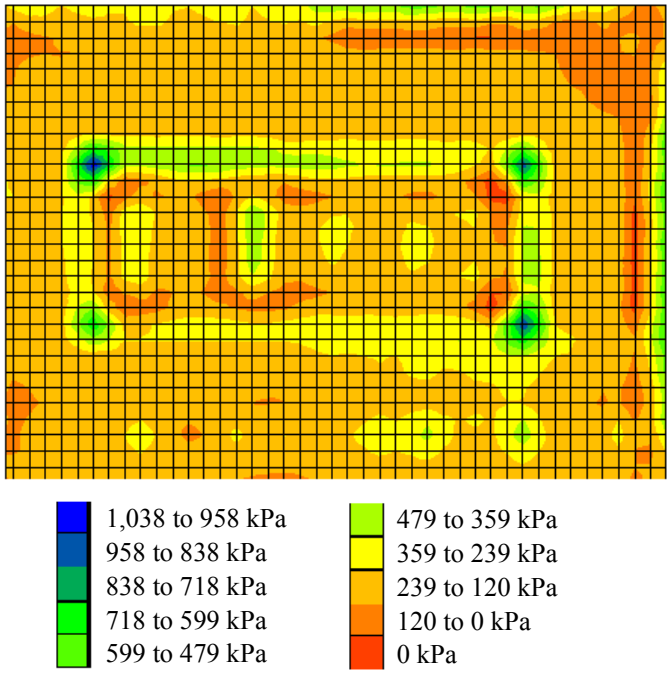


Fig. 5. Mat Contact Pressure Contours – Mat Foundation with Settlement Reducing Piles

Following a series of iterations, including significant collaboration with the project's structural engineer and architect, predicted settlement of the combined mat-core-settlement reducing pile model was reduced to less than about 2.54 cm (1 in). The predicted settlement was acceptable to the designers and resulted in an overall settlement reduction of about 80 to 90% when compared to the mat foundation system models analyzed without the use of settlement reducing piles.

INSTALLATION, FIELD TESTING, MONITORING, AND MODEL REFINEMENT

The ACIP piles were constructed at the positions determined by our geotechnical model. Sequencing of the installation was critical since all of the ACIP piles were installed prior to placement of the concrete mat. Due to the tight site constraints, some difficulty was encountered in installation due to pile position and installation of instrumentation equipment and cables which required continuous coordination with the contractor. The 45.7 cm (18 in) diameter piles were installed with traditional continuous flight auger equipment. A single center bar was installed the full length of the ACIP pile and steel cage was installed within the upper approximate 4.6 to 6.1 m (15 to 20 ft). Typical spacing of the piles within the core was about 4.6 m (15 ft) and about 6.1 to 7.6 m (20 to 25 ft) spacing outside of the core area. Full-time observation indicated acceptable penetration, tip depth, and grout take throughout construction.

During demolition of the existing parking garage structure, four seismographs were installed in/near adjacent structures including the existing Phase 1 building and a historic church immediately north of the site. The recorded vibration peak vector sum values were typically less than about 3 mm/s (0.12 in/s). The majority of peak values occurred from traffic and nearby stadium events. The vibration monitoring concluded that the demolition and subsequent construction activities did not adversely impact adjacent structures.

Inclinometers were installed at eight locations along the perimeter of the approximate 9 to 12 m (30 to 40 ft) excavation. The soldier pile and lagging system included multiple rows of tiebacks and prior earth

retention systems were encountered during excavation. Monthly readings provided the project team with the confidence that the earth retention system was performing and any concerns could be readily addressed.

A total of three pile load tests were performed within the footprint of the mat foundation. The load testing program consisted of tipping a pile within the lakebed soils for evaluation of shorter piles; however, the pile "plunged" before the design load was achieved. The model showed that the geotechnical capacity and corresponding settlement of the piles tipping in the less competent lakebed materials exceeded design assumptions. In contrast, a load test was performed on an ACIP pile tipping into the underlying shale and limestone bedrock. The load test results confirmed that the high capacity coupled with the approximate 2.5 cm (1 in.) settlement, when placed in the three-dimensional model will structurally "fail" due to the high building loads. A load test was performed with a pile tipping within the stiffer transitional zone between the lakebed materials and bedrock. The 14 m (46 ft.) long pile deflected about 9.4 cm (3.7 in.) under a load of 127 metric tons (140 tons). The resulting load-deflection information from this load test was used to calibrate the soil-structure model, and resulting predicted settlements and contact pressures. As a result of the load test data and foundation response, several additional ACIP piles were added to the model.

Strain gages were installed at approximate 1.5 m (5 ft) intervals at eight locations along the length of the load test pile tipping above the bedrock. The strain gages measured the load distribution along the pile. A plot comparing pile length with applied load as compared to the load measured in the strain gages is shown in Fig. 6. The load reaching the pile tip ranged from about 15 to 30 percent of the applied load which confirmed the assumption that the piles would not be overstressed in our model. The plotted load-displacement curve also compared relatively well with the model prediction. Actual movement at the maximum load of 272 metric tons (300 tons) was measured to be about 76 mm (3 in) while the model predicted movement of about 51 mm (2 in).

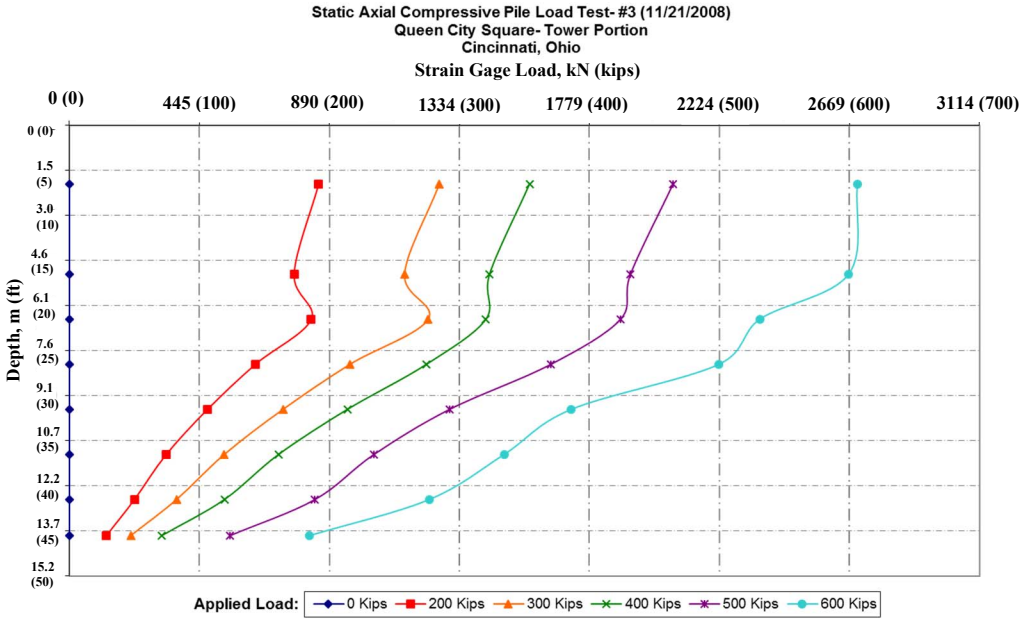


Fig. 6. Load Test Strain Distribution

Strain gages were installed at twelve selected production pile locations, along with two pressure cells and one settlement sensor. One pressure cell was installed under the core area of the tower and the other was installed near the edge of the mat for comparison. Each cell was installed about 0.5 m (18 in) below the mat subgrade. The settlement sensor consisted of a protected LVDT instrument which was mounted to the top of one of the sacrificial reaction piles and embedded in the bottom of the concrete mat foundation. The data

from each device was collected using a 16-channel data logger data acquisition system. The logger was wirelessly connected to the office using web-based technology. The results of the strain gage and earth pressure cell for a selected pile location are shown in Fig. 7.

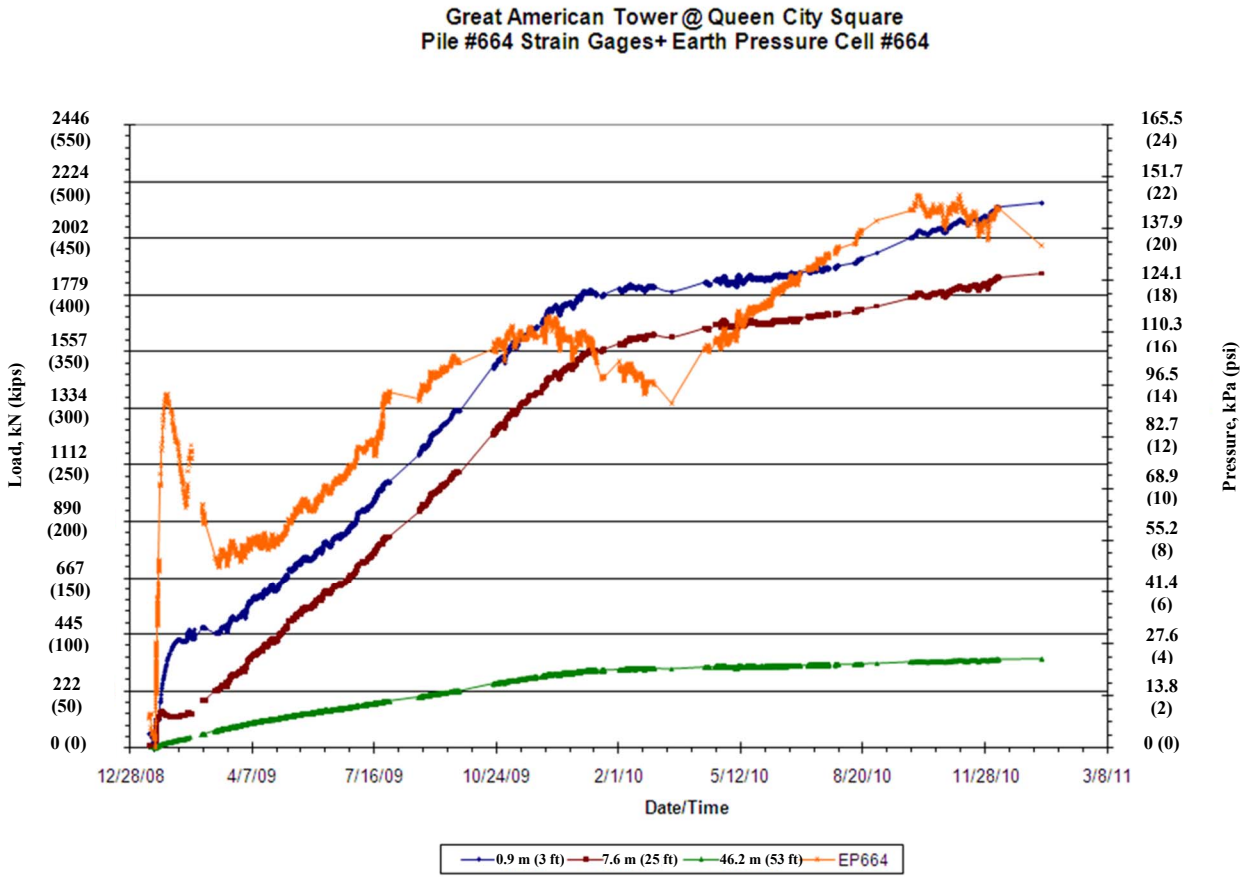


Fig. 7. Strain Gage and Earth Pressure Distribution

The initial elevated earth pressure readings are attributed to disturbance during construction. Construction of the final level of the tower was completed within about 12 months of the initial mat construction, which corresponds with the leveling off of the measured strains. The continued upward trend is a result of interior construction and finishing. Movement was observed to correspond with water level readings in the nearby Ohio River. The measured strain and pressure development compared well with model assumptions.

SUMMARY

Using advanced soil-structure interaction software, along with instrumentation in the field to substantiate model assumptions, a unique foundation system was successfully realized. The tools and methods used to develop the three-dimensional model not only promoted the state-of-practice, but also resulted in significant construction cost savings. The result was a total of 281 “settlement-reducing” ACIP piles strategically located below a mat foundation for support of the Great American Tower. The use of instrumentation during and following construction assisted the designers in fine-tuning the geotechnical model. As a result, stress/strain development was reasonably consistent with model predictions. Such data has since been used in evaluation of stress/strain development on other projects. Combining traditional mat and ACIP pile foundations into a unique soil-structure interaction based foundation system combined with instrumentation technology, resulted in a successful project and advancement of geotechnical analysis and design.

CHARACTERISTIC FEATURES OF DEEP EXCAVATIONS IN THE METROPOLIS AND THE PROBABLE HAZARDS.

Prof. Sudhir Kumar Das, FIE (I) FIGS FIRT MASCE (USA) IRSE (RETD)
Department of Civil Engineering, Techno-India Group, Kolkata, India.

Abstract

The exorbitant price of the land in the metropolis has restricted the horizontal expansion and compelled the owners, the developers and the engineers to opt for vertical expansion. This has resulted in the construction of high rises by extending floors of the existing buildings and developing the new ones for which deep excavation is a must. The multistoried buildings up to a certain height can be founded on shallow depth if the soil beneath can withstand the load. If not, the soil can be stabilized by the latest improvement technology to change the properties of soil to cater the desired load of the superstructures. By such practice the cost and time of completion of the substructures can be reduced in comparison to the substructures needed for deep excavation.

The necessity of deep excavation cannot be ignored to create housings, underground parking lots and the other public amenities for the urban migrants in the metropolis.

Although most of the metropolis have underground mapping the developers, before starting excavation should be hundred percent sure about the alignment and depth of the utilities so that the excavators do not snap the same to bring cut in water supply, power lines, telephone lines etc, resulting in hue and cry in the neighborhoods of the metropolis due to no availability of the essential services The building/structures coming on the influence zones of the deep excavation should be monitored in all sequences of excavations.

In case of building underground corridors for rail or road through open deep excavation under a traffic road the developers, before commencing excavation should shift/divert the dry and wet utilities coming on the way of excavation to suitable locations. The surface traffic need to be diverted either temporarily to an adjacent alternative road or allowed to pass over a decking built over the trench of excavation for the affected length of construction. The soil support system is necessary longitudinally on the two sides covering the width of trench for building corridors. In case of building substructures of flyovers built at different plots along the alignment of the flyover or a multistoried complex built at an isolated plot, the soil support system would be necessary on all the sides covering the plot of construction.

The material of construction of soil support depends on the depth, type of soil and the type of permanent structure to be developed. Probable geo-hazards inviting casualties in the deep excavation projects occur due to caving of soil, leakage of wet utilities, seepage through honey comb concrete surfaces, failure of pump used for dewatering etc.

A detailed comprehensive planning, management and determination of the project authority is essential for marginalizing the casualties. These prevent unforeseen expenditure in mitigation and help to control the time and the cost over run of overall project. The engineer at site should be more a professional manager than an engineer at site. He should be conversant with the safety and environment rules and regulations applicable to deep underground projects.

Key words: horizontal expansion; vertical expansion; metropolis; deep excavation; underground mapping; soil support; geo-hazards; comprehensive planning.

1.0 Introduction:

India being a developing nation, may not afford to go for tunneling methodology for underground corridor for rail or road for few kilometers in a metropolis. The reason behind the same is the tunneling is a costlier methodology compared to open one. The deep excavation may be needed for building substructures for flyovers, expressways, an isolated multistoried complex or founding a tall tower within a metropolis where open excavation is a must. The exorbitant cost of the land in the metropolis has restricted the horizontal expansion and the owners, the developers and the engineers are encouraged for vertical expansion resulting in construction of high rises by extending floors of the existing buildings and building the new ones in different plots of land necessitating the deep excavation in the metropolis.

Any substructure should penetrate the desired soil level for which the superstructure is designed. The properties of soil at shallow level may not cater the requisites of safety of the substructures. Modern technology provides ample scope for improvement of soil at shallow depth to change the properties of soil to cater the higher load of a superstructure where deep excavation may be avoided. In case deep excavation is a must in a metropolis for building underground constructions, the engineers and the developers should be alert about the thousands of utilities beneath the road level of a metropolis.

Although most of the metropolis have underground mapping the developers, before starting excavation should be hundred percent sure about the alignment and depth of the utilities so that the excavators do not snap the same to bring cut in water supply, power lines, telephone lines etc, resulting in hue and cry in the neighborhoods of the metropolis due to no availability of the essential services.

In case of building underground corridors for rail or road in a congested metropolis it is advisable to bring the tunneling depth at a deeper level to have safe cushion of soil above the top of the tunnel and below all the utilities' level. In tunneling methodology, stationing and disposal of huge quantities of excavated spoils of open excavation are avoided in the busy metropolis. This is no doubt a plus point for the tunneling technology where diversion of surface traffic and underground supporting of utilities or their diversion needed in open excavation are totally eliminated.

If the deep excavation is carried open on a traffic road longitudinally for a kilometer or so, the engineer's onus will be to divert the traffic to an alternative road for the affected length or allow the traffic at restricted speed over a decking constructed temporarily over the supports of the open excavation. Proper barricading of site of construction is essential so that outsiders should not have access to do away with any type of accident or unforeseen happenings.

2.0 Soil support technology

2.01 In case of underground corridor bearing rail or road in a megacity, retain walling made of either steel or concrete is necessary longitudinally on two sides of the desired width of deep excavation necessary for constructing the proposed corridor. In case of substructures of flyovers or multistoried complex with/without basements in metropolis, retain walling is needed on all sides covering square, rectangular, pentagonal shape of substructures of the flyovers built at different plots along the alignment of the flyover or substructures of the multistoried complex built at an isolated plot of land. Before commencements of excavation of retain walling all out effort is to be made to locate the underground utilities coming on the way of excavation and then either to remove temporarily or to shift/divert as warranted at site so that essential services are not disturbed.

2.02 The building/structures coming on the influence zones of the deep excavation should be monitored in all sequences of excavations. If any cracks appear on any part of the influenced adjacent buildings/structures, tell-tale mortars are to be pasted over the cracks so as to examine the mortar remain stable during further stages of excavation. The mortar will tear if the earlier cracks get further widened. The engineer at site should investigate the degree of danger of the widening of cracks in regard to the geotechnical safety of the building and inform to the competent authority about the need of vacating of the occupants of the affected buildings, specially the old ones and rehabilitating them in suitable places till the time the buildings are repaired in original conditions or the excavation works are completed, whichever is earlier.

3.0 Stability of deep excavation

3.01 Before carrying out deep excavation, the stability of the cut at any stage of construction need to be checked against heaving of soil from below the excavation at that stage. If the load of earth supported by the retaining wall at the excavation level added with other superimposed load at the top of excavation is not exceeded the bearing capacity below that level (applying a reasonable factor of safety) the heaving against bursting the base of excavation is totally eliminated.[Fig.3 Annex A]. The permissible bearing capacity is to be calculated from the soil properties of the concerned bore holes data analyzed in the soil laboratory.

4.0 Prerequisites for carrying out deep excavation

4.01. Before commencing the excavation work, the topography of the area of construction including the hydrology has to be studied in depth to ascertain the nature of ground profile and the ground water table. The ground water table varies from cities to cities and place to place. In some cities for example in Kolkata, one of the metropolises of India, the ground water table reaches the ground level in monsoon. If the water table is higher than any stage of excavation level, the water table need to be lowered below the excavation level by

dewatering through well point or any suitable pumping system for onward excavation below that stage.

4.02 The soil strata drawing are to be prepared after obtaining the properties of soil from the thorough analysis of bore hole data in the laboratory. The soil strata drawings are the indicators to place the bottom of the underground substructure whether it is a multistoried basement of a high rise complex or an underground corridor for rail or road. .

4.03 In carrying out deep excavation in a metropolis it is essential to collect from the concerned authorities, the underground maps showing the locations of embedded dry and wet utilities. If maps are not available the utilities are to be located by pre-trenching or by applying sensor indicators. After the alignment and depth of the utilities are ascertained, the engineer at site shall make all arrangement to divert temporarily some of the utilities over ground so to ease the cutting and disposal of earth spoils. The same utilities are required to be restored in their original location after the permanent structure is built. The utilities which cannot be diverted over ground are kept hanged from the strutting members or supported on the strutting members of the braced excavation. [Fig.1. Annex A]

4.04 It is to be seen that such utilities are in no way hit by the machine excavation so as to prevent snapping of dry utilities like telephone and electrical cables and leaking of wet pipelines. If such precautions are not taken at site there are chances of failure of communication, electricity and water supply in the neighborhood. Due to any leak in the sewer line, the excavated trench can be inundated in no time resulting in withholding all the construction activities. The construction works cannot be restored till the sewage is removed from the trench and properly sanitized.

4.05 The buildings and the structures especially old and multi-storied lying within the influence zone of the deep excavation shall be monitored for any visible cracks or fissures. [Fig.2.Annex.A]. This is necessary to bring confidence of the owners of the building about the safety of habitation. During monitoring, if any cracks found at any point of the building due to any of the construction activities, retrofitting and rehabilitation measures need to be immediately undertaken by the site engineer to avoid further casualties.. In case any old building appears vulnerable for habitation during the course of excavation, the inhabitants are to be rescued and shifted to alternative accommodation arranged by the competent authority.

5.0 Construction methodology

5.01 There are different construction methodologies for the deep excavation undertaken in the metropolis depending on site, condition of soil, surrounding environment, budget sanctioned, time of completion, restriction of work if any, need of the people etc.

5.02 The type of material the soil support walling to be made of depends on the depth of deep excavation. If the depth of cut varies from 6 to 9 meters, the soil support may be made of steel sheet piles of smaller sections. For more than nine to twenty meters or so, interlocking steel sheet piles of heavier sections, cast/in-situ concrete bored piles of requisite section @0.5 to 1.0 meter center to center, suitable H-section soldier piles @ 1m center to

center laced with timber laggings or reinforced concrete diaphragm walls of designed thickness should be constructed to serve as soil support wallings. The excavated trench is required to be braced by strutting and waling made of steel sections which remain temporarily till the permanent structure is built. Despite the bracing members are considered temporary, the members are to be designed as permanent members to avoid failure during any sequence of construction. The bracing technology is called cut and cover construction because it involves cut, excavate, construct and cover. [Fig.1 Annex-A]

5.03 In the cut and cover construction the excavated trench being open, is prone to dusting of soil despite grabbing the soil by the modern excavators.[Fig4.Annex-A] To eliminate such dusting the width and length of the proposed excavated trench is covered by steel decking prior to commence excavation through a predetermined hole in the decking. The system then changes to cover and cut construction in lieu of cut and cover construction. Both the methods are conventional and cost effective open excavation methods for the metropolis of India.

6.0 Probable geo-hazards in deep excavation (from the practical experience of the author)

6.01 In case sheet pile used as soil support: During driving of interlocking sheet piles from top of ground, despite making attempt to maintain verticality of piles along the alignment some pile is driven out of the alignment resulting in difficulty in interlocking with the next pile. This creates gap which remain unnoticed from top of ground. The gap created at any point below ground level becomes a source of seepage behind the retaining wall (sheet piling) into the deep excavation. Since noise created during driving becomes noise pollution, it should be considered as a geohazard. So attempt need to be made to reduce the noise decibel to minimum.

6.02 In case diaphragm walling is used as soil support: While grabbing soil in between the guide walls before concreting diaphragm wall, any underground utility which remained unnoticed due to oversight may be cut by the grab causing the concerned utility service not available to the users before the same is restored back in operation.

6.03 Despite taking all precautions of pouring the concrete vertically from top and maintaining the consistency of bentonite slurry, there may be caving of soil from the side of the trench supported by bentonite slurry resulting in mixing with concrete producing weak spots. These weak spots become vulnerable for seepage from outside the constructed diaphragm walls into the deep excavation trench.

6.04 Despite taking all precautions of pouring the concrete vertically from top with the intention of making dense concreting of diaphragm there may be honey combing in few spots whose appearance could be seen in the concerned sequence of construction. These honey combing spots become vulnerable for seepage from outside the diaphragm walls into the deep excavation trench.

6.05 The deep excavation trench is liable to be inundated by the seepages described in the 3 para above.. As a result the construction activities will come to a dead lock condition. The activities could be restored only after stopping the seepages by undertaking extensive cement grouting (depending on the volume of seepage water) and other treatment works as warranted at site and finally dewatering the residual water of the excavated trench.

6.06 Any leakage in any of the underground wet utilities within the deep excavation occurred due to any construction activities is vulnerable for inundation of the trench at any stage of construction. The inundation will result in withholding of all construction activities. These can be restored only after the sewage water (from the leakage in sewer) is removed by pumping and the dry trench is properly sanitized to make it work friendly.

6.07 During the course of deep excavation the foundations of the buildings and structures lying within the influence zone of the deep cut [Fig.4.Annex-A] may be subjected to differential settlement resulting in appearance of cracks in the buildings. The affected buildings need to be monitored regularly about the widening of existing cracks and appearance of new cracks. Strutting and waling steel members are to be tightened to keep the verticality of the retaining structures in tact leaving any chance of deformation of retained soil behind the retaining wall. Retrofitting and rehabilitation measures are to be undertaken soon after the cracks appeared to get the confidence of the owners of the buildings and to continue the progress of the project without agitation from the owners and their tenants. In case any building especially old is found vulnerable despite after taking safety precautions, the occupants of the affected building need to be vacated and rehabilitated as deemed fit.

6.08 The bracings of the braced trench may fail due to unsafe design considering temporary constructions. It may lead to complication and destabilize the trench endangering the workmen. All the activities need to be stopped and could be restored only after the braced cut is made stable through rectification.

6.09 There may be failure of dewatering pumps inviting inundation of ground water leading to stoppage of all activities. The activities could be restored only after the water from the trench is pumped out and the faults of the dewatering pump system are rectified.

6.10 Last but not the least the heaving of soil from the bottom of excavation may burst the excavated trench [Fig.3-Annex-A] due to geo technical miscalculation with erratic soil properties.

7.0 Safety precautions

7.01 Safe access and egress to all excavation sites including providing ladder, steps, ramps and other safe means of exit for employees working in deep cut trenches. The underground workers need to be protected against hazardous atmosphere in deep excavation by providing respiratory protection and regularly monitoring all measures/controls used to reduce atmospheric contamination to safe level.

7.02 All surface obstacles that may create hazard should be removed or minimized from the deep excavation site. Warning vests or other reflective or high-visibility garments are required to be worn while the workers are exposed to vehicular traffic to avoid accident.

7.03 Wearing of helmets and anti-slip shoes during working /inspecting hours either in underground or over ground in deep underground projects, shall be made mandatory for the workers including the supervisors and the officials of the project.

8.0 Quality Control

By quality of steel or concrete one should understand as to what degree of perfection, a steel product or a concrete product is made according to standard design and specifications. The quality of steel used as soil support or bracing members of a braced cut excavation and the quality of concrete used as diaphragm walling for soil support or used as permanent concrete structures should never be compensated for speedy construction to achieve the target date of completion. The quality depends on the application of materials, men, machines, equipments and on the whole on the manufacturing parameters. Since variation of raw materials can alter the quality of the finished product say concrete, the quality control should cover statistical sampling (concrete cubes) and testing in the laboratory to affirm concrete strength before the same is accepted by the competent authority. Quality control is more concerned with making things right rather than discovering and rejecting the wrong ones. The right workability of concrete by providing a right (higher) water cement ratio in the congested reinforcements will result in achieving concreting without any honey combing in the finished product.

9.0 Conclusion

9.01 The safety of the temporary structures which are constructed to build the permanent structure should be maintained till the permanent structure is built completely and the strength of the temporary structures become redundant for the deep excavation works.

9.02 The underground wet utilities which were supported or hanged within the deep excavation should be protected and kept in operation till the same are restored in their original condition after completion of the permanent structure and other ancillaries.

9.03 Casualties in a deep excavation project can absolutely avoided if the safety measures and the quality parameters are strongly enforced. However, a detailed comprehensive planning, management and determination can reduce the damage to the minimum extent. Minimum damage at site is an indicator of good governance of the site engineer. Such a strategy would help the project authorities to control the cost and time over run without incurring any extra expenditure like massive cement grouting treatment works to stop seepages from outside the soil supports seeping into the excavated trench.

9.04 A right developer having adequate experiences of underground engineering, equipped with men, materials and machineries, conversant with latest rules and regulations for protecting the environment, having adequate fund in hand should be entrusted for deep underground projects. Prequalification of contractors and the key personnel need to be an yardstick to involve the experienced geo-foundation engineers and the contractors in critical

and difficult geotechnical projects. The engineer at site should be more a professional manager than an engineer while dealing with the mitigation activities to counter the geo-hazard failures.

ANNEXURE-A

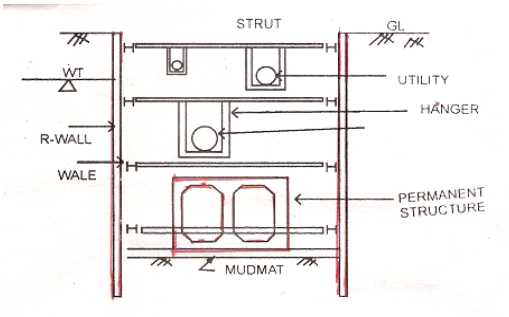


Fig.1



Fig.4

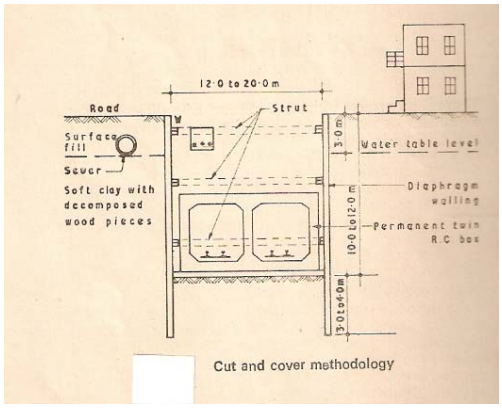


Fig. 2

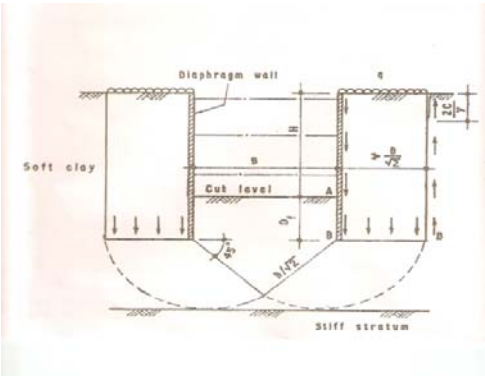


Fig.3

9.0 REFERENCES

.1. Alekseev, S.N. & Ivanovo, F.M. *Durable concrete structures*

2. Stewart, D.A. *The Design & Placing of High Quality Concrete*

3. Tsytovich, N. *Soil Mechanics*

4. Choudhury. S. *Project Management*

5*The Indian Concrete Journal***,** Vol.55, Number12, Dec.1981

6. DMRC (2002): *Geotechnical Interpretative Report*, Delhi Metro Rail Corporation, India

7. Das. S. K. *'The Engineer at a construction site is more a professional manager than an Engineer"* Proceedings of the fourth International Structural Engineering and Construction Conference (ISEC- 4), Melbourne, Australia, 26-28, September, 2007.Vol.2 Page1449-51

DYNAMIC RESPONSE OF SHORT PILES UNDER LATERAL TRANSIENT LOAD

Indrajit Chowdhury, Research Scholar, Indian Institute of Engineering Science & Technology, Howrah India, 9874605676, ixchowdh@gmail.com

Rituparna Dey, Junior research fellow Indian Institute of Engineering Science & Technology, Howrah India, rituprndy16@gmail.com

Ambarish Ghosh, Professor, Department of Civil Engineering; Indian Institute of Engineering Science &Technology, Howrah India, ambarish@civil.iiests.ac.in

ABSTRACT

In port and harbor facilities, jetties and cargo berth terminals are usually installed on piles that remain partially embedded in soil, while a part of it behaves as columns supporting top deck. Technology in vogue adapts a pseudo static analysis in computer where the top deck including piles are analyzed as an integrated system based on finite element method when the piles are modeled as beam elements, while the soil in which it is embedded is modeled as linear or nonlinear springs. Typical berthing force of the ship is considered as a pseudo static force where the dynamic characteristics of the force is taken into consideration by an equivalent impact factor and little study exists on the actual behavior of these type of piles under the transient shock due to berthing impact. Present paper proposes an analytical solution based on which one can compute the dynamic response of such jetty piles considering shear modulus of soil constant with depth. Considering the solution is analytical in nature no special software is needed and can well be adapted for design office practice using generic utility software like MATHCAD, MATLAB etc. that makes the proposed model computationally very efficient.

Keywords: Short piles, transient load, dynamic response.

INTRODUCTION

Response of piles under dynamic load has been an important study in the realms of civil engineering, where significant research has been carried out on its dynamic behavior under harmonic loads like one experienced in a machine foundation or under seismic force.

A number of researchers have given solution to this problem like Parmelee et al (1964), Tajimi (1966), Penzien (1970), Novak et al (1974, 1983), Banerjee and Sen (1987), Dobry and Gazetas (1988), Chowdhury and Dasgupta (2008).

However, most of these theories are based on piles loaded under harmonic load and valid for long piles where structural failure precedes the soil failure considering the piles are long and flexible.

In many cases due to soil condition prevailing at site or for the loading conditions one is compelled to install short piles (having slenderness ratio less than 20) below a number of structures like jetties, water tanks on ground, machine foundation, bridge pier etc, and many of them are subjected to transient shocks like impact from ships, blast loading, impact from moving vehicles that can induce significant load on the structure foundation system. Unfortunately little is known about its behavior under such transient shocks.

Literature review shows there has been little research on both static and dynamic response of short piles under lateral load. Except for the theory as proposed by Brinch Hansen (1961) and Broms(1965), there are practically no theory available to address the issue under static loading. Similarly for dynamic loading, literature review shows that work is very sparse and except for the paper of Chowdhury and Dasgupta (2010) researchers could not identify any notable work that has tried to elaborate on this particular topic. Present paper thus tries to develop a mathematical model on dynamic response of short piles under transient lateral shock that remains an important study for jetty piles under vessel impact.

PROPOSED METHOD

Shown in Figure 1 is a typical jetty structure with its typical transverse cross section. In most cases, considering the jetties are subjected to heavy loads (especially if it is a cargo berthing terminal) and having sloping ground profile below water line, the diameter of the piles are large and are embedded into ground to a depth where depth of embedment to the radius of piles are less than 20 making them behave as short piles (here soil failure precedes the structural failure), while a part of pile above soil line, acts as a column to the top deck, making the top deck system being supported on partially embedded short piles. There is no direct solution to this problem till date in terms of dynamic response/ transient load and engineers have to often resort to numerical analysis to arrive at an approximate solution.

One of the major difficulties in handling a short pile analytically is unlike long piles where the load influence dies down quickly below pile head gives the computational advantage of ignoring the boundary conditions of the pile tip. In case of short piles this cannot be ignored making the unknown boundary conditions as four in lieu of two (as in case of long piles) making the computation difficult [Desai and Christiansen (1983)].

The general solution for such finite beams on elastic foundation can be represented by Karnovsky and Lebed (2002)

$$u(z) = C_0 V_0(pz) + C_1 V_1(pz) + C_2 V_2(pz) + C_3 V_3(pz) \qquad [1]$$

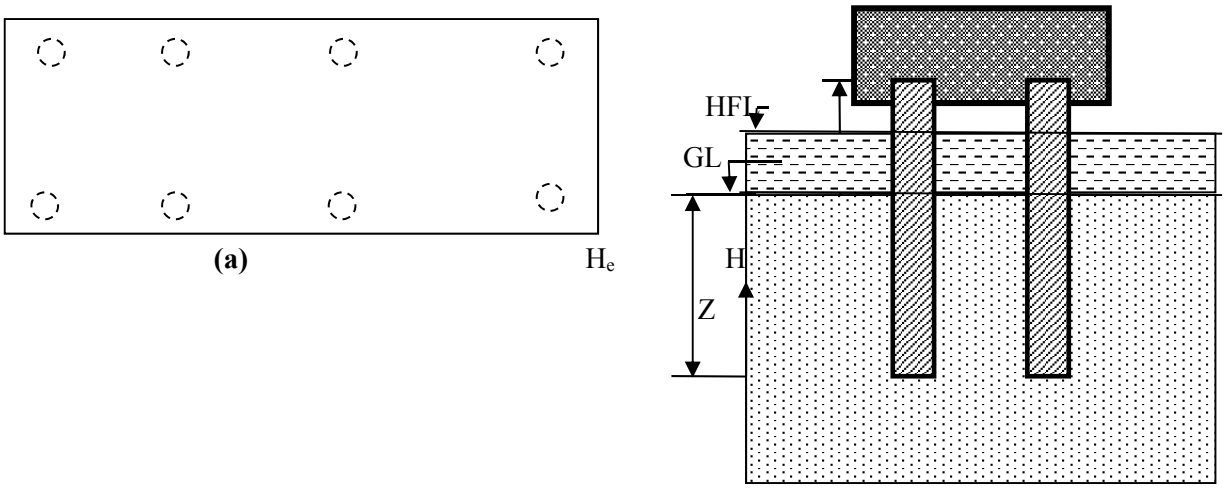


Fig. 1. Plan and sectional view of a jetty structure

Here

u(z)= Displacement of body in horizontal direction and varies with depth z, C_0, C_1,C_2,C_3= Integration constants, $p = \sqrt[4]{\frac{k_s D_{eff}}{4EI}}$ an interaction parameter, and is function of relative stiffness of the pile and surrounding soil, k_s= Dynamic sub-grade modulus of soil, E= Young's modulus of pile material, I= Moment of inertia of pile cross section, D_{eff}= Effective width of pile expressed as $0.5\pi D_w$, D_w= Diameter of pile, $V_0(pz)$, $V_1(pz)$,$V_2(pz)$, $V_3(pz)$= Puzrevsky functions [Karnovsky and Lebed (2002)], and are expressed as

$$V_0(pz) = \cosh(pz)\cos(pz) \quad [2]$$

$$V_1(pz) = \frac{1}{\sqrt{2}}\left[\cosh(pz)\sin(pz) + \sinh(pz)\cos(pz)\right] \quad [3]$$

$$V_2(pz) = \sinh(pz)\sin(pz) \quad [4]$$

$$V_3(pz) = \frac{1}{\sqrt{2}}\left[\cosh(pz)\sin(pz) - \sinh(pz)\cos(pz)\right] \quad [5]$$

When the ship induces a velocity V_0 to the pile head due to impact while berthing, the pile will deform as semi rigid cantilever beam when the boundary conditions are

- At z=0 , u(z)=0 and u'(z)=0
- At z=H, u(z)=u_H and u'(z)= u_H/H for very small rotations

For u=0 at z=0 we have C_0=0 and for u'=0 at z=0 we have C_1=0

Now considering $\alpha = pH$ we have

$$u(z) = C_2 V_2(\alpha\frac{z}{H}) + C_3 V_3(\alpha\frac{z}{H}) \quad [6]$$

Where $\alpha = \sqrt[4]{\frac{k_s D_{eff} H^4}{4EI}}$, a dimensionless number.

Now considering at z=H u=u_H and u'=u_H/H we have two equations

$$C_2 V_2(\alpha) + C_3 V_3(\alpha) = u_H \quad [7]$$

And $C_2 \frac{\alpha\sqrt{2}}{H} V_1(\alpha) + C_3 \frac{\alpha\sqrt{2}}{H} V_2(\alpha) = \frac{u_H}{H}$ [8]

Equation [7] and [8] can be expressed in matrix form as

$$\begin{bmatrix} V_2(\alpha) & V_3(\alpha) \\ \frac{\alpha\sqrt{2}}{H} V_1(\alpha) & \frac{\alpha\sqrt{2}}{H} V_2(\alpha) \end{bmatrix} \begin{Bmatrix} C_2 \\ C_3 \end{Bmatrix} = \begin{Bmatrix} u_H \\ \frac{u_H}{H} \end{Bmatrix} \quad [9]$$

Solution of Equation [9] finally gives

$$C_2 = \left[\frac{\alpha\sqrt{2}}{H} V_2(\alpha) - \frac{V_3(\alpha)}{H} \right] \frac{u_H}{\Delta} \quad [10]$$

And $C_3 = \left[\frac{-\alpha\sqrt{2}}{H} V_1(\alpha) + \frac{V_2(\alpha)}{H} \right] \frac{u_H}{\Delta}$ [11]

Here $\Delta = \frac{\alpha\sqrt{2}}{H} \left[V_2^{\,2}(\alpha) - V_1(\alpha) V_3(\alpha) \right]$ [12]

Now substituting the value of C_2 and C_3 in Equation [9] we finally have

$$\frac{u(z)}{u_H} = \left[\frac{\alpha\sqrt{2} V_2(\alpha) - V_3(\alpha)}{H\Delta} \right] V_2\left(\frac{\alpha z}{H} \right) + \left[\frac{V_2(\alpha) - \alpha\sqrt{2} V_1(\alpha)}{H\Delta} \right] V_3\left(\frac{\alpha z}{H} \right) \quad [13]$$

Equation [13], is a dimensionless term and is the shape function of pile deformation and can be expressed as

$$\phi(z) = \left[\frac{\alpha\sqrt{2} V_2(\alpha) - V_3(\alpha)}{\alpha\sqrt{2}\left(V_2^{\,2}(\alpha) - V_1(\alpha) V_3(\alpha) \right)} \right] V_2\left(\frac{\alpha z}{H} \right) + \left[\frac{V_2(\alpha) - \alpha\sqrt{2} V_1(\alpha)}{\alpha\sqrt{2}\left(V_2^{\,2}(\alpha) - V_1(\alpha) V_3(\alpha) \right)} \right] V_3\left(\frac{\alpha z}{H} \right) \quad [14]$$

Considering $\xi = z/H$, Equation (14) can be expressed in natural co-ordinate as

$$\phi(\xi) = \left[\frac{\alpha\sqrt{2} V_2(\alpha) - V_3(\alpha)}{\alpha\sqrt{2}\left(V_2^{\,2}(\alpha) - V_1(\alpha) V_3(\alpha) \right)} \right] V_2(\alpha\xi) + \left[\frac{V_2(\alpha) - \alpha\sqrt{2} V_1(\alpha)}{\alpha\sqrt{2}\left(V_2^{\,2}(\alpha) - V_1(\alpha) V_3(\alpha) \right)} \right] V_3(\alpha\xi)$$

$$\rightarrow \phi(\xi) = A V_2(\alpha\xi) + B V_3(\alpha\xi) \quad [15]$$

Equation [15] is the shape function when the pile is fully embedded, however in this case a part of the pile acts as a column supporting the top deck and it is embedded up-to a depth H_e when we have

$\alpha_e = \sqrt[4]{\frac{k_s D_{eff} H_e^{\,4}}{4EI}}$ where

$$\phi_e(\xi) = \left[\frac{\alpha_e\sqrt{2}V_2(\alpha_e) - V_3(\alpha_e)}{\alpha_e\sqrt{2}\left(V_2^{\,2}(\alpha_e) - V_1(\alpha_e)V_3(\alpha_e)\right)}\right]V_2(\alpha_e\xi) + \left[\frac{V_2(\alpha_e) - \alpha_e\sqrt{2}V_1(\alpha_e)}{\alpha_e\sqrt{2}\left(V_2^{\,2}(\alpha_e) - V_1(\alpha_e)V_3(\alpha_e)\right)}\right]V_3(\alpha_e\xi)$$

$$\rightarrow \phi_e(\xi) = A_eV_2(\alpha_e\xi) + B_eV_3(\alpha_e\xi) \qquad [16]$$

Here the subscript e represents a partially embedded pile. The stiffness of pile in fundamental mode can thus be expressed as

$$K_w = EI\int_0^H \phi_e''(z)^2\,dz + k_sD_{eff}\int_0^{H_e}\phi_e^{\,2}(z)dz \qquad [17]$$

Equation [17] in natural co-ordinate can be expressed as

$$K_w = \frac{4EI\alpha_e^{\,4}}{H^3}\int_0^1 \phi_e''(\xi)^2\,d\xi + k_sD_{eff}H_e\int_0^{\eta_e}\phi_e^{\,2}(\xi)d\xi \qquad [18]$$

$$\rightarrow K_w = \frac{4EI\alpha_e^{\,4}}{H^3}\left[\int_0^1 \left[A_eV_0(\alpha_e\xi) + B_eV_1(\alpha_e\xi)\right]^2 d\xi + k_sD_{eff}H_e\int_0^{\eta_e}\left[A_eV_2(\alpha_e\xi) + B_eV_3(\alpha_e\xi)\right]^2 d\xi\right] \qquad [19]$$

Here η_e is the ratio of embedded depth to full depth of well H_e/H, where $0 \le \eta_e \le 1.0$.

Equation [19] can be written in a simplified compact form as

$$K_w = \frac{4EI\alpha_e^{\,4}}{H^3}\left[I_1 + \eta_eI_2\right] \rightarrow k_sD_{eff}H_e\eta_e^{\,3}\left[I_1 + \eta_eI_2\right] \qquad [20]$$

Equation [20] can be expressed as

$$K_w^b = \frac{4EI}{H^3}\chi^b \qquad [21]$$

Where $\chi^b = \alpha^4\left(I_1 + \eta_eI_2\right)$ is a stiffness coefficient and the superscript b stands for the term bending.

Here, $I_1 = \int_0^1 \left[A_eV_0(\alpha_e\xi) + B_eV_1(\alpha_e\xi)\right]^2 d\xi$ and $I_2 = \int_0^{\eta_e}\left[A_eV_2(\alpha_e\xi) + B_eV_3(\alpha_e\xi)\right]^2 d\xi$ are integration constants that can be computed numerically.

STIFFNESS DUE TO SHEAR DEFORMATION

Considering the large diameter of pile, the pile shaft can have significant stiffness in shear deformation. Equation of equilibrium in this case can be expressed as

$$\eta GA\frac{d^2u}{dz^2} + k_sD_{eff}u = 0 \qquad [22]$$

Here G= Shear modulus of pile. A=Area of cross-section of pile, k_s= dynamic sub-grade modulus.

Equation [16] is a standard second order linear differential equation whose solution can be expressed as

$$u(z) = C\cos qz + D\sin qz \qquad [23]$$

Here $q = \sqrt{k_s D_{eff} / GA}$ a standard parameter. Now considering $\beta = qH$, Equation (23) can be expressed as

$$u(z) = C\cos\frac{\beta z}{H} + D\sin\frac{\beta z}{H} \quad [24]$$

Applying the boundary condition at z=0 u=0 we have C=0.Again considering at z=H u=u_H we have $D = u_H / \sin\beta$. From which we have

$$\frac{u(z)}{u_H} = \frac{1}{\sin\beta}\sin\left(\frac{\beta z}{H}\right) \quad [25]$$

Converting Equation (25) to natural co-ordinate and also taking the embedment up to depth H_e we have

$$\phi_e^s(\xi) = \frac{1}{\sin\beta_e}\sin\left(\frac{\beta_e z}{H}\right) \quad [26]$$

Here $\beta_e = \sqrt{k_s D_{eff} H_e^{\,2} / GA}$ where e stands for embedment and superscript s stand for shear.

The shear stiffness of the pile can be expressed as

$$K_w^s = \eta GA\int_0^H \left(\phi_e'^s\right)^2(z)dz + k_s D_{eff}\int_0^{H_e}\left(\phi_e^s\right)^2(z)dz$$

$$\rightarrow K_w^s = \frac{\eta GA}{H}\int_0^1 \left(\phi_e'^s(\xi)\right)^2 d\xi + k_s D_{eff} H\int_0^{\eta_e}\left(\phi_e^s(\xi)\right)^2 d\xi \quad [27]$$

Considering the shape functions are simple in this case can be analytically solved directly which finally gives

$$K_w^s = \frac{\eta GA\beta_e^{\,2}}{2H\sin^2\beta_e}\left[1 + \frac{\sin 2\beta_e}{2\beta_e} + \frac{1}{\eta_e^{\,2}}\left(\eta_e - \frac{\sin 2\beta_e\eta_e}{2\beta_e}\right)\right] \quad [28]$$

Equation [28] can be expressed in a compact form as

$$K_w^s = \frac{\eta GA}{2H}\chi^s \quad [29]$$

Here $\chi^s = \frac{\beta_e^{\,2}}{\sin^2\beta_e}\left[1 + \frac{\sin 2\beta_e}{2\beta_e} + \frac{1}{\eta_e^{\,2}}\left(\eta_e - \frac{\sin 2\beta_e\eta_e}{2\beta_e}\right)\right]$ [30]

CONSIDERATION OF EFFECTIVE STIFFNESS

The effective stiffness of the pile can be expressed as Chowdhury (2013)

$$\frac{1}{K_w^e} = \frac{1}{K_w^b} + \frac{1}{K_w^s} \quad [31]$$

Substituting Equations [21] and [29] in [31] will finally give

$$K_w^e = \frac{4EI}{H^3}\chi^b \left[\frac{1}{1+\frac{16(1+\nu)}{\eta\lambda^2}\left(\frac{\chi^b}{\chi^s}\right)} \right] \quad [32]$$

In Equation [32], $\lambda = H/r$ the slenderness ratio of the pile shaft. ν = Poisson's ratio and η = Shear correction factor for circular pile. It will be observed that when the pile has large diameter and short length, shear deformation significantly affects the stiffness as λ is small.

The only value that needs to be computed now is the dynamic sub-grade modulus of soil k_s and is derived hereafter.

DETERMINATION OF DYNAMIC SUB GRADE MODULUS k_S

For a rigid cylinder embedded in ground the lateral stiffness is expressed as Wolf (1985) as

$$K_x = \frac{8Gr_0}{2-\nu}\left[1+\frac{e}{r_0}\right] \quad [33]$$

Where the first term within the bracket depicts the stiffness from bearing and the second term represents the stiffness from the foundation wall.

Thus ignoring the first term and assuming e=dz an infinitely small segment, we can express Equation [33] as

$$dK_x = \frac{8Gdz}{2-\nu} \quad [34]$$

Thus the second term of Equation [33] that represents soil stiffness can be expressed as

$$K_{soil} = \frac{8GH_e}{2-\nu}\int_0^{\eta_e}\left[A_e V_2(\alpha_e\xi) + B_e V_3(\alpha_e\xi)\right]^2 d\xi \quad [35]$$

Equating this to the second term of Equation [19] one finally obtains

$$k_s = \frac{16G}{\pi D(2-\nu)} \quad [36]$$

Here G= Dynamic shear modulus of soil, ν= Poisson's ratio of soil, D= Diameter of well

CONSIDERATION OF MASS AND DAMPING VALUE OF THE PILE

The mass matrix of the pile can be expressed as

$$M_w = \frac{\gamma_p AH}{g}\int_0^1 \left[\phi_e^b(z)\right]^2 dz \rightarrow \frac{\gamma_p AH}{g} I_3. + \frac{P}{g}\phi_e^b(H)^2 \quad [37]$$

Here γ_p = Weight density that represents the total weight of pile and P=Allowable static vertical load from top deck for which the pile is designed for.

The damping effect of pile can be expressed as Chowdhury et al (2013)

$$C_w = \frac{\gamma_s D_{eff} H_e V_s}{g} \int_0^{\eta_e} \left[\phi_e^b(z)\right]^2 dz \rightarrow \frac{\gamma_s D_{eff} H_e V_s}{g} I_3. \quad [38]$$

Here V_s= Shear wave velocity of soil.

Under free vibration condition the equation of equilibrium is expressed as

$$M_w \ddot{u} + C_w \dot{u} + K_w u = 0 \quad [39]$$

Solution of Equation [39] can be expressed as Meirovitch (1985) as

$$u = e^{-\zeta \omega_n t}\left[A \sin \omega_n \sqrt{1-\zeta^2}\, t + B \cos \omega_n \sqrt{1-\zeta^2}\, t \right] \quad [40]$$

In equation [40] $\omega_n = \sqrt{K_w / M_w}$ the natural frequency of the system and $\zeta = C_w / \left(2\sqrt{K_w M_w}\right)$, the damping ratio of the system.

Now considering the boundary condition at t=0 u=0 and at t=0 du/dt=V_0 we have

$$u = \frac{V_0}{\omega_n \sqrt{1-\zeta^2}} e^{-\zeta \omega n t} \sin \omega_n \sqrt{1-\zeta^2}\, t \quad [41]$$

It is apparent one has to carry out a time history plot to obtain the maximum amplitude of the pile. Once this is obtained, variation of the same along pile length can be expressed as

$$u(z) = u(t)_{\max}\left[A V_2(\alpha\xi) + B V_3(\alpha\xi) \right] \quad [42]$$

The moment and shear in pile are expressed as

$$M(z) = -EI \frac{d^2 u(z)}{dz^2} \text{ and } V(z) = -EI \frac{d^3 u(z)}{dz^3} \quad [43]$$

Equation [41] to [43] gives the complete solution to a short pile under dynamic load.

A CASE STUDY

To study the proposed model, a raw water jetty supported on piles (Figure-2) subjected to impact load from berthing is studied hereafter. The site is situated at Panihati West Bengal, and the field soil data is as furnished hereafter from the project geotechnical report in Table1.

The diameter of piles are 1.0 and 0.75 meter embedded within the ground to a depth of 7.134m while has a free upstanding length of 15.4m after complete scouring (under worst condition). The dynamic shear modulus of soil is co-related from Hardin and Drnevich (1973) formula for cohesive soil. Considering the soil has more or less uniform property from 3 to 9 m an average value of G constant over the embedded depth of pile is assumed where G_{av}= 55192.71 kN/m^2.The computed allowable load on each pile as per IS-2911 is 354 kN. Computed time period T=1.427 sec. and critical damping ratio= 0.593.However as

recommended by Novak, damping considered is maximum 50% of computed value .Velocity induced at pile head due to ship berthing is 2.5m/sec.

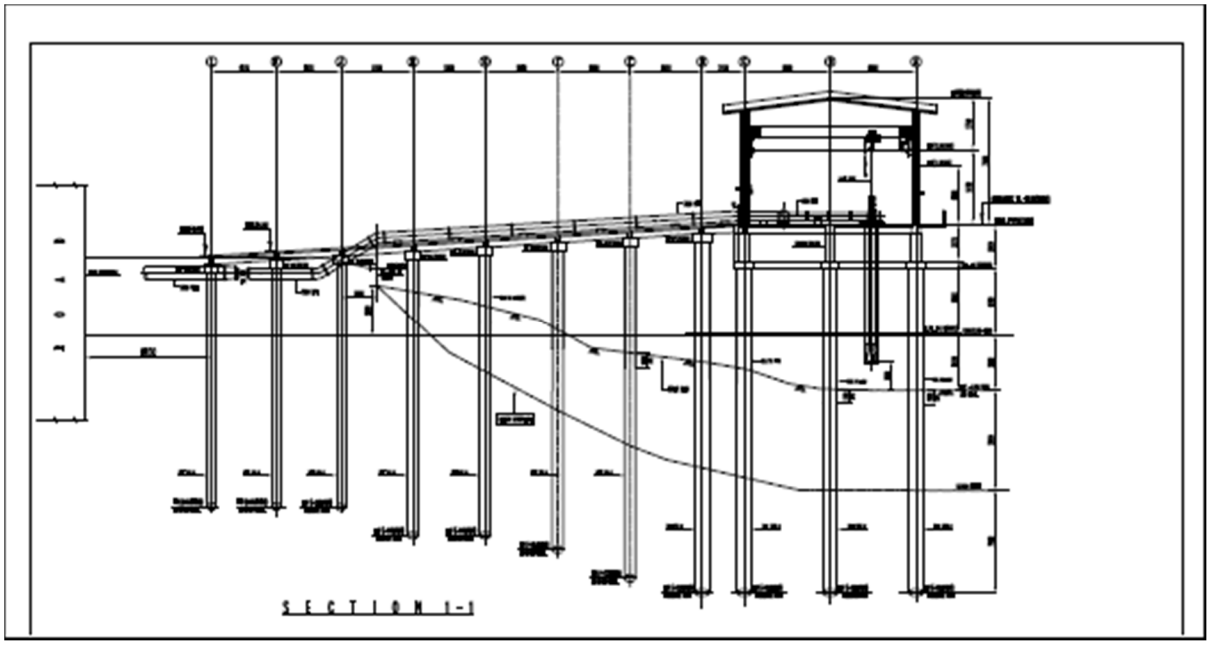


Figure-2 Sectional view of the Raw Water Jetty

Table1: Relevant Soil data from project geotechnical report.

Bore hole #	Depth	γ_b	c	ϕ	LL	PL	e_0	Sand Size	Silt Size	Clay Size
BH-1/UDS-1/1	3.0-3.45	19	45	5	72.5	34	0.93	17	39	44
BH-1/UDS-1/2	6.50-6.95	20	43	6	64	27.5	1.0219	15	45	40
BH-1/UDS-1/3	9.0-9.45	19	51.5	7	71	31	1.22	11	47.5	41.5
BH-1/SPT-1/4	10.5-10.95	-	-	-	48.5	25	-	-	-	-
BH-1/SPT-1/6	14.5-14.95	-	-	-	53	25	-	-	-	-
BH-1/SPT-1/12	23.5-23.95	-	-	-	64.5	25	-	-	-	-
BH-1/SPT-1/16	30-30.45	-	-	-	62.5	26	-	-	-	-

The time history plot of the amplitude of vibration is as shown in Figure 3

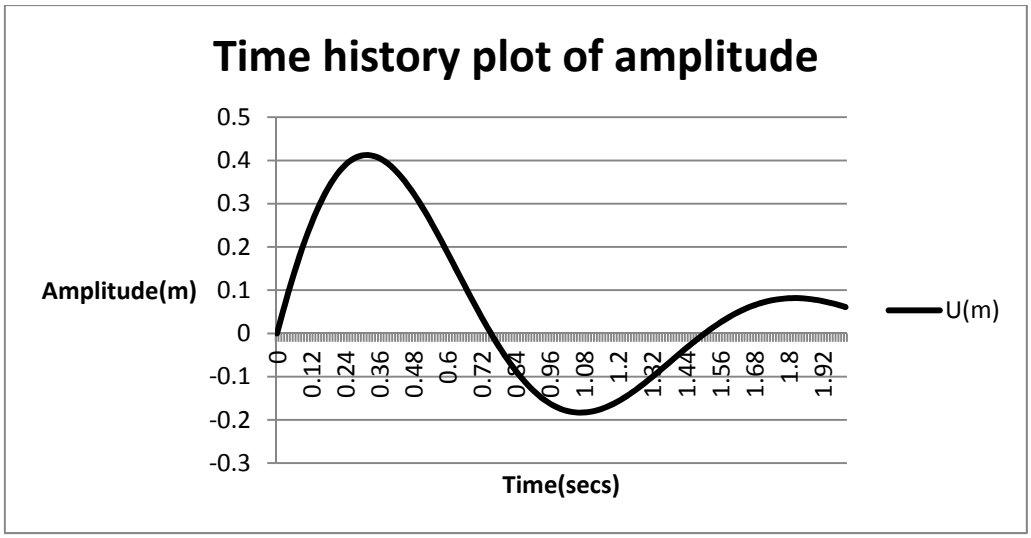


Figure-3 Time history plot of the amplitude of vibration of short piles.

Bending moment and shear force induced in the pile are shown in Figure 4 and 5. It is observed that unlike long piles the behavior is completely different and load is distributed along the whole length of pile unlike a long pile where the moment and shear is restricted to top few meters.

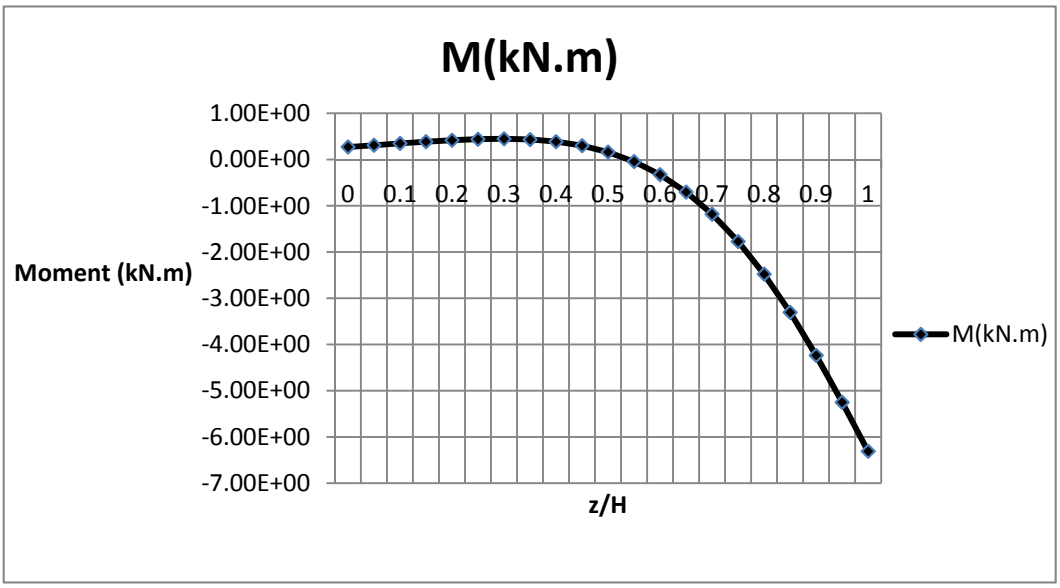


Figure 4 Bending Moment plot of pile under impact load

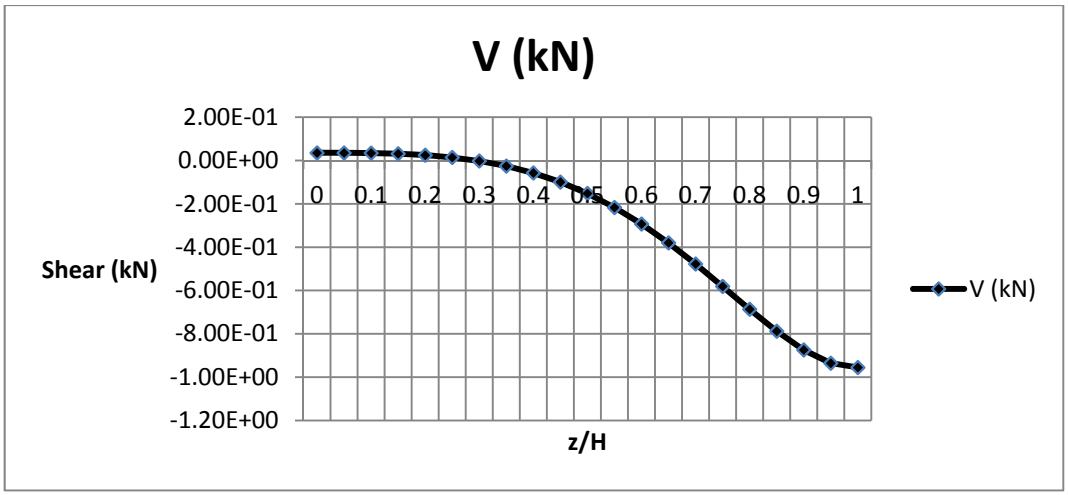


Figure 5 Shear force plot of pile under impact load

It is observed that though the displacement is high (410 mm) the moment and shear induced in the pile is not high. This can be attributed to the large unsupported length of the pile that makes it considerably flexible resulting in low values of moment and shear. In this particular case possibly the buckling load of pile and secondary moment due to $P\Delta$ effect would govern the structural design of the supporting pile. As the moment and shear induced in the pile is low the pile below the scour line that behaves as short pile is not subjected to any significant load and would not induce significant stress in the surrounding soil inducing any failure

CONCLUSION

A comprehensive mathematical model for dynamic response of short jetty piles under transient load is presented herein that gives an insight to its behavior under transient type loads. The solution being analytical in nature, no special software need to be developed and can well be carried out in standard commercially available utility packages like a spread sheet or software like MATHCAD, MATLAB etc.

REFERENCES

Banerjee, P.K and Sen, R. [1987]. "Dynamic behaviour of axially and laterally loaded piles and pile groups" in Developments in Soil Mechanics and Foundation Engineering, Vol. 3, (Banerjee, P.K. and Butterfield, R. ed.)Elsevier Applied Science, London.

Brinch Hansen J (1961) The ultimate resistance of rigid piles against transversal force. Danish Geotechnical Buletin # 12 Copenhegan pp 5-9.

Broms B.B.[1965]. "Design of Laterally loaded piles", J. of Soil Mech. and Found Engg. Div. ASCE, 91 No SM-3 pp79-98.

Chowdhury I and Dasgupta S.P. [2008]. Dynamics of Structures and Foundations – A unified approach, Vol 1& 2; CRC Press, Leiden, Holland.

Chowdhury I and Dasgupta S.P. (2010) Estimation of lateral load capacity of short piles under earthquake force.Proceeding, 5th International Conference on Recent Advances in Soil Dynamics and Earthquake Engineering San Diego California USA.

Chowdhury I and Dasgupta S.P. (2013) Dynamic response of a partially embedded cylindrical structure under seismic force considering foundation compliance 22nd International Conference in Structural Mechanics in Reactor Technology San Francisco USA pp 18-23.

Desai C.S. and Christiansen J.T. (1985), Numerical Methods in Geotechnical Engineering. McGraw Hill publications, USA.

Dobry, R. and Gazetas, G. [1988]. "Simple Method for dynamic stiffness and damping of floating piles groups", Geotechnique, 38, No 4, pp-557-574.

Hardin B.O. and Drnevich V.P. (1973) Shear Modulus and damping in soil, design equations and charts. JSMFD ASCE Vol. 98.

IS -2911 Code of practice for analysis and design of pile foundations, Bureau of Indian Standards India.

Karnovsky I and Lebed O [2002]. Formulas for Structural Dynamics; McGraw-Hill Publication, NY.

Meirovitch, L. [1985]. Analytical Methods in Vibration, Macmillan Publication, London.

Novak, M. [1974], "Dynamic stiffness and damping of piles", Can. Geotech. J., Vol.11, pp.574-598.

Novak, .M. and El Sharnouby. B. [1983], "Stiffness and damping constants for single piles", J. Geotech. Engg. Div., ASCE, 109, pp. 961 –974.

Parmelee, .R.A., Penzien J, Scheffey, C.F, Seed, H.B and Thiers, G. [1964]. "Seismic effects on structures supported on piles extending through deep sensitive clays", University of California, Berkeley, Report SESM 64-2.

Penzien, J. [1970]. Soil Pile Foundation Interaction in Earthquake engineering, (R.L. Wiegel, ed) Prentice Hall, Englewood Cliff, New Jersey.

Shames, I.H. and Dym, C.L. [1995]. Energy and Finite Element Method in Structural Mechanics, New Age,International Publishers Ltd., New Delhi.

Tajimi H. [1966]. "Earthquake response of Foundation Structures (in Japanese)", Report, Faculty of Science and Engineering, Nihon University Tokyo 1.1-3.5.

Wolf J [1985]. Dynamic Soil Structure Interaction in Time Domain, Prentice Hall, New York.

DEEP EXCAVATION FOR LOOP PIT

Manos De, Tata Consulting Engineers Limited, Jamshedpur, Jharkhand, India, Phone - (0657)6696456, email - mde@tce.co.in
Pathik Deb Mallik, Tata Steel Processing and Distribution Limited, Kolkata, West Bengal, India, Phone – (033)66130600, email – pathik@tspdl.com
Shyamal K. Mitra, S.K.Mitra & Associates, Kolkata, West Bengal, India, Phone – +91 9903072403, email – skma99@gmail.com
Shuvranshu Rout, Tata Consulting Engineers Limited, Jamshedpur, Jharkhand, India, Phone - (0657)6696235, email - skrout@tce.co.in
Rajiv Kishore, Tata Consulting Engineers Limited, Jamshedpur, Jharkhand, India, Phone - (0657)6696585, email - rkishore@tce.co.in

ABSTRACT

This paper presents a case study on the design and construction of a deep underground pit structure constructed inside almost a century old existing plant building. The complexity and challenge for the design and construction lay in executing the work in a difficult subsoil condition especially the presence of deep mica schist. The limited space availability in the existing plant for construction work without hampering regular production in other adjoining areas of the plant made the execution more challenging. Experience with difficult subsoil and proximity to old foundations entailed a non-conventional engineering approach while ensuring complete safety in spite of maintaining the normal operation.

Keywords: deep excavation, mica schist, loop pit, factor of safety, slope stability

INTRODUCTION

Tata Steel Processing and Distribution Limited (TSPDL) is a subsidiary unit of Tata Steel Limited (TSL) having a CR processing facility inside the premises of Tata Steel Limited. TSPDL intended to install equipment for a new slitting line inside the existing shed including construction of very deep structure called “loop pit” where the strips from cut CR sheets collect in the form of loops and are recovered as scrap. The entire plant is located within the shed of existing plant. The construction of all foundations including the loop pit is to be executed in the limited area without disturbance to normal production work in balance areas of the plant and also maintain safety and integrity of existing structures.

The existing shed is an old structure constructed approximately 80 years ago. The building column foundations are gravity type design of brick masonry supporting only the vertical load from the columns. This type of foundation designed with no eccentricity of loading provides no allowance for implementing any foundation stabilizing design. The present project required civil construction for the new equipment foundations safely within this area.

LAYOUT

The loop pit structure has plan dimensions of 5.5m X 2.1m with depth to pit floor of 11.2m below existing floor level of the CR plant. The centreline of the pit is located at 9500mm from the centreline of columns on Row-A; the clear distance from edge of pit wall to edge of column foundation is approximately 6m. The limited space available on the side of A-row columns posed serious constraint on making excavation plan for this deep structure without destabilizing the foundation system of the existing shed columns.

The layout of the loop pit within the existing plant shed is shown in Fig.1.

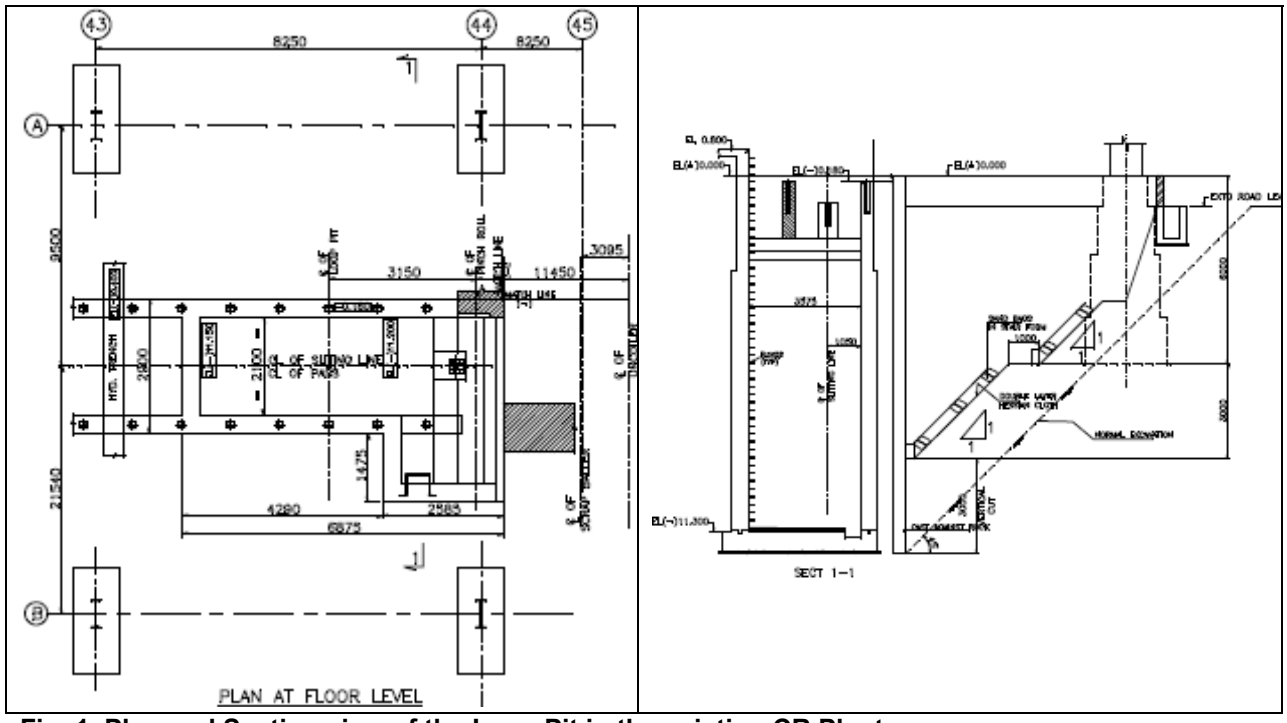


Fig. 1. Plan and Section view of the Loop Pit in the existing CR Plant

SITE CONDITIONS AND CONSTRAINTS

Due to limited space, open excavation with stable slopes having intermediate benches was not found to be feasible from all sides of the pit. Space for making sloped cut for excavation was available from three sides of the structure; only the edge on column row-A side is critical for excavation. It was further observed from the borehole log data provided in the soil report that highly weathered rock exist from about 8.0 m below the existing ground level. Hence, any kind of protection system made of driving method was also not found to be feasible. The earth retaining system was planned by adopting some kind of boring method.

After considering all the design and constructional aspects, it was suggested that contiguous bored cast-in-situ piles parallel to A-row would be most suitable retaining system for the project. Contiguous bored piles designed to retain the earth above the dredge line by cantilever action (stabilizing passive resistance being greater than the destabilizing active earth pressures), require large depth of embedment of bored piles below the dredge line. To retain 12.5 m of earth/weathered rock, required depth of embedment of piles below the dredge line was calculated as more than 10 m. This meant that the pile length would be more than 22.5 m from the existing ground level. Achieving such embedment below the dredge line in moderately weathered rock would have been very difficult within practical time limit.

GEOTECHNICAL INVESTIGATION AND SUBSOIL DESCRIPTION

Detail geotechnical investigation was carried out at the site comprising of 2 (two) boreholes (BH-1 & BH-2) taken to depth of 15m each below plant floor level. The general borehole data and soil stratification for the site as extracted from the geotechnical investigation report are presented in Table 1.

The depth of soil boring was found varying from 4.5m (BH-1) to 6.5m (BH-2) and depth of rock drilling was found varying from 10.5m(BH-1) to 8.5m(BH-2). The standing water level in BH-1 was 2.6m and BH-2 was 3.8m. The total soil depth was classified broadly into five strata. In boarder perspective, the top two strata in the upper horizon constituted the overburden sandy type soil mixed with brickbats, lateritic soil with nodules etc. The overburden soil was followed by mica-schist rock strata of varying weathering state. Degree of weathering of underlying rock varied from completely weathered to moderately weathered state.

Table 1. Sub-soil Stratification

Strata No	**Material Description**	**Ava. Thickness(m)**	**Ava. N-value**	CR (%)	RQD (%)
I	Heterogeneous Sandy Fill	2-4	6-9		
II	Silty Clay	2-2.5	7-18		
IIIA	Completely weathered Mica-Schist	2	>100		
IIIB	Highly Weathered Mica-Schist	2-3.5		30-48	0-29
IIIC	Moderately weathered Mica-Schist	> 5		51-86	0-78

PRELIMINARY EXCAVATION SCHEMES

Based on the constraints mentioned above and the subsurface stratigraphy, it was suggested to adopt braced excavation technique comprising bored cast-in-situ concrete piles and wales and struts of rolled steel sections as its principal components. The drawing showing this excavation scheme is shown in Fig.2.

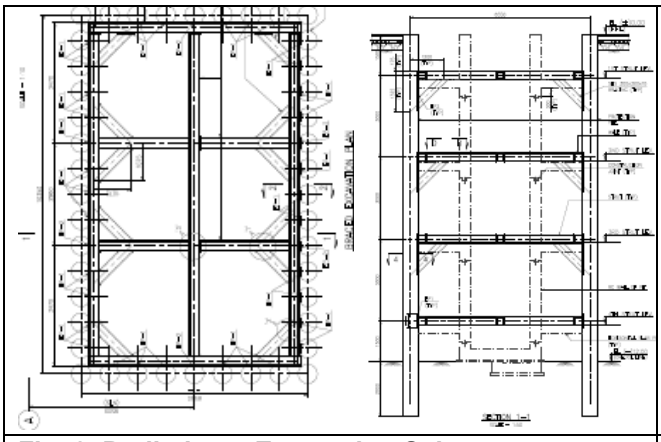


Fig. 2. Preliminary Excavation Scheme

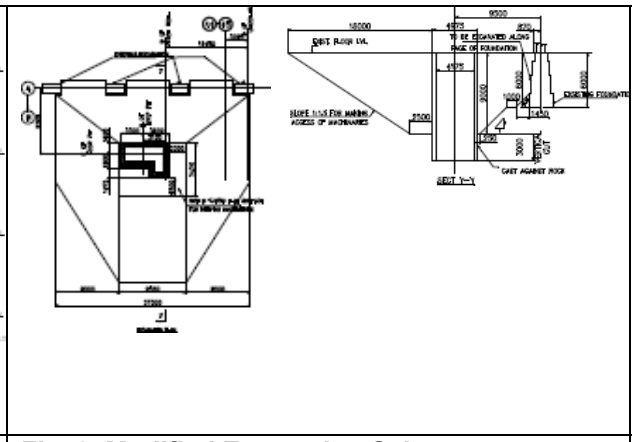


Fig. 3. Modified Excavation Scheme

This scheme shown in Fig.2 suffered from the difficulty in terms of both cost and execution time and could not be taken up for execution. New scheme was developed which involved part open excavation and part protection micro-piling (using sal-bullah/ concrete filled pipe piles) along the line of column foundations as shown in Fig. 3. Work was started at site for installation of the pipes along the A-row columns using soil boring equipment. However, the progress of work on advancement of the boreholes was very poor firstly due to presence of hard rock pieces and secondly on account of interference with the operating overhead crane which was interfering with the boring rig. This scheme also had to be abandoned after unsatisfactory progress during a period two weeks of work.

MODIFIED EXCAVATION SCHEME

The progress of excavation work had come to a standstill and complete re-engineering for a feasible excavation scheme was required. Since all means of protected excavation had to be abandoned, open excavation with suitable slope was the only option left for execution. It was found that on A-row, a dado wall of 1.0m height existed flush with the outside edge of building column. It was planned to dismantle this wall which would provide additional 2.4m space on this side of the pit. This additional space was to be utilized to accommodate the slope of the excavation line towards A-row columns. The excavation slope was extended to the edge of RCC drain on the road side. This scheme was discussed at site and preliminary sketch developed. The existing situation in the work area prior to start of the deep excavation and preliminary sketch for the alternate excavation scheme is shown in Fig. 4 and Fig.5 respectively.



Fig. 4. Existing site condition

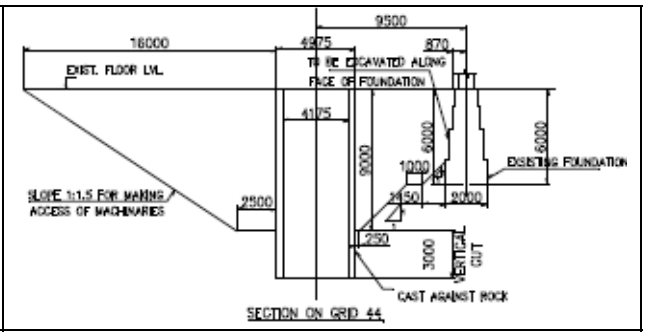


Fig. 5. Sketch for proposed excavation scheme

STABILITY ANALYSIS OF EXCAVATION SLOPE

Method of Stability Analysis

This scheme developed during the site meeting was analysed to evaluate the stability factor for the proposed excavation slope. The initial scheme was also modified slightly to introduce a bench at (-) 6.0M level to enhance the stability. The slope was analysed for stability through slope stability calculations to assess the factor of safety. The soil properties and inferred data used for the analysis are as presented in Table-2 below.

Table 2. Design Geotechnical Parameters

Strata No	Material	Unit Weight (kN/m^3)	Cohesion(C) (kPa)	Angle of Internal Friction (ϕ) deg
I	Heterogeneous Sandy Fill	18	0	28
II	Silty Clay	18	20	20
IIIA	Completely weathered Mica-Schist	20	200	25
IIIB	Highly Weathered Mica-Schist	22	500	30
IIIC	Moderately weathered Mica-Schist	25	750	35

Slope Stability Software Program:

Commercial computer programs Slope/W and Seep/W 2007 by Geoslope were used for the stability analysis of the proposed excavation slope. This software uses two-dimensional geometry and calculates the factor of safety against slope failure through limit equilibrium method. The various options are:
Simplified Bishop's method of slices – assumes a circular failure plane.
Simplified Janbu's method of slices – uses failure surface of general shape.
Spencer's method of slices – assumes failure surface in general or circular shape.

Factor of Safety

Results of slope stability analysis are indicative of failure mechanism of excavated face i.e. whether the slope is adequately safe or at risk of incipient failure. The factor of safety (FoS) is considered as indicator of safety margin to decide on risk of failure and acceptable level of FoS for specific condition.

No specific guideline on minimum FoS is available for the temporary excavations. Under the circumstance references on FoS as advocated in texts and publications, standards, codes are reviewed. It is noted that suggested values are based on use of in-situ and realistic geotechnical parameters, analysis of sufficient number of probable failure surfaces to determine critical failure plane and carrying out the construction with proper quality control complying with design requirements.

In general for static loading condition, a minimum value of factor of safety of 1.5 is commonly employed for permanent or long term performance (Lambe and Whitman, 1969). Based on recommendations of other national & international standards recommended FoS values are summarised below.

Table 3. Desired Factor of Safety

Condition	Desired Min. FoS	Reference
Long Term Performance (static)	1.5	US, UK, Canadian standards
Short Term Performance (static)	1.2-1.3	US, UK, Canadian standards
Construction condition	1.3	IS:7894-1975, Appendix A
Steady seepage with sustained rainfall	1.3	IS:7894-1975, Appendix A

The proposed slope for the excavation was analysed through all the available methods in the software to arrive at the minimum FoS. Since the soil burden to bottom of excavation is removed, the column load which is almost equal to this overburden is not considered. The summary of the methods employed, main features of the theory, limitations and resultant value of FoS are presented in Table 3 below:

Table 4. Calculated Factor of Safety

Method	Assumptions	Limitations	FoS
Fellenius' Ordinary method of slices	Resultant of the inter-slice forces for all slices is inclined at an angle that is parallel to the base of the slice.	Neglects all inter-slice forces, does not satisfy force equilibrium for individual slices and the slide mass.	1.214
Bishop's Simplified Method	Inter-slice shear forces are assumed zero. Vertical force equilibrium satisfied for each slice; overall moment equilibrium satisfied about centre of rotation.	Horizontal force equilibrium will not be satisfied for one slice.	1.331
Janbu's Simplified Method	No inter-slice forces considered. Vertical force equilibrium satisfied for each slice. Overall horizontal force equilibrium satisfied for entire mass.	Does not completely satisfy moment equilibrium condition. A correction factor has been used to account for this inadequacy.	1.159.

Method	Assumptions	Limitations	FoS
Spencer's Method	Complete static equilibrium conditions are satisfied. Assumes constant value of resultant inter-slice force with unknown inclination that is determined during the analysis.		1.223.

The following figures 6, 7, 8 and 9 show the computer generated output for the failed soil mass with lowest FoS for each method analysed:

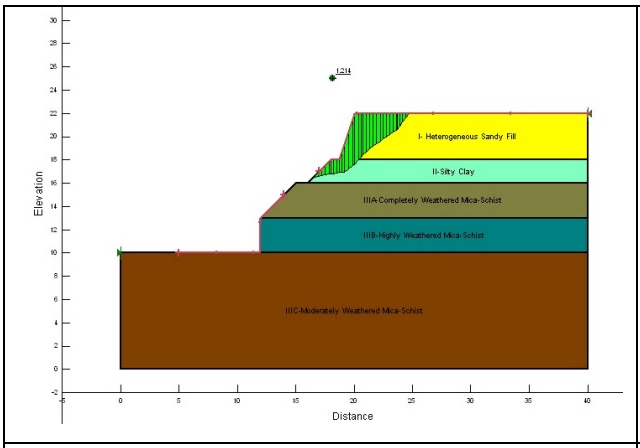


Fig. 6. Method of Ordinary Slices

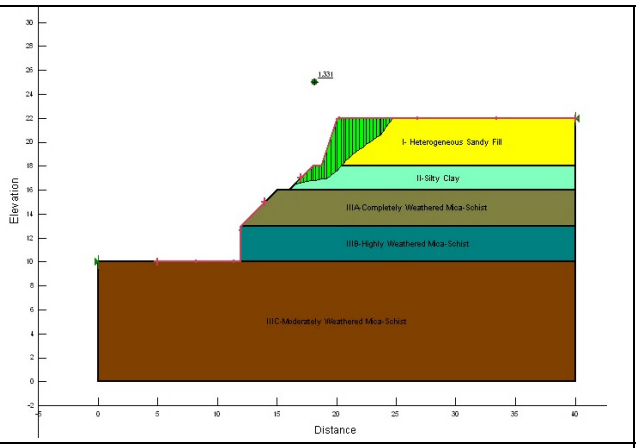


Fig. 7. Bishop's Method

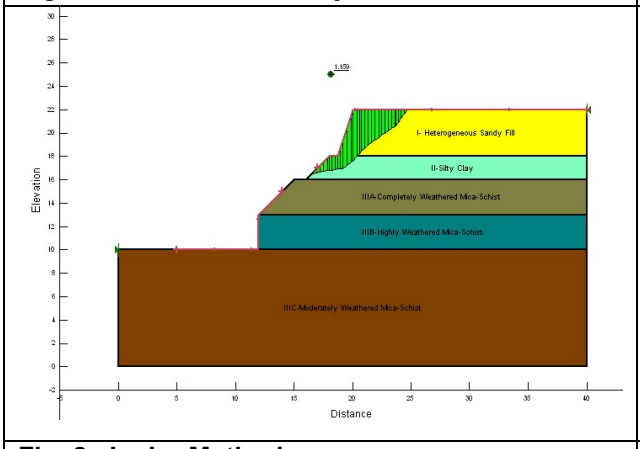


Fig. 8. Janbu Method

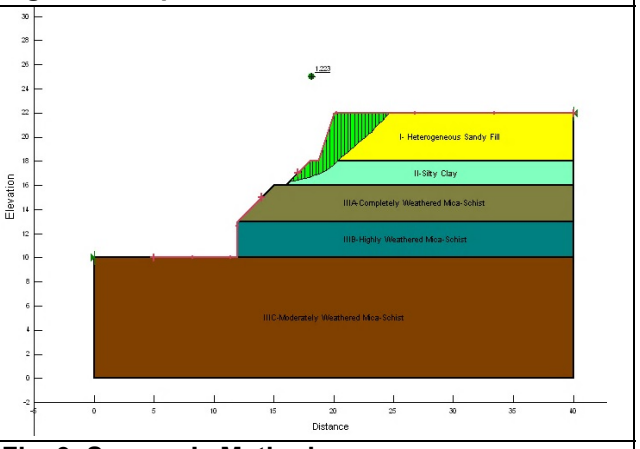


Fig. 9. Spencer's Method

Pore water Pressure

In effective stress analysis, pore water pressures are estimated at relevant locations in the slope. These pore pressures are usually estimated from ground water conditions that may be specified by phreatic surface and piezometer data.

The soil investigation work had been carried out during monsoon when water table was high (2.6m to 3.8m), while the actual execution work was being carried out in the dry months of January-February.

Also, initial trial pits made to depths of 4~6m did not reveal presence of ground water during the start of excavation work. Therefore, presence of ground water is considered at 10.0m depth from ground level for the analysis based on actual site excavation. However, potential seepage was considered from nearby areas at depth of 4m below ground level. In this case steady seepage conditions have been analysed by examining water levels in open excavations pits. Drainage sump with pump out arrangement was provided at the bottom of excavation to keep the mica-schist is dry condition as much as practicable.

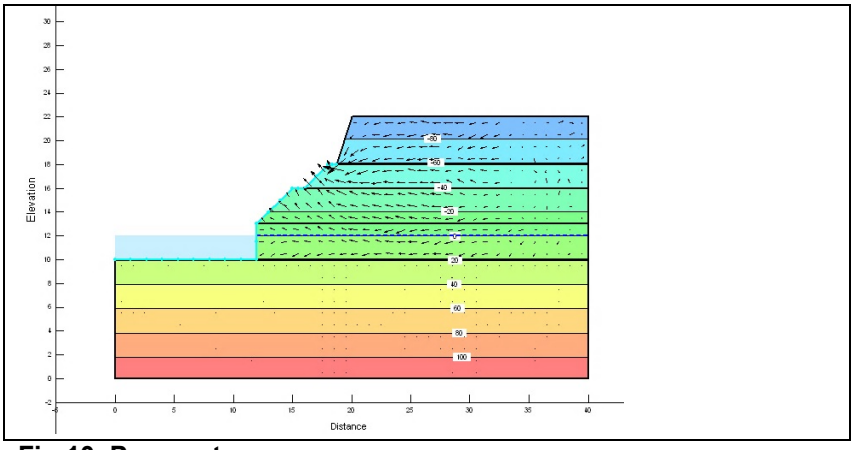


Fig.10. Pore water pressure

SUMMARY AND CONCLUSION

The project required construction of foundations for installation of new equipment inside an existing Coil Rolling unit shed. The most critical unit to be constructed was the loop pit having depth of 12m below the grade level inside the plant. The major difficulties involved space restrictions inside operating plant, proximity to adjacent equipment and building columns, presence of mica schist soil with its particular characteristics which impose severe restrictions on the type of excavation and soil protection scheme to be employed. The difficulties were further compounded by unavailability of tools and materials by the execution contractor to suit site conditions.

The situation required complete revised planning for the execution of the excavation work and a new methodology was drawn up to implement open excavation for the pit. The stability of the slope was analysed using software tools to ensure that adequate safety is ensured for the excavation including the effect of pore water pressure.

The designed slope was found to have minimum factor of safety of 1.159 to 1.331 as per various slope stability methods analysed. This was found acceptable for this temporary work.

Layer of geotextile was provided on the excavated surface, covered with two layers of sandbag to provide additional surcharge weight to increase factor of safety, relieve build-up of pore pressure by allowing the seepage water to flow out into a sump at bottom of slope and prevent scouring of material from slope.

Modified excavation drawing was issued and the work progressed successfully in scheduled time and in safe manner. The alternate concept based on site conditions backed by appropriate design calculations to simulate the site conditions, knowledge and experience on the behaviour of mica-schist formation which

exhibit good strength in dry condition achieved the project requirement where conventional design solutions could not yield desired results.

No instrument for monitoring behaviour of slope was used. Use of suitable instruments for measuring pore water pressure and slope movements will enhance the safety of the work through monitoring of probable destabilizing factors and plan appropriate corrective action.

FIGURES – PHOTOGRAPHS DEPICTING CONSTRUCTION STAGES



Fig.11. Excavation started



Fig.12. Excavation reaches (-)4.0M



Fig.13. Excavation reaches (-) 6.0M



Fig.14. Excavation reaches (-) 9.0M



Fig.15. Excavation reaches (-) 12.0M



Fig.16. Loop Pit Construction started



Fig.17. Loop Pit Construction proceeds



Fig.18. Loop Pit Construction reached top

ACKNOWLEDGEMENTS

We would like to thank Tata Steel Processing and Distribution Limited, Jamshedpur, India for facilitating necessary statutory approvals to Tata Consulting Engineers to work as "Consultant" in such a complex brown field project. We are also taking this opportunity to highlight their continuous support on site specific inputs throughout project execution.

We would like to thank SKM Geosurvey, Kolkata, India for the geotechnical investigation report, interpretation of field and laboratory results and active support in formulation of site specific solution for the deep excavation.

REFERENCES

Abramson, L.W., Lee, T.S., Sharma, S., and Boyce, G.M., 2001. Slope Stability and Stabilization Methods, 2nd edition, John Wiley and Sons, New York, 736 P.

Gadd, P. E. ,1988. Sand bag slope protection: design, construction and performance, Arctic Costal processes and slope protection design, ASCE, New York, pp. 145-165.

Lambe, T.W.,and Whitman, R.V., 1969. Soil Mechanics, John Wiley and Sons, New York, 576 P.

Puller, M., 2003. Deep Excavations: A practical manual, 2nd edition, Thomas Telford, London, 571 P.

Terzaghi, K., 1943. Theoretical Soil Mechanics, John Wiley and Sons, New York, 510 P.

Terzaghi, K., and Peck, R.B., 1967. Soil Mechanics in Engineering Practice, John Wiley and Sons, New York, 549 P.

Twine, D., and Roscoe, H.C., 1999. Temporary Propping of Deep Excavations-Guidance on Design, CIRIA, C517.

RELIABILITY ASSESSMENT OF THE CAPACITY OF SINGLE PILE SUBJECTED TO VERTICAL LOADING

Rajarshi Pramanik, IITKharagpur, Kharagpur, West Bengal, India, +919434520539, rpramanik@iitkgp.ac.in
Dilip K. Baidya, IITKharagpur, Kharagpur, West Bengal, India, +919434065386, baidya@civil.iitkgp.ernet.in
Nirjhar Dhang, IITKharagpur, Kharagpur, West Bengal, India, +919434027565, nirjhar@civil.iitkgp.ernet.in

ABSTRACT

This paper performs the reliability evaluation of pile foundation under vertical loading condition using the concept of fuzzy set theory. The uncertain parameters are expressed as fuzzy numbers. Monte Carlo simulation technique in conjunction with fuzzy set theory and fuzzy reliability index approach are implemented in evaluation of the probability of failure of pile foundations. The results are validated through some well established methods such as, First Order Reliability Method (FORM), Second Order Reliability Method (SORM), and direct Monte Carlo Simulation (MCS). Response surface method (RSM) is used to approximate the original limit state equation through second order polynomial. The effect of the position of the water table is also highlighted. Finally, the effect of the variation of applied load is examined and it is observed that the fuzzy reliability analysis gives more conservative estimate of failure probability than the other methods.

Keywords: fuzzy number, membership function, random variable, pile foundation

INTRODUCTION

Civil engineering structures, such as high rise buildings, bridges, offshore platforms etc. are always subjected to vertical as well as horizontal loads. To support these structures, pile foundations are generally the solution in most of the situation. It transmits load from the superstructure to soil at a reasonably great depth. This transfer may be by vertical distribution of the load along the pile shaft or a direct application of load to a lower stratum through the pile tip. Different methods are available to estimate the capacity of piles embedded in different types of soil and under the application of vertical and horizontal loading. To consider the variability in soil and other unforeseen able situation, generally a reasonable value of factor of safety is used to estimate the designed capacity of the pile. Recent developments have shown a trend to place the treatment of uncertainty on a more formal basis, in particular by applying the results of reliability theory to geotechnical engineering. Keeping in mind the importance of pile foundation in the engineering structures it is essential to maintain a high structural safety which result in increase in reliability. The probability theory has been proved to be a powerful tool for representing variability in mathematical models. The variability associated with soil parameters and the modeling uncertainties are needed to be considered for the reliability assessment purpose.

Recent development (Zhang et al. 2005; Misra and Roberts 2006; Haldar and Babu 2008; Basu and Salgado 2012; Teixeira et al. 2012; Pula and Rozanski 2012; and Chan and Low 2012) showed that the reliability analysis of pile foundations subjected to axial as well as lateral load has been one of the important current research topic in geotechnical field. Probabilistic based performance criteria were quantified for a single pile and pile groups in cohesionless soil by Eloseily et al. (2002). A *p*-multiplier approach was incorporated into the analysis to modify the p-y curve for a single pile to obtain the p-y curve for individual piles in a pile group. A statistical analysis of set up capacity of pile was carried out from the database of a large number of pile testing data in clay by Yang and Liang (2006). Load and resistance factor design (LRFD) using FORM was used for examining the different load and resistance factor for different target reliability index. Limit state analysis of drilled shaft was performed by Misra and Roberts (2006) in probabilistic framework. The fuzzy based reliability analysis (Dodagoudar and Venkatachalam 2000; and Park et al. 2012) of the earth slope was reported in the literature. Dodagoudar

and Venkatachalam (2000) presented a new approach, called fuzzy point estimate method (FPEM) for reliability evaluation of earth slope. Park et al. (2012) reported a hybrid approach, fuzzy set theory in conjunction with Monte Carlo simulation technique, to determine the failure probability of earth slope. Second Order Reliability Method (SORM) (Kiureghian et al. 1987; Breitung 1984; and Chan and Low 2012a) applied to many geotechnical problems for the approximation of the failure probability reasonably. Chan and Low (2012a) represented an efficient SORM approach based on approximating paraboloid fitted to the limit state surface (Kiureghian et al. 1987) in the neighborhood of the design point and applied to some geotechnical problem. Reliability analysis using response surface method (RSM) (Babu and Srivastava 2007; Chan and Low 2012b; Ji and Low 2012; and Zhang et al. 2015) was applied to many engineering problem for its approximation power to depict the original limit state equation. Babu and Srivastava (2007) analyzed the failure probability of shallow foundation under bearing capacity and settlement criteria failure using RSM. In this analysis two level factorial design concept was used to construct the response surface. Zhang et al. (2015) used the concept of RSM by calibrating the design points in each iteration and also developed a modified response method to overcome the shortcoming associated with the classical RSM.

In classical reliability method, FORM, SORM, direct MCS are adequately incorporate physical randomness, statistical and modeling uncertainty but they are unable to capture the vagueness or fuzziness and ambiguity of the parameters which is systematically incorporate in fuzzy reliability analysis. On the other hand, in conventional reliability theory, the variables are assumed as random maintaining a probability distribution such as normal, lognormal, beta etc. The prediction of the distribution pattern of the random variable needs a large number of data set which remains unknown to us in most of the situation. In fuzzy reliability concept, we overcome this deficiency by considering the variables as fuzzy numbers rather than random variables.

In this paper, fuzzy set theory concepts (Zadeh 1965) are used for reliability evaluation of pile foundation under vertical loading condition. The uncertainty is quantified through fuzzy reliability index and probability of failure obtained from fuzzy Monte Carlo simulation technique. The results are validated through some well established methods such as, FORM, direct MCS and SORM. Finally, response surface method (RSM) is used to approximate the original limit state equation through second order polynomial. The effect of the position of the water table is also highlighted. Finally, the effect of the variation of applied load is examined.

CONCEPTS OF FUZZY SET THEORY

A fuzzy set, introduced by Zadeh (1965), can be defined mathematically by assigning to each possible individual in the universe of discourse a value representing its grade of membership in the fuzzy set. This grade corresponds to the degree to which that individual is similar or compatible with the concept represented by the fuzzy set. Thus, individuals may belong in the fuzzy set to a greater or lesser degree as indicated by a larger or smaller membership grade. These membership grades are often represented by real number values ranging in the closed interval between 0 and 1.

Fuzzy set and membership function

If X is a collection of objects denoted generically by x then a fuzzy set A in X is a set of ordered pairs (Zimmermann 2001):

$$A = \{(x, \mu_A(x)) \mid x \in X\} \quad [1]$$

$\mu_A(x)$ is called the membership function or membership grade of x in A which can be defined as $\mu_A(x) : X \rightarrow \{0,1\}$. This membership function can predict the degree of possibility of occurrence for each members of the fuzzy set. Triangular and trapezoidal shapes of membership functions are used more often for representing fuzzy numbers. In this paper, trapezoidal membership function has been used and this

type of membership function can be expressed in the form of a quadruple as follows (Dodagoudar and Venkatachalam 2000):

$$A = [a, b, c, d] \quad [2]$$

where *a* and *d* are, respectively, the lower and upper *x* values of the trapezoid at $\mu_A(x) = 0$, and *b* and *c* are the *x* values that correspond to $\mu_A(x) = 1$ (Fig. 1).

α-cut and extremities of fuzzy number

The set of elements that belong to the fuzzy set *A* at least to the degree *α* is called the *α*-level set. It is defined as follows (Zimmermann 2001):

$$A_\alpha = \{x \in X \mid \mu_A(x) \geq \alpha\} \quad [3]$$

the *α*-cut of a fuzzy set *A* is the crisp set A_α that contains all the elements of the universal set *X* whose membership grades in *A* are greater than or equal to the specified value of *α*. The basic idea of the *α*-cut concept is the discretization of a fuzzy number into a group of *α*-cut intervals. For each of the uncertain parameters, the *α*-cut of a fuzzy set will give an interval having two points, i.e. upper and lower bound values for a particular *α*-cut (Fig. 1). Any particular fuzzy set *A* can be transformed into an infinite number of *α*-cut sets, because there are an infinite number of *α* values on the interval [0,1]. Each uncertain parameter is described by their mean value and standard deviation. The dispersion, i.e. value of *a* and *d*, of each variable is defined by two parameters k_1 and k_2. k_1 and k_2 are the number of sigma units which will take values 0.5 to 3.0 depending on the data available and accuracy of the results desired (Dodagoudar and Venkatachalam 2000). The value of the parameters of the trapezoidal fuzzy number are: $a = E[X] - k_1\sigma[X]$, $b = E[X] - k_2\sigma[X]$, $c = E[X] + k_2\sigma[X]$ and $d = E[X] + k_1\sigma[X]$. Where, *E[X]* and *σ[X]* are the expected value and standard deviation of the variable respectively. For each *α*-cut level, each parameter gives an upper bound and a lower bound value. The values can be obtained as given below (Dodagoudar and Venkatachalam 2000):

$$x_{\alpha_i^+} = c + V_{\alpha_i} \quad [4a]$$

$$x_{\alpha_i^-} = b - V_{\alpha_i} \quad [4b]$$

Where V_{α_i} = the value to be added or subtracted to obtain the corresponding parameter point considering its membership function, $x_{\alpha_i^+}$ and $x_{\alpha_i^-}$ = the vector of coordinates of the uncertain parameters.

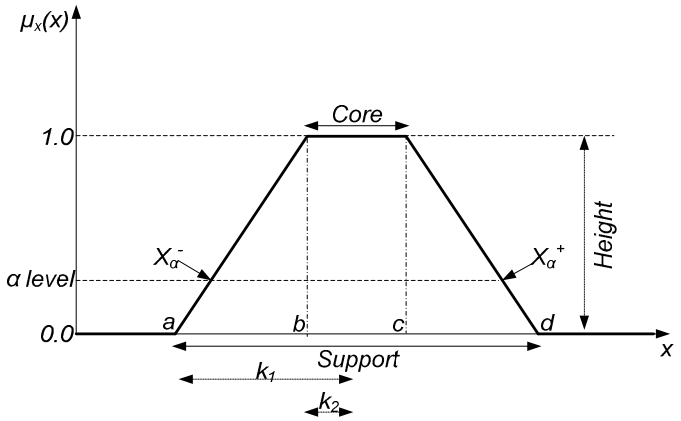


Fig. 1 Fuzzy membership function and α-cut level

Fuzzy reliability analysis

In this method, resistance and load both are assumed as fuzzy number whose membership function varies as trapezoidal membership function. Performance function (difference between resistance and load) is also assumed as fuzzy number and trapezoidal membership function is also defined its characteristic. Resistance and load can be defined as interval from Eq. 2:

$$R = [r_1(\alpha), r_2(\alpha), r_3(\alpha), r_4(\alpha)] \quad [5]$$

$$Q = [q_1(\alpha), q_2(\alpha), q_3(\alpha), q_4(\alpha)] \quad [6]$$

According to fuzzy arithmetic (Zimmermann 2001; Park et al. 2012) performance function can also be defined as interval:

$$Z = R - Q = [z_1(\alpha), z_2(\alpha), z_3(\alpha), z_4(\alpha)] = [r_1(\alpha)-q_4(\alpha), r_2(\alpha)-q_2(\alpha), r_3(\alpha)-q_3(\alpha), r_4(\alpha)-q_1(\alpha)] \quad [7]$$

Fuzzy reliability index (FR) can be defined by the probability that the membership function of the performance function (Z) is larger than 0. This is calculated as the ratio of the area of the membership function for which Z is greater than 0 to the total area of the membership of Z and is given by (Park et al. 2012):

$$FR = \frac{\int_{z>0} \mu_z(z)dz}{\int_z \mu_z(z)dz} \quad [8]$$

Fuzzy based Monte Carlo simulation

Fuzzy based Monte Carlo simulation (FMCS) is a hybrid technique which incorporates Monte Carlo simulation in conjunction with the fuzzy interval of random α-cut values in random number generation procedure (Park et al. 2012). Random numbers generation is done in two stages. First, α-level values are randomly chosen between 0 and 1. Thus each fuzzy variable gives a lower and an upper limit for each α-level. Next, another random number generation is used in order to randomly select the element values between the upper and lower bound value for each iteration. These values are used as input parameter values to evaluate factor of safety for the pile foundation (Fig. 2). Thus a large number of different factor of safety are obtained, and fuzzy probability of failure can be evaluated with the help of the approach used for conventional MCS. In this approach, Supremum (Sup) and Infimum (Inf) of the output parameter was evaluated after conducting Monte Carlo simulation.

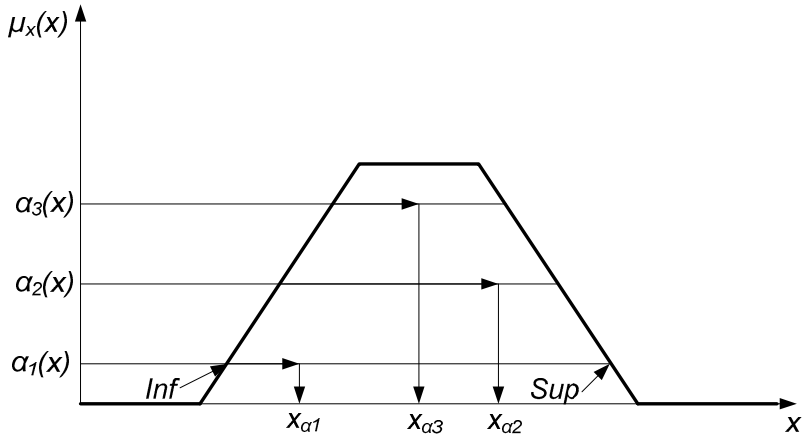


Fig. 2 Concept of fuzzy based Monte Carlo simulation

APPLICATION TO A SINGLE PILE UNDER VERTICAL LOADING

The above methods were applied to many engineering problems (Dodagoudar and Venkatachalam 2000; Sadeghi et al. 2010; and Park et al. 2012) and attempt is made to check the applicability of the same in pile foundation. In order to verify the performance and feasibility of the above methods, the methods are applied to a single pile subjected to vertical loading. Classical probability theory and fuzzy set theory are applied for the sake of uncertainty measurement.

The methods are applied to a single pile embedded in cohesionless layered soil medium (Fig. 3) subjected to axial loading. The water table is on the ground surface. The load carrying capacity of a single pile is given by:

$$Q_u = Q_b + Q_f = q_b A_b + q_f A_s \quad [9]$$

where Q_u = Ultimate bearing capacity of a single pile; Q_b = Ultimate end bearing capacity; Q_f = Ultimate skin friction resistance; q_b = Ultimate unit bearing capacity of the pile at the base; A_b = Bearing area of the tip of the pile; q_f = Ultimate unit skin friction resistance; A_s = Total surface area of the pile embedded below ground surface. Ultimate end bearing capacity is given by:

$$Q_b = (cN_c + \bar{q}N_q + 0.5\gamma' dN_\gamma) \times \frac{\pi d^2}{4} \quad [10]$$

and for cohesionless soil ultimate skin friction resistance is given by:

$$Q_f = P\sum_{i=1}^{N} \bar{\sigma}_v K \tan\delta \Delta L_i \quad [11]$$

where c = cohesion of the soil; N_c, N_q, N_γ = bearing capacity factors; $\bar{q}$ = effective overburden pressure at the tip of the pile; γ' = effective unit weight of the soil; d = diameter of the pile; P = perimeter of the pile shaft; $\bar{\sigma}_v$ = average effective overburden pressure at the middle of the each layer; K = earth pressure coefficient; δ = angle of skin friction between soil and pile material, assumed as 0.75 times of the angle of shearing resistance. ΔL_i = depth of the each layer. Diameter and length of the pile are assumed as 540.0 mm and 16.0m respectively.

Angle of shearing resistance (ϕ) and saturated unit weight of soil (γ_{sat}) are assumed as fuzzy numbers with trapezoidal membership function. The statistical parameters of the soil parameters are shown in Table 1. The COV values are taken from Phoon and Kulhawy (1999). Beside this, applied load coming to the pile top is also assumed as fuzzy number with same membership function. The mean value and coefficient of variation (COV) of the applied load (Q) are assumed as 3500.0 kN and 20.0% respectively. Although, COV value varies from low to high range, in the present study, the assumption of the COV value of the applied load is on the higher side. The values of [a,b,c,d] of each fuzzy number are determined using the method proposed by Dodagoudar and Venkatachalam (2000). In this paper, three cases: (a) Case A, k_1 = 1.5 and k_2 = 0.5; (b) Case B, k_1 = 2.0 and k_2 = 0.5; (c) Case C, k_1 = 2.0 and k_2 = 1.0 are studied. For example, the value of [a,b,c,d] for ϕ_1 is [24.0, 27.0, 33.0, 36.0] for Case A. Similarly, the ranges for the other variables are determined in the similar way.

Results of Fuzzy based Monte Carlo simulation (FMCS)

In the Fuzzy based Monte Carlo simulation (FMCS) technique, random numbers between 0 and 1 are generated and, these values are used as α-cut level value. For each α-cut level, each fuzzy number gives a lower and upper bound value. Trapezoidal membership functions are used for all fuzzy numbers. Then again random numbers are generated in between these two bounded values for each variable. These values are used in the calculation of performance function (Eq. 7). The analysis is done in MATLAB

environment. The probability of failure (p_F) obtained from the FMCS for the three cases are summarized in Table 2. From Table 2, it can be seen that for Case B and C the difference in the p_F value is small whereas, for Case A the p_F value is close to zero. So, it is quite obvious that the influence of k_1 value on failure probability is bigger but the change in p_F value is also occurred for changing k_2 value. So, the dependency of the p_F values always lies on both k_1 and k_2 value.

Table 1 Statistical parameter of random variables

Layer No.	Soil parameter	Mean value (μ)	Coefficient of Variation** (COV) (%)
I	ϕ_1	30.0	10.0
	γ_1^*	20.17	5.0
II	ϕ_2	33.0	10.0
	γ_2^*	20.38	5.0
III	ϕ_3	35.0	10.0
	γ_3^*	20.06	5.0

* saturated unit weight of soil; ** Phoon and Kulhawy (1999)

Table 2 Comparison of the values of the probability of failure

Case No.	FMCS	Fuzzy based reliability index analysis	
	p_F	FR*	p_F (1-FR)
A ($k_1 = 1.5$, $k_2 = 0.5$)	3.80×10^{-5}	0.9795	2.05×10^{-2}
B ($k_1 = 2.0$, $k_2 = 0.5$)	2.60×10^{-3}	0.9308	6.92×10^{-2}
C ($k_1 = 2.0$, $k_2 = 1.0$)	3.90×10^{-3}	0.9319	6.81×10^{-2}

* From Eq. [8]

Results of Fuzzy based reliability index analysis

In fuzzy based reliability index analysis, same membership functions (trapezoidal) are used for all the fuzzy numbers similar to that are used in FMCS. Trapezoidal membership function obtained for resistance and load for Case A are as follow:

R = TrFN [3014.0, 3426.5, 4561.8, 5361.3] [12]

Q = TrFN [2100.0, 2800.0, 4200.0, 4900.0] [13]

Now the performance function is obtained from Eq. 7 as follow:

Z = TrFN [-1886.0, 626.5, 361.8, 3261.3] [14]

Similarly, the membership functions for other two cases (Case B and Case C) are determined. The results for the three cases are summarized in Table 2. It can be seen from Table 2 that the probabilities of failure values differ for different k_1 and k_2 values but the order of magnitudes are same for three cases.

Comparison of results with First Order Reliability Method (FORM) and Direct MCS

In the next stage of the analysis, First Order Reliability Method (FORM) (Low and Tang 1997; and Low and Tang 2004) and direct Monte Carlo Simulation (MCS) are used to compare the results that are obtained from fuzzy set theory. All random variables are assumed to be normally distributed for this analysis and statistical parameters are as shown in Table 1. Here also the applied load (Q) is assumed as a random variable with mean and coefficient of variation are 3500.0kN and 20% respectively. The reliability index (β) value obtained from FORM is 2.1740 and the corresponding probability of failure [$p_F = \Phi(-\beta)$] value is 0.0149. It can be seen from Table 2 that the p_F value obtained from FORM is close to the value obtained from fuzzy based reliability index analysis for Case A but the difference is little bigger for Case B and C. Determination of β is a optimization problem and MATLAB built-in Sequential

Quadratic Programming (SQP) (Metya and Bhattacharya 2014; and Rao 2009) algorithm are used to determine β. The probability of failure (p_F) obtained from direct MCS is 0.0133. The analysis is carried out by simulating 50000 variables in MATLAB environment. This p_F value is quite close to the value obtained from FORM.

Comparison of results with Second Order Reliability Method (SORM)

Now the analysis is carried out using Second Order Reliability Method (SORM). The point fitted paraboloid method originally proposed by Kiureghian et al. (1987) is used in the analysis. The probability of failure value obtained from the analysis is 0.0133 which is smaller than the value obtained from FORM method because the performance function is explicit in nature. This kind of problem was also reported by Chan and Low (2012) for Example 1. The SORM is more efficient than FORM when the β value is quite high and performance function is implicit in nature (Halder and Mahadevan 2003).

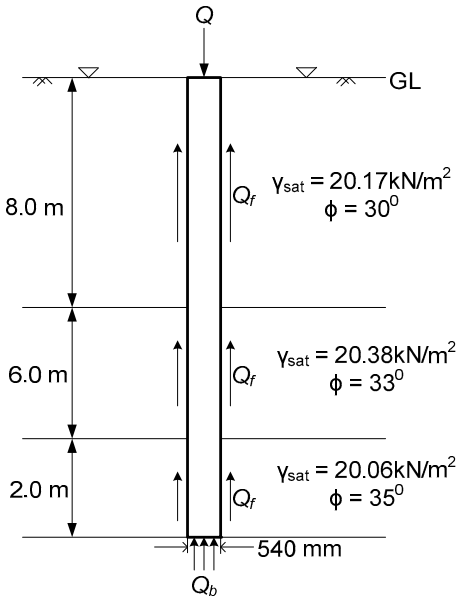


Fig. 3 Pile embedded in layered cohesionless soil strata

Reliability index using Response Surface Method (RSM)

In the next stage, Reliability analysis of the vertically loaded pile are carried out using classical RSM (Zhang et al. 2015) with m = 1, 2 and 3 respectively. All the random variables are assumed to be normally distributed. The reliability index is calculated using FORM. The results for each m values are shown in Table 3. The total number of iteration required to converge the β value for all m value is 3. It can be seen that the β values using RSM are same as that obtained from conventional approach.

Table 3 Reliability index using RSM and FORM

	Design points ($\mathbf{x_D}$)							Reliability index
	ϕ_1	ϕ_2	ϕ_3	γ_1	γ_2	γ_3	Q	(β)
m = 1	29.4	31.3	33.9	19.9	20.3	19.1	4780.3	2.1740
m = 2	29.4	31.2	33.9	19.9	20.3	19.1	4776.7	2.1742
m = 3	29.4	31.1	33.8	19.9	20.3	19.1	4770.5	2.1750

Influence of water table in the analysis

In the previous analysis, the water table was assumed to be on the ground surface and saturated unit weights of soil was considered as random variables. Now, the analysis is carried out for different depth of the water table from the ground surface. Fig. 4 shows the results obtained from four different methods. Only Case A has been examined for the fuzzy reliability index analysis. Soil above the water table is assumed to be in dry condition and the dry unit weight of the soil is assumed as 16.50kN/m^3 and the friction angle has remained unchanged. For each method, it is observed that the depth of water table has a significant effect on the failure probability as the failure probability is reduced on increasing the depth of the water table.

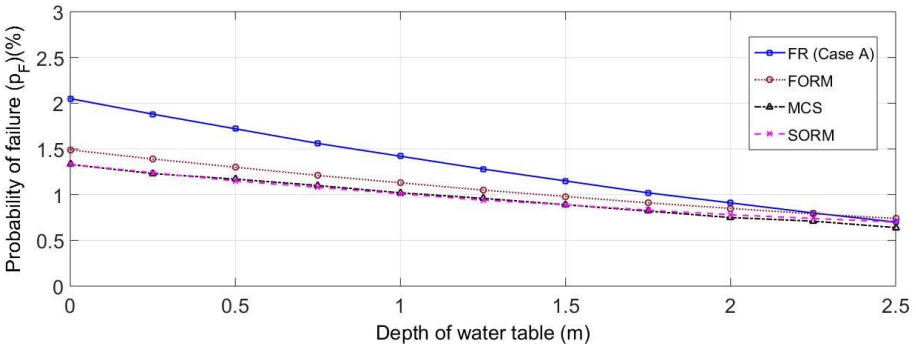


Fig. 4 Variation of p_F with the depth of water table

Effect of variation of applied load

Figure 5 shows the variation of p_F values for different COVs of applied load. The COV values are varied from 10% to 30%. It can be seen from the figure that the failure probability is raised up to 6% for the highest variation of the applied load. Case A is analysed for the fuzzy based reliability analysis and it can be seen that fuzzy based reliability analysis gives conservative estimate of failure probability for higher COV values.

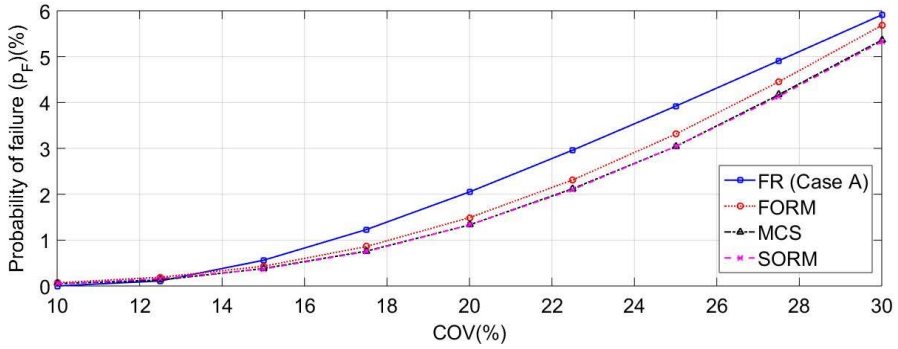


Fig. 5 Variation of p_F for different COV values of applied load

CONCLUSIONS

Based on the studies performed in this paper, the following concluding remarks can be made:

1. The values of probability of failure (p_F) obtained from FMCS and fuzzy based reliability index differ significantly for different cases and the failure probability is high for larger k_1 and k_2

values. Although the difference in p_F values between both methods in each case is high, the increasing trend of p_F values with larger k_1 and k_2 values is similar for both methods.

2. Based on the Second Order Reliability Method (SORM) the probability of failure value obtained is less than the value obtained from FORM. In this case, the efficiency of the SORM does not well observed because the performance function is explicit.
3. The response surface method (RSM) is applied to the analysis and it is found that the value of reliability index is similar to that obtained from the limit state equation.
4. The effect of water table is examined and it is observed that the depth of water table has a significant effect on the failure probability as the failure probability is decreased on increasing the depth of the water table for all the methods. From Fig. 4, it can be seen that the differences in p_F values between FR (Case A) and the other methods are large. This is because the variables are random maintaining normal distribution in all other methods except in fuzzy reliability analysis, where, the variables are assumed as fuzzy numbers.
5. The effect of COV values of applied load is next investigated and it is found that the failure probability is increased with the increase in COV values for all the methods and fuzzy based reliability method always predicts failure probability conservatively.

REFERENCES

Babu, G.L. Sivakumar, and Srivastava, Anil 2007. Reliability analysis of allowable pressure on shallow foundation using response surface method. Computers and Geotechnics, Vol. 34 (2007) pp. 187–194.

Basu, D., and Salgado, Rodrigo 2012. Load and Resistance Factor Design of Drilled Shafts in Sand. Journal of Geotechnical and Geological Engineering, 138(12), 1455-1469.

Breitung, Karl 1984. Asymptotic approximations for multinormal integrals. Journal of Engineering Mechanics, Vol. 110(3), pp. 357-366.

Chan, Chin Loong, and Low, Bak Kong 2012a. Practical second-order reliability analysis applied to foundation engineering. International Journal for Numerical and Analytical Methods in Geomechanics, 36(2012), 1387-1409.

Chan, Chin Loong, and Low, Bak Kong 2012b. Probabilistic analysis of laterally loaded pile using response surface and neural network approaches. Computers and Geotechnics, Vol. 43(2012), pp. 101-110.

Dodagoudar, G.R., and Venkatachalam, G. 2000. Reliability analysis of slopes using fuzzy sets theory. Computers and Geotechnics, Vol. 27, 101-115.

Eloseily, K.H., Ayyub, B.M., and Patev, Robert 2002. Reliability Assessment of Pile Groups in Sand. Journal of Structural Engineering, 128(10), 1346-1353.

Haldar, Achintya, and Mahadevan, Sankaran 2000. Probability, Reliability, and Statistical Methods in Engineering Design, New York, John Wiley & Sons, 304p.

Haldar, Sumanta, and Babu, G.L. Sivakumar 2008. Load Resistance Factor Design of Axially Loaded Pile Based on Load Test Results. Journal of Geotechnical and Geological Engineering, 134(8), 1106-1117.

Ji, Jian, and Low, B.K. 2012. Stratified response surfaces for system probabilistic evaluation of slopes. Journal of Geotechnical and Geological Engineering, 138(11), 1398-1406.

Kim, Dongwook, and Lee, Junhwan 2012. Resistance factor contour plot analyses of load and resistance factor design of axially-loaded driven piles in clays. Computers and Geotechnics, 44(2012), 9-19.

Kiureghian, A.D., Lin, Hong-Zong, and Hwang, Shyh-Jiann 1987. Second-order reliability approximations. Journal of Engineering Mechanics, Vol. 113(8), pp. 1208-1225.

Low, B.K., and Tang, W.H., 1997. Efficient reliability evaluation using spreadsheet. Journal of Engineering Mechanics, Vol. 123(7), pp. 749-752.

Low, B.K., and Tang, W.H., 2004. Reliability analysis using object-oriented constrained optimization. Structural Safety, Vol. 26, pp. 69-89.

Metya, S., Bhattacharya, G. 2014. Probabilistic critical slip surface for earth slopes based on the first order reliability method. Indian Geotechnical Journal, Vol. 44(3), pp. 329-340.

Misra, Anil, and Roberts, Lance A. 2006. Axial service limit state analysis of drilled shafts using probabilistic approach. Journal of Geotechnical and Geological Engineering, 24, 1561-1580.

Park, H.J., Um, Jeongi-Gi, Woo, Ik, Kim, J.W. 2012. Application of fuzzy set theory to evaluate the probability of failure in rock slopes. Engineering Geology, 125 (2012), pp. 92-101.

Phoon, Kok-Kwang, Kulhawy, F.H. 1999. Characterization of geotechnical variability. Canadian Geotechnical Journal, 36, 612-624.

Pula, W., and Rozanski, A. 2012. Reliability of rigid piles subjected to lateral loads. Archives of Civil and Mechanical Engineering, 12(2012), 205-218.

Rao, S.S. 2009. Engineering optimization. theory and practice, 4th edn. Wiley, New York, pp. 422-428.

Sadeghi, N., Fayek, A.R., Pedrycz,W., 2010. Fuzzy Monte Carlo simulation and risk assessment in construction. Computer-Aided Civil and Infrastructure Engineering, Vol. 25, pp. 238-252.

Teixeira, Ana, Honjo, Yusuke, Correia, Antonia Gomes, and Henriques, Antonia Abel 2012. Sensitivity analysis of vertically loaded pile reliability. Soils and Foundations, 52(6), 1118-1129.

Yang, Luo, and Liang, Robert 2006. Incorporating set-up into reliability-based design of driven piles in clay. Canadian Geotechnical Journal, 43, 946-955.

Zadeh, L.A., 1965. Fuzzy sets. Information and Control, Vol. 8, pp. 338-353.

Zhang, L.M., Li, D.Q., and Tang, Wilson H. 2005. Reliability of bored pile foundations considering bias in failure criteria. Canadian Geotechnical Journal, 42, 1086-1093.

Zhang, J., Chen, H.Z., Huang, H.W., and Luo, Z. 2015. Efficient response surface method for practical geotechnical reliability analysis. Computers and Geotechnics, Vol. 69 (2015), pp. 496-505.

Zimmermann, H.J., 2001. Fuzzy Set Theory and its Applications. Kluwer Academic Boston. 514p.

Indicator Pile Program at Port of Oakland, California

By Partha Sircar,
Retired Geotechnical Engineer, California, USA

Abstract

For Berth 22 modifications at the Port of Oakland, nearly 600 octagonal 24-inch 'diameter' precast-prestressed concrete piles were driven, some piles over 160 feet long. Prior to production pile driving, an indicator/test pile program was performed, which included extensive use of dynamic load testing with (Pile Driving Analyzer (PDA) & CAPWAP analyses. The indicator test-pile program resulted in requiring significantly longer piles than the original design based on subsurface borings. The cause of this discrepancy is investigated in light of the available geotechnical information, soil mechanics principles and standard techniques for pile capacity computations. Several interesting phenomena emerged. These include relatively low resistances offered by crushed rockfill than would conventionally be assumed, non-homogeneity of an apparently uniform formation and the effects of jetting on pile side friction. Also revealing was the significant increase in capacity between 1 and 3 weeks of driving for long piles in clay. Recommendations were developed for pile capacity for future use as "lessons learned".

Introduction

The foundation for the replaced Berth 22 structure at the Port of Oakland in California involved driving approximately 570, 24-inch octagonal precast prestressed concrete piles. A plan and a section for the pile locations are presented in Figure 1.

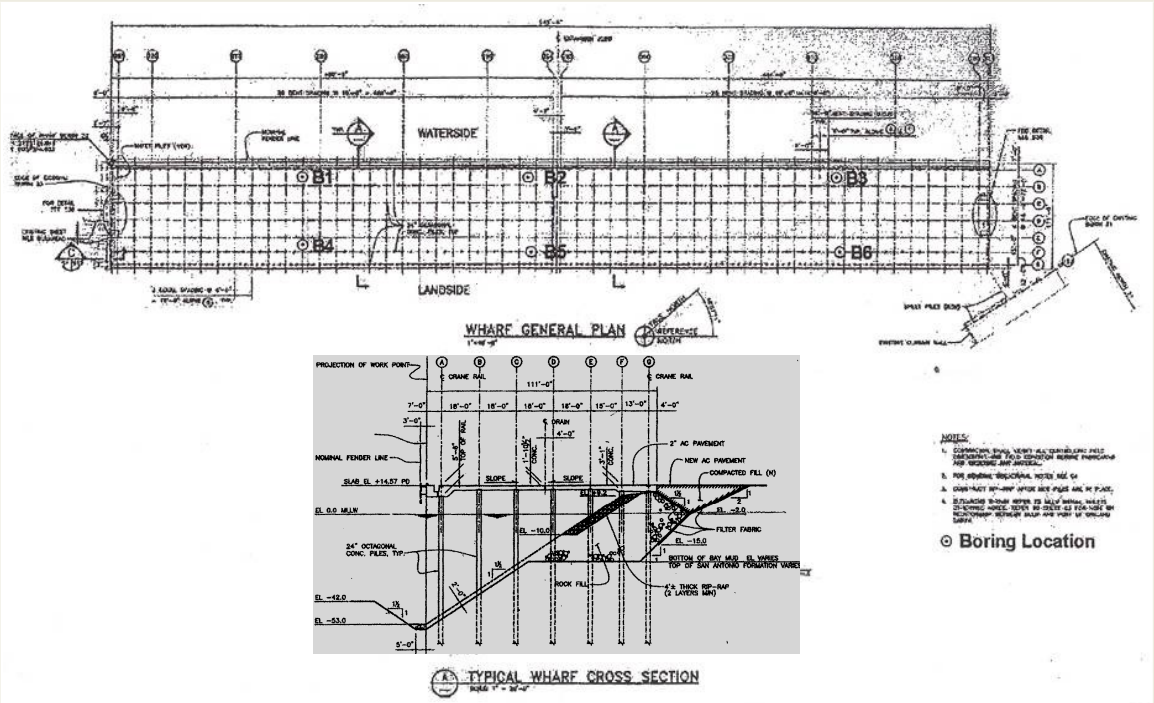


Figure 1 - Site Plan and Wharf Cross Section

The ultimate loads on the piles used in the design are presented in Table 1 – the loads are quite heavy.

Table 1 Pile Design Loads and Recommend Lengths

Row	Ultimate Vertical Load (kips)	Ultimate Uplift Load (kips)	Elevation of Top of Pile (ft)	Elevation of Top of Rockfill (ft)	Pile Penetration Below Top of Rockfill (ft)	Pile Tip Elevations (ft)	Total Pile Length (ft)
A	1356	--	9.32	-47.5	107.0	-154.5	163.8
B	925	--	12,53	-35.5	82.0	-117.5	130.0
C	920	--	12.53	-23.5	81.0	-104.5	117.0
D	822	--	12.53	-11.5	39.0	-50.5	63.0
E	756	--	12.53	0.7	36.7	-36.0	48.5
F	388	119	11.51	9.2	36.7	-36.0	47.5
G	614	133	11.51	9.2	36.7	-36.0	47.5

The foundation design was followed by an extensive Indicator Pile Program. The contractors (Manson Construction Co. of Richmond, California) opted to use a Delmag D62-02 diesel hammer (Rated Maximum Energy – 165 kip-feet). Per the project specifications, the same hammer was used for both indicator and production pile driving. The production piles of appropriate lengths were ordered based on thr results of the Indicator Pile Program. A number of interesting results were found from the Indicator Program, which is discussed in this paper.

Indicator Pile Program

The Indicator Pile Program consisted of monitoring selected piles using the Pile Driving Analyzer (PDA) both during driving and restrike after a few days to assess the effect of increased capacity due to set-up. The piles to be monitored were driven using the same hammer cushion assembly proposed by the Contractor for production piles to be meaningful. The PDA was developed by Goble, Rausche, Likins (GRL) of Cleveland, Ohio in USA. Wires are attached on the pile sides approximately near the top and connected to a control box, which measured accelerations and strains at the top of a pile for a hammer blow on top of the pile. The accelerations and strains were converted into loads and displacements on the pile using a Wave Equation algorithm. It measures the energy actually delivered to the pile and the stresses during driving. Thereby, excessive stresses during driving and consequent potential damage to the pile may be identified. In addition, output from the PDA can be utilized to estimate the downward capacity of the pile using a proprietary program called CAPWAP (Case Pile Wave Analysis Program), also developed by GRL. The CAPWAP program through a matching procedure calculates the skin friction, end bearing and the total capacity of a pile for the hammer blow based on the output from the PDA. It also estimates the skin friction distribution along the length of the pile for the specific hammer blow. Thus, it provides an estimate of the skin friction, end bearing and total capacity of a pile if a restrike is performed after a few days of driving to assess the increased capacity due to set-up, which is an important consideration for piles driven through significant thicknesses of clayey soils. The PDA and CAPWAP services were provided by Steve Abe of Lafayette, California.

Original plans were to drive 32 indicator piles and to restrike 7 piles, all in the outer (waterside) rows. Plans were to monitor 9 piles using the PDA and perform CAPWAP analyses for 16 cases. Subsequently, the program was increased substantially in response to the changed conditions relative to the original design assumptions. 38 indicator piles were driven and 25 restrikes were performed, including two restrikes on four Row A piles. 29 piles were monitored using the PDA.

CAPWAP analyses were performed on 41 cases. Analyses have been performed on both 'during driving' and restrike conditions. The 'during driving' results were used where the pile was embedded primarily in sandy soils, where significant increase in capacity is not expected. **CAPWAP analysis results were assumed as the basis for the ultimate pile capacities. Proposed production pile lengths and criteria for pile driving and refusal were based on the CAPWAP results and pile driveability analyses using the computer program GRLWEAP.**

Attempts have been made to match the pile capacities computed using CAPWAP with pile capacities computed using the FHWA Method as incorporated in the APILE computer program (Ensoft, 1998). The FHWA Method was chosen above the other methods available in APILE, since (a) it has specific curves pertaining to friction for precast concrete piles; (b) accommodates the effect of magnitude of soil displaced by the pile, which could be significant for larger diameters; and (c) the end bearing capacity factor grows exponentially with increasing friction angle of the surrounding soil. Conclusions regarding the parameters (usually friction angle) with the best matches could be established. It is acknowledged that CAPWAP analyses are not sacrosanct and therefore, conclusions are generally based on trends from several piles.

Soil Profile

As may be seen from the section in Figure 1, natural soils were dredged our in front of the wharf essentially to the bottom of the Bay Mud and replaced with 6-in. crushed rock.

A soil profile along the north-south direction of the wharf (prior to the dredging) is presented in Figure 2.

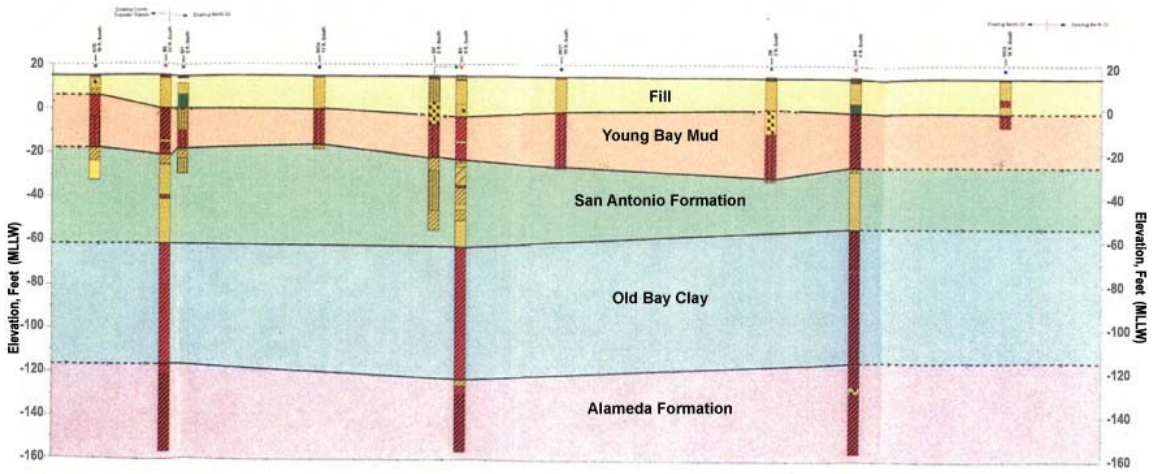


Figure 2 – Soil Profile in North – South Direction

The soil layer thicknesses (assuming the Bay Mud has been removed) are quite uniform throughout the area. The profile may be idealized as (PB, 2003):

Rockfill: 6-in. size crushed rock from top of dike to El. -26

San Antonio Formation: Medium dense to very dense sandy soils with occasional zones rich in silt or clay (El -26 to El -55)

Old Bay Clay: Stiff to very stiff clays of medium to high plasticity (El -55 to El -118)

Alameda Formation: Stiff to very stiff clays of high plasticity. These clays are generally stiffer than the Old Bay Clay (below El -118)

The required tip elevations per the original design are also presented in Table 1. As may be seen from the table, the piles in rows D, E, F and G were designed to tip in the San Antonio Formation, whereas the outer piles, e.g. in Rows A, B and C were designed to penetrate the San Antonio formation tip in the stiff clays below. Also, to avoid premature refusal in the San Antonio formation, the project specifications allow piles in the outer three rows to be jetted through the San Antonio Formation.

The proposed production pile lengths subsequent to the indicator pile program are presented in Table 2. Significant increases from the original design lengths are readily apparent, particularly for Rows D, E, F and G.

Table 2 Recommended Pile Lengths after Indicator Pile Program

Row	Elev. of Top of Pile (ft)	Bent No.	Pile Tip Elevations (ft)	Total Pile Length (ft)
A	9.32	268 to 302	-154.7	164.0
	ditto	302+ to 321	-150.7	160.0
B	12.53	268 to 280	-117.5	130.0
	ditto	281 to 300	-122.5	135.0
	ditto	300 to 321	-117.5	130.0
C	12.53	268 to 280	-117.5	130.0
	ditto	281 to 300	-122.5	135.0
	ditto	300 to 321	-112.5	125.0
D	12.53	268 to 283	-112.5*	125.0
	ditto	284 to 293	-52.5	65.0
	ditto	294 to 302	-50.5	63.0
	ditto	303 to 314	-49.5	62.0
	ditto	315 to 321	-106.5*	119.0
E	12.53	268 to 281	-102.5*	115.0
	ditto	282 to 293	-52.5	65.0
	ditto	294 to 302	-50.5	63.0
	ditto	303 to 314	-49.5	62.0
	ditto	315 to 321	-98.5*	111.0
F	11.51	268 to 275	-45.0	56.5
	ditto	275+ to 284	-41.5	53.0
	ditto	284+ to 321	-61.5*	73.0
G	11.51	268 to 275	-73.5*	85.0
	ditto	275+ to 293	-51.5	63.0
	ditto	293+ to 315	-49.5	61.0
	ditto	315+ to 321	-84.5*	96.0

*Very Dense San Antonio Formation was not encountered at these locations

The increases in pile length in Rows D, E, F and G, which were designed to tip into the San Antonio Formation, occurred due to:

(a) The pile-soil skin friction from the rockfill layer was consistently much lower than would normally be assumed.
(b) The San Antonio Formation was neither as dense nor as uniform as assumed in the design.

These issues are discussed below in greater detail.

Skin Friction in the Rockfill

From the start of the program, it was readily noticed that the piles were driving extremely easy through the rockfill. Even at a penetration of over 30 feet, the pile drove at no more than 4-6 blows per foot. This was quite unexpected. Values of skin friction versus depth extracted from CAPWAP results are plotted on Figure 3. Pile-skin friction versus depth for phi angles of 25 and

30 degrees, based on the FHWA procedure (Ensoft, 1998), are also presented in the figure. It appears that the skin friction in the rockfill is best modeled using a friction angle of around 25 degrees, whereas, based on the stable slopes of the wharf dike a friction angle of 35 degrees or greater is probably more appropriate.

It therefore appears that the skin friction of the pile through the rockfill cannot be modeled using algorithms for piles through sand, where the surrounding sand is treated as a continuum. The relatively much smaller number of contact points per unit area in the pile-rockfill interface, compared to that of in a pile-sand interface probably renders the sand model untenable for the present purpose. The low side friction may also be a reflection of a significantly lower lateral earth pressure on the pile sides for a pile driven into rockfill material, compared to a pile penetrating a sand layer.

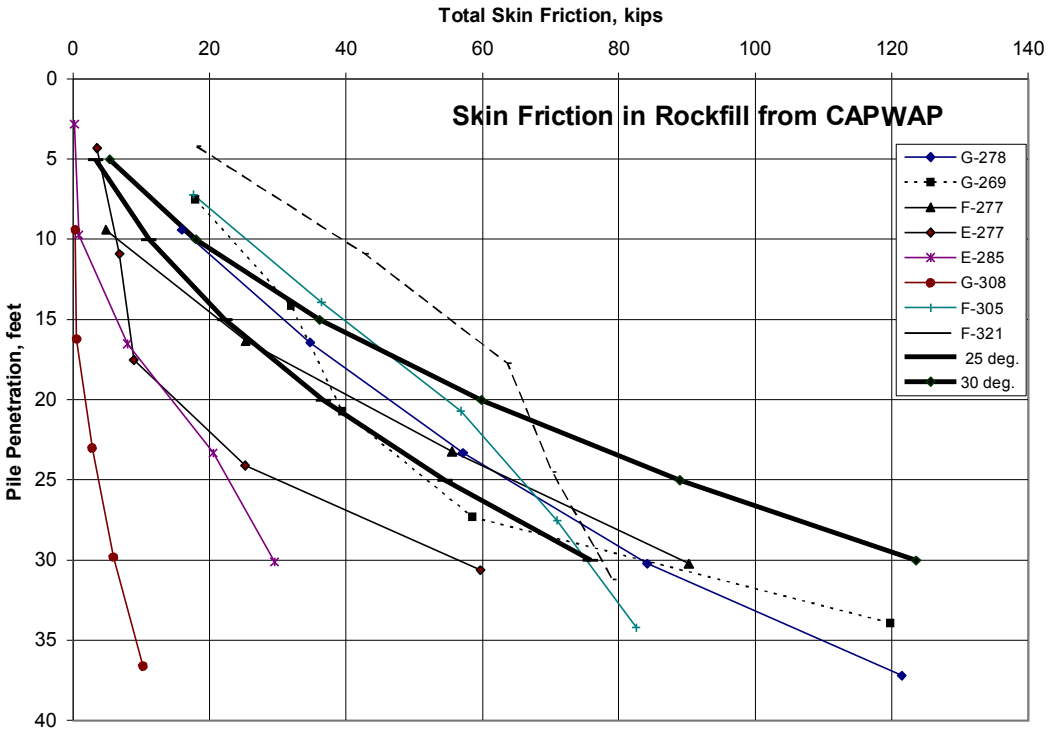


Figure 3 – Skin Friction in Rockfill from CAPWAP

It is not immediately clear from the limited information if the pile-soil skin friction in the rockfill layer is affected by the overburden pressure. Nevertheless, tentatively, a friction angle of 25 degrees is recommended along with the FHWA method.

Pile Behavior in the San Antonio Formation

Pile driving through the San Antonio Formation revealed two important findings:

(a) Blow counts varied widely within the San Antonio Formation, both in the vertical and lateral directions.

(b) Very high blow counts (refusal) were encountered in a zone over approximately half the length of the wharf in the middle.

The wide variation in blow counts is reflective of the variability of the San Antonio Formation. Presented in Figure 4 are plots of blow counts versus depth in the San Antonio Formation for the six borings drilled by Fugro in 2002. The boring locations are shown in Figure 1. If the blow counts at any point decrease with depth in the San Antonio Formation it may be inferred that the pile tip is in a silty layer or perhaps even a clayey layer. Obviously, if the pile tips in such a layer, it will exhibit a lower end bearing. Therefore, for a conservative, yet rational estimation of pile capacities in the San Antonio Formation with its variable nature, the following is proposed. The skin friction for the pile should be based on a higher friction angle, say 35 degrees and the end bearing should be based on a lower friction angle, say 25 degrees.

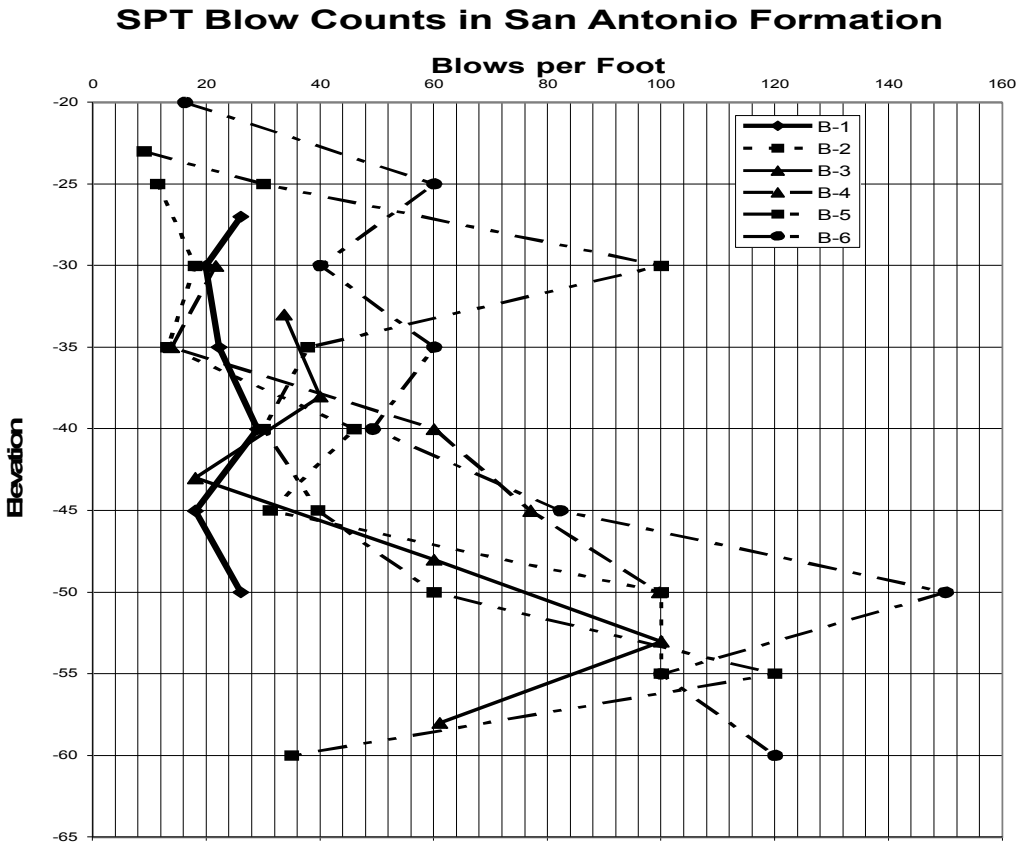


Figure 4 – SPT Blow Counts in San Antonio Formation
(Note: Blow Counts for Standard California Sampler, where used, have been corrected)

Very Dense Layer in San Antonio Formation

Very high blow counts (blow counts of 60 or greater) are indicated in all borings except B-1, indicating a 'Very Dense Layer' at around below El. -45. The pile locations where the very high blow counts were encountered are presented in Table 3. In all cases the top of the very dense layer lies between El -47 and El -49. This agrees fairly well with boring logs.

Table 3 Elevations for Top of the Very Dense Layer in San Antonio Formation

Row	Bent No.	Tip Elevation (ft.)	Blow Counts for last 5 feet	Inferred Top of Very Dense Layer (ft.)
C	293	-52.72	30, 55, 47, 194, 259	-50.0
D	293	-50.52	21, 26, 50, 140, 67/6"	-49.0
	305	-49.7	7, 9, 31, 108, 186/9"	-48.0
	313	-49.0	12, 53, 86, 138, 77/6"	-47.4
E	285	-51.97	18, 25, 39, 58, 121	-49.0
	306	-48.5	10, 13, 13, 46, 157?8"	-47.5
	314	-49.6	34, 81, 94, 110, 115	-47.6
G	278	-51.52	17, 15, 17, 40, 96	-49.5
	308	-47.9	12, 14, 16, 24, 186/9"	-47.1

Back calculation of the end bearing capacity factor Nq in this dense sand layer indicates a value ranging from 43 to over 100. Some of the lower values may be due to insufficient penetration of the pile into the very dense layer – values of Nq may increase additional penetration.
This corresponds to a friction angle range of 37 to over 40 degrees for this very dense layer by the FHWA Method (Ensoft, 1998). It is felt that the friction angle of this layer is considerably higher (at least 40 degrees).

The locations where the 'Very Dense Layer' would not be encountered, as inferred from the Indicator Pile Program would result in significantly longer piles as shown in Table 2.

Effect of Jetting on Skin Friction

As noted earlier, the longer piles (in Rows A, B and C) were jetted down through the San Antonio formation to preclude the possibility of premature refusal. (In fact, premature refusal was encountered in pile at C-293, where the Contractor forgot the jetting.) Plots of skin friction versus depth in the San Antonio Formation are presented in Figure 5 below for three piles where the piles were jetted through greater than 30 feet of San Antonio Formation. All the three results are for 7-day restrikes. The plots show that a conservative value of 35 degrees appears satisfactory for the present and may be used. This implies that except for the very dense layers, soils are not significantly loosened due to jetting.

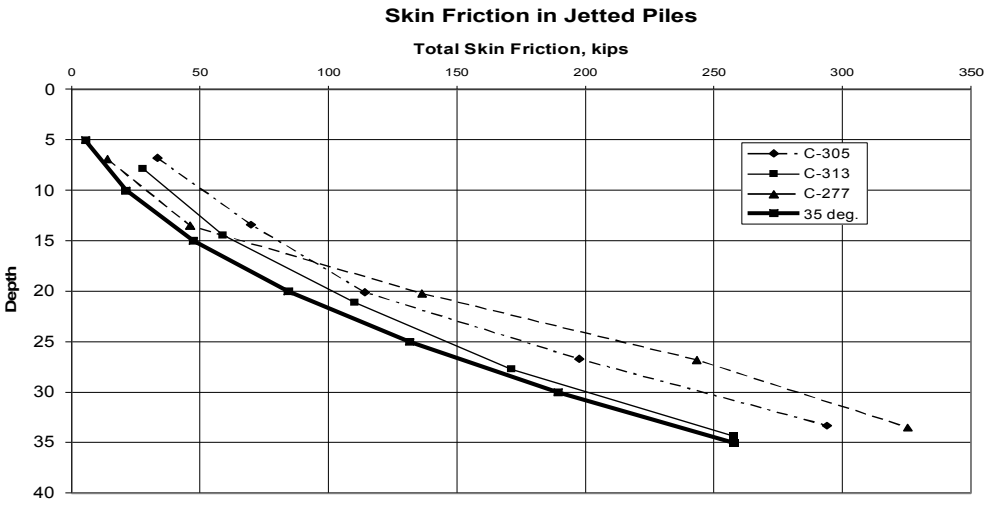


Figure 5 – Skin Friction in Jetted Piles

Set-up Times for the Long Piles

Project specifications required a set-up time of one week for the piles in Rows A, B and C before they were restruck to assess the increase in capacity with time (set-up). CAPWAP results on all the one-week restrikes on the Row A piles showed the ultimate capacities to be 25-30 percent lower than required (see Table 4). Based on available literature, a further gain of more than 10-15 percent in the long term could not be assumed with any confidence without additional testing. The 164-foot long piles represented the limits of the planned equipment – longer piles would therefore require major modifications to the plans. Thus restrikes after at least 2 weeks after driving were proposed with the hope that the capacity would have picked up by then and the pile length would thus be acceptable. The results noted in Table 4 clearly indicate that adequate pile capacities have been attained by all the 7 piles in Row A, which were restruck 2-3 weeks after initial driving.

Table 4 CAPWAP Results on Row A Piles

Bent No.	Initial Driving				One Week Restrike				Two Plus Week Restrike			
	Date	Total Capacity (kips)	Skin Friction (kips)	End Bearing (kips)	Date	Total Capacity (kips)	Skin Friction (kips)	End Bearing (kips)	Date	Total Capacity (kips)	Skin Friction (kips)	End Bearing (kips)
277	3 Aug.	424	342	82	13 Aug	1120	1020	100	31 Aug	1368	1261	107
284	4 Aug.								31 Aug	1292	1144	148
293	5 Aug.	308	218	90	13 Aug	1154	1012	142	31 Aug	1318	1176	142
305	20 Oct.	388	337	51	1 Nov.	1220	1090	130				
313	26 Oct.				1 Nov.	1152	1090	62	15 Nov	1480	1375	105
321	26 Oct.				1 Nov.	1080	977	103	15 Nov	1423	1288	135

The magnitude of this increase in capacity with time, though somewhat surprising, is not wholly unexpected. Essentially all the capacities for the Row A piles are derived from the Old Bay Clay and the Alameda Formation. Both the clays have relatively high degrees of plasticity. During pile driving, due to the 'undrained' nature of the loading, pore pressures are developed in the clays around the vicinity of the pile. With time, the pore pressures dissipate, resulting in reconsolidation and consequent increase in soil strength around the pile and thus the increased resistance to pile driving during restrikes. This is known as pile 'set up'. Rate of dissipation of pore pressures and increase in resistance during driving depend, among other factors, on the permeability of the surrounding soil and the size of the zone around which significant pore pressures have developed. Clays of high plasticity have low permeabilities and therefore greater times are involved for pore pressure dissipation. In addition, larger the pile diameter, larger is the zone of influence and therefore greater times would be involved for dissipation and consequent gain in strength. In addition, during pile driving, surrounding undisturbed clays lose strength due to remolding, due to breakdown of the undisturbed clay structure – the degree in loss in strength due to remolding depends on the 'sensitivity' of the clay. Part of this strength is regained with time due to partial recovery of the clay structure, a phenomenon known as 'thixotropy', which may also account for part of the increased resistance during restrike.

Conclusions –Lessons Learnt

1. Skin friction in the crushed rock was seen to be unexpectedly low, perhaps reflecting the inapplicability of standard pile driving experiences and computation procedures to the large sized rock particles. A friction angle of 25 degrees is tentatively recommended.

2. The San Antonio Formation sands are highly variable in gradation and density, often with silt and sometimes clay rich layers. Except for the zone with the very dense sands, the rest may be reasonably designed using a 35-degree friction angle for skin friction and a 25-degree angle for end bearing. The FHWA method is recommended for pile capacity calculations.

3. In approximately half the project area, approximately 10 feet of the bottom of the San Antonio formation is very dense. Piles will encounter refusal unless jetting or other measures are used. A bearing capacity factor (Nq) of 60 is recommended for computation of the tip capacity for piles bearing in this layer.

4. Proper assessment of the highly variable characteristics of the San Antonio formation prompted the use of a larger number of indicator piles and CAPWAP analyses than generally performed. As an afterthought, a creative scattering of the distribution of the indicator piles could perhaps be used to advantage.

5. There was no clear indication of reduction in skin friction in the San Antonio formation for piles jetted through the formation. A friction angle of 35 degrees may be used for skin friction, with the FHWA method.

6. A minimum of two-week set-up time is required for the Row A piles. These piles are the longest in the project: 164 feet long; 100.5 feet penetration primarily through clays of high plasticity.

References

1. Ensoft, "Computer Program APILE Plus, Version 3.0", A program for the Analysis of Axial Capacity of Driven Piles by L. C. Reese. S. T. Wang and J. Arrellaga, 1998

2. Parsons, Brinckerhoff, Quade and Douglas (PB), "Final Geotechnical Study, Berth 22 Wharf Replacement, Port of Oakland, Oakland, California, Prepared for the Port of Oakland, March 14, 2003

3. Rausche, F., Pile Dynamics, Inc., "Pile Driving Analyzer (PDA) and CAPWAP, Proven Pile Testing Technology: Principles and Recent Advances"

INFLUENCE OF PILE GEOMETRY ON THE DYNAMIC RESPONSE OF AN UNDER-REAMED PILE

Muzammil, M, Jr. Research Engineer, RDSO, Lucknow, Uttar Pradesh, India, muzammil.amu@gmail.com
Bharathi, M, Research Scholar, IIT Roorkee, Roorkee, Uttarakhand, India, bharathi.iitr@gmail.com
Saran, S, Emeritus Professor (Retd.), IIT Roorkee, Roorkee, Uttarakhand, India, saranfce@iitr.ac.in
Mukerjee, S, Visiting Faculty, IIT Roorkee, Roorkee, Uttarakhand, India, shyamal.mukerjee@gmail.com

ABSTRACT

This paper presents the results of in-situ tests conducted on a set of under-reamed piles in a silty sand deposit. Three piles (i.e. vertical, vertical with one bulb and vertical with two bulbs) of diameter 0.2 m were cast upto a depth of 5 m. The pile cap had four foundation bolts cast into it so that a mechanical oscillator-motor assembly could be mounted centrally on it. The oscillator-motor assembly was used to generate purely sinusoidal dynamic forces, in either horizontal or vertical directions. For both horizontal and vertical vibration cases, it was observed that (i) the natural frequencies decreased with an increase in the excitation force level, (ii) for the same excitation level, the natural frequencies as well as the maximum amplitude of vibration are almost the same irrespective of the pile geometry i.e. number of bulbs in the pile, indicating that the full pile length is not being excited. For the vertical vibration case, the soil-pile stiffness at frequencies, before resonance, were observed to be higher than those at frequencies after resonance. In the horizontal vibration case, the stiffness of the soil-pile system was found to be decreasing with an increase in the excitation force level. The damping ratio was found to be increasing with an increase in the excitation force level.

Keywords: Under-reamed piles, forced vibration tests, Soil-pile stiffness, damping ratios

INTRODUCTION

Under-reamed piles are piles, normally upto a depth of 6 m, with one or more bulbs along the pile stem. These have been used for structures like transmission towers, structures on expansive soils etc. for a very long time, however it is only in the last 30 years that dynamic response of a pile has been studied. Evaluation of dynamic soil-pile interaction is a very complex problem as the conditions and properties of soil are highly variable and unpredictable. Various models and approaches have been suggested by various investigators for evaluating the dynamic soil-pile interaction problem, but most of them are based on the assumptions that the behaviour of soil is linear and the soil surrounding the pile is strongly adhered to it. But in practice, it is not so. The soil surrounding the pile is always somewhat loosened and undergoes some deformation when a sinusoidal load is applied. This causes the soil-pile system to behave nonlinearly.

In earlier studies by Novak, (1974), Novak and Aboul-Ella, (1978) etc. a linear elastic behaviour of soil was assumed. This approach was very useful in understanding the mechanism of soil-pile interaction to a large extent. Subsequently various models were suggested like the lumped mass models with nonlinear discrete springs, dashpots and friction elements Matlock et al. (1978), weak cylindrical zone around the pile model Novak and Sheta, (1980), ideal boundary zone model with non-reflective interface, Han and Sabin, (1995) etc. These approximate solutions give an idea about the mechanism of dynamic pile-soil interaction to a large extent. However, in reality both separation and slippage can occur due to the formation of a weak bond at the contact surface between the soil and the pile when a dynamic load is applied. In addition, the soil column adjacent to the pile experiences large deformations under dynamic loads and thus behaves nonlinearly.

Some computer aided model studies on the dynamic response of under-reamed piles have been reported, however, very few insitu dynamic tests on under-reamed piles are reported. Dynamic tests on piles were carried out by Novak and Grigg (1976) on small scale single piles and pile groups in the field. Similar field tests on small scale piles were conducted to study the nonlinear behaviour of a single pile and a pile group under strong harmonic excitation by Han and Novak (1988), Han and Vaziri (1992), Burr et al. (1997), Manna and Baidya (2010) etc. The majority of these experimental studies were focussed on the response of the specific pile groups and compared with the results of a single pile. Hence there was a need to study the influence of pile geometry on the dynamic response of an under-reamed pile from insitu tests.

INVESTIGATION PROGRAM

The site was located at the Department of Earthquake Engineering, IIT Roorkee. In order to identify the soil stratum at the site, where these tests were planned, one boring up to 9.2m depth, supplemented with SPT tests at every 1.0m interval, was done. Soil samples were collected carefully from the split-spoon sampler and tested in the laboratory for determining unit weight and moisture content. Sieve analyses were also carried out on each sample for soil classification. Angle of internal friction, ϕ, was estimated from the relation between ϕ and SPT N value. Table 1 shows the properties of the soil at the test site.

Table 1. Soil properties at the Test Site

Soil type	SM
Uniformity coefficient (C_u)	4.26
Coefficient of curvature (C_c)	1.99
Mean specific gravity (G)	2.66
Angle of internal friction (ϕ)	30^o

Three bored cast insitu piles were cast upto a depth of 5 m. The first pile (P1) was a normal vertical pile with no bulb. The second (P2) and third piles (P3) had one and two bulbs respectively. The diameter of the piles was 0.2 m and the diameter of the under-reamed bulb was 0.5 m. The locations of the bulbs, from the bottom, were 0.43 m for the first bulb and 1.43 m for the second bulb. Fig. 1 shows the layout of the test piles. The dimension of pile cap was 0.7 m × 0.7 m × 0.3 m (height) and had four foundation bolts cast into it so that a mechanical oscillator-motor assembly could be mounted centrally on it. The oscillator-motor assembly was used to generate purely sinusoidal dynamic forces, in either vertical or horizontal directions.

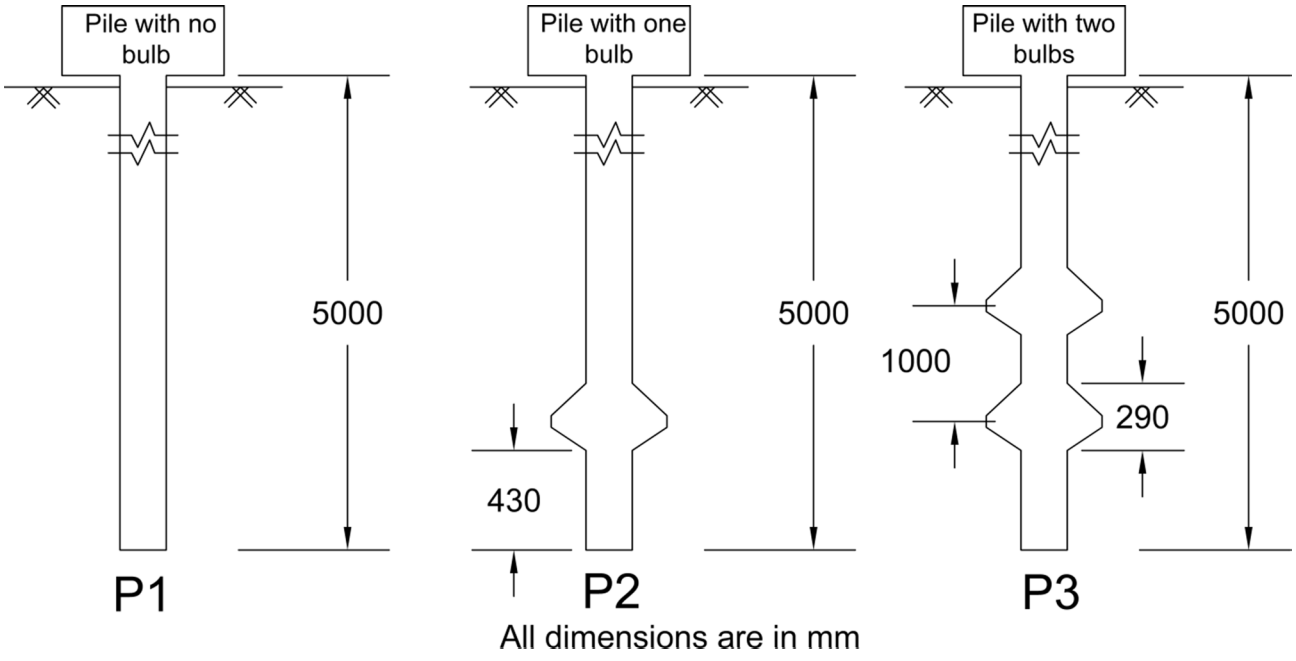


Fig. 1 Geometry of piles

In the first phase of the investigation program, forced vertical vibration tests were conducted on each of the three piles. The motor-oscillator assembly was fixed on the pile cap such that purely vertical sinusoidal forces are generated. The force level was varied by (i) changing the eccentricity setting within the mechanical oscillator or (ii) varying the electric motor speed using a speed control unit. Three eccentricity settings of 30^o, 60^o and 90^o were used in the testing programme and for each eccentricity setting the motor speed was varied from 3 to 45 Hz. The induced vertical accelerations were monitored using two accelerometers suitably fixed on the pile cap top. Fig. 2 shows the test set up for the vertical vibration test.



Fig. 2. Vertical Vibration Test

In the second phase of the investigation program, forced horizontal vibration tests were conducted on each of the three piles. The motor-oscillator assembly was fixed on the pile cap such that purely horizontal sinusoidal forces are generated. The force level was varied by (i) changing the eccentricity setting within the mechanical oscillator or (ii) varying the electric motor speed using a speed control unit. Three eccentricity settings of 30^o, 45^o and 60^o were used in the testing programme and for each eccentricity setting the motor speed was varied from 3 to 45 Hz. The induced horizontal accelerations were monitored using three accelerometers suitably fixed on the vertical face of the pile cap. Fig. 3 shows the test set up for the horizontal vibration test.



Fig. 3. Horizontal Vibration Test

RESULTS AND ANALYSIS

Details of Vertical and Horizontal Vibration Tests performed are given in Table 2.

Table 2. Details of tests conducted

Test Type	Length of Pile (m)	Pile No.	Eccentricity Settings (θ)
Vertical Vibration Test	5	P1	30^o, 60^o, 90^o
		P2	30^o, 60^o, 90^o
		P3	30^o, 60^o, 90^o
Horizontal Vibration Test	5	P1	30^o, 45^o, 60^o
		P2	30^o, 45^o, 60^o
		P3	30^o, 45^o, 60^o

Vertical vibration test

In the Vertical vibration tests, data obtained in terms of acceleration amplitude was converted into displacement amplitude and then a displacement versus frequency plot was drawn. Fig. 4 shows a typical plot for vertical vibration test. From such plots, resonant frequency (f_{nz}) and maximum displacement amplitude $(A_z)_{max}$ were obtained for the vertical vibration tests and these are reported in Table 3.

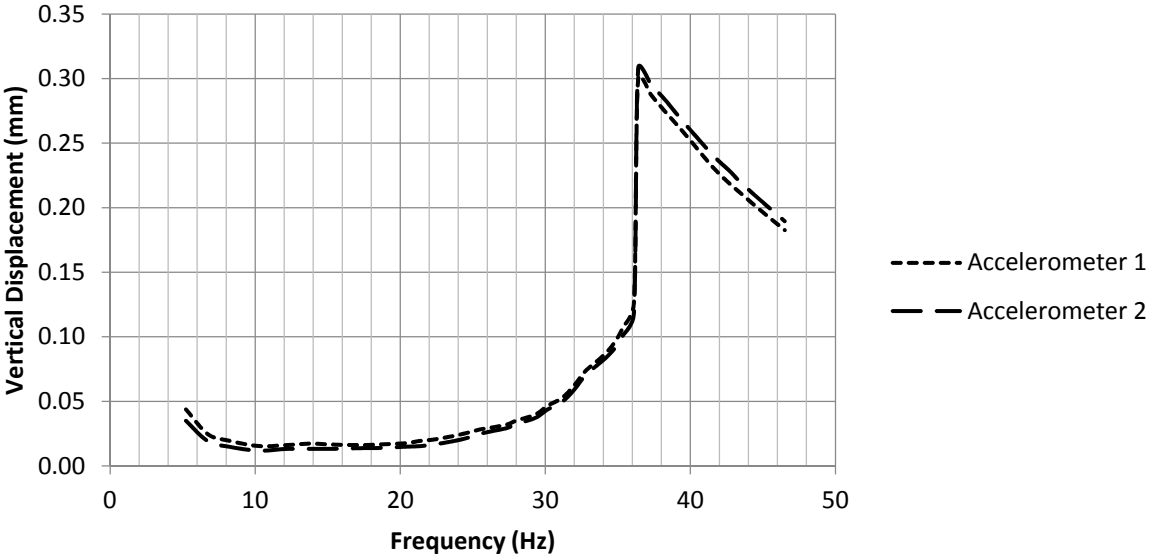


Fig. 4. Vertical displacement vs frequency for pile P3 (eccentricity = 30°)

Table 3. Natural frequencies and maximum displacement amplitude for different piles (Vertical Vibration Test)

Pile No.	Eccentricity (θ) (deg)	Resonant Frequency (f_{nz}) (c/s)	Displacement Amplitude $(A_z)_{max}$ (mm)
P1	30	35	0.26
	60	28	0.48
	90	23	0.72
P2	30	37	0.27
	60	25.5	0.53
	90	21.5	0.85
P3	30	36.5	0.31
	60	27.5	0.64
	90	22	0.88

Vertical vibration test data was used to evaluate the soil-pile stiffness in the vertical direction (K_Z) and damping ratio (ξ) of the soil-pile system and to assess the effect of number of bulbs, in the under-reamed piles, on the soil-pile stiffness. To evaluate stiffness in the vertical direction (K_Z) and damping ratio (ξ) of the soil-pile system, the following iterative procedure was adopted. A value of damping ratio was assumed, then undamped resonant frequency, magnification factor, static displacement, exciting force were calculated for each frequency. The slope of the curve between exciting force and static displacement gives the stiffness of the soil-pile system for the assumed damping ratio. Using this stiffness value, damping ratio was recalculated. Iteration was performed until both the assumed and calculated damping ratios converged. The converged value of damping ratio is the true damping ratio of the soil-pile system. Using this damping ratio stiffness of the soil-pile system was recalculated. The results are reported in Tables 4, 5 and 6.

Table 4. Stiffness and damping ratios for pile P1

θ	Resonant Frequency, f_{nz} (c/s)	$(A_z)_{max}$ (mm)	Before Resonance		After Resonance		Strain Level ($\times 10^{-4}$)
			Damping ξ (%)	Stiffness, K_Z (N/mm)	Damping ξ (%)	Stiffness, K_Z (N/mm)	
30	35	0.26	5.12	489003	18.21	131033	3.71
60	28	0.48	5.58	305872	18.28	87965.5	6.86
90	23	0.72	5.22	205837	19.62	51761.8	10.43

Table 5. Stiffness and damping ratios for pile P2

θ	Resonant Frequency, f_{nz} (c/s)	$(A_z)_{max}$ (mm)	Before Resonance		After Resonance		Strain Level ($\times 10^{-4}$)
			Damping ξ (%)	Stiffness, K_Z (N/mm)	Damping ξ (%)	Stiffness, K_Z (N/mm)	
30	37	0.27	4.1	666256	15.1	175244	3.86
60	25.5	0.53	5.54	230121	18.41	66111.2	7.57
90	21.5	0.85	5.6	142407	18.66	40716.1	12.29

Table 6. Stiffness and damping ratios for pile P3

θ	Resonant Frequency, f_{nz} (c/s)	$(A_z)_{max}$ (mm)	Before Resonance		After Resonance		Strain Level ($\times 10^{-4}$)
			Damping ξ (%)	Stiffness, K_Z (N/mm)	Damping ξ (%)	Stiffness, K_Z (N/mm)	
30	36.5	0.31	3.93	600277	14.62	156523	4.43
60	27.5	0.64	4.54	264964	14.79	78960.9	9.14
90	22	0.88	4.34	186401	15	52266.4	12.71

Horizontal vibration test

In the Horizontal vibration tests, data obtained in terms of acceleration amplitude was converted into displacement amplitude and then a displacement versus frequency plot was drawn. Fig. 5 shows a typical plot for horizontal vibration test. In the horizontal vibration test, three accelerometers were used to measure induced accelerations along the pile cap height. From these acceleration values displacements were calculated and plotted along the pile cap height to obtain rotational amplitude, corresponding to each excitation frequency. A plot of rotational amplitude versus frequency was made and resonant frequency (f_{nz}) and maximum rotational amplitude $(A_\theta)_{max}$ were obtained and these are reported in Table 7.

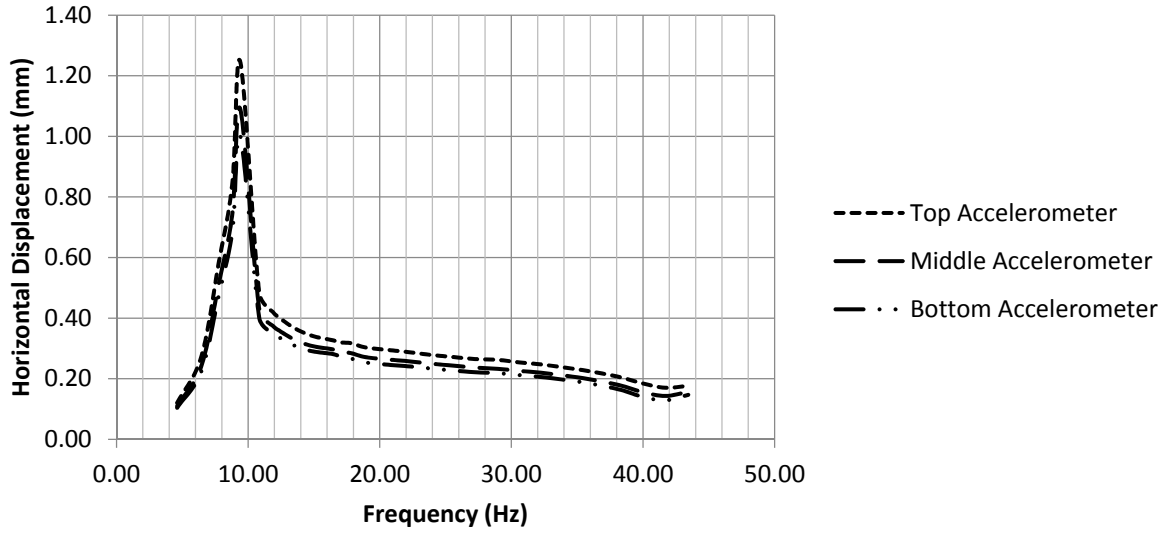


Fig. 5. Horizontal displacement vs frequency plot for pile P3 (eccentricity = 45°)

Table 7. Natural frequencies and maximum rotational amplitude for different piles (Horizontal Vibration Test)

Pile No.	Eccentricity (θ) (deg)	Resonant Frequency (f_{nz}) (c/s)	Rotational Amplitude $(A_\theta)_{max}$ (rad)
P1	30	12.7	0.014
	45	9	0.015
	60	7.5	0.016
P2	30	14.5	0.048
	45	13	0.059
	60	12.83	0.075
P3	30	12.6	0.023
	45	9.3	0.07
	60	8.5	0.092

Horizontal vibration test data was used to evaluate the soil-pile stiffness in the lateral direction (K_θ) and damping ratio (ξ) of the soil-pile system and to assess the effect of number of bulbs, in the under-reamed pile, on the soil-pile stiffness. No sliding movement of the pile was assumed to occur as it was embedded firmly in the soil. Hence, only one resonant peak was observed instead of two peaks as is expected in a two degree of freedom system. To evaluate stiffness in the lateral direction (K_θ) and damping ratio (ξ) of the soil-pile system, the following iterative procedure was adopted. A value of damping ratio was assumed, then undamped resonant frequency, magnification factor, static displacement and exciting moment were calculated for each frequency. The slope of the curve between exciting moment and static displacement gives the stiffness of the soil-pile system for the assumed damping ratio. Using this stiffness value, damping ratio was recalculated. Iteration was performed until both the assumed and calculated damping ratios converged. The converged value of damping ratio is the true damping ratio of the soil-pile system. Using this damping value, stiffness of the soil-pile system was recalculated. The results are reported in Tables 8, 9 and 10.

Table 8. Stiffness and damping ratios for pile P1

θ	Resonant Frequency, f_{nz} (c/s)	$(A_\theta)_{max}$ (rad)	Damping ξ (%)	Rotational Stiffness, K_θ (Nm/rad)	Strain Level ($\times 10^{-4}$)
30	12.7	0.014	5.35	365114	3.71
60	7.5	0.016	8.22	123811	10.43

Table 9. Stiffness and damping ratios for pile P2

θ	Resonant Frequency, f_{nz} (c/s)	$(A_\theta)_{max}$ (rad)	Damping ξ (%)	Rotational Stiffness, K_θ (Nm/rad)	Strain Level ($\times 10^{-4}$)
30	14.5	0.048	5.89	129262	3.86
45	13	0.059	7.78	94422.8	7.57
60	12.83	0.075	10	72923.5	12.29

Table 10. Stiffness and damping ratios for pile P3

θ	Resonant Frequency, f_{nz} (c/s)	$(A_\theta)_{max}$ (rad)	Damping ξ (%)	Rotational Stiffness, K_θ (Nm/rad)	Strain Level ($\times 10^{-4}$)
30	13.6	0.023	5.35	220454	4.43
45	9.3	0.07	6.9	46108.3	9.14
60	8.5	0.092	7.1	37217.3	12.71

CONCLUSIONS

On the basis of the experimental results obtained the following conclusions are arrived at;

Piles subjected to vertical vibration

1. The resonant frequency of the soil-pile system decreases with an increase in the exciting force level.
2. It is observed that the values of resonant frequency and maximum displacement amplitude of vibration are nearly the same for the different piles, (P1, P2 and P3), excited to the same force level. Hence it may be said that the number of bulbs in the under-reamed pile has no influence on the resonant frequency and maximum displacement amplitude of vibration.
3. The soil-pile stiffness at frequencies, before resonance, was observed to be higher than those at frequencies after resonance. This is an important observation as the soil-pile stiffness calculated at frequencies lower than resonance can be used in the design of low frequency machines whereas the soil-pile stiffness value obtained at frequencies beyond resonance can be employed in the design of high frequency machines.
4. The stiffness of the soil-pile system decreases with an increase in the induced strain level.
5. Damping ratio of the soil-pile system increases marginally with an increase in the induced strain level.

Piles subjected to horizontal vibration

1. The resonant frequency of the soil-pile system decreases with an increase in the exciting force level.
2. It has been observed that the values of resonant frequency and maximum rotational amplitude of vibration are nearly the same for the different piles, (P1, P2 and P3), excited to the same force level. Hence it may be said that the number of bulbs in the under-reamed pile has no effect on resonant frequency and maximum rotational amplitude of vibration.
3. For the same soil-pile system the values of resonant frequency and rotational amplitude were observed to be much smaller than those observed in the vertical vibration case, at the same force level.
4. The rotational stiffness of the soil-pile system was found to be decreasing with an increase in the induced strain level.
5. The damping ratio was found to be increasing with an increase in the induced strain level.

ACKNOWLEDGMENT

The authors are grateful to IIT Roorkee for providing the facilities for this investigation. The research work presented herein was funded through an Institute Fellowship (2011-2013), to the first author, from the Ministry of Human Resource and Development, Government of India.

REFERENCES

1. Burr, J. P., Pender, M. J. and Larkin, T. J. (1997). Dynamic Response of Laterally Excited Pile Groups. Journal of Geotechnical and Geoenvironmental Engineering, ASCE, 123(1), pp. 1-8.
2. Dobry, R., and Gazetas, G. (1988). Simple method for dynamic stiffness and damping of floating pile groups. Geotechnique, London, England, 38(4), 557 -574.
3. Gazetas, G., and Makris, N. (1991). Dynamic pile-soil-pile interaction. Part 1: Analysis of axial vibration. Earthquake Engineering and Structural Dynamics, Chichester, England, 20, 115-132.
4. Han, Y. and Vaziri, H. (1992). Dynamic response of pile groups under lateral loading. Soil Dyn. Earthquake Eng., 11, 87-99.
5. Han, Y. C. and Novak, M. (1988). Dynamic Behaviour of Single Piles Under Strong Harmonic Excitation. Canadian Geotechnical Journal, 25, pp. 523-534.

6. Han, Y. C., (1997). Dynamic Vertical Response of Piles in Nonlinear Soil. Journal of Geotechnical and Geoenvironmental Engineering.

7. Manna, B. (2010). Dynamic nonlinear response of pile foundations under vertical vibration-Theory versus experiment. Soil Dynamics and Earthquake Engineering, 201006.

8. Manna, B., and Baidya, D. K., (2010). Dynamic Response of Pile Foundations under Coupled Vibration. IGC Roorkee, pp. 55-66.

9. Matlock, H. and Reese, L. C. (1962). Generaliszed Solutions for Laterally Loaded Piles. Transactions of the American Society of Civil Engineers, Vol. 127, Part I, pp. 1220-1247.

10. Matlock, H., Foo, H. C. and Bryant, L. M. (1978). Simulation of Lateral Pile Behaviour under Earthquake Motion. Proc. ASCE. Specialty Conf. on Earthquake Engineering and Soil Dynamics, Pasadna, CA, 11, pp. 600-619.

11. Muzammil M. (2013). Influence of Pile Geometry on the Dynamic Response of Under-reamed Piles. M. Tech Thesis, Department of Earthquake Engineering, IIT Roorkee.

12. Novak, M. (1974). Dynamic Stiffness and Damping of Piles. Canadian Geotechnical Journal, 11, pp. 574-598.

13. Novak, M. and Aboul-Ella, F. (1978). Impedance Functions of Piles in Layered Media. Journal of Engineering Mechanics, ASCE, 104(3), pp. 643-661.

14. Novak, M., and El-Sharnouby, B. (1983). Stiffness and damping constants of single piles. J. Geotech. Div., ASCE, Vol. 109, No. 7, pp. 961-974.

15. Novak, M., and Grigg, R. F. (1984). Dynamic experiments with small pile foundations. Can. Geotech. J., Ottawa, Canada, 13(6), 738-756.

16. Novak, M., and Sheta, M. (1980). Approximate approach to contact effects of piles. Dynamic Response of Pile Foundations: Analytical Aspects, ASCE, New York, N.Y., 53-79.

PILES THROUGH SOFT CLAY FOR A METRO PROJECT

Ravi Sundaram, Cengrs Geotechnica Pvt. Ltd., Noida, U.P., India 0120-4206771 ravi@cengrs.com
Sanjay Gupta, Cengrs Geotechnica Pvt. Ltd., Noida, U.P, India 0120-4206771 sanjay@cengrs.com
Sorabh Gupta, Cengrs Geotechnica Pvt. Ltd., Noida, U.P., India 0120-4206771 sorabh@cengrs.com
Abraham Varghese, Cengrs Geotechnica Pvt. Ltd., Noida, U.P., India 0120-4206771 abraham@cengrs.com

ABSTRACT

Geotechnical investigation for the Kochi Metro revealed a critical section of the Viaduct near Ernakulam Junction Railway Station. Four piers, located over a 220 m stretch, were passing through an area with substantial thickness of soft clay. The scope of the geotechnical investigation included two boreholes and a static cone penetration test at each pier location. In the boreholes, field vane shear test was conducted at different depths in addition to the routine SPT. The design of heavily loaded piles in such strata is a challenge due to the liquefaction of the shallow sands and negative skin friction / down-drag in the soft under-consolidated clay. Bored cast-in-situ piles of 1500 mm diameter extending to 50-60 m depth were used to carry 500-600 tonnes load.

Keywords: metro piers, soft clay, field vane shear tests, bored piles, negative skin friction

INTRODUCTION

The first phase of the rapid transit system at Kochi, Kerala (See Fig. 1) whose elevated route spans from Aluva to Thripunithura covers a total distance of about 25 kilometers. One of the more critical sections of the viaduct exists near the Ernakulam Junction Railway station where the alignment takes a sharp curve to move towards Vyttila, crossing the railway tracks and running partially over the approach of South over-bridge.

In this section, four piers located on either side of the railway tracks near the Route Relay Cabin of Ernakulam Junction Railway Station pass through an area with substantial thickness of soft under-consolidated clay.

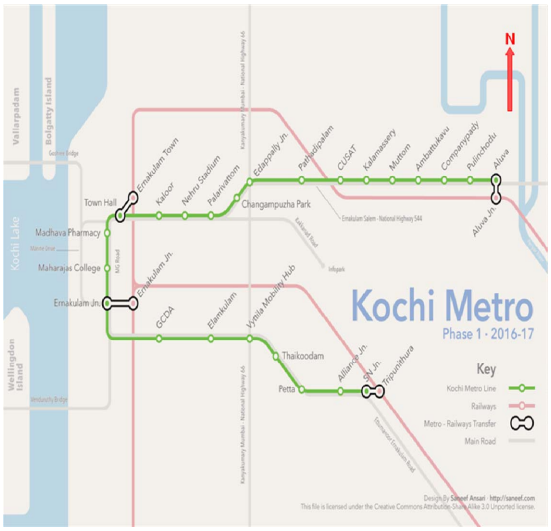


Fig. 1. Metro Route Alignment

The alignment is geotechincally challenging due to the presence of loose liquefiable sand and soft under-consolidated and sensitive clay.

Initial investigations by the owner based on limited boreholes only yielded conservative and inconclusive pile capacities. For a thorough understanding of the soil behaviour, a detailed geotechnical investigation was carried out to assess the engineering behaviour of the soil strata.

The scope of the geotechnical investigation included two boreholes and a static cone penetration test at each pier location. In the boreholes, field vane shear tests were conducted at different depths in addition to the routine SPT.

Photographs of the field investigation in progress are presented on Fig. 2.

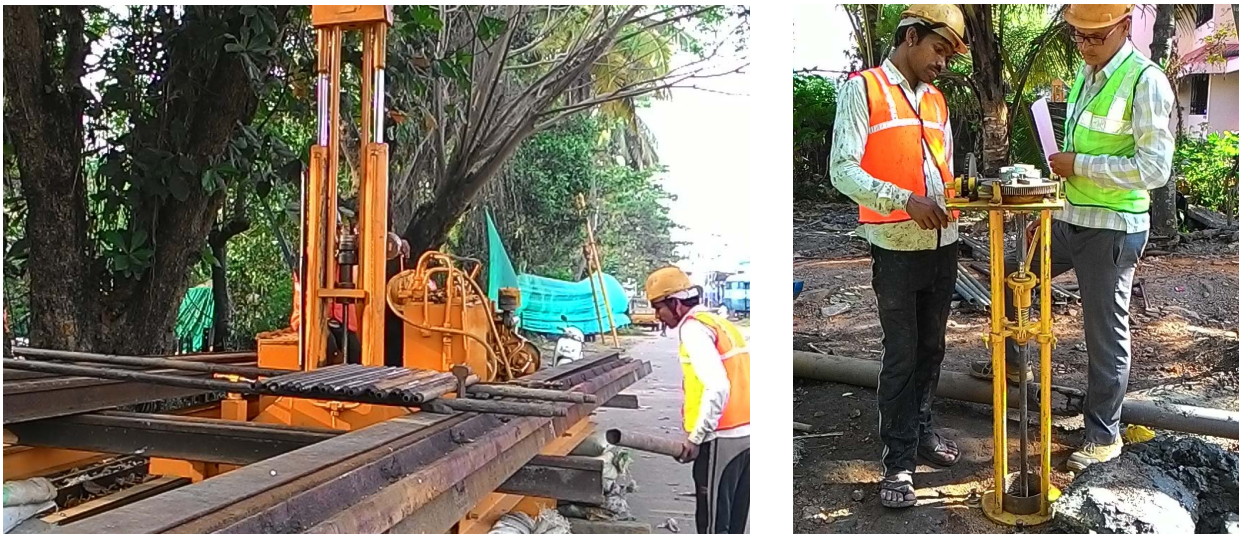


Fig. 2. Field investigation in progress. Photograph on left shows dead load placed over the Static cone penetrometer rig since the anchors could not provide sufficient reaction. Photograph on right shows field vane shear test in progress

REGIONAL GEOLOGY

Kochi is an alluvial plain on the southwest coast of India, in the southern state of Kerala. The city lies at the sea mouth of seven major rivers which start from the Western Ghats and travel through Kerala's midlands, lowlands and coastal areas, to drain out into the Arabian Sea. The alluvial formations occurring in this coastal belt constitute sand, silt, clay of the lagoonal and back water deposits, beach deposits and the river/flood plain deposits in mid-land areas (Narayana & Priju, 2006).

SITE STRATIGRAPHY

The four piers are located over a 220 m stretch. The piers are numbered 750, 751, 751B and 752. In spite of the relatively small distance of 50-100 m between the pier locations, the investigations revealed substantial variations in stratigraphy from one pier to the next.

In general, there is a surficial silty sand stratum to 5-11 m depth. Groundwater is shallow and met at less than 1 m depth. This sand layer is liquefiable to 4-7.5 m depth during earthquakes.

Below this, soft to firm silty clay is met to 20-25 m depth. The clay has high moisture content, close to the liquid limit. It is under-consolidated to normally consolidated in nature with SPT values of 1-5. The cone tip resistances (q_c) range from 0 to 25 kg/cm^2. Field vane shear tests in this stratum indicated undrained shear strength in the range of 0.25 to 0.7 kg/cm^2 for undisturbed condition. The remoulded undrained shear strength is in the range of 0.06 to 0.4 kg/cm^2 indicating that the clay is sensitive with sensitivity of 4 to 6.

Below the soft clay, stiff to hard clay is met to 62-65 m depth underlain by hard organic clay (peat) with intermediate discontinuous sand layers. SPT in this deposit generally exceeds 30-40. The cone tip resistances (q_c) range from 30 to as high as 200 kg/cm^2. Refusal (N>100) is met below 54-60 m depth. The peat has a low bulk density of about 1.40 gm/cm^3 due to the low specific gravity of peat. However,

SPT values in the peat are high, ranging from 90 to more than 100. The peat stratum is underlain by a hard white clay layer with SPT values of 40-100.

A cross-sectional profile along the route alignment is presented on Fig. 3.

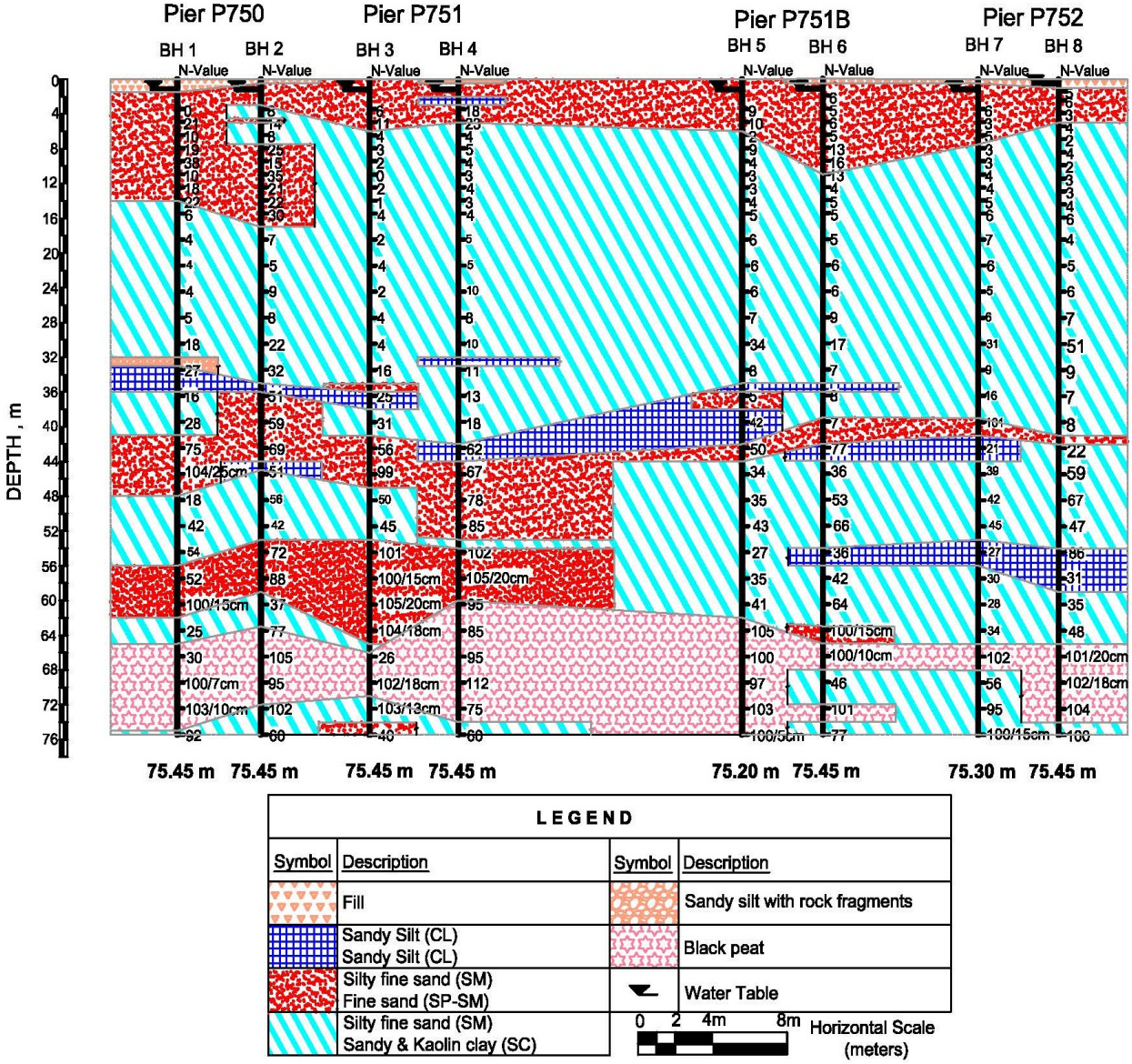


Fig. 3. Cross-Sectional Profile

Soil Characteristics at Each Pier Location

The soil characteristics at each pier location were evaluated in detail to assess the safe pile capacity. Typical soil properties including N-values, cone tip resistance and undrained shear strength profiles at Piers 751 and 752 are presented on Figs. 4 and 5.

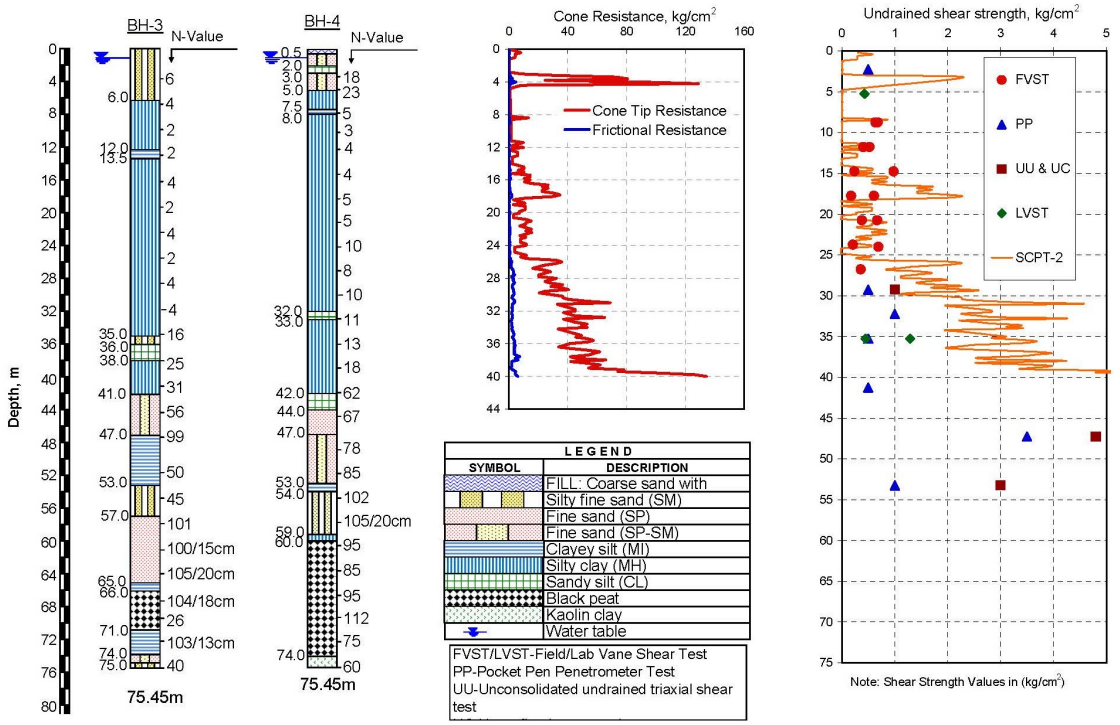


Fig. 4. Soil Characteristics at Pier 751

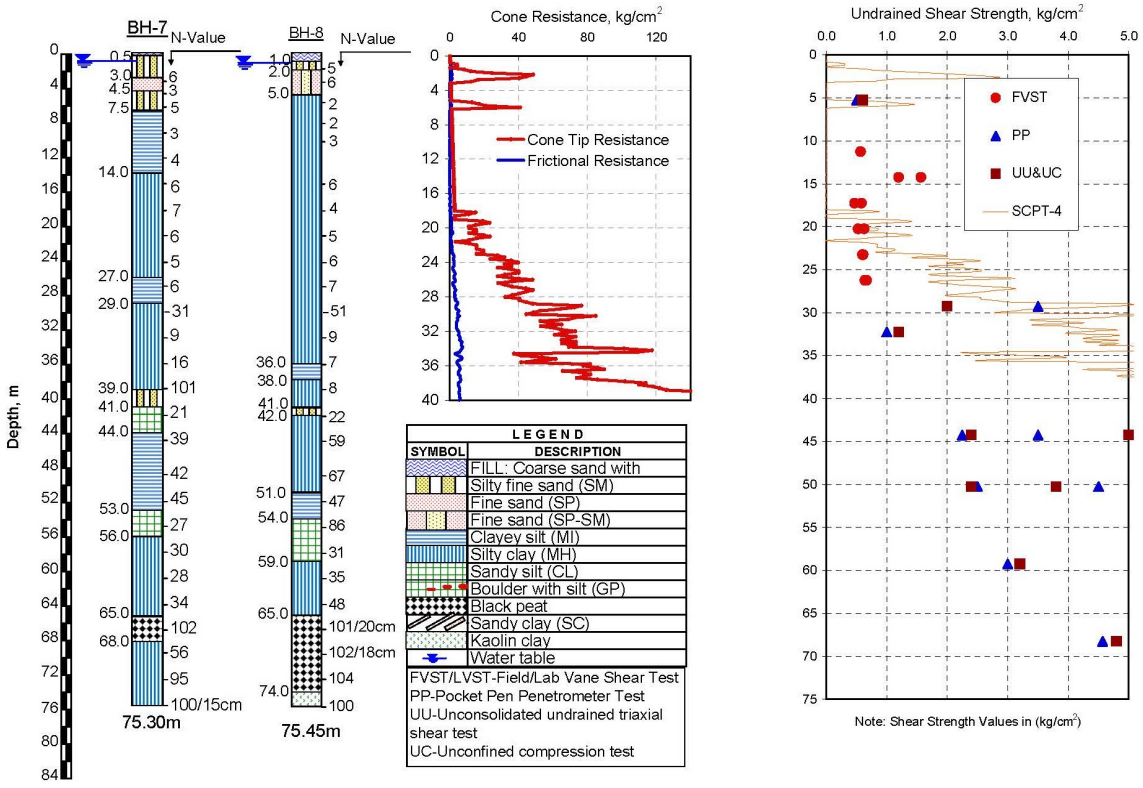


Fig. 5. Soil Characteristics at Pier 752

Engineering Characteristics of the Soft Clay

The soft clay is under-consolidated to normally-consolidated. A typical consolidation test conducted on it is presented on Fig. 6. It is highly sensitive with significant loss of shear strength on remoulding. The sensitivity ranges from 4 to 6 as illustrated in Fig. 7.

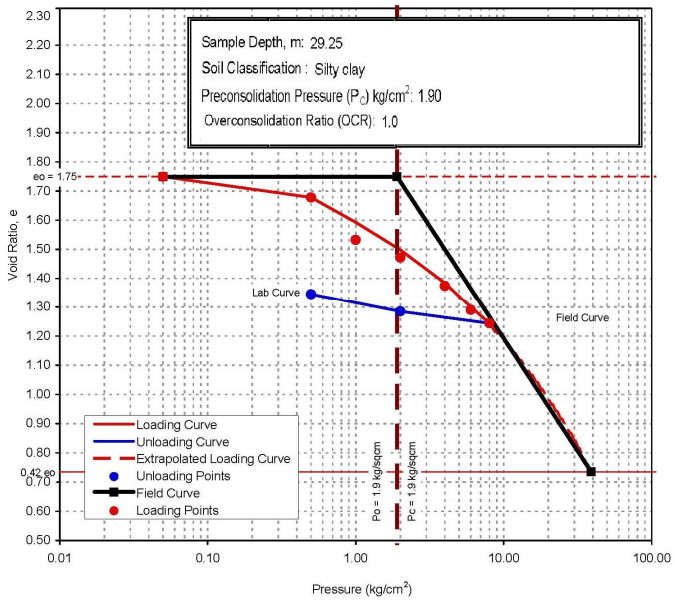


Fig. 6. Typical Consolidation Test Results

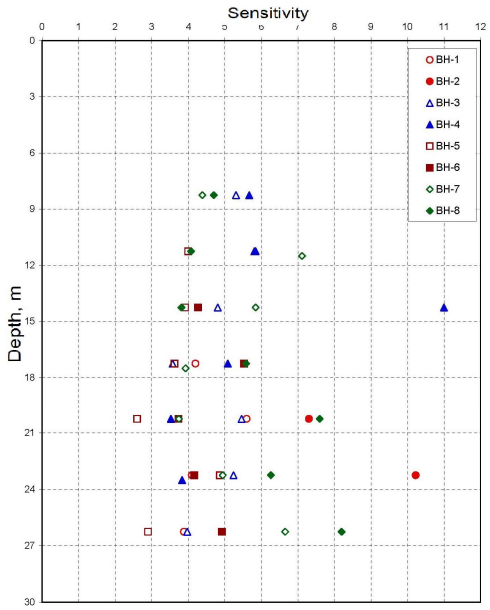


Fig. 7. Sensitivity versus Depth

FOUNDATION DESIGN

Liquefaction Susceptibility Assessment

As per IS: 1893 (Part-1) – 2002, the project area is in Earthquake Zone 3. The design parameters for liquefaction analysis used are as follows:

Earthquake magnitude on Richter scale : 6.0
Peak ground acceleration : 0.16g
Design Groundwater level : at ground level
Silt content in shallow fine sand layer : 3-5%

The liquefaction susceptibility assessment was performed as per the Summary Report of NCEER (Youd and Idris, 2001). Liquefaction analysis was done based on the SPT and q_c values. Since the investigation did not include measurement of shear wave velocities, the analysis was restricted to SPT and q_c.

As per the simplified procedure, the factor of safety (FS) against liquefaction is given by the following equation:

$$FS = \left[\frac{CRR_{7.5}}{CSR}\right] MSF \qquad [1]$$

Where

CSR = Cyclic Stress Ratio, generated by the earthquake shaking
$CRR_{7.5}$ = Cyclic Resistance Ratio for magnitude 7.5 earthquakes; and
MSF = Magnitude Scaling Factor, used to scale the calculated $CRR_{7.5}$ values to the design earthquake magnitude.

A Magnitude Scaling Factor (MSF) of 1.990 (based on a mean of Scaling Factors defined by various investigators recommended by the NCEER Summary Report, 2001) was applied to the $CRR_{7.5}$ value, to adjust the clean sand curves to the design earthquake magnitude of 6.0. The results are summarized in Table 1.

Table 1. Assessment of Liquefaction Susceptibility

Pier	Liquefaction Susceptibility Assessment
750	Liquefaction potential between 1.5-3.0 m depth
751	Liquefaction potential to 4.5 m depth
751B	Liquefaction potential to 5.0 m depth
752	Liquefaction potential to 5-7.5 m depth

Pile Capacities

Reinforced Cement Concrete (RCC) bored cast in-situ piles of 1500 mm diameter were planned to be used to support the piers. As per the design, the downward compression load on each pile was about 600 tonnes.

In spite of the relatively small distances between the pier and test locations, the investigations revealed substantial variations in stratigraphy. The soft clay stratum is encountered at the pier locations from 5 to 8 m and from 18 to 24 m depths at Piers P-751, P-751B and P-752. At Pier P-750 location, the soft stratum is encountered between about 14 m and 30 m depth. In these depth zones, negative skin friction / downdrag have been considered on the piles. Pile capacities have been calculated based on the following boundary conditions:

Pile Cut-Off-Level (COL) : 3.0 m depth below EGL
Design Groundwater Level : At Ground Level
Depth of Liquefaction Potential : 3.0 m depth below EGL
Overburden pressure considered to become constant below 15 pile diameters

Typical design profile for Pier 751 is shown in Table 2.

Table 2. Design profile for Pier 751

Layer No.	Depth, m From	Depth, m To	Soil Classification	SPT values	q_c values kg/cm^2	c T/m^2	ϕ degrees	γ T/m^3
1	0.0	3.0	Fill	-	2	Ignored		1.60
2	3.0	5.0	Loose silty sand	9	11	0	30	1.65
3	5.0	24.0	Very soft silty clay	3	5	2.5	0	1.55
4	24.0	32.0	Firm silty clay	6	30	4.0	4	1.50
5	32.0	42.0	Very stiff silty clay	17	50	6.0	5	1.70
6	42.0	60.0	Very dense fine sand	60	-	0	32	1.85
7	60.0	74.0	Peat	95	-	14.0	4	1.40
8	74.0	75.0	Hard clay	50	-	20.0	6	1.90

Negative skin friction was considered in the soft clay stratum between 5 and 24 m depth.

Based on the analysis, safe pile capacities for 1500 mm diameter bored cast-in-situ piles computed in accordance with IS 2911 (Part 1/Section 2): 2010 are summarized in Table 2 below. The values include a factor of 2.5 under compression load and 3.0 for uplift.

Table 3. Computed Safe Pile Capacities – 1500 mm diameter Bored Piles

Pier	Pile Length below COL, m	Computed Safe Pile Capacities, Tonnes		Magnitude of Negative Skin Friction (in ultimate capacity), Tonnes	Remarks
		Compression (FS=2.5)	Uplift (FS=3.0)		
Pier P750	50	430	277	81.5	Pile tip in hard clay
	53	646	307		Pile tip in dense sand
Pier P751	52	561	281	96.8	Pile Tip in dense sand
	55	611	310		
Pier P751B	65	585	380	71.3	Sand zones not met. Pile tip in hard clay
	70	646	418		
Pier P752	66	564	369	61.1	Sand zones not met. Pile tip in hard clay
	71	622	406		

The piling system has been designed using the above capacities. As may be seen in the above table, the pile tip level has to be decided depending upon the bearing strata. Where thick sand zones are met, pile length is relatively less.

The contractor was advised to perform pile load tests at all four pier locations since the results cannot be generalized over the stretch. The negative skin friction is a long-term phenomenon and will not be mobilized during the load test on the test pile which is usually conducted over a 36 to 48 hour period. To ensure that the piles are safe under the design loads, the applied load on the test pile has to be at least equal to the computed ultimate pile capacity load plus the magnitude of negative skin friction.

CONCLUDING REMARKS

The geotechnical investigation program should be planned carefully to incorporate appropriate tests as per the strata conditions. Project specifications should be formulated accordingly as against the current practice of having standard specifications for all ground conditions.

The design of piles in strata containing soft clay and loose sand requires a detailed and thorough geotechnical investigation. Static cone penetration tests and field vane shear tests should supplement the routine investigation by boreholes so as to add value to the geotechnical data and characterize the soils properly. The design should be optimized after assessing the thickness of the zone that may experience negative skin friction. Pile load tests should consider the influence of negative skin friction on the test results.

REFERENCES

IS 1893 (Part-1): 2002. Indian Standard Criteria for Earthquake Design of Structures, Part 1: General Provisions and Buildings. 5th revision. Bureau of Indian Standards, New Delhi.

IS 2911 (Part 1/Section 2): 2010. Indian Standard. Design and Construction of Pile Foundations – Code of Practice. Part 1 Concrete Piles. Section 2 Bored Cast-in Situ Concrete Piles. 2nd revision. Bureau of Indian Standards, New Delhi.

Narayana, A.C, and Priju, C.P. 2006. Evolution of coastal landforms and sedimentary environment of the late Quaternary period along Central Kerala, southwest coast of India. Journal of Coastal Research, Special Issue 39. Proceedings, 8th International Coastal Symposium, Brazil, 2004. pp 1898-1902

Youd, T.L., and Idriss, I.M. 2001. Liquefaction Resistance of Soils: Summary Report from the 1996 NCEER and 1998 NCEER/NSF Workshops on Evaluation of Liquefaction Resistance of Soils. Journal of Geotechnical and Geo-environmental Engineering, April 2001. pp 297-313.

.